Effects of variable organic matter C:N:P stoichiometry on carbon cycling in the northwest European shelf seas

Dissertation zur Erlangung des Doktorgrades der Naturwissenschaften (Dr. rer. nat.)
an der Fakultät für Mathematik, Informatik und Naturwissenschaften
im Fachbereich Erdsystemwissenschaften
der Universität Hamburg

vorgelegt von

Kubilay Timur Demir

aus Dormagen

Hamburg, 2025

Fachbereich Erdsystemwissenschaften

Datum der Disputation:	23.01.2026
Gutachter:innen der Dissertation:	Prof. Dr. Corinna Schrum
	Prof. Dr. Helmuth Thomas
Zusammensetzung der Prüfungskommission:	Prof. Dr. Corinna Schrum
	Prof. Dr. Helmuth Thomas
	Dr. Moritz Mathis
	Prof. Dr. Jörn Behrens
	Prof. Dr. Christin Bernhold
Vorsitzender des Fach-Promotionsausschusses Erdsystemwissenschaften:	Prof. Dr. Dirk Notz
Dekan der MIN Fakultät:	Prof. Dr. Ing. Norbert Ritter

Abstract

Marine ecosystems couple the flows of carbon and nutrients from their assimilation by primary producers, through food webs and microbial ecosystems, to their eventual release through respiration back into the environment. Since Alfred C. Redfield first observed consistent ratios of carbon, nitrogen, and phosphorus across global phytoplankton communities and in the uptake of inorganic nutrients, the coupling of these elemental cycles in marine ecosystems has widely been described by the canonical Redfield ratios of C:N:P = 106:16:1 in biomass or C:N:P = 105:15:1 in the uptake of inorganic carbon and nutrients. This framework has informed the representation of living cells, including phytoplankton and heterotrophs, as well as non-living or detrital organic matter in regional and global biogeochemical models. However, observations over recent decades have revealed systematic deviations from these ratios, with differences among living cells and non-living organic matter, as well as across size and lability fractions. This variability challenges the assumption of constant stoichiometry in organic matter cycling in marine ecosystems, calling for a reassessment of existing model representations with fixed elemental ratios.

This dissertation addresses this uncertainty in Redfield stoichiometry-based model representations by examining the effects of observed variations in organic matter C:N:P stoichiometry on marine carbon cycling. It first synthesizes global observations across living cells, including phytoplankton and heterotrophs, as well as non-living dissolved and particulate organic matter. By evaluating the environmental drivers of this variability, exploring its implications for biogeochemical cycles, and reviewing past model implementations of variable stoichiometry, this review provides a foundation for subsequent model development and regional impact assessment, which form the main body of this work.

Building on the global synthesis of observed stoichiometric variability, the dissertation explores its regional implications by quantifying the effects of variable organic matter C:N:P stoichiometry on carbon cycling in the northwest European shelf seas. This is achieved by incorporating variable stoichiometry into the representation of dissolved and particulate organic matter in a coupled physical–biogeochemical modeling system. Two process representations are implemented, including the preferential remineralization of organic nitrogen and phosphorus relative to carbon, and the extracellular release of carbon-rich dissolved organic matter by phytoplankton. The assessment focuses on how these processes, individually and in combination, affect the balance between carbon fixation and respiration, as well as seasonal and annual air–sea CO_2 exchange, and cross-shelf

exchanges with the northeastern Atlantic Ocean.

The results show that variable C:N:P stoichiometry enhances seasonal biological drawdown of CO_2 by strengthening pre-existing seasonal, vertical, and lateral gradients in net community production. These effects are most pronounced in the deep, seasonally stratified regions of the central and northern North Sea, the Norwegian Trench, and along the steep shelf edge, where biological CO_2 drawdown is most efficient due to the vertical separation of production and respiration. The resulting increase in the seasonal vertical gradient of dissolved inorganic carbon drives a higher annual oceanic CO_2 uptake by approximately 10–30 percent and enhances the cross-shelf export of dissolved inorganic carbon, accounting for roughly 60–90 percent of the additionally sequestered CO_2. Impacts on organic carbon stocks and fluxes are smaller and more variable. In addition to the annual increase in oceanic CO_2 uptake, the maximum uptake is shifted from winter to spring and summer due to increased biological control of the surface partial pressure of CO_2.

These insights demonstrate that regional physical and biogeochemical conditions strongly influence the effects of variable stoichiometry, emphasizing the need to represent C:N:P variability in both regional models and global representations of the coastal ocean. They also suggest that shifts in organic matter stoichiometry under environmental change can influence the efficiency of carbon export through the biological carbon pump. By quantifying the regional effects of variable C:N:P stoichiometry in the northwest European shelf seas, this dissertation offers a first glimpse into the regional variability of these effects and contributes to sustained improvements in the model representation of biogeochemical cycles at both regional and global scales.

Zusammenfassung

Marine Ökosysteme koppeln die Elementkreisläufe von Kohlenstoff und Nährstoffen von ihrer Aufnahme durch Primärproduzenten über die Nahrungskette und mikrobielle Prozesse bis hin zu ihrer Freisetzung durch Zellatmung in die Umgebung. Seit Alfred C. Redfield erstmals beobachtete, dass die Verhältnisse von Kohlenstoff, Stickstoff und Phosphor in Phytoplankton-Gemeinschaften und bei der Aufnahme anorganischer Nährstoffe global konsistenten Verhältnissen folgen, wird die Kopplung dieser Elementkreisläufe in marinen Ökosystemen durch die etablierten Redfield-Verhältnisse von C:N:P = 106:16:1 in Plankton-Biomasse oder C:N:P = 105:15:1 bei der Kohlenstoff- und Nährstoffaufnahme beschrieben. Dieser Zusammenhang prägt seitdem die Repräsentation lebender Zellen, einschließlich Phytoplankton und Heterotrophen, sowie nicht lebender oder detritischer organischer Substanzen in regionalen und globalen biogeochemischen Modellen. Beobachtungen der letzten Jahrzehnte haben jedoch systematische Abweichungen von diesen Verhältnissen aufgezeigt, mit Unterschieden zwischen lebenden Zellen und nicht lebender organischer Substanz sowie zwischen verschiedenen Größen- und Labilitätsfraktionen. Diese Variabilität stellt die Annahme konstanter C:N:P-Verhältnisse in der Produktion und Dekomposition organischer Substanz in marinen Ökosystemen in Frage und erfordert eine Neubewertung bestehender Modelldarstellungen mit festen Elementverhältnissen.

Diese Dissertation adressiert die Unsicherheit in den auf Redfield-Verhältnissen basierenden Modelldarstellungen, indem sie die Auswirkungen der beobachteten Abweichungen in den C:N:P-Verhältnissen organischer Stoffe auf den marinen Kohlenstoffkreislauf untersucht. Zunächst werden globale Beobachtungen über lebende Zellen, einschließlich Phytoplankton und heterotrophen Organismen, sowie nicht lebende gelöste und partikuläre organische Stoffe in einer Übersichtsarbeit zusammengefasst. Diese bewertet die Umweltbedingungen, die die Variabilität der C:N:P-Verhältnisse beeinflussen, untersucht ihre Auswirkungen auf biogeochemische Stoffkreisläufe und vergleicht frühere Modellimplementierungen. Diese Kontextualisierung bildet eine Grundlage für die anschließende Modellentwicklung und die regionale Folgenabschätzung, die den Hauptteil dieser Arbeit darstellen.

Aufbauend auf der globalen Synthese der beobachteten Variabilität in C:N:P Verhältnissen untersucht die Dissertation deren regionale Relevanz und quantifiziert die Auswirkungen der variablen C:N:P-Verhältnisse auf den Kohlenstoffkreislauf in den nordwesteuropäischen Schelfmeeren. Dies wird erreicht, indem die variable Stöchiometrie in die Darstellung gelöster und partikulärer organischer Substanzen

eines gekoppelten physikalisch-biogeochemischen Modellsystems integriert wird. Diese wird durch zwei Prozessdarstellungen implementiert, darunter die bevorzugte Remineralisierung von organischem Stickstoff und Phosphor im Verhältnis zu Kohlenstoff sowie die extrazelluläre Freisetzung kohlenstoffreichen gelösten organischen Materials durch Phytoplankton. Die Bewertung konzentriert sich auf den Einfluss dieser Prozesse, einzeln und in Kombination, auf das Gleichgewicht zwischen der Bindung und Freisetzung von Kohlenstoff, auf die saisonale und jährliche CO_2-Aufnahme, sowie auf Austauschflüsse mit dem Nordostatlantik über die Schelfkante.

Die Ergebnisse zeigen, dass variable C:N:P-Verhältnisse die saisonale biologische CO_2-Absenkung in tiefere Schichten intensivieren, indem sie die bereits bestehenden saisonalen, vertikalen und lateralen Gradienten in der Netto-Produktionsbilanz des Ökosystems verstärken. Diese Effekte sind am ausgeprägtesten in den tiefen, saisonal stratifizierten Regionen der zentralen und nördlichen Nordsee, im Norwegischen Graben und entlang der Schelfkante, wo die biologische CO_2-Absenkung aufgrund der vertikalen Trennung von Produktion und Dekomposition organischer Stoffe am effizientesten ist. Der daraus resultierende Anstieg des saisonalen vertikalen Gradienten von gelöstem anorganischem Kohlenstoff führt zu einer um etwa 10 bis 30 Prozent höheren CO_2-Aufnahme durch den Ozean und zu einem verstärkten Export von gelöstem anorganischem Kohlenstoff über die Schelfkante hinaus, was etwa 60 bis 90 Prozent des zusätzlich gebundenen CO_2 ausmacht. Die Auswirkungen auf die organischen Kohlenstoffspeicher und Kohlenstoffflüsse sind geringer und variabler. Zusätzlich zum jährlichen Anstieg der CO_2-Aufnahme verschiebt sich das saisonale Maximum der Aufnahme von Winter in den Frühling und Sommer, da der CO_2-Partialdruck an der Oberfläche verstärkt durch biologische CO_2-Bindung kontrolliert wird.

Diese Erkenntnisse zeigen, dass regionale physikalische und biogeochemische Bedingungen die Auswirkungen variabler C:N:P Stöchiometrie stark beeinflussen, was die Notwendigkeit hervorhebt, diese Variabilität in C:N:P-Verhältnissen sowohl in regionalen Modellen als auch in globalen Darstellungen der Küstenmeere zu berücksichtigen. Sie deuten auch darauf hin, dass Änderungen in der Stöchiometrie organischer Stoffe unter Umweltveränderungen die Effizienz des Kohlenstoffexports in tiefere Schichten durch die biologische Kohlenstoffpumpe beeinflussen können. Durch die Quantifizierung der regionalen Auswirkungen variabler C:N:P-Verhältnisse in den nordwesteuropäischen Schelfmeeren bietet diese Dissertation einen ersten Einblick in die regionale Variabilität dieser Auswirkungen und leistet einen Beitrag zur fortlaufenden Verbesserung der Modellierung biogeochemischer Kreisläufe auf regionaler wie auch auf globaler Ebene.

List of Publications

Publications related to this dissertation:

Article I (Appendix A):
Demir, K. T., Mathis, M., Daewel, U., Thomas, H., and Schrum, C. C:N:P stoichiometry of marine organic matter in the global coastal and open oceans: Patterns and predictors, biogeochemical implications, and model representations. (*to be submitted*)

Article II (Appendix B):
Demir, K. T., Mathis, M., Kossack, J., Liu, F., Daewel, U., Stegert, C., Thomas, H., and Schrum, C. (2025b). Variable organic matter stoichiometry enhances the biological drawdown of CO_2 in the northwest European shelf seas. *Biogeosciences*, 22, 2569–2599, doi: 10.5194/bg-22-2569-2025

Article III (Appendix C):
Demir, K. T., Mathis, M., Kossack, J., Liu, F., Daewel, U., Stegert, C., Thomas, H., and Schrum, C. (2025a). Organic matter stoichiometry regulates the continental shelf carbon pump efficiency of the northwest European shelf seas. ESS Open Archive [Preprint]. Submitted to *Global Biogeochemical Cycles* (*under review*), doi: 10.22541/essoar.175088438.85557149/v1

Table of Contents

Abstract iii

Zusammenfassung v

List of Publications vii

Table of Contents viii

Unifying essay: Effects of variable organic matter C:N:P stoichiometry on carbon cycling in the northwest European shelf seas

1 Introduction 1

2 Global variations in the C:N:P stoichiometry of marine organic matter 7

3 Influence of variable C:N:P stoichiometry on net community production and air–sea CO_2 exchange in the northwest European shelf seas 15

4 Effects of variable C:N:P stoichiometry on the carbon budget and export contributions of the northwest European shelf seas 22

5 Summary and Outlook 27

Bibliography 29

Appendix A: *Article* I 39

Appendix B: *Article* II 116

Appendix C: *Article* III 201

Acknowledgements 254

Unifying essay:

Effects of variable organic matter C:N:P stoichiometry on carbon cycling in the northwest European shelf seas

1 Introduction

This dissertation re-examines the interactions between the continuous production and recycling of organic matter (OM) in marine ecosystems, and the coupling of the elemental cycles of carbon (C), nitrogen (N), and phosphorus (P) in the context of biogeochemical model representations. The assimilation of carbon and nutrients by primary producers, including the macronutrients nitrogen and phosphorus, as well as other elements such as sulfur and iron, which are required in smaller amounts, is inherently linked through their allocation to cellular macromolecules (e.g., proteins, lipids, carbohydrates, nucleic acids) that form biomass and sustain metabolic functions. This relationship is described within the framework of ecological stoichiometry (Meunier et al., 2025; Sterner & Elser, 2002). Certain elements are essential only for particular taxa rather than for primary producers in general. For example, these include silicon, which is used to build diatom frustules, or calcium, which is used to form coccoliths in coccolithophores. The ecological stoichiometry of heterotrophic organisms continues to couple the flows of carbon, nutrients, and energy through trophic interactions in marine food webs and across entire ecosystems, until respiration returns them to the environment as inorganic compounds (Fig. 1.1). The production and decomposition of OM further links dissolved oxygen in seawater to the cycling of carbon and other elements, as photosynthesis releases oxygen while assimilating CO_2, whereas respiration consumes oxygen while releasing CO_2.

As a result, the coupling of carbon and nutrient cycles through the C:N:P stoichiometry of organisms and non-living or detrital OM has consequences not only for marine ecosystems, but also for broader Earth system dynamics and society. It is central to three of the nine planetary boundaries, whose thresholds are critical for defining a safe operating space for humanity: climate change, ocean acidification, and global biogeochemical fluxes of nitrogen and phosphorus (Richardson et al.,

2023; Rockström et al., 2009). The coupling of elemental cycles influences these planetary boundaries through the relative fluxes of carbon and nutrients between compartments and their sequestration in OM, with the resulting balance between carbon fixation and respiration affecting both the efficiency of the biological carbon pump and air–sea CO_2 exchange (del Giorgio & Duarte, 2002; Hopkinson & Vallino, 2005). Given its role in planetary boundaries and in marine carbon cycling and ecosystems, this carbon–nutrient coupling is relevant to the United Nations Sustainable Development Goals 13 (climate action) and 14 (life below water), which target sustainable adaptation to maintain environmental conditions and ecosystem services for society (United Nations, Department of Economic and Social Affairs, 2025), and to international research efforts, including the Integrated Ocean Carbon Research program of the UNESCO Intergovernmental Oceanographic Commission (Aricò et al., 2021). Aricò et al. (2021) stressed the need to revisit the coupling of carbon and nutrients in OM cycling, emphasizing exchanges between the coastal and open ocean, where the stoichiometry in imports and exports can influence regional air–sea CO_2 exchange, and to refine its representation in marine biogeochemical models, which often rely on fixed elemental ratios, thereby neglecting regional variability and potential shifts under future environmental conditions (Bauer et al., 2013; Dai et al., 2022; Liu et al., 2025).

Alfred C. Redfield (1890–1983; Sterner & Elser 2002) formulated a global approximation of constant ratios of C:N:P = 106:16:1 in phytoplankton biomass, and C:N:P = 105:15:1 in the uptake of inorganic carbon and nutrients (Redfield, 1934, 1958; Redfield et al., 1963). These are known as the Redfield ratios, which have since provided a framework for this coupling in marine ecosystems. Based on measurements of phytoplankton composition across ocean regions (measured as seston, i.e., bulk suspended particulate matter; Sterner & Elser 2002), Redfield (1958) concluded that the average elemental stoichiometry of phytoplankton communities remains close to these ratios, and is reflected in the uptake of nutrients and dissolved inorganic carbon from surrounding waters. Although Redfield acknowledged differences across taxa and environments, he assumed that differences would largely balance out across broad ocean regions.

Secondly, Redfield noted that the N:P ratios of inorganic nutrients in seawater match those of living organisms, whereas carbon, being far more abundant, was not limiting. Rather than assuming that phytoplankton adaptation had adjusted cellular N:P ratios to match the environmental nutrient abundance, he proposed that the average composition of phytoplankton largely determines the relative nutrient abundance in the ocean, with processes such as nitrogen fixation from the atmosphere possibly having adjusted nutrient ratios to meet the requirements of primary producers over the past. At the same time, he already suggested potential deviations from these ratios, particularly with respect to the coastal ocean linked to land–sea coupling, and

in organic degradation products due to the faster recycling of organic phosphorus relative to nitrogen. These constant Redfield ratios have since been widely used in biogeochemical models to represent the composition of phytoplankton, heterotrophs, and detrital OM, to couple simulated elemental fluxes, and to derive relative nutrient and carbon fluxes from observations.

In recent decades, however, observational and experimental evidence, including mesocosm experiments, has repeatedly shown considerable and systematic deviations from this approximation (Geider & La Roche, 2002; Liang et al., 2023; Martiny et al., 2013; Tanioka, Garcia, et al., 2022). Collectively, these studies have revealed process-specific differences between living and non-living OM, and between fractions of dissolved (DOM) and particulate organic matter (POM) that differ in size and biological accessibility. In this context, dissolved organic carbon, nitrogen, and phosphorus (DOC, DON, DOP) and particulate organic carbon, nitrogen, and phosphorus (POC, PON, POP) are referred to as the elemental components of DOM and POM, respectively. A consistent carbon enrichment in DOM and POM, the tendency for carbon content to increase with depth due to the preferential recycling of nutrients, and instances of carbon overconsumption (i.e., where additional dissolved inorganic carbon uptake exceeds what would be expected from Redfield-equivalent nutrient uptake) together demonstrate global variability in C:N:P stoichiometry (Hopkinson & Vallino, 2005; Liang et al., 2023; Osterroht & Thomas, 2000; Tanioka et al., 2021; Thomas et al., 1999). These observations challenge the idea of constant C:N:P ratios in vertical and lateral OM fluxes and call for a re-evaluation of existing model frameworks based on this assumption, as well as their implications for the representation of biogeochemical cycles.

Revisiting such long-standing assumptions has previously advanced related areas of research. For instance, progress in analytical techniques and the expanded spatial coverage of global DOC surveys have overturned the view of this reservoir as homogeneous and passive, revealing pronounced variability across ocean basins and with depth, and an active role of DOM in the biological carbon pump (Hansell et al., 2009; Hopkinson & Vallino, 2005; Roshan & DeVries, 2017). Similarly, by broadening the scope to the observed variability in elemental C:N:P ratios of marine OM, centered around but extending beyond the classical Redfield ratio assumption, this dissertation re-examines the coupling of OM cycling and elemental fluxes. It highlights the limitations of assuming a spatially and temporally constant ratio that is uniform across all OM fractions, explores the implications of stoichiometric variability for biogeochemical cycles, and outlines directions for improving these representations in biogeochemical models through a more differentiated consideration of OM cycling and its stoichiometry.

Specifically, this work examines the effects of variable OM C:N:P stoichiometry on marine carbon cycling, first by synthesizing globally observed variability and its

implications based on literature, and second by quantifying its regional impact on the northwest European shelf seas. It emphasizes the balance between carbon fixation and respiration, as well as the resulting oceanic carbon uptake and export, including vertical and lateral fluxes between coastal and open ocean regions. To build a foundation for the subsequent model development and regional assessment, Section 2 discusses the main findings from *Article* I (Appendix A), examining global variability in OM C:N:P stoichiometry across different fractions and in both coastal and open oceans, providing a compilation of ranges for bulk DOM and POM (i.e., the total of all fractions), as well as phytoplankton and heterotrophs, and discussing their drivers and implications. It then compares past model implementations of OM cycling and variable C:N:P representations, covering both living cells and detrital POM and DOM, and offering guidance for future model development. Through this section, the dissertation addresses the following questions, aimed at quantifying variability in and developing model representations of the C:N:P stoichiometry in marine OM:

1. How do living cells and bulk DOM and POM compare in their average C:N:P stoichiometry, and how do these ratios vary across regions and depths?

2. What biological and environmental factors drive variability in the C:N:P stoichiometry of living cells and bulk DOM and POM fractions, and what are the implications for biogeochemical cycles?

3. How has variable OM C:N:P stoichiometry been incorporated into past regional and global biogeochemical models, and how do these representations differ in complexity?

4. How can future biogeochemical models achieve accurate representations of OM C:N:P stoichiometry while balancing complexity and computational cost, and considering observational constraints?

Building on this foundation, the dissertation centers on a regional impact assessment for the northwest European shelf seas, a temperate continental shelf that acts as a sink for atmospheric CO_2 (Frankignoulle & Borges, 2001; Kitidis et al., 2019; Legge et al., 2020; Thomas et al., 2005). Global applications have revealed an influence of C:N:P stoichiometry on the projected nitrogen fixation, food quality, carbon uptake and export under present, future, and glacial conditions (Kwiatkowski et al., 2018; Letscher & Moore, 2015; Matsumoto & Tanioka, 2020; Sullivan et al., 2024; Tanioka & Matsumoto, 2017; Tanioka et al., 2021), with vertical carbon export shown to be 9–20% higher when variable C:N:P stoichiometry is considered. However, the regional implications, particularly for coastal and marginal seas, remain largely unquantified. This dissertation addresses this gap through a two-part regional impact study. Section 3 synthesizes findings from *Article* II (Appendix B) on how variable C:N:P

stoichiometry affects the balance between carbon fixation and respiration, and the resulting annual and seasonal changes in air–sea CO_2 exchange. Section 4 contextualizes results from *Article* III (Appendix C) in terms of changes in the organic and inorganic carbon budgets, focusing on how shifts in carbon export contributions drive the previously found impact on air–sea CO_2 exchange. Together, these sections address the following questions regarding the regional impact of variable stoichiometry:

5. How does variable OM C:N:P stoichiometry influence the balance between carbon fixation and respiration in the northwest European shelf seas, as compared to constant Redfield stoichiometry?

6. How do these changes in carbon fixation and respiration affect the annual and seasonal air–sea CO_2 exchange, as compared to constant Redfield stoichiometry?

7. How does the response of CO_2 uptake to variable OM C:N:P stoichiometry in the northwest European shelf seas compare to global estimates? What role does regional variability play in shaping this response?

8. How is the response to variable OM C:N:P stoichiometry reflected in the organic and inorganic carbon budgets of the northwest European shelf seas?

9. Which changes in regional carbon export contributions are responsible for the resulting changes in the air–sea CO_2 exchange?

10. Can the impact of variable OM stoichiometry on air–sea CO_2 exchange and carbon export in the northwest European shelf seas be generalized across the global coastal ocean, or does the response depend on prevailing regional export pathways?

In addressing these questions, this work provides a first glimpse, through a first comprehensive and quantitative regional assessment, into the regional variability in the effects of variable OM C:N:P stoichiometry on regional carbon cycling, which is neglected in Redfield stoichiometry-based models. As such, it quantifies the resulting uncertainty of assuming Redfield stoichiometry in carbon cycle representations by illustrating it through a model-based case study of the northwest European shelf seas. It not only quantifies its impact on the regional carbon cycle on the shelf but also extends to the impact on cross-shelf exchanges with the open ocean, underscoring their potential significance for global biogeochemical cycles. This analysis thus contributes to a broader understanding of the role of continental shelves in the marine carbon cycle, mediating carbon exchanges between the land, atmosphere, and open ocean, and influencing biogeochemical cycles from regional to global scales.

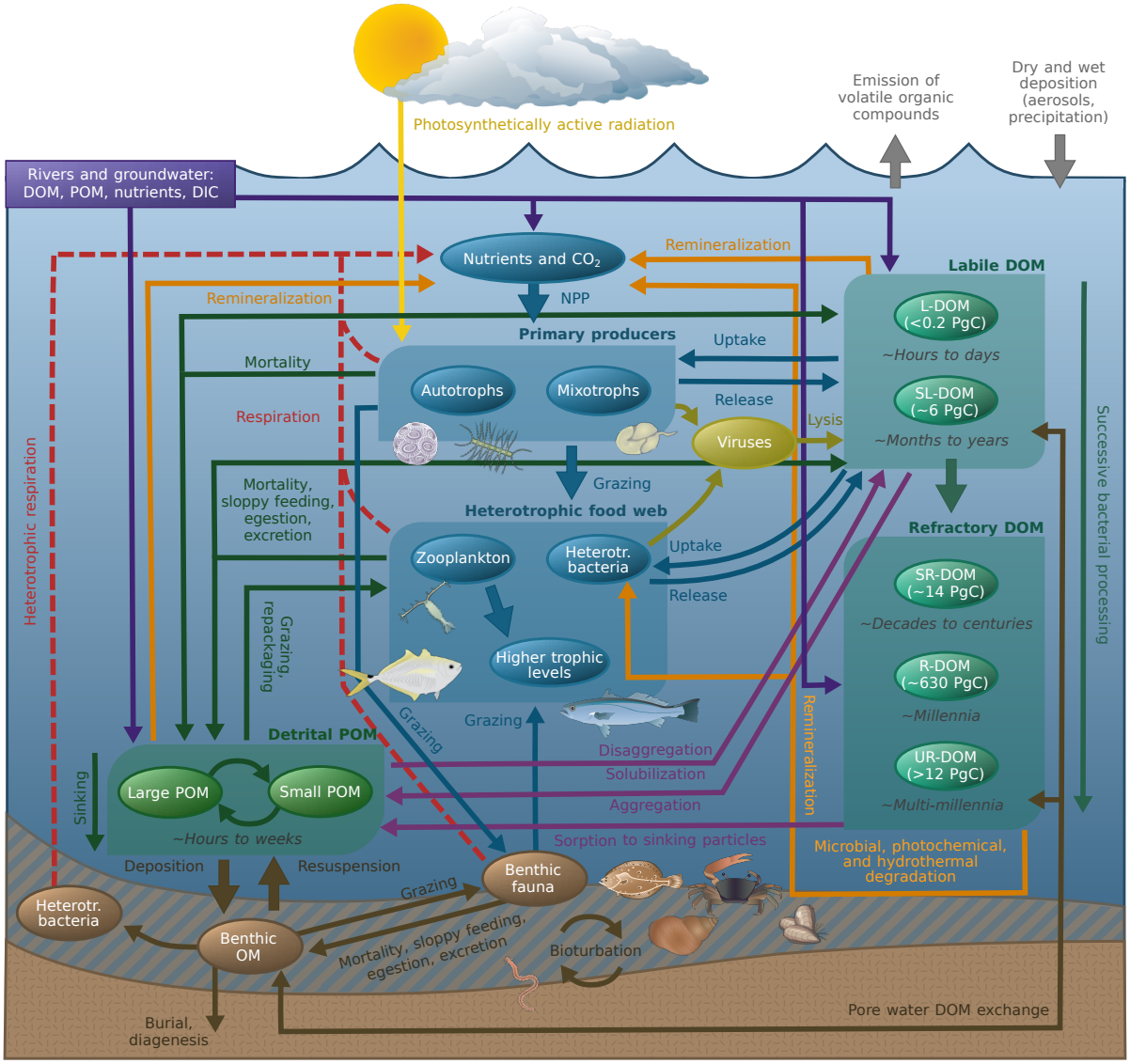

Figure 1.1: *Overview of organic matter (OM) cycling in the ocean, showing production, transformation, and removal pathways of particulate (POM) and dissolved organic matter (DOM). OM originates in the euphotic zone via primary production, with additional terrestrial and atmospheric inputs. POM enters the heterotrophic food web through grazing and is respired back to inorganic carbon and nutrients, aggregated into faster-sinking particles, or solubilized into DOM, with additional POM and DOM released through mortality, sloppy feeding, egestion, and excretion. A small fraction reaches the sediments and is partially preserved through diagenesis, after continued uptake and degradation by benthic fauna and heterotrophic bacteria. DOM is also produced by phytoplankton exudation, viral lysis, and POM solubilization, and is continuously transformed or removed via microbial uptake, respiration returning it to inorganic carbon and nutrients, particle sorption, and abiotic processes such as photooxidation. DOM consists of a diverse mixture of chemical compounds, with its continuum of lability categorized into discrete pools including labile (L-DOM), semi-labile (SL-DOM), semi-refractory (SR-DOM), refractory (R-DOM), and ultra-refractory (UR-DOM), with nomenclature, stocks, and lifetimes based on Hansell (2013). Labile DOM is transformed into more refractory forms by microbial and abiotic processes, contributing to long-term carbon sequestration via the microbial carbon pump as conceptualized by Jiao et al. (2011). Arrows indicate the direction of carbon and nutrient fluxes, with food web interactions shown from prey to predator. Figure objects were taken and partly modified from the UMCES IAN Media Library under a Creative Commons license CC BY-SA 4.0. The figure is reproduced from Article* I*, included in Appendix A.*

2 Global variations in the C:N:P stoichiometry of marine organic matter

Article I (Appendix A) reviews the global distribution, cycling, and C:N:P stoichiometry of marine OM, including living biomass and bulk DOM and POM, and provides the basis for the subsequent model development and the regional study on the northwest European shelf seas. It addresses questions 1–4 on variability in C:N:P stoichiometry, its drivers, biogeochemical implications, and past model representations. Before discussing stoichiometric variability, this section briefly overviews the global distribution and cycling of OM, and the contributions of DOM and POM to organic carbon export via the biological carbon pump, providing essential context for interpreting the drivers and implications of variable elemental C:N:P ratios.

At an estimated 700 Pg C, marine OM holds close to the 890 Pg C of carbon currently stored in atmospheric CO_2 (Friedlingstein et al., 2025). DOM constitutes the largest form of reduced carbon in the ocean with 662 ± 32 Pg C (Carlson et al., 2024; Hansell et al., 2009), operationally defined as material passing through a filter with a nominal size of 0.7 µm. DOM is categorized into discrete fractions of varying age and reactivity, with labile DOM (0.2 Pg C) recycled within days, semi-labile DOM (6 Pg C) accumulating seasonally in the epipelagic (0–200 m), semi-refractory DOM (14 Pg C) persisting on decadal timescales and being exported to the mesopelagic or twilight zone (200–1000 m), and long-lived refractory and ultra-refractory DOM (630 Pg C and 12 Pg C) with lifetimes exceeding deep ocean mixing timescales and therefore being well mixed (Hansell, 2013) (Fig. 1.1). In the surface ocean, DOC concentrations range roughly from 50–80 µM, with accumulation of semi-labile and semi-refractory fractions in addition to refractory DOC, declining with depth to 34–48 µM as semi-labile DOC decreases (Hansell, 2013; Hansell et al., 2009) (Tables 1–3, Appendix A). Both concentrations and vertical gradients are controlled by net DOC production and redistribution through large-scale ocean circulation (Hansell, 2013; Hansell et al., 2009; Roshan & DeVries, 2017). In coastal and marginal seas, DOC concentrations are higher, depending on residence time, water volume, and terrestrial inputs, exceeding 100 µM in the northwest European shelf seas (Tables 1–3, Appendix A).

Material that does not pass through this 0.7 µm filter is classified as POM, including living biomass and detritus. POM is seasonally produced and decomposed, with lifetimes of hours to weeks, and thus lacks the long-term persistence of DOM (Wakeham & Lee, 1993). Its vertical distribution decreases from maximum concentrations in the euphotic zone to near-zero at depth. The short-lived nature,

low concentrations, and strong seasonal variability make direct measurements challenging, so vertical POM distribution is typically estimated from export fluxes attenuating exponentially with depth, as described by the Martin curve (Buesseler & Boyd, 2009; Buesseler et al., 2020; J. H. Martin et al., 1987). Satellite-based estimates suggest a global POM stock of 3 Pg C, with roughly 2.3 Pg C in the upper 200 meters (Fox et al., 2024; Stramska, 2009), while marine biomass is estimated at 3–6 Pg C (Bar-On & Milo, 2019; Bar-On et al., 2018; Friedlingstein et al., 2025). Globally, surface POC concentrations average roughly 6 µM in the open ocean, ranging 2–17 µM depending on latitude and season (Fox et al., 2024; Martiny et al., 2014; Stramska, 2009; Tanioka, Larkin, et al., 2022) (Table 4, Appendix A). Low-latitude oceans range 2–7 µM, high-latitude regions 6–10 µM, with higher accumulation in coastal and marginal seas, reaching average concentrations up to 16 µM in the northwest European shelf seas (Chaichana et al., 2019). Thus, while the bulk DOC pool is over 200 times larger than POC, with surface concentrations 5–40 times higher, much of it cycles only on millennial timescales, so despite lower concentrations, POC plays a central role in carbon export.

This observed distribution of marine OM results from a dynamic balance between continuous production, transformation, and removal of POM and DOM (Carlson et al., 2024; Wakeham & Lee, 1993) (Fig. 1.1). POM and DOM are formed through primary production in the euphotic zone, with additional contributions from terrestrial and atmospheric inputs (Bianchi, 2011; Field et al., 1998; Xie et al., 2023). POM is produced as phytoplankton biomass, while DOM is also released through phytoplankton exudation, viral lysis, and solubilization of POM (Cai & Jiao, 2023; Carlson et al., 2024; Mühlenbruch et al., 2018; Thornton, 2014). POM enters the heterotrophic food web via grazing on lower trophic levels and the repackaging of detrital POM. Heterotrophic respiration of grazers, as well as bacterial uptake and respiration of DOM continuously release CO_2 and nutrients (Rivkin & Legendre, 2001). Both POM and DOM are also released through mortality, sloppy feeding, egestion, and excretion (Carlson et al., 2024; Møller, 2007; Møller et al., 2003; Wakeham & Lee, 1993). Dynamic exchanges occur along a continuum of particle sizes, including colloids and marine gels, with aggregation of DOM or small POM into larger aggregates and solubilization of POM to DOM (He et al., 2016). While most labile DOM is rapidly recycled through the microbial loop (Moran et al., 2022), a small fraction is progressively transformed into more recalcitrant forms through microbial processing, contributing to long-term carbon sequestration via the microbial carbon pump (Cai & Jiao, 2023; Dittmar et al., 2021; Jiao et al., 2011; Moran et al., 2022).

In interaction with these OM cycling processes, carbon and nutrients are redistributed through sinking, migration, and ocean circulation. One major consequence of this is the export of organic carbon to depth via POM and DOM. This export, conceptualized as the biological carbon pump, is a major mechanism for oceanic CO_2 uptake, with

carbon fixed at the surface by primary production and released through respiration at depth. POC is transported by sinking and circulation, with a small fraction reaching the sediments and stored up to multi-millennial timescales through burial and diagenesis, while the majority is remineralized within the water column. In contrast, DOM is transported solely by circulation and eventually remineralized in the water column, with associated CO_2 returned to the surface on the ocean mixing timescale (DeVries & Primeau, 2011; Hansell et al., 2009; Roshan & DeVries, 2017). On average, DOC contributes roughly 20% to total carbon export below 100 meters (i.e., POC contributes 80%), decreasing with depth (Hansell et al., 2009), with relative DOC export averaging 5–15% in equatorial and polar regions and up to about 40% in subtropical regions, reflecting regional differences in net production and circulation (Roshan & DeVries, 2017). The distribution, cycling, and export of OM are key for understanding its observed C:N:P stoichiometry and provide the basis for the following discussion.

Article I highlights differences in average C:N:P stoichiometry, variability, and drivers between bulk DOM, POM, and the ecological stoichiometry of phytoplankton and heterotrophs (Tables 5–8, Appendix A), and their implications for carbon cycling and export. Overall, bulk DOM is carbon-rich and phosphorus-poor compared to elemental Redfield ratios. Globally, water column–integrated bulk DOM has an average composition of DOC:DON = 14–17, DOC:DOP = 778–810, and DON:DOP = 48–54, reflecting a mixture of semi-labile and refractory fractions (Hopkinson & Vallino, 2005; Liang et al., 2023) (Fig. 2.1, Tables 5–7, Appendix A). Semi-labile DOM, produced seasonally and exported on seasonal to interannual timescales, has a C:N:P stoichiometry intermediate between Redfield and bulk DOM, with DOC:DON = 8.9–10.7, DOC:DOP = 179–199, and DON:DOP = 20. In contrast, refractory DOM is strongly carbon-rich and phosphorus-poor, with DOC:DON = 15.7–18, DOC:DOP = 1373–3512, and DON:DOP = 10–202 (Hopkinson & Vallino, 2005; Liang et al., 2023). Refractory DOM turns over at low rates over millennial timescales and contributes little to seasonal or interannual carbon and nutrient cycling. With depth, decreasing semi-labile and semi-refractory DOM concentrations cause bulk DOM to approach refractory DOM composition, while surface DOM is closer to semi-labile DOM stoichiometry with averages of DOC:DON = 14–14.6, DOC:DOP = 374–387, DON:DOP = 26–27 (Hopkinson & Vallino, 2005; Liang et al., 2023). Newly produced DOM stoichiometry can also vary due to differences in the elemental C:N:P ratios during production and respiration, for example, from extracellular release of carbon-enriched DOM by phytoplankton under nutrient limitation (Mühlenbruch et al., 2018; Thornton, 2014), or preferential nutrient uptake by mixotrophic or heterotrophic organisms (Liang et al., 2023). As semi-labile DOM largely controls seasonal carbon export, DOM is exported with an intermediate stoichiometry between Redfield ratios and bulk DOM stoichiometry, meaning it is slightly carbon-enriched and phosphorus

poor, but not as strongly as the bulk DOM or refractory DOM pools (Hopkinson & Vallino, 2005; Liang et al., 2023).

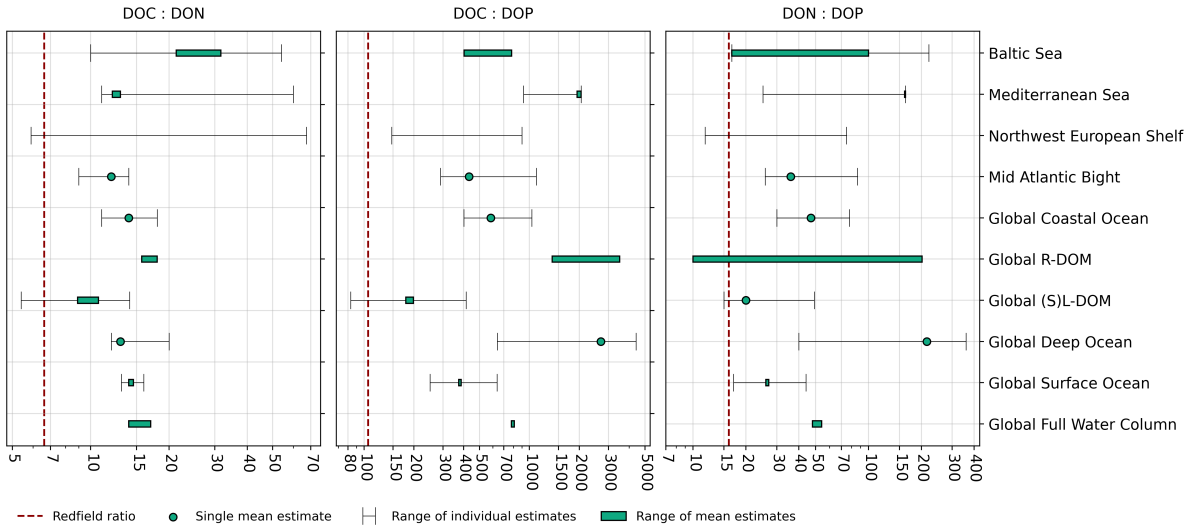

Figure 2.1: *Molar ratios of dissolved organic carbon (DOC), nitrogen (DON), and phosphorus (DOP) for bulk dissolved organic matter (DOM) across different ocean regions, alongside global ranges for refractory or recalcitrant DOM (R-DOM) and (semi-)labile DOM (SL-DOM). Vertical dashed red lines indicate the canonical Redfield ratios (C:N = 6.625, C:P = 106, N:P = 16) for reference. Error bars represent reported ranges of individual estimates. Turquoise boxes indicate the range of estimated mean values when multiple estimates were available, while turquoise points indicate single available estimates. The figure is reproduced from Article* I*, included in Appendix A, with the data compiled from Tables 5–7 of the article.*

In contrast to DOM, the short-lived POM pool has a C:N:P stoichiometry more closely linked to newly produced material, reflecting a mixture of living cells and detrital POM, which complicates understanding its relative composition and drivers. The stoichiometry of POM ranges from below to above Redfield ratios, with averages between Redfield ratios and semi-labile DOM. Globally, the average surface composition is estimated at POC:PON = 6.5–7.7, POC:POP = 137–163, and PON:POP = 20–22 (Fig. 2.2, Table 8, Appendix A). Ratios of carbon and nitrogen to phosphorus are higher in nutrient-depleted low-latitude gyres (POC:PON:POP = 195:28:1) and intermediate in nutrient-rich upwelling regions (137:18:1), both higher than Redfield ratios. These are lower at cold, nutrient-replete high latitudes (78:13:1) (Martiny et al., 2013), below Redfield ratios, which is reflected in regional averages despite substantial variability within basins (Fig. 2.2). With depth, average POC:POP ratios increase to 294 in the mesopelagic zone, reflecting preferential remineralization of phosphorus (Tanioka et al., 2021). On global scales, variability in POM stoichiometry is primarily linked to phytoplankton community composition, with smaller taxa such as cyanobacteria or coccolithophores with higher C:P ratios dominating low latitudes, and larger taxa such as diatoms with lower C:P ratios dominating high

latitudes, along with plasticity of individual species (Liefer et al., 2024; Lomas et al., 2021; Tanioka, Garcia, et al., 2022). At high latitudes, sea surface temperature and macronutrient availability have been identified as main predictors of this variability. In contrast, relative nitrogen and phosphorus availability and nutricline depth (i.e., the depth at which primary production ceases) are most predictive at lower latitudes (Tanioka, Garcia, et al., 2022). Detrital POM stoichiometry has been underrepresented as a potential driver of bulk POM stoichiometry, despite making up a large fraction of the observed pool. Overall, POM has C:N:P ratios between Redfield and semi-labile DOM, with a consistent latitudinal gradient influencing the efficiency and variability of carbon export via the biological carbon pump (Sullivan et al., 2024).

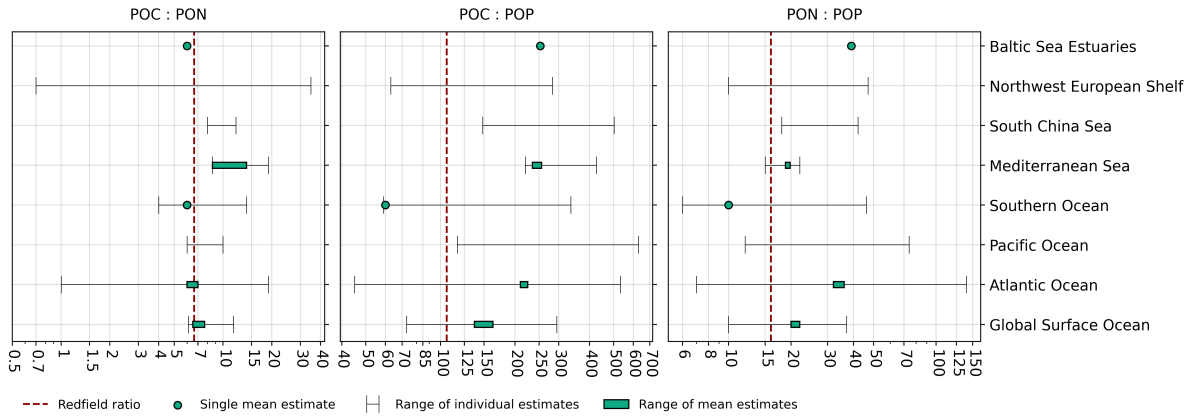

Figure 2.2: *Molar ratios of particulate organic carbon (POC), nitrogen (PON), and phosphorus (POP) across different ocean regions. POM includes both living biomass and detrital POM. Vertical dashed red lines indicate the canonical Redfield ratios (C:N = 6.625, C:P = 106, N:P = 16) for reference. Error bars represent reported ranges of individual estimates. Turquoise boxes indicate the range of estimated mean values when multiple estimates were available, while turquoise points indicate single available estimates. The figure is reproduced from Article* I*, included in Appendix A, with the data compiled from Table 8 of the article.*

Experimental evidence shows that marine phytoplankton and heterotrophs vary substantially in C:N:P stoichiometry, with ranges and averages distinct from bulk DOM and POM, ranging from below to above Redfield ratios depending on taxa and environmental conditions (Fig. 2.3). Under nutrient-replete conditions, phytoplankton across taxa average near Redfield ratios (C:N 6.6–7.8, C:P 107–132, N:P 16–18), but broader ranges (C:N 4.9–12.3, C:P 42–222, N:P 5–38) have been observed between individual species (Garcia et al., 2018; Ho et al., 2003; Quigg et al., 2003, 2010). Nutrient limitation has been shown to strongly affect the stoichiometry of phytoplankton assimilation, with P-limitation increasing C:P to 600–1300, N:P to 48–115, and N-limitation increasing C:N to 12.6–20, producing elemental ratios well above Redfield stoichiometry under strong nutrient-depletion (Geider & La Roche, 2002; Goldman et al., 1979). Other environmental factors, including irradiance,

temperature, and pCO_2, have shown smaller or inconsistent effects on the C:N:P stoichiometry of phytoplankton.

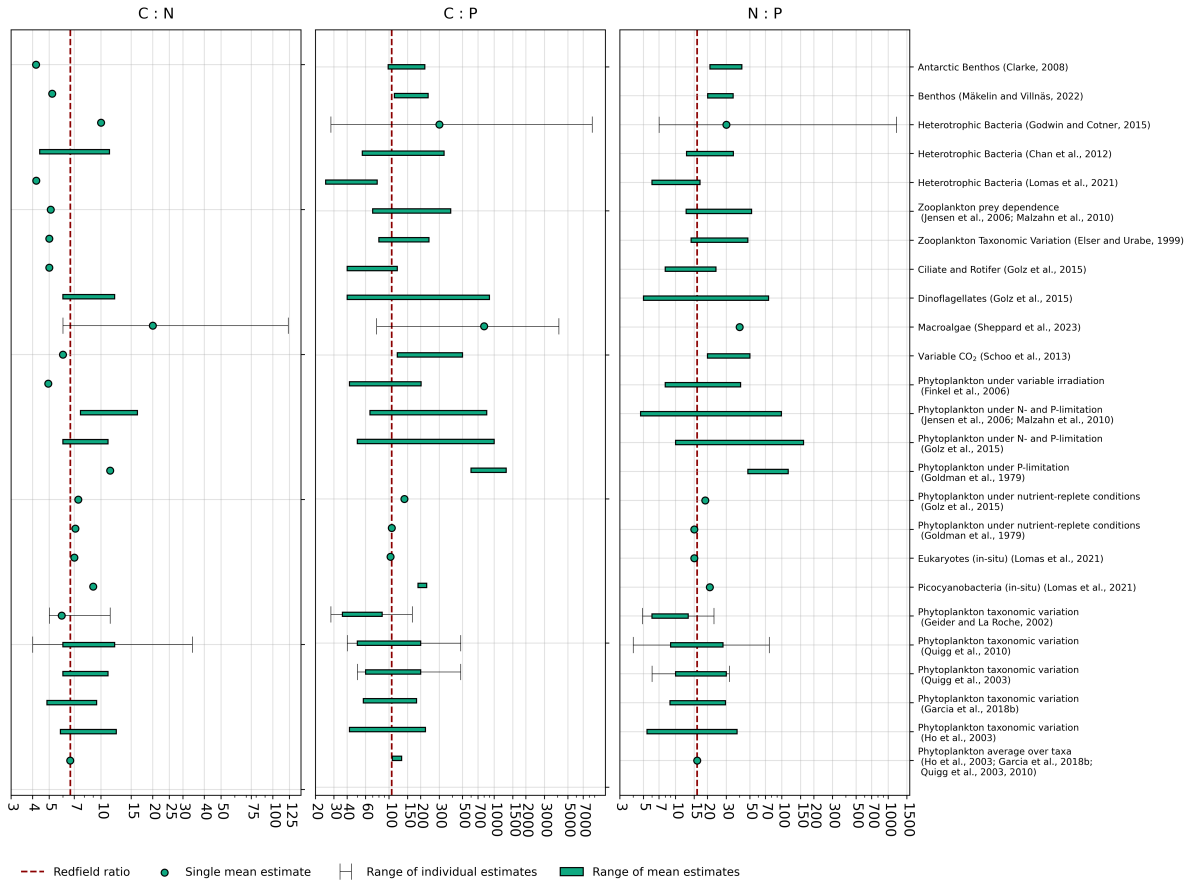

Figure 2.3: *Molar C:N, C:P, and N:P ratios representing the ecological stoichiometry of marine organisms, including phytoplankton, zooplankton, heterotrophic bacteria, and marine benthos. For phytoplankton, ranges reflect variation among taxonomic groups, nutrient-replete versus nutrient-limited conditions, and responses to different light and pCO_2 levels. While most values are derived from experimental studies, two estimates for phytoplankton are based on global in-situ measurements, as indicated in the labels. Zooplankton stoichiometry is shown to vary across taxa and in response to food quality. Heterotrophic bacterial ratios are presented from three studies with divergent reported ranges. Vertical dashed red lines indicate the canonical Redfield ratios (C:N = 6.625, C:P = 106, N:P = 16) for reference. Error bars represent reported ranges of individual estimates. Turquoise boxes indicate the range of estimated mean values when multiple estimates were available, while turquoise points indicate single available estimates. The figure is reproduced from Article* I*, included in Appendix A, with the data compiled from literature ranges cited in Article* I*, as indicated in the labels.*

Zooplankton stoichiometry has been shown to depend mainly on prey composition and homeostatic regulation. Some taxa maintain narrow ranges, as ciliates with C:N 5.0–5.7 and C:P 40–120, and others reflect prey variability, as dinoflagellates with C:N 6–12 and C:P 40–900, demonstrating that heterotroph stoichiometry can also vary substantially above and below Redfield ratios (Golz et al., 2015). Heterotrophic bacteria are often more nutrient-rich than phytoplankton

or zooplankton, with C:N 4–5 and C:P 25–77, typically below Redfield ratios (Fagerbakke et al., 1996; White et al., 2019; Zimmerman et al., 2014), though some recent studies report larger ranges (Chan et al., 2012; Godwin & Cotner, 2015).

In summary, semi-labile DOM is carbon-rich and phosphorus-poor relative to Redfield ratios, but to a lesser extent than bulk DOM, with POM between Redfield ratios and semi-labile DOM. The ecological stoichiometry of phytoplankton and heterotrophs ranges from above to below Redfield values, with averages across different phytoplankton taxa near Redfield ratios and larger differences between taxonomy and under different nutrient conditions.

This variability across OM fractions has implications for global biogeochemical cycles, necessitating a differentiated representation of OM cycling and its C:N:P stoichiometry in biogeochemical models. Higher C:N and C:P ratios in seasonally produced semi-labile DOM and sinking detrital POM, the main vehicles of carbon export, suggest higher carbon fixation, new production, and carbon export per unit of nutrients relative to Redfield ratios (Anderson & Pondaven, 2003; Hopkinson & Vallino, 2005). Preferential remineralization of organic nitrogen and phosphorus over carbon due to higher bioavailability (Lønborg & Álvarez-Salgado, 2012) further decouples carbon and nutrient cycles, enhancing nutrient recycling, while retaining organic carbon and increasing carbon export efficiency (Anderson & Pondaven, 2003; Hopkinson & Vallino, 2005; Liang et al., 2023; Thomas et al., 1999).

Latitudinal and regional differences in DOM and POM C:N:P drive spatial differences in carbon export efficiency and lateral exchanges, influencing seasonal DIC drawdown and air–sea CO_2 exchange (Fransner et al., 2018; Martiny et al., 2013; Roshan & DeVries, 2017; Tanioka, Garcia, et al., 2022; Tanioka et al., 2021). Environmentally-driven shifts in C:N:P ratios of phytoplankton and heterotrophs, from changes in community composition, physiological adaptation, or food-web interactions, may further influence carbon export and nutrient cycling over time (Kwiatkowski et al., 2018; Liu et al., 2025; van de Waal et al., 2010). Terrestrial OM inputs with distinct stoichiometry and degradability also contribute to regional carbon and nutrient budgets, which would require explicit consideration to assess their transformation and exchanges within the marine environment (Bauer et al., 2013; Bianchi, 2011). Together, this spatial and temporal variability across OM size and lability fractions emphasizes the need for biogeochemical models to explicitly account for variable C:N:P ratios to represent carbon–nutrient coupling and resulting ocean–climate feedbacks.

Marine ecosystem models increasingly incorporate variable C:N:P stoichiometry into their OM representation. This is either limited to detrital POM and DOM or extending to phytoplankton and, in some cases, zooplankton and heterotrophic bacteria, using inverse biogeochemical models (Sullivan et al., 2024; Teng et al., 2014) or nutrient-phytoplankton-zooplankton-detritus (NPZD)-type models (Butenschön

et al., 2016; Kühn et al., 2010; Letscher et al., 2015; Neumann et al., 2022). Variability in DOM and POM production and respiration has been represented through data-driven optimization (Letscher et al., 2015), preferential remineralization of nitrogen and phosphorus (Anderson & Pondaven, 2003; Letscher & Moore, 2015; Somes & Oschlies, 2015), or extracellular release of carbon-rich DOM under nutrient limitation (Kühn et al., 2010; Neumann et al., 2022), sometimes including multiple DOM fractions (Letscher et al., 2015), or an explicit representation of the microbial loop (Butenschön et al., 2016; Smith et al., 2005), and DOM–POM exchanges (Kreus et al., 2015; Neumann et al., 2022). Variable stoichiometry in phytoplankton has been implemented via statistical functions relating uptake to environmental and physiological conditions (Bonachela et al., 2013; Garcia et al., 2016), Droop or cell quota models decoupling nutrient uptake from growth (Butenschön et al., 2016; Kwiatkowski et al., 2018; Zakem & Levine, 2019), and mechanistic cell models for macromolecular allocation (Armin & Inomura, 2021; Inomura et al., 2022, 2020; Wirtz & Kerimoglu, 2016). In heterotrophs, models account for variable stoichiometry through prey composition, stoichiometric regulation via excretion of excess carbon or nutrients, nutrient-selective DOM uptake, or extended cell quota models (Butenschön et al., 2016; Fransner et al., 2018; Kreus et al., 2015; Polimene et al., 2017; Zakem & Levine, 2019). Applications range from one-dimensional models (Anderson & Pondaven, 2003; Smith et al., 2005) to regional three-dimensional models of the North and Baltic Seas (Fransner et al., 2018; Kühn et al., 2010; Neumann et al., 2022), and global simulations (Chien et al., 2023; Kwiatkowski et al., 2018; Letscher & Moore, 2015; Matsumoto & Tanioka, 2020; Somes & Oschlies, 2015).

These applications demonstrate that variable OM C:N:P stoichiometry has been incorporated at different levels of complexity, ranging from limited to detrital POM and DOM to extended across ecosystem compartments. More comprehensive implementations include variable C:N:P stoichiometry in autotrophs, heterotrophs, POM, and DOM, with distinct lability fractions and, in some cases, an explicit microbial loop, providing a more complete representation of stoichiometric variability. These high-complexity implementations, however, come with increased computational cost and require extensive data and tuning, with many key processes and parameters remaining uncertain. By contrast, models that only consider variable stoichiometry in detrital POM and DOM may reproduce major influences on carbon export at a lower cost, which could provide an advantage for high-resolution simulations at regional and global scales. Looking forward, accurate C:N:P representation will depend on balancing realism with computational efficiency and available observational constraints (A. P. Martin et al., 2024). Modular model implementations, where variable stoichiometry is selectively incorporated into specific OM components depending on research objectives, spatial scale, and data availability for validation, offer one promising pathway for future developments.

3 Influence of variable C:N:P stoichiometry on net community production and air–sea CO_2 exchange in the northwest European shelf seas

Article II (Appendix B) examines how variable OM C:N:P stoichiometry affects carbon cycling in the northwest European shelf seas, addressing questions 5–7 on its influence on the balance between carbon fixation and respiration, seasonal and annual air–sea CO_2 exchange, and how the regional response compares to global estimates. This section presents the core findings of *Article* II, along with background information on the geography and carbon cycling of the northwest European shelf seas, and a description of the implementation used to assess the role of variable C:N:P stoichiometry in POM and DOM production and removal processes. Building on this, Section 4 continues with results from *Article* III, which extend the analysis to cross-shelf exchanges and their implications for the carbon budget and export contributions to global biogeochemical cycles.

The northwest European shelf seas provide a suitable testbed for the analyses in *Articles* II and III for two reasons. First, they are among the most comprehensively researched shelf systems, with extensive observational datasets, dedicated regional modeling studies, and established frameworks for operational forecasting, providing a strong basis for model validation. Observational coverage includes data from the International Council for the Exploration of the Sea (ICES) on biological, chemical, and physical properties of European shelf waters, the Global Ocean Data Analysis Project (GLODAP) compiling global measurements of inorganic carbon and related properties, and the Surface Ocean CO_2 Atlas (SOCAT) with high-resolution surface ocean CO_2 fugacity observations. These datasets were used in this work to validate the model representation of nutrients and carbonate system properties. Second, the region is subject to multiple anthropogenic pressures, including competing societal uses such as wind farms, hydrogen infrastructure, shipping, fishing, and marine protected areas. This makes it particularly important to assess uncertainties in the carbon cycle to better inform future projections under changing conditions.

The northwest European shelf seas extend from the shallow southern North Sea and the adjacent continental margins of Europe northward to the steep shelf break that runs along a curved path from the Armorican Shelf to the Norwegian coast, and connect the northern North Sea eastward to the Baltic Sea through the narrow, shallow Danish Straits in the Kattegat–Skagerrak region (Fig. 3.1). They include inner shelf regions of the UK and Ireland, such as the Celtic and Irish Seas, as well as outer shelf regions including the Malin and Hebrides shelves and the Armorican Shelf off

the coast of France. The shelf is characterized by a cyclonic residual circulation and efficient exchange with the northeast Atlantic, with net volume inputs from north of the Shetland Islands, from the Celtic Sea through the English Channel, and from the Baltic Sea, with net volume outflow primarily through the Norwegian Trench (Holt et al., 2009; Huthnance et al., 2009, 2022; Thomas et al., 2005).

Shallow regions are permanently well mixed, as tidal mixing at the seafloor and wind-driven mixing at the surface keep the two frictional boundary layers close together, limiting vertical separation of carbon production and respiration. In contrast, the deeper northern areas and the shelf edge are seasonally stratified, generating a seasonal vertical DIC gradient due to surface autotrophy and subsurface respiration (Thomas et al., 2004). In combination with a net on-shelf transport of surface waters and off-shelf transport at depth, this gradient drives a net export of DIC. This interaction of the regional circulation and biological carbon drawdown, known as the continental shelf carbon pump (Holt et al., 2009; Legge et al., 2020; Thomas et al., 2005, 2004; Wakelin et al., 2012), drives an annual uptake of atmospheric CO_2 estimated between 1.3 and 3.3 Tmol C yr^{-1} (Kitidis et al., 2019; Legge et al., 2020; Wakelin et al., 2012). The wide range reflects limited spatiotemporal coverage, high natural variability, and systematic measurement uncertainties.

As a basis for assessing the effects of variable C:N:P stoichiometry on carbon cycling in the northwest European shelf seas, this work evaluates hindcast simulations employing the NWES-LR configuration of the three-dimensional physical–biogeochemical modeling system SCHISM-ECOSMO-CO_2 (Kossack et al., 2024, 2023). This configuration resolves baroclinic circulation and tracer transport across the model domain at 4.5–15 km horizontal resolution and 3–53 vertical layers using the Semi-implicit Cross-scale Hydroscience Integrated System Model (SCHISM) (Zhang et al., 2016). Based on these physical conditions, the NPZD-type lower-trophic-level ecosystem model ECOSMO II (Daewel & Schrum, 2013; Schrum et al., 2006) represents ecosystem dynamics, cycling of OM and nutrients, and the resulting uptake and release of DIC and total alkalinity, while the remaining carbonate system state and air–sea CO_2 fluxes are determined by a coupled carbonate system module based on Blackford & Gilbert (2007).

To represent the observed variability in the C:N:P stoichiometry of DOM and POM, the ECOSMO II model was further developed to include two contributing processes motivated by observational and experimental evidence (Fig. 3.2). First, the extracellular release of carbon-enriched DOM by phytoplankton under nutrient limitation was implemented as a direct uptake of DIC and nutrients into DOM, with additional flocculation from DOM to POM representing transparent exopolymer particle formation, both adapted from Neumann et al. (2022). Second, the preferential remineralization of organic nitrogen and phosphorus relative to carbon was implemented by assigning higher relative remineralization rates to these elements,

reflecting their greater bioavailability, which results in higher uptake and respiration by mixotrophic and heterotrophic organisms. For this, independent state variables were introduced for pelagic DOC, DON, and DOP, as well as pelagic (i.e., within the water column) and benthic (i.e., in the surface sediments) POC, PON, and POP.

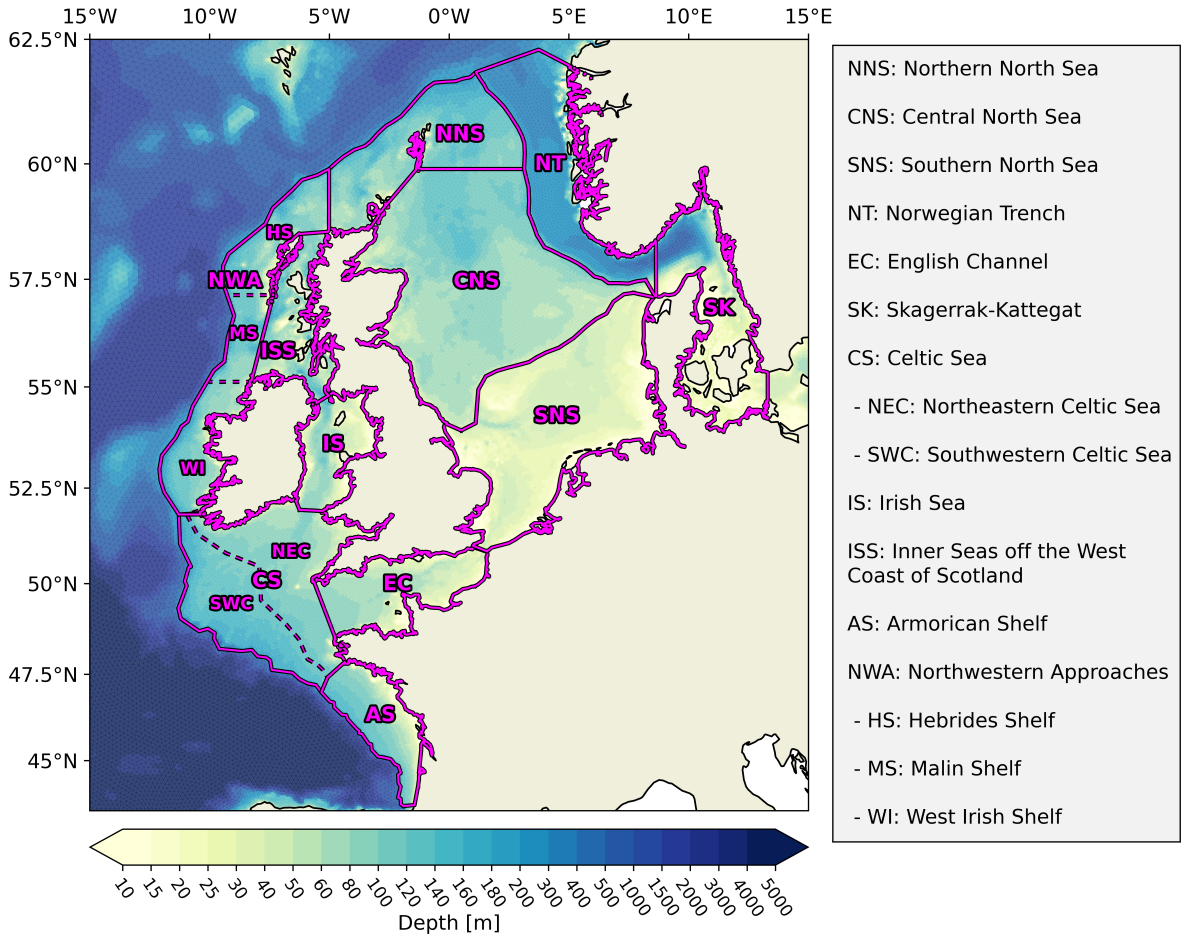

Figure 3.1: *Sub-regions and bathymetry of the northwest European shelf seas (NWES) based on a combination of bathymetric features and both physical and biogeochemical variability. The division of the NWES into sub-regions with relatively homogeneous physical and biogeochemical characteristics allows for the identification of consistent carbon cycle responses. The figure is reproduced from Demir et al. (2025b), included as Article* II *in Appendix B.*

The implementation focuses on DOM and POM as the primary drivers of carbon export, assuming Redfield stoichiometry in primary and secondary producers. This assumption enables the attribution of modeled changes to the two added process implementations and keeps computational costs feasible. The study compares four model configurations to assess the individual and combined effects of the two processes. These include a reference with constant Redfield stoichiometry (RS), one considering the extracellular release of carbon-enriched DOM (ER), one considering the preferential remineralization of organic nitrogen and phosphorus

relative to carbon (PR), and a combined configuration (ER&PR) including both process implementations with a reduced contribution. All configurations were calibrated to reproduce observed means and ranges of DOM and POM concentrations and C:N:P stoichiometry based on the findings from *Article* I.

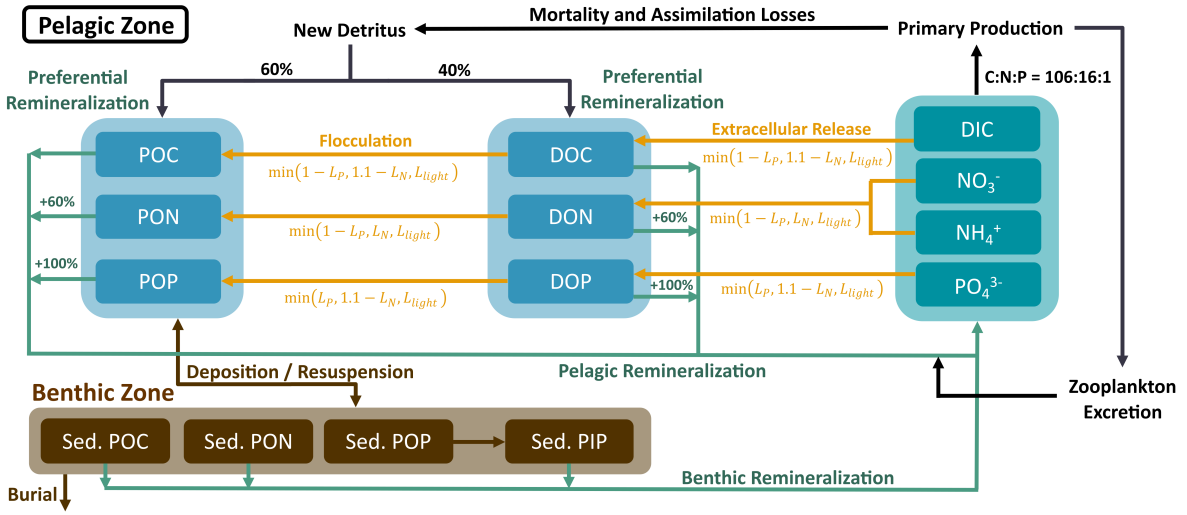

Figure 3.2: *Schematic diagram showing the OM cycling in the variable stoichiometry ECOSMO II implementation, including the preferential remineralization of organic nitrogen and phosphorus, as well as the extracellular release of carbon-enriched DOM with the associated particle formation. The figure is reproduced from Demir et al. (2025b), included as Article* II *in Appendix B.*

Article II shows that, compared to a Redfield stoichiometry-based model, accounting for the observed stoichiometry of DOM and POM in ECOSMO II substantially increases biological CO_2 drawdown and the resulting annual and seasonal oceanic uptake of atmospheric CO_2 (Fig. 3.3–3.5). This underscores the importance of considering variable OM stoichiometry in both regional and global biogeochemical models for an accurate representation of marine carbon cycling. In the northwest European shelf seas, incorporating variable OM stoichiometry increases the annual CO_2 uptake by 9–31 % compared to the Redfield stoichiometry configuration, from 1.11 Tmol C yr^{-1} to 1.21–1.44 Tmol C yr^{-1} (Fig. 7, Appendix B), while shifting the seasonal maximum uptake from winter to spring and summer (Fig. 3.5). These changes are driven by an intensification of pre-existing seasonal, vertical, and lateral gradients in net community production (NCP; i.e., the balance between carbon fixation by autotrophy taking up CO_2 and respiration releasing CO_2). The impact is largest in the deep and seasonally stratified northern areas of the North Sea and along the shelf edge, where biological export of carbon is most efficient. All changes are consistent across configurations in their spatial distribution, but they are smallest when considering the preferential remineralization of organic nitrogen and phosphorus, largest when including the extracellular release of carbon-enriched

DOM, and intermediate in the combined configuration, where both processes are considered with a reduced contribution.

The enhanced seasonal, vertical, and lateral gradients in NCP result from increases both in surface productivity during the spring bloom and sub-surface respiration in autumn and winter (Fig. 8, Appendix B). Consequently, the seasonal maximum in net organic carbon production during May increases by up to 8–72%, while the minimum NCP in October, associated with sub-surface respiration, decreases by up to 13–72% (Fig. 3.3b). Vertically, the upper 50 meters become 7–34% more autotrophic, while sub-surface layers become 6–41% more net heterotrophic, reflecting enhanced carbon fixation at the surface and respiration at depth (Fig. 10, Appendix B). The pre-existing lateral gradient, with net organic carbon production in the central North Sea and subsequent respiration in the Norwegian Trench, is intensified, suggesting potential CO_2 export from surface waters of the central North Sea into the deep Norwegian Trench (Fig. 3.3a).

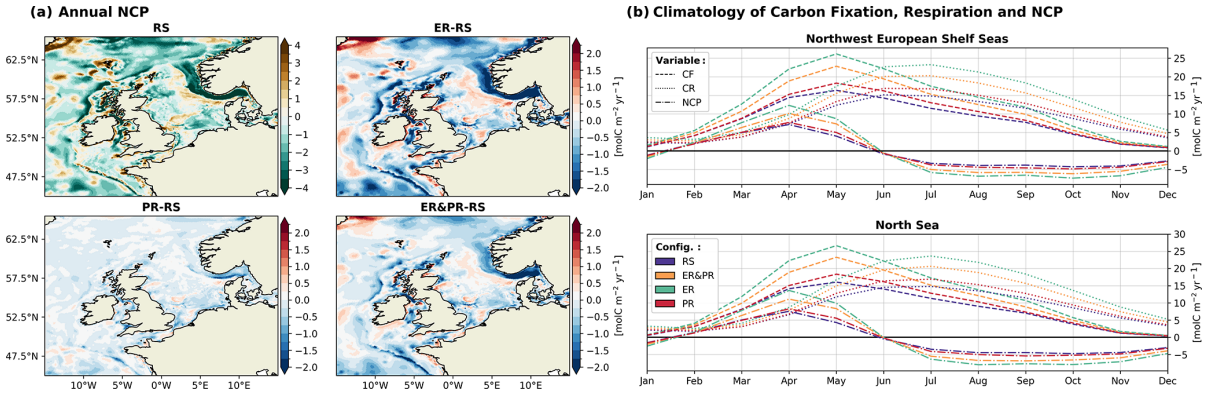

Figure 3.3: *(a) Spatial distribution of annual vertically integrated net community production (NCP) for the Redfield Stoichiometry (RS) configuration and differences for the Extracellular Release (ER), Preferential Remineralization (PR), and combined (ER&PR) configurations over the simulation period of 2000–2010. (b) Respective monthly 11-year mean of carbon fixation (CF, dashed), carbon respiration (CR, dotted), including benthic and pelagic remineralization, and NCP (dash–dot). The figure is reproduced from Demir et al. (2025b), included as Article* II *in Appendix B.*

These changes in NCP translate into differences in the seasonal export of carbon. Increases in both POC and DOC production contribute to a larger seasonal export of DIC from the surface when including extracellular DOM release, whereas only increased POC accumulation contributes when considering the preferential remineralization (Fig. 15 and 16, Appendix B). As a result, the seasonal minimum in surface DIC and pCO_2 increases more when DOM release is included, improving the representation of seasonality and correlation with observations, but the lack of organic carbon retention causes an earlier return to winter concentrations and pressures starting in autumn compared to observations (Fig. 13 and 14, Appendix B).

The marked annual increase in CO_2 uptake across the northwest European shelf seas (Fig. 3.4) results from pronounced seasonal changes in air–sea CO_2 fluxes (Fig. 3.5). Winter uptake is slightly reduced by 0.2–0.8 mol C m^{-2} yr^{-1}, while spring and summer uptake increase by 0.1–0.7 and 0.4–1.3 mol C m^{-2} yr^{-1}, respectively. In autumn, there is an enhanced north–south gradient from uptake in the northern half to outgassing in the southern half, with up to 0.2 mol C m^{-2} yr^{-1} stronger overall outgassing. These shifts reflect a stronger biological contribution to the seasonal air–sea CO_2 exchange, driven by intensified NCP gradients across the northwest European shelf seas. The seasonal changes, which drive the net annual increase, improve the representation of monthly air–sea CO_2 fluxes compared to monthly mean observations from Kitidis et al. (2019).

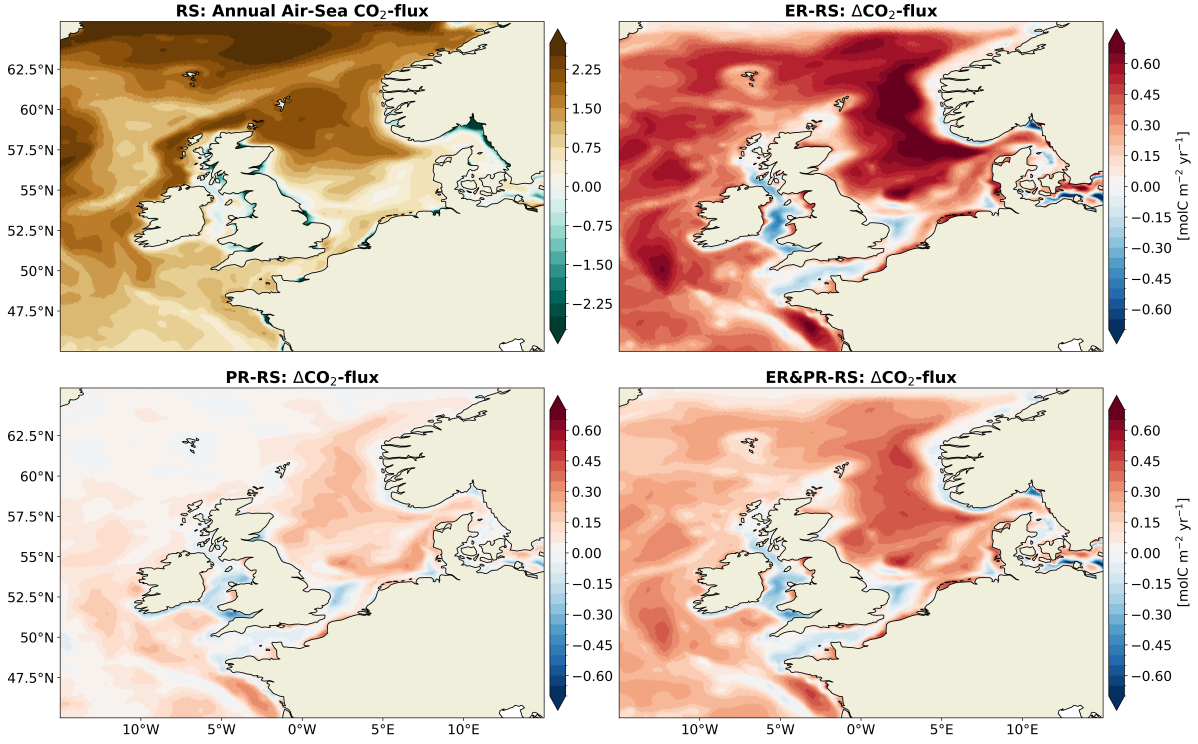

Figure 3.4: *Annual mean air–sea CO_2 exchange for the RS configuration and differences for the ER, PR, and ER&PR configurations over the simulation period of 2000–2010. The direction of the flux is defined as downward, meaning a positive air–sea CO_2 exchange indicates an oceanic uptake and a negative one an outgassing of CO_2. Similarly, positive differences represent an increase in uptake or a decrease in outgassing and vice versa. The figure is reproduced from Demir et al. (2025b), included as Article* II *in Appendix B.*

While the magnitude of the increase in annual CO_2 uptake of 9–31% is consistent with global estimates of 9–20% higher carbon uptake or vertical export when considering variable C:N:P stoichiometry (Kwiatkowski et al., 2018; Letscher & Moore, 2015; Matsumoto & Tanioka, 2020; Sullivan et al., 2024; Tanioka & Matsumoto, 2017; Tanioka et al., 2021), the spatial distribution of this response in the northwest European shelf seas is strongly shaped by regional variability. The largest increase

in CO_2 uptake occurs in the deep northern North Sea and along the shelf edge, where strong NCP gradients combined with downwelling circulation enhance the transfer of carbon to sub-surface waters, whereas the biological drawdown of CO_2 is weaker in the shallow and permanently well-mixed southern North Sea and the inner shelf regions. This contrast demonstrates that regional variability in physical and biogeochemical conditions directly influences the magnitude and spatial distribution of the effects of variable C:N:P stoichiometry on carbon cycling, highlighting the need to account for this variability in regional and global biogeochemical models.

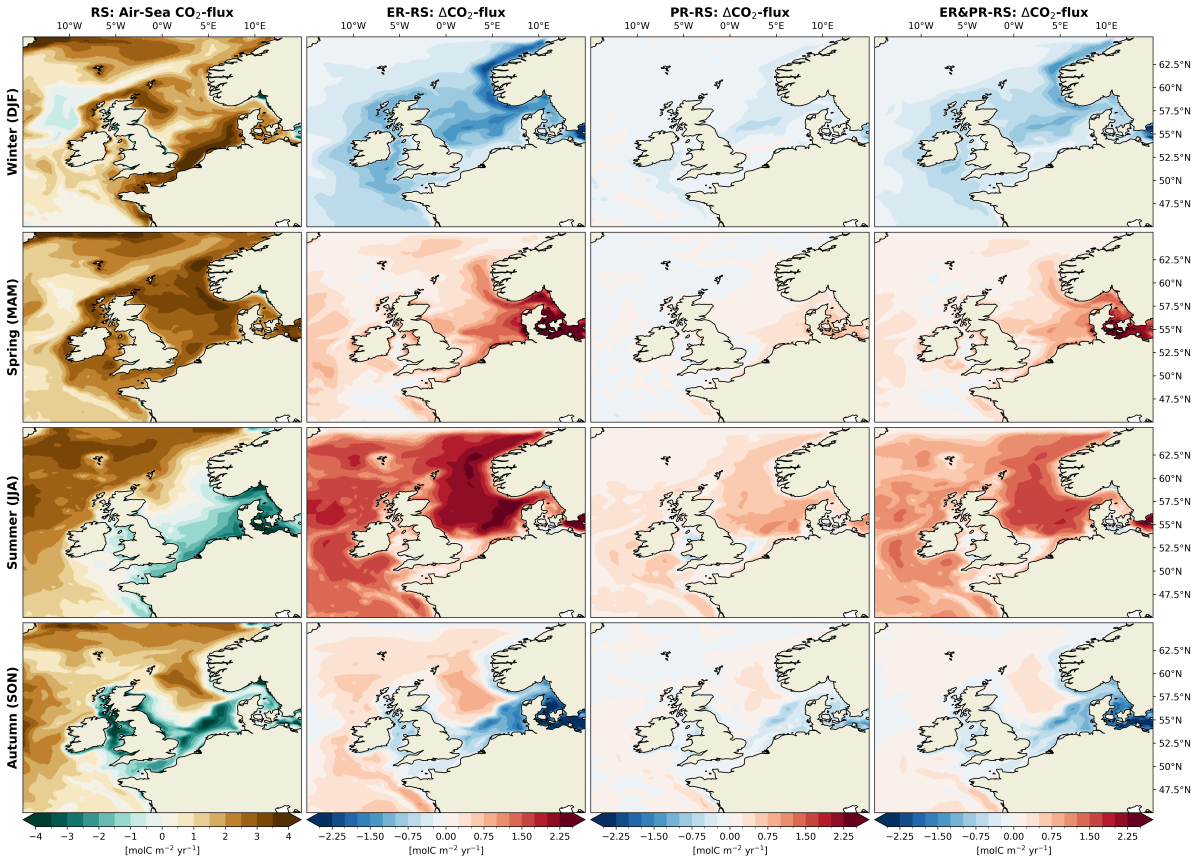

Figure 3.5: *Seasonal mean air–sea CO_2 exchange for the RS configuration and differences for the ER, PR, and ER&PR configurations over the simulation period of 2000–2010. The figure is reproduced from Demir et al. (2025b), included as Article* II *in Appendix B.*

4 Effects of variable C:N:P stoichiometry on the carbon budget and export contributions of the northwest European shelf seas

Article III (Appendix C) examines the effects of variable OM C:N:P stoichiometry on the carbon budget, and carbon export contributions in the northwest European shelf seas. With this, it addresses questions 8–10 on how changes in organic and inorganic carbon fluxes drive the previously quantified changes in air–sea CO_2 exchange, and how regional variability may compare to responses across the global open and coastal oceans. Building on the findings from *Article* II, this regional assessment completes the evaluation of variable stoichiometry on shelf carbon cycling. The core findings from *Article* III are presented below in the context of previous carbon budget estimates.

A recent carbon budget analysis by Legge et al. (2020), combining observational and model-based estimates, provides ranges for carbon stocks and fluxes in the northwest European shelf seas, allowing the results of this study to be discussed in the context of existing uncertainties. Reported values for the uptake of atmospheric CO_2 range from 1.3–3.3 Tmol C yr^{-1}, with a net cross-shelf DIC export of 3.45–6.4 Tmol C yr^{-1} and additional riverine inputs of 2.3–5.0 Tmol C yr^{-1}, of which 0.2–2.4 Tmol C yr^{-1} are organic carbon. The cross-shelf transport of organic carbon varies widely among previous studies, estimating a net export of 0.01–1.84 Tmol C yr^{-1}, which results in a total carbon export of 3.5–8.2 Tmol C yr^{-1}. Benthic–pelagic organic carbon exchange is particularly uncertain, with reported values between −2.2 and 6.0 Tmol C yr^{-1}. These ranges emphasize the considerable uncertainties that persist in observed and simulated organic and inorganic carbon fluxes.

Article III begins by assessing the simulated cross-shelf volume fluxes across individual shelf break sections, as these exchanges strongly influence carbon export and the interannual variability of carbon inventories. These net cross-shelf volume exchanges are consistent with the characteristic cyclonic residual circulation of the northwest European shelf seas (Holt et al., 2009; Huthnance et al., 2009, 2022; Thomas et al., 2005) (Fig. 4.1). Major inflows occur along the southwestern and northern shelf break, with 0.56 Sv entering through the Celtic Sea, 0.40 Sv through the West Shetland Shelf, and an additional 0.45 Sv entering between the West Irish and Hebrides shelf breaks. The northern inflow is primarily balanced by net export through the Norwegian Trench in the northeast with 1.17 Sv and the Armorican Shelf in the southwest with 0.25 Sv, offsetting part of the Celtic Sea inflow. Minor additional sources and sinks include the North Sea–Baltic Sea exchange (0.010 Sv)

and river discharge (0.005 Sv). The physical circulation is identical across all simulations, so differences in tracer concentrations and carbon fluxes arise solely from the implemented representations of variable C:N:P stoichiometry.

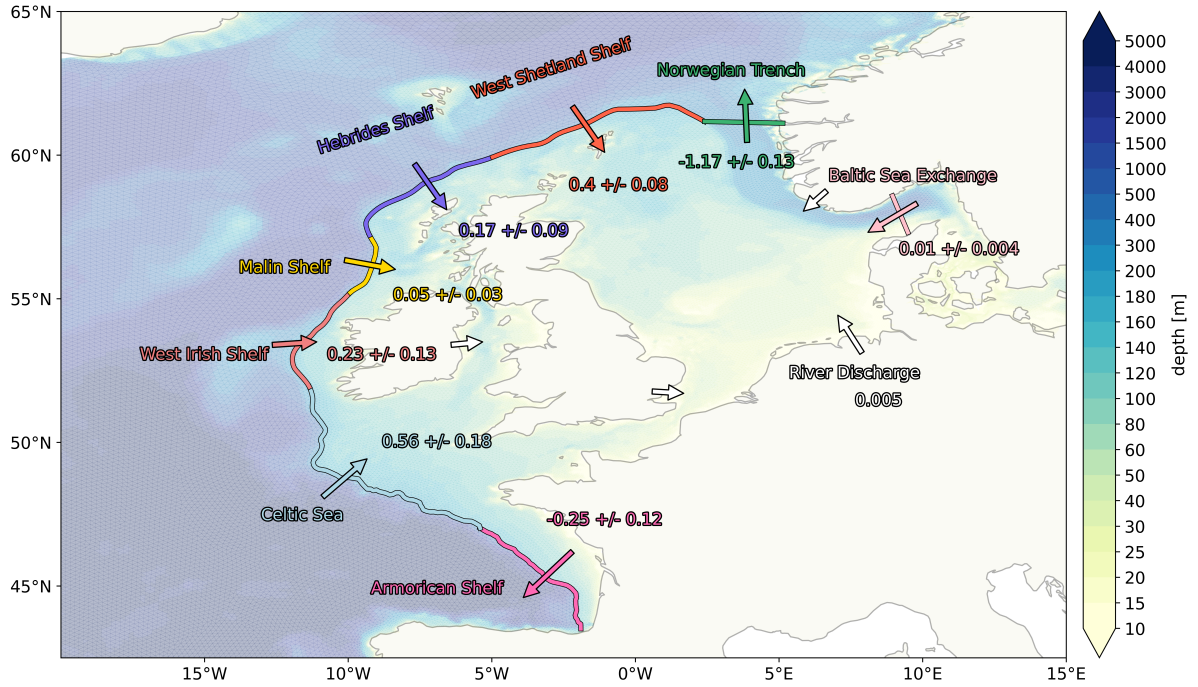

Figure 4.1: *Cross-shelf net volume transports in Sverdrup (Sv, 1 Sv = 10^6 m $^3s^{-1}$) across shelf break sections of the northwest European shelf seas and North Sea-Baltic Sea net volume exchange. All vertically-integrated net transports are presented as 11-year means over the simulation period from 2000 to 2010, with standard deviations between annual means indicating interannual variability. River discharge from continental Europe, Norway, the United Kingdom, and Ireland is indicated by white arrows, but reported as a single total value for the volume budget. Arrow direction indicates net transport direction, while the colormap shows bathymetry, and lines delineate individual triangular grid cells. The figure is reproduced from Demir et al. (2025a), included as Article* III *in Appendix C.*

Article III demonstrates that considering variable C:N:P stoichiometry in DOM and POM most substantially affects the inorganic carbon budget of the northwest European shelf seas, while the organic carbon budget exhibits comparatively smaller and more variable changes. It links the previously shown increase of 0.102–0.339 Tmol C yr^{-1} in CO_2 uptake from *Article* II to an increase in net cross-shelf DIC export of 0.060–0.301 Tmol C yr^{-1} (Fig. 4.2). The contribution to the increase in net DIC export occurs through the Norwegian Trench with 0.040–0.185 Tmol C yr^{-1}, with a second large contribution by a reduction in net DIC import across the northwestern shelf break from the West Shetland Shelf to the West Irish Shelf of 0.022–0.135 Tmol C yr^{-1}. Increased net on-shelf and reduced net off-shelf DIC transport across the Celtic Sea, Armorican Shelf, and the Baltic Sea effectively offset a small fraction of this export. Some DIC is taken up by enhanced pelagic NCP, but released back through additional

net deposition and subsequent benthic remineralization. In contrast to the inorganic carbon budget, changes in the organic carbon budget are limited to modest increases in pelagic TOC stocks and shifts in cross-shelf TOC exchanges, with more variable impacts in time and across configurations.

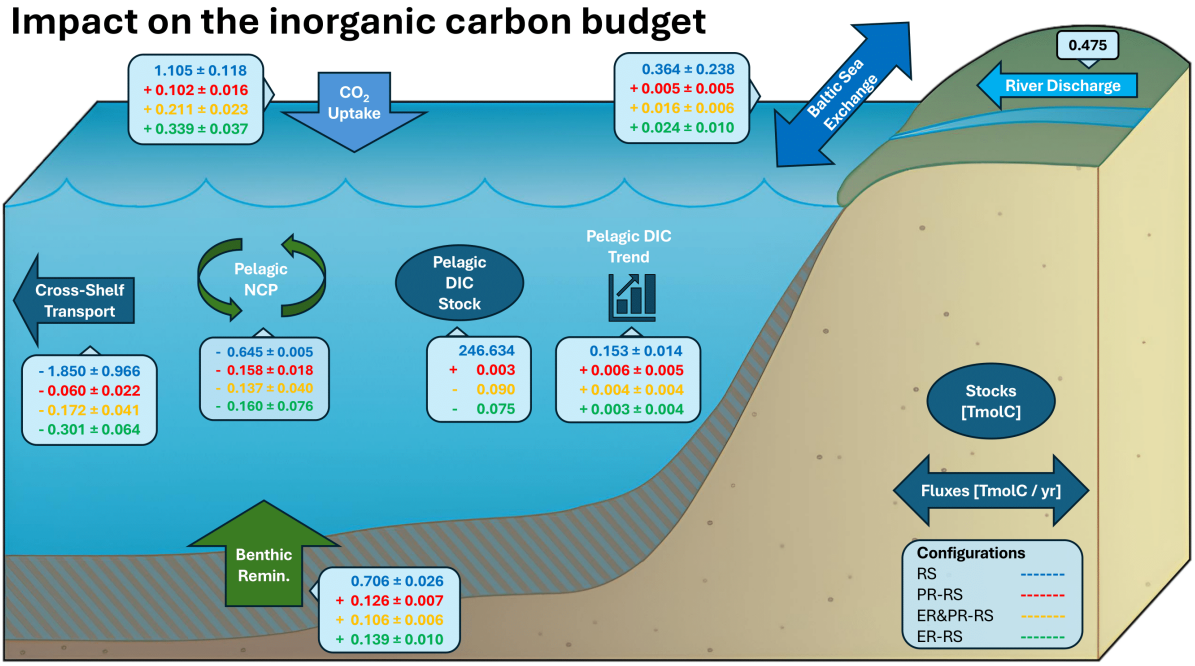

Figure 4.2: *Impacts of variable stoichiometry on the inorganic carbon budget of the NWES. All carbon stocks are shown in Tmol C, and fluxes are provided in Tmol C* yr^{-1}*. Green arrows indicate the conversion between organic and inorganic carbon. The absolute stocks and fluxes are shown for the Redfield stoichiometry (RS) configuration, with the differences shown for the extracellular release (ER), preferential remineralization (PR), and the combined configuration (ER&PR). The figure background was created in part using modified images from the UMCES IAN Media Library under a Creative Commons license CC BY-SA 4.0. The figure is reproduced from Demir et al. (2025a), included as Article* III *in Appendix C.*

Based on these changes in the organic and inorganic carbon budgets, *Article* III quantifies the relative export contributions driving the additional CO_2 uptake (Fig. 4.3). The dominant change in carbon export contribution is the increased net cross-shelf export of DIC across the shelf edge, accounting for 59–89% of the uptake, largest in the ER and smallest in the PR configuration. The increased net DIC export across the Norwegian Trench accounts for 39–55% of the additional uptake, while the reduced net DIC import across the northwestern shelf break accounts for another 22–40%, with a small and strongly variable opposite contribution of 2–7% from the southwestern shelf edge. Only in the PR configuration do organic fluxes and stock trends contribute more substantially and consistently, with a reduced cross-shelf TOC import, contributing 15%, and small positive trends in pelagic DIC and TOC stocks. In the ER and ER&PR configurations, these contributions are small

and strongly variable. The contributions from trends in the DIC and TOC stocks in the PR configuration are unlikely to persist over longer timescales, as accumulated carbon would eventually be remineralized or exported. These results demonstrate that variable OM C:N:P stoichiometry regulates the efficiency of the continental shelf carbon pump. By enhancing the biological drawdown of CO_2, as shown in *Article* II, and thereby increasing the vertical DIC gradient, the carbon-enrichment in POM and DOM compared to Redfield stoichiometry increases the efficiency in CO_2 uptake and DIC export.

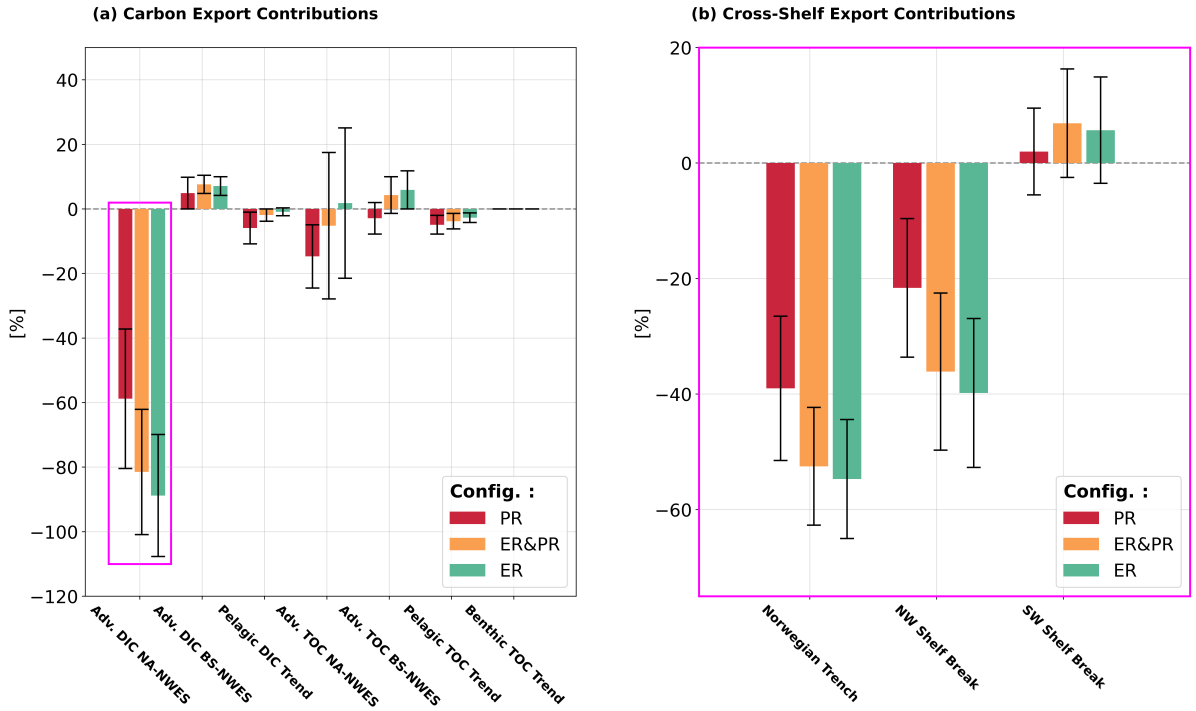

Figure 4.3: *(a) Contributions of export fluxes and trends in carbon stock to the additional uptake of atmospheric CO_2 in the variable stoichiometry configurations. The mean contribution represents the average over the period 2000–2010, with error bars indicating interannual variability as standard deviation for carbon fluxes and normal error for the differences in trends. (b) The advective (Adv.) cross-shelf exchanges of both DIC and TOC are separated into the net cross-shelf exchange with the North Atlantic (NA) and with the Baltic Sea (BS). The northwestern (NW) shelf break ranges from the West Shetland Shelf to the West Irish Shelf, with the southwestern (SW) shelf break including the Celtic Sea and Armorican Shelf. The figure is reproduced from Demir et al. (2025a), included as Article* III *in Appendix C.*

Through this regional assessment, *Articles* II and III show that the regional influence of variable C:N:P stoichiometry on marine carbon cycling depends on the predominant carbon export pathways. In the northwest European shelf seas, uptake is driven by the continental shelf carbon pump. Here, the biological drawdown of CO_2 creates a DIC gradient, which, together with the regional circulation, drives CO_2 uptake through an off-shelf transport of DIC. In other systems, however, with

different physical and biogeochemical conditions and resulting export pathways, such as POC burial or cross-shelf organic carbon export, the regional response may differ substantially. While the consistent increase in CO_2 sequestration aligns with global model results, the regional response is system-specific. This motivates the incorporation of variable OM C:N:P stoichiometry into regional biogeochemical models, as well as into the representation of the coastal ocean in global models.

5 Summary and Outlook

Drawing on *Articles* I–III, this dissertation examines how variable OM C:N:P stoichiometry influences marine carbon cycling, from a global assessment of variability to a two-part regional impact study in the northwest European shelf seas. *Article* I identifies systematic variations across OM fractions, depths, and regions, addressing both their implications for carbon cycling and their implementation in biogeochemical models. The two-part regional impact study in *Articles* II and III shows that variable stoichiometry affects the balance between carbon fixation and respiration, enhancing CO_2 drawdown through increased NCP gradients, which in turn increases oceanic CO_2 uptake and its subsequent cross-shelf export to the northeastern Atlantic. While the estimated impact on CO_2 uptake is consistent with previous global estimates, the regional variability stresses the importance of considering regional physical and biogeochemical conditions. This motivates the consideration of variable stoichiometry in biogeochemical models, both regionally and in the representation of the coastal ocean in global models. These results provide a first glimpse into the regional impacts of variable OM C:N:P stoichiometry, but they do not capture all aspects of this variability or other important sources of uncertainty, leaving open avenues for future research.

Several drivers of variability in C:N:P stoichiometry and their biogeochemical impacts could not be considered in this study. These include the role of terrestrial OM, including its composition, stoichiometry, and degradability in the marine environment, which remain poorly constrained by observations (Bauer et al., 2013; Bianchi, 2011). Other aspects beyond the scope of this work are the variable stoichiometry of phytoplankton and heterotrophs and the influence of prey quality on higher trophic levels, which would require a more complex ecosystem representation. Shifts in C:N:P stoichiometry linked to plankton community composition or to the adaptation of individual species under environmental change, and their potential consequences for ecosystem–climate interactions, also remain to be addressed (Liu et al., 2025). Changes in the stoichiometry and lability of DOM through microbial uptake and release could not be considered due to the lack of explicit representation of DOM fractions and of DOM uptake and release by mixotrophic and heterotrophic organisms. Many of these processes are still poorly constrained by observations, particularly in their regional variability, leaving these variations and their impacts on marine carbon cycling uncertain.

Future model developments should aim to consider variable stoichiometry across compartments, including autotrophs, heterotrophs, POM, and DOM, while balancing

realism, computational demands, and the availability of observational data (A. P. Martin et al., 2024). However, when resources or data are limited, focusing on non-living pools can still provide a more accurate representation of the biological carbon pump's efficiency. In addition, a more differentiated representation of DOM lifetimes and an explicit consideration of the microbial loop through DOM uptake by mixotrophic and heterotrophic organisms are relevant to the representation of long-term carbon sequestration via the microbial carbon pump and the efficiency of the biological carbon pump. Accounting for these mechanisms will reduce uncertainty in estimates of the ocean carbon sink and improve projections of ecosystem–climate interactions under changing environmental conditions.

Beyond uncertainties in the representation of OM C:N:P stoichiometry, other observational limitations lead to large uncertainties in global and regional carbon fluxes, as shown above for the northwest European shelf seas. For instance, in all of the European shelf seas, limited observations of pelagic and benthic production and respiration below the euphotic zone leave the overall trophic state poorly constrained (Gazeau et al., 2004). Benthic stocks and benthic–pelagic coupling are also highly uncertain, with strongly spatially varying organic carbon stocks and accumulation rates across continental shelves, which contributes to the large uncertainty in regional carbon budgets (Diesing et al., 2021). These uncertainties, among many others, contribute to a wide range of model-based estimates for carbon fluxes, including air–sea CO_2 exchange and lateral DIC and organic carbon transport between the coastal ocean and the open ocean, depending on the representation of biological productivity and the trophic state. By quantifying the effects of variable OM C:N:P stoichiometry on regional carbon fluxes, this work addresses one of many sources of uncertainty and represents an incremental step toward improving regional and global marine biogeochemical models and the representation of the global coastal ocean, as increasing resolution will require more detailed process representations.

Bibliography

Anderson, T. R., & Pondaven, P. (2003). Non-Redfield carbon and nitrogen cycling in the Sargasso Sea: Pelagic imbalances and export flux. *Deep Sea Research Part I: Oceanographic Research Papers*, *50*(5), 573–591. doi: 10.1016/S0967-0637(03)00034-7

Aricò, S., Arrieta, J. M., Bakker, D. C. E., Boyd, P. W., Cotrim da Cunha, L., Chai, F., … Rojas Aldana, A. (2021). *Integrated ocean carbon research: A summary of ocean carbon research, and vision of coordinated ocean carbon research and observations for the next decade* (Tech. Rep. No. 158). Paris: UNESCO Intergovernmental Oceanographic Commission. doi: 10.25607/h0gj-pq41

Armin, G., & Inomura, K. (2021). Modeled temperature dependencies of macromolecular allocation and elemental stoichiometry in phytoplankton. *Computational and Structural Biotechnology Journal*, *19*, 5421–5427. doi: 10.1016/j.csbj.2021.09.028

Bar-On, Y. M., & Milo, R. (2019). The biomass composition of the oceans: A blueprint of our blue planet. *Cell*, *179*(7), 1451–1454. doi: 10.1016/j.cell.2019.11.018

Bar-On, Y. M., Phillips, R., & Milo, R. (2018). The biomass distribution on Earth. *Proceedings of the National Academy of Sciences*, *115*(25), 6506–6511. doi: 10.1073/pnas.1711842115

Bauer, J., Cai, W. J., Raymond, P., & et al. (2013). The changing carbon cycle of the coastal ocean. *Nature*, *504*, 61–70. doi: 10.1038/nature12857

Bianchi, T. S. (2011). The role of terrestrially derived organic carbon in the coastal ocean: A changing paradigm and the priming effect. *Proceedings of the National Academy of Sciences*, *108*(49), 19473-19481. doi: 10.1073/pnas.1017982108

Blackford, J., & Gilbert, F. (2007). pH variability and CO_2 induced acidification in the North Sea. *Journal of Marine Systems*, *64*(1), 229-241. doi: 10.1016/j.jmarsys.2006.03.016

Bonachela, J. A., Allison, S. D., Martiny, A. C., & Levin, S. A. (2013). A model for variable phytoplankton stoichiometry based on cell protein regulation. *Biogeosciences*, *10*(6), 4341–4356. doi: 10.5194/bg-10-4341-2013

Buesseler, K. O., & Boyd, P. W. (2009). Shedding light on processes that control particle export and flux attenuation in the twilight zone of the open ocean. *Limnology and Oceanography*, *54*(4), 1210–1232. doi: 10.4319/lo.2009.54.4.1210

Buesseler, K. O., Boyd, P. W., Black, E. E., & Siegel, D. A. (2020). Metrics that matter for assessing the ocean biological carbon pump. *Proceedings of the National Academy of Sciences*, *117*(18), 9679–9687. doi: 10.1073/pnas.1918114117

Butenschön, M., Clark, J., Aldridge, J. N., Allen, J. I., Artioli, Y., Blackford, J., … Torres, R. (2016). Ersem 15.06: a generic model for marine biogeochemistry and the ecosystem dynamics of the lower trophic levels. *Geoscientific Model Development*, *9*(4), 1293–1339. doi: 10.5194/gmd-9-1293-2016

Cai, R., & Jiao, N. (2023). Recalcitrant dissolved organic matter and its major production and removal processes in the ocean. *Deep Sea Research Part I: Oceanographic Research Papers*, *191*, 103922. doi: 10.1016/j.dsr.2022.103922

Carlson, C. A., Liu, S., Stephens, B. M., & English, C. J. (2024). Chapter 5 - DOM production, removal, and transformation processes in marine systems. In D. A. Hansell & C. A. Carlson (Eds.), *Biogeochemistry of marine dissolved organic matter (third edition)* (pp. 137–246). Academic Press. doi: 10.1016/B978-0-443-13858-4.00013-7

Chaichana, S., Jickells, T., & Johnson, M. (2019). Interannual variability in the summer dissolved organic matter inventory of the North Sea: Implications for the continental shelf pump. *Biogeosciences*, *16*(5), 1073–1096. doi: 10.5194/bg-16-1073-2019

Chan, L.-K., Newton, R. J., Sharma, S., Smith, C. B., Rayapati, P., Limardo, A. J., … Moran, M. A. (2012). Transcriptional changes underlying elemental stoichiometry shifts in a marine heterotrophic bacterium. *Frontiers in Microbiology, Volume 3 - 2012*. doi: 10.3389/fmicb.2012.00159

Chien, C.-T., Pahlow, M., Schartau, M., Li, N., & Oschlies, A. (2023). Effects of phytoplankton physiology on global ocean biogeochemistry and climate. *Science Advances*, *9*(30), eadg1725. doi: 10.1126/sciadv.adg1725

Daewel, U., & Schrum, C. (2013). Simulating long-term dynamics of the coupled North Sea and Baltic Sea ecosystem with ECOSMO II: Model description and validation. *Journal of Marine Systems*, *119-120*, 30-49. doi: 10.1016/j.jmarsys.2013.03.008

Dai, M., Su, J., Zhao, Y., Hofmann, E. E., Cao, Z., Cai, W.-J., … Wang, Z. (2022). Carbon fluxes in the coastal ocean: Synthesis, boundary processes, and future trends. *Annual Review of Earth and Planetary Sciences*, *50*, 593-626. doi: 10.1146/annurev-earth-032320-090746

del Giorgio, P., & Duarte, C. M. (2002). Respiration in the open ocean. *Nature*, *420*, 379–384. doi: 10.1038/nature01165

Demir, K. T., Mathis, M., Kossack, J., Liu, F., Daewel, U., Stegert, C., … Schrum, C. (2025a). Organic matter stoichiometry regulates the continental shelf carbon pump efficiency of the northwest European shelf seas. *ESS Open Archive [Preprint]. Submitted to Global Biogeochemical Cycles (under review)*. doi: 10.22541/essoar.175088438.85557149/v1

Demir, K. T., Mathis, M., Kossack, J., Liu, F., Daewel, U., Stegert, C., … Schrum, C. (2025b). Variable organic matter stoichiometry enhances the biological

drawdown of CO_2 in the northwest European shelf seas. *Biogeosciences*, *22*(11), 2569–2599. doi: 10.5194/bg-22-2569-2025

DeVries, T., & Primeau, F. (2011). Dynamically and observationally constrained estimates of water-mass distributions and ages in the global ocean. *Journal of Physical Oceanography*, *41*(12), 2381–2401. doi: 10.1175/JPO-D-11-03.1

Diesing, M., Thorsnes, T., & Bjarnadóttir, L. R. (2021). Organic carbon densities and accumulation rates in surface sediments of the North Sea and Skagerrak. *Biogeosciences*, *18*(6), 2139–2160. doi: 10.5194/bg-18-2139-2021

Dittmar, T., Lennartz, S. T., Buck-Wiese, H., Hansell, D. A., Santinelli, C., Vanni, C., … Hehemann, J.-H. (2021). Enigmatic persistence of dissolved organic matter in the ocean. *Nature Reviews Earth & Environment*, *2*, 570-583. doi: 10.1038/s43017-021-00183-7

Doney, S. C., Ruckelshaus, M., Duffy, J. E., Barry, J. P., Chan, F., English, C. A., … Talley, L. D. (2012). Climate change impacts on marine ecosystems. *Annual Review of Marine Science*, *4*, 11–37. doi: 10.1146/annurev-marine-041911-111611

Fagerbakke, K. M., Heldal, M., & Norland, S. (1996). Content of carbon, nitrogen, oxygen, sulfur and phosphorus in native aquatic and cultured bacteria. *Aquatic Microbial Ecology*, *10*, 15–27. doi: 10.3354/ame010015

Field, C. B., Behrenfeld, M. J., Randerson, J. T., & Falkowski, P. (1998). Primary production of the biosphere: Integrating terrestrial and oceanic components. *Science*, *281*(5374), 237-240. doi: 10.1126/science.281.5374.237

Fox, J., Behrenfeld, M. J., Halsey, K. H., & Graff, J. R. (2024). Global estimates of particulate organic carbon concentration from the surface ocean to the base of the mesopelagic. *Global Biogeochemical Cycles*, *38*(10), e2024GB008149. doi: 10.1029/2024GB008149

Frankignoulle, M., & Borges, A. V. (2001). European continental shelf as a significant sink for atmospheric carbon dioxide. *Global Biogeochemical Cycles*, *15*(3), 569–576. doi: 10.1029/2000GB001307

Fransner, F., Gustafsson, E., Tedesco, L., Vichi, M., Hordoir, R., Roquet, F., … Nycander, J. (2018). Non-Redfieldian dynamics explain seasonal pCO_2 drawdown in the Gulf of Bothnia. *Journal of Geophysical Research: Oceans*, *123*(1), 166-188. doi: 10.1002/2017JC013019

Friedlingstein, P., O'Sullivan, M., Jones, M. W., Andrew, R. M., Hauck, J., Landschützer, P., … Zeng, J. (2025). Global carbon budget 2024. *Earth System Science Data*, *17*(3), 965–1039. doi: 10.5194/essd-17-965-2025

Garcia, N. S., Bonachela, J. A., & Martiny, A. C. (2016). Interactions between growth-dependent changes in cell size, nutrient supply and cellular elemental stoichiometry of marine *synechococcus*. *The ISME Journal*, *10*(11), 2715–2724. doi: 10.1038/ismej.2016.50

Garcia, N. S., Bonachela, J. A., & Martiny, A. C. (2018). Interactions between growth-dependent changes in cell size, nutrient supply and cellular elemental stoichiometry of marine synechococcus. *The ISME Journal*, *10*(11), 2715–2724. doi: 10.1038/ismej.2016.50

Gazeau, F., Smith, S. V., Gentili, B., Frankignoulle, M., & Gattuso, J.-P. (2004). The European coastal zone: Characterization and first assessment of ecosystem metabolism. *Estuarine, Coastal and Shelf Science*, *60*(4), 673-694. doi: 10.1016/j.ecss.2004.03.007

Geider, R., & La Roche, J. (2002). Redfield revisited: Variability of C:N:P in marine microalgae and its biochemical basis. *European Journal of Phycology*, *37*(1), 1–17. doi: 10.1017/S0967026201003456

Godwin, C. M., & Cotner, J. B. (2015). Aquatic heterotrophic bacteria have highly flexible phosphorus content and biomass stoichiometry. *The ISME Journal*, *9*(10), 2324-2327. doi: 10.1038/ismej.2015.34

Goldman, J. C., McCarthy, J. J., & Peavey, D. G. (1979). Growth rate influence on the chemical composition of phytoplankton in oceanic waters. *Nature*, *279*, 210–215. doi: 10.1038/279210a0

Golz, A.-L., Burian, A., & Winder, M. (2015). Stoichiometric regulation in micro- and mesozooplankton. *Journal of Plankton Research*, *37*(2), 293–305. doi: 10.1093/plankt/fbu109

Hansell, D. A. (2013). Recalcitrant dissolved organic carbon fractions. *Annual Review of Marine Science*, *5*, 421-445. doi: 10.1146/annurev-marine-120710-100757

Hansell, D. A., Carlson, C. A., Repeta, D. J., & Schlitzer, R. (2009). Dissolved organic matter in the ocean: A controversy stimulates new insights. *Oceanography*, *22*(4), 202–211. doi: 10.5670/oceanog.2009.109

He, W., Chen, M., Schlautman, M. A., & Hur, J. (2016). Dynamic exchanges between DOM and POM pools in coastal and inland aquatic ecosystems: A review. *Science of The Total Environment*, *551-552*, 415-428. doi: 10.1016/j.scitotenv.2016.02.031

Ho, T.-Y., Quigg, A., Finkel, Z. V., Milligan, A. J., Wyman, K., Falkowski, P. G., & Morel, F. M. M. (2003). The elemental composition of some marine phytoplankton. *Journal of Phycology*, *39*(6), 1145–1159. doi: 10.1111/j.0022-3646.2003.03-090.x

Holt, J., Wakelin, S., & Huthnance, J. M. (2009). Down-welling circulation of the northwest European continental shelf: A driving mechanism for the continental shelf carbon pump. *Geophysical Research Letters*, *36*(14). doi: 10.1029/2009GL038997

Hopkinson, C., & Vallino, J. (2005). Efficient export of carbon to the deep ocean through dissolved organic matter. *Nature*, *433*, 142–145. doi: 10.1038/nature03191

Huthnance, J. M., Holt, J. T., & Wakelin, S. L. (2009). Deep ocean exchange with west-European shelf seas. *Ocean Science*, *5*(4), 621–634. doi: 10.5194/os-5-621-2009

Huthnance, J. M., Hopkins, J., Berx, B., Dale, A., Holt, J., Hosegood, P., ... Spingys, C. (2022). Ocean shelf exchange, nw European shelf seas: Measurements, estimates and comparisons. *Progress in Oceanography*, *202*, 102760. doi: 10.1016/j.pocean.2022.102760

Inomura, K., Deutsch, C., Jahn, O., & et al. (2022). Global patterns in marine organic matter stoichiometry driven by phytoplankton ecophysiology. *Nature Geoscience*, *15*, 1034–1040. doi: 10.1038/s41561-022-01066-2

Inomura, K., Omta, A. W., Talmy, D., Bragg, J., Deutsch, C., & Follows, M. J. (2020). A mechanistic model of macromolecular allocation, elemental stoichiometry, and growth rate in phytoplankton. *Frontiers in Microbiology*, *11*. doi: 10.3389/fmicb.2020.00086

Jiao, N., Herndl, G., Hansell, D., et al. (2011). The microbial carbon pump and the oceanic recalcitrant dissolved organic matter pool. *Nature Reviews Microbiology*, *9*, 555. doi: 10.1038/nrmicro2386-c5

Kitidis, V., Shutler, J. D., Ashton, I., et al. (2019). Winter weather controls net influx of atmospheric CO_2 on the north-west European shelf. *Scientific Reports*, *9*, 20153. doi: 10.1038/s41598-019-56363-5

Klausmeier, C. A., Litchman, E., Daufresne, T., & Levin, S. A. (2004). Optimal nitrogen-to-phosphorus stoichiometry of phytoplankton. *Nature*, *429*, 171–174. doi: 10.1038/nature02454

Kossack, J., Mathis, M., Daewel, U., Liu, F., Demir, K. T., Thomas, H., & Schrum, C. (2024). Tidal impacts on air-sea CO_2 exchange on the north-west European shelf. *Frontiers in Marine Science*, *11*, 1406896. doi: 10.3389/fmars.2024.1406896

Kossack, J., Mathis, M., Daewel, U., Zhang, Y. J., & Schrum, C. (2023). Barotropic and baroclinic tides increase primary production on the northwest European shelf. *Frontiers in Marine Science*, *10*, 1206062. doi: 10.3389/fmars.2023.1206062

Kreus, M., Schartau, M., Engel, A., Nausch, M., & Voss, M. (2015). Variations in the elemental ratio of organic matter in the central Baltic Sea: Part I—linking primary production to remineralization. *Continental Shelf Research*, *100*, 25–45. doi: 10.1016/j.csr.2014.06.015

Kwiatkowski, L., Aumont, O., Bopp, L., & Ciais, P. (2018). The impact of variable phytoplankton stoichiometry on projections of primary production, food quality, and carbon uptake in the global ocean. *Global Biogeochemical Cycles*, *32*(4), 516-528. doi: 10.1002/2017GB005799

Kühn, W., Pätsch, J., Thomas, H., Borges, A. V., Schiettecatte, L.-S., Bozec, Y., & Prowe, A. E. F. (2010). Nitrogen and carbon cycling in the North Sea and exchange with the North Atlantic – A model study, part II: Carbon budget and fluxes. *Continental Shelf Research*, *30*(16), 1701–1716. doi: 10.1016/j.csr.2010.07.001

Legge, O., Johnson, M., Hicks, N., Jickells, T., Diesing, M., Aldridge, J., ... Williamson, P. (2020). Carbon on the northwest European shelf: Contemporary budget and future influences. *Frontiers in Marine Science*, *7*. doi: 10.3389/fmars.2020.00143

Letscher, R. T., & Moore, J. K. (2015). Preferential remineralization of dissolved organic phosphorus and non-Redfield DOM dynamics in the global ocean: Impacts on marine productivity, nitrogen fixation, and carbon export. *Global Biogeochemical Cycles*, *29*(3), 325–340. doi: 10.1002/2014GB004904

Letscher, R. T., Moore, J. K., Teng, Y.-C., & Primeau, F. W. (2015). Variable C:N:P stoichiometry of dissolved organic matter cycling in the community earth system model. *Biogeosciences*, *12*(1), 209–221. doi: 10.5194/bg-12-209-2015

Liang, Z., Letscher, R. T., & Knapp, A. N. (2023). Global patterns of surface ocean dissolved organic matter stoichiometry. *Global Biogeochemical Cycles*, *37*(12), e2023GB007788. doi: 10.1029/2023GB007788

Liefer, J. D., White, A. E., Finkel, Z. V., Irwin, A. J., Dugenne, M., Inomura, K., ... Follows, M. J. (2024). Latitudinal patterns in ocean C:N:P reflect phytoplankton acclimation and macromolecular composition. *Proceedings of the National Academy of Sciences*, *121*(46), e2404460121. doi: 10.1073/pnas.2404460121

Liu, J., Wang, H., Mou, J., Peñuelas, J., Delgado-Baquerizo, M., Martiny, A. C., ... Chen, J. (2025). Global-scale shifts in marine ecological stoichiometry over the past 50 years. *Nature Geoscience*, *18*, 819–827. doi: 10.1038/s41561-025-01735-y

Lomas, M. W., Baer, S. E., Mouginot, C., Terpis, K. X., Lomas, D. A., Altabet, M. A., & Martiny, A. C. (2021). Varying influence of phytoplankton biodiversity and stoichiometric plasticity on bulk particulate stoichiometry across ocean basins. *Communications Earth & Environment*, *2*, 143. doi: 10.1038/s43247-021-00212-9

Lønborg, C., & Álvarez-Salgado, X. A. (2012). Recycling versus export of bioavailable dissolved organic matter in the coastal ocean and efficiency of the continental shelf pump. *Global Biogeochemical Cycles*, *26*(3). doi: 10.1029/2012GB004353

Martin, A. P., Dominguez, A. B., Baker, C. A., Baumas, C. M. J., Bisson, K. M., Cavan, E., ... Yool, A. (2024). When to add a new process to a model – and when not: A marine biogeochemical perspective. *Ecological Modelling*, *498*, 110870. doi: 10.1016/j.ecolmodel.2024.110870

Martin, J. H., Knauer, G. A., Karl, D. M., & Broenkow, W. W. (1987). VERTEX: Carbon cycling in the northeast Pacific. *Deep Sea Research Part A. Oceanographic Research Papers*, *34*(2), 267–285. doi: 10.1016/0198-0149(87)90086-0

Martiny, A. C., Pham, C. T. A., Primeau, F. W., Vrugt, J. A., Lomas, M. W., & Moore, J. K. (2013). Strong latitudinal patterns in the elemental ratios of marine plankton and organic matter. *Nature Geoscience*, *6*, 279–283. doi: 10.1038/ngeo1757

Martiny, A. C., Vrugt, J., & Lomas, M. (2014). Concentrations and ratios of particulate organic carbon, nitrogen, and phosphorus in the global ocean. *Scientific Data*,

1, 140048. doi: 10.1038/sdata.2014.48

Matsumoto, K., Rickaby, R., & Tanioka, T. (2020). Carbon export buffering and CO_2 drawdown by flexible phytoplankton C:N:P under glacial conditions. *Paleoceanography and Paleoclimatology*, *35*(7), e2019PA003823. doi: 10.1029/2019PA003823

Matsumoto, K., & Tanioka, T. (2020). Shifts in regional production as a driver of future global ocean production stoichiometry. *Environmental Research Letters*, *15*(12), 124027. doi: 10.1088/1748-9326/abc4b0

Meunier, C. L., Buchkowski, R., Elser, J. J., Laspoumaderes, C., Metson, G. S., Sethna, L. R., & Boersma, M. (2025). Editorial: Advances in ecological stoichiometry. *Frontiers in Ecology and Evolution*. doi: 10.3389/fevo.2025.1632107

Moran, M. A., Kujawinski, E. B., Schroer, W. F., Amin, S. A., Bates, N. R., Bertrand, E. M., ... Vardi, A. (2022). Microbial metabolites in the marine carbon cycle. *Nature Microbiology*, *7*, 508-523. doi: 10.1038/s41564-022-01090-3

Møller, E. F. (2007). Production of dissolved organic carbon by sloppy feeding in the copepods acartia tonsa, centropages typicus, and temora longicornis. *Limnology and Oceanography*, *52*(1), 79-84. doi: 10.4319/lo.2007.52.1.0079

Møller, E. F., Thor, P., & Nielsen, T. G. (2003). Production of DOC by calanus finmarchicus, c. glacialis and c. hyperboreus through sloppy feeding and leakage from fecal pellets. *Marine Ecology Progress Series*, *262*, 185-191. doi: 10.3354/meps262185

Mühlenbruch, M., Grossart, H.-P., Eigemann, F., & Voss, M. (2018). Mini-review: Phytoplankton-derived polysaccharides in the marine environment and their interactions with heterotrophic bacteria. *Environmental Microbiology*, *20*(8), 2671-2685. doi: 10.1111/1462-2920.14302

Neumann, T., Radtke, H., Cahill, B., Schmidt, M., & Rehder, G. (2022). Non-Redfieldian carbon model for the Baltic Sea (ERGOM version 1.2) – implementation and budget estimates. *Geoscientific Model Development*, *15*(22), 8473–8540. doi: 10.5194/gmd-15-8473-2022

Osterroht, C., & Thomas, H. (2000). New production enhanced by nutrient supply from non-Redfield remineralisation of freshly produced organic material. *Journal of Marine Systems*, *25*(1), 33-46. doi: 10.1016/S0924-7963(00)00007-5

Polimene, L., Sailley, S., Clark, D., Mitra, A., & Allen, J. I. (2017). Biological or microbial carbon pump? the role of phytoplankton stoichiometry in ocean carbon sequestration. *Journal of Plankton Research*, *39*(2), 180-186. doi: 10.1093/plankt/fbw091

Quigg, A., Finkel, Z. V., Irwin, A. J., Rosenthal, Y., Ho, T.-Y., Reinfelder, J. R., ... Falkowski, P. G. (2003). The evolutionary inheritance of elemental stoichiometry in marine phytoplankton. *Nature*, *425*, 291–294. doi: 10.1038/nature01953

Quigg, A., Irwin, A. J., & Finkel, Z. V. (2010). Evolutionary inheritance of elemental stoichiometry in phytoplankton. *Proceedings of the Royal Society B: Biological Sciences*, *278*(1705), 526–534. doi: 10.1098/rspb.2010.1356

Redfield, A. C. (1934). On the proportions of organic derivatives in sea water and their relation to the composition of plankton. In R. J. Daniel (Ed.), *James johnstone memorial volume* (pp. 176–192). University of Liverpool.

Redfield, A. C. (1958). The biological control of chemical factors in the environment. *American Scientist*, *46*, 205–221. Retrieved from http://www.jstor.org/stable/27827150

Redfield, A. C., Ketchum, B. H., & Richards, F. A. (1963). The influence of organisms on the composition of seawater. In M. N. Hill (Ed.), *The sea* (Vol. 2, pp. 26–77). Interscience Publishers.

Richardson, K., Steffen, W., Lucht, W., Bendtsen, J., Cornell, S. E., Donges, J. F., … Rockström, J. (2023). Earth beyond six of nine planetary boundaries. *Science Advances*, *9*(37), eadh2458. doi: 10.1126/sciadv.adh2458

Rivkin, R. B., & Legendre, L. (2001). Biogenic carbon cycling in the upper ocean: Effects of microbial respiration. *Science*, *291*(5512), 2398-2400. doi: 10.1126/science.291.5512.2398

Rockström, J., Steffen, W., Noone, K., Persson, , Chapin, F. S., Lambin, E. F., … Foley, J. A. (2009). A safe operating space for humanity. *Nature*, *461*(7263), 472–475. doi: 10.1038/461472a

Roshan, S., & DeVries, T. (2017). Efficient dissolved organic carbon production and export in the oligotrophic ocean. *Nature Communications*, *8*, 2036. doi: 10.1038/s41467-017-02227-3

Schrum, C., Alekseeva, I., & John, M. S. (2006). Development of a coupled physical–biological ecosystem model ECOSMO: Part I: Model description and validation for the North Sea. *Journal of Marine Systems*, *61*(1), 79-99. doi: 10.1016/j.jmarsys.2006.01.005

Sheppard, E. J., Hurd, C. L., Britton, D. D., Reed, D. C., & Bach, L. T. (2023). Seaweed biogeochemistry: Global assessment of C:N and C:P ratios and implications for ocean afforestation. *Journal of Phycology*, *59*(5), 879–892. doi: 10.1111/jpy.13381

Smith, S. L., Yamanaka, Y., & Kishi, M. J. (2005). Attempting consistent simulations of stn. ALOHA with a multi-element ecosystem model. *Journal of Oceanography*, *61*, 1–23. doi: 10.1007/s10872-005-0016-4

Somes, C. J., & Oschlies, A. (2015). On the influence of non-Redfield dissolved organic nutrient dynamics on the spatial distribution of N_2 fixation and the size of the marine fixed nitrogen inventory. *Global Biogeochemical Cycles*, *29*(7), 973–993. doi: 10.1002/2014GB005050

Sterner, R. W., & Elser, J. J. (2002). *Ecological stoichiometry: The biology of elements from molecules to the biosphere*. Princeton, NJ: Princeton University Press. Retrieved

from http://www.jstor.org/stable/j.ctt1jktrp3

Stramska, M. (2009). Particulate organic carbon in the global ocean derived from SeaWiFS ocean color. *Deep Sea Research Part I: Oceanographic Research Papers*, *56*(9), 1459–1470. doi: 10.1016/j.dsr.2009.04.009

Sullivan, M. R., Primeau, F. W., Hagstrom, G. I., Wang, W.-L., & Martiny, A. C. (2024). Integrating trait-based stoichiometry in a biogeochemical inverse model reveals links between phytoplankton physiology and global carbon export. *Global Biogeochemical Cycles*, *38*(3), e2023GB007986. doi: https://doi.org/10.1029/2023GB007986

Tanioka, T., Garcia, C. A., Martiny, A. C., Fichot, C. G., Matsumoto, K., Larkin, A. A., … Fagan, A. (2022). Global patterns and predictors of C:N:P in marine ecosystems. *Communications Earth & Environment*, *3*, 271. doi: 10.1038/s43247-022-00603-6

Tanioka, T., Larkin, A. A., Moreno, A. R., Brock, M. L., Fagan, A. J., Garcia, C. A., … Martiny, A. C. (2022). Global ocean particulate organic phosphorus, carbon, oxygen for respiration, and nitrogen ($go - popcorn$). *Scientific Data*, *9*, 688. doi: 10.1038/s41597-022-01809-1

Tanioka, T., & Matsumoto, K. (2017). Buffering of ocean export production by flexible elemental stoichiometry of particulate organic matter. *Global Biogeochemical Cycles*, *31*(10), 1528-1542. doi: 10.1002/2017GB005670

Tanioka, T., Matsumoto, K., & Lomas, M. W. (2021). Drawdown of atmospheric pCO_2 via variable particle flux stoichiometry in the ocean twilight zone. *Geophysical Research Letters*, *48*(22), e2021GL094924. doi: 10.1029/2021GL094924

Teng, Y.-C., Primeau, F. W., Moore, J. K., Lomas, M. W., & Martiny, A. C. (2014). Global-scale variations of the ratios of carbon to phosphorus in exported marine organic matter. *Nature Geoscience*, *7*, 895–898. doi: 10.1038/ngeo2303

Thomas, H., Bozec, Y., de Baar, H. J. W., Elkalay, K., Frankignoulle, M., Schiettecatte, L.-S., … Borges, A. V. (2005). The carbon budget of the North Sea. *Biogeosciences*, *2*(1), 87–96. doi: 10.5194/bg-2-87-2005

Thomas, H., Bozec, Y., Elkalay, K., & de Baar, H. J. W. (2004). Enhanced open ocean storage of CO_2 from shelf sea pumping. *Science*, *304*(5673), 1005–1008. doi: 10.1126/science.1095491

Thomas, H., Ittekkot, V., Osterroht, C., & Schneider, B. (1999). Preferential recycling of nutrients—the ocean's way to increase new production and to pass nutrient limitation? *Limnology and Oceanography*, *44*(8), 1999-2004. doi: 10.4319/lo.1999.44.8.1999

Thornton, D. C. (2014). Dissolved organic matter (DOM) release by phytoplankton in the contemporary and future ocean. *European Journal of Phycology*, *49*(1), 20-46. doi: 10.1080/09670262.2013.875596

United Nations, Department of Economic and Social Affairs. (2025). *The Sustainable*

Development Goals Report 2025 (Technical Report). United Nations. Retrieved from https://unstats.un.org/sdgs/report/2025/

van de Waal, D. B., Verschoor, A. M., Verspagen, J. M., van Donk, E., & Huisman, J. (2010). Climate-driven changes in the ecological stoichiometry of aquatic ecosystems. *Frontiers in Ecology and the Environment*, *8*(3), 145–152. doi: 10.1890/080178

Wakeham, S. G., & Lee, C. (1993). Production, transport, and alteration of particulate organic matter in the marine water column. In F. G. Stehli, D. S. Jones, M. H. Engel, & S. A. Macko (Eds.), *Organic geochemistry* (Vol. 11, pp. 145–169). Springer US. doi: 10.1007/978-1-4615-2890-6_6

Wakelin, S. L., Holt, J. T., Blackford, J. C., Allen, J. I., Butenschön, M., & Artioli, Y. (2012). Modeling the carbon fluxes of the northwest European continental shelf: Validation and budgets. *Journal of Geophysical Research: Oceans*, *117*(C5). doi: 10.1029/2011JC007402

White, A. E., Giovannoni, S. J., Zhao, Y., Vergin, K., & Carlson, C. A. (2019). Elemental content and stoichiometry of sar11 chemoheterotrophic marine bacteria. *Limnology and Oceanography Letters*, *4*(2), 44–51. doi: 10.1002/lol2.10103

Wirtz, K. W., & Kerimoglu, O. (2016). Autotrophic stoichiometry emerging from optimality and variable co-limitation. *Frontiers in Ecology and Evolution*, *4*, 131. doi: 10.3389/fevo.2016.00131

Xie, L., Gao, X., Liu, Y., Zhao, J., & Xing, Q. (2023). The joint effects of atmospheric dry and wet deposition on organic carbon cycling in a mariculture area in north china. *Science of The Total Environment*, *876*, 162715. doi: 10.1016/j.scitotenv.2023.162715

Zakem, E. J., & Levine, N. M. (2019). Systematic variation in marine dissolved organic matter stoichiometry and remineralization ratios as a function of lability. *Global Biogeochemical Cycles*, *33*(11), 1389–1407. doi: 10.1029/2019GB006375

Zhang, Y. J., Stanev, E., & Grashorn, S. (2016). Unstructured-grid model for the North Sea and Baltic Sea: Validation against observations. *Ocean Modelling*, *97*, 91-108. doi: 10.1016/j.ocemod.2015.11.009

Zimmerman, A. E., Allison, S. D., & Martiny, A. C. (2014). Phylogenetic constraints on elemental stoichiometry and resource allocation in heterotrophic marine bacteria. *Environmental Microbiology*, *16*(5), 1398–1410. doi: 10.1111/1462-2920.12329

Appendix A: *Article* I

This chapter contains a manuscript that has not yet been published:

Demir, K. T., Mathis, M., Daewel, U., Thomas, H., and Schrum, C. C:N:P stoichiometry of marine organic matter in the global coastal and open oceans: Patterns and predictors, biogeochemical implications, and model representations. (*to be submitted*)

The author contributions of Kubilay Timur Demir (KTD) and others to this paper are as follows:

KTD was responsible for conceptualization, methodology, formal analysis, investigation, data curation, and visualization. KTD also prepared the original draft of the manuscript. Writing, review, and editing were carried out by KTD, MM, UD, HT, and CS. MM, UD, HT, and CS provided supervision. Project administration, as well as resource and funding acquisition, were led by CS.

C:N:P stoichiometry of marine organic matter in the global coastal and open oceans: Patterns and predictors, biogeochemical implications, and model representations

Kubilay Timur Demir[1], Moritz Mathis[1], Ute Daewel[1], Helmuth Thomas[2,3], Corinna Schrum[1,4]

[1]Institute of Coastal Systems—Analysis and Modeling, Helmholtz-Zentrum Hereon, Geesthacht, Germany
[2]Institute of Carbon Cycles, Helmholtz-Zentrum Hereon, Geesthacht, Germany
[3]Institute for Chemistry and Biology of the Marine Environment, Carl von Ossietzky University of Oldenburg, Oldenburg, Germany
[4]Institute of Oceanography, University of Hamburg, Hamburg, Germany

Correspondence to: Kubilay Timur Demir (Kubilay.Demir@hereon.de)

Abstract. The ratios of carbon, nitrogen, and phosphorus in the production, transformation, and decomposition of marine organic matter (OM) play a central role in coupling the global oceanic carbon and nutrient cycles. This review synthesizes current understanding of the distribution, cycling, and elemental C:N:P stoichiometry of dissolved (DOM) and particulate organic matter (POM) across different coastal and open ocean regions. We begin by describing the diverse cycling pathways of OM, from production by autotrophs, through assimilation and transformation within the microbial loop and larger heterotrophic food web, to continued processing throughout the water column and interactions across the DOM–POM continuum. The review then examines how these cycling processes shape the distribution of DOM and POM across depths and regions, and evaluates their resulting contributions to export production. We highlight systematic variability in OM stoichiometry across size and lability fractions, depths, and geographic regions, and assess how the ecological stoichiometry of producers and consumers contributes to variations in the C:N:P ratios of POM. Further, we explore the biological and environmental drivers that influence OM stoichiometry, including community composition and phytoplankton acclimation in response to nutrient stress, temperature, irradiance, and partial pressure of CO_2. The review also considers emerging trends under climate change and discusses how deviations from Redfield stoichiometry affect biogeochemical cycling, particularly in relation to carbon export and new production. Finally, we evaluate current biogeochemical model representations of variable C:N:P stoichiometry in OM production and transformation across living cells and detrital or non-living POM and DOM. Building on these insights, the review outlines future directions for observations and modeling to advance understanding of OM cycling and its role in global biogeochemical cycles.

1 Introduction

This review synthesizes findings from the past several decades on the distribution and C:N:P stoichiometry of marine organic matter (OM) in both the coastal and open oceans, with a focus on variability across size and lability fractions with depth. As

part of this synthesis, we also cover recent advances in the understanding of OM cycling, with an emphasis on dissolved organic matter (DOM), given its central role in controlling the distribution and time scales of variability in OM concentrations and C:N:P ratios in the global ocean, with consequences for long-term carbon sequestration. We further discuss drivers that have been suggested to shape this variability, its implications for biogeochemical cycling, and current representations in models. We explore differences between the coastal and open oceans, in light of the essential role of the coastal ocean in the land-ocean coupling of biogeochemical cycles. Our central aim is to provide a comprehensive overview of C:N:P ratios in marine OM and their significance for carbon and nutrient cycles across spatial and temporal scales to support future developments of OM representations in regional and global biogeochemical models.

Marine OM contains approximately 700 petagrams of carbon (Pg C), as reported in recent global carbon budget reports (Friedlingstein et al., 2025; Intergovernmental Panel on Climate Change (IPCC), 2023), which is a comparable amount to the 890 Pg C currently stored in atmospheric CO_2 (Friedlingstein et al., 2025). The diverse mixture of organic compounds in marine OM is characterized by varying chemical composition, physical structures, and reactivity (Nagata, 2008), forms a continuous spectrum of size and lability that is commonly classified into operational fractions (Dittmar et al., 2021; Hansell, 2013; Nagata, 2008; Ogawa and Tanoue, 2003). These fractions exhibit broadly consistent characteristics such as composition, reactivity, and sinking speed, which allow the conceptualization of differences in their production, transformation, and removal processes (Carlson et al., 2024; Dittmar and Lennartz, 2024; Hansell, 2013; Nagata, 2008; Wakeham and Lee, 1993).

With an estimated 662 ± 32 Pg C (Carlson et al., 2024; Hansell et al., 2009), dissolved organic carbon (DOC) constitutes the dominant component of the ocean's reservoir of reduced carbon. DOC is operationally defined as the fraction that passes through filters with pore sizes of 0.2–0.7 µm, but most commonly 0.7 µm (Carlson et al., 2024; Nagata, 2008; Ogawa and Tanoue, 2003; Wells, 1998). This definition contrasts with strict chemical dissolution as a homogeneous molecular mixture in a solution. Thus, DOC includes colloids and organisms, including bacteria and viruses smaller than the filter size (Nagata, 2008; Ogawa and Tanoue, 2003; Wells, 1998). Material retained by this filter size is classified as particulate organic matter (POM), comprising both living plankton cells and non-living detritus (Nagata, 2008; Wakeham and Lee, 1993). At the intersection of DOM and POM, there is a continuum of size fractions, including colloids and marine gels with dynamic DOM-POM exchanges (Azam, 1998; Azam et al., 1994; Azam and Malfatti, 2007; He et al., 2016; Lee, 2024; Nagata, 2008; Verdugo et al., 2004; Wells, 1998). In the surface ocean, the relative proportions of DOM, detritus, and biomass of living plankton have been estimated at approximately 200:10:1 (Nagata, 2008), although these ratios likely vary considerably between regions and throughout the seasonal cycle in the production and decomposition of OM.

Two recent studies (Bar-On et al., 2018; Bar-On and Milo, 2019) estimate global carbon stocks in marine biota at 6 Pg C by upscaling previous observations, doubling the 3 Pg C reported in the latest carbon budget and IPCC assessment (Friedlingstein et al., 2025; Intergovernmental Panel on Climate Change (IPCC), 2023). Their analysis further highlights that marine biomass is nearly two orders of magnitude smaller than terrestrial biomass and, compared to terrestrial ecosystems, has a larger fraction of consumers (animals, non-photosynthetic protists, heterotrophic bacteria), and a lower fraction of producers (photosynthetic protists, cyanobacteria, and plants such as green algae and seagrasses), most of which are planktonic. Estimates of total POC

stocks and individual fractions remain uncertain due to substantial seasonal variability and the difficulty in distinguishing non-living detritus from living cells, but recent assessments combining satellite and in situ observations suggest a global stock of approximately 3 Pg C, with about 2.3 Pg C in the upper 200 m (Fox et al., 2024; Stramska, 2009). While these global carbon stocks offer a helpful perspective on the partitioning of organic carbon in the global ocean, understanding the role of these fractions in nutrient recycling and air–sea CO_2 exchange also requires consideration of their turnover timescales.

More than 90% of DOM in the ocean is classified as refractory or recalcitrant DOM (R-DOM) (Hansell, 2013), meaning it resists rapid microbial degradation, accumulates, and therefore contributes little to new production (Cai and Jiao, 2023; Dittmar et al., 2021; Hopkinson and Vallino, 2005). Radiocarbon dating suggests an average lifetime of R-DOM between 4000 and 6000 years (Bauer et al., 1992), exceeding an estimated deep ocean mixing timescale of up to 1400–1500 years (DeVries and Primeau, 2011). As a result, concentrations of refractory or recalcitrant dissolved organic carbon (R-DOC) are nearly homogeneous across the global deep ocean, with only minor gradients in DOM concentrations ranging from 34–48 µM (Aminot and Kérouel, 2004; Hansell and Carlson, 1998a; Hopkinson and Vallino, 2005; Liang et al., 2023). This resistance to microbial degradation is thought to result either from an emergent recalcitrance due to the extreme dilution of individual compounds, rendering them biologically inaccessible, their inherent chemical recalcitrance, or a combination of both (Baltar et al., 2021; Cai and Jiao, 2023; Dittmar et al., 2021; Jiao et al., 2011, 2014, 2018).

While long-term changes in the stock, composition, and reactivity of R-DOM and ultra-refractory DOM (UR-DOM) (Hansell, 2013) may influence air–sea CO_2 exchange and hence climate on multi-millennial timescales (Cai and Jiao, 2023; Lee, 2024; Lønborg et al., 2020; Rothman et al., 2003; Sexton et al., 2011; Shen and Benner, 2018), carbon cycling, nutrient regeneration, and trophic interactions on seasonal to interannual scales are primarily driven by the production and degradation of POM, and the more reactive and intermediate fractions of DOM. Semi-labile DOM (SL-DOM), which accounts for an estimated 15–20% of global net community production (NCP) (Hansell et al., 2009; Hansell and Carlson, 1998b), and has a lifetime ranging from months to years (Hansell, 2013; Hansell et al., 2009; Ogawa and Tanoue, 2003), accumulates in the epipelagic zone and contributes to seasonal carbon export from surface waters through downwelling (Carlson et al., 1994, 2024; Hansell et al., 2009; Nagata, 2008; Ogawa and Tanoue, 2003). Semi-refractory DOM (SR-DOM) contributes to carbon export into the mesopelagic zone through ocean circulation on timescales of decades to centuries (Carlson et al., 2024; Hansell, 2013). POM is exported to depth both through gravitational sinking and physical transport by ocean circulation. (Hansell et al., 2009; Nagata, 2008; Wakeham and Lee, 1993). In contrast to SL-DOM, labile DOM (L-DOM) is rapidly recycled through the microbial loop by heterotrophic prokaryotes on timescales of seconds to days (Azam, 1998; Azam et al., 1983, 1994), playing a key role in the immediate turnover of organic carbon and nutrient regeneration (Carlson et al., 2024; Hansell, 2013; Hansell et al., 2009; Moran et al., 2022b, a; Ogawa and Tanoue, 2003). However, due to its short residence time, it does not accumulate, is not exported to depth, and contributes less than a percent to the measured concentrations and overall composition of DOM in the global ocean (Hansell, 2013; Hansell et al., 2009; Nagata, 2008; Ogawa and Tanoue, 2003). These differences in turnover timescales, in combination with large-scale ocean circulation, determine the distribution and vertical structure of DOM in the global ocean and the potential for long-term carbon sequestration (Hansell, 2013; Hansell et al., 2009, 2024).

As part of this continuous OM recycling, the elemental ratios of carbon, nitrogen, and phosphorus in all fractions of marine OM form a critical link between carbon and nutrient cycles in the ocean (Hopkinson and Vallino, 2005). For decades, the elemental Redfield stoichiometry of C:N:P=106:16:1 provided a foundational framework for understanding this coupling (Redfield, 1958; Redfield et al., 1963). However, a growing body of observations has revealed substantial deviations from these canonical ratios, with consistent differences across various OM pools, challenging the idea of a universal and constant stoichiometry (Aminot and Kérouel, 2004; Chaichana et al., 2019; Geider and La Roche, 2002; Ho et al., 2003; Hopkinson and Vallino, 2005; Letscher and Moore, 2015; Liang et al., 2023; Liu et al., 2025; Loh and Bauer, 2000; Lønborg et al., 2024; Martiny et al., 2013; Moreno and Martiny, 2018; Painter et al., 2017, 2018; Pujo-Pay et al., 2011; Tanioka et al., 2022b).

Healthy phytoplankton tend to exhibit average elemental ratios close to the Redfield C:N:P of 106:16:1 under nutrient-replete conditions, when averaged across diverse taxa at the global scale (Ho et al., 2003). However, substantial deviations are observed between taxa and in response to environmental variability, particularly nutrient availability and shifts in community composition, with observed C:N:P ratios ranging from below to above Redfield stoichiometry (Burkhardt et al., 1999; Finkel et al., 2006; Garcia et al., 2018b; Geider and La Roche, 2002; Leonardos and Geider, 2004; Quigg et al., 2003, 2010; Schoo et al., 2013; Sheward et al., 2023; Tanioka and Matsumoto, 2020). Global observations of bulk POM show substantial latitudinal variability in elemental ratios, but on average exhibit higher C:P and N:P ratios, indicating overall carbon and nitrogen enrichment relative to Redfield ratios (Inomura et al., 2022; Kwiatkowski et al., 2018; Liefer et al., 2024; Liu et al., 2025; Tanioka et al., 2022a, b; Tanioka and Matsumoto, 2020). As bulk POM represents a mixture of living cells and detrital material, this enrichment likely reflects a combination of carbon enrichment in detrital POM and variations in the ecological stoichiometry of plankton.

Detrital OM fractions are generally carbon-enriched due to the preferential remineralization of nutrients, which are more bioavailable relative to carbon (Graeber et al., 2021; Lønborg et al., 2009; Lønborg and Álvarez-Salgado, 2012). Consequently, carbon enrichment increases with age, with the strongest enrichment found in R-DOM (Aminot and Kérouel, 2004; Hopkinson and Vallino, 2005; Liang et al., 2023; Lønborg and Álvarez-Salgado, 2012), followed by SL-DOM (Aminot and Kérouel, 2004; Hoikkala et al., 2015; Hopkinson and Vallino, 2005; Liang et al., 2023; Lønborg and Álvarez-Salgado, 2012), and the lowest carbon-enrichment in POM (Chaichana et al., 2017, 2019; Davis et al., 2014, 2019; Doval et al., 1999; Frigstad et al., 2013; Hung et al., 2007; Liang et al., 2023; Loh and Bauer, 2000; Lucea et al., 2003; Martiny et al., 2014; Painter et al., 2017; Pujo-Pay et al., 2011; Singh et al., 2015; Suratman et al., 2009; Tanioka et al., 2022b). Bulk DOM has C:N:P ratios that fall between those of SL-DOM and R-DOM (Lønborg et al., 2024), approaching R-DOM stoichiometry with depth as SL-DOM and SR-DOM concentrations decline (Aminot and Kérouel, 2004; Hopkinson and Vallino, 2005; Letscher and Moore, 2015). Observations have confirmed these differences by size and lability to be broadly consistent across the global surface ocean (Liang et al., 2023; Tanioka et al., 2022b).

Hopkinson and Vallino (2005) highlighted the inconsistency of assuming Redfield stoichiometry between carbon and nutrient fluxes in light of substantial deviations observed in DOM stoichiometry, and similar concerns about the stoichiometry of exported POM have been raised (Osterroht and Thomas, 2000; Schneider et al., 2004; Tanioka et al., 2021; Thomas et al.,

1999; Williams et al., 1980). If estimates of DOC and POC export are accurate, while OM stoichiometry differs markedly from Redfield ratios, understanding the mechanisms governing the C:N:P stoichiometry in the production, export, and remineralization of both DOM and POM becomes essential for accurately representing the coupling of elemental cycles (Hopkinson and Vallino, 2005). Addressing these questions is critical for improving estimates and the representation of carbon and nutrient fluxes in models under changing environmental conditions, such as climate change and ocean acidification, and their potential impacts on OM and ecosystem stoichiometry (Finkel et al., 2010; Hutchins and Tagliabue, 2024; Kwiatkowski et al., 2018; Liu et al., 2025; Sardans et al., 2012). To improve our understanding of the driving mechanisms, studies have explored a range of potential predictors of variations in OM stoichiometry based on global observations (Hutchins and Tagliabue, 2024; Inomura et al., 2022; Liang et al., 2023; Liefer et al., 2024; Tanioka et al., 2022b; Tanioka and Matsumoto, 2020).

Model representations have increasingly incorporated variable C:N:P stoichiometry in the represented OM compartments. These studies differ in their focus on non-living OM (Anderson and Pondaven, 2003; Demir et al., 2025b; Lan Smith et al., 2005; Letscher et al., 2015; Neumann et al., 2022), or including variable cellular C:N:P in phytoplankton (Butenschön et al., 2016; Chien et al., 2023; Kwiatkowski et al., 2018; Matsumoto et al., 2021; Wirtz and Kerimoglu, 2016), and in the complexity of OM cycling representation. These approaches vary from using fixed empirical relationships to dynamic, mechanistic representations that allow elemental ratios to respond to environmental conditions, such as nutrient availability. This is, for instance, through variable C:N:P assimilation rates during phytoplankton growth, depending on inorganic nutrient availability (Galbraith and Martiny, 2015; Matsumoto et al., 2020b), internal cell quota models with a decoupling of uptake and growth (Butenschön et al., 2016; Zakem and Levine, 2019), representations of the macromolecular allocation in autotrophic cells (Armin and Inomura, 2021; Wirtz and Kerimoglu, 2016), or extracellular DOM release by phytoplankton, with C:N:P depending on nutrient availability (Demir et al., 2025b; Lan Smith et al., 2005; Neumann et al., 2022; Pätsch and Kühn, 2008). However, few models integrate a complete and differentiated representation of C:N:P ratios across OM pools in their production and decomposition processes, particularly in capturing the distinct reactivity and lifetimes of DOM fractions and variations throughout the heterotrophic food web. Besides computational cost and limited observational constraints for validating regional variability, the absence of a synthesized conceptual framework limits progress in model development.

Fully understanding the coupling of biogeochemical cycles requires the consideration of OM cycling, its elemental C:N:P stoichiometry, the relative partitioning among different pools, their interactions, and their distinct turnover timescales. These factors are crucial for improving model representations and predicting the future evolution of biogeochemical cycles in the ocean. Accurately capturing regional variability in the coastal ocean, its exchange with the open ocean, and its coupling with the land will be important to quantify the future coastal carbon sink, given the diversity in prevailing carbon export pathways (Resplandy et al., 2024; Roobaert et al., 2019, 2024a, b). The variability of the C:N:P stoichiometry of marine OM is one of the many interacting factors that have been shown to influence biogeochemical cycles under present-day and expected or projected future conditions (Bauer et al., 2013; Canuel et al., 2012; Dai et al., 2022; Flanjak et al., 2025; Lee, 2024; Lønborg et al., 2020).

Several fundamental questions remain despite extensive interdisciplinary research. This specifically pertains to the composition, reactivity, and stoichiometry of DOM and POM, as well as the relative importance of their production, transformation, and removal pathways concerning regional variability, and their contribution to export production, especially under ongoing environmental change. (Cai and Jiao, 2023; Carlson et al., 2024; Dittmar et al., 2021; Flanjak et al., 2025; Lee, 2024; Wakeham and Lee, 2019). Motivated by these knowledge gaps and their implications for conceptual understanding and model development, we aim to contextualize recent findings and provide a structured synthesis of our current knowledge on the C:N:P stoichiometry of marine OM in this review.

Section 2 summarizes the key production, transformation, and removal processes of POM and DOM, along with their distribution. Section 3 then examines patterns in the C:N:P stoichiometry of DOM and POM as well as the ecological stoichiometry of producers and consumers. Section 4 describes the suggested predictors and environmental drivers that shape the distribution of OM stoichiometry, some suggested climate change-driven trends, and implications for biogeochemical cycles with respect to the limited representation of constant Redfield stoichiometry. Section 5 provides an overview of current biogeochemical modeling strategies for incorporating variable C:N:P stoichiometry into their OM representation. Finally, section 6 concludes with a summary and outlines key directions for future research.

2 POM and DOM Cycling and distribution

2.1 POM production, transformation, and removal processes

2.1.1 POM production and external sources

In the global ocean, the majority of marine OM is autochthonous, meaning it is ultimately derived from marine primary production, mainly by photoautotrophs in the euphotic zone at a rate of 45–52 Pg C yr^{-1} (Carr et al., 2006; Field et al., 1998; Westberry et al., 2008), and to a much smaller extent by chemoautotrophs in the deep ocean at a rate of 0.77 Pg C yr^{-1} (Bell et al., 2017; Middelburg, 2011; Nakagawa and Takai, 2008) (Fig. 1). External, or allochthonous, OM inputs include terrestrial sources delivered via river discharge, coastal erosion, and groundwater flow (Bianchi, 2011; Connolly et al., 2020; Webb et al., 2019), as well as atmospheric dry and wet deposition (Iavorivska et al., 2016; Jurado et al., 2008; Xie et al., 2023). A small fraction of the OM produced in the ocean is also emitted to the atmosphere in the form of biogenic and abiotically produced volatile organic compounds (VOCs), primary marine aerosols, and secondary organic aerosols (SOAs) (Beaupré et al., 2019; Conte et al., 2020; Kieber et al., 2016; Kim et al., 2017; Wang et al., 2025; Yu and Li, 2021; Zhao et al., 2023a).

Net primary production (NPP) is strongly seasonally and regionally variable, depending on growth conditions such as nutrient and light availability, temperature, and community composition (Fernández-González et al., 2022), which are influenced by the ocean circulation, bathymetry, stratification, atmospheric conditions, and both terrestrial carbon and nutrients inputs (Sharples et al., 2019). Many of these controlling factors are themselves sensitive to ongoing and future environmental changes

(Fernández-González et al., 2022), with potential consequences, not only for the magnitude of NPP (Hochfeld and Hinners, 2024b), but also for the microbial community and food web structure (Doney et al., 2012), and the partitioning, transformation, and degradation pathways of all OM fractions (Lønborg et al., 2020; Ridgwell and Arndt, 2015; Shen and Benner, 2018; Thornton, 2014; Van de Waal and Litchman, 2020; Wagner et al., 2020).

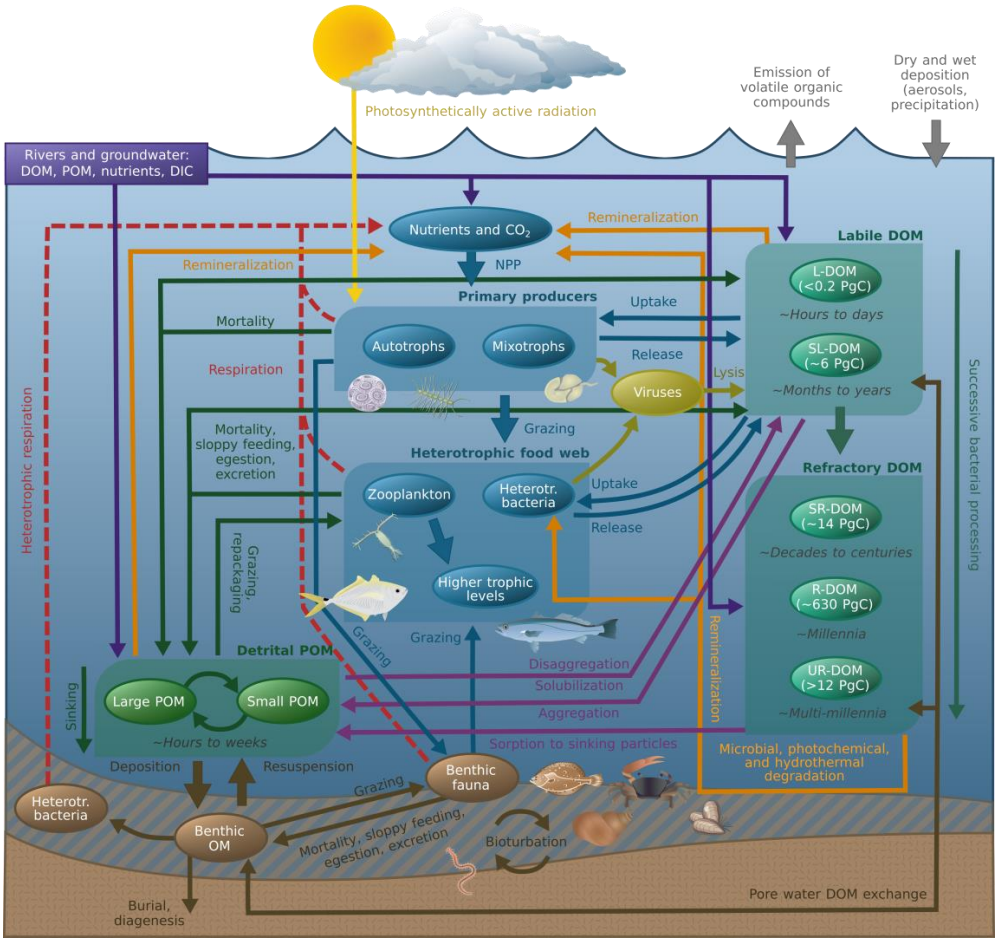

Figure 1: Overview of organic matter (OM) cycling in the ocean, illustrating key production, transformation, and removal pathways of particulate (POM) and dissolved organic matter (DOM). OM is primarily produced through marine primary production by phytoplankton in the euphotic zone, with additional contributions from chemoautotrophs and external terrestrial and atmospheric sources. POM enters the heterotrophic food web, undergoing grazing by zooplankton and higher trophic levels, microbial degradation by heterotrophic bacteria, aggregation into larger, faster-sinking particles, and solubilization into DOM. A small proportion of POM reaches marine sediments, where it continues to be transformed by benthic fauna and microbial activity, with only a minor fraction ultimately preserved through diagenesis. DOM is produced directly through extracellular release or exudation by phytoplankton, and secondarily via trophic interactions, viral lysis, and solubilization of POM. Both POM and DOM are released through mortality, sloppy feeding, egestion, and excretion. DOM is continuously transformed and removed through microbial uptake and respiration, sorption onto sinking particles, and abiotic processes such

as photooxidation. DOM pool spans a continuum of lability, categorized into labile (L-DOM), semi-labile (SL-DOM), semi-refractory (SR-DOM), refractory (R-DOM), and ultra-refractory (UR-DOM) fractions by Hansell (2013), who also estimated the corresponding stocks and lifetimes indicated in the schematic. While most DOM is rapidly recycled, a small fraction is transformed from labile into refractory DOM fractions via microbial and abiotic processes, contributing to long-term carbon storage via the microbial carbon pump, as conceptualized by Jiao et al. (2011). Arrows point in the direction of mass or carbon and nutrient fluxes, with predator-prey interactions pointing from prey to predator. Objects in the figure were taken, and in part modified, from the UMCES IAN Media Library under a Creative Commons license CC BY-SA 4.0.

2.1.2 POM food web dynamics

The majority of NPP is incorporated into phytoplankton biomass, contributing to POM accumulation in surface waters (Baines and Pace, 1991; Conan et al., 2007; Wakeham and Lee, 1993). Living POM enters the heterotrophic food web (HFW) through grazing and assimilation of ingested material, as well as through interactions with heterotrophic bacteria and viruses (Nagata, 2008; Wakeham and Lee, 1993). POM is consumed by zooplankton and higher trophic levels, including pelagic and demersal fish, and benthic fauna, with losses to the detrital DOM and POM pools via mortality, sloppy feeding, incomplete assimilation, and excretion (Nagata, 2008; Wakeham and Lee, 1993). Cellular respiration for maintaining metabolic functions and supporting additional biological activities continuously converts POM back to CO_2 and nutrients (Carlson et al., 2007; del Giorgio and Duarte, 2002; Robinson, 2008). Detrital POM differs from living biomass in composition, structure, and reactivity, as it is undergoing continuous transformation through microbial degradation, aggregation and disaggregation, circulation, and gravitational sinking, processes that collectively modify its size, bioavailability, sinking, and dispersion (Nagata, 2008; Wakeham and Lee, 1993). Together, these interacting pathways drive the continuous recycling of OM and nutrients in the epipelagic zone, sustaining upper ocean productivity and mediating vertical fluxes of carbon and nutrients (Carlson et al., 2024; Nagata, 2008; Wakeham and Lee, 1993).

2.1.3 POM-DOM continuum and interactions

Detrital POM is dynamically linked to DOM and to a continuum of particle sizes through ongoing processes of aggregation and disaggregation (He et al., 2016; Nagata, 2008; Wakeham and Lee, 1993). In the euphotic zone, DOM and small POM fractions aggregate into larger assemblages, for instance through the formation of organic gels (Engel et al., 2020; He et al., 2016; Mari et al., 2017). A major source of precursors to these gels is phytoplankton exudation, particularly acidic polysaccharides that form a significant component of extracellular polymeric substances (EPS), from which marine gels assemble (Engel, 2002; Engel et al., 2020; Mopper et al., 1995; Passow, 2002; Thornton, 2014). These include carbohydrate- and therefore carbon-rich transparent exopolymer particles (TEP), as well as protein-rich Coomassie stainable particles (CSP) (Engel et al., 2020; He et al., 2016; Mari et al., 2017; Verdugo et al., 2004). Together, gels and colloids form a compositional continuum, mediating the transition from dissolved to particulate phases (Verdugo et al., 2004; Wells, 1998). As adhesive matrices, they facilitate the formation of larger heterogeneous aggregates as marine snow, comprising organic gels, detritus,

microbial cells, and mineral particles, which play a central role in vertical POC export from the surface ocean (Alldredge and Silver, 1988; Engel, 2002; Engel et al., 2020; Nagata, 2008; Schneider et al., 2004).

As POM sinks, it undergoes progressive disaggregation and solubilization, biochemically through microbial degradation, grazing, and repackaging, and physically through fragmentation, producing smaller particles and DOM (Alcolombri et al., 2021; He et al., 2016; Nagata, 2008; Turner, 2015; Wakeham and Lee, 1993). Simultaneously, microbial degradation and enzymatic processes remineralize fractions of POM and DOM into CO_2 and nutrients (Carlson et al., 2007; Nagata, 2008; Robinson, 2008; Wakeham and Lee, 1993). These ongoing transformations occur across a broad size continuum, from colloidal DOM to large aggregates, and shape microbial accessibility, degradation pathways, and ultimately regulate the efficiency of vertical carbon export through the biological pump (He et al., 2016; Lee et al., 2012; Verdugo et al., 2004; Wells, 1998).

2.1.4 POM export and sedimentation

Only a small fraction of POM produced, in the euphotic zone escapes rapid recycling and is transferred to depth, typically following an exponential decline described by the Martin curve (De La Rocha and Passow, 2007; Gloege et al., 2017; Henson et al., 2019; Martin et al., 1987; Omand et al., 2020). Export fluxes from the euphotic zone are estimated to range from 5% to over 40% of NPP (Boyd and Trull, 2007; Buesseler, 1998; Buesseler and Boyd, 2009; De La Rocha and Passow, 2007; Gloege et al., 2017; Henson et al., 2011; Martin et al., 1987), yet the majority of this material is remineralized in the mesopelagic or twilight zone (De La Rocha and Passow, 2007; Giering et al., 2014; Gloege et al., 2017; Steinberg et al., 2008). As a result, only about 1–3% of the initially produced POM reaches the deep ocean, and even less is deposited in sediments after continued degradation (De La Rocha and Passow, 2007; Gloege et al., 2017; Omand et al., 2020; Wakeham and Lee, 1993).

After deposition in sediments, POM is subject to further remineralization via aerobic and anaerobic oxidation in the permeable, oxygenated surface layer by microbial activity (Ahmerkamp et al., 2020; Marchant et al., 2017). POM is also recycled and redistributed through benthic food web interactions of epifauna and infauna (Chen et al., 2021; Kröncke and Bergfeld, 2003). Within marine sediments, bioturbation, as the biological reworking of sediments, has both stabilizing and destabilizing effects through processes such as bio-mixing, bio-irrigation, burrow ventilation, bio-deposition, and bio-resuspension (Bianchi et al., 2021; Kristensen et al., 2012; Meysman et al., 2006). Where shallow water depths allow for sufficient light penetration, benthic primary producers such as macroalgae produce new biomass and contribute to the burial of organic carbon (Duarte, 2017; Duarte et al., 2022). In some areas, further resuspension by tidal or wind-driven currents, as well as through anthropogenic activities as demersal fishing, returns POM to the water column, making it available to remineralization and grazing, thereby reducing net sediment accumulation (Eigaard et al., 2017; Tiano et al., 2019).

Only a small fraction of material that escapes remineralization and reworking in the surface sediments gets buried more deeply, where it can be preserved over geological timescales through progressive diagenesis and eventually catagenesis (Arndt et al., 2013; Emerson and Hedges, 2003; Henrichs, 1993; Kristensen, 2000; Wakeham and Lee, 1993). As a result, only a minor proportion of the initially produced POM is ultimately preserved in the sedimentary record. For a more detailed account of

POM production, transformation, and removal processes throughout the water column the reader is referred to Wakeham and Lee (1993), and for OM-bacteria interactions to Nagata (2008).

2.2 DOM production, transformation, and removal processes

2.2.1 Dissolved primary production

Compared to POM production, a more variable fraction of NPP is released as DOM, comprising compounds such as monosaccharides, oligosaccharides, polysaccharides, amino acids, proteins, lipids, and organic acids (Carlson et al., 2024; Mühlenbruch et al., 2018; Thornton, 2014). Additional DOM is produced through trophic pathways that recycle readily produced POM (Carlson et al., 2024; Møller, 2007; Møller et al., 2003; Saba et al., 2011). DOM is released through processes, including extracellular release by phytoplankton and macroalgae (Borchard and Engel, 2012; Børsheim et al., 2005; Carlson et al., 2024; Granum et al., 2002; Myklestad, 1995), sloppy feeding, or incomplete assimilation and subsequent egestion or excretion by grazers (Møller, 2007; Møller et al., 2003), and release of intracellular DOM via viral lysis (Lønborg et al., 2013; Ma et al., 2018) or apoptosis (i.e., programmed cell death) (Bidle, 2016; Cai and Jiao, 2023; Veldhuis et al., 2001; Wang et al., 2024) (Fig. 1).

Extracellular release of DOM by phytoplankton is commonly divided conceptually into passive and active release (Carlson et al., 2024; Mühlenbruch et al., 2018; Thornton, 2014; Wear et al., 2015a). Passive DOM release by diffusion across the cell membrane is driven by concentration gradients, is a function of biomass rather than productivity, and yields DOM with a stoichiometry similar to that of the cell interior (Carlson et al., 2024; Thornton, 2014). Active DOM release involves the exudation of carbon-rich exopolysaccharides as an overflow mechanism to dissipate excess energy, maintain internal stoichiometric balance, and keeping the cell's photosynthetic machinery active, as well as the active exudation of DOM for extracellular benefits to the cell such as protection against UV radiation, reduction of oxidative stress, cryoprotection, or attracting bacterioplankton communities for later nutrient or trace metal regeneration (Carlson et al., 2024; Mühlenbruch et al., 2018; Thornton, 2014). Carlson et al. (2024) suggest that, given variable and mixed evidence for either mechanism, the different mechanisms for DOM release are likely not mutually exclusive. However, their respective contributions depend on environmental conditions, such as light and nutrients, as well as community structure.

The percentage of NPP released as extracellular DOM (percentage extracellular release; PER) remains poorly constrained. Reported values vary widely across studies, with estimates generally ranging from 2% to 50%, with average contributions of 3.7 to 25%, depending on species, physiological state, and growth stage, with some observations temporarily reaching up to 80% (Baines and Pace, 1991; Borchard and Engel, 2012; Carlson et al., 2024; Moran et al., 2022a; Thornton, 2014; Wear et al., 2015a, b). The composition of the released DOM in terms of macronutrients and elemental stoichiometry depends on environmental conditions and the individual process contributions (Moran et al., 2022a; Mühlenbruch et al., 2018; Thornton, 2014), with implications for the later release of carbon and nutrients (Eigemann et al., 2022; Moran et al., 2022a). PER has

shown both increases and decreases with total primary productivity across systems from oligotrophic to eutrophic states, but generally shows a larger and more variable contribution in oligotrophic systems with lower particulate primary production (Alonso-Sáez et al., 2008; Carlson et al., 2024; Karl et al., 1998; López-Sandoval et al., 2011; Teira et al., 2003).

Although it is less understood, extracellular release of DOM by macroalgae, including diverse classes of compounds, has similarly been linked to environmental conditions and plays a role in ecosystem-DOM interactions (Mueller et al., 2016; Nelson et al., 2023; Paine et al., 2023; Reed et al., 2015; Weigel and Pfister, 2021; Zhao et al., 2023b). With an average of 17%, PER of macroalgae is comparable to that of phytoplankton, and decreases with increasing particulate primary production (Carlson et al., 2024). However, based on the contribution of 1–3% to global and 20% to coastal marine NPP (Carlson et al., 2024; Duarte et al., 2022; Field et al., 1998), Carlson et al. (2024) conclude that their relevance is limited to shallow coastal waters, with global DOM release largely dominated by phytoplankton. They further note that macroalgal DOC production may still be important to R-DOM production and carbon sequestration, as a fraction of 28–78% of their DOC production is resistant to heterotrophic remineralization (Li et al., 2022; Wada et al., 2008; Watanabe et al., 2020). In addition to DOM release by photoautotrophic phytoplankton and macroalgae in surface waters, a small fraction of DOM is released by chemoautotrophs and chemoheterotrophs (Bayer et al., 2023; Carlson et al., 2024; Meador et al., 2020). These have diverse metabolic functions, such as micro-environmental stability, mutualistic beneficial or antagonistic functions, and extracellular digestion (Amin et al., 2009; Arnosti, 2011; Carlson et al., 2024; Imai et al., 1993).

2.2.2 Grazing-mediated and microbial DOM production

Apart from dissolved primary production via extracellular release, DOM is also indirectly produced through food web and bacteria-OM interactions (which break down living and detrital POM), cell lysis induced by phytoplankton, bacteria, and viruses, which releases intracellular DOM, as well as solubilization of POM (Carlson et al., 2024; He et al., 2016; Lønborg et al., 2013; Møller, 2007; Møller et al., 2003; Moran et al., 2022a, b; Nagata, 2008; Saba et al., 2011). During the transfer of energy and nutrients in the form of POM from auto- and mixotrophs over micro- and mesozooplankton to higher trophic levels, including fish, grazing and repackaging of detrital POM releases DOM through sloppy feeding, excretion of non-assimilated and egestion of undigested OM, leaching from fecal pellets, as well as mortality, and subsequent dissolution of gelatinous zooplankton (Carlson et al., 2024; Caron et al., 1985; Luo et al., 2020; Møller, 2007; Møller et al., 2003; Saba et al., 2011; Steinberg et al., 2000; Steinberg and Landry, 2017; Urban-Rich, 1999).

Cell lysis is the rupture of the cell membrane that results in the release of intracellular DOM. It can be triggered by allelopathy, where organisms release defensive biochemicals to deter predators (Tillmann, 2003; Weissbach et al., 2010; Wolfe, 2000). Lysis can also occur through the enzymatic breakdown of the cell membrane by bacteria (Imai et al., 1993; Li et al., 1998; Stewart and Brown, 1969). Viral infections can lead to lysis when viruses exploit the host's metabolic machinery to replicate and ultimately cause the cell to rupture and release viral progeny (Lønborg et al., 2013; Ma et al., 2018; Wilhelm and Suttle, 1999; Zimmerman et al., 2020). Additionally, lysis may result from programmed or autocatalytic cell death under

environmental stress or to protect the surrounding population from an infection (Bidle, 2016; Bramucci and Case, 2019; Franklin et al., 2006; Wang et al., 2020).

Carlson et al. (2024) estimate a gross DOC production of 36 Pg C yr^{-1}, with 13.3 (3–19) Pg C yr^{-1} from extracellular release by Phytoplankton, 7.5 (3–13) Pg C yr^{-1} from DOC release by microzooplankton, 4.8 (2–8) Pg C yr^{-1} from viral lysis of bacteria, 4.5 (2–10) Pg C yr^{-1} from DOC release by mesozooplankton, 3.2 (1–5) Pg C yr^{-1} from viral lysis of phytoplankton, 2.7 (0–11) Pg C yr^{-1} from sloppy feeding of mesozooplankton, and lastly 0.2 Pg C yr^{-1} from extracellular release by macroalgae, based on several previous studies (Møller, 2007; Moran et al., 2022b; Saba et al., 2011; Wilhelm and Suttle, 1999).

2.2.3 DOM transformation and removal pathways

The majority of this produced DOM is transformed or removed through biotic and abiotic pathways, which release CO_2 and nutrients through respiration, but also convert DOM to POM through particle aggregation or repackaging into bacterioplankton biomass, thereby re-entering the HFW (Arnosti, 2011; Arnosti et al., 2018, 2021; Azam, 1998; Azam et al., 1994; Carlson et al., 2024; Ducklow et al., 1986; He et al., 2016; Moran et al., 2022b; Reintjes et al., 2019; Rivkin and Legendre, 2001). Bacterioplankton hydrolyze polymeric high molecular weight (HMW) DOM as proteins, polysaccharides, and lipids into low molecular weight (LMW) mono- or oligomeric DOM for transport across the cell membrane, or in some cases directly take up HMW DOM, following different uptake strategies and DOM sources of different size and reactivity (Amon and Benner, 1994, 1996; Arnosti, 2011; Arnosti et al., 2018, 2021; Reintjes et al., 2017, 2019). Here, the assimilation or bacterial growth efficiency, and with this the partitioning between release of CO_2 and nutrients via bacterial respiration, waste products, and assimilated biomass, depends on several environmental and biotic conditions, as well as the available source of detrital OM (Carlson et al., 2007; Church, 2008; del Giorgio and Cole, 1998; Robinson, 2008; Sherr and Sherr, 2008). In the absence of inorganic nitrogen and phosphorus sources, some mixotrophic and photoheterotrophic organisms also utilize abundant DOM as a nutrient and energy source for growth (Antia et al., 1991; Edwards, 2019; Fitzsimons et al., 2020; Kolber et al., 2001; Mulholland and Lee, 2009; Muñoz-Marín et al., 2020). Other organisms contributing to DOM removal include filter-feeding metazoans such as sponges, bivalves, and anemones, as well as protists, and mycoplankton (Bart et al., 2021; Breyer and Baltar, 2023; Mayers et al., 2023; Ribes et al., 2023; Tranvik et al., 1993; Welsh et al., 2020).

In addition to the biotic removal and transformation pathways for DOM, there are additional abiotic pathways including photooxidation (Miller and Zepp, 1995; Mopper et al., 1991), sorption to particles (Druffel and Williams, 1990; Hewson and Fuhrman, 2003), emission of VOCs and aerosols (Beaupré et al., 2019; Kim et al., 2017; Wang et al., 2025), and removal in hydrothermal vents (Hawkes et al., 2015). Photooxidation transforms DOM under exposure to UV radiation from sunlight by oxidizing some DOM completely into CO_2 and inorganic nutrients, partially oxidizing DOM into more labile compounds that enhance bacterial remineralization, and producing VOCs which can be further oxidized to SOAs (Conte et al., 2020; Miller and Zepp, 1995; Mopper et al., 1991; Wang et al., 2025; Yu and Li, 2021). DOM is also removed through transformation into sinking POM via sorption of detrital DOM and viruses onto particles (Coppola et al., 2014; Druffel et al., 1996; Druffel and

Williams, 1990; Hewson and Fuhrman, 2003; Mayers et al., 2023; Yamashita et al., 2022), as well as through the formation of marine gels as TEPs from EPS produced during DOM release, such as through exudation by phytoplankton or viral lysis, thereby reintroducing it into the HFW, and increasing removal via respiration and vertical carbon export (Borchard and Engel, 2012; Engel, 2002; Mari et al., 2017; Mayers et al., 2023; Mojica and Brussaard, 2014; Mopper et al., 1995; Passow, 2002). Apart from the emission of VOCs and SOAs to the atmosphere, primary marine aerosols are released through bubbles at the air–sea interface (Beaupré et al., 2019; Keene et al., 2007; Kieber et al., 2016). A reduction in DOC concentrations of outflow from hydrothermal vents also suggests a potential removal pathway (Hawkes et al., 2015; Lang et al., 2006; Lin et al., 2019).

2.2.4 R-DOM production and removal pathways

While most DOM is rapidly recycled through the aforementioned transformation and removal processes, up to an estimated 0.4% of NCP resists microbial degradation and contributes to the formation of R-DOM (Osterholz et al., 2015). Despite growing interest, the dominant production and removal pathways of R-DOM remain uncertain, and their relative contributions are poorly constrained. However, recent syntheses have highlighted key mechanisms contributing to R-DOM formation and persistence in the marine environment (Cai and Jiao, 2023; Carlson et al., 2024; Dittmar et al., 2021; Dittmar and Lennartz, 2024; Jiao et al., 2010, 2011, 2014, 2018; Osterholz et al., 2015). These studies emphasize the importance of both the intrinsic recalcitrance and the dilution of individual compounds in rendering otherwise bioavailable DOM inaccessible, and the role of microbial diversification in the transformation from L-DOM to R-DOM (Baltar et al., 2021; Cai and Jiao, 2023; Dittmar et al., 2021). Beyond the intrinsic quality of DOM, environmental factors influence its reactivity, such that both microbial communities and external conditions can shape DOM composition (Berggren et al., 2022; Creed et al., 2018; Hach et al., 2020; Kujawinski, 2011; Kujawinski et al., 2016; Zhao et al., 2019). As a result, its stability can change with relocation, shifting community structure, or environmental conditions (Liu et al., 2022).

Production of R-DOM occurs biotically along with initially formed L-DOM through DOM release by phytoplankton and both auto- and heterotrophic bacteria (Aluwihare and Repeta, 1999; Kaiser and Benner, 2008), viral lysis (Cai and Jiao, 2023; Lønborg et al., 2013; Ma et al., 2018; Moran et al., 2022a), protist grazing, and egestion (Cai and Jiao, 2023; Moran et al., 2022a; Nagata and Kirchman, 1992; Strom et al., 1997; Taylor et al., 1985), but mainly through successive bacterial processing of L-DOM to R-DOM (Cai et al., 2019; Hach et al., 2020; Jiao et al., 2010; Jørgensen et al., 2014; Kujawinski, 2011; Lian et al., 2021; Lønborg et al., 2015; Osterholz et al., 2015; Zhao et al., 2019). These biotic contributions are conceptually summarized as the microbial carbon pump (MCP) (Cai and Jiao, 2023; Carlson et al., 2024; Dittmar et al., 2021; Jiao et al., 2010; Moran et al., 2022a; Osterholz et al., 2015). Selective removal of SL-DOM and SR-DOM by filter-feeders can also shift DOM composition to be more refractory (Hildebrand et al., 2022).

Previously suggested abiotic production processes include polymerization of LMW DOM via photochemical reactions (Gonsior et al., 2009; Paerl et al., 2020; Scully et al., 2003; Sun et al., 2021), adsorption of L-DOM to colloids (Carlson et al., 2024; Kirchman et al., 1989; Nagata and Kirchman, 1992), sulfurization of DOM (Carlson et al., 2024; Pohlabeln et al., 2017;

Raven et al., 2018), and black carbon from hydrothermal vents (Yamashita et al., 2023). Additional allochthonous sources include rivers, submarine groundwater discharge (Bauer et al., 2013; Bianchi, 2011), and dissolved black carbon originating from aerosols and terrestrial inputs (Bao et al., 2017; Dittmar and Paeng, 2009). Removal involves both biotic and abiotic processes, including microbial and photochemical degradation (Cai et al., 2019; Medeiros et al., 2015; Mopper et al., 1991), circulation through hydrothermal vents (Hawkes et al., 2015), sorption onto sinking particles (Cai and Jiao, 2023; Carlson et al., 2024), via emission of primary marine aerosols through bubbles at the air–sea interface (Beaupré et al., 2019), and through the priming effect, where the addition of L-DOM increases the decomposition of R-DOM (Cai and Jiao, 2023; Carlson et al., 2024).

For a more comprehensive discussion of DOM and R-DOM production, transformation, and removal pathways, the reader is referred to Carlson et al. (2024). A detailed account of R-DOM production and removal processes, its constituents and characterization, as well as the MCP can be found in Dittmar et al. (2021), Dittmar and Lennartz (2024), and Cai and Jiao (2023). The recycling of L-DOM via the microbial loop (Azam, 1998; Azam et al., 1983, 1994), as well as the release, consumption, and exchange of short-lived metabolites by marine phytoplankton, bacteria, grazers, and viruses are discussed by Moran et al. (2022a, b), including its role in the microbial loop and the formation of R-DOM via the MCP. A consistent classification and terminology of labile and recalcitrant DOM fractions and their biogeochemical relevance is provided by Hansell (2013).

2.3 OM distribution and vertical export contributions

2.3.1 DOM distribution

Despite the considerable uncertainty in marine primary productivity and contributions of OM production and removal processes, the global distribution of DOC has been quantified across the global open ocean through extensive hydrographic surveys, with concentrations remaining within a narrow range of approximately 34–80 µM (Hansell, 2013; Hansell et al., 2009, 2024; Roshan and DeVries, 2017). Differences across basins in both surface and bottom water concentrations have been linked to the transports across the main ocean gyres, mainly redistributing the intermediate SL-DOM and SR-DOM fractions (Hansell, 2013), which are not well mixed in contrast to R-DOM and UR-DOM (Carlson et al., 2024; Hansell, 2013; Hansell et al., 2009, 2024). These differences in DOC accumulation have consequences for DOC export and the relative contribution to export production compared to POC (Roshan and DeVries, 2017). Given that the global DOC distribution of the open ocean has readily been described in detail, we only briefly summarize the main findings, and then go on to discuss differences in comparison to coastal and marginal seas, which have not yet been addressed, based on a literature compilation of concentration ranges (Tables 1–3).

In terms of the average vertical distribution across the water column, bulk DOC can be approximated by a superposition of R-DOC and UR-DOC with vertically homogeneous background concentrations of 34–48 µM (Aminot and Kérouel, 2004;

Hansell and Carlson, 1998a; Hopkinson and Vallino, 2005; Liang et al., 2023), SR-DOC accumulating in the epi- and mesopelagic zones, and SL-DOC mainly in the epipelagic zone, adding roughly 10–40 µM to surface concentrations, quickly decreasing towards close to zero deep water concentrations below 1000 meters (Carlson et al., 2024; Dittmar et al., 2021; Hansell, 2013; Hansell et al., 2009; Nagata, 2008; Ogawa and Tanoue, 2003; Roshan and DeVries, 2017). The L-DOC fraction can be assumed to be negligible to DOC accumulation, contributing less than 1 µM to measured concentrations (Hansell, 2013; Nagata, 2008; Ogawa and Tanoue, 2003). Accordingly, bulk DOC concentrations decrease from roughly 50–80 µM at the surface towards relatively homogeneous deep-water R-DOC concentrations.

However, there are marked differences in the accumulation and vertical export of DOM across the surface and deep ocean (Hansell, 2013; Hansell et al., 2009, 2024; Hansell and Carlson, 1998a; Roshan and DeVries, 2017). In particular, strong stratification and upwelling in the equatorial to subtropical Atlantic, Pacific, and Indian Oceans lead to the highest surface DOC concentrations of ~70–80 µM (Hansell, 2013; Hansell et al., 2009, 2024). Similar concentrations are observed in the Arctic Ocean, likely due to high terrestrial inputs (Dittmar and Kattner, 2003; Hansell et al., 2009). In contrast, DOC accumulation is lowest in the surface waters of the Southern Ocean, where a combination of upwelling, intermediate- and bottom-water formation mixes surface and deep waters, resulting in low vertical gradients and concentrations ranging from ~40 µM at depth to ~45–50 µM at the surface (Hansell, 2013; Hansell et al., 2009, 2024). DOC concentration gradients in the global deep ocean have been linked to radiocarbon-based water mass ages, which determine the time available for SR-DOC removal over decadal to centennial timescales following export to depth via overturning circulation (Hansell et al., 2012). This relationship is further supported by circulation-derived water age estimates, which indicate last passage times of 410, 760, and 1060 years in the Atlantic, Indian, and Pacific Oceans, respectively (DeVries and Primeau, 2011), and corresponding deep water DOC concentrations of roughly 41–44, 39–40, and 34–39 µM reported by Hansell et al. (2009), indicating a decrease in DOC concentrations with increasing water mass age.

In comparison to the open ocean, the shallow coastal and marginal seas generally exhibit higher DOM accumulation depending on a combination of factors, including the ratio of terrestrial OM input to water volume, the balance between riverine influence and open ocean exchange, variability in NCP, and differences in water residence times. The global CoastDOMv1 dataset supports this (Lønborg et al., 2024), which spans coastal regions from 1978 to 2022 and includes 62,338 measurements of DOC, 20,356 of DON, and 13,533 of DOP, with concentrations of 103 (77–228) µM for DOC, 8.0 (5.5–15.8) µM for DON, and 0.18 (0.11–0.30) µM for DOP (Table 1). By contrast, recent estimates from global open ocean surface waters report lower concentrations of 65.8 (52.4–73.5) µM for DOC, 4.5 (3.7–5.3) µM for DON, and 0.17 (0.11–0.27) µM for DOP across major biogeochemical regions (Liang et al., 2023) (Table 1).

In regions like the Mid-Atlantic Bight and Georges Bank, the higher surface accumulation of DOM results in more pronounced vertical gradients, with mean concentrations or ranges, and ranges based on individual measurements (in parentheses), ranging from 65–125 (61–201) µM for DOC, 5–10.2 (4.2–14.3) µM for DON, and 0.17–0.30 (0.07–0.42) µM for DOP at the surface to 46.7–50 (41–55) µM for DOC, 2.76–3 (2.6–4.0) µM for DON, and 0.02–0.03 (0.01–0.08) µM for DOP in slope and bottom waters (Hopkinson et al., 1997, 2002; Hopkinson and Vallino, 2005) (Table 1). The latter approach the global open ocean

refractory pool, which has estimated mean concentrations of 33.8–48.1 µM for DOC, 2.7–3.0 µM for DON, and 0.03–0.05 µM for DOP (Aminot and Kérouel, 2004; Hansell and Carlson, 1998a; Hopkinson and Vallino, 2005; Liang et al., 2023) (Table 2). Similar ranges of mean values and ranges of surface concentrations are observed in the northwest European shelf seas with 46.9–108.7 (32.7–224.8) µM for DOC, 5.2–9.0 (1.0–16.4) µM for DON, and 0.26 (0.13–0.46) µM for DOP, the Mediterranean Sea with (37.5–120) µM for DOC, (0–7.2) µM for DON, and (0.0–0.4) µM for DOP, and the South and East China Seas, with (43–132) µM for DOC, (6–9.6) µM for DON, and (0.05–0.25) µM for DOP.

A much larger DOM accumulation is measured in the Baltic Sea with 290–466 (242–1230) µM for DOC, 17.2 (7.8–203) µM for DON, and (0.06–0.9) µM for DOP (Table 2), likely due to the residence times of several decades, combined with large terrestrial inputs and low water volume. Specifically, the quantification of (semi-)labile, biodegradable, or bioavailable DOM remains limited, but with some estimates providing mean concentrations of 23.3–25.0 (0–198) µM for DOC, 1.2–2.8 (0–15.2) µM for DON, and 0.04–0.14 (0.01–0.34) µM for DOP, with more variable concentrations across individual measurements as for bulk DOM (Table 3). Despite growing observational coverage, important gaps remain in the differentiation of DOM fractions and the ability to trace the abundance and fate of terrestrial inputs, which are critical to constraining the composition, lability, and export contribution of DOM in coastal and marginal seas.

Table 1: Literature compilation of observational data on concentrations of bulk dissolved organic carbon (DOC), nitrogen (DON), and phosphorus (DOP), including all fractions of dissolved organic matter (DOM). Individual numbers without parentheses represent averages over regions or a series of measurements, whereas values in parentheses show ranges between individual measurements or sub-regions. Ranges of concentrations with a double-asterisk represent estimates from figures in the respective references. For the data from Lønborg et al. (2024), we report the median along with the 25th and 75th percentiles, as these better represent the distribution of the large dataset, avoiding the influence of outliers on the mean and range. Modified from Table S3 in (Demir et al., 2025b).

Location	Sub-Region or Focus	Bulk DOM Concentrations			Source
		DOC $[\mu M]$	DON $[\mu M]$	DOP $[\mu M]$	
Global Ocean	Surface Ocean Biogeochemical Regions	65.8 (52.4–73.5)	4.5 (3.7–5.3)	0.17 (0.11–0.27)	(Liang et al., 2023)
	Full Water Column	(46.2–65.3)	(2.1–4.5)	(0.04–0.19)	(Letscher et al., 2015; Letscher and Moore, 2015)
	Coastal Ocean	(50–60)	(4.5–45)	(0.08–0.50)	(Lønborg and Álvarez-Salgado, 2012)
	Coastal Ocean	103 (77–228)	8.0 (5.5–15.8)	0.18 (0.11–0.30)	(Lønborg et al., 2024)
	Shelf, Slope, and Open Ocean (surface only 0–100m)	(30–160)**	(1–11)**	(0.00–0.45)**	(Hopkinson and Vallino, 2005)
Atlantic Ocean	Georges Bank (Surface Ocean)	65–92	5	0.17	(Hopkinson et al., 1997)
	Georges Bank (Deep Waters)	50	3	0.02	(Hopkinson et al., 1997)
	Mid-Atlantic Bight (Surface Ocean)	125 (81–201)	10.2 (7.1–14.3)	0.30 (0.14–0.42)	(Hopkinson et al., 2002)
	Mid-Atlantic Bight (Deep Slope Waters)	46.7	2.76	0.03	(Hopkinson et al., 2002)

	Northeastern Atlantic (Surface Waters)	(61–83)	(4.2–6.1)	(0.07–0.14)	(Aminot and Kérouel, 2004)
	Northeastern Atlantic (Deep Waters)	(41–55)	(2.6–4.0)	(0.01–0.08)	(Aminot and Kérouel, 2004)
Pacific Ocean	Eastern North Pacific	(35–72)	(1.5–4.5)	(0.013–0.229)	(Loh and Bauer, 2000)
	North Pacific Subtropical Gyre	(63–105)	(3.7–6.2)	(0.10–0.27)	(Church et al., 2002)
Southern Ocean	-	(39–53)	(2.5–5.2)	(0.061–0.225)	(Loh and Bauer, 2000)
Mediterranean Sea	Southern Adriatic Basin (Surface)	(49–79)	(2.3–7.2)	(0.02–0.08)	(Santinelli et al., 2012)
	Southern Adriatic Basin (Intermediate Waters)	(45–54)	(1.8–5.3)	(0.02–0.06)	(Santinelli et al., 2012)
	Southern Adriatic Basin (Deep Waters)	(47–60)	(2.9–6.2)	(0.02–0.08)	(Santinelli et al., 2012)
	Northwestern Mediterranean	(44–95)	(2.8–6.2)	-	(Doval et al., 1999)
	Northwestern Mediterranean	(40–120)**	(0–6)**	(0.0–0.4)**	(Lucea et al., 2003)
	Northwestern Mediterranean (Surface Waters)	(67–69)	(4.0–4.2)	(0.08–0.08)	(Aminot and Kérouel, 2004)
	Northwestern Mediterranean (Deep Waters)	(46–48)	(2.7–3.0)	(0.03–0.04)	(Aminot and Kérouel, 2004)
	Northwestern Mediterranean	(80–100)	(4.5–5.5)	(0.06–0.10)	(Raimbault et al., 1999)
	Western Basin	(37.6–69.4)	(2.5–5.5)	(0–0.09)	(Pujo-Pay et al., 2011)
	Eastern Basin	(37.5–72.4)	(2.1–6.3)	(0–0.10)	(Pujo-Pay et al., 2011)
East China Sea	-	(60–120)	(6–9.6)	(0.05–0.25)	(Hung et al., 2003)
South China Sea	Northern Parts	(43–132)	-	-	(Hung et al., 2007)
Northwest European Shelf	Norwegian Coastal Waters	-	(8–11.5)**	-	(Frigstad et al., 2013)
	Celtic Sea	(65–70)	(3.9–6)	(0.19–0.35)	(Davis et al., 2019)
	North Sea	46.9–107.5 (32.7–224.8)	5.2–9.0 (2.8–13.7)	-	(Chaichana et al., 2017, 2019)
	Northern North Sea (Surface)	60.7–73.8 (32.7–104.2)	5.3–6.6 (3.0–8.7)	-	(Chaichana et al., 2017, 2019)
	Northern North Sea (Bottom)	46.9–73.8 (36.8–120.1)	5.2–5.9 (1.0–11.7)	-	(Chaichana et al., 2017, 2019)
	Southern North Sea	65.5–97.5 (36.3–224.8)	5.3–9.0 (2.8–13.7)	-	(Chaichana et al., 2017, 2019)
	Central North Sea	(68–318)	(2–11)**	-	(Suratman et al., 2009)

	North Sea	108.7 (61.7–185.0)	6.6 (3.5–16.4)	0.26 (0.13–0.46)	(Painter et al., 2018)
Baltic Sea	Bothnian Sea	466	-	-	(Rowe et al., 2018)
	Bothnian Bay	416	-	-	(Rowe et al., 2018)
	Gulf of Finland	(290–724)	(8.6–38.5)	(0.06–0.80)	(Hoikkala et al., 2012, 2015)
	Gulf of Bothnia	(241–520)	(7.8–14.8)	(0.12–0.18)	(Hoikkala et al., 2015)
	Gulf of Riga	(400–1230)	(10–38)	(0.5–0.9)	(Hoikkala et al., 2015)
	Baltic Proper	(259–708)	(10.2–203)	-	(Hoikkala et al., 2015; Rowe et al., 2018)
	Estuaries	(318.41–736.74)	(14.14–45.22)	(0.14–0.38)	(Voss et al., 2021)
	Southwestern Baltic Sea (Heiligendamm)	290	17.2	-	(Osterholz et al., 2021)
	Gotland Basin	-	-	(0.20–0.29)	(Nausch et al., 2008)

Table 2: Literature compilation of observational data on concentrations of refractory or recalcitrant dissolved organic carbon (R-DOC), nitrogen (R-DON), and phosphorus (R-DOP). Individual numbers or ranges (e.g., between sub-regions or different years) without parentheses represent averages over regions or a series of measurements, whereas values in parentheses show ranges between individual measurements. Modified from Table S5 in (Demir et al., 2025b).

Location	Sub-Region or Focus	Refractory or Recalcitrant DOM Concentrations			Source
		R-DOC $[\mu M]$	R-DON $[\mu M]$	R-DOP $[\mu M]$	
Global Ocean	Surface Ocean	46 (45–49)	2.7 (2.5–2.8)	-	(Liang et al., 2023)
	Deep Ocean	42	3.0	0.05	(Liang et al., 2023)
	Surface Ocean	42	-	-	(Hopkinson and Vallino, 2005)
	Deep Ocean	34	-	-	(Hopkinson and Vallino, 2005)
	Deep Ocean	33.8–48.1	-	-	(Hansell and Carlson, 1998a)
Atlantic and Mediterranean	NE Atlantic and NW Mediterranean	44.9 (43.8–45.9)	2.85 (2.73–3.00)	0.029 (0.023–0.034)	(Aminot and Kérouel, 2004)

Table 3: Literature compilation of observational data on concentrations of biodegradable or (semi-)labile dissolved organic carbon (L-DOC), nitrogen (L-DON), and phosphorus (L-DOP). Individual numbers or ranges (e.g., between sub-regions or different years) without parentheses represent averages over regions or a series of measurements, whereas values in parentheses show ranges between individual measurements.

The given percentage indicates the fraction of labile dissolved organic carbon, nitrogen, and phosphorus in relation to the bulk pool. Modified from Table S4 in (Demir et al., 2025b).

Location	Sub-Region or Focus	Biodegradable or (Semi-)Labile DOM Concentrations			Source
		L-DOC $[\mu M]$	L-DON $[\mu M]$	L-DOP $[\mu M]$	
Global Ocean	Surface Ocean Biogeochemical Regions	25.0 (10.5–29.1)	2.8 (1.9–3.5)	0.14 (0.06–0.22)	(Liang et al., 2023)
	Shelf, Slope, and Open Ocean	(15–80)	-	-	(Hopkinson and Vallino, 2005)
	Coastal Ocean	(1–199) (2–51%)	(0.6–15.2) (10–65%)	(0.04–0.33) (30–96%)	(Lønborg and Álvarez-Salgado, 2012)
Atlantic Ocean	Northeastern Atlantic	(16.0–16.3) (26–27%)	(1.5–1.6) (34–36%)	(0.04–0.10) (60–78%)	(Aminot and Kérouel, 2004)
Mediterranean Sea	Northwestern Mediterranean	23.3 34%	1.2 30%	0.04 60%	(Aminot and Kérouel, 2004)
Baltic Sea	Open Sea Only	(0–82) (0–17%)	(0–6.5) (0–41%)	(0.01–0.34) (8–65%)	(Hoikkala et al., 2012, 2015)

2.3.2 POM distribution

As a seasonally produced and rapidly decomposed pool with short lifetimes, POM lacks the long-term persistence of DOM and consequently decreases from maximum productivity and concentrations in the euphotic zone to near-zero at depth, rather than converging to a stable background concentration as DOM does. Due to limited direct measurements and their substantial seasonal variability, the vertical distribution of POM is typically inferred from export fluxes that decline exponentially with depth (Buesseler et al., 2020; Buesseler and Boyd, 2009; Martin et al., 1987), further discussed below in comparison to vertical DOM export. Here, we compare some available global and regional surface concentration ranges, both from in-situ measurements and remote sensing-derived estimates (Table 4), to provide a general perspective relative to DOM.

The range of global concentrations is relatively consistent across different sources, with significant variations by latitude, and an increased abundance of POM in coastal and marginal seas, especially for the Baltic Sea. Global average concentrations and ranges (in parentheses) are estimated at 6.4 (2.3–17.2) µM for POC, 0.83 (0.32–2.2) µM for PON, and 40 (10–170) nM for POP (Table 4). Across the open ocean, estimated average POC concentrations as well as their seasonal variation are lowest at lower latitudes, with 5–7, 3.5–4.5, and 5–6 µM for the South Atlantic, South Pacific, and Indian Ocean, respectively. At higher latitudes, average concentrations and seasonal ranges are higher with 6–10, 4–7, and 3.5–8 µM for the North Atlantic, North Pacific, and Southern Ocean, with slightly higher overall ranges by latitude of roughly 3.5–15 from Stramska (2009), and 4–10 from Fox et al. (2024) (Table 4). In-situ measurements for coastal and marginal seas show higher, but strongly variable mean concentrations and ranges, likely in part due to small-scale variability not captured by coarser satellite products, with

(0.70–15) µM for POC, (0.01–0.17) µM for PON, and (0–55) nM for POP in the Mediterranean Sea, 7.3–16.0 (1.1–43.8) µM for POC, 1.5–2.2 (0.2–5.9) µM for PON, and (1–14) nM for POP in the northwest European shelf seas, and 33 (8.3–388) µM for POC, 4.8 (0.7–13.42) µM for PON, and (140–390) nM for POP in the Baltic Sea (Table 4). Given the high concentrations in adjacent estuaries, higher POM accumulation in the Baltic Sea can likely be attributed to terrestrial sources and long residence times, which is consistent with the higher DOM accumulation.

Table 4: Literature compilation of observational data on concentrations of particulate organic carbon (POC), nitrogen (PON), and phosphorus (POP). Individual numbers or ranges (e.g., between sub-regions or different years) without parentheses represent averages over regions or a series of measurements, whereas values in parentheses show ranges between individual measurements. Ranges of concentrations with a double-asterisk represent estimates from figures in the respective references. Strong outliers in the measurement referenced as "Patch" were excluded from Nausch et al. (2008). Estimates in mg C m^{-3} were converted to µM for consistency, with the estimates from Stramska (2009) based on horizontally averaged climatological time series, and from Fox et al. (2024) from the global surface POC distribution. Modified from Table S6 in (Demir et al., 2025b).

Location	Sub-Region or Focus	POM Concentrations			Source
		POC $[\mu M]$	PON $[\mu M]$	POP $[nM]$	
Global Ocean	Surface Ocean Biogeochemical Regions	6.4 (2.3–17.2)	0.83 (0.32–2.2)	40 (10–170)	(Liang et al., 2023; Martiny et al., 2014; Tanioka et al., 2022a)
	Horizontally-Averaged Surface Concentration	5–6**	-	-	(Stramska, 2009)
	Time-Averaged Surface Concentration by Latitude	3.5–15**	-	-	(Stramska, 2009)
	Surface Ocean	4–10**	-	-	(Fox et al., 2024)
Atlantic Ocean	North Atlantic Mean Surface Concentration	6–10**	-	-	(Stramska, 2009)
	South Atlantic Mean Surface Concentration	5–7**	-	-	(Stramska, 2009)
Pacific Ocean	Eastern North Pacific	(0.09–5.76)	(0.012–0.917)	(0.45–37.32)	(Loh and Bauer, 2000)
	North Pacific Mean Surface Concentration	4–7**	-	-	(Stramska, 2009)
	South Pacific Mean Surface Concentration	3.5–4.5**	-	-	(Stramska, 2009)
Indian Ocean	Mean Surface Concentration	5–6**	-	-	(Stramska, 2009)
Southern Ocean	South of the Tasman Sea	(0.05–3.48)	(0.004–0.490)	(0.25–13.48)	(Loh and Bauer, 2000)
	Mean Surface Concentration	3.5–8**	-	-	(Stramska, 2009)
Mediterranean Sea	NW Mediterranean	(0.9–14.9)	(0.1–1.7)	-	(Doval et al., 1999)

	NW Mediterranean	(4–15)**	(0.2–0.7)**	(0–55)**	(Lucea et al., 2003)
	Western Basin	(0.74–8.70)	(0.01–0.87)	(1–45)	(Pujo-Pay et al., 2011)
	Eastern Basin	(0.70–5.41)	(0.01–0.66)	(1–30)	(Pujo-Pay et al., 2011)
South China Sea	Northern Parts	(1.1–13)	-	-	(Hung et al., 2007)
Northwest European Shelf	Hebrides Shelf	(4.73–6.74)	(0.37–0.76)	(1–10)	(Painter et al., 2017)
	Norwegian Coastal Waters	(6–14)**	(0.8–2.5)**	(6–14)**	(Frigstad et al., 2013)
	Celtic Sea	(2–15)**	(0.2–3)**	(1–13)**	(Davis et al., 2019)
	North Sea	7.3–16.0 (1.1–43.8)	1.5–2.2 (0.3–5.9)	-	(Chaichana et al., 2017, 2019)
	Northern North Sea (Surface)	10.5 (2.7–21.8)	2.0 (0.6–2.9)	-	(Chaichana et al., 2017, 2019)
	Northern North Sea (Bottom)	7.3 (1.1–16.2)	1.5 (0.3–2.7)	-	(Chaichana et al., 2017, 2019)
	Southern North Sea	16.0 (5.8–43.8)	2.2 (0.6–5.9)	-	(Chaichana et al., 2017, 2019)
	Central North Sea	(1.9–38.4)	(0.2–5.8)**	-	(Suratman et al., 2009)
Baltic Sea	Estuaries	(29.8–388)	-	-	(Voss et al., 2021)
	Gotland and Gdansk Deep	(8.3–79.9)	(0.7–11.4)	-	(Winogradow et al., 2019)
	SW Baltic Sea (Heiligendamm)	33	4.8	-	(Osterholz et al., 2021)
	Gotland Basin	(27.98–93.92)	(3.88–13.42)	(140–390)	(Nausch et al., 2008)

530

2.3.3 DOM and POM export contributions

DOC has long been assumed to be homogeneously distributed across the ocean and hence neglected as a contributor to the export of carbon from surface waters. However, progress in analytical measurements and an increasing number of observations revealed that, while POC dominates global export production, DOC significantly contributes, with an estimated contribution
535 of 20% to export at 100m depth (Hansell et al., 2009). The export contributions decrease with depth from 20% to below 10%, as most SL-DOC is remineralized within months to years in the epipelagic zone, while a larger fraction of POC is exported deeper through sinking and downwelling (Hansell et al., 2009). A recent study based on data assimilation of satellite and in-situ data into a biogeochemical model reports similar contributions of 9.1 Pg C yr^{-1} (~85%) exported below the euphotic zone

as POC and 1.6 Pg C yr^{-1} (~15%) as DOC (DeVries and Weber, 2017), with previous estimates for total carbon export ranging from 4 to 12 Pg C yr^{-1} (Dunne et al., 2005; Henson et al., 2011; Laws et al., 2000; Schlitzer, 2002, 2004; Siegel et al., 2014). However, there is considerable variability in the estimated fractions of POC and DOC in NCP and export, as well as in the efficiency of carbon export through the biological carbon pump across the global ocean (DeVries and Weber, 2017; Henson et al., 2012; Roshan and DeVries, 2017), and seasonally (Henson et al., 2015). Some drivers of this variability include community composition and heterotrophic food web structure (Buesseler, 1998; Buesseler and Boyd, 2009; De La Rocha and Passow, 2007; Henson et al., 2019), particle characteristics (Omand et al., 2020; Riley et al., 2012), and the C:N:P stoichiometry of exported OM (Hopkinson and Vallino, 2005; Letscher and Moore, 2015; Tanioka et al., 2021). In addition, estimated export contributions can be sensitive to the metrics used to assess vertical flux attenuation, introducing further uncertainty (Buesseler et al., 2020; Gloege et al., 2017).

Roshan and DeVries (2017) identified strong latitudinal differences in the relative NCP and export contributions. They show the smallest ratios of net DOC production and DOC export to total carbon export in equatorial and polar regions, both at approximately 5–15%, with maximum contributions in subtropical regions of ~20–40% for net DOC production and ~40% (30–80%) for DOC export. Apart from differences in DOC production, they attribute these differences to equatorial upwelling and poleward transport, leading to a substantial accumulation and downwelling of DOC in the subtropics. The high net DOC production in oligotrophic regions is consistent with the high and variable DOM release and PER reported by Carlson et al. (2024). In agreement with previous estimates, the average contribution of DOC to carbon export is 20 ± 9%.

Overall, these studies confirm that POC has the globally dominant contribution to vertical organic carbon export, but DOC contributes significantly, and in some regions even equally or even more to carbon export. At the same time, it should be considered that all DOC is eventually remineralized in the water column, exporting dissolved inorganic carbon (DIC) to deeper waters. However, only POC contributes to long-term storage in marine sediments.

3 C:N:P stoichiometry of marine OM

3.1 Marine OM classification

The ranges and variations in the C:N:P stoichiometry of marine OM differ widely by size and lability fractions (Hopkinson and Vallino, 2005; Liang et al., 2023; Martiny et al., 2013; Tanioka et al., 2022b). To account for this, we here distinguish between ranges of POM and DOM stoichiometry from literature, and further subdivide DOM into L-DOM and R-DOM fractions. POM is discussed as a bulk pool, encompassing both living biomass and detritus, reflecting the greater availability of observational data that typically do not differentiate between these components. In addition to bulk POM stoichiometry, we separately discuss marine ecological stoichiometry and specifically internal plankton stoichiometry, as mainly measured in experimental studies, which provides a physiological context for the elemental composition of living biomass under varying environmental conditions and in response to potential future changes.

For DOM, we first consider bulk DOM stoichiometry, which is more widely reported in observational studies. In addition, we estimate L-DOM and R-DOM stoichiometry from a subset of studies where these fractions were explicitly distinguished. We use a simplified two-compartment classification that groups the five classes proposed by Hansell et al. (2013) into two broader lability fractions. This reflects the limitations of most observational datasets, which typically do not resolve several classes, but instead aggregate DOM into more operationally defined reactive and non-reactive pools based on lability or depth. The L-DOM pool described here includes both L-DOM and SL-DOM components, with the latter dominating due to the rapid microbial uptake and low concentrations of L-DOM. The R-DOM pool mainly includes R-DOM and UR-DOM. As SR-DOM is not typically distinguished as a separate class and occurs in both surface and deeper waters, it may be represented to some extent in either our L-DOM or R-DOM fraction.

3.2 Global DOM stoichiometry

A large range of C:N:P ratios is observed in bulk DOM across the global ocean, but generally much more carbon-rich relative to elemental Redfield ratios of C:N:P = 106:16:1 (Hopkinson and Vallino, 2005; Redfield, 1958; Redfield et al., 1963) (Table 5). One major control of differences in bulk DOM stoichiometry is the vertical shift in the relative contributions of L-DOM and R-DOM fractions, and an associated increase in nutrient depletion of DOM with depth as the L-DOM fraction decreases, as described by a two pool conceptualization in Hopkinson and Vallino (2005). Global water column-integrated bulk DOM composition is estimated at DOC:DON = 14–17, DOC:DOP = 778–810, and DON:DOP = 48–54 (Table 5, Fig. 2). Surface waters have comparable C:N, but roughly half the C:P and N:P ratios, with an estimated mean composition and ranges (in parentheses) of DOC:DON = 14–14.6 (13.0–16.1), DOC:DOP = 374–387 (251–638), and DON:DOP = 26–27 (17–44) (Table 5). In contrast, deep waters are much more P-depleted, with a bulk DOM composition of DOC:DON = 13 (12–20), DOC:DOP = 2700 (640–4404), and DON:DOP = 215 (40–360) (Table 5). Hence, surface waters are close to the estimated ranges of L-DOM composition with L-DOC:L-DON = 8.9–10.7 (5.4–14.1), L-DOC:L-DOP = 179–199 (83–414), and L-DON:L-DOP = 20 (15–49) (Table 6), and deep water concentrations align with ranges of R-DOM composition estimates with R-DOC:R-DON = 15.7–18, R-DOC:R-DOP = 1373–3512, and R-DON:R-DOP = 10–202 (Table 7). With regards to differences across ocean basins, Liang et al. (2023) found bulk DOC:DON ratios to be relatively consistent, but DOC:DOP and DON:DOP ratios to be more variable and highest in the subtropical gyres, particularly in the Atlantic Ocean. Both ratios were generally lower in equatorial, polar, and subpolar regions as well as in the Pacific and Southern Oceans, which aligns with lower DOC:DOP ratios compared to the Atlantic Ocean from other sources (Table 5).

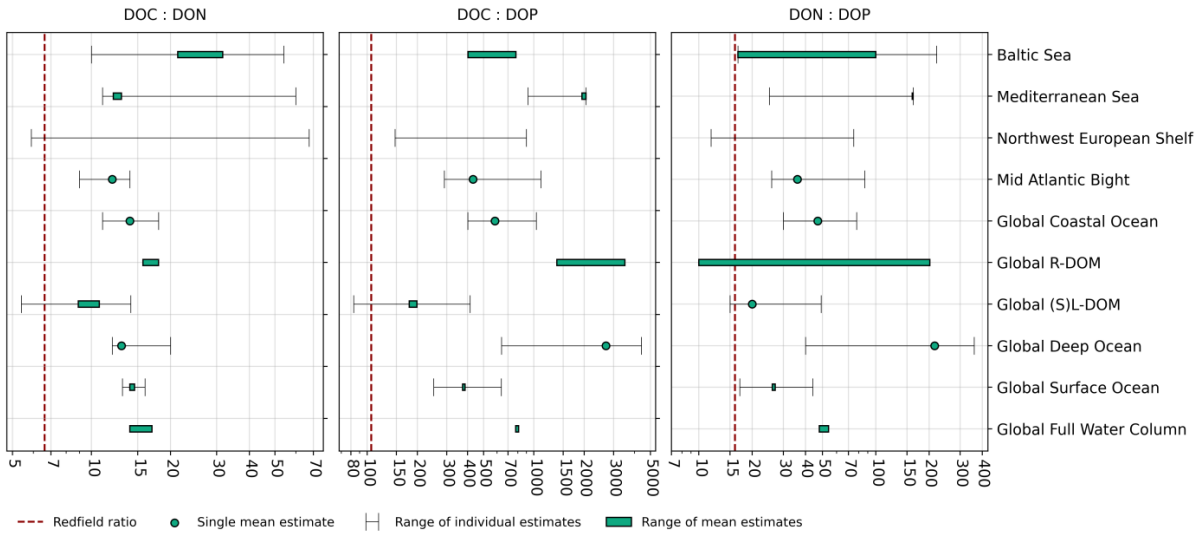

Figure 2: Molar ratios of dissolved organic carbon (DOC), nitrogen (DON), and phosphorus (DOP) for bulk DOM across different ocean regions, alongside global ranges for refractory or recalcitrant DOM (R-DOM) and (semi-)labile DOM (SL-DOM). Vertical dashed red lines indicate the canonical Redfield ratios (C:N = 6.625, C:P = 106, N:P = 16) for reference. Error bars represent reported ranges of individual estimates. Turquoise boxes indicate the range of estimated mean values when multiple estimates were available, while turquoise points indicate single available estimates. Data compiled from Tables 5–7.

Coastal and marginal seas vary in bulk DOM composition. The median concentrations and ranges (in parentheses) of the CoastDOMv1 dataset globally show comparable DOC:DON ratios, but a higher P-depletion in the coastal ocean with DOC:DON = 14 (11–18), DOC:DOP = 583 (401–1034), and DON:DOP = 47 (30–78) (Table 5, Fig. 2). Continental shelves with active open ocean exchange have a more variable composition compared to surface waters of the open ocean, estimated at DOC:DON = 12 (9–14), DOC:DOP = 431 (290–1101), and DON:DOP = 36 (25.8–86.7) in the Mid-Atlantic Bight, and DOC:DON = (5.9–67.4), DOC:DOP = (147–900), and DON:DOP = (11.7–75) in the northwest European shelf seas (Table 5). Semi-enclosed marginal seas show more substantial deviations from elemental Redfield ratios with DOC:DON = 12.1–13.0 (11–60), DOC:DOP = 1941–2055 (920–2055), and DON:DOP = 160.8–162.7 (25–162.7) for the Mediterranean Sea, and DOC:DON = 21.3–31.6 (10–54), DOC:DOP = 402.6–780.7, and DON:DOP = 16.6–100 (16.6–221) for the Baltic Sea, likely due to a combination of terrestrial sources and long water residence times (Table 5). The Baltic Sea in particular shows high DOC:DON ratios typically found in riverine environments, while the Mediterranean Sea is more P-depleted than the global coastal ocean. Differences in L-DOM composition between the open and coastal oceans are minor except for the Mediterranean Sea, which shows substantially higher L-DOC:L-DON and L-DOC:L-DOP ratios of 19.2 and 530, respectively (Table 6). Together, these observations highlight substantial variability in DOM stoichiometry across regions and lability fractions, indicating that representing all DOM fractions with uniform Redfield ratios would misrepresent their composition and cycling in biogeochemical models, underscoring the need to differentiate DOM fractions. A more detailed account of the global variations in DOM stoichiometry is provided by Liang et al. (2023).

620 **Table 5:** Literature compilation of observational data on elemental ratios of carbon, nitrogen, and phosphorus in bulk dissolved organic matter (DOM). Individual numbers or ranges (e.g., between sub-regions or different years) without parentheses represent averages over regions or a series of measurements, whereas values in parentheses show ranges between individual measurements. A single asterisk indicates implicit estimates of individual DOC:DON, DOC:DOP or DON:DOP ratios from provided ranges of DOC:DON:DOP ratios where they were not provided explicitly. Ranges of values with a double-asterisk represent estimates from figures in the respective references. For the
625 data from Lønborg et al. (2024), we report the median along with the 25th and 75th percentiles, as these better represent the distribution of the large dataset, avoiding the influence of outliers on the mean and range. Modified from Table S7 in (Demir et al., 2025b).

Location	Sub-region or focus	Bulk DOM stoichiometry			Source
		DOC:DON	DOC:DOP	DON:DOP	
Global ocean	Global surface ocean (biogeochemical regions)	14.6 (13.0–16.1)	387 (251–638)	26 (17–44)	(Liang et al., 2023)
	Full water column	17*	810	48	(Letscher et al., 2015; Letscher and Moore, 2015)
	Coastal ocean	9*	1164	123	(Lønborg and Álvarez-Salgado, 2012)
	Coastal ocean	14 (11–18)	583 (401–1034)	47 (30–78)	(Lønborg et al., 2024)
	Shelf, slope, and open ocean	14*	778	54	(Hopkinson and Vallino, 2005)
	Shelf, slope, and open ocean (surface only 0–100m)	14	374	27	(Hopkinson and Vallino, 2005)
Atlantic Ocean	Georges Bank (Surface Ocean)	(11–15)	(400–800)	(24–55)	(Hopkinson et al., 1997)
	Geroges Bank (Deep Waters)	(14–20)	(700–2500)	(40–140)	(Hopkinson et al., 1997)
	Mid-Atlantic Bight (Surface Ocean)	12 (9–14)*	431 (290–1101)	36 (25.8–86.7)	(Hopkinson et al., 2002)
	Mid-Atlantic Bight (Deep Slope Waters)	13 (12–14)*	2700 (986–4404)	215 (70–360)	(Hopkinson et al., 2002)
	NE Atlantic (Surface Waters)	(13.1–14.3)	(440–850)	(31–62)	(Aminot and Kérouel, 2004)
	NE Atlantic (Deep Waters)	(12.6–16.4)	(640–3100)	(45–200)	(Aminot and Kérouel, 2004)
Pacific Ocean	Eastern North Pacific	(13–30)	(277–537)	(13–34)	(Loh and Bauer, 2000)
	North Pacific Subtropical Gyre	(14.8–16.4)	(390–483)	(24.0–31.4)	(Church et al., 2002)
Southern Ocean	South of the Tasman Sea	(9–18)	(229–682)	(12–49)	(Loh and Bauer, 2000)
Mediterranean Sea	Southern Adriatic Basin (Surface)	(14–16)	(1189–1411)	(86–88)	(Santinelli et al., 2012)
	Southern Adriatic Basin (Intermediate Waters)	(13–14)	(1107–1279)	(83–97)	(Santinelli et al., 2012)
	Southern Adriatic Basin (Deep Waters)	(11–15)	(993–1693)	(85–108)	(Santinelli et al., 2012)
	NW Mediterranean	15.5	-	-	(Doval et al., 1999)
	NW Mediterranean	(30–60)*	(1510–1984)	(25–66)	(Lucea et al., 2003)

	NW Mediterranean (Surface Waters)	(16.7–16.9)	(920–970)	(55–57)	(Aminot and Kérouel, 2004)
	NW Mediterranean (Deep Waters)	(15.1–17.2)	(1100–1800)	(64–106)	(Aminot and Kérouel, 2004)
	Western Basin	12.1	1941	162.7	(Pujo-Pay et al., 2011)
	Eastern Basin	13.0	2055	160.8	(Pujo-Pay et al., 2011)
East China Sea	-	(8.9–15.3)	(200–853)	(19–83.6)	(Hung et al., 2003)
South China Sea	Northern Parts	(11–13)*	(322–510)	(29–39)	(Hung et al., 2007)
Sea of Japan (East Sea)	-	17*	374	22	(Kim and Kim, 2013)
Northwest European Shelf	Norwegian Coastal Waters	-	-	(59.8–73.6)	(Frigstad et al., 2013)
	Celtic Sea	(12–17)*	(281–416)	(17–33)	(Davis et al., 2014)
	Celtic Sea	(11.0–17.4)	(147–377)	(11.7–31.7)	(Davis et al., 2019)
	North Sea	(5.9–36.5)	-	-	(Chaichana et al., 2017, 2019)
	Central North Sea	(9.5–67.4)	-	-	(Suratman et al., 2009)
	North Sea	(10–25)**	(200–900)**	(15–75)**	(Painter et al., 2018)
Baltic Sea	Baltic Proper	31.6	527.0	16.6	(Rowe et al., 2018)
	Bothnian Sea	21.3	402.6	18.9	(Rowe et al., 2018)
	Bothnian Bay	23.1	780.7	33.8	(Rowe et al., 2018)
	Gulf of Finland	(10–54)	-	(25–419)	(Hoikkala et al., 2012, 2015)
	Gulf of Bothnia	(25–28)	-	100	(Hoikkala et al., 2015)
	Gulf of Riga	-	-	(20–60)	(Hoikkala et al., 2015)
	Baltic Proper	(17–26)	-	(20–30)	(Hoikkala et al., 2015)
	Estuaries	(16–23)*	(1199–3714)	(52–221)	(Voss et al., 2021)
	Rivers	31*	2790	91	(Stepanauskas et al., 2002)
	Southwestern Baltic Sea (Heiligendamm)	(12.5–20)**	-	-	(Osterholz et al., 2021)

Table 6: Literature compilation of observational data on elemental ratios of carbon, nitrogen, and phosphorus in biodegradable or (semi-) labile dissolved organic matter (L-DOM). Individual numbers or ranges (e.g., between sub-regions or different years) without parentheses represent averages over regions or a series of measurements, whereas values in parentheses show ranges between individual measurements.

A single asterisk indicates implicit estimates from provided ranges of L-DOC:L-DON:L-DOP ratios where they were not provided explicitly. Modified from Table S8 in (Demir et al., 2025b).

Location	Sub-region or focus	Biodegradable or (semi-)labile DOM stoichiometry			Source
		L-DOC:L-DON	L-DOC:L-DOP	L-DON:L-DOP	
Global ocean	Global surface ocean (biogeochemical regions)	8.9 (5.4–12.0)	179 (83–414)	20 (15–49)	(Liang et al., 2023)
	Coastal ocean	(8–9)*	(197–216)	(24–25)	(Lønborg and Álvarez-Salgado, 2012)
	Shelf, slope, and open ocean	10.7 (8.7–14.1)	199 (154–245)	20 (15.6–25)	(Hopkinson and Vallino, 2005)
Atlantic	NE Atlantic	(10.1–10.7)	(159–380)	(14.8–38)	(Aminot and Kérouel, 2004)
	Mid-Atlantic Bight	(10.0–14.1)	(193–203)	(15.6–20.2)	(Hopkinson and Vallino, 2005)
	Georges Bank	9.8	245	25	(Hopkinson and Vallino, 2005)
Pacific Ocean	Hawaiian Ocean	8.7	154	17.8	(Hopkinson and Vallino, 2005)
Mediterranean Sea	NW Mediterranean	19.2	530	28	(Aminot and Kérouel, 2004)
Baltic Sea	Gulf of Finland	(0.8–11.7)	-	-	(Hoikkala et al., 2012, 2015)

Table 7: Literature compilation of observational data on elemental ratios of carbon, nitrogen, and phosphorus in refractory or recalcitrant dissolved organic matter (R-DOM). Individual numbers or ranges (e.g., between sub-regions or different years) without parentheses represent averages over regions or a series of measurements whereas values in parentheses show ranges between individual measurements. A single asterisk indicates implicit estimates from provided ranges of R-DOC:R-DON:R-DOP ratios where they were not provided explicitly. Modified from Table S9 in (Demir et al., 2025b).

Location	Refractory or recalcitrant DOM stoichiometry			Source
	R-DOC:R-DON	R-DOC:R-DOP	R-DON:R-DOP	
Global ocean	17.0 (16.5–18.1)	1373 (900–2300)	82 (50–140)	(Liang et al., 2023)
Coastal ocean	18*	2835	159	(Lønborg and Álvarez-Salgado, 2012)
Shelf, slope, and open ocean	17*	3511	202	(Hopkinson and Vallino, 2005)
NE Atlantic and NW Mediterranean	15.7	1570	10	(Aminot and Kérouel, 2004)

3.3 Global POM stoichiometry

Overall, the globally observed POM stoichiometry is much less variable in comparison to bulk DOM stoichiometry. On average, the composition is intermediate between Redfield stoichiometry and L-DOM composition, but with ranges from modestly below Redfield ratios to ratios exceeding them (Table 8). In the surface ocean, the average POM composition and

ranges (in parentheses) are estimated at POC:PON = 6.5–7.7 (6.1–11.6), POC:POP = 137–163 (73–295), and PON:POP = 20–22 (10–37) (Table 8, Fig. 3).

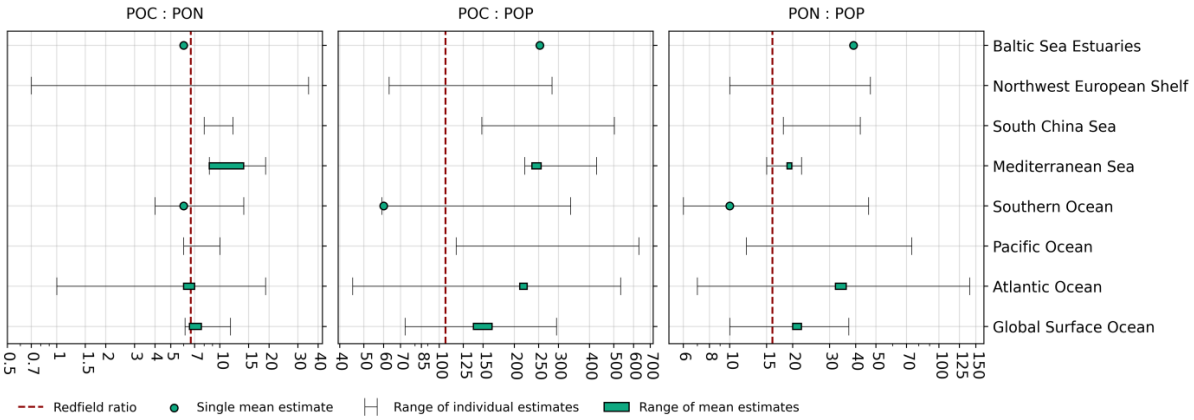

Figure 3: Molar ratios of particulate organic carbon (POC), nitrogen (PON), and phosphorus (POP) across different ocean regions. POM includes both living biomass and detrital POM. Vertical dashed red lines indicate the canonical Redfield ratios (C:N = 6.625, C:P = 106, N:P = 16) for reference. Error bars represent reported ranges of individual estimates. Turquoise boxes indicate the range of estimated mean values when multiple estimates were available, while turquoise points indicate single available estimates. Data compiled from Table 8.

Martiny et al. (2013) identified strong latitudinal patterns in relation to nutrient availability, with POC:PON:POP above Redfield ratios at 195:28:1 in warm and nutrient-depleted low latitude gyres, 137:18:1 in warm and nutrient-rich upwelling regions, and below Redfield ratios at 78:13:1 in cold and nutrient-rich high latitudes. This poleward gradient is also supported by more recent observations from Tanioka et al. (2022b), estimating the highest POC:PON:POP ratios at 225:32:1 in the western North Atlantic, and the lowest poleward of the southern Subtropical Convergence, with ratios below Redfield stoichiometry at 60:10:1. Both Tanioka et al. (2022b) and Teng et al. (2014) further show peak POC:PON, POC:POP, and PON:POP ratios in both northern and southern subtropical regions, with reduced values near the equator and the lowest ratios observed at high latitudes, along with generally higher P-depletion in the northern hemisphere.

In comparison to differences across latitudes, variations across ocean basins and longitudes are quite variable (Tanioka et al., 2022a, b). A clearer dependency is observed with depth, where POM composition becomes increasingly P-depleted, leading to a mean and range in POC:POP ratios in the mesopelagic or twilight zone of 294 (83–500), compared to a POC:POP ratio of 137–163 (73–295) at the surface (Tanioka et al., 2021) (Table 8, Fig. 3). While regional data remains very limited, available case studies suggest a POM composition in coastal waters on the upper end of estimates for the open ocean, with ratios of POC:PON = 8.6–14.0 (8.6–19), POC:POP = 235–256 (220–426), and PON:POP = 18.8–19.8 (15–22) in the Mediterranean Sea, POC:PON = (8–12), POC:POP = (148–502), and PON:POP = (18–42) in the South China Sea, and POC:PON = (0.7–34.9), POC:POP = (63–283), and PON:POP = (10–47) in the northwest European shelf seas (Table 8 , Fig. 3). In particular POC:PON ratios are higher and show a larger range than the global open ocean, likely due to carbon-rich terrestrial OM inputs (Bauer et al., 2013). While the variability of POM stoichiometry is generally lower than in the bulk DOM pool, there are

substantial global variations, comparable to L-DOM, which are likely to have implications for global biogeochemical cycles, especially considering the larger contribution to export production. A more comprehensive account of global POM stoichiometry and its spatial variability is given by Martiny et al. (2013, 2014) and Tanioka et al. (2022a, b).

Table 8: Literature compilation of observational data on elemental ratios of carbon, nitrogen, and phosphorus in particulate organic matter (POM). Individual numbers represent averages over regions or a series of measurements whereas values in parentheses show ranges between sub-regions or measurements. A single asterisk indicates implicit estimates from provided ranges of POC:PON:POP ratios, where they were not provided as individual ratios explicitly. Ranges of values with a double-asterisk represent estimates from figures in the respective references. Global surface ocean POC:PON:POP ratios from Liang et al. (2023) are provided in their supplementary material and based on previously published data from Martiny et al. (2014) and Tanioka et al. (2022a). Modified from Table S10 in (Demir et al., 2025b).

Location	Sub-region or focus	POM stoichiometry			Source
		POC:PON	POC:POP	PON:POP	
Global Ocean	Surface ocean	7.7 (6.1–9.2)	160 (73–295)	21 (10–37)	(Liang et al., 2023; Martiny et al., 2014; Tanioka et al., 2022a)
	Surface Ocean (0–1000m)	6.55 (6.54–6.57)	141 (140–142)	20.8 (20.6–21.0)	(Liu et al., 2025)
	Global Median	6.6	163	22	(Martiny et al., 2014)
	Global Area-Weighted Mean	7.3*	146	20	(Martiny et al., 2013)
	Global Area-Weighted Mean (<30m)	6.7 (6.1–11.6)	137 (96–155)	21 (12–23)	(Tanioka et al., 2022a)
	Twilight zone (100–1000m)	-	294 (83–500)	-	(Tanioka et al., 2021)
Atlantic Ocean	Bermuda Atlantic	6 (1–19)	210 (45–532)	36 (7–140)	(Singh et al., 2015)
	Western North Atlantic	7*	225	32	(Tanioka et al., 2022b)
Pacific Ocean	Eastern North Pacific	(6–10)	(117–630)	(12–74)	(Loh and Bauer, 2000)
Southern Ocean	-	(4–14)	(59–336)	(6–46)	(Loh and Bauer, 2000)
	Poleward of Southern Subtropical Convergence	6*	60	10	(Tanioka et al., 2022b)
Mediterranean Sea	NW Mediterranean	8.6	-	-	(Doval et al., 1999)
	NW Mediterranean	(14–19)*	(220–426)	(15–22)	(Lucea et al., 2003)
	Western Basin	13.3	256	19.8	(Pujo-Pay et al., 2011)
	Eastern Basin	14.0	235	18.8	(Pujo-Pay et al., 2011)
South China Sea	Northern Parts	(8–12)*	(148–502)	(18–42)	(Hung et al., 2007)
Northwest European Shelf	Hebrides Shelf	(8.26–13.67)	(142.4–259.97)	(16.4–26.32)	(Painter et al., 2017)
	Norwegian Coastal Waters	(7.1–7.4)	(110.8–125.2)	(14.6–17.6)	(Frigstad et al., 2013)

	Celtic Sea	(5–6)*	(63–223)	(10–38)	(Davis et al., 2014)
	Celtic Sea	(4.3–11.6)	(144–283)	(24–47)	(Davis et al., 2019)
	North Sea	(0.7–16.8)	-	-	(Chaichana et al., 2017, 2019)
	Central North Sea	(2.5–34.9)	-	-	(Suratman et al., 2009)
Baltic Sea	Estuaries	6*	253	39	(Voss et al., 2021)
	Gotland and Gdansk Deep	(5.8–10.8)	-	-	(Winogradow et al., 2019)
	SW Baltic Sea (Heiligendamm)	(2.5–11)**	-	-	(Osterholz et al., 2021)

3.4 Ecological stoichiometry of marine organisms

3.4.1 Concepts and quantification of ecological stoichiometry

Compared to inorganic nutrients and organic degradation products, the cellular C:N:P stoichiometry of living organisms, referred to as ecological or biological stoichiometry, is more strongly constrained by the nutrient requirements for the synthesis and balanced composition of biological macromolecules such as proteins, lipids, carbohydrates, nucleic acids, and pigments needed for maintaining homeostasis and supporting essential biological functions (Meunier et al., 2025; Sterner and Elser, 2002). In marine ecosystems, the C:N:P stoichiometry of phytoplankton cells is shaped by community composition and environmental conditions, including nutrient availability, light, temperature, and pCO_2 (Finkel et al., 2006; Garcia et al., 2018b; Geider and La Roche, 2002; Ho et al., 2003; Leonardos and Geider, 2004; Schoo et al., 2013; Sheward et al., 2023; Tanioka and Matsumoto, 2020). It regulates the carbon fixation and nutrient uptake by primary production and determines the elemental quality of prey available to zooplankton, fish, and benthic consumers, thereby controlling the stoichiometry of assimilated biomass (Elser and Hassett, 1994; Hassett et al., 1997; Moorthi et al., 2016; Pertola et al., 2002). Food web processes influence ecosystem stoichiometry and nutrient availability, both through bottom-up effects on consumer nutrition and bacterial composition (Chan et al., 2012; Scott et al., 2012), and top-down effects such as compensatory or selective feeding, or the release of excess carbon or nutrients by consumers (Meunier et al., 2012; Moorthi et al., 2016).

Assessing the average and ranges of ecological stoichiometry of both marine primary producers and consumers remains challenging, as individual components of POM cannot easily be separated. For this reason, some studies directly link global changes in POM stoichiometry to phytoplankton physiology, with the advantage of ample spatial coverage (Galbraith and Martiny, 2015; Liefer et al., 2024; Liu et al., 2025; Moreno and Martiny, 2018; Sterner, 2015). However, a more mechanistic understanding of drivers of physiological changes can be derived from direct measurements in culture or mesocosm experiments (Tanioka and Matsumoto, 2020), which, on the other hand, are challenging to scale up to global ecosystem

stoichiometry, given the considerable diversity in community composition and possible differences in the adaptation to environmental conditions. Nevertheless, several laboratory experiments considering varying nutrient, light, and temperature conditions provide some indication of the range of ecological C:N:P stoichiometry of phytoplankton (Burkhardt et al., 1999; Finkel et al., 2006; Garcia et al., 2018b; Geider and La Roche, 2002; Ho et al., 2003; Kim et al., 2018; Leonardos and Geider, 2004; Quigg et al., 2003, 2010; Schoo et al., 2013; Sheward et al., 2023; Tanioka and Matsumoto, 2020), zooplankton (Elser and Hassett, 1994; Hassett et al., 1997; Moorthi et al., 2016; Pertola et al., 2002), heterotrophic bacteria (Chan et al., 2012; Scott et al., 2012), and higher trophic levels such as marine benthos (Clarke, 2008; Mäkelin and Villnäs, 2022).

3.4.2 Ecological stoichiometry of marine phytoplankton

Four studies quantifying the C:N:P stoichiometry of 7–29 species of marine eukaryotic phytoplankton under equal and nutrient-replete conditions found that, although the mean or median elemental ratios over all species were close to Redfield ratios of C:N:P=106:16:1, there was substantial variability between individual species and functional groups (Garcia et al., 2018b; Ho et al., 2003; Quigg et al., 2003, 2010). The reported average phytoplankton C:N:P stoichiometries were 124:16:1 (Ho et al., 2003), 107.3:16.2:1 (Garcia et al., 2018b), 125:16:1 (Quigg et al., 2003), and 132:18:1 (Quigg et al., 2010), providing a range of mean ratios of C:N = 6.62–7.81, C:P = 107.3–132, and N:P = 16–18 (Fig. 4). Between the 15 considered species, Ho et al. (2003) found elemental ratios of C:N = 5.8–12.3, C:P = 42–222, and N:P = 5.4–38, with slightly narrower ranges when grouped and averaged by phyla. Garcia et al. (2018b) estimated a less variable elemental composition from 30 isolates across 7 classes of phytoplankton, with C:N = 4.85–9.44, C:P = 56.9–182.4, and N:P = 8.89–29.58, but also centered around Redfield stoichiometry. Quigg et al. (2003, 2010) do not explicitly report the range of estimates, but based on figures in the main text and supplementary material, the range of average elemental composition by functional group is approximately C:N = 6–11, C:P = 60–200 (50–480), N:P = 10–30 (6–32) (Quigg et al., 2003), and C:N = 6–12 (4–34), C:P = 50–200 (40–480), N:P = 9–28 (4–76) (Quigg et al., 2010), where values in parentheses indicate ranges between individual species.

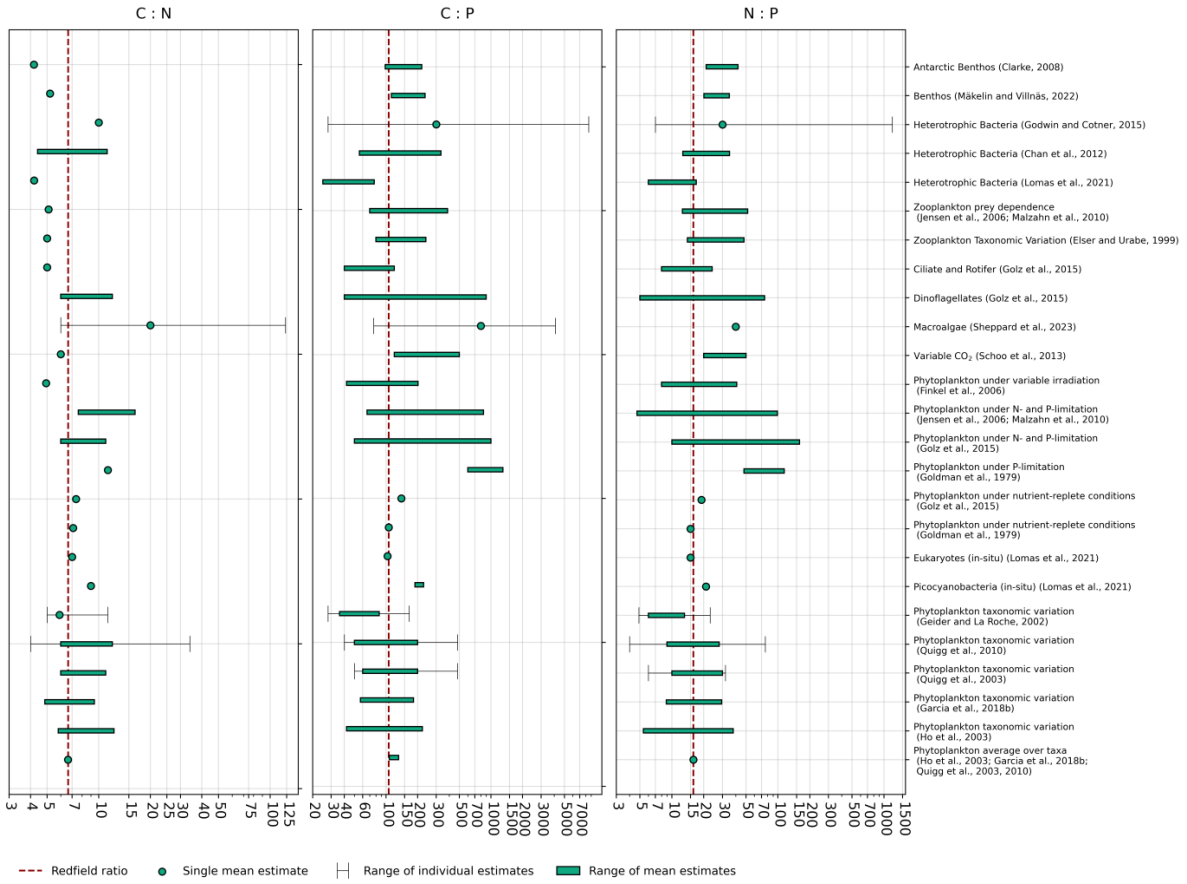

Figure 4: Molar C:N, C:P, and N:P ratios representing the ecological stoichiometry of marine organisms, including phytoplankton, zooplankton, heterotrophic bacteria, and marine benthos. For phytoplankton, ranges reflect variation among taxonomic groups, nutrient-replete versus nutrient-limited conditions, and responses to different light and pCO_2 levels. While most values are derived from experimental studies, two estimates for phytoplankton are based on global in situ measurements, as indicated in the labels. Zooplankton stoichiometry is shown as varying across taxa and in response to food quality. Heterotrophic bacterial ratios are presented from three studies with divergent reported ranges. Vertical dashed red lines indicate the canonical Redfield ratios (C:N = 6.625, C:P = 106, N:P = 16) for reference. Error bars represent reported ranges of individual estimates. Turquoise boxes indicate the range of estimated mean values when multiple estimates were available, while turquoise points indicate single available estimates. Data sources are provided in the figure and referenced in the main text.

Based on a collection of earlier studies (Burkhardt et al., 1999; Goldman et al., 1992; La Roche et al., 1993; Nielsen, 1992, 1996; Parsons, 1961; Sakshaug et al., 1983, 1984; Terry et al., 1983), two further analyses under nutrient-replete conditions report mean C:N:P ratios and ranges (in parentheses) of C:N = 5.9–8.1 (5.0–11.3), C:P = 36–86 (28–166), N:P = 6.0–13.2 (4.9–23), and N:P = 9 (5–19), respectively, with average C:P and N:P consistently below Redfield stoichiometry (Geider and La Roche, 2002; Leonardos and Geider, 2004) (Fig. 4). However, Ho et al. (2003) links this to the earlier of the two studies mainly considering diatoms and dinoflagellates, which also showed lower N:P ratios in their analysis as well compared to other species. To our knowledge, only one study has directly measured species-specific C:N:P composition across ocean basins

and found differences between two picocyanobacteria species with mean ratios of C:N = 9–11, C:P = 188–228, and N:P = 21–22, and the remaining eukaryotic phytoplankton with C:N = 7, C:P = 103, and N:P = 15 (Lomas et al., 2021). Together, these experimental and observational studies consistently demonstrate strong variability in the internal C:N:P stoichiometry of phytoplankton across species, suggesting that community composition can determine the average stoichiometry of phytoplankton and hence primary production, with important implications for potential future changes in global marine carbon and nutrient cycles.

Besides community composition, environmental conditions have also been shown to influence the C:N:P stoichiometry of individual phytoplankton species. Goldman et al. (1979) show that, under N- and P-limited conditions, cellular C:N:P ratios depend strongly on growth rates. Under P-limited conditions, elemental ratios change from C:N = 7.1, C:P = 106, N:P = 15 to C:N = 11.3–12.5, C:P = 600–1300, and N:P = 48–115 (Fig. 4), with a change from 90% to 10% of the maximum growth rate. Similarly, under N-limited conditions, C:N ratios change from 7.0–7.1 at 90% to 12.6–20.0 at 10% of the maximum growth rate, with inconsistent changes in C:P ratios from strong increases to decreases, but generally stable N:P ratios. Hence, there is a 2–3-fold increase in C:N ratios under N-limitation, and a 5–10-fold increase in C:P ratios under P-limitation, in both cases when growth rates become low. A similar range of changes has been found in a meta-analysis of the calcifying marine phytoplankton *Emiliania huxleyi*, with C:N:P = 124:16:1 under nutrient-replete conditions, showing roughly a 3-fold increase in N:P and 5-folding in C:P ratios under P-depletion, and a doubling in C:N under N-depletion (Sheward et al., 2023). Similar ranges of increases in C:P and C:N ratios with P-depletion, and in C:N ratios with N-limitation are further supported by Golz et al. (2015), and a meta-analysis by Tanioka and Matsumoto (2020), combining several previous syntheses mainly from experimental evidence, but also including in situ POM measurements (Flynn et al., 2010; Geider and La Roche, 2002; Hillebrand et al., 2013; Moreno and Martiny, 2018; Persson et al., 2010; Thrane et al., 2016; Villar-Argaiz et al., 2018; Yvon-Durocher et al., 2015). Both meta-analyses highlight macronutrient availability as the leading environmental driver of cellular C:N:P stoichiometry of phytoplankton.

While Tanioka and Matsumoto (2020) also conclude a lesser, but still significant increase in C:N and C:P ratios with increasing irradiation, as well as in the C:P ratio with increased temperature, Sheward et al. (2023) do not find a consistent impact of light or temperature on C:N:P ratios, but only a marginal decrease in C:N and C:P under lower light conditions. Velthuis et al. (2022) equally conclude no consistent impact of warming on C:N:P stoichiometry. Finkel et al. (2006) assessed five phytoplankton species from four different phyla under varying light conditions and found that C:P and N:P ratios in some species decreased consistently with increasing light from C:N:P = 202:41:1 to C:N:P = 42:8:1, while others showed inconsistent responses (Fig. 4). Furthermore, phylogenetic differences at all irradiance levels were comparable to those induced by changes in light conditions, with C:P ranging from 14 to 202 and N:P from 1.5 to 41.0. Hence, the effects of irradiance and temperature appear to be strongly species dependent and thus less generalizable.

Evidence for the effect of increased partial pressure of CO_2 (pCO_2) on C:N and C:P stoichiometry is also inconsistent. One study shows a doubling in the C:N ratio (C:N < 6 to C:N > 10) and a quadrupling in the C:P ratio (C:P ≈ 120 to C:P > 500) with increasing pCO_2 from 200 to 800 µatm in longer incubation periods of 14 days, and generally higher carbon content in

shorter incubation periods of 3 days (Schoo et al., 2013) (Fig. 4). Other studies suggest smaller and less consistent increases across different phytoplankton species (Burkhardt et al., 1999; Velthuis et al., 2022), or even no effect of pCO_2 levels on C:N:P stoichiometry over a range from 0 to more than 1000 µatm (Kim et al., 2018; Sheward et al., 2023). While these results do not precisely constrain the impact of pCO_2 levels on phytoplankton stoichiometry, they suggest a reduction in C:N and C:P ratios to be unlikely, with a possibility of increasing carbon content with rising CO_2 concentrations.

Global assemblages of macroalgae have been found to have mean C:N and C:P ratios 2.8 and 4 times higher, respectively, than those of phytoplankton, based on data from 444 species across over 400 locations, with means and ranges of C:N = 20 (6–123) and C:P = 801 (76–4102), indicating a higher carbon fixation per unit of nutrients (Sheppard et al., 2023) (Fig. 4). As is the case for phytoplankton, both nutrient availability and differences between phyla showed the strongest influence on macroalgal C:N:P ratios. Average C:N ratios and their ranges decreased from 27.5 (7.6–122.5) for brown macroalgae, through 17.8 (6.2–54.3) for green macroalgae, to 14.8 (5.6–77.6) for red macroalgae.

3.4.3 Ecological stoichiometry of marine heterotrophs

Some studies have assessed the impacts of variable C:N:P ratios in phytoplankton on the heterotrophic food web, including zooplankton, heterotrophic bacteria, and benthic organisms. The ecological stoichiometry of zooplankton in microcosm experiments has been shown to depend not only on prey composition, but also on metabolic conditions, such as temperature and consumer body mass (Moorthi et al., 2016). Variations in C:N:P composition of zooplankton have further been found to be less variable than their prey due to stoichiometric regulation for maintaining homeostasis, but with the strength of this regulation depending on the species (Golz et al., 2015).

For instance, compared to a 50% increase in the C:N and 3–7-folding in the C:P ratio of phytoplankton stoichiometry under N- and P-depletion, respectively (C:N ≈ 6–11, C:P ≈ 50–1000, N:P ≈ 10–160), from C:N:P = 140:19:1 under nutrient-replete conditions, Golz et al. (2015) show that two dinoflagellate species show an almost equal increase with prey composition (C:N ≈ 6–12, C:P ≈ 40–900, N:P ≈ 5–75), while a ciliate and rotifer species show strong regulation and close to no sensitivity in C:N:P to prey composition (C:N ≈ 5.0–5.7, C:P ≈ 40–120, N:P ≈ 8–24) (Fig. 4). These ranges indicate the range of variations across species and nutrient conditions which we estimated based on respective mean compositions from figures in Golz et al. (2015). Despite the considerable variation under substantial nutrient limitation, under nutrient-replete and intermediate conditions, Golz et al. (2015) show that all zooplankton species have a C:N:P composition close to or below Redfield ratios.

They further show that C:N:P in response to prey composition changes from two previous studies show a more consistent regulation and elemental compositions of C:N = 5.1–8.5, C:P = 70–385, and N:P = 12.6–52, with more variable prey composition of C:N = 7.6–16.3, C:P = 66–847.9, and N:P = 4.7–98.9 (Jensen et al., 2006; Malzahn et al., 2010) (Fig. 4). Besides prey composition, there is also similar variability in composition between zooplankton species, with Elser and Urabe (1999) comparing three species with ranges of C:N = 5–6, C:P = 80–240, and N:P = 14–48. Food web structure, such as

zooplankton diversity, can also affect prey quality and thus secondarily affect zooplankton composition itself (Plum et al., 2015; Plum and Hillebrand, 2019).

Compared to zooplankton, heterotrophic bacteria are generally thought to have a C:N:P composition below Redfield, with estimated mean ratios of C:N = 4.2–5, C:P = 25–77, N:P = 6–17 (Fagerbakke et al., 1996; White et al., 2019; Zimmerman et al., 2014) (Fig. 4). However, some studies show similar ranges of variability in C:N:P composition as for phyto- and zooplankton, with ranges of C:N = 4.4–11.2, C:P = 55.6–333.3, and N:P = 12.7–35.0 (Chan et al., 2012), and C:P = 40–217 under P-sufficient, or C:P = 55–548 under P-deficient conditions (Scott et al., 2012). A recent study states that variations in aquatic heterotrophic bacteria are larger than those of any other species or assemblages, with C:N:P ratios ranging from 28:7:1 to 8500:1200:1 (Godwin and Cotner, 2015). As the median of roughly C:N:P = 300:30:1 is at the higher end of the abovementioned studies, this extensive range may be limited to extreme environmental conditions or individual cells, and is likely less relevant to the average global composition.

Evidence for the elemental composition of marine higher trophic levels remains limited, but some available observations suggest a similar composition, with a narrower range of C:N:P ratios in benthic grazers compared to lower trophic levels (Clarke, 2008; Mäkelin and Villnäs, 2022). Benthic consumers show seasonal variations for benthic species and communities with available prey composition, with ranges of C:N = 5.2–7.0, C:P = 112.5–235.0, and N:P = 20.1–34.8 (Mäkelin and Villnäs, 2022) (Fig. 4). On average, six species of Antarctic marine benthos show similar ranges of C:N = 4.19–6.73, C:P = 97.9–219.1, and N:P = 21.1–42.0, indicating relatively N-rich but P-poor compositions compared to Redfield ratios (Clarke, 2008). While this only provides a partial representation of the C:N:P stoichiometry across the food web, it indicates that the composition of higher trophic levels, to some extent, follows prey composition.

Overall, these findings indicate that, while the average phytoplankton composition across a range of species under nutrient-replete conditions is typically close to Redfield stoichiometry, there are substantial variations with community composition and environmental conditions, in particular under nutrient stress. Compared to primary producers, variations across consumers and heterotrophic bacteria are less understood, and in addition to prey composition, have been shown to depend on several factors, including metabolic conditions, the extent of stoichiometric regulation of individual species, and consumer diversity. Still, the drivers of ecological stoichiometry, their implications for biogeochemical cycles, and their representation in biogeochemical models remain an open field of investigation (Hutchins and Tagliabue, 2024; Inomura et al., 2022; Liefer et al., 2024; Liu et al., 2025; Meunier et al., 2025; Moreno and Martiny, 2018; Sterner, 2015).

4 Predictors, trends, and implications of variable OM stoichiometry

4.1 Biogeographical predictors of POM stoichiometry

While studies on the ecological C:N:P stoichiometry of primary producers and consumers can identify mechanistic drivers through controlled experiments, as described above, drivers of global variations in POM and DOM stoichiometry can only be

inferred from statistical relationships or model reconstructions, identifying predictors such as environmental conditions or ecosystem properties like community composition. Directly attributing stoichiometric changes to specific variables based on statistics, however, is comparatively more challenging, as secondary effects such as temperature-driven changes in stratification and hence nutrient availability (Richardson and Bendtsen, 2019), or selection of well-adapted plankton species with different elemental composition (Lomas et al., 2021; Sharoni and Halevy, 2020), may be attributed to the effect of a single correlated variable, if not separately accounted for. Nevertheless, some recent studies have identified consistent patterns in the stoichiometry of POM (Galbraith and Martiny, 2015; Garcia et al., 2018a; Inomura et al., 2022; Lee et al., 2021; Liefer et al., 2024; Liu et al., 2025; Lomas et al., 2021; Matsumoto and Tanioka, 2020; Moreno and Martiny, 2018; Sterner, 2015; Talarmin et al., 2016; Tanioka et al., 2022b; Yvon-Durocher et al., 2015).

Variations in the C:N:P stoichiometry of POM are primarily linked to changes in phytoplankton physiology, diversity, and the resulting C:N:P of primary production, due to its short lifetime and stronger dependence on the quality of the initially produced material compared to DOM. Based on a generalized additive model analysis, combining global data on plankton genomic diversity and POM stoichiometry distribution, Tanioka et al. (2022b) identified differences in predictors of C:N:P in nutrient-replete high latitude subpolar and polar regions, poleward of 45°N and 45°S, compared to more nutrient-limited low latitudes from equatorial to subtropical regions. They found that an increase in C:P and N:P ratios from polar to subpolar regions was mainly driven by an increase in temperature, and an associated shift in phytoplankton community composition from diatoms to coccolithophores and cyanobacteria, with macronutrient availability as a secondary driver. They suggested that this reflected greater cellular P-allocation under cold, nutrient-replete conditions (Toseland et al., 2013). In contrast, at lower latitudes, nutricline depth and element-specific nutrient stress together drive C:N:P variability, with deeper nutriclines leading to higher C:P and N:P under P-limitation, and to higher C:N under N-limitation, likely reflecting shifts in plasticity under different types and intensities of nutrient stress. Liefer et al. (2024) link this latitudinal gradient in carbon to nutrient ratios to a shift in macromolecular composition and an associated physiological acclimation of phytoplankton.

These findings align with earlier work, suggesting a higher influence of nutrient stress in low latitude oligotrophic environments, and of temperature in nutrient-replete high latitude waters, both in response to changes in phytoplankton community (Moreno and Martiny, 2018). A combination of field data and experimental evidence also supports the influence of temperature on C:N:P stoichiometry, showing a 2.6-fold increase in C:P and N:P from 0 to 30°C (Yvon-Durocher et al., 2015), and similar increases as well as an associated shift in community composition in mesocosm experiments, with no effect of warming on C:N ratios (Yvon-Durocher et al., 2017). Galbraith and Martiny (2015) were able to reproduce the latitudinal distribution of POM stoichiometry solely based on the linear dependence of C:N:P in phytoplankton assimilation rates on ambient nutrient concentrations, where C:N ratios scaled with N-availability and C:P with P-availability. With a global ecosystem model consisting of two phytoplankton size classes, Inomura et al. (2022) find that variations in C:N ratios are generally adapted by phytoplankton plasticity, while changes in C:P ratios are controlled by selection of taxonomic groups Their results further suggest a higher presence of small phytoplankton taxa with lower P-storage at low latitudes and larger taxa with higher P-storage at high latitudes, which aligns with the equatorward shift from diatoms to coccolithophores and

cyanobacteria at high latitudes described by Tanioka et al. (2022b). Together, these individual assessments on the influence of nutrient availability, temperature, and community composition, based on observations and model reconstructions, support the statistically derived predictors and potential drivers of C:N:P stoichiometry in POM from Tanioka et al. (2022b).

With direct measurements of cellular phytoplankton C:N:P composition across ocean basins, distinguished by the three categories *Prochlorococcus*, *Synechococcus*, and eukaryotes, with the latter defined as larger autofluorescing cells that could not be categorized by the applied gating scheme, Lomas et al. (2021) quantified the impact of environmental conditions on C:N:P ratios in distinct autotrophic species. Based on the correlation of depth, as a proxy for irradiance, temperature, and the nitrate-to-phosphate flux ratio across the nutricline with elemental C:N:P ratios of each species, they found higher C:P and N:P ratios with increasing nitrate-to-phosphate flux ratio and for cyanobacteria compared to eukaryotic phytoplankton, which is consistent with prior estimates (Bertilsson et al., 2003; Weber and Deutsch, 2010). However, they did not find a consistent correlation with temperature or depth across species. For two of the three groups, they found an increase in C:P ratios with increasing temperature, but changes in C and P content were varied. In agreement with the aforementioned studies, they attribute the variations in C:N:P stoichiometry to a combination of community composition, associated taxonomic differences, and the plasticity or acclimation within species. Lomas et al. (2021) further highlight the higher plasticity of cyanobacteria as a reason for higher variations in C:P and N:P ratios, and the potential mixotrophy of larger eukaryotic phytoplankton supplementing nutrient requirements and allowing them to remain more homeostatic.

Despite numerous assessments of predictive variables for the C:N:P stoichiometry of POM, the main drivers of its variability are still under discussion. Given the strong consistency between experimental evidence, discussed in the previous subsection, and global statistical analyses showing that nutrient availability and community composition are primary drivers of variations in C:N:P ratios of POM, it is likely that both phytoplankton plasticity and interspecific differences influence the global biogeography of C:N:P composition, mainly in response to nutrient availability, but also with a more variable response to temperature and possibly other environmental conditions. These analyses have, however, mainly focused on the physiological controls of primary producers, but the contribution of heterotrophic organisms and variations in the decomposition of the large detrital fraction in POM are underrepresented, despite their potential relevance and differences in composition (Frigstad et al., 2011; Minor et al., 1998; Talmy et al., 2016). For instance, Frigstad et al. (2011) suggest that the preferential remineralization of nutrients and the relative fractions of phytoplankton, heterotrophs, and detritus may influence the global distribution in C:N:P stoichiometry, which is supported by Minor et al. (1998), who describe systematic differences in the macromolecular composition of phytoplankton and detritus. Consequently, Lomas et al. (2021) point out the necessity to assess the drivers of C:N:P stoichiometry not purely based on bulk POM composition, but based on specific taxonomic groups.

4.2 Biogeographical predictors of DOM stoichiometry

In contrast to POM, variations in DOM stoichiometry are not directly linked to production processes. Instead, the wide range of DOM reactivity timescales results in a decoupling from primary production and a more substantial influence of microbial

transformation and degradation (Hach et al., 2020). DOM is produced through several pathways, including DOM release by phytoplankton, but also through secondary processes such as grazing-mediated release and microbial solubilization of particles, which further complicates the quantification of mechanisms driving changes in C:N:P ratios. As discussed in Section 3.2, DOM stoichiometry largely reflects the relative contributions of SL-DOM and R-DOM fractions, with progressive nutrient depletion as DOM ages (Hopkinson and Vallino, 2005; Liang et al., 2023). Changes in DOM stoichiometry thus reflect shifts in the balance between seasonally produced L-DOM and SL-DOM, long-lived R-DOM fractions (Carlson et al., 2024; Hansell et al., 2024), and carbon-rich terrestrial DOM (Bauer et al., 2013; Bianchi, 2011). However, the drivers of global differences in DOM stoichiometry across its production, composition, and transformation remain poorly understood.

Some indirect evidence is provided by global estimates of net production and accumulation of DOC (Hansell et al., 2024; Roshan and DeVries, 2017), observed DOM distributions and stoichiometry (Hansell, 2013; Hansell et al., 2009; Hopkinson and Vallino, 2005; Liang et al., 2023), and studies linking variations in C:N:P and quantity of released DOM to environmental factors such as nutrient and light conditions (Carlson et al., 2024; Mühlenbruch et al., 2018; Thornton, 2014). Liang et al. (2023) propose that global variability in bulk DOM stoichiometry is primarily driven by changes in SL-DOM composition in surface waters. Based on weaker correlations between DON and DOP concentrations and NPP compared to DOC, they suggest that decoupling from DOC occurs due to additional uptake by mixotrophy. Liang et al. (2025) further link this uptake to SL-DON and SL-DOP production in equatorial waters and transport to oligotrophic subtropical regions, consistent with patterns of net DOC production (Roshan and DeVries, 2017) and the preferential remineralization of DON and DOP over DOC (Hopkinson and Vallino, 2005). Thus, variations in DOM stoichiometry may reflect differences in both the production, transformation, and redistribution through circulation of SL-DOM, though this remains to be thoroughly investigated.

4.3 Climate change impacts on C:N:P stoichiometry

Climate change and other anthropogenic stressors are reshaping marine ecosystems through diverse physical and biological changes (Doney et al., 2012), with likely consequences for the ecological stoichiometry of marine autotrophs, pelagic food webs, (van de Waal et al., 2010), and their coupling to global biogeochemical cycles (Hutchins and Tagliabue, 2024). This section provides an overview of proposed climate-driven consequences for OM cycling, distribution, and C:N:P stoichiometry, including implications for elemental ratios in phytoplankton assimilation and export.

Multiple global and regional model projections suggest that warming-induced shifts in phytoplankton community composition and physiological acclimation lead to altered cellular C:N:P ratios (Cael et al., 2021; Hochfeld and Hinners, 2024a, b; Matsumoto et al., 2020b; Matsumoto and Tanioka, 2020). In global ecosystem model simulations, a shift toward cyanobacteria and a phytoplankton acclimation to higher C:P ratios were found to contribute to a modest overall increase in export C:N:P (Matsumoto et al., 2020b), alongside the influence of regional changes in productivity (Matsumoto and Tanioka, 2020). Enhanced stratification and the expansion of oligotrophic regions are expected to promote higher C:P and N:P ratios, either through physiological plasticity or adaptation (Sheward et al., 2023; Toseland et al., 2013), or community shifts (Fernández-

González et al., 2022; Matsumoto et al., 2020b), potentially buffering the decline in carbon export under reduced productivity (Teng et al., 2014; van de Waal et al., 2010). This is consistent with model experiments showing a minor reduction in export production under warming when variable stoichiometry is represented, compared to fixed Redfield-ratio assumptions (Tanioka and Matsumoto, 2017).

In addition to primary producer responses, secondary effects on food web structure and nutrient transfer have also been projected. Changes in phytoplankton size distribution and prey quality are expected to drive shifts in zooplankton abundance and size structure, with potential consequences for nutrient recycling and trophic transfer efficiency (Benedetti et al., 2021; Cael et al., 2021; van de Waal et al., 2010). Model experiments in the Baltic Sea also emphasize the importance of accounting for phytoplankton adaptation to warming, as neglecting acclimation may overestimate shifts in community composition (Hochfeld and Hinners, 2024a, b). Observationally, a global analysis of bulk POM from 1971 to 2020 shows rising C:P and N:P ratios until around 2007, followed by a decline, potentially reflecting changes in anthropogenic nutrient inputs (Liu et al., 2025). While these trends do not confirm a continued rise in phytoplankton C:P as predicted by some models, the dataset includes both living and detrital material, complicating comparisons with model-based projections and impeding a direct attribution to phytoplankton composition. To better isolate the drivers of changes in OM stoichiometry and pool partitioning, experimental studies provide valuable additional insight into underlying processes and food web interactions under controlled climate perturbations.

Experimental studies have explored how future climate conditions may alter the elemental composition and partitioning of OM between dissolved and particulate pools, including changes in extracellular release by phytoplankton and interactions with zooplankton. In mesocosm experiments simulating warming under varying zooplankton densities, DOC and POC accumulation, as well as C:N and C:P ratios in both pools, increased with temperature under low copepod abundance, while this effect was counteracted under high copepod densities, indicating that zooplankton grazing can modulate the temperature-driven OM accumulation through top-down control (Biermann et al., 2015). Other experiments under elevated temperature similarly report increased DOM and POM accumulation, enhanced release of carbohydrate-rich DOM, rising C:N ratios, and elevated formation of TEPs (Engel et al., 2011; Taucher et al., 2012). These findings are consistent with enhanced phytoplankton exudation under stratification-induced nutrient limitation (Thornton, 2014). In contrast, Wohlers-Zöllner et al. (2012) observed a redistribution from POM to DOM without a significant change in stoichiometric ratios, potentially reflecting enhanced DOM release or preferential POM uptake.

Despite the growing body of research, many observed and projected effects remain specific to particular conditions, due to the complex interplay between physical and biogeochemical drivers. As a result, the cumulative impact of climate-driven changes on OM distribution and stoichiometry across different regions and OM fractions is still poorly constrained. Based on current evidence, climate-driven shifts in C:N:P stoichiometry are unlikely to represent a major overlooked feedback on oceanic carbon uptake. However, accounting for the observed variability in the stoichiometry of phytoplankton, POM, and DOM can significantly influence carbon export in climate change projections (Matsumoto et al., 2020a; Tanioka and Matsumoto, 2017; Teng et al., 2014). In addition to shifts in OM stoichiometry, a potentially more consequential question is whether climate

change will alter the size and persistence of the global DOM reservoir (Lee, 2024). Since DOC represents the majority of marine organic carbon, shifts in DOM accumulation or stability could have a more substantial impact on air–sea CO_2 exchange than changes in C:N:P ratios. However, the processes controlling DOM storage and reactivity remain poorly understood, making future changes difficult to constrain (Lønborg et al., 2020; Shen and Benner, 2018; Wagner et al., 2020).

4.4 Implications for global biogeochemical cycles

The aforementioned variability in the C:N:P stoichiometry of OM across different size and lability fractions, as well as between living cells and detrital bulk POM and DOM pools, has to be considered alongside diverse production and removal pathways and complex interactions across a range of timescales (Hopkinson and Vallino, 2005; Liang et al., 2023; Lønborg and Álvarez-Salgado, 2012; Martiny et al., 2013; Tanioka et al., 2022b). Together, this variability challenges the common simplification of applying fixed Redfield ratios of C:N:P = 106:16:1 to represent the global coupling of carbon and nutrient cycles across all OM fractions. Instead, accurately capturing biogeochemical cycles requires a differentiated representation of OM stoichiometry and cycling across distinct fractions, each shaped by specific ecological and environmental drivers. This variability limits the ability of simulations based on fixed Redfield stoichiometry to represent OM cycling and the broader biogeochemical implications of variable stoichiometry.

One significant consequence of variable C:N:P stoichiometry in OM production, remineralization, and export is the decoupling of carbon and nutrient cycles, with the carbon-enrichment in DOM and POM pools resulting in greater carbon export per unit of nitrogen and phosphorus than predicted by elemental Redfield ratios (Anderson and Pondaven, 2003; Demir et al., 2025b; Hopkinson and Vallino, 2005; Lønborg and Álvarez-Salgado, 2012; Tanioka et al., 2021). Differences with depth, specifically the carbon-enrichment in DOM and POM with the preferential remineralization of nitrogen and phosphorus over carbon, lead to vertical gradients in OM composition, enhancing nutrient recycling and new production, while retaining more carbon at depth and thus fueling new surface production without equivalent release of inorganic carbon (Anderson and Pondaven, 2003; Demir et al., 2025b; Hopkinson and Vallino, 2005; Letscher and Moore, 2015; Lønborg and Álvarez-Salgado, 2012; Tanioka et al., 2021; Thomas et al., 1999).

The stoichiometry of both production and export also varies geographically, with POM typically showing lower C:N:P at high latitudes and higher C:N:P at low latitudes (Martiny et al., 2013; Tanioka et al., 2022b), and this spatial variability, combined with differing DOM and POM export contributions (Roshan and DeVries, 2017), shapes the overall C:N:P ratios of newly produced and exported OM. This control on carbon export is relevant to the global oceanic carbon sink, but also annual and seasonal air–sea CO_2 exchange, and coastal carbon export fluxes at a regional level (Demir et al., 2025a, b; Matsumoto et al., 2020a; Tanioka et al., 2021).

In addition to spatial gradients, temporal variability in OM stoichiometry under changing environmental conditions can arise from shifts in ecological stoichiometry, changes in the microbial decomposition of detrital POM and DOM, and restructuring of food webs, all of which influence the production and removal of OM and its coupling with biogeochemical cycles over time

(Doney et al., 2012; Liu et al., 2025; Ratnarajah et al., 2023; van de Waal et al., 2010). While shifts in elemental stoichiometry remain difficult to constrain, they may contribute to feedback processes affecting carbon export efficiency, the strength of the oceanic carbon sink, and broader ecosystem adaptation to changing conditions. Variable stoichiometry in phytoplankton has readily been shown to affect projections of primary production, food quality, and carbon uptake (Kwiatkowski et al., 2018). The consideration of variable stoichiometry is further important to the consideration of terrestrially OM inputs, with distinct stoichiometry and degradability, which require explicit consideration to assess their fate, transformation, and potential contribution to marine carbon cycling (Bauer et al., 2013; Bianchi, 2011). Together, these spatial and temporal dimensions of stoichiometric variability across OM size and lability fractions emphasize the need for biogeochemical models to explicitly consider variable C:N:P ratios to improve the representation of carbon-nutrient coupling and ocean-climate feedback processes.

5 Model representation of variable OM stoichiometry

5.1 Variable cellular phytoplankton C:N:P

Variable C:N:P stoichiometry has been incorporated into a wide range of marine ecosystem models, spanning different spatial scales, structural complexities, and scientific objectives. Theoretical models describe variability in autotrophic uptake and growth in various ways, including statistical functions representing physiological adaptation and macromolecular allocation in response to environmental drivers such as nutrient supply, temperature, and internal quotas (Bonachela et al., 2013; Garcia et al., 2016; Klausmeier et al., 2004). Others employ mechanistic models of macromolecular allocation in autotrophic cells (Armin and Inomura, 2021; Inomura et al., 2020; Wirtz and Kerimoglu, 2016), or internal cell quota models, also referred to as Droop-type models, with decoupled environmentally controlled uptake and internally regulated growth (Butenschön et al., 2016; Zakem and Levine, 2019). All of these types of functions, including environmental conditions, macromolecular models, and cell quota models, have been applied to lower-trophic-level nutrient-phytoplankton-zooplankton-detritus (NPZD) or simpler ecosystem model applications, with varying objectives.

At the global scale, variations in cellular phytoplankton C:N:P have been applied to reconstruct the global distribution of POM stoichiometry directly from inorganic nutrient distribution based on separate C:N and C:P uptake functions (Galbraith and Martiny, 2015), or based on a macromolecular allocation model for C:N:P uptake applied to two different size classes of phytoplankton (Inomura et al., 2020, 2022). Global applications have revealed impacts of cellular C:N:P on nutrient distribution and nitrogen fixation (Chien et al., 2023), export production and carbon export under present, future or glacial conditions based (Matsumoto et al., 2020a, b, 2021; Matsumoto and Tanioka, 2020; Ödalen et al., 2020; Tanioka et al., 2020; Tanioka and Matsumoto, 2017), highest in the oligotrophic ocean (Fillman et al., 2023), community composition (Kwiatkowski et al., 2018; Matsumoto et al., 2020a; Matsumoto and Tanioka, 2020), and changes in projections of NPP, food quality and carbon uptake (Kwiatkowski et al., 2018). Increased carbon export with variable C:P stoichiometry in phytoplankton

production has also been predicted by data-based inverse model approaches, deriving global phytoplankton stoichiometry from inorganic nutrient concentrations (Sullivan et al., 2024; Teng et al., 2014). Regional simulations in the Gulf of Bothnia, a northern basin of the Baltic Sea, have shown that considering both the variable C:N:P uptake by four functional groups of phytoplankton, based on a cell quota model, and extracellular DOM release affect the seasonal drawdown of pCO_2 (Fransner et al., 2018).

5.2 Variable C:N:P in detrital POM and DOM

Apart from cellular C:N:P of phytoplankton, other model implementations focus on the representation of detrital POM and DOM stoichiometry, given their central role in carbon export and recycling and redistribution of nutrients. This approach further limits computational expenses for large-scale high-resolution applications by maintaining the simplification of Redfield stoichiometry in both autotrophs and heterotrophs, thereby reducing the number of state variables. For representing the observed variations in DOM and POM stoichiometry, these representations consider the preferential remineralization of organic N and P in DOM, POM, or both through variations in relative remineralization rates (Anderson and Pondaven, 2003; Demir et al., 2025b; Lan Smith et al., 2005; Letscher and Moore, 2015; Somes and Oschlies, 2015; Zakem and Levine, 2019), or the extracellular release or exudation of DOM by phytoplankton, implemented as a direct uptake from nutrients, and with the C:N or C:N:P stoichiometry based on nutrient availability, also referred to as excess or overflow production (Demir et al., 2025b; Kühn et al., 2010; Lan Smith et al., 2005; Lorkowski et al., 2012; Neumann et al., 2022; Pätsch and Kühn, 2008; Prowe et al., 2009). The latter increases with decreasing nutrient availability and becomes more carbon-rich relative to nitrogen, phosphorus, or both, under sufficient light conditions, as described in section 2.2.1.

While most use a fixed ratio between base remineralization rates of C, N, and P, Lan Smith et al. (2005) incorporate the preferential remineralization through a representation of the microbial food web, with uptake and respiration of L-DOM and SL-DOM through heterotrophic bacteria. Other formulations include global data-based optimization of production and remineralization rates for DOC, DON, and DOP, distinguished into SL-DOM and R-DOM classes, with the advantage of considering other, potentially overlooked processes, but at the cost of lacking the mechanistic representation of DOM production (Letscher et al., 2015; Letscher and Moore, 2015). The target regions of coupled physical-biogeochemical model applications range from local 1D-water column models in the Sargasso Sea (Anderson and Pondaven, 2003) and the ALOHA station near Hawaii (Lan Smith et al., 2005), through regional 3D models for the North Sea (Kühn et al., 2010; Lorkowski et al., 2012; Pätsch and Kühn, 2008; Prowe et al., 2009), the entire northwest European shelf seas (Demir et al., 2025b, a), and the Baltic Sea (Neumann et al., 2022), to global model applications (Letscher et al., 2015; Letscher and Moore, 2015; Somes and Oschlies, 2015). For the consideration of variable C:N:P in DOM and POM, the research questions focus on the carbon cycle representations with respect to carbon fixation, export production, regional carbon budgets, air–sea CO_2 exchange, and nitrogen fixation.

5.3 Variable C:N:P in heterotrophs and across OM fractions

Beyond the representation of variable C:N:P stoichiometry in autotrophs and detrital DOM and POM fractions, some models further include a representation of variable C:N:P ratios of heterotrophs, including zooplankton and heterotrophic bacteria (Butenschön et al., 2016; Fransner et al., 2018; Polimene et al., 2017; Zakem and Levine, 2019), while other models assume homeostatic zooplankton with responses only in growth rate, depending on prey quality (Kwiatkowski et al., 2018). By integrating variable stoichiometry into all OM components, these models can represent variable carbon and nutrient fluxes across the whole planktonic and microbial food web.

For instance, Butenschön et al. (2016), as well as subsequent work based on the same model framework (Fransner et al., 2018; Polimene et al., 2017), represent four functional groups of pelagic phytoplankton with variable C:N:P ratios through a Droop cell quota model. Two of the three zooplankton groups are affected by prey quality but release N and P for stoichiometric regulation. The model also includes three pelagic POM size classes and L-DOM with variable stoichiometry, as well as benthic degradable and refractory OM, while assuming fixed stoichiometry for mesozooplankton, benthic fauna, and pelagic SL-DOM and SR-DOM. Imbalances are released as inorganic nutrients. Further, pelagic heterotrophic bacteria take up pelagic OM depending on the model configuration. In the static model, they take up only L-DOM, which is produced from the decomposition of all other DOM and POM pools. The release of inorganic nutrients generally compensates for any stoichiometric imbalances. In the dynamic model, heterotrophic bacteria take up all POM and DOM pools but do not assimilate inorganic nutrients. The dynamic implementation incorporates the microbial carbon pump for representing multiple degradation timescales of L-DOM, SL-DOM, and SR-DOM. Benthic heterotrophic bacteria take up benthic POM, with a preferential uptake of organic N and P over C, and access to inorganic nutrients when accessible OM is nutrient-depleted. In an updated formulation, the model also considers extracellular release of carbon-rich DOM through exudation for a more accurate representation of the balance between the biological and microbial carbon pump (Polimene et al., 2017).

Other variable C:N:P representations across OM fractions include Kreus et al. (2015) with a 1D-water column representation of the BY15 station located in the central eastern Gotland Basin of the Baltic Sea. Their model implementation includes variable C:N:P ratios in two phytoplankton groups, including one of nitrogen-fixing cyanobacteria, one general group of heterotrophs, detrital POM, and L-DOM. Additionally, SL-DOM in the form of dissolved polysaccharides is represented as carbon only, with an additional representation of marine gels with flexible C:N ratios formed from these polymeric exudates and additionally adsorbing L-DOM, thereby modulating the C:N composition. In contrast to the previous approach, this implementation formulates phytoplankton uptake as a function of both inorganic nutrient availability and cellular C:N and N:P ratios, with an exudation of polysaccharides increasing with N-limitation. Through the gel formation and L-DOM adsorption, DOM is further aggregated to detrital POM, which is in turn linked back to DOM through degradation. Heterotrophs here only graze on both phytoplankton groups, and partially regulate imbalances in C:N:P from food quality through a relaxation term, with imbalances released by excretion and respiration.

A lower-complexity microbial ecosystem model implementation by Zakem and Levine (2019) incorporates a cell quota or Droop model in both phytoplankton and heterotrophs for representing variable C:N:P assimilation, growth, and excretion. Heterotrophs additionally take up inorganic nutrients in the absence of organic sources to satisfy demands for biomass synthesis. As in both previous approaches, there is additional loss through mortality, respiration, and excretion, with excretion releasing excess carbon or nutrients.

To represent variable stoichiometry of higher trophic levels, such as function groups or species of fish, theoretical models have been developed by linking energy balance and elemental fluxes through bioenergetic and stoichiometric principles, accounting for species- and size-specific limitations in carbon, nitrogen, and phosphorus based on food quality, trophic group, and life stage (Schiettekatte et al., 2020; Schindler and Eby, 1997). To our knowledge, such formulations have not yet been implemented in coupled physical-biogeochemical models that include a variable stoichiometry representation across all trophic levels, from primary producers to higher consumers, in an end-to-end model representation. As such, the extension of variable C:N:P stoichiometry to higher trophic levels still presents an avenue for future research.

5.4 Model realism, complexity, observational constraints, and computational cost

These varying implementations of variable C:N:P stoichiometry in the OM representation of biogeochemical models illustrate the variety of possible levels of complexity and potential applications. The most suitable level of complexity and number of processes represented strongly depend on the required degree of process resolution to address the scientific question, but also on the computational cost afforded at the intended scale, resolution, and length of simulation. Striking the right balance between realism, computational feasibility, and accurate parameter configurations based on the available constraints from observations remains a key challenge in model design (Martin et al., 2024).

In absence of resource limitations, and with abundance of observational data for constraining the required parameters, model development should aim for an integrated approach, including mechanistic descriptions of variability in C:N:P ratios of autotrophs, zooplankton and heterotrophic bacteria, detrital POM and DOM, under consideration of other aspects as pelagic and benthic community composition, higher trophic levels, size and lability fractions of POM and DOM, respectively, with an explicit representation of the microbial loop or microbial carbon pump, and the dynamic POM-DOM continuum and interactions. This would likely result in the most accurate representation of the coupling of marine OM cycling with global carbon and nutrient cycles. Conversely, in favor of low computational cost, as for large-scale high-resolution simulations over long time periods, reduced complexity representations may be favorable, and a consideration of variable C:N:P stoichiometry only in detrital POM and DOM may suffice for a reasonable representation of global export production and the coupling of biogeochemical cycles, without considering complex intracellular variations and species interactions. A promising direction is the use of modular model design (Vijayakumaran et al., 2025), which enables flexible inclusion or omission of components depending on application needs and desired complexity. Future model frameworks may also support the selective activation of C:N:P variability, though this could remain a technical challenge in most current model implementations.

6 Summary and outlook

In this review, we have described the diverse cycling pathways of marine OM, from its production by autotrophic cells to its assimilation and transformation by microbial interactions and within the broader heterotrophic food web, continued processing throughout the water column, and interactions across the DOM-POM continuum. These pathways lead to systematic variations in C:N:P stoichiometry across size and lability fractions, depths, and geographic regions. OM accumulation is generally higher in coastal oceans, primarily driven by terrestrial DOM inputs, although the extent varies depending on the relative influence of ocean margins versus riverine sources. This is reflected in higher carbon enrichment in both DOM and POM, particularly notable in the Baltic and Mediterranean Seas.

The resulting deviations from elemental Redfield ratios have important implications for global biogeochemical cycles and their representation in regional and global biogeochemical models. Previous studies have demonstrated that accounting for variable C:N:P stoichiometry of phytoplankton, detrital POM, and DOM affects current estimates and future projections of carbon export, nitrogen fixation, NPP, and food quality (Demir et al., 2025b; Kwiatkowski et al., 2018; Letscher and Moore, 2015; Matsumoto et al., 2020a, b; Tanioka and Matsumoto, 2017). In addition, climate-driven changes in OM stoichiometry due to changing community composition or acclimation of phytoplankton may introduce further variability with considerable impacts on biogeochemical processes and the strength of the ocean carbon sink under present and future conditions (Cael et al., 2021; Hochfeld and Hinners, 2024b; Liu et al., 2025; van de Waal et al., 2010).

For future development, the challenge remains to balance model realism and computational cost, with modular frameworks enabling selective inclusion of variable C:N:P stoichiometry, ranging from DOM and POM representations for large scale simulations to more mechanistic integrated models that capture variability across autotrophs, heterotrophs, pelagic and benthic communities, size and lability classes of POM and DOM, respectively, and explicit microbial loop and POM-DOM interactions, which are essential for accurately representing OM cycling and biogeochemical feedbacks.

At the same time, critical knowledge gaps persist regarding the quality and transformation of terrestrial DOM in the marine environment as well as the composition and controls on the lability of DOM fractions. Addressing these uncertainties requires improved, more differentiated observations of C:N:P stoichiometry, particularly distinguishing among lability fractions of DOM and between living and detrital POM components, as well as species-specific composition and trends. Such targeted measurements are crucial for isolating the key drivers of stoichiometric variability and for constraining and validating model representations. This, together with improving existing model representations, for example by incorporating environmental dependencies of phytoplankton and heterotrophic uptake stoichiometry, will be essential for advancing our understanding of the coupling of OM with global biogeochemical cycles.

Author contributions. KTD was responsible for conceptualization, methodology, formal analysis, investigation, data curation, and visualization. KTD also prepared the original draft of the manuscript. Writing, review, and editing were carried out by

KTD, MM, UD, HT, and CS. MM, UD, HT, and CS provided supervision. Project administration, as well as resource and funding acquisition, were led by CS.

Competing interests. The contact author has declared that none of the authors has any competing interests.

Acknowledgements. The research was funded by the Deutsche Forschungsgemeinschaft (DFG, German Research Foundation) under Germany's Excellence Strategy – EXC 2037 'CLICCS - Climate, Climatic Change, and Society'–Project Number: 390683824 and contributes to the CLICCS subproject A5 The Land-Ocean Transition Zone.

References

Ahmerkamp, S., Marchant, H. K., Peng, C., Probandt, D., Littmann, S., Kuypers, M. M. M., and Holtappels, M.: The effect of sediment grain properties and porewater flow on microbial abundance and respiration in permeable sediments, Sci Rep, 10, 3573, https://doi.org/10.1038/s41598-020-60557-7, 2020.

Alcolombri, U., Peaudecerf, F. J., Fernandez, V. I., Behrendt, L., Lee, K. S., and Stocker, R.: Sinking enhances the degradation of organic particles by marine bacteria, Nat. Geosci., 14, 775–780, https://doi.org/10.1038/s41561-021-00817-x, 2021.

Alldredge, A. L. and Silver, M. W.: Characteristics, dynamics and significance of marine snow, Progress in Oceanography, 20, 41–82, https://doi.org/10.1016/0079-6611(88)90053-5, 1988.

Alonso-Sáez, L., Vázquez-Domínguez, E., Cardelús, C., Pinhassi, J., Sala, M. M., Lekunberri, I., Balagué, V., Vila-Costa, M., Unrein, F., Massana, R., Simó, R., and Gasol, J. M.: Factors Controlling the Year-Round Variability in Carbon Flux Through Bacteria in a Coastal Marine System, Ecosystems, 11, 397–409, https://doi.org/10.1007/s10021-008-9129-0, 2008.

Aluwihare, L. I. and Repeta, D. J.: A comparison of the chemical characteristics of oceanic DOM and extracellular DOM produced by marine algae, Marine Ecology Progress Series, 186, 105–117, https://doi.org/10.3354/meps186105, 1999.

Amin, S. A., Green, D. H., Hart, M. C., Küpper, F. C., Sunda, W. G., and Carrano, C. J.: Photolysis of iron–siderophore chelates promotes bacterial–algal mutualism, Proceedings of the National Academy of Sciences, 106, 17071–17076, https://doi.org/10.1073/pnas.0905512106, 2009.

Aminot, A. and Kérouel, R.: Dissolved organic carbon, nitrogen and phosphorus in the N-E Atlantic and the N-W Mediterranean with particular reference to non-refractory fractions and degradation, Deep Sea Research Part I: Oceanographic Research Papers, 51, 1975–1999, https://doi.org/10.1016/j.dsr.2004.07.016, 2004.

Amon, R. M. W. and Benner, R.: Rapid cycling of high-molecular-weight dissolved organic matter in the ocean, Nature, 369, 549–552, https://doi.org/10.1038/369549a0, 1994.

Amon, R. M. W. and Benner, R.: Bacterial utilization of different size classes of dissolved organic matter, Limnology and Oceanography, 41, 41–51, https://doi.org/10.4319/lo.1996.41.1.0041, 1996.

Anderson, T. R. and Pondaven, P.: Non-Redfield carbon and nitrogen cycling in the Sargasso Sea: Pelagic imbalances and export flux, Deep-Sea Research Part I: Oceanographic Research Papers, 50, 573–591, https://doi.org/10.1016/S0967-0637(03)00034-7, 2003.

Antia, N. J., Harrison, P. J., and Oliveira, L.: The role of dissolved organic nitrogen in phytoplankton nutrition, cell biology and ecology, Phycologia, 30, 1–89, https://doi.org/10.2216/i0031-8884-30-1-1.1, 1991.

Armin, G. and Inomura, K.: Modeled temperature dependencies of macromolecular allocation and elemental stoichiometry in phytoplankton, Computational and Structural Biotechnology Journal, 19, 5421–5427, https://doi.org/10.1016/j.csbj.2021.09.028, 2021.

Arndt, S., Jørgensen, B. B., LaRowe, D. E., Middelburg, J. J., Pancost, R. D., and Regnier, P.: Quantifying the degradation of organic matter in marine sediments: A review and synthesis, Earth-Science Reviews, 123, 53–86, https://doi.org/10.1016/j.earscirev.2013.02.008, 2013.

Arnosti, C.: Microbial Extracellular Enzymes and the Marine Carbon Cycle, Annual Review of Marine Science, 3, 401–425, https://doi.org/10.1146/annurev-marine-120709-142731, 2011.

Arnosti, C., Reintjes, G., and Amann, R.: A mechanistic microbial underpinning for the size-reactivity continuum of dissolved organic carbon degradation, Marine Chemistry, 206, 93–99, https://doi.org/10.1016/j.marchem.2018.09.008, 2018.

Arnosti, C., Wietz, M., Brinkhoff, T., Hehemann, J.-H., Probandt, D., Zeugner, L., and Amann, R.: The Biogeochemistry of Marine Polysaccharides: Sources, Inventories, and Bacterial Drivers of the Carbohydrate Cycle, Annual Review of Marine Science, 13, 81–108, https://doi.org/10.1146/annurev-marine-032020-012810, 2021.

Azam, F.: Microbial Control of Oceanic Carbon Flux: The Plot Thickens, Science, 280, 694–696, https://doi.org/10.1126/science.280.5364.694, 1998.

Azam, F. and Malfatti, F.: Microbial structuring of marine ecosystems, Nat Rev Microbiol, 5, 782–791, https://doi.org/10.1038/nrmicro1747, 2007.

Azam, F., Fenchel, T., Field, J., Gray, J., Meyer-Reil, L., and Thingstad, F.: The Ecological Role of Water-Column Microbes in the Sea, Mar. Ecol. Prog. Ser., 10, 257–263, https://doi.org/10.3354/meps010257, 1983.

Azam, F., Smith, D. C., Steward, G. F., and Hagström, Å.: Bacteria-organic matter coupling and its significance for oceanic carbon cycling, Microb Ecol, 28, 167–179, https://doi.org/10.1007/BF00166806, 1994.

Baines, S. B. and Pace, M. L.: The production of dissolved organic matter by phytoplankton and its importance to bacteria: Patterns across marine and freshwater systems, Limnology and Oceanography, 36, 1078–1090, https://doi.org/10.4319/lo.1991.36.6.1078, 1991.

Baltar, F., Alvarez-Salgado, X. A., Arístegui, J., Benner, R., Hansell, D. A., Herndl, G. J., and Lønborg, C.: What Is Refractory Organic Matter in the Ocean?, Frontiers in Marine Science, 8, 642637, https://doi.org/10.3389/fmars.2021.642637, 2021.

Bao, H., Niggemann, J., Luo, L., Dittmar, T., and Kao, S.-J.: Aerosols as a source of dissolved black carbon to the ocean, Nat Commun, 8, 510, https://doi.org/10.1038/s41467-017-00437-3, 2017.

Bar-On, Y. M. and Milo, R.: The Biomass Composition of the Oceans: A Blueprint of Our Blue Planet, Cell, 179, 1451–1454, https://doi.org/10.1016/j.cell.2019.11.018, 2019.

Bar-On, Y. M., Phillips, R., and Milo, R.: The biomass distribution on Earth, Proceedings of the National Academy of Sciences, 115, 6506–6511, https://doi.org/10.1073/pnas.1711842115, 2018.

Bart, M. C., Mueller, B., Rombouts, T., van de Ven, C., Tompkins, G. J., Osinga, R., Brussaard, C. P. D., MacDonald, B., Engel, A., Rapp, H. T., and de Goeij, J. M.: Dissolved organic carbon (DOC) is essential to balance the metabolic demands of four dominant North-Atlantic deep-sea sponges, Limnology and Oceanography, 66, 925–938, https://doi.org/10.1002/lno.11652, 2021.

Bauer, J., Williams, P., and Druffel, E.: C-14 activity of dissolved organic carbon fractions in the North Central Pacific and Sargasso Sea, Nature, 357, 667–670, https://doi.org/10.1038/357667a0, 1992.

Bauer, J. E., Cai, W.-J., Raymond, P. A., Bianchi, T. S., Hopkinson, C. S., and Regnier, P. A. G.: The changing carbon cycle of the coastal ocean, Nature, 504, 61–70, https://doi.org/10.1038/nature12857, 2013.

Bayer, B., McBeain, K., Carlson, C. A., and Santoro, A. E.: Carbon content, carbon fixation yield, and dissolved organic carbon release from diverse marine nitrifiers, Limnology and Oceanography, 68, 84–96, https://doi.org/10.1002/lno.12252, 2023.

Beaupré, S. R., Kieber, D. J., Keene, W. C., Long, M. S., Maben, J. R., Lu, X., Zhu, Y., Frossard, A. A., Kinsey, J. D., Duplessis, P., Chang, R. Y.-W., and Bisgrove, J.: Oceanic efflux of ancient marine dissolved organic carbon in primary marine aerosol, Science Advances, 5, eaax6535, https://doi.org/10.1126/sciadv.aax6535, 2019.

Bell, J. B., Woulds, C., and Oevelen, D. van: Hydrothermal activity, functional diversity and chemoautotrophy are major drivers of seafloor carbon cycling, Sci Rep, 7, 12025, https://doi.org/10.1038/s41598-017-12291-w, 2017.

Benedetti, F., Vogt, M., Elizondo, U. H., Righetti, D., Zimmermann, N. E., and Gruber, N.: Major restructuring of marine plankton assemblages under global warming, Nat Commun, 12, 5226, https://doi.org/10.1038/s41467-021-25385-x, 2021.

Berggren, M., Guillemette, F., Bieroza, M., Buffam, I., Deininger, A., Hawkes, J. A., Kothawala, D. N., LaBrie, R., Lapierre, J.-F., Murphy, K. R., Al-Kharusi, E. S., Rulli, M. P. D., Hensgens, G., Younes, H., and Wünsch, U. J.: Unified understanding of intrinsic and extrinsic controls of dissolved organic carbon reactivity in aquatic ecosystems, Ecology, 103, e3763, https://doi.org/10.1002/ecy.3763, 2022.

Bertilsson, S., Berglund, O., Karl, D. M., and Chisholm, S. W.: Elemental composition of marine Prochlorococcus and Synechococcus: Implications for the ecological stoichiometry of the sea, Limnology and Oceanography, 48, 1721–1731, https://doi.org/10.4319/lo.2003.48.5.1721, 2003.

Bianchi, T. S.: The role of terrestrially derived organic carbon in the coastal ocean: A changing paradigm and the priming effect, Proceedings of the National Academy of Sciences, 108, 19473–19481, https://doi.org/10.1073/pnas.1017982108, 2011.

Bianchi, T. S., Aller, R. C., Atwood, T. B., Brown, C. J., Buatois, L. A., Levin, L. A., Levinton, J. S., Middelburg, J. J., Morrison, E. S., Regnier, P., Shields, M. R., Snelgrove, P. V. R., Sotka, E. E., and Stanley, R. R. E.: What global biogeochemical consequences will marine animal–sediment interactions have during climate change?, Elementa: Science of the Anthropocene, 9, 00180, https://doi.org/10.1525/elementa.2020.00180, 2021.

Bidle, K. D.: Programmed Cell Death in Unicellular Phytoplankton, Current Biology, 26, R594–R607, https://doi.org/10.1016/j.cub.2016.05.056, 2016.

Biermann, A., Lewandowska, A. M., Engel, A., and Riebesell, U.: Organic matter partitioning and stoichiometry in response to rising water temperature and copepod grazing, Marine Ecology Progress Series, 522, 49–65, https://doi.org/10.3354/meps11148, 2015.

Bonachela, J. A., Allison, S. D., Martiny, A. C., and Levin, S. A.: A model for variable phytoplankton stoichiometry based on cell protein regulation, Biogeosciences, 10, 4341–4356, https://doi.org/10.5194/bg-10-4341-2013, 2013.

Borchard, C. and Engel, A.: Organic matter exudation by Emiliania huxleyi under simulated future ocean conditions, Biogeosciences, 9, 3405–3423, https://doi.org/10.5194/bg-9-3405-2012, 2012.

Børsheim, K. Y., Vadstein, O., Myklestad, S. M., Reinertsen, H., Kirkvold, S., and Olsen, Y.: Photosynthetic algal production, accumulation and release of phytoplankton storage carbohydrates and bacterial production in a gradient in daily nutrient supply, Journal of Plankton Research, 27, 743–755, https://doi.org/10.1093/plankt/fbi047, 2005.

Boyd, P. W. and Trull, T. W.: Understanding the export of biogenic particles in oceanic waters: Is there consensus?, Progress in Oceanography, 72, 276–312, https://doi.org/10.1016/j.pocean.2006.10.007, 2007.

Bramucci, A. R. and Case, R. J.: Phaeobacter inhibens induces apoptosis-like programmed cell death in calcifying Emiliania huxleyi, Sci Rep, 9, 5215, https://doi.org/10.1038/s41598-018-36847-6, 2019.

Breyer, E. and Baltar, F.: The largely neglected ecological role of oceanic pelagic fungi, Trends in Ecology & Evolution, 38, 870–888, https://doi.org/10.1016/j.tree.2023.05.002, 2023.

Buesseler, K. O.: The decoupling of production and particulate export in the surface ocean, Global Biogeochemical Cycles, 12, 297–310, https://doi.org/10.1029/97GB03366, 1998.

Buesseler, K. O. and Boyd, P. W.: Shedding light on processes that control particle export and flux attenuation in the twilight zone of the open ocean, Limnology and Oceanography, 54, 1210–1232, https://doi.org/10.4319/lo.2009.54.4.1210, 2009.

Buesseler, K. O., Boyd, P. W., Black, E. E., and Siegel, D. A.: Metrics that matter for assessing the ocean biological carbon pump, Proceedings of the National Academy of Sciences, 117, 9679–9687, https://doi.org/10.1073/pnas.1918114117, 2020.

Burkhardt, S., Zondervan, I., and Riebesell, U.: Effect of CO2 concentration on C:N:P ratio in marine phytoplankton: A species comparison, Limnology and Oceanography, 44, 683–690, https://doi.org/10.4319/lo.1999.44.3.0683, 1999.

Butenschön, M., Clark, J., Aldridge, J. N., Allen, J. I., Artioli, Y., Blackford, J., Bruggeman, J., Cazenave, P., Ciavatta, S., Kay, S., Lessin, G., Leeuwen, S. V., Molen, J. V. D., Mora, L. D., Polimene, L., Sailley, S., Stephens, N., and Torres, R.: ERSEM 15.06: A generic model for marine biogeochemistry and the ecosystem dynamics of the lower trophic levels, Geoscientific Model Development, 9, 1293–1339, https://doi.org/10.5194/gmd-9-1293-2016, 2016.

Cael, B. B., Dutkiewicz, S., and Henson, S.: Abrupt shifts in 21st-century plankton communities, Science Advances, 7, eabf8593, https://doi.org/10.1126/sciadv.abf8593, 2021.

Cai, R. and Jiao, N.: Recalcitrant dissolved organic matter and its major production and removal processes in the ocean, Deep Sea Research Part I: Oceanographic Research Papers, 191, 103922, https://doi.org/10.1016/j.dsr.2022.103922, 2023.

Cai, R., Zhou, W., He, C., Tang, K., Guo, W., Shi, Q., Gonsior, M., and Jiao, N.: Microbial Processing of Sediment-Derived Dissolved Organic Matter: Implications for Its Subsequent Biogeochemical Cycling in Overlying Seawater, Journal of Geophysical Research: Biogeosciences, 124, 3479–3490, https://doi.org/10.1029/2019JG005212, 2019.

Canuel, E. A., Cammer, S. S., McIntosh, H. A., and Pondell, C. R.: Climate change impacts on the organic carbon cycle at the land-ocean interface, Annual Review of Earth and Planetary Sciences, 40, 685–711, https://doi.org/10.1146/annurev-earth-042711-105511, 2012.

Carlson, C. A., Ducklow, H. W., and Michaels, A. F.: Annual flux of dissolved organic carbon from the euphotic zone in the northwestern Sargasso Sea, Nature, 371, 405–408, https://doi.org/10.1038/371405a0, 1994.

Carlson, C. A., Del Giorgio, P. A., and Herndl, G. J.: Microbes and the Dissipation of Energy and Respiration: From Cells to Ecosystems, Oceanography, 20, 89–100, https://doi.org/10.5670/oceanog.2007.52, 2007.

Carlson, C. A., Liu, S., Stephens, B. M., and English, C. J.: Chapter 5 - DOM production, removal, and transformation processes in marine systems, in: Biogeochemistry of Marine Dissolved Organic Matter (Third Edition), edited by: Hansell, D. A. and Carlson, C. A., Academic Press, 137–246, https://doi.org/10.1016/B978-0-443-13858-4.00013-7, 2024.

Caron, D. A., Goldman, J. C., Andersen, O. K., and Dennett, M. R.: Nutrient cycling in a microflagellate food chain: II. Population dynamics and carbon cycling, Marine Ecology Progress Series, 24, 243–254, https://doi.org/10.3354/meps024243, 1985.

Carr, M.-E., Friedrichs, M. A. M., Schmeltz, M., Noguchi Aita, M., Antoine, D., Arrigo, K. R., Asanuma, I., Aumont, O., Barber, R., Behrenfeld, M., Bidigare, R., Buitenhuis, E. T., Campbell, J., Ciotti, A., Dierssen, H., Dowell, M., Dunne, J., Esaias, W., Gentili, B., Gregg, W., Groom, S., Hoepffner, N., Ishizaka, J., Kameda, T., Le Quéré, C., Lohrenz, S., Marra, J., Mélin, F., Moore, K., Morel, A., Reddy, T. E., Ryan, J., Scardi, M., Smyth, T., Turpie, K., Tilstone, G., Waters, K., and Yamanaka, Y.: A comparison of global estimates of marine primary production from ocean color, Deep Sea Research Part II: Topical Studies in Oceanography, 53, 741–770, https://doi.org/10.1016/j.dsr2.2006.01.028, 2006.

Chaichana, S., Jickells, T., and Johnson, M.: Distribution and C/N stoichiometry of dissolved organic matter in the North Sea in summer 2011-12, Biogeosciences Discuss, 1–33, https://doi.org/10.5194/bg-2017-387, 2017.

Chaichana, S., Jickells, T., and Johnson, M.: Interannual variability in the summer dissolved organic matter inventory of the North Sea: Implications for the continental shelf pump, Biogeosciences, 16, 1073–1096, https://doi.org/10.5194/bg-16-1073-2019, 2019.

Chan, L.-K., Newton, R. J., Sharma, S., Smith, C. B., Rayapati, P., Limardo, A. J., Meile, C., and Moran, M. A.: Transcriptional Changes Underlying Elemental Stoichiometry Shifts in a Marine Heterotrophic Bacterium, Front. Microbiol., 3, 159, https://doi.org/10.3389/fmicb.2012.00159, 2012.

Chen, Y.-Y., Edgar, G. J., and Fox, R. J.: The Nature and Ecological Significance of Epifaunal Communities within Marine Ecosystems, in: Oceanography and Marine Biology, CRC Press, 2021.

Chien, C.-T., Pahlow, M., Schartau, M., Li, N., and Oschlies, A.: Effects of phytoplankton physiology on global ocean biogeochemistry and climate, Science Advances, 9, eadg1725, https://doi.org/10.1126/sciadv.adg1725, 2023.

Church, M. J.: Resource Control of Bacterial Dynamics in the Sea, in: Microbial Ecology of the Oceans, John Wiley & Sons, Ltd, 335–382, https://doi.org/10.1002/9780470281840.ch10, 2008.

Church, M. J., Ducklow, H. W., and Karl, D. M.: Multiyear increases in dissolved organic matter inventories at Station ALOHA in the North Pacific Subtropical Gyre, Limnology and Oceanography, 47, 1–10, https://doi.org/10.4319/lo.2002.47.1.0001, 2002.

Clarke, A.: Ecological stoichiometry in six species of Antarctic marine benthos, Marine Ecology Progress Series, 369, 25–37, https://doi.org/10.3354/meps07670, 2008.

Conan, P., Søndergaard, M., Kragh, T., Thingstad, F., Pujo-Pay, M., Williams, P. J. le B., Markager, S., Cauwet, G., Borch, N. H., Evans, D., and Riemann, B.: Partitioning of organic production in marine plankton communities: The effects of

inorganic nutrient ratios and community composition on new dissolved organic matter, Limnology and Oceanography, 52, 753–765, https://doi.org/10.4319/lo.2007.52.2.0753, 2007.

Connolly, C. T., Cardenas, M. B., Burkart, G. A., Spencer, R. G. M., and McClelland, J. W.: Groundwater as a major source of dissolved organic matter to Arctic coastal waters, Nat Commun, 11, 1479, https://doi.org/10.1038/s41467-020-15250-8, 2020.

Conte, L., Szopa, S., Aumont, O., Gros, V., and Bopp, L.: Sources and Sinks of Isoprene in the Global Open Ocean: Simulated Patterns and Emissions to the Atmosphere, Journal of Geophysical Research: Oceans, 125, e2019JC015946, https://doi.org/10.1029/2019JC015946, 2020.

Coppola, A. I., Ziolkowski, L. A., Masiello, C. A., and Druffel, E. R. M.: Aged black carbon in marine sediments and sinking particles, Geophysical Research Letters, 41, 2427–2433, https://doi.org/10.1002/2013GL059068, 2014.

Creed, I. F., Bergström, A.-K., Trick, C. G., Grimm, N. B., Hessen, D. O., Karlsson, J., Kidd, K. A., Kritzberg, E., McKnight, D. M., Freeman, E. C., Senar, O. E., Andersson, A., Ask, J., Berggren, M., Cherif, M., Giesler, R., Hotchkiss, E. R., Kortelainen, P., Palta, M. M., Vrede, T., and Weyhenmeyer, G. A.: Global change-driven effects on dissolved organic matter composition: Implications for food webs of northern lakes, Global Change Biology, 24, 3692–3714, https://doi.org/10.1111/gcb.14129, 2018.

Dai, M., Su, J., Zhao, Y., Hofmann, E. E., Cao, Z., Cai, W.-J., Gan, J., Lacroix, F., Laruelle, G. G., Meng, F., Müller, J. D., Regnier, P. A. G., Wang, G., and Wang, Z.: Carbon Fluxes in the Coastal Ocean: Synthesis, Boundary Processes, and Future Trends, Annu. Rev. Earth Planet. Sci., 50, 593–626, https://doi.org/10.1146/annurev-earth-032320-090746, 2022.

Davis, C. E., Mahaffey, C., Wolff, G. A., and Sharples, J.: A storm in a shelf sea: Variation in phosphorus distribution and organic matter stoichiometry, Geophysical Research Letters, 41, 8452–8459, https://doi.org/10.1002/2014GL061949, 2014.

Davis, C. E., Blackbird, S., Wolff, G., Woodward, M., and Mahaffey, C.: Seasonal organic matter dynamics in a temperate shelf sea, Progress in Oceanography, 177, 101925, https://doi.org/10.1016/j.pocean.2018.02.021, 2019.

De La Rocha, C. L. and Passow, U.: Factors influencing the sinking of POC and the efficiency of the biological carbon pump, Deep Sea Research Part II: Topical Studies in Oceanography, 54, 639–658, https://doi.org/10.1016/j.dsr2.2007.01.004, 2007.

Demir, K. T., Mathis, M., Kossack, J., Liu, F., Daewel, U., Stegert, C., Thomas, H., and Schrum, C.: Organic matter stoichiometry regulates the continental shelf carbon pump efficiency of the northwest European shelf seas, ESS Open Archive [Preprint], https://doi.org/10.22541/essoar.175088438.85557149/v1, 2025a.

Demir, K. T., Mathis, M., Kossack, J., Liu, F., Daewel, U., Stegert, C., Thomas, H., and Schrum, C.: Variable organic matter stoichiometry enhances the biological drawdown of CO_2 in the northwest European shelf seas, Biogeosciences, 22, 2569–2599, https://doi.org/10.5194/bg-22-2569-2025, 2025b.

DeVries, T. and Primeau, F.: Dynamically and Observationally Constrained Estimates of Water-Mass Distributions and Ages in the Global Ocean, 41, 2381–2409, https://doi.org/10.1175/JPO-D-10-05011.1, 2011.

DeVries, T. and Weber, T.: The export and fate of organic matter in the ocean: New constraints from combining satellite and oceanographic tracer observations, Global Biogeochemical Cycles, 31, 535–555, https://doi.org/10.1002/2016GB005551, 2017.

Dittmar, T. and Kattner, G.: The biogeochemistry of the river and shelf ecosystem of the Arctic Ocean: a review, Marine Chemistry, 83, 103–120, https://doi.org/10.1016/s0304-4203(03)00105-1, 2003.

Dittmar, T. and Lennartz, S. T.: Chapter 13 - Reasons behind the long-term stability of dissolved organic matter, in: Biogeochemistry of Marine Dissolved Organic Matter (Third Edition), edited by: Hansell, D. A. and Carlson, C. A., Academic Press, 613–655, https://doi.org/10.1016/B978-0-443-13858-4.00006-X, 2024.

Dittmar, T. and Paeng, J.: A heat-induced molecular signature in marine dissolved organic matter, Nature Geosci, 2, 175–179, https://doi.org/10.1038/ngeo440, 2009.

Dittmar, T., Lennartz, S. T., Buck-Wiese, H., Hansell, D. A., Santinelli, C., Vanni, C., Blasius, B., and Hehemann, J.-H.: Enigmatic persistence of dissolved organic matter in the ocean, Nat Rev Earth Environ, 2, 570–583, https://doi.org/10.1038/s43017-021-00183-7, 2021.

Doney, S. C., Ruckelshaus, M., Duffy, J. E., Barry, J. P., Chan, F., English, C. A., Galindo, H. M., Grebmeier, J. M., Hollowed, A. B., Knowlton, N., Polovina, J., Rabalais, N. N., Sydeman, W. J., and Talley, L. D.: Climate Change Impacts on Marine Ecosystems, Annual Review of Marine Science, 4, 11–37, https://doi.org/10.1146/annurev-marine-041911-111611, 2012.

Doval, M. D., Pérez, F. F., and Berdalet, E.: Dissolved and particulate organic carbon and nitrogen in the Northwestern Mediterranean, Deep Sea Research Part I: Oceanographic Research Papers, 46, 511–527, https://doi.org/10.1016/S0967-0637(98)00072-7, 1999.

Druffel, E. R. M. and Williams, P. M.: Identification of a deep marine source of particulate organic carbon using bomb 14C, Nature, 347, 172–174, https://doi.org/10.1038/347172a0, 1990.

Druffel, E. R. M., Bauer, J. E., Williams, P. M., Griffin, S., and Wolgast, D.: Seasonal variability of particulate organic radiocarbon in the northeast Pacific Ocean, Journal of Geophysical Research: Oceans, 101, 20543–20552, https://doi.org/10.1029/96JC01850, 1996.

Duarte, C. M.: Reviews and syntheses: Hidden forests, the role of vegetated coastal habitats in the ocean carbon budget, Biogeosciences, 14, 301–310, https://doi.org/10.5194/bg-14-301-2017, 2017.

Duarte, C. M., Gattuso, J.-P., Hancke, K., Gundersen, H., Filbee-Dexter, K., Pedersen, M. F., Middelburg, J. J., Burrows, M. T., Krumhansl, K. A., Wernberg, T., Moore, P., Pessarrodona, A., Ørberg, S. B., Pinto, I. S., Assis, J., Queirós, A. M., Smale, D. A., Bekkby, T., Serrão, E. A., and Krause-Jensen, D.: Global estimates of the extent and production of macroalgal forests, Global Ecology and Biogeography, 31, 1422–1439, https://doi.org/10.1111/geb.13515, 2022.

Ducklow, H. W., Purdie, D. A., Williams, P. J. LeB., and Davies, J. M.: Bacterioplankton: A Sink for Carbon in a Coastal Marine Plankton Community, Science, 232, 865–867, https://doi.org/10.1126/science.232.4752.865, 1986.

Dunne, J. P., Armstrong, R. A., Gnanadesikan, A., and Sarmiento, J. L.: Empirical and mechanistic models for the particle export ratio, Global Biogeochemical Cycles, 19, GB4026, https://doi.org/10.1029/2004GB002390, 2005.

Edwards, K. F.: Mixotrophy in nanoflagellates across environmental gradients in the ocean, Proceedings of the National Academy of Sciences, 116, 6211–6220, https://doi.org/10.1073/pnas.1814860116, 2019.

Eigaard, O. R., Bastardie, F., Hintzen, N. T., Buhl-Mortensen, L., Buhl-Mortensen, P., Catarino, R., Dinesen, G. E., Egekvist, J., Fock, H. O., Geitner, K., Gerritsen, H. D., González, M. M., Jonsson, P., Kavadas, S., Laffargue, P., Lundy, M., Gonzalez-Mirelis, G., Nielsen, J. R., Papadopoulou, N., Posen, P. E., Pulcinella, J., Russo, T., Sala, A., Silva, C., Smith, C.

J., Vanelslander, B., and Rijnsdorp, A. D.: The footprint of bottom trawling in European waters: distribution, intensity, and seabed integrity, ICES Journal of Marine Science, 74, 847–865, https://doi.org/10.1093/icesjms/fsw194, 2017.

Eigemann, F., Rahav, E., Grossart, H.-P., Aharonovich, D., Sher, D., Vogts, A., and Voss, M.: Phytoplankton exudates provide full nutrition to a subset of accompanying heterotrophic bacteria via carbon, nitrogen and phosphorus allocation, 24, 2467–248, https://doi.org/10.1111/1462-2920.15933, 2022.

Elser, J. J. and Hassett, R. P.: A stoichiometric analysis of the zooplankton–phytoplankton interaction in marine and freshwater ecosystems, Nature, 370, 211–213, https://doi.org/10.1038/370211a0, 1994.

Elser, J. J. and Urabe, J.: The Stoichiometry of Consumer-Driven Nutrient Recycling: Theory, Observations, and Consequences, Ecology, 80, 735–751, https://doi.org/10.1890/0012-9658(1999)080%255B0735:TSOCDN%255D2.0.CO;2, 1999.

Emerson, S. and Hedges, J.: 6.11 - Sediment Diagenesis and Benthic Flux, in: Treatise on Geochemistry, edited by: Holland, H. D. and Turekian, K. K., Pergamon, Oxford, 293–319, https://doi.org/10.1016/B0-08-043751-6/06112-0, 2003.

Engel, A.: Direct relationship between CO2 uptake and transparent exopolymer particles production in natural phytoplankton, Journal of Plankton Research, 24, 49–53, https://doi.org/10.1093/plankt/24.1.49, 2002.

Engel, A., Händel, N., Wohlers, J., Lunau, M., Grossart, H.-P., Sommer, U., and Riebesell, U.: Effects of sea surface warming on the production and composition of dissolved organic matter during phytoplankton blooms: results from a mesocosm study, Journal of Plankton Research, 33, 357–372, https://doi.org/10.1093/plankt/fbq122, 2011.

Engel, A., Endres, S., Galgani, L., and Schartau, M.: Marvelous Marine Microgels: On the Distribution and Impact of Gel-Like Particles in the Oceanic Water-Column, Front. Mar. Sci., 7, 405, https://doi.org/10.3389/fmars.2020.00405, 2020.

Fagerbakke, K. M., Heldal, M., and Norland, S.: Content of carbon, nitrogen, oxygen, sulfur and phosphorus in native aquatic and cultured bacteria, Aquatic Microbial Ecology, 10, 15–27, https://doi.org/10.3354/ame010015, 1996.

Fernández-González, C., Tarran, G. A., Schuback, N., Woodward, E. M. S., Arístegui, J., and Marañón, E.: Phytoplankton responses to changing temperature and nutrient availability are consistent across the tropical and subtropical Atlantic, Commun Biol, 5, 1–13, https://doi.org/10.1038/s42003-022-03971-z, 2022.

Field, C. B., Behrenfeld, M. J., Randerson, J. T., and Falkowski, P.: Primary Production of the Biosphere: Integrating Terrestrial and Oceanic Components, Science, 281, 237–240, https://doi.org/10.1126/science.281.5374.237, 1998.

Fillman, N., Schmittner, A., and Kvale, K. F.: Variable Stoichiometry Effects on Glacial/Interglacial Ocean Model Biogeochemical Cycles and Carbon Storage, ESS Open Archive [Preprint] (Submitted), 2023.

Finkel, Z. V., Quigg, A., Raven, J. A., Reinfelder, J. R., Schofield, O. E., and Falkowski, P. G.: Irradiance and the elemental stoichiometry of marine phytoplankton, Limnology and Oceanography, 51, 2690–2701, https://doi.org/10.4319/lo.2006.51.6.2690, 2006.

Finkel, Z. V., Beardall, J., Flynn, K. J., Quigg, A., Rees, T. A. V., and Raven, J. A.: Phytoplankton in a changing world: cell size and elemental stoichiometry, Journal of Plankton Research, 32, 119–137, https://doi.org/10.1093/plankt/fbp098, 2010.

Fitzsimons, M. F., Probert, I., Gaillard, F., and Rees, A. P.: Dissolved organic phosphorus uptake by marine phytoplankton is enhanced by the presence of dissolved organic nitrogen, Journal of Experimental Marine Biology and Ecology, 530–531, 151434, https://doi.org/10.1016/j.jembe.2020.151434, 2020.

Flanjak, L., Wienkers, A., and Laufkötter, C.: Dissolved organic carbon dynamics in a changing ocean: A COBALTv2–ESM2M coupled model analysis, EGUsphere, 1–27, https://doi.org/10.5194/egusphere-2025-1639, 2025.

Flynn, K. J., Raven, J. A., Rees, T. A. V., Finkel, Z., Quigg, A., and Beardall, J.: Is the Growth Rate Hypothesis Applicable to Microalgae?, Journal of Phycology, 46, 1–12, https://doi.org/10.1111/j.1529-8817.2009.00756.x, 2010.

Fox, J., Behrenfeld, M. J., Halsey, K. H., and Graff, J. R.: Global Estimates of Particulate Organic Carbon Concentration From the Surface Ocean to the Base of the Mesopelagic, Global Biogeochemical Cycles, 38, e2024GB008149, https://doi.org/10.1029/2024GB008149, 2024.

Franklin, D. J., Brussaard, C. P. D., and Berges, J. A.: What is the role and nature of programmed cell death in phytoplankton ecology?, European Journal of Phycology, 41, 1–14, https://doi.org/10.1080/09670260500505433, 2006.

Fransner, F., Gustafsson, E., Tedesco, L., Vichi, M., Hordoir, R., Roquet, F., Spilling, K., Kuznetsov, I., Eilola, K., Mörth, C. M., Humborg, C., and Nycander, J.: Non-Redfieldian Dynamics Explain Seasonal pCO2 Drawdown in the Gulf of Bothnia, Journal of Geophysical Research: Oceans, 123, 166–188, https://doi.org/10.1002/2017JC013019, 2018.

Friedlingstein, P., O'Sullivan, M., Jones, M. W., Andrew, R. M., Hauck, J., Landschützer, P., Le Quéré, C., Li, H., Luijkx, I. T., Olsen, A., Peters, G. P., Peters, W., Pongratz, J., Schwingshackl, C., Sitch, S., Canadell, J. G., Ciais, P., Jackson, R. B., Alin, S. R., Arneth, A., Arora, V., Bates, N. R., Becker, M., Bellouin, N., Berghoff, C. F., Bittig, H. C., Bopp, L., Cadule, P., Campbell, K., Chamberlain, M. A., Chandra, N., Chevallier, F., Chini, L. P., Colligan, T., Decayeux, J., Djeutchouang, L. M., Dou, X., Duran Rojas, C., Enyo, K., Evans, W., Fay, A. R., Feely, R. A., Ford, D. J., Foster, A., Gasser, T., Gehlen, M., Gkritzalis, T., Grassi, G., Gregor, L., Gruber, N., Gürses, Ö., Harris, I., Hefner, M., Heinke, J., Hurtt, G. C., Iida, Y., Ilyina, T., Jacobson, A. R., Jain, A. K., Jarníková, T., Jersild, A., Jiang, F., Jin, Z., Kato, E., Keeling, R. F., Klein Goldewijk, K., Knauer, J., Korsbakken, J. I., Lan, X., Lauvset, S. K., Lefèvre, N., Liu, Z., Liu, J., Ma, L., Maksyutov, S., Marland, G., Mayot, N., McGuire, P. C., Metzl, N., Monacci, N. M., Morgan, E. J., Nakaoka, S.-I., Neill, C., Niwa, Y., Nützel, T., Olivier, L., Ono, T., Palmer, P. I., Pierrot, D., Qin, Z., Resplandy, L., Roobaert, A., Rosan, T. M., Rödenbeck, C., Schwinger, J., Smallman, T. L., Smith, S. M., Sospedra-Alfonso, R., Steinhoff, T., et al.: Global Carbon Budget 2024, Earth System Science Data, 17, 965–1039, https://doi.org/10.5194/essd-17-965-2025, 2025.

Frigstad, H., Andersen, T., Hessen, D. O., Naustvoll, L.-J., Johnsen, T. M., and Bellerby, R. G. J.: Seasonal variation in marine C:N:P stoichiometry: can the composition of seston explain stable Redfield ratios?, Biogeosciences, 8, 2917–2933, https://doi.org/10.5194/bg-8-2917-2011, 2011.

Frigstad, H., Andersen, T., Hessen, D. O., Jeansson, E., Skogen, M., Naustvoll, L.-J., Miles, M. W., Johannessen, T., and Bellerby, R. G. J.: Long-term trends in carbon, nutrients and stoichiometry in Norwegian coastal waters: Evidence of a regime shift, Progress in Oceanography, 111, 113–124, https://doi.org/10.1016/j.pocean.2013.01.006, 2013.

Galbraith, E. D. and Martiny, A. C.: A simple nutrient-dependence mechanism for predicting the stoichiometry of marine ecosystems, Proceedings of the National Academy of Sciences, 112, 8199–8204, https://doi.org/10.1073/pnas.1423917112, 2015.

Garcia, C. A., Baer, S. E., Garcia, N. S., Rauschenberg, S., Twining, B. S., Lomas, M. W., and Martiny, A. C.: Nutrient supply controls particulate elemental concentrations and ratios in the low latitude eastern Indian Ocean, Nat Commun, 9, 4868, https://doi.org/10.1038/s41467-018-06892-w, 2018a.

Garcia, N. S., Bonachela, J. A., and Martiny, A. C.: Interactions between growth-dependent changes in cell size, nutrient supply and cellular elemental stoichiometry of marine Synechococcus, The ISME Journal, 10, 2715–2724, https://doi.org/10.1038/ismej.2016.50, 2016.

Garcia, N. S., Sexton, J., Riggins, T., Brown, J., Lomas, M. W., and Martiny, A. C.: High Variability in Cellular Stoichiometry of Carbon, Nitrogen, and Phosphorus Within Classes of Marine Eukaryotic Phytoplankton Under Sufficient Nutrient Conditions, Front. Microbiol., 9, 543, https://doi.org/10.3389/fmicb.2018.00543, 2018b.

Geider, R. and La Roche, J.: Redfield revisited: variability of C:N:P in marine microalgae and its biochemical basis, European Journal of Phycology, 37, 1–17, https://doi.org/10.1017/S0967026201003456, 2002.

Giering, S. L. C., Sanders, R., Lampitt, R. S., Anderson, T. R., Tamburini, C., Boutrif, M., Zubkov, M. V., Marsay, C. M., Henson, S. A., Saw, K., Cook, K., and Mayor, D. J.: Reconciliation of the carbon budget in the ocean's twilight zone, Nature, 507, 480–483, https://doi.org/10.1038/nature13123, 2014.

del Giorgio, P. A. and Cole, J. J.: BACTERIAL GROWTH EFFICIENCY IN NATURAL AQUATIC SYSTEMS, Annual Review of Ecology, Evolution, and Systematics, 29, 503–541, https://doi.org/10.1146/annurev.ecolsys.29.1.503, 1998.

del Giorgio, P. A. and Duarte, C. M.: Respiration in the open ocean, Nature, 420, 379–384, https://doi.org/10.1038/nature01165, 2002.

Gloege, L., McKinley, G. A., Mouw, C. B., and Ciochetto, A. B.: Global evaluation of particulate organic carbon flux parameterizations and implications for atmospheric pCO_2, Global Biogeochemical Cycles, 31, 1192–1215, https://doi.org/10.1002/2016GB005535, 2017.

Godwin, C. M. and Cotner, J. B.: Aquatic heterotrophic bacteria have highly flexible phosphorus content and biomass stoichiometry, The ISME Journal, 9, 2324–2327, https://doi.org/10.1038/ismej.2015.34, 2015.

Goldman, J., Hansell, D., and Dennett, M.: Chemical characterization of three large oceanic diatoms: potential impact on water column chemistry, Mar. Ecol. Prog. Ser., 88, 257–270, https://doi.org/10.3354/meps088257, 1992.

Goldman, J. C., McCarthy, J. J., and Peavey, D. G.: Growth rate influence on the chemical composition of phytoplankton in oceanic waters, Nature, 279, 210–215, https://doi.org/10.1038/279210a0, 1979.

Golz, A.-L., Burian, A., and Winder, M.: Stoichiometric regulation in micro- and mesozooplankton, Journal of Plankton Research, 37, 293–305, https://doi.org/10.1093/plankt/fbu109, 2015.

Gonsior, M., Peake, B. M., Cooper, W. T., Podgorski, D., D'Andrilli, J., and Cooper, W. J.: Photochemically Induced Changes in Dissolved Organic Matter Identified by Ultrahigh Resolution Fourier Transform Ion Cyclotron Resonance Mass Spectrometry, Environ. Sci. Technol., 43, 698–703, https://doi.org/10.1021/es8022804, 2009.

Graeber, D., Tenzin, Y., Stutter, M., Weigelhofer, G., Shatwell, T., von Tümpling, W., Tittel, J., Wachholz, A., and Borchardt, D.: Bioavailable DOC: reactive nutrient ratios control heterotrophic nutrient assimilation—An experimental proof of the macronutrient-access hypothesis, Biogeochemistry, 155, 1–20, https://doi.org/10.1007/s10533-021-00809-4, 2021.

Granum, E., Kirkvold, S., and Myklestad, S. M.: Cellular and extracellular production of carbohydrates and amino acids by the marine diatom Skeletonema costatum: diel variations and effects of N depletion, Marine Ecology Progress Series, 242, 83–94, https://doi.org/10.3354/meps242083, 2002.

Hach, P. F., Marchant, H. K., Krupke, A., Riedel, T., Meier, D. V., Lavik, G., Holtappels, M., Dittmar, T., and Kuypers, M. M. M.: Rapid microbial diversification of dissolved organic matter in oceanic surface waters leads to carbon sequestration, Sci Rep, 10, 13025, https://doi.org/10.1038/s41598-020-69930-y, 2020.

Hansell, D. A.: Recalcitrant Dissolved Organic Carbon Fractions, Annual Review of Marine Science, 5, 421–445, https://doi.org/10.1146/annurev-marine-120710-100757, 2013.

Hansell, D. A. and Carlson, C. A.: Deep-ocean gradients in the concentration of dissolved organic carbon, Nature, 395, 263–266, https://doi.org/10.1038/26200, 1998a.

Hansell, D. A. and Carlson, C. A.: Net community production of dissolved organic carbon, Global Biogeochemical Cycles, 12, 443–453, https://doi.org/10.1029/98GB01928, 1998b.

Hansell, D. A., Carlson, C., Repeta, D., and Schlitzer, R.: Dissolved Organic Matter in the Ocean: A Controversy Stimulates New Insights, Oceanog., 22, 202–211, https://doi.org/10.5670/oceanog.2009.109, 2009.

Hansell, D. A., Carlson, C. A., and Schlitzer, R.: Net removal of major marine dissolved organic carbon fractions in the subsurface ocean, Global Biogeochemical Cycles, 26, 2011GB004069, https://doi.org/10.1029/2011GB004069, 2012.

Hansell, D. A., Romera-Castillo, C., and Lopez, C. N.: Chapter 17 - Dynamics of dissolved organic carbon in the global ocean, in: Biogeochemistry of Marine Dissolved Organic Matter (Third Edition), edited by: Hansell, D. A. and Carlson, C. A., Academic Press, 769–802, https://doi.org/10.1016/B978-0-443-13858-4.00004-6, 2024.

Hassett, R. P., Cardinale, B., Stabler, L. B., and Elser, J. J.: Ecological stoichiometry of N and P in pelagic ecosystems: Comparison of lakes and oceans with emphasis on the zooplankton-phytoplankton interaction, Limnology and Oceanography, 42, 648–662, https://doi.org/10.4319/lo.1997.42.4.0648, 1997.

Hawkes, J. A., Rossel, P. E., Stubbins, A., Butterfield, D., Connelly, D. P., Achterberg, E. P., Koschinsky, A., Chavagnac, V., Hansen, C. T., Bach, W., and Dittmar, T.: Efficient removal of recalcitrant deep-ocean dissolved organic matter during hydrothermal circulation, Nature Geosci, 8, 856–860, https://doi.org/10.1038/ngeo2543, 2015.

He, W., Chen, M., Schlautman, M. A., and Hur, J.: Dynamic exchanges between DOM and POM pools in coastal and inland aquatic ecosystems: A review, Science of The Total Environment, 551–552, 415–428, https://doi.org/10.1016/j.scitotenv.2016.02.031, 2016.

Henrichs, S. M.: Early Diagenesis of Organic Matter: The Dynamics (Rates) of Cycling of Organic Compounds, in: Organic Geochemistry: Principles and Applications, edited by: Engel, M. H. and Macko, S. A., Springer US, Boston, MA, 101–117, https://doi.org/10.1007/978-1-4615-2890-6_4, 1993.

Henson, S., Le Moigne, F., and Giering, S.: Drivers of Carbon Export Efficiency in the Global Ocean, Global Biogeochemical Cycles, 33, 891–903, https://doi.org/10.1029/2018GB006158, 2019.

Henson, S. A., Sanders, R., Madsen, E., Morris, P. J., Le Moigne, F., and Quartly, G. D.: A reduced estimate of the strength of the ocean's biological carbon pump, Geophysical Research Letters, 38, L04606, https://doi.org/10.1029/2011GL046735, 2011.

Henson, S. A., Sanders, R., and Madsen, E.: Global patterns in efficiency of particulate organic carbon export and transfer to the deep ocean, Global Biogeochemical Cycles, 26, GB1028, https://doi.org/10.1029/2011GB004099, 2012.

Henson, S. A., Yool, A., and Sanders, R.: Variability in efficiency of particulate organic carbon export: A model study, Global Biogeochemical Cycles, 29, 33–45, https://doi.org/10.1002/2014GB004965, 2015.

Hewson, I. and Fuhrman, J. A.: Viriobenthos Production and Virioplankton Sorptive Scavenging by Suspended Sediment Particles in Coastal and Pelagic Waters, Microb Ecol, 46, 337–347, https://doi.org/10.1007/s00248-002-1041-0, 2003.

Hildebrand, T., Osterholz, H., Bunse, C., Grotheer, H., Dittmar, T., and Schupp, P. J.: Transformation of dissolved organic matter by two Indo-Pacific sponges, Limnology and Oceanography, 67, 2483–2496, https://doi.org/10.1002/lno.12214, 2022.

Hillebrand, H., Steinert, G., Boersma, M., Malzahn, A., Meunier, C. L., Plum, C., and Ptacnik, R.: Goldman revisited: Faster-growing phytoplankton has lower N : P and lower stoichiometric flexibility, Limnology and Oceanography, 58, 2076–2088, https://doi.org/10.4319/lo.2013.58.6.2076, 2013.

Ho, T.-Y., Quigg, A., Finkel, Z. V., Milligan, A. J., Wyman, K., Falkowski, P. G., and Morel, F. M. M.: The Elemental Composition of Some Marine Phytoplankton, Journal of Phycology, 39, 1145–1159, https://doi.org/10.1111/j.0022-3646.2003.03-090.x, 2003.

Hochfeld, I. and Hinners, J.: Evolutionary adaptation to steady or changing environments affects competitive outcomes in marine phytoplankton, Limnology and Oceanography, 69, 1172–1186, https://doi.org/10.1002/lno.12559, 2024a.

Hochfeld, I. and Hinners, J.: Phytoplankton adaptation to steady or changing environments affects marine ecosystem functioning, Biogeosciences, 21, 5591–5611, https://doi.org/10.5194/bg-21-5591-2024, 2024b.

Hoikkala, L., Lahtinen, T., Perttilä, M., and Lignell, R.: Seasonal dynamics of dissolved organic matter on a coastal salinity gradient in the northern Baltic Sea, Continental Shelf Research, 45, 1–14, https://doi.org/10.1016/j.csr.2012.04.008, 2012.

Hoikkala, L., Kortelainen, P., Soinne, H., and Kuosa, H.: Dissolved organic matter in the Baltic Sea, Journal of Marine Systems, 142, 47–61, https://doi.org/10.1016/j.jmarsys.2014.10.005, 2015.

Hopkinson, C. S. and Vallino, J. J.: Efficient export of carbon to the deep ocean through dissolved organic matter, Nature, 433, 142–145, https://doi.org/10.1038/nature03191, 2005.

Hopkinson, C. S., Fry, B., and Nolin, A. L.: Stoichiometry of dissolved organic matter dynamics on the continental shelf of the northeastern U.S.A., 17, 473–489, https://doi.org/10.1016/S0278-4343(96)00046-5, 1997.

Hopkinson, C. S., Vallino, J. J., and Nolin, A.: Decomposition of dissolved organic matter from the continental margin, Deep Sea Research Part II: Topical Studies in Oceanography, 49, 4461–4478, https://doi.org/10.1016/S0967-0645(02)00125-X, 2002.

Hung, J.-J., Chen, C.-H., Gong, G.-C., Sheu, D.-D., and Shiah, F.-K.: Distributions, stoichiometric patterns and cross-shelf exports of dissolved organic matter in the East China Sea, Deep Sea Research Part II: Topical Studies in Oceanography, 50, 1127–1145, https://doi.org/10.1016/S0967-0645(03)00014-6, 2003.

Hung, J.-J., Wang, S.-M., and Chen, Y.-L.: Biogeochemical controls on distributions and fluxes of dissolved and particulate organic carbon in the Northern South China Sea, Deep Sea Research Part II: Topical Studies in Oceanography, 54, 1486–1503, https://doi.org/10.1016/j.dsr2.2007.05.006, 2007.

Hutchins, D. A. and Tagliabue, A.: Feedbacks between phytoplankton and nutrient cycles in a warming ocean, Nat. Geosci., 17, 495–502, https://doi.org/10.1038/s41561-024-01454-w, 2024.

Iavorivska, L., Boyer, E. W., and DeWalle, D. R.: Atmospheric deposition of organic carbon via precipitation, Atmospheric Environment, 146, 153–163, https://doi.org/10.1016/j.atmosenv.2016.06.006, 2016.

Imai, I., Ishida, Y., and Hata, Y.: Killing of marine phytoplankton by a gliding bacterium Cytophaga sp., isolated from the coastal sea of Japan, Marine Biology, 116, 527–532, https://doi.org/10.1007/BF00355470, 1993.

Inomura, K., Omta, A. W., Talmy, D., Bragg, J., Deutsch, C., and Follows, M. J.: A Mechanistic Model of Macromolecular Allocation, Elemental Stoichiometry, and Growth Rate in Phytoplankton, Front. Microbiol., 11, 86, https://doi.org/10.3389/fmicb.2020.00086, 2020.

Inomura, K., Deutsch, C., Jahn, O., Dutkiewicz, S., and Follows, M. J.: Global patterns in marine organic matter stoichiometry driven by phytoplankton ecophysiology, Nat. Geosci., 15, 1034–1040, https://doi.org/10.1038/s41561-022-01066-2, 2022.

Intergovernmental Panel on Climate Change (IPCC) (Ed.): Global Carbon and Other Biogeochemical Cycles and Feedbacks, in: Climate Change 2021 – The Physical Science Basis: Working Group I Contribution to the Sixth Assessment Report of the Intergovernmental Panel on Climate Change, Cambridge University Press, Cambridge, 673–816, https://doi.org/10.1017/9781009157896.007, 2023.

Jensen, T. C., Anderson, T. R., Daufresne, M., and Hessen, D. O.: Does excess carbon affect respiration of the rotifer Brachionus calyciflorus Pallas?, Freshwater Biology, 51, 2320–2333, https://doi.org/10.1111/j.1365-2427.2006.01653.x, 2006.

Jiao, N., Herndl, G. J., Hansell, D. A., Benner, R., Kattner, G., Wilhelm, S. W., Kirchman, D. L., Weinbauer, M. G., Luo, T., Chen, F., and Azam, F.: Microbial production of recalcitrant dissolved organic matter: long-term carbon storage in the global ocean, Nat Rev Microbiol, 8, 593–599, https://doi.org/10.1038/nrmicro2386, 2010.

Jiao, N., Herndl, G. J., Hansell, D. A., Benner, R., Kattner, G., Wilhelm, S. W., Kirchman, D. L., Weinbauer, M. G., Luo, T., Chen, F., and Azam, F.: The microbial carbon pump and the oceanic recalcitrant dissolved organic matter pool, Nat Rev Microbiol, 9, 555–555, https://doi.org/10.1038/nrmicro2386-c5, 2011.

Jiao, N., Robinson, C., Azam, F., Thomas, H., Baltar, F., Dang, H., Hardman-Mountford, N. J., Johnson, M., Kirchman, D. L., Koch, B. P., Legendre, L., Li, C., Liu, J., Luo, T., Luo, Y.-W., Mitra, A., Romanou, A., Tang, K., Wang, X., Zhang, C., and Zhang, R.: Mechanisms of microbial carbon sequestration in the ocean – future research directions, Biogeosciences, 11, 5285–5306, https://doi.org/10.5194/bg-11-5285-2014, 2014.

Jiao, N., Cai, R., Zheng, Q., Tang, K., Liu, J., Jiao, F., Wallace, D., Chen, F., Li, C., Amann, R., Benner, R., and Azam, F.: Unveiling the enigma of refractory carbon in the ocean, National Science Review, 5, 459–463, https://doi.org/10.1093/nsr/nwy020, 2018.

Jørgensen, L., Stedmon, C. A., Granskog, M. A., and Middelboe, M.: Tracing the long-term microbial production of recalcitrant fluorescent dissolved organic matter in seawater, Geophysical Research Letters, 41, 2481–2488, https://doi.org/10.1002/2014GL059428, 2014.

Jurado, E., Dachs, J., Duarte, C. M., and Simó, R.: Atmospheric deposition of organic and black carbon to the global oceans, Atmospheric Environment, 42, 7931–7939, https://doi.org/10.1016/j.atmosenv.2008.07.029, 2008.

Kaiser, K. and Benner, R.: Major bacterial contribution to the ocean reservoir of detrital organic carbon and nitrogen, Limnology and Oceanography, 53, 99–112, https://doi.org/10.4319/lo.2008.53.1.0099, 2008.

Karl, D. M., Hebel, D. V., Björkman, K., and Letelier, R. M.: The role of dissolved organic matter release in the productivity of the oligotrophic North Pacific Ocean, Limnology and Oceanography, 43, 1270–1286, https://doi.org/10.4319/lo.1998.43.6.1270, 1998.

Keene, W. C., Maring, H., Maben, J. R., Kieber, D. J., Pszenny, A. A. P., Dahl, E. E., Izaguirre, M. A., Davis, A. J., Long, M. S., Zhou, X., Smoydzin, L., and Sander, R.: Chemical and physical characteristics of nascent aerosols produced by

bursting bubbles at a model air-sea interface, Journal of Geophysical Research: Atmospheres, 112, D05209, https://doi.org/10.1029/2007JD008464, 2007.

Kieber, D. J., Keene, W. C., Frossard, A. A., Long, M. S., Maben, J. R., Russell, L. M., Kinsey, J. D., Tyssebotn, I. M. B., Quinn, P. K., and Bates, T. S.: Coupled ocean-atmosphere loss of marine refractory dissolved organic carbon, Geophysical Research Letters, 43, 2765–2772, https://doi.org/10.1002/2016GL068273, 2016.

Kim, J.-M., Lee, K., Suh, Y.-S., and Han, I.-S.: Phytoplankton Do Not Produce Carbon-Rich Organic Matter in High CO2 Oceans, Geophysical Research Letters, 45, 4189–4197, https://doi.org/10.1029/2017GL075865, 2018.

Kim, M. J., Novak, G. A., Zoerb, M. C., Yang, M., Blomquist, B. W., Huebert, B. J., Cappa, C. D., and Bertram, T. H.: Air-Sea exchange of biogenic volatile organic compounds and the impact on aerosol particle size distributions, Geophysical Research Letters, 44, 3887–3896, https://doi.org/10.1002/2017GL072975, 2017.

Kim, T.-H. and Kim, G.: Factors controlling the C:N:P stoichiometry of dissolved organic matter in the N-limited, cyanobacteria-dominated East/Japan Sea, Journal of Marine Systems, 115–116, 1–9, https://doi.org/10.1016/j.jmarsys.2013.01.002, 2013.

Kirchman, D. L., Henry, D. L., and Dexter, S. C.: Adsorption of proteins to surfaces in seawater, Marine Chemistry, 27, 201–217, https://doi.org/10.1016/0304-4203(89)90048-0, 1989.

Klausmeier, C. A., Litchman, E., Daufresne, T., and Levin, S. A.: Optimal nitrogen-to-phosphorus stoichiometry of phytoplankton, Nature, 429, 171–174, https://doi.org/10.1038/nature02454, 2004.

Kolber, Z. S., Gerald, F., Plumley, Lang, A. S., Beatty, J. T., Blankenship, R. E., VanDover, C. L., Vetriani, C., Koblizek, M., Rathgeber, C., and Falkowski, P. G.: Contribution of Aerobic Photoheterotrophic Bacteria to the Carbon Cycle in the Ocean, Science, 292, 2492–2495, https://doi.org/10.1126/science.1059707, 2001.

Kreus, M., Schartau, M., Engel, A., Nausch, M., and Voss, M.: Variations in the elemental ratio of organic matter in the central Baltic Sea: Part I-Linking primary production to remineralization, Continental Shelf Research, 100, 25–45, https://doi.org/10.1016/j.csr.2014.06.015, 2015.

Kristensen, E.: Organic matter diagenesis at the oxic/anoxic interface in coastal marine sediments, with emphasis on the role of burrowing animals, in: Life at Interfaces and Under Extreme Conditions, Dordrecht, 1–24, https://doi.org/10.1007/978-94-011-4148-2_1, 2000.

Kristensen, E., Penha-Lopes, G., Delefosse, M., Valdemarsen, T., Quintana, C., and Banta, G.: What is bioturbation? The need for a precise definition for fauna in aquatic sciences, Mar. Ecol. Prog. Ser., 446, 285–302, https://doi.org/10.3354/meps09506, 2012.

Kröncke, I. and Bergfeld, C.: North sea benthos: a review, Senckenbergiana maritima, 33, 205–268, https://doi.org/10.1007/BF03043049, 2003.

Kühn, W., Pätsch, J., Thomas, H., Borges, A. V., Schiettecatte, L. S., Bozec, Y., and Prowe, A. E. F.: Nitrogen and carbon cycling in the North Sea and exchange with the North Atlantic-A model study, Part II: Carbon budget and fluxes, Continental Shelf Research, 30, 1701–1716, https://doi.org/10.1016/j.csr.2010.07.001, 2010.

Kujawinski, E. B.: The Impact of Microbial Metabolism on Marine Dissolved Organic Matter, Annual Review of Marine Science, 3, 567–599, https://doi.org/10.1146/annurev-marine-120308-081003, 2011.

Kujawinski, E. B., Longnecker, K., Barott, K. L., Weber, R. J. M., and Kido Soule, M. C.: Microbial Community Structure Affects Marine Dissolved Organic Matter Composition, Front. Mar. Sci., 3, 45, https://doi.org/10.3389/fmars.2016.00045, 2016.

Kwiatkowski, L., Aumont, O., Bopp, L., and Ciais, P.: The Impact of Variable Phytoplankton Stoichiometry on Projections of Primary Production, Food Quality, and Carbon Uptake in the Global Ocean, Global Biogeochemical Cycles, 32, 516–528, https://doi.org/10.1002/2017GB005799, 2018.

La Roche, J., Geider, R. J., Graziano, L. M., Murray, H., and Lewis, K.: Induction of Specific Proteins in Eukaryotic Algae Grown Under Iron-, Phosphorus-, or Nitrogen-Deficient Conditions, Journal of Phycology, 29, 767–777, https://doi.org/10.1111/j.0022-3646.1993.00767.x, 1993.

Lan Smith, S., Yamanaka, Y., and Kishi, M. J.: Attempting Consistent Simulations of Stn. ALOHA with a Multi-Element Ecosystem Model, J Oceanogr, 61, 1–23, https://doi.org/10.1007/s10872-005-0016-4, 2005.

Lang, S. Q., Butterfield, D. A., Lilley, M. D., Paul Johnson, H., and Hedges, J. I.: Dissolved organic carbon in ridge-axis and ridge-flank hydrothermal systems, Geochimica et Cosmochimica Acta, 70, 3830–3842, https://doi.org/10.1016/j.gca.2006.04.031, 2006.

Laws, E. A., Falkowski, P. G., Smith Jr., W. O., Ducklow, H., and McCarthy, J. J.: Temperature effects on export production in the open ocean, Global Biogeochemical Cycles, 14, 1231–1246, https://doi.org/10.1029/1999GB001229, 2000.

Lee, B. J., Fettweis, M., Toorman, E., and Molz, F. J.: Multimodality of a particle size distribution of cohesive suspended particulate matters in a coastal zone, Journal of Geophysical Research: Oceans, 117, C04017, https://doi.org/10.1029/2011JC007552, 2012.

Lee, C.: Chapter 1 - Why dissolved organics matter: Take 3—The messiness of nature, in: Biogeochemistry of Marine Dissolved Organic Matter (Third Edition), edited by: Hansell, D. A. and Carlson, C. A., Academic Press, 1–12, https://doi.org/10.1016/B978-0-443-13858-4.00020-4, 2024.

Lee, J. A., Garcia, C. A., Larkin, A. A., Carter, B. R., and Martiny, A. C.: Linking a Latitudinal Gradient in Ocean Hydrography and Elemental Stoichiometry in the Eastern Pacific Ocean, Global Biogeochemical Cycles, 35, e2020GB006622, https://doi.org/10.1029/2020GB006622, 2021.

Leonardos, N. and Geider, R. J.: Effects of nitrate : phosphate supply ratio and irradiance on the C : N : P stoichiometry of Chaetoceros muelleri, European Journal of Phycology, 39, 173–180, https://doi.org/10.1080/0967026042000201867, 2004.

Letscher, R. T. and Moore, J. K.: Preferential remineralization of dissolved organic phosphorus and non-Redfield DOM dynamics in the global ocean: Impacts on marine productivity, nitrogen fixation, and carbon export, Global Biogeochemical Cycles, 29, e2014GB004904, https://doi.org/10.1002/2014GB004904, 2015.

Letscher, R. T., Moore, J. K., Teng, Y.-C., and Primeau, F.: Variable C : N : P stoichiometry of dissolved organic matter cycling in the Community Earth System Model, Biogeosciences, 12, 209–221, https://doi.org/10.5194/bg-12-209-2015, 2015.

Li, H., Zhang, Z., Xiong, T., Tang, K., He, C., Shi, Q., Jiao, N., and Zhang, Y.: Carbon Sequestration in the Form of Recalcitrant Dissolved Organic Carbon in a Seaweed (Kelp) Farming Environment, Environ. Sci. Technol., 56, 9112–9122, https://doi.org/10.1021/acs.est.2c01535, 2022.

Li, Z., Clarke, A. J., and Beveridge, T. J.: Gram-Negative Bacteria Produce Membrane Vesicles Which Are Capable of Killing Other Bacteria, Journal of Bacteriology, 180, 5478–5483, https://doi.org/10.1128/jb.180.20.5478-5483.1998, 1998.

Lian, J., Zheng, X., Zhuo, X., Chen, Y.-L., He, C., Zheng, Q., Lin, T.-H., Sun, J., Guo, W., Shi, Q., Jiao, N., and Cai, R.: Microbial transformation of distinct exogenous substrates into analogous composition of recalcitrant dissolved organic matter, Environmental Microbiology, 23, 2389–2403, https://doi.org/10.1111/1462-2920.15426, 2021.

Liang, Z., Letscher, R. T., and Knapp, A. N.: Global Patterns of Surface Ocean Dissolved Organic Matter Stoichiometry, Global Biogeochemical Cycles, 37, e2023GB007788, https://doi.org/10.1029/2023GB007788, 2023.

Liang, Z., Letscher, R. T., and Knapp, A. N.: Oligotrophic Ocean New Production Supported by Lateral Transport of Dissolved Organic Nutrients, Global Biogeochemical Cycles, 39, e2024GB008345, https://doi.org/10.1029/2024GB008345, 2025.

Liefer, J. D., White, A. E., Finkel, Z. V., Irwin, A. J., Dugenne, M., Inomura, K., Ribalet, F., Armbrust, E. V., Karl, D. M., Fyfe, M. H., Brown, C. M., and Follows, M. J.: Latitudinal patterns in ocean C:N:P reflect phytoplankton acclimation and macromolecular composition, Proceedings of the National Academy of Sciences, 121, e2404460121, https://doi.org/10.1073/pnas.2404460121, 2024.

Lin, H.-T., Repeta, D. J., Xu, L., and Rappé, M. S.: Dissolved organic carbon in basalt-hosted deep subseafloor fluids of the Juan de Fuca Ridge flank, Earth and Planetary Science Letters, 513, 156–165, https://doi.org/10.1016/j.epsl.2019.02.008, 2019.

Liu, J., Wang, H., Mou, J., Penuelas, J., Delgado-Baquerizo, M., Martiny, A. C., Zhou, G., Hutchins, D. A., Inomura, K., Lomas, M. W., Fakhraee, M., Pellegrini, A., Kohler, T. J., Deutsch, C. A., Planavsky, N., Lapointe, B., Zhang, Y., Li, Y., Zhou, J., Zhang, Y., Sun, S., Li, Y., Zhang, W., Cao, J., and Chen, J.: Global-scale shifts in marine ecological stoichiometry over the past 50 years, Nat. Geosci., 18, 769–778, https://doi.org/10.1038/s41561-025-01735-y, 2025.

Liu, S., Longnecker, K., Kujawinski, E. B., Vergin, K., Bolaños, L. M., Giovannoni, S. J., Parsons, R., Opalk, K., Halewood, E., Hansell, D. A., Johnson, R., Curry, R., and Carlson, C. A.: Linkages Among Dissolved Organic Matter Export, Dissolved Metabolites, and Associated Microbial Community Structure Response in the Northwestern Sargasso Sea on a Seasonal Scale, Front. Microbiol., 13, 833252, https://doi.org/10.3389/fmicb.2022.833252, 2022.

Loh, A. N. and Bauer, J. E.: Distribution, partitioning and fluxes of dissolved and particulate organic C, N and P in the eastern North Pacific and Southern Oceans, Deep Sea Res. Pt. I, 47, 2287–2316, https://doi.org/10.1016/S0967-0637(00)00027-3, 2000.

Lomas, M. W., Baer, S. E., Mouginot, C., Terpis, K. X., Lomas, D. A., Altabet, M. A., and Martiny, A. C.: Varying influence of phytoplankton biodiversity and stoichiometric plasticity on bulk particulate stoichiometry across ocean basins, Commun Earth Environ, 2, 143, https://doi.org/10.1038/s43247-021-00212-9, 2021.

Lønborg, C. and Álvarez-Salgado, X. A.: Recycling versus export of bioavailable dissolved organic matter in the coastal ocean and efficiency of the continental shelf pump, Global Biogeochemical Cycles, 26, GB3018, https://doi.org/10.1029/2012GB004353, 2012.

Lønborg, C., Davidson, K., Álvarez–Salgado, X. A., and Miller, A. E. J.: Bioavailability and bacterial degradation rates of dissolved organic matter in a temperate coastal area during an annual cycle, Marine Chemistry, 113, 219–226, https://doi.org/10.1016/j.marchem.2009.02.003, 2009.

Lønborg, C., Middelboe, M., and Brussaard, C. P. D.: Viral lysis of Micromonas pusilla: impacts on dissolved organic matter production and composition, Biogeochemistry, 116, 231–240, https://doi.org/10.1007/s10533-013-9853-1, 2013.

Lønborg, C., Yokokawa, T., Herndl, G. J., and Antón Álvarez-Salgado, X.: Production and degradation of fluorescent dissolved organic matter in surface waters of the eastern north Atlantic ocean, Deep Sea Research Part I: Oceanographic Research Papers, 96, 28–37, https://doi.org/10.1016/j.dsr.2014.11.001, 2015.

Lønborg, C., Carreira, C., Jickells, T., and Álvarez-Salgado, X. A.: Impacts of Global Change on Ocean Dissolved Organic Carbon (DOC) Cycling, Front. Mar. Sci., 7, 466, https://doi.org/10.3389/fmars.2020.00466, 2020.

Lønborg, C., Carreira, C., Abril, G., Agustí, S., Amaral, V., Andersson, A., Arístegui, J., Bhadury, P., Bif, M. B., Borges, A. V., Bouillon, S., Calleja, M. L., Cotovicz Jr., L. C., Cozzi, S., Doval, M., Duarte, C. M., Eyre, B., Fichot, C. G., García-Martín, E. E., Garzon-Garcia, A., Giani, M., Gonçalves-Araujo, R., Gruber, R., Hansell, D. A., Hashihama, F., He, D., Holding, J. M., Hunter, W. R., Ibánhez, J. S. P., Ibello, V., Jiang, S., Kim, G., Klun, K., Kowalczuk, P., Kubo, A., Lee, C.-W., Lopes, C. B., Maggioni, F., Magni, P., Marrase, C., Martin, P., McCallister, S. L., McCallum, R., Medeiros, P. M., Morán, X. A. G., Muller-Karger, F. E., Myers-Pigg, A., Norli, M., Oakes, J. M., Osterholz, H., Park, H., Lund Paulsen, M., Rosentreter, J. A., Ross, J. D., Rueda-Roa, D., Santinelli, C., Shen, Y., Teira, E., Tinta, T., Uher, G., Wakita, M., Ward, N., Watanabe, K., Xin, Y., Yamashita, Y., Yang, L., Yeo, J., Yuan, H., Zheng, Q., and Álvarez-Salgado, X. A.: A global database of dissolved organic matter (DOM) concentration measurements in coastal waters (CoastDOM v1), Earth System Science Data, 16, 1107–1119, https://doi.org/10.5194/essd-16-1107-2024, 2024.

López-Sandoval, D. C., Fernández, A., and Marañón, E.: Dissolved and particulate primary production along a longitudinal gradient in the Mediterranean Sea, Biogeosciences, 8, 815–825, https://doi.org/10.5194/bg-8-815-2011, 2011.

Lorkowski, I., Pätsch, J., Moll, A., and Kühn, W.: Interannual variability of carbon fluxes in the North Sea from 1970 to 2006 - Competing effects of abiotic and biotic drivers on the gas-exchange of CO 2, Estuarine, Coastal and Shelf Science, 100, 38–57, https://doi.org/10.1016/j.ecss.2011.11.037, 2012.

Lucea, A., Duarte, C. M., Agustí, S., and Søndergaard, M.: Nutrient (N, P and Si) and carbon partitioning in the stratified NW Mediterranean, Journal of Sea Research, 49, 157–170, https://doi.org/10.1016/S1385-1101(03)00005-4, 2003.

Luo, J. Y., Condon, R. H., Stock, C. A., Duarte, C. M., Lucas, C. H., Pitt, K. A., and Cowen, R. K.: Gelatinous Zooplankton-Mediated Carbon Flows in the Global Oceans: A Data-Driven Modeling Study, Global Biogeochemical Cycles, 34, e2020GB006704, https://doi.org/10.1029/2020GB006704, 2020.

Ma, X., Coleman, M. L., and Waldbauer, J. R.: Distinct molecular signatures in dissolved organic matter produced by viral lysis of marine cyanobacteria, Environmental Microbiology, 20, 3001–3011, https://doi.org/10.1111/1462-2920.14338, 2018.

Mäkelin, S. and Villnäs, A.: Food sources drive temporal variation in elemental stoichiometry of benthic consumers, Limnology and Oceanography, 67, 784–799, https://doi.org/10.1002/lno.12034, 2022.

Malzahn, A. M., Hantzsche, F., Schoo, K. L., Boersma, M., and Aberle, N.: Differential effects of nutrient-limited primary production on primary, secondary or tertiary consumers, Oecologia, 162, 35–48, https://doi.org/10.1007/s00442-009-1458-y, 2010.

Marchant, H. K., Ahmerkamp, S., Lavik, G., Tegetmeyer, H. E., Graf, J., Klatt, J. M., Holtappels, M., Walpersdorf, E., and Kuypers, M. M. M.: Denitrifying community in coastal sediments performs aerobic and anaerobic respiration simultaneously, The ISME Journal, 11, 1799–1812, https://doi.org/10.1038/ismej.2017.51, 2017.

Mari, X., Passow, U., Migon, C., Burd, A. B., and Legendre, L.: Transparent exopolymer particles: Effects on carbon cycling in the ocean, Progress in Oceanography, 151, 13–37, https://doi.org/10.1016/j.pocean.2016.11.002, 2017.

Martin, A. P., Dominguez, A. B., Baker, C. A., Baumas, C. M. J., Bisson, K. M., Cavan, E., Freilich, M., Galbraith, E., Galí, M., Henson, S., Kvale, K. F., Lemmen, C., Luo, J. Y., McMonagle, H., Viríssimo, F. de M., Möller, K. O., Richon, C., Suresh, I., Wilson, J. D., Woodstock, M. S., and Yool, A.: When to add a new process to a model – and when not: A marine biogeochemical perspective, Ecological Modelling, 498, 110870, https://doi.org/10.1016/j.ecolmodel.2024.110870, 2024.

Martin, J. H., Knauer, G. A., Karl, D. M., and Broenkow, W. W.: VERTEX: carbon cycling in the northeast Pacific, Deep Sea Research Part A. Oceanographic Research Papers, 34, 267–285, https://doi.org/10.1016/0198-0149(87)90086-0, 1987.

Martiny, A. C., Pham, C. T. A., Primeau, F. W., Vrugt, J. A., Moore, J. K., Levin, S. A., and Lomas, M. W.: Strong latitudinal patterns in the elemental ratios of marine plankton and organic matter, Nature Geoscience, 6, 279–283, https://doi.org/10.1038/ngeo1757, 2013.

Martiny, A. C., Vrugt, J. A., and Lomas, M. W.: Concentrations and ratios of particulate organic carbon, nitrogen, and phosphorus in the global ocean, Sci Data, 1, 140048, https://doi.org/10.1038/sdata.2014.48, 2014.

Matsumoto, K. and Tanioka, T.: Shifts in regional production as a driver of future global ocean production stoichiometry, Environ. Res. Lett., 15, 124027, https://doi.org/10.1088/1748-9326/abc4b0, 2020.

Matsumoto, K., Rickaby, R., and Tanioka, T.: Carbon Export Buffering and CO2 Drawdown by Flexible Phytoplankton C:N:P Under Glacial Conditions, Paleoceanography and Paleoclimatology, 35, e2019PA003823, https://doi.org/10.1029/2019PA003823, 2020a.

Matsumoto, K., Tanioka, T., and Rickaby, R.: Linkages Between Dynamic Phytoplankton C:N:P and the Ocean Carbon Cycle Under Climate Change, Oceanography, 33, 44–52, https://www.jstor.org/stable/26937739, 2020b.

Matsumoto, K., Tanioka, T., and Zahn, J.: MESMO 3: Flexible phytoplankton stoichiometry and refractory dissolved organic matter, Geosci. Model Dev., 14, 2265–2288, https://doi.org/10.5194/gmd-14-2265-2021, 2021.

Mayers, K. M. J., Kuhlisch, C., Basso, J. T. R., Saltvedt, M. R., Buchan, A., and Sandaa, R.-A.: Grazing on Marine Viruses and Its Biogeochemical Implications, mBio, 14, e01921-21, https://doi.org/10.1128/mbio.01921-21, 2023.

Meador, T. B., Schoffelen, N., Ferdelman, T. G., Rebello, O., Khachikyan, A., and Könneke, M.: Carbon recycling efficiency and phosphate turnover by marine nitrifying archaea, Science Advances, 6, eaba1799, https://doi.org/10.1126/sciadv.aba1799, 2020.

Medeiros, Patricia. M., Seidel, M., Powers, L. C., Dittmar, T., Hansell, D. A., and Miller, W. L.: Dissolved organic matter composition and photochemical transformations in the northern North Pacific Ocean, Geophysical Research Letters, 42, 863–870, https://doi.org/10.1002/2014GL062663, 2015.

Meunier, C. L., Hantzsche, F. M., Cunha-Dupont, A. Ö., Haafke, J., Oppermann, B., Malzahn, A. M., and Boersma, M.: Intraspecific selectivity, compensatory feeding and flexible homeostasis in the phagotrophic flagellate Oxyrrhis marina: three ways to handle food quality fluctuations, Hydrobiologia, 680, 53–62, https://doi.org/10.1007/s10750-011-0900-4, 2012.

Meunier, C. L., Buchkowski, R., Elser, J. J., Laspoumaderes, C., Metson, G. S., Sethna, L. R., and Boersma, M.: Editorial: Advances in ecological stoichiometry, Front. Ecol. Evol., 13, https://doi.org/10.3389/fevo.2025.1632107, 2025.

Meysman, F. J. R., Middelburg, J. J., and Heip, C. H. R.: Bioturbation: a fresh look at Darwin's last idea, Trends in Ecology & Evolution, 21, 688–695, https://doi.org/10.1016/j.tree.2006.08.002, 2006.

Middelburg, J. J.: Chemoautotrophy in the ocean, Geophysical Research Letters, 38, L17607, https://doi.org/10.1029/2011GL049725, 2011.

Miller, W. L. and Zepp, R. G.: Photochemical production of dissolved inorganic carbon from terrestrial organic matter: Significance to the oceanic organic carbon cycle, Geophysical Research Letters, 22, 417–420, https://doi.org/10.1029/94GL03344, 1995.

Minor, E. C., Eglinton, T. I., Olson, R., and Boon, J. J.: The compositional heterogeneity of particulate organic matter from the surface ocean: an investigation using flow cytometry and DT-MS, 29, 1561–1582, https://doi.org/10.1016/S0146-6380(98)00161-2, 1998.

Mojica, K. D. A. and Brussaard, C. P. D.: Factors affecting virus dynamics and microbial host–virus interactions in marine environments, FEMS Microbiology Ecology, 89, 495–515, https://doi.org/10.1111/1574-6941.12343, 2014.

Møller, E. F.: Production of dissolved organic carbon by sloppy feeding in the copepods Acartia tonsa, Centropages typicus, and Temora longicornis, Limnology and Oceanography, 52, 79–84, https://doi.org/10.4319/lo.2007.52.1.0079, 2007.

Møller, E. F., Thor, P., and Nielsen, T. G.: Production of DOC by Calanus finmarchicus, C. glacialis and C. hyperboreus through sloppy feeding and leakage from fecal pellets, Marine Ecology Progress Series, 262, 185–191, https://doi.org/10.3354/meps262185, 2003.

Moorthi, S. D., Schmitt, J. A., Ryabov, A., Tsakalakis, I., Blasius, B., Prelle, L., Tiedemann, M., and Hodapp, D.: Unifying ecological stoichiometry and metabolic theory to predict production and trophic transfer in a marine planktonic food web, Philosophical Transactions of the Royal Society B: Biological Sciences, 371, 20150270, https://doi.org/10.1098/rstb.2015.0270, 2016.

Mopper, K., Zhou, X., Kieber, R. J., Kieber, D. J., Sikorski, R. J., and Jones, R. D.: Photochemical degradation of dissolved organic carbon and its impact on the oceanic carbon cycle, Nature, 353, 60–62, https://doi.org/10.1038/353060a0, 1991.

Mopper, K., zhou, J., Sri Ramana, K., passow, U., dam, H. G., and Drapeau, D. T.: The role of surface-active carbohydrates in the flocculation of a diatom bloom in a mesocosm, Deep Sea Research Part II: Topical Studies in Oceanography, 42, 47–73, https://doi.org/10.1016/0967-0645(95)00004-A, 1995.

Moran, M. A., Kujawinski, E. B., Schroer, W. F., Amin, S. A., Bates, N. R., Bertrand, E. M., Braakman, R., Brown, C. T., Covert, M. W., Doney, S. C., Dyhrman, S. T., Edison, A. S., Eren, A. M., Levine, N. M., Li, L., Ross, A. C., Saito, M. A., Santoro, A. E., Segrè, D., Shade, A., Sullivan, M. B., and Vardi, A.: Microbial metabolites in the marine carbon cycle, Nat Microbiol, 7, 508–523, https://doi.org/10.1038/s41564-022-01090-3, 2022a.

Moran, M. A., Ferrer-González, F. X., Fu, H., Nowinski, B., Olofsson, M., Powers, M. A., Schreier, J. E., Schroer, W. F., Smith, C. B., and Uchimiya, M.: The Ocean's labile DOC supply chain, Limnology and Oceanography, 67, 1007–1021, https://doi.org/10.1002/lno.12053, 2022b.

Moreno, A. R. and Martiny, A. C.: Ecological Stoichiometry of Ocean Plankton, Annu. Rev. Mar. Sci., 10, 43–69, https://doi.org/10.1146/annurev-marine-121916-063126, 2018.

Mueller, B., den Haan, J., Visser, P. M., Vermeij, M. J. A., and van Duyl, F. C.: Effect of light and nutrient availability on the release of dissolved organic carbon (DOC) by Caribbean turf algae, Sci Rep, 6, 23248, https://doi.org/10.1038/srep23248, 2016.

Mühlenbruch, M., Grossart, H.-P., Eigemann, F., and Voss, M.: Mini-review: Phytoplankton-derived polysaccharides in the marine environment and their interactions with heterotrophic bacteria, Environmental Microbiology, 20, 2671–2685, https://doi.org/10.1111/1462-2920.14302, 2018.

Mulholland, M. R. and Lee, C.: Peptide hydrolysis and the uptake of dipeptides by phytoplankton, Limnology and Oceanography, 54, 856–868, https://doi.org/10.4319/lo.2009.54.3.0856, 2009.

Muñoz-Marín, M. C., Gómez-Baena, G., López-Lozano, A., Moreno-Cabezuelo, J. A., Díez, J., and García-Fernández, J. M.: Mixotrophy in marine picocyanobacteria: use of organic compounds by Prochlorococcus and Synechococcus, The ISME Journal, 14, 1065–1073, https://doi.org/10.1038/s41396-020-0603-9, 2020.

Myklestad, S. M.: Release of extracellular products by phytoplankton with special emphasis on polysaccharides, Science of The Total Environment, 165, 155–164, https://doi.org/10.1016/0048-9697(95)04549-G, 1995.

Nagata, T.: Organic Matter–Bacteria Interactions in Seawater, in: Microbial Ecology of the Oceans, John Wiley & Sons, Ltd, 207–241, https://doi.org/10.1002/9780470281840.ch7, 2008.

Nagata, T. and Kirchman, D. L.: Release of macromolecular organic complexes by heterotrophic marine flagellates, Marine Ecology Progress Series, 83, 233–240, 1992.

Nakagawa, S. and Takai, K.: Deep-sea vent chemoautotrophs: diversity, biochemistry and ecological significance, FEMS Microbiology Ecology, 65, 1–14, https://doi.org/10.1111/j.1574-6941.2008.00502.x, 2008.

Nausch, M., Nausch, G., Wasmund, N., and Nagel, K.: Phosphorus pool variations and their relation to cyanobacteria development in the Baltic Sea: A three-year study, Journal of Marine Systems, 71, 99–111, https://doi.org/10.1016/j.jmarsys.2007.06.004, 2008.

Nelson, C. E., Kelly, L. W., and Haas, A. F.: Microbial Interactions with Dissolved Organic Matter Are Central to Coral Reef Ecosystem Function and Resilience, Annual Review of Marine Science, 15, 431–460, https://doi.org/10.1146/annurev-marine-042121-080917, 2023.

Neumann, T., Radtke, H., Cahill, B., Schmidt, M., and Rehder, G.: Non-Redfieldian carbon model for the Baltic Sea (ERGOM version 1.2) – implementation and budget estimates, Geosci. Model Dev., 15, 8473–8540, https://doi.org/10.5194/gmd-15-8473-2022, 2022.

Nielsen, M. V.: Irradiance and daylength effects on growth and chemical composition of Gyrodinium aureolum Hulburt in culture, Journal of Plankton Research, 14, 811–820, https://doi.org/10.1093/plankt/14.6.811, 1992.

Nielsen, M. V.: Growth and chemical composition of the toxic dinoflagellate Gymnodinium galatheanum in relation to irradiance, temperature and salinity, Marine Ecology Progress Series, 136, 205–211, https://doi.org/10.3354/meps136205, 1996.

Ödalen, M., Nycander, J., Ridgwell, A., Oliver, K. I. C., Peterson, C. D., and Nilsson, J.: Variable C/P composition of organic production and its effect on ocean carbon storage in glacial-like model simulations, Biogeosciences, 17, 2219–2244, https://doi.org/10.5194/bg-17-2219-2020, 2020.

Ogawa, H. and Tanoue, E.: Dissolved Organic Matter in Oceanic Waters, Journal of Oceanography, 59, 129–147, https://doi.org/10.1023/A:1025528919771, 2003.

Omand, M. M., Govindarajan, R., He, J., and Mahadevan, A.: Sinking flux of particulate organic matter in the oceans: Sensitivity to particle characteristics, Sci Rep, 10, 5582, https://doi.org/10.1038/s41598-020-60424-5, 2020.

Osterholz, H., Niggemann, J., Giebel, H.-A., Simon, M., and Dittmar, T.: Inefficient microbial production of refractory dissolved organic matter in the ocean, Nat Commun, 6, 7422, https://doi.org/10.1038/ncomms8422, 2015.

Osterholz, H., Burmeister, C., Busch, S., Dierken, M., Frazão, H. C., Hansen, R., Jeschek, J., Kremp, A., Kreuzer, L., Sadkowiak, B., Waniek, J. J., and Schulz-Bull, D. E.: Nearshore Dissolved and Particulate Organic Matter Dynamics in the Southwestern Baltic Sea: Environmental Drivers and Time Series Analysis (2010–2020), Frontiers in Marine Science, 8:795028, https://doi.org/10.3389/fmars.2021.795028, 2021.

Osterroht, C. and Thomas, H.: New production enhanced by nutrient supply from non-Redfield remineralisation of freshly produced organic material, Journal of Marine Systems, 25, 33–46, https://doi.org/10.1016/S0924-7963(00)00007-5, 2000.

Paerl, R. W., Claudio, I. M., Shields, M. R., Bianchi, T. S., and Osburn, C. L.: Dityrosine formation via reactive oxygen consumption yields increasingly recalcitrant humic-like fluorescent organic matter in the ocean, Limnology and Oceanography Letters, 5, 337–345, https://doi.org/10.1002/lol2.10154, 2020.

Paine, E. R., Brewer, E. A., Schmid, M., Diaz-Pulido, G., Boyd, P. W., and Hurd, C. L.: Strong seasonal patterns of DOC release by a temperate seaweed community: Implications for the coastal ocean carbon cycle, Journal of Phycology, 59, 738–750, https://doi.org/10.1111/jpy.13352, 2023.

Painter, S. C., Hartman, S. E., Kivimäe, C., Salt, L. A., Clargo, N. M., Daniels, C. J., Bozec, Y., Daniels, L., Allen, S., Hemsley, V. S., Moschonas, G., and Davidson, K.: The elemental stoichiometry (C, Si, N, P) of the Hebrides Shelf and its role in carbon export, Progress in Oceanography, 159, 154–177, https://doi.org/10.1016/j.pocean.2017.10.001, 2017.

Painter, S. C., Lapworth, D. J., Woodward, E. M. S., Kroeger, S., Evans, C. D., Mayor, D. J., and Sanders, R. J.: Terrestrial dissolved organic matter distribution in the North Sea, Science of The Total Environment, 630, 630–647, https://doi.org/10.1016/j.scitotenv.2018.02.237, 2018.

Parsons, T. R.: On the chemical composition of eleven species of marine phytoplankton, J Fish Res Bd Can, 18, 1001–1016, 1961.

Passow, U.: Transparent exopolymer particles (TEP) in aquatic environments, Progress in Oceanography, 55, 287–333, https://doi.org/10.1016/S0079-6611(02)00138-6, 2002.

Pätsch, J. and Kühn, W.: Nitrogen and carbon cycling in the North Sea and exchange with the North Atlantic—A model study. Part I. Nitrogen budget and fluxes, Continental Shelf Research, 28, 767–787, https://doi.org/10.1016/j.csr.2007.12.013, 2008.

Persson, J., Fink, P., Goto, A., Hood, J. M., Jonas, J., and Kato, S.: To be or not to be what you eat: regulation of stoichiometric homeostasis among autotrophs and heterotrophs, Oikos, 119, 741–751, https://doi.org/10.1111/j.1600-0706.2009.18545.x, 2010.

Pertola, S., Koski, M., and Viitasalo, M.: Stoichiometry of mesozooplankton in N- and P-limited areas of the Baltic Sea, Marine Biology, 140, 425–434, https://doi.org/10.1007/s00227-001-0723-3, 2002.

Plum, C. and Hillebrand, H.: Multiple zooplankton species alter the stoichiometric interactions between producer and consumer levels, Mar Biol, 166, 163, https://doi.org/10.1007/s00227-019-3609-y, 2019.

Plum, C., Hüsener, M., and Hillebrand, H.: Multiple vs. single phytoplankton species alter stoichiometry of trophic interaction with zooplankton, Ecology, 96, 3075–3089, https://doi.org/10.1890/15-0393.1, 2015.

Pohlabeln, A. M., Gomez-Saez, G. V., Noriega-Ortega, B. E., and Dittmar, T.: Experimental Evidence for Abiotic Sulfurization of Marine Dissolved Organic Matter, Front. Mar. Sci., 4, 364, https://doi.org/10.3389/fmars.2017.00364, 2017.

Polimene, L., Sailley, S., Clark, D., Mitra, A., and Allen, J. I.: Biological or microbial carbon pump? The role of phytoplankton stoichiometry in ocean carbon sequestration, Journal of Plankton Research, 39, 180–186, https://doi.org/10.1093/plankt/fbw091, 2017.

Prowe, A. E. F., Thomas, H., Pätsch, J., Kühn, W., Bozec, Y., Schiettecatte, L.-S., Borges, A. V., and Baar, H. J. W. de: Mechanisms controlling the air–sea CO2 flux in the North Sea, Continental Shelf Research, 29, 1801–1808, https://doi.org/10.1016/j.csr.2009.06.003, 2009.

Pujo-Pay, M., Conan, P., Oriol, L., Cornet-Barthaux, V., Falco, C., Ghiglione, J.-F., Goyet, C., Moutin, T., and Prieur, L.: Integrated survey of elemental stoichiometry (C, N, P) from the western to eastern Mediterranean Sea, Biogeosciences, 8, 883–899, https://doi.org/10.5194/bg-8-883-2011, 2011.

Quigg, A., Finkel, Z. V., Irwin, A. J., Rosenthal, Y., Ho, T.-Y., Reinfelder, J. R., Schofield, O., Morel, F. M. M., and Falkowski, P. G.: The evolutionary inheritance of elemental stoichiometry in marine phytoplankton, Nature, 425, 291–294, https://doi.org/10.1038/nature01953, 2003.

Quigg, A., Irwin, A. J., and Finkel, Z. V.: Evolutionary inheritance of elemental stoichiometry in phytoplankton, Proceedings of the Royal Society B: Biological Sciences, 278, 526–534, https://doi.org/10.1098/rspb.2010.1356, 2010.

Raimbault, P., Pouvesle, W., Diaz, F., Garcia, N., and Sempéré, R.: Wet-oxidation and automated colorimetry for simultaneous determination of organic carbon, nitrogen and phosphorus dissolved in seawater, Marine Chemistry, 66, 161–169, https://doi.org/10.1016/S0304-4203(99)00038-9, 1999.

Ratnarajah, L., Abu-Alhaija, R., Atkinson, A., Batten, S., Bax, N. J., Bernard, K. S., Canonico, G., Cornils, A., Everett, J. D., Grigoratou, M., Ishak, N. H. A., Johns, D., Lombard, F., Muxagata, E., Ostle, C., Pitois, S., Richardson, A. J., Schmidt, K., Stemmann, L., Swadling, K. M., Yang, G., and Yebra, L.: Monitoring and modelling marine zooplankton in a changing climate, Nat Commun, 14, 564, https://doi.org/10.1038/s41467-023-36241-5, 2023.

Raven, M. R., Fike, D. A., Gomes, M. L., Webb, S. M., Bradley, A. S., and McClelland, H.-L. O.: Organic carbon burial during OAE2 driven by changes in the locus of organic matter sulfurization, Nat Commun, 9, 3409, https://doi.org/10.1038/s41467-018-05943-6, 2018.

Redfield, A. C.: The biological control of chemical factors in the environment., American Scientist, 46, 205–221, 1958.

Redfield, A. C., Ketchum, B. H., and Richards, F. A.: The influence of organisms on the composition of seawater, in: The Sea, vol. 2, edited by: Hill, M. N., Intersience Publishers, New York, NY, 26–77, 1963.

Reed, D. C., Carlson, C. A., Halewood, E. R., Nelson, J. C., Harrer, S. L., Rassweiler, A., and Miller, R. J.: Patterns and controls of reef-scale production of dissolved organic carbon by giant kelp Macrocystis pyrifera, Limnology and Oceanography, 60, 1996–2008, https://doi.org/10.1002/lno.10154, 2015.

Reintjes, G., Arnosti, C., Fuchs, B. M., and Amann, R.: An alternative polysaccharide uptake mechanism of marine bacteria, The ISME Journal, 11, 1640–1650, https://doi.org/10.1038/ismej.2017.26, 2017.

Reintjes, G., Arnosti, C., Fuchs, B., and Amann, R.: Selfish, sharing and scavenging bacteria in the Atlantic Ocean: a biogeographical study of bacterial substrate utilisation, The ISME Journal, 13, 1119–1132, https://doi.org/10.1038/s41396-018-0326-3, 2019.

Resplandy, L., Hogikyan, A., Müller, J. D., Najjar, R. G., Bange, H. W., Bianchi, D., Weber, T., Cai, W.-J., Doney, S. C., Fennel, K., Gehlen, M., Hauck, J., Lacroix, F., Landschützer, P., Le Quéré, C., Roobaert, A., Schwinger, J., Berthet, S., Bopp, L., Chau, T. T. T., Dai, M., Gruber, N., Ilyina, T., Kock, A., Manizza, M., Lachkar, Z., Laruelle, G. G., Liao, E., Lima, I. D., Nissen, C., Rödenbeck, C., Séférian, R., Toyama, K., Tsujino, H., and Regnier, P.: A Synthesis of Global Coastal Ocean Greenhouse Gas Fluxes, Global Biogeochemical Cycles, 38, e2023GB007803, https://doi.org/10.1029/2023GB007803, 2024.

Ribes, M., Yahel, G., Romera-Castillo, C., Mallenco, R., Morganti, T. M., and Coma, R.: The removal of dissolved organic matter by marine sponges is a function of its composition and concentration: An in situ seasonal study of four Mediterranean species, Science of The Total Environment, 871, 161991, https://doi.org/10.1016/j.scitotenv.2023.161991, 2023.

Richardson, K. and Bendtsen, J.: Vertical distribution of phytoplankton and primary production in relation to nutricline depth in the open ocean, Marine Ecology Progress Series, 620, 33–46, https://doi.org/10.3354/meps12960, 2019.

Ridgwell, A. and Arndt, S.: Chapter 1 - Why Dissolved Organics Matter: DOC in Ancient Oceans and Past Climate Change, in: Biogeochemistry of Marine Dissolved Organic Matter (Second Edition), edited by: Hansell, D. A. and Carlson, C. A., Academic Press, Boston, 1–20, https://doi.org/10.1016/B978-0-12-405940-5.00001-7, 2015.

Riley, J. S., Sanders, R., Marsay, C., Le Moigne, F. a. C., Achterberg, E. P., and Poulton, A. J.: The relative contribution of fast and slow sinking particles to ocean carbon export, Global Biogeochemical Cycles, 26, GB1029, https://doi.org/10.1029/2011GB004085, 2012.

Rivkin, R. B. and Legendre, L.: Biogenic Carbon Cycling in the Upper Ocean: Effects of Microbial Respiration, Science, 291, 2398–2400, https://doi.org/10.1126/science.291.5512.2398, 2001.

Robinson, C.: Heterotrophic Bacterial Respiration, in: Microbial Ecology of the Oceans, John Wiley & Sons, Ltd, 299–334, https://doi.org/10.1002/9780470281840.ch9, 2008.

Roobaert, A., Laruelle, G. G., Landschützer, P., Gruber, N., Chou, L., and Regnier, P.: The Spatiotemporal Dynamics of the Sources and Sinks of CO_2 in the Global Coastal Ocean, Global Biogeochemical Cycles, 33, 1693–1714, https://doi.org/10.1029/2019GB006239, 2019.

Roobaert, A., Regnier, P., Landschützer, P., and Laruelle, G. G.: A novel sea surface pCO_2-product for the global coastal ocean resolving trends over 1982–2020, Earth System Science Data, 16, 421–441, https://doi.org/10.5194/essd-16-421-2024, 2024a.

Roobaert, A., Resplandy, L., Laruelle, G. G., Liao, E., and Regnier, P.: Unraveling the Physical and Biological Controls of the Global Coastal CO_2 Sink, Global Biogeochemical Cycles, 38, e2023GB007799, https://doi.org/10.1029/2023GB007799, 2024b.

Roshan, S. and DeVries, T.: Efficient dissolved organic carbon production and export in the oligotrophic ocean, Nat Commun, 8, 2036, https://doi.org/10.1038/s41467-017-02227-3, 2017.

Rothman, D. H., Hayes, J. M., and Summons, R. E.: Dynamics of the Neoproterozoic carbon cycle, Proceedings of the National Academy of Sciences, 100, 8124–8129, https://doi.org/10.1073/pnas.0832439100, 2003.

Rowe, O. F., Dinasquet, J., Paczkowska, J., Figueroa, D., Riemann, L., and Andersson, A.: Major differences in dissolved organic matter characteristics and bacterial processing over an extensive brackish water gradient, the Baltic Sea, Marine Chemistry, 202, 27–36, https://doi.org/10.1016/j.marchem.2018.01.010, 2018.

Saba, G. K., Steinberg, D. K., and Bronk, D. A.: The relative importance of sloppy feeding, excretion, and fecal pellet leaching in the release of dissolved carbon and nitrogen by *Acartia tonsa* copepods, Journal of Experimental Marine Biology and Ecology, 404, 47–56, https://doi.org/10.1016/j.jembe.2011.04.013, 2011.

Sakshaug, E., Andresen, K., Myklestad, S., and Olsen, Y.: Nutrient status of phytoplankton communities in Norwegian waters (marine, brackish, and fresh) as revealed by their chemical composition1, Journal of Plankton Research, 5, 175–196, https://doi.org/10.1093/plankt/5.2.175, 1983.

Sakshaug, E., Graneli, E., Elbrächter, M., and Kayser, H.: Chemical composition and alkaline phosphatase activity of nutrient-saturated and P-deficient cells of four marine dinoflagellates, Journal of Experimental Marine Biology and Ecology, 77, 241–254, https://doi.org/10.1016/0022-0981(84)90122-9, 1984.

Santinelli, C., Ibello, V., Lavezza, R., Civitarese, G., and Seritti, A.: New insights into C, N and P stoichiometry in the Mediterranean Sea: The Adriatic Sea case, Continental Shelf Research, 44, 83–93, https://doi.org/10.1016/j.csr.2012.02.015, 2012.

Sardans, J., Rivas-Ubach, A., and Peñuelas, J.: The C:N:P stoichiometry of organisms and ecosystems in a changing world: A review and perspectives, Perspectives in Plant Ecology, Evolution and Systematics, 14, 33–47, https://doi.org/10.1016/j.ppees.2011.08.002, 2012.

Schiettekatte, N. M. D., Barneche, D. R., Villéger, S., Allgeier, J. E., Burkepile, D. E., Brandl, S. J., Casey, J. M., Mercière, A., Munsterman, K. S., Morat, F., and Parravicini, V.: Nutrient limitation, bioenergetics and stoichiometry: A new model to predict elemental fluxes mediated by fishes, Functional Ecology, 34, 1857–1869, https://doi.org/10.1111/1365-2435.13618, 2020.

Schindler, D. E. and Eby, L. A.: Stoichiometry of Fishes and Their Prey: Implications for Nutrient Recycling, Ecology, 78, 1816–1831, https://doi.org/10.1890/0012-9658(1997)078%255B1816:SOFATP%255D2.0.CO;2, 1997.

Schlitzer, R.: Carbon export fluxes in the Southern Ocean: results from inverse modeling and comparison with satellite-based estimates, Deep Sea Research Part II: Topical Studies in Oceanography, 49, 1623–1644, https://doi.org/10.1016/s0967-0645(02)00004-8, 2002.

Schlitzer, R.: Export Production in the Equatorial and North Pacific Derived from Dissolved Oxygen, Nutrient and Carbon Data, Journal of Oceanography, 60, 53–62, https://doi.org/10.1023/B:JOCE.0000038318.38916.e6, 2004.

Schneider, B., Engel, A., and Schlitzer, R.: Effects of depth- and CO2-dependent C:N ratios of particulate organic matter (POM) on the marine carbon cycle, Global Biogeochemical Cycles, 18, GB2015, https://doi.org/10.1029/2003GB002184, 2004.

Schoo, K. L., Malzahn, A. M., Krause, E., and Boersma, M.: Increased carbon dioxide availability alters phytoplankton stoichiometry and affects carbon cycling and growth of a marine planktonic herbivore, Mar Biol, 160, 2145–2155, https://doi.org/10.1007/s00227-012-2121-4, 2013.

Scott, T., Cotner, J., and LaPara, T.: Variable Stoichiometry and Homeostatic Regulation of Bacterial Biomass Elemental Composition, Front. Microbiol., 3, 42, https://doi.org/10.3389/fmicb.2012.00042, 2012.

Scully, N. M., Cooper, W. J., and Tranvik, L. J.: Photochemical effects on microbial activity in natural waters: the interaction of reactive oxygen species and dissolved organic matter, FEMS Microbiology Ecology, 46, 353–357, https://doi.org/10.1016/S0168-6496(03)00198-3, 2003.

Sexton, P. F., Norris, R. D., Wilson, P. A., Pälike, H., Westerhold, T., Röhl, U., Bolton, C. T., and Gibbs, S.: Eocene global warming events driven by ventilation of oceanic dissolved organic carbon, Nature, 471, 349–352, https://doi.org/10.1038/nature09826, 2011.

Sharoni, S. and Halevy, I.: Nutrient ratios in marine particulate organic matter are predicted by the population structure of well-adapted phytoplankton, Science Advances, 6, eaaw9371, https://doi.org/10.1126/sciadv.aaw9371, 2020.

Sharples, J., Mayor, D. J., Poulton, A. J., Rees, A. P., and Robinson, C.: Shelf Sea Biogeochemistry: Nutrient and carbon cycling in a temperate shelf sea water column, Progress in Oceanography, 177, 102182, https://doi.org/10.1016/j.pocean.2019.102182, 2019.

Shen, Y. and Benner, R.: Mixing it up in the ocean carbon cycle and the removal of refractory dissolved organic carbon, Sci Rep, 8, 2542, https://doi.org/10.1038/s41598-018-20857-5, 2018.

Sheppard, E. J., Hurd, C. L., Britton, D. D., Reed, D. C., and Bach, L. T.: Seaweed biogeochemistry: Global assessment of C:N and C:P ratios and implications for ocean afforestation, Journal of Phycology, 59, 879–892, https://doi.org/10.1111/jpy.13381, 2023.

Sherr, E. and Sherr, B.: Understanding Roles of Microbes in Marine Pelagic Food Webs: A Brief History, in: Microbial Ecology of the Oceans, John Wiley & Sons, Ltd, 27–44, https://doi.org/10.1002/9780470281840.ch2, 2008.

Sheward, R. M., Liefer, J. D., Irwin, A. J., and Finkel, Z. V.: Elemental stoichiometry of the key calcifying marine phytoplankton Emiliania huxleyi under ocean climate change: A meta-analysis, Global Change Biology, 29, 4259–4278, https://doi.org/10.1111/gcb.16807, 2023.

Siegel, D. A., Buesseler, K. O., Doney, S. C., Sailley, S. F., Behrenfeld, M. J., and Boyd, P. W.: Global assessment of ocean carbon export by combining satellite observations and food-web models, Global Biogeochemical Cycles, 28, 181–196, https://doi.org/10.1002/2013GB004743, 2014.

Singh, A., Baer, S. E., Riebesell, U., Martiny, A. C., and Lomas, M. W.: C : N : P stoichiometry at the Bermuda Atlantic Time-series Study station in the North Atlantic Ocean, Biogeosciences, 12, 6389–6403, https://doi.org/10.5194/bg-12-6389-2015, 2015.

Somes, C. J. and Oschlies, A.: On the influence of “non-Redfield” dissolved organic nutrient dynamics on the spatial distribution of N2 fixation and the size of the marine fixed nitrogen inventory, Global Biogeochemical Cycles, 29, 973–993, https://doi.org/10.1002/2014GB005050, 2015.

Steinberg, D. K. and Landry, M. R.: Zooplankton and the Ocean Carbon Cycle, Annual Review of Marine Science, 9, 413–444, https://doi.org/10.1146/annurev-marine-010814-015924, 2017.

Steinberg, D. K., Carlson, C. A., Bates, N. R., Goldthwait, S. A., Madin, L. P., and Michaels, A. F.: Zooplankton vertical migration and the active transport of dissolved organic and inorganic carbon in the Sargasso Sea, Deep Sea Research Part I: Oceanographic Research Papers, 47, 137–158, https://doi.org/10.1016/S0967-0637(99)00052-7, 2000.

Steinberg, D. K., Van Mooy, B. A. S., Buesseler, K. O., Boyd, P. W., Kobari, T., and Karl, D. M.: Bacterial vs. zooplankton control of sinking particle flux in the ocean's twilight zone, Limnology and Oceanography, 53, 1327–1338, https://doi.org/10.4319/lo.2008.53.4.1327, 2008.

Stepanauskas, R., JØrgensen, N. O. G., Eigaard, O. R., Žvikas, A., Tranvik, L. J., and Leonardson, L.: Summer Inputs of Riverine Nutrients to the Baltic Sea: Bioavailability and Eutrophication Relevance, Ecological Monographs, 72, 579–597, https://doi.org/10.1890/0012-9615(2002)072%255B0579:SIORNT%255D2.0.CO;2, 2002.

Sterner, R. W.: Ocean stoichiometry, global carbon, and climate, Proceedings of the National Academy of Sciences, 112, 8162–8163, https://doi.org/10.1073/pnas.1510331112, 2015.

Sterner, R. W. and Elser, J. J.: Ecological Stoichiometry: The Biology of Elements from Molecules to the Biosphere, Princeton University Press, 2002.

Stewart, J. R. and Brown, R. M.: Cytophaga That Kills or Lyses Algae, Science, 164, 1523–1524, https://doi.org/10.1126/science.164.3887.1523, 1969.

Stramska, M.: Particulate organic carbon in the global ocean derived from SeaWiFS ocean color, Deep Sea Research Part I: Oceanographic Research Papers, 56, 1459–1470, https://doi.org/10.1016/j.dsr.2009.04.009, 2009.

Strom, S. L., Benner, R., Ziegler, S., and Dagg, M. J.: Planktonic grazers are a potentially important source of marine dissolved organic carbon, Limnology and Oceanography, 42, 1364–1374, https://doi.org/10.4319/lo.1997.42.6.1364, 1997.

Sullivan, M. R., Primeau, F. W., Hagstrom, G. I., Wang, W.-L., and Martiny, A. C.: Integrating Trait-Based Stoichiometry in a Biogeochemical Inverse Model Reveals Links Between Phytoplankton Physiology and Global Carbon Export, Global Biogeochemical Cycles, 38, e2023GB007986, https://doi.org/10.1029/2023GB007986, 2024.

Sun, L., Xu, C., Lin, P., Quigg, A., Chin, W.-C., and Santschi, P. H.: Photo-oxidation of proteins facilitates the preservation of high molecular weight dissolved organic nitrogen in the ocean, Marine Chemistry, 229, 103907, https://doi.org/10.1016/j.marchem.2020.103907, 2021.

Suratman, S., Weston, K., Jickells, T., and Fernand, L.: Spatial and seasonal changes of dissolved and particulate organic C in the North Sea, Hydrobiologia, 628, 13–25, https://doi.org/10.1007/s10750-009-9730-z, 2009.

Talarmin, A., Lomas, M. W., Bozec, Y., Savoye, N., Frigstad, H., Karl, D. M., and Martiny, A. C.: Seasonal and long-term changes in elemental concentrations and ratios of marine particulate organic matter, Global Biogeochemical Cycles, 30, 1699–1711, https://doi.org/10.1002/2016GB005409, 2016.

Talmy, D., Martiny, A. C., Hill, C., Hickman, A. E., and Follows, M. J.: Microzooplankton regulation of surface ocean POC:PON ratios, Global Biogeochemical Cycles, 30, 311–332, https://doi.org/10.1002/2015GB005273, 2016.

Tanioka, T. and Matsumoto, K.: Buffering of Ocean Export Production by Flexible Elemental Stoichiometry of Particulate Organic Matter, Global Biogeochemical Cycles, 31, 1528–1542, https://doi.org/10.1002/2017GB005670, 2017.

Tanioka, T. and Matsumoto, K.: A meta-analysis on environmental drivers of marine phytoplankton C:N:P, Biogeosciences, 17, 2939–2954, https://doi.org/10.5194/bg-17-2939-2020, 2020.

Tanioka, T., Fichot, C. G., and Matsumoto, K.: Toward Determining the Spatio-Temporal Variability of Upper-Ocean Ecosystem Stoichiometry From Satellite Remote Sensing, Front. Mar. Sci., 7, 604893, https://doi.org/10.3389/fmars.2020.604893, 2020.

Tanioka, T., Matsumoto, K., and Lomas, M. W.: Drawdown of Atmospheric pCO2 Via Variable Particle Flux Stoichiometry in the Ocean Twilight Zone, Geophysical Research Letters, 48, e2021GL094924, https://doi.org/10.1029/2021GL094924, 2021.

Tanioka, T., Larkin, A. A., Moreno, A. R., Brock, M. L., Fagan, A. J., Garcia, C. A., Garcia, N. S., Gerace, S. D., Lee, J. A., Lomas, M. W., and Martiny, A. C.: Global Ocean Particulate Organic Phosphorus, Carbon, Oxygen for Respiration, and Nitrogen (GO-POPCORN), Sci Data, 9, 688, https://doi.org/10.1038/s41597-022-01809-1, 2022a.

Tanioka, T., Garcia, C. A., Larkin, A. A., Garcia, N. S., Fagan, A. J., and Martiny, A. C.: Global patterns and predictors of C:N:P in marine ecosystems, Communications Earth & Environment, 3, 271, https://doi.org/10.1038/s43247-022-00603-6, 2022b.

Taucher, J., Schulz, K. G., Dittmar, T., Sommer, U., Oschlies, A., and Riebesell, U.: Enhanced carbon overconsumption in response to increasing temperatures during a mesocosm experiment, Biogeosciences, 9, 3531–3545, https://doi.org/10.5194/bg-9-3531-2012, 2012.

Taylor, G. T., Iturriaga, R., and Sullivan, C. W.: Interactions of bactivorous grazers and heterotrophic bacteria with dissolved organic matter, Marine Ecology Progress Series, 23, 129–141, 1985.

Teira, E., Pazó, M. J., Quevedo, M., Fuentes, M. V., Niell, F. X., and Fernández, E.: Rates of dissolved organic carbon production and bacterial activity in the eastern North Atlantic Subtropical Gyre during summer, Marine Ecology Progress Series, 249, 53–67, https://doi.org/10.3354/meps249053, 2003.

Teng, Y.-C., Primeau, F. W., Moore, J. K., Lomas, M. W., and Martiny, A. C.: Global-scale variations of the ratios of carbon to phosphorus in exported marine organic matter, Nature Geosci, 7, 895–898, https://doi.org/10.1038/ngeo2303, 2014.

Terry, K. L., Hirata, J., and Laws, E. A.: Light-limited growth of two strains of the marine diatom *Phaeodactylum tricornutum* Bohlin: Chemical composition, carbon partitioning and the diel periodicity of physiological processes, Journal of Experimental Marine Biology and Ecology, 68, 209–227, https://doi.org/10.1016/0022-0981(83)90054-0, 1983.

Thomas, H., Ittekkot, V., Osterroht, C., and Schneider, B.: Preferential recycling of nutrients—the ocean's way to increase new production and to pass nutrient limitation?, Limnology and Oceanography, 44, 1999–2004, https://doi.org/10.4319/lo.1999.44.8.1999, 1999.

Thornton, D. C. O.: Dissolved organic matter (DOM) release by phytoplankton in the contemporary and future ocean, European Journal of Phycology, 49, 20–46, https://doi.org/10.1080/09670262.2013.875596, 2014.

Thrane, J.-E., Hessen, D. O., and Andersen, T.: The impact of irradiance on optimal and cellular nitrogen to phosphorus ratios in phytoplankton, Ecology Letters, 19, 880–888, https://doi.org/10.1111/ele.12623, 2016.

Tiano, J. C., Witbaard, R., Bergman, M. J. N., van Rijswijk, P., Tramper, A., van Oevelen, D., and Soetaert, K.: Acute impacts of bottom trawl gears on benthic metabolism and nutrient cycling, ICES Journal of Marine Science, 76, 1917–1930, https://doi.org/10.1093/icesjms/fsz060, 2019.

Tillmann, U.: Kill and eat your predator: a winning strategy of the planktonic flagellate Prymnesium parvum, Aquatic Microbial Ecology, 32, 73–84, https://doi.org/10.3354/ame032073, 2003.

Toseland, A., Daines, S. J., Clark, J. R., Kirkham, A., Strauss, J., Uhlig, C., Lenton, T. M., Valentin, K., Pearson, G. A., Moulton, V., and Mock, T.: The impact of temperature on marine phytoplankton resource allocation and metabolism, Nature Clim Change, 3, 979–984, https://doi.org/10.1038/nclimate1989, 2013.

Tranvik, L. J., Sherr, E. B., and Sherr, B. F.: Uptake and utilization of “colloidal DOM” by heterotrophic flagellates in seawater, Marine Ecology Progress Series, 92, 301–309, https://doi.org/10.3354/meps092301, 1993.

Turner, J. T.: Zooplankton fecal pellets, marine snow, phytodetritus and the ocean’s biological pump, Progress in Oceanography, 130, 205–248, https://doi.org/10.1016/j.pocean.2014.08.005, 2015.

Urban-Rich, J.: Release of dissolved organic carbon from copepod fecal pellets in the Greenland Sea, Journal of Experimental Marine Biology and Ecology, 232, 107–124, https://doi.org/10.1016/S0022-0981(98)00104-X, 1999.

Van de Waal, D. B. and Litchman, E.: Multiple global change stressor effects on phytoplankton nutrient acquisition in a future ocean, Philosophical Transactions of the Royal Society B: Biological Sciences, 375, 20190706, https://doi.org/10.1098/rstb.2019.0706, 2020.

Veldhuis, M. J. W., Kraay, G. W., and Timmermans, K. R.: Cell death in phytoplankton: correlation between changes in membrane permeability, photosynthetic activity, pigmentation and growth, European Journal of Phycology, 36, 167–177, https://doi.org/10.1017/S0967026201003110, 2001.

Velthuis, M., Keuskamp, Joost. A., Bakker, E. S., Boersma, M., Sommer, U., van Donk, E., and Van de Waal, D. B.: Differential effects of elevated pCO2 and warming on marine phytoplankton stoichiometry, Limnology and Oceanography, 67, 598–607, https://doi.org/10.1002/lno.12020, 2022.

Verdugo, P., Alldredge, A. L., Azam, F., Kirchman, D. L., Passow, U., and Santschi, P. H.: The oceanic gel phase: a bridge in the DOM–POM continuum, Marine Chemistry, 92, 67–85, https://doi.org/10.1016/j.marchem.2004.06.017, 2004.

Vijayakumaran, V., Daewel, U., Millington, R., Bruggeman, J., Powley, H., Lessin, G., Lindenthal, A., and Schrum, C.: The effect of coupling higher trophic level modules on the dynamics of three models of lower trophic level , Copernicus Meetings, https://doi.org/10.5194/egusphere-egu25-7123, 2025.

Villar-Argaiz, M., Medina-Sánchez, J. M., Biddanda, B. A., and Carrillo, P.: Predominant Non-additive Effects of Multiple Stressors on Autotroph C:N:P Ratios Propagate in Freshwater and Marine Food Webs, Front. Microbiol., 9, 69, https://doi.org/10.3389/fmicb.2018.00069, 2018.

Voss, M., Asmala, E., Bartl, I., Carstensen, J., Conley, D. J., Dippner, J. W., Humborg, C., Lukkari, K., Petkuviene, J., Reader, H., Stedmon, C., Vybernaite-Lubiene, I., Wannicke, N., and Zilius, M.: Origin and fate of dissolved organic matter in four shallow Baltic Sea estuaries, Biogeochemistry, 154, 385–403, https://doi.org/10.1007/s10533-020-00703-5, 2021.

van de Waal, D. B., Verschoor, A. M., Verspagen, J. M., van Donk, E., and Huisman, J.: Climate-driven changes in the ecological stoichiometry of aquatic ecosystems, Frontiers in Ecology and the Environment, 8, 145–152, https://doi.org/10.1890/080178, 2010.

Wada, S., Aoki, M. N., Mikami, A., Komatsu, T., Tsuchiya, Y., Sato, T., Shinagawa, H., and Hama, T.: Bioavailability of macroalgal dissolved organic matter in seawater, Marine Ecology Progress Series, 370, 33–44, https://doi.org/10.3354/meps07645, 2008.

Wagner, S., Schubotz, F., Kaiser, K., Hallmann, C., Waska, H., Rossel, P. E., Hansman, R., Elvert, M., Middelburg, J. J., Engel, A., Blattmann, T. M., Catalá, T. S., Lennartz, S. T., Gomez-Saez, G. V., Pantoja-Gutiérrez, S., Bao, R., and Galy, V.: Soothsaying DOM: A Current Perspective on the Future of Oceanic Dissolved Organic Carbon, Front. Mar. Sci., 7, 341, https://doi.org/10.3389/fmars.2020.00341, 2020.

Wakeham, S. G. and Lee, C.: Production, Transport, and Alteration of Particulate Organic Matter in the Marine Water Column, in: Organic Geochemistry, vol. 11, edited by: Engel, M. H. and Macko, S. A., Springer US, Boston, MA, 145–169, https://doi.org/10.1007/978-1-4615-2890-6_6, 1993.

Wakeham, S. G. and Lee, C.: Limits of our knowledge, part 2: Selected frontiers in marine organic biogeochemistry, Marine Chemistry, 212, 16–46, https://doi.org/10.1016/j.marchem.2019.02.005, 2019.

Wang, H., Chen, F., Mi, T., Liu, Q., Yu, Z., and Zhen, Y.: Responses of Marine Diatom Skeletonema marinoi to Nutrient Deficiency: Programmed Cell Death, Applied and Environmental Microbiology, 86, e02460-19, https://doi.org/10.1128/AEM.02460-19, 2020.

Wang, J., Li, J., Tsona Tchinda, N., and Du, L.: Marine Biogenic Volatile Organic Compounds: Production, Emission, Atmospheric Transformation, and Climate Effects, Curr Pollution Rep, 11, 37, https://doi.org/10.1007/s40726-025-00365-7, 2025.

Wang, R., Wang, S., Cao, R., Han, J., Huang, T., and Wen, G.: The apoptosis of *Chlorella vulgaris* and the release of intracellular organic matter under metalimnetic oxygen minimum conditions, Science of The Total Environment, 907, 168001, https://doi.org/10.1016/j.scitotenv.2023.168001, 2024.

Watanabe, K., Yoshida, G., Hori, M., Umezawa, Y., Moki, H., and Kuwae, T.: Macroalgal metabolism and lateral carbon flows can create significant carbon sinks, Biogeosciences, 17, 2425–2440, https://doi.org/10.5194/bg-17-2425-2020, 2020.

Wear, E. K., Carlson, C. A., Windecker, L. A., and Brzezinski, M. A.: Roles of diatom nutrient stress and species identity in determining the short- and long-term bioavailability of diatom exudates to bacterioplankton, Marine Chemistry, 177, 335–348, https://doi.org/10.1016/j.marchem.2015.09.001, 2015a.

Wear, E. K., Carlson, C. A., James, A. K., Brzezinski, M. A., Windecker, L. A., and Nelson, C. E.: Synchronous shifts in dissolved organic carbon bioavailability and bacterial community responses over the course of an upwelling-driven phytoplankton bloom, Limnology and Oceanography, 60, 657–677, https://doi.org/10.1002/lno.10042, 2015b.

Webb, J. R., Santos, I. R., Maher, D. T., Tait, D. R., Cyronak, T., Sadat-Noori, M., Macklin, P., and Jeffrey, L. C.: Groundwater as a source of dissolved organic matter to coastal waters: Insights from radon and CDOM observations in 12 shallow coastal systems, Limnology and Oceanography, 64, 182–196, https://doi.org/10.1002/lno.11028, 2019.

Weber, T. S. and Deutsch, C.: Ocean nutrient ratios governed by plankton biogeography, Nature, 467, 550–554, https://doi.org/10.1038/nature09403, 2010.

Weigel, B. L. and Pfister, C. A.: The dynamics and stoichiometry of dissolved organic carbon release by kelp, Ecology, 102, e03221, https://doi.org/10.1002/ecy.3221, 2021.

Weissbach, A., Tillmann, U., and Legrand, C.: Allelopathic potential of the dinoflagellate *Alexandrium tamarense* on marine microbial communities, Harmful Algae, 10, 9–18, https://doi.org/10.1016/j.hal.2010.05.007, 2010.

Wells, M. L.: A neglected dimension, Nature, 391, 530–531, https://doi.org/10.1038/35248, 1998.

Welsh, J. E., Steenhuis, P., de Moraes, K. R., van der Meer, J., Thieltges, D. W., and Brussaard, C. P. D.: Marine virus predation by non-host organisms, Sci Rep, 10, 5221, https://doi.org/10.1038/s41598-020-61691-y, 2020.

Westberry, T., Behrenfeld, M. J., Siegel, D. A., and Boss, E.: Carbon-based primary productivity modeling with vertically resolved photoacclimation, Global Biogeochemical Cycles, 22, GB2024, https://doi.org/10.1029/2007GB003078, 2008.

White, A. E., Giovannoni, S. J., Zhao, Y., Vergin, K., and Carlson, C. A.: Elemental content and stoichiometry of SAR11 chemoheterotrophic marine bacteria, Limnol Oceanogr Letters, 4, 44–51, https://doi.org/10.1002/lol2.10103, 2019.

Wilhelm, S. W. and Suttle, C. A.: Viruses and Nutrient Cycles in the Sea: Viruses play critical roles in the structure and function of aquatic food webs, BioScience, 49, 781–788, https://doi.org/10.2307/1313569, 1999.

Williams, P. M., Carlucci, A. F., and Olson, R.: A deep profile of some biologically important properties in the central North Pacific gyre, Oceanologica Acta, 3, 471–476, https://archimer.ifremer.fr/doc/00122/23291/21119.pdf, 1980.

Winogradow, A., Mackiewicz, A., and Pempkowiak, J.: Seasonal changes in particulate organic matter (POM) concentrations and properties measured from deep areas of the Baltic Sea, Oceanologia, 61, 505–521, https://doi.org/10.1016/j.oceano.2019.05.004, 2019.

Wirtz, K. W. and Kerimoglu, O.: Autotrophic Stoichiometry Emerging from Optimality and Variable Co-limitation, Frontiers in Ecology and Evolution, 4, 131, https://doi.org/10.3389/fevo.2016.00131, 2016.

Wohlers-Zöllner, J., Biermann, A., Engel, A., Dörge, P., Lewandowska, A. M., von Scheibner, M., and Riebesell, U.: Effects of rising temperature on pelagic biogeochemistry in mesocosm systems: a comparative analysis of the AQUASHIFT Kiel experiments, Mar Biol, 159, 2503–2518, https://doi.org/10.1007/s00227-012-1958-x, 2012.

Wolfe, G.: The chemical defense ecology of marine unicellular plankton: constraints, mechanisms, and impacts, The Biological Bulletin, 198, 225–244, https://doi.org/10.2307/1542526, 2000.

Xie, L., Gao, X., Liu, Y., Zhao, J., and Xing, Q.: The joint effects of atmospheric dry and wet deposition on organic carbon cycling in a mariculture area in North China, Science of The Total Environment, 876, 162715, https://doi.org/10.1016/j.scitotenv.2023.162715, 2023.

Yamashita, Y., Nakane, M., Mori, Y., Nishioka, J., and Ogawa, H.: Fate of dissolved black carbon in the deep Pacific Ocean, Nat Commun, 13, 307, https://doi.org/10.1038/s41467-022-27954-0, 2022.

Yamashita, Y., Mori, Y., and Ogawa, H.: Hydrothermal-derived black carbon as a source of recalcitrant dissolved organic carbon in the ocean, Science Advances, 9, eade3807, https://doi.org/10.1126/sciadv.ade3807, 2023.

Yu, Z. and Li, Y.: Marine volatile organic compounds and their impacts on marine aerosol—A review, Science of The Total Environment, 768, 145054, https://doi.org/10.1016/j.scitotenv.2021.145054, 2021.

Yvon-Durocher, G., Dossena, M., Trimmer, M., Woodward, G., and Allen, A. P.: Temperature and the biogeography of algal stoichiometry, Global Ecology and Biogeography, 24, 562–570, https://doi.org/10.1111/geb.12280, 2015.

Yvon-Durocher, G., Schaum, C.-E., and Trimmer, M.: The Temperature Dependence of Phytoplankton Stoichiometry: Investigating the Roles of Species Sorting and Local Adaptation, Front. Microbiol., 8, 2003, https://doi.org/10.3389/fmicb.2017.02003, 2017.

Zakem, E. J. and Levine, N. M.: Systematic Variation in Marine Dissolved Organic Matter Stoichiometry and Remineralization Ratios as a Function of Lability, Global Biogeochemical Cycles, 33, 1389–1407, https://doi.org/10.1029/2019GB006375, 2019.

Zhao, D., Yang, Y., Tham, Y. J., and Zou, S.: Emission of marine volatile organic compounds (VOCs) by phytoplankton— a review, Marine Environmental Research, 191, 106177, https://doi.org/10.1016/j.marenvres.2023.106177, 2023a.

Zhao, Z., Gonsior, M., Schmitt-Kopplin, P., Zhan, Y., Zhang, R., Jiao, N., and Chen, F.: Microbial transformation of virus-induced dissolved organic matter from picocyanobacteria: coupling of bacterial diversity and DOM chemodiversity, The ISME Journal, 13, 2551–2565, https://doi.org/10.1038/s41396-019-0449-1, 2019.

Zhao, Z.-F., Huang, Z.-J., Sun, Z.-D., Liu, Z.-Y., Qin, S., Han, T., Qi, X.-Y., Sun, X.-Y., and Zhong, Z.-H.: Effects of instantaneous changes in temperature, light, and salinity on the dynamics of dissolved organic carbon release by *Sargassum thunbergii*, Marine Pollution Bulletin, 190, 114865, https://doi.org/10.1016/j.marpolbul.2023.114865, 2023b.

Zimmerman, A. E., Allison, S. D., and Martiny, A. C.: Phylogenetic constraints on elemental stoichiometry and resource allocation in heterotrophic marine bacteria, Environmental Microbiology, 16, 1398–1410, https://doi.org/10.1111/1462-2920.12329, 2014.

Zimmerman, A. E., Howard-Varona, C., Needham, D. M., John, S. G., Worden, A. Z., Sullivan, M. B., Waldbauer, J. R., and Coleman, M. L.: Metabolic and biogeochemical consequences of viral infection in aquatic ecosystems, Nat Rev Microbiol, 18, 21–34, https://doi.org/10.1038/s41579-019-0270-x, 2020.

Appendix B: *Article* II

This appendix contains the following published article in Biogeosciences:

Demir, K. T., Mathis, M., Kossack, J., Liu, F., Daewel, U., Stegert, C., Thomas, H., and Schrum, C. (2025b). Variable organic matter stoichiometry enhances the biological drawdown of CO_2 in the northwest European shelf seas. *Biogeosciences*, 22, 2569–2599, doi: 10.5194/bg-22-2569-2025

The author contributions of Kubilay Timur Demir (KTD) and others to this paper are as follows:

KTD was responsible for the conceptualization of the study, while the methodology was developed collaboratively by KTD, MM, JK, and CSc. Software development was undertaken by KTD, JK, FL, and CSt, with the validation carried out by KTD, JK, and FL. KTD performed the formal analysis, and the investigation was conducted by KTD, MM, CSc, and HT. MM and CSc provided the necessary resources, and data curation was managed by KTD. The original draft of the manuscript was prepared by KTD, and subsequent writing, review, and editing were contributed by KTD, MM, JK, FL, UD, CSt, HT, and CSc. KTD also took responsibility for visualization. Supervision of the project was provided by MM, UD, HT, and CSc. Finally, CSc handled the project administration and funding acquisition.

Biogeosciences, 22, 2569–2599, 2025
https://doi.org/10.5194/bg-22-2569-2025

Biogeosciences Open Access EGU

Variable organic matter stoichiometry enhances the biological drawdown of CO_2 in the northwest European shelf seas

Kubilay Timur Demir[1], Moritz Mathis[1], Jan Kossack[1], Feifei Liu[1], Ute Daewel[1], Christoph Stegert[2], Helmuth Thomas[3,4], and Corinna Schrum[1,5]

[1]Matter Transport and Ecosystem Dynamics, Institute of Coastal Systems – Analysis and Modeling, Helmholtz-Zentrum Hereon, Geesthacht, Germany
[2]Bundesamt für Seeschifffahrt und Hydrographie, Hamburg, Germany
[3]Institute of Carbon Cycles, Helmholtz-Zentrum Hereon, Geesthacht, Germany
[4]Institute for Chemistry and Biology of the Marine Environment, Carl von Ossietzky University of Oldenburg, Oldenburg, Germany
[5]Institute of Oceanography, University of Hamburg, Hamburg, Germany

Correspondence: Kubilay Timur Demir (kubilay.demir@hereon.de)

Received: 5 November 2024 – Discussion started: 20 November 2024
Revised: 24 February 2025 – Accepted: 12 March 2025 – Published: 6 June 2025

Abstract. Variations in the elemental ratios of carbon, nitrogen, and phosphorus in marine organic matter (OM) and their influence on the marine carbon cycle remain poorly understood for both the open and coastal oceans. Observations consistently show an enrichment of carbon and a depletion of phosphorus relative to elemental Redfield ratios. However, many biogeochemical models are constrained to Redfield stoichiometry, neglecting the effects of variable stoichiometry on carbon cycling and typically underestimating biological carbon fixation. This impedes the accurate representation of OM cycling and the resulting carbon fluxes, especially in productive temperate shelf seas such as the northwest European shelf seas (NWES). Here, the efficiency of oceanic CO_2 uptake strongly depends on the biological uptake of inorganic carbon and its export to the North Atlantic, both of which are influenced by OM stoichiometry. In this study, we provide a first comprehensive and quantitative assessment of the effects of variable OM stoichiometry on carbon cycling in the NWES. For this purpose, we integrate two pathways for variable OM stoichiometry, motivated by observational and experimental results, into the regional high-resolution coupled 3D physical–biogeochemical modeling system SCHISM-ECOSMO-CO_2 (Semi-implicit Cross-scale Hydroscience Integrated System Model – ECOSystem MOdel): first, the release of carbon-enriched dissolved OM under nutrient limitation and, second, the preferential remineralization of organic nitrogen and phosphorus. With these extensions we reproduce the observed OM stoichiometry and evaluate its impact on marine carbon cycling, with a focus on OM cycling and the resulting air–sea CO_2 exchange. Compared to the reference simulation with fixed Redfield stoichiometry, the variable stoichiometry configurations show an increase in the annual net CO_2 uptake of 10 %–33 % in the North Sea and 9 %–31 % in the entire NWES, depending on the relative contribution of the two new implementations. As the main driver of the additional CO_2 uptake, we identify a corresponding intensification of annual and seasonal OM cycling, resulting in higher net autotrophy in surface waters and higher net heterotrophy in sub-surface layers. This enhanced gradient in net community production leads to an increased biological drawdown of inorganic carbon, most pronounced in the Norwegian Trench. By increasing the biological control on the surface partial pressure of CO_2, this leads to higher summer and lower winter uptake. Our results highlight the importance of variable stoichiometry for an accurate representation of the shelf carbon pump mechanism in the NWES, as it significantly influences the efficiency of carbon sequestration. Since the response depends largely on regional physical conditions and pre-existing carbon export mechanisms, regional assessments are essential to understand the sensitivity of the carbon cycle to OM stoichiometry, which should be included

Published by Copernicus Publications on behalf of the European Geosciences Union.

in global models to accurately represent the coastal carbon cycle.

1 Introduction

Marine organic matter (OM) is a major global reservoir of reduced carbon (Friedlingstein et al., 2023; Hansell et al., 2009) and plays a key role in sequestering atmospheric CO_2 in the ocean (Carlson and Hansell, 2015; Falkowski et al., 1998; Hansell et al., 2009). The balance between OM production and decomposition controls the transformation and transports of both organic and inorganic carbon (del Giorgio and Duarte, 2002; Smith and Hollibaugh, 1993), especially in the shallow and highly productive temperate shelf seas (Barrón and Duarte, 2015; Bauer et al., 2013; Canuel et al., 2012; Dai et al., 2022; Gattuso et al., 1998). Through its chemical composition, OM further regulates the coupling between the elemental cycles of carbon, nitrogen, and phosphorus, with implications for the relative magnitudes of elemental fluxes, nutrient availability, and OM production (Hopkinson and Vallino, 2005). In this way, variations in OM composition may affect the biological carbon drawdown and thereby the air–sea CO_2 exchange through both changes in carbon fixation and variations in the composition of the OM that is available for lateral and vertical transports (Hopkinson and Vallino, 2005; Loh and Bauer, 2000; Lønborg and Álvarez-Salgado, 2012; Tanioka et al., 2021; Williams, 1995; Zakem and Levine, 2019).

Despite observational evidence for large global and regional variations in elemental C : N : P ratios in dissolved (DOM) and particulate (POM) organic matter (Hopkinson and Vallino, 2005; Liang et al., 2023; Loh and Bauer, 2000; Lønborg et al., 2024; Martiny et al., 2013; Tanioka et al., 2022b), many biogeochemical models assume a constant Redfield stoichiometry of C : N : P = 106 : 16 : 1 or similar, originally derived as an average ratio for the entire global ocean (Redfield, 1963). As a consequence, these models tend to underestimate carbon fixation, especially during nutrient limitation in summer, which is indicated by their deficiency in representing the seasonality of the dissolved inorganic carbon (DIC) concentration and partial pressure of CO_2 (pCO_2) in surface waters (Bozec et al., 2006; Kähler and Koeve, 2001; Prowe et al., 2009). Hence, variable stoichiometry in OM production and decomposition is essential for the adequate representation of biogeochemical fluxes and especially their seasonality (Anderson and Pondaven, 2003; Bozec et al., 2006). Previous experiments using Earth system models suggest that the globally observed carbon enrichment in both DOM and POM significantly enhances global carbon and nitrogen fixation, drawdown of CO_2, and export production when compared to Redfield-stoichiometry-based estimates (Letscher et al., 2015; Letscher and Moore, 2015; Tanioka et al., 2021). However, the regional impact on coastal seas and its spatiotemporal variability remain uncertain due to the scarcity of measurements and the resulting missing consideration in regional studies (Aricò et al., 2021).

The global coastal ocean disproportionately contributes to the sequestration of atmospheric CO_2 in relation to its areal extent through carbon transport to the deep ocean and burial in sediments (Bauer et al., 2013; Dai et al., 2022; Laruelle et al., 2014). Its role is suggested to have changed from a weak pre-industrial net source to a significant contemporary net sink of CO_2 due to both rising atmospheric CO_2 concentrations and enhanced productivity driven by higher terrestrial nutrient inputs (Bauer et al., 2013; Lacroix et al., 2021; Laruelle et al., 2018; Mathis et al., 2024). With a regionally significant contribution (Frankignoulle and Borges, 2001), the northwest European shelf seas (NWES) efficiently export atmospheric CO_2 to the North Atlantic Ocean through the shelf carbon pump mechanism (Tsunogai et al., 1999; Thomas et al., 2004; Bozec et al., 2005; Legge et al., 2020).

In the seasonally stratified parts of the central and northern North Sea, the spatial separation of production in the surface mixed layer and respiration in the sub-surface layer lead to a seasonally occurring drawdown of CO_2, resulting in a vertical gradient of DIC. Subsequently, the DIC-enriched subsurface waters are transported across the shelf edge, leading to a net export of DIC (Thomas et al., 2004). This DIC export is further driven by riverine and Baltic Sea discharge of DIC and net heterotrophy, where the net import of organic carbon, largely from cross-shelf transports, increases net respiration and thereby adds DIC to the system (Thomas et al., 2005). With a smaller contribution, particulate organic carbon (POC) is exported by net deposition and burial in sediments, mainly in the deep regions of the Norwegian Trench, the Skagerrak, and along the shelf edge (Legge et al., 2020; Thomas et al., 2005). The sedimentation of POC is associated with high uncertainties and may play a larger role on long timescales (Legge et al., 2020; Thomas et al., 2005).

This regional carbon export mechanism in the NWES may strongly depend on the observed variations in OM stoichiometry, which makes them essential for regional model-based carbon budget estimates (Chaichana et al., 2019; Davis et al., 2019). Reproducing the observed OM stoichiometry may account for the typically underestimated carbon fixation (Humphreys et al., 2019; Prowe et al., 2009) and consequently affect the estimated net air–sea CO_2 exchange, cross-shelf transport of DIC, and vertical transport of organic carbon in the NWES through changes in the biological carbon pump and the resulting drawdown of DIC.

In this work, we assess the effects of observed variations in OM stoichiometry on carbon fixation, respiration, biological drawdown of inorganic carbon, and the implications for the air–sea CO_2 exchange in the NWES. This serves as a first step in identifying the regional impact on marine carbon cycling, with a focus on the continental shelf carbon pump mechanism. For this, we integrate two pathways of variable OM stoichiometry, motivated by observational and experi-

mental results, into a regional high-resolution coupled 3D physical–biogeochemical ocean model.

Firstly, we introduce an extracellular release of carbon-enriched DOM under nutrient limitation, modified from Neumann et al. (2022). While primary production at Redfield stoichiometry dominates biological carbon fixation under nutrient-replete conditions, the extracellular release allows for additional carbon fixation beyond nutrient limitation and, with variable OM stoichiometry, depending on nutrient availability. This release of carbon-enriched DOM has been observed as an extracellular release of carbohydrates under nutrient stress by phytoplankton cells in mesocosm experiments (Børsheim et al., 2005; Fajon et al., 1999; Søndergaard et al., 2000), as well as field measurements during bloom periods (Myklestad, 1995; Wear et al., 2015b; Williams, 1995). Estimates suggest that the extracellular release of DOC on average contributes 10 %–20 % but temporarily up to 80 % of primary productivity (Wear et al., 2015a). Accordingly, global observations suggest that stoichiometric variations depend on macronutrient availability, specifically nitrogen-versus-phosphorous stress, in addition to temperature (Tanioka et al., 2022b).

Secondly, we include the preferential remineralization of organic nitrogen and phosphorus with the sequence P>N>C for both DOM and POM. Both observations (Clark et al., 1998; Hopkinson et al., 1997, 2002; Loh and Bauer, 2000; Thomas et al., 1999; Williams et al., 1980) and experimental evidence (Hach et al., 2020; Lønborg et al., 2009; Lønborg and Álvarez-Salgado, 2012) suggest the preferential utilization of organic nitrogen and phosphorus over carbon due to higher bioavailability as a mechanism for variable OM stoichiometry. Assuming remineralization at Redfield ratios thus implies underestimating the recycling of nutrients, new production, and carbon export (Hach et al., 2020; Lønborg and Álvarez-Salgado, 2012). This process is thought to contribute to the slow formation of strongly nutrient-depleted and carbon-enriched refractory DOM from labile DOM (Cai and Jiao, 2023; Hach et al., 2020), with refractory DOM having an estimated average lifetime of approximately 6000 years (Bauer et al., 1992).

While previous studies have simulated OM cycling with variable OM stoichiometry for the North Sea (Butenschön et al., 2016; Lorkowski et al., 2012) and the Baltic Sea (Neumann et al., 2022), this work represents the first comprehensive and quantitative assessment of the effects of observed variations in OM stoichiometry on marine carbon cycling in the NWES. This study quantifies the regional impacts of two pathways for variable OM stoichiometry on OM cycling and the resulting air–sea CO_2 exchange in the NWES. In doing so, it will improve our understanding of these implications for marine carbon cycling and the limitations of Redfield-stoichiometry-based estimates. To achieve an accurate representation of the magnitude of both mechanisms, we account for the observed range of POM and labile DOM stoichiometry. We assess the effects of the individual and combined mechanisms by comparing four hindcast simulations: a reference configuration using Redfield stoichiometry, separate configurations for each mechanism, and a final one that integrates both with a reduced contribution. These simulations are conducted using the SCHISM-ECOSMO-CO_2 modeling system from Kossack et al. (2023, 2024) and span the period from 1995 to 2010, covering the NWES, the Baltic Sea, and parts of the northeastern Atlantic Ocean.

2 Materials and methods

2.1 SCHISM-ECOSMO-CO_2 modeling system

The SCHISM-ECOSMO-CO_2 modeling system couples 3D hydrodynamic, biogeochemical, and carbonate system models through the Framework for Aquatic Biogeochemical Models (FABM; Bruggeman and Bolding, 2014). This one-way coupling allows us to consider the control of dynamic forcing conditions on ecosystem and carbon dynamics, as well as the effects of biological production, respiration, and the physical state on carbon cycling (Fig. 1). The Semi-implicit Cross-scale Hydroscience Integrated System Model (SCHISM; Zhang et al., 2016b) simulates the physical state and the resulting tracer transports over the ocean domain. Under these physical forcing conditions, the here-introduced variable stoichiometry version of the ecosystem model ECOSMO II (ECOSystem MOdel; Daewel and Schrum, 2013; Schrum et al., 2006) prognostically calculates tracer concentrations through local sources and sinks from biogeochemical processes. Based on simulated temperature, pressure, salinity, and two prognostic carbonate system variables provided by ECOSMO II, the carbonate system model by Blackford and Gilbert (2007) diagnostically computes the missing carbonate system variables and the air–sea CO_2 exchange under equilibrium conditions. The carbonate system calculations follow the HALTAFALL algorithm (Ingri et al., 1967) for the composition of equilibrium mixtures.

2.1.1 Hydrodynamic model SCHISM

The hydrodynamical model component SCHISM is capable of efficiently resolving 3D baroclinic ocean circulation in the NWES and adjacent areas across a range of depths from the shallow southern North Sea to the deep waters of the northeastern Atlantic (Zhang et al., 2016a). This is achieved through the use of an unstructured triangular horizontal grid (Zhang et al., 2016b) in combination with localized sigma coordinates with shaved cells (LSC^2) for the vertical grid structure (Zhang et al., 2015). Previous studies have demonstrated that SCHISM is able to accurately resolve transports across shelf slopes and canyons (Wang et al., 2022). This makes it particularly suitable for simulating cross-shelf transports and resolving the Norwegian Trench, the Skagerrak, and shelf slope areas in the NWES. The adaptive vertical resolution further enhances the representation of

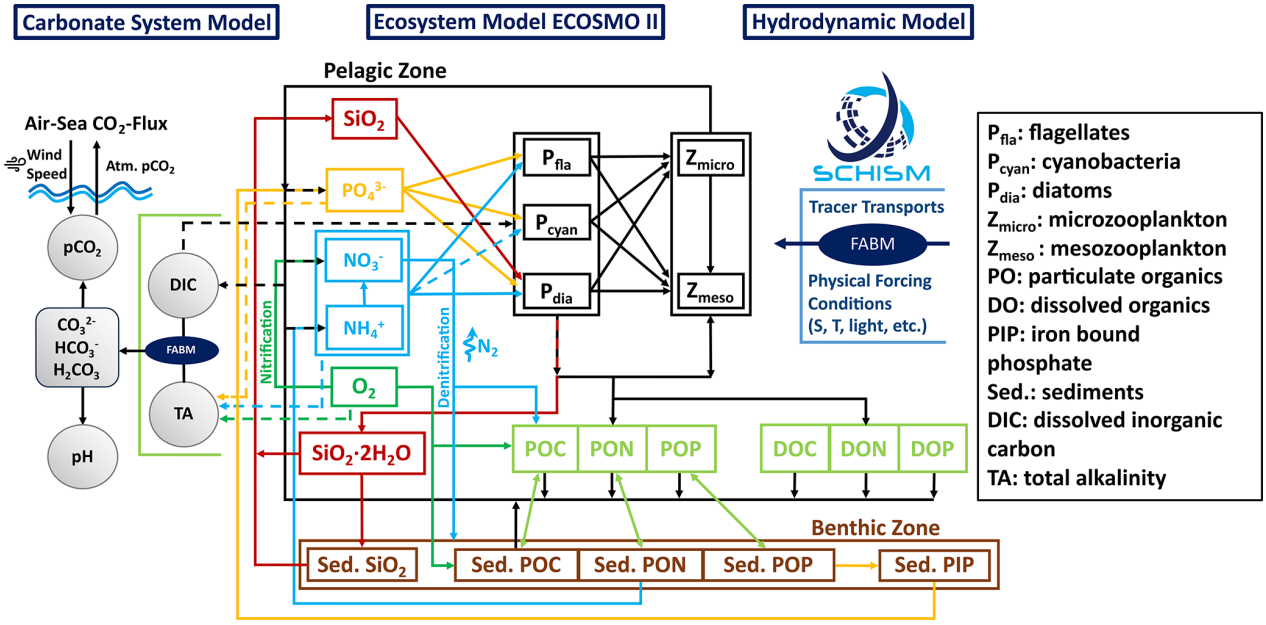

Figure 1. Schematic diagram of the coupled physical–biogeochemical modeling system SCHISM-ECOSMO-CO_2 based on the FABM framework. The modeling system couples the 3D baroclinic circulation model SCHISM, an extended version of the lower-trophic-level ecosystem model ECOSMO II, and a carbonate system model based on the HALTAFALL algorithm to calculate the composition of equilibrium mixtures.

bottom and slope currents, with relevance for the resulting benthic pelagic coupling. By employing a third-order finite-volume transport scheme built upon the weighted essentially non-oscillatory (WENO) formalism, SCHISM is capable of simulating mesoscale eddies in the open ocean (Ye et al., 2019), thereby facilitating cross-scale applications.

The model simulations for this study employ the NWES-LR grid, initialization, and forcing configuration from Kossack et al. (2023, 2024) and Porz et al. (2024), which successfully reproduced temperature, nutrient, and carbonate system variability in the NWES. Our simulations cover the ocean domain from 40–66° N and 20° W–30° E, including the NWES, the Baltic Sea, and parts of the northeastern Atlantic Ocean for the years 1995 to 2010, with a time step of 200 s. For the purposes of this analysis, the initial 5 years are excluded as a spin-up period. With 140 152 triangular grid elements and a maximum of 53 vertical layers, the horizontal resolution ranges from about 4.5 to 10 km, with increasing depth on the continental shelf, and reaches up to 15 km in the Atlantic Ocean. While the Baltic Sea and parts of the northeast Atlantic are included for the explicit resolution of exchange fluxes, the focus of this study is on the North Sea and the entire NWES. In accordance with Kossack et al. (2023, 2024), we subdivide the NWES into sub-areas based on a combination of bathymetry and both physical and biogeochemical variability (Fig. 2). The boundary of the NWES along the shelf edge is defined by the 200 m isobath, with the exception of the Norwegian Trench, which is included because of its important role in cross-shelf exchange fluxes.

2.1.2 Ecosystem model ECOSMO II

The lower-trophic-level ecosystem model ECOSMO II describes the interactions of nutrient cycles and functional groups of phytoplankton, zooplankton, detritus, and surface sediments with 16 state variables (Daewel and Schrum, 2013). Here, nutrient cycles include phosphate (PO_4), oxygen (O_2), silicate (SiO_2), and nitrogen as both ammonium (NH_4) and nitrate (NO_3). ECOSMO II represents three functional groups of phytoplankton: flagellates, limited by nitrogen and phosphate; diatoms, additionally limited by silicate; and cyanobacteria with the ability to fix nitrogen from the atmosphere at the water surface. Light limits primary production for all functional groups, with the consideration of self-shading by plankton and organic matter. Cyanobacteria production is additionally temperature-dependent and only possible under sufficient light and under low-salinity conditions in the Baltic Sea. The two zooplankton groups differ in their herbivorous and omnivorous feeding behavior.

Detritus is present in the form of POM, DOM, and biogenic opal ($SiO_2 \times 2H_2O$), with different rates of temperature-dependent remineralization. POM and DOM contain carbon, nitrogen, and phosphorus at Redfield ratios of C : N : P = 106 : 16 : 1 (Redfield, 1963). New detritus from assimilation losses and mortality separates into 60 %

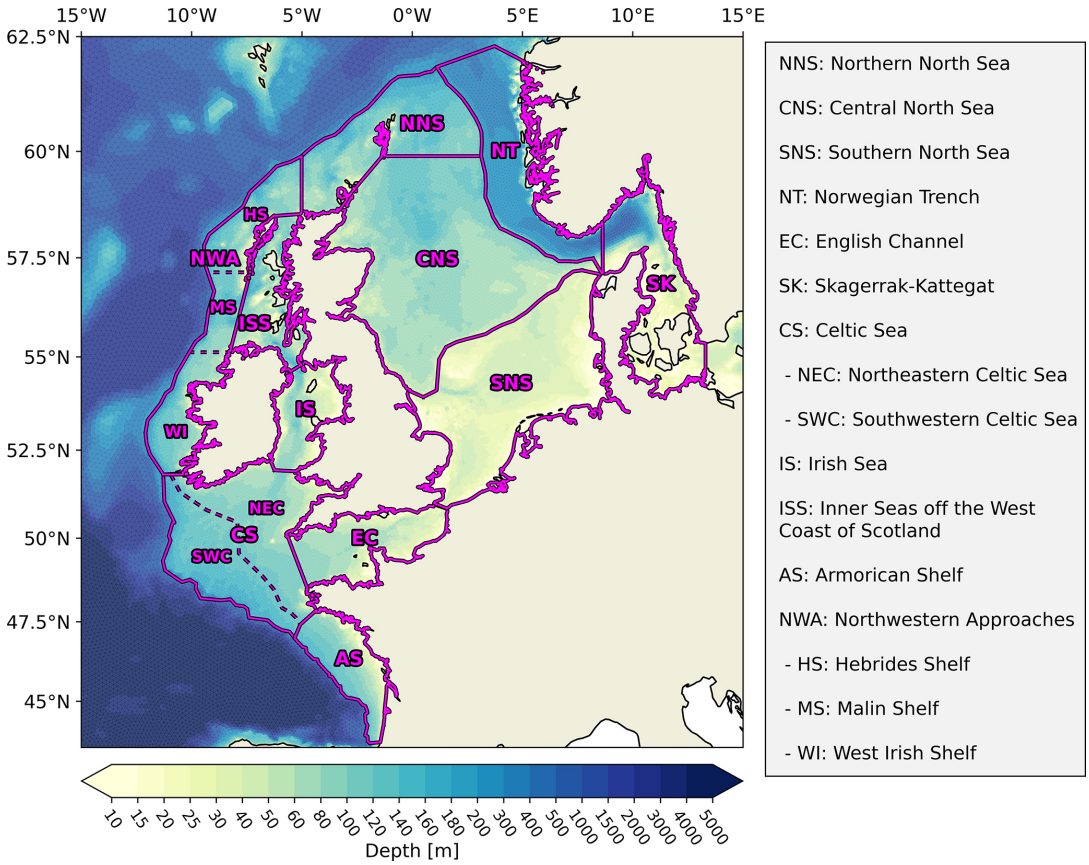

Figure 2. Sub-regions and bathymetry of the northwest European shelf seas (NWES) based on a combination of bathymetric features and both physical and biogeochemical variability. The division of the NWES into sub-regions with relatively homogeneous physical and biogeochemical characteristics allows for the identification of consistent carbon cycle responses.

POM and 40 % DOM, with diatom losses further enriching biogenic opal. While POM and biogenic opal sink at constant velocities, DOM is only transported through advection and diffusion. Below a critical bottom-shear stress, both POM and opal accumulate by deposition in two corresponding sediment pools. Above this critical shear stress, they are resuspended back into the water column. Burial permanently removes both POM and silicate from the sediment pools at a constant percentage rate. Benthic remineralization releases DIC and silicate to the water column as a function of temperature only, whereas nitrogen and phosphorous release from sedimentary POM also depends on oxygen concentrations. Under oxic conditions, remineralization of particulate organic nitrogen (PON) from sediments releases ammonium. Under anoxic conditions, the release of ammonium doubles, and denitrification additionally converts nitrate as an oxidation agent into gaseous nitrogen, which becomes unavailable for photosynthesis. Remineralization converts particulate organic phosphorus (POP) into iron-bound particulate inorganic phosphorous (PIP), the third sediment pool. Dissolution of this PIP then releases phosphate back to the water column. This process increases with increasing temperature and decreasing oxygen concentrations, reaching its maximum under anoxic conditions.

2.1.3 Variable stoichiometry in ECOSMO II

We here extend the ECOSMO II formulation of pelagic and benthic OM, formerly constrained to elemental Redfield ratios, to represent variable OM stoichiometry and its consequences for carbon and nutrient cycling. For this, we introduce independent state variables for pelagic dissolved organic carbon (DOC), nitrogen (DON), and phosphorus (DOP), as well as pelagic and benthic particulate organic carbon (POC), nitrogen (PON), and phosphorus (POP). However, the internal stoichiometry of phyto- and zooplankton biomass remains at constant Redfield ratios. In accordance with Neumann et al. (2022), we assume that this provides a reasonable simplification, as healthy phytoplankton cells only marginally deviate from Redfield ratios compared to DOM and POM (Ho et al., 2003), while also limiting computational cost with reduced model complexity. However, re-

gional variations and future trends in ecosystem stoichiometry may motivate further model developments (Finkel et al., 2010; Geider and La Roche, 2002; Sardans et al., 2021). Concentrations and rates continue to use units of grams of carbon equivalent according to Redfield ratios in conformity with the model implementation. Rates depending on OM concentrations now scale with the respective C, N, or P content. Based on these changes, we implement two pathways for variable OM stoichiometry in both carbon fixation and respiration, motivated by observational evidence.

Firstly, we include an extracellular release of carbon-enriched DOM adapted from Neumann et al. (2022). While primary and secondary production are still constrained to Redfield stoichiometry, the extracellular release allows for DOM production and hence carbon fixation beyond nutrient limitation, with variable stoichiometry depending on the nutrient conditions. The release of DOM results in a corresponding uptake of DIC and nutrients independent of phytoplankton biomass, which is described as part of the full set of ecosystem model equations in the Supplement (Sect. S2). The extracellular release base rate E defined in Eq. (1) is a function of phytoplankton biomass C_{P_j}, the respective maximum uptake rates σ_j, an optional temperature dependence β_{T_j} (here only relevant for cyanobacteria), and a constant scaling factor B_{ER}, which controls the range of stoichiometric variations and organic carbon concentrations to ensure an accurate representation. It is summed over all phytoplankton groups P_j and ensures that extracellular release only persists as long as phytoplankton biomass is present and remains on a comparable scale to primary production. As the extracellular release does not generate additional phytoplankton biomass, it will eventually decline in absence of primary production.

In contrast to primary production, the extracellular release is not co-limited by the nutrient availability of nitrogen and phosphorus. Instead, nutrient and light conditions control the balance between the release of DOC, DON, and DOP. The release rates E_{DON} and E_{DOP} defined in Eqs. (2) and (3) are limited by the respective nutrient limitations β_{N} and β_{P} of nitrogen and phosphorus but also by the inverse nutrient limitations $1-\beta_{\mathrm{P}}$ and $1.1-\beta_{\mathrm{N}}$, such that the release is highest in the absence of the other nutrient source. Consequently, when primary production is limited only by one nutrient source, extracellular release increases for the less limiting nutrient source. In the absence of both nutrient sources, the extracellular release shifts to release only DOC at a rate E_{DOC}, limited by both inverse nutrient limitations, as defined in Eq. (4). Any release of DON and DOP also releases DOC, such that the release of DOM is always carbon-rich relative to elemental Redfield ratios. As it is inherent to the implementation, all limiting terms and maximum uptake rates have been adapted to align with the existing terms for primary production in ECOSMO II.

$$E = B_{\mathrm{ER}} \times \Sigma_{j=1}^{3}(\sigma_j C_{P_j} \beta_{Tj}) \tag{1}$$

$$E_{\mathrm{DON}} = \begin{cases} E \times \min\left(1-\beta_{\mathrm{P}}, \beta_{\mathrm{N}}, \alpha\left(I\right)\right), \\ \quad \beta_N > 0.1 \,\mathrm{and}\, \beta_{\mathrm{P}} < 1 \\ 0, \ \beta_N \leq 0.1 \,\mathrm{or}\, \beta_{\mathrm{P}} \geq 1 \end{cases} \tag{2}$$

$$E_{\mathrm{DOP}} = \begin{cases} E \times \min\left(\beta_{\mathrm{P}}, 1.1-\beta_{\mathrm{N}}, \alpha(I)\right), \\ \quad \beta_{\mathrm{P}} > 0.1 \,\mathrm{and}\, \beta_{\mathrm{N}} < 1.1 \\ 0, \ \beta_{\mathrm{P}} \leq 0.1 \,\mathrm{or}\, \beta_{\mathrm{N}} \geq 1.1 \end{cases} \tag{3}$$

$$E_{\mathrm{DOC}} = E_{\mathrm{DON}} + E_{\mathrm{DOP}} + \begin{cases} E \times \min\left(\max(1-\beta_{\mathrm{P}}, 1.1-\beta_{\mathrm{N}}), \alpha(I)\right), \\ \quad \beta_{\mathrm{P}} < 1 \,\mathrm{and}\, \beta_{\mathrm{N}} < 1.1 \\ 0, \ \beta_{\mathrm{P}} \geq 1 \,\mathrm{or}\, \beta_{\mathrm{N}} \geq 1.1 \end{cases} \tag{4}$$

To account for the formation of transparent exopolymer particles (Engel, 2002; Mari et al., 2017) from the released DOM, as proposed by Neumann et al. (2022), we include a flocculation rate from DOM to POM. The particle formation is thought to linearly depend on the resulting DIC uptake (Engel, 2002; Neumann et al., 2022), for which we adapt the formulation to be a function of the same limitations as the extracellular release itself. The base rate of flocculation F in Eq. (5) is defined by a constant rate F_{DOM2POM} and the scaling factor B_{ER}, both of which are specified in the configuration. The resulting fluxes F_{DON2PON}, F_{DOP2POP}, and F_{DOC2POC} as defined in Eqs. (6)–(8) are depended upon the base rate F and the respective tracer concentrations $\mathrm{C_{DON}}$, $\mathrm{C_{DOP}}$, and $\mathrm{C_{DOC}}$, as well as the same limiting factors as those that apply to the extracellular release itself. To account for the increased carbon contents in observed POM concentrations, we add the flocculation rate for nitrogen and phosphorus to the rate F_{DOC2POC} for carbon. Consequently, the POC formation is the largest under any conditions, as is the release of DOC itself.

$$F = F_{\mathrm{DOM2POM}} \times B_{\mathrm{ER}} \tag{5}$$

$$F_{\mathrm{DON2PON}} = \begin{cases} F \times \mathrm{C_{DON}} \times \min\left(1-\beta_{\mathrm{P}}, \beta_{\mathrm{N}}, \alpha(I)\right), \\ \quad \beta_{\mathrm{N}} > 0.1 \,\mathrm{and}\, \beta_{\mathrm{P}} < 1 \\ 0, \ \beta_{\mathrm{N}} \leq 0.1 \,\mathrm{or}\, \beta_{\mathrm{P}} \geq 1 \end{cases} \tag{6}$$

$$F_{\mathrm{DOP2POP}} = \begin{cases} F \times \mathrm{C_{DOP}} \times \min\left(\beta_{\mathrm{P}}, 1.1-\beta_{\mathrm{N}}, \alpha\left(I\right)\right), \\ \quad \beta_{\mathrm{P}} > 0.1 \,\mathrm{and}\, \beta_{\mathrm{N}} < 1.1 \\ 0, \ \beta_{\mathrm{P}} \leq 0.1 \,\mathrm{or}\, \beta_{\mathrm{N}} \geq 1.1 \end{cases} \tag{7}$$

$$F_{\mathrm{DOC2POC}} = F_{\mathrm{DON2PON}} + F_{\mathrm{DOP2POP}} + \begin{cases} F \times \mathrm{C_{DOC}} \\ \quad \times \min\left(\max(1-\beta_{\mathrm{P}}, 1.1-\beta_{\mathrm{N}}), \alpha(I)\right), \\ \quad \beta_{\mathrm{P}} < 1 \,\mathrm{and}\, \beta_{\mathrm{N}} < 1.1 \\ 0, \ \beta_{\mathrm{P}} \geq 1 \,\mathrm{or}\, \beta_{\mathrm{N}} \geq 1.1 \end{cases} \tag{8}$$

Under strongly nutrient-limited conditions, $\beta_{\mathrm{N}} \leq 0.1$ or $\beta_{\mathrm{P}} \leq 0.1$, the extracellular release and flocculation for DON or DOP are reduced to zero to prevent an excessive depletion of nutrients. Should $1-\beta_{\mathrm{P}}$ or $1.1-\beta_{\mathrm{N}}$ fall below zero, the respective terms are also set to zero, as the formulation would otherwise permit negative production. In practice, this state

is, however, not reached since the limitations stay within these bounds.

As a second mechanism for variable OM stoichiometry, we incorporate the preferential remineralization of organic nitrogen and phosphorus expressed through higher relative remineralization rates. The remineralization rates ϵ for all of the OM variables are defined in Eqs. (9)–(14). All rates depend on the same temperature function, here expressed in Eq. (9) for POC with the constant reference temperature T_{ref} and the simulated temperature T. The remineralization rate for DOC is defined relative to POC at a constant ratio, $\epsilon_{\text{DOC:POC}}$. Similarly, the ratios between the percentage rates of PON, POP, DON, and DOP compared to POC and DOC are defined by the constant ratios $\epsilon_{\text{POC:PON}}$, $\epsilon_{\text{POC:POP}}$, $\epsilon_{\text{DOC:DON}}$, and $\epsilon_{\text{DOC:DOP}}$, all of which are specified in the configuration. In the model configurations for this study, we selected values between zero and 1 to reflect the greater bioavailability of nitrogen and phosphorus relative to carbon. The lower the ratio, the higher the respective bioavailability. This allows for the approximation of the observed mean DOM and POM stoichiometry through a faster recycling of nutrients compared to carbon.

$$\epsilon_{\text{POC}}(T) = 0.006 \times \left(1 + 20 \times \left(\frac{T^2}{T_{\text{ref}}^2 + T^2}\right)\right) \tag{9}$$

$$\epsilon_{\text{PON}}(T) = \frac{\epsilon_{\text{POC}}(T)}{\epsilon_{\text{POC:PON}}} \tag{10}$$

$$\epsilon_{\text{POP}}(T) = \frac{\epsilon_{\text{POC}}(T)}{\epsilon_{\text{POC:POP}}} \tag{11}$$

$$\epsilon_{\text{DOC}}(T) = \epsilon_{\text{DOC:POC}} \times \epsilon_{\text{POC}}(T) \tag{12}$$

$$\epsilon_{\text{DON}}(T) = \frac{\epsilon_{\text{DOC}}(T)}{\epsilon_{\text{DOC:DON}}} \tag{13}$$

$$\epsilon_{\text{DOP}}(T) = \frac{\epsilon_{\text{DOC}}(T)}{\epsilon_{\text{DOC:DOP}}} \tag{14}$$

A complementary schematic of the OM cycling in the variable stoichiometry version of ECOSMO II is shown in Fig. 3, which illustrates how these two additional parameterizations are incorporated into the existing model structure. The full model description is provided in the Supplement (Sect. S2). This model version includes the prognostic equations for dissolved inorganic carbon (DIC) and total alkalinity (TA) for the coupling to the carbonate system model described below. These were previously introduced in Kossack et al. (2024).

2.1.4 Carbonate system model

The carbonate system model by Blackford and Gilbert (2007) describes marine carbonate chemistry based on four main state variables: DIC, TA, pH, and pCO_2. Additionally, it provides the speciation of DIC into carbonic acid (H_2CO_3), bicarbonate (HCO_3^-), and carbonate ions (CO_3^{2-}). Given two of the main state variables, the model estimates the remaining variables iteratively using the HALTAFALL algorithm (Ingri et al., 1967), a method for calculating the composition of equilibrium mixtures. Here, ECOSMO II prognostically simulates DIC and TA, thereby enabling the carbonate system model to diagnostically calculate pH, pCO_2, and the carbonate speciation based on temperature, pressure, and salinity, as in Kossack et al. (2024). For the carbonate speciation, the necessary dissociation constants are based on Millero et al. (2006).

In ECOSMO II, DIC is released into the water column by two processes: pelagic and benthic remineralization of organic carbon and zooplankton excretion. Conversely, carbon fixation by net primary production and the extracellular release of DOC consume DIC. At the ocean surface, the exchange of CO_2 with the atmosphere results in the addition or removal of DIC from the water column. The air–sea CO_2 exchange depends on the difference between the simulated surface pCO_2 and monthly prescribed atmospheric CO_2 concentrations from the Mace Head station (Lan et al., 2023) and on wind speed as described by the gas transfer parametrization in Wanninkhof (2014). Changes in TA are caused by biological uptake and release of nitrate, ammonium, and phosphate, as described in the prognostic TA formulation by Wolf-Gladrow et al. (2007) and Gustafsson (2013). A complete description of the DIC and TA equations can also be found in the full model description in the Supplement (Sect. S2). A number of previous studies have already examined carbon dynamics in the North Sea and the NWES using versions of this carbonate system model in combination with different physical and ecosystem models (Artioli et al., 2012, 2014; Blackford et al., 2017; Blackford and Gilbert, 2007; Wakelin et al., 2012).

2.1.5 Model configuration and experiments

To assess the individual and combined effects of the release of carbon-enriched DOM and the preferential remineralization of organic nitrogen and phosphorus, we compare four model configurations with identical initial conditions and forcing. The first configuration (RS), which serves as a reference simulation, adheres to Redfield stoichiometry by considering equal remineralization rates for carbon, nitrogen, and phosphorus and by neglecting the extracellular release of DOM. The second configuration (known as ER) considers the DOM release with a scaling factor of $B_{\text{ER}} = 0.4$ and equal remineralization rates. The third configuration (known as PR) includes the preferential remineralization of nitrogen and phosphorus with $+60\,\%$ and $+100\,\%$ higher bioavailability for POM and DOM, respectively. Lastly, the fourth configuration (ER&PR) combines the extracellular release and PR, both with a reduced contribution. This is expressed by a lower extracellular release scaling factor, $B_{\text{ER}} = 0.2$, and a reduced increase in bioavailability of $+30\,\%$ and $+50\,\%$ for nitrogen and phosphorus, respectively. These configurations have been developed to represent the mean sto-

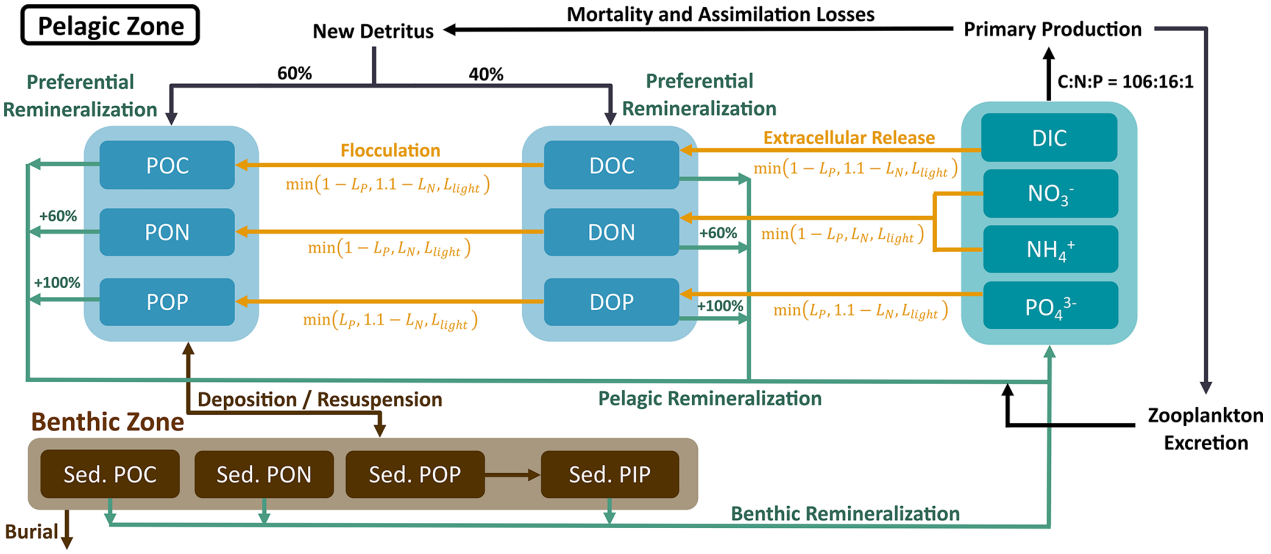

Figure 3. Schematic diagram showing the organic matter (OM) cycling in the variable stoichiometry ECOSMO II including the preferential remineralization of organic nitrogen and phosphorous, as well as the extracellular release of carbon-enriched DOM with the associated particle formation.

ichiometry of labile DOM and POM within observational bounds (Sect. 2.2.2).

All relevant parameters for the four configurations are listed in the Supplement (Table S1). The initial conditions and river discharge, open-boundary, and atmospheric forcing conditions are identical to the NWES-LR configuration in Kossack et al. (2023, 2024), except for the surface deposition of ammonium and nitrate. The spatially resolved surface deposition is now prescribed monthly rather than by a climatological mean. The monthly means are derived from EMEP MSC-W data (Simpson et al., 2012). Additional variables for DON, DOP, PON, and POP are calculated from the DOM and POM concentrations assuming Redfield stoichiometry in the initial and forcing conditions. Accordingly, any discrepancies from elemental Redfield ratios can be attributed to the aforementioned parameterizations.

Initial fields and monthly climatological means for the open-boundary conditions of temperature, salinity, nutrients, and oxygen are interpolated from the World Ocean Atlas 2018 (WOA18) data products (Garcia et al., 2018a, b; Locarnini et al., 2018; Zweng et al., 2019). For DIC and TA, the initial and boundary conditions are based on interpolated climatological fields from NNGv2LDEO (Broullón et al., 2019, 2020), a neural network (NN) approach combining the Global Ocean Data Analysis Project version 2 (Gv2) and the Lamont–Doherty Earth Observatory (LDEO) datasets. For the Baltic Sea, the TA initial conditions are instead derived from the salinity relation in Hjalmarsson et al. (2008). To account for globally increasing atmospheric CO_2 concentrations, an interannual trend from global ICON-Coast simulations (Mathis et al., 2022) is added to the DIC open-boundary conditions. Measurements from the Mace Head station (Lan et al., 2023) provide monthly mean atmospheric CO_2 forcing for the air–sea CO_2 exchange calculation. All initial sediment fields are based on ECOSMO simulations conducted by Fabian Werner (personal communication, 2023) and Samuelsen et al. (2022).

River loads of nutrients, DIC, and TA are prescribed along with river discharge for the 172 largest rivers in the model domain, while the remaining loads are set to zero. A regional dataset introduced by Daewel and Schrum (2013) and extended by Zhao et al. (2019) provides daily nutrient loads from a 21-year mean over 1995–2015. Annual mean concentrations from Pätsch and Lenhart (2004) and Neal and Davies (2003) additionally supply DIC, DOC, and TA river loads for the Scheldt, Meuse, Rhine, Ems, Elbe, Humber, Wear, Tweed, Great Ouse, and Thames. Where possible, missing TA loads are derived from the salinity relation in Hjalmarsson et al. (2008) and Artioli et al. (2012). For the remaining rivers, we use average DIC loads of 2700 µM from Pätsch and Lenhart (2004) and an average TA in the NWES of 2050 µM. Missing DOC loads are estimated to be 1/10 of the corresponding DIC concentration. Riverine DOC is assumed to be only 10 % bioavailable, as suggested by Kühn et al. (2010). This fraction is considered to be remineralized and hence is directly added to DIC.

2.2 Organic matter stoichiometry: representation and validation

2.2.1 Observed organic matter stoichiometry

The spatial and temporal variability of C : N : P stoichiometry in DOM and POM remains poorly constrained. However, case studies and global observations permit the estimation of their range of variations. Due to scarcity of measurements within the NWES, we rely on a mixture of global and regional observations. For reference, a literature compilation of both concentrations and the stoichiometry of OM in the global open ocean and various marginal seas is provided in the Supplement (Tables S3–S10). These observations indicate globally consistent compositional differences between DOM and POM, as well as between different lability fractions of DOM (Hopkinson and Vallino, 2005; Liang et al., 2023). Furthermore, some latitudinal and vertical patterns and predictors have previously been identified, including temperature and nutrient availability (Liang et al., 2023; Martiny et al., 2013; Tanioka et al., 2022b). Ecosystem stoichiometry may also change under shifting environmental conditions such as temperature, stratification, and CO_2 concentrations (Finkel et al., 2010; Moreno and Martiny, 2018; Sardans et al., 2012, 2021), which could contribute to future trends in DOM and POM composition.

In the surface layer of the global open ocean, the observed average stoichiometry of bulk DOM exhibits ranges of DOC : DON : DOP = 387–1164 : 26–123 : 1 (Hopkinson and Vallino, 2005; Letscher and Moore, 2015; Liang et al., 2023; Lønborg and Álvarez-Salgado, 2012), which is more carbon-rich than POM, with an estimated average composition of DOC : DON : DOP = 146–294 : 21–36 : 1 (Liang et al., 2023; Martiny et al., 2014; Singh et al., 2015; Tanioka et al., 2021, 2022a). For both DOM and POM, there is a persistent vertical trend that indicates increasing C : N, C : P, and N : P ratios with depth. This relation is thought to arise as organic nitrogen and phosphorus is preferentially respired, leaving older and deeper material more carbon-rich (Hopkinson and Vallino, 2005; Letscher and Moore, 2015; Painter et al., 2017; Tanioka et al., 2021).

In the case of DOM, this vertical gradient is more pronounced, which is linked to old and strongly nutrient-depleted refractory material. The continuous spectrum of lability in DOM is typically simplified into two or three pools of (semi-)labile (LDOM) and refractory DOM (RDOM) (Hansell et al., 2009). While the labile and semi-labile fractions have a life time of days to years, the refractory pool has an average age of approximately 6000 years (Bauer et al., 1992; Hansell et al., 2009). Over time, the bioavailable compounds are removed, leaving the remaining refractory material highly carbon-rich, with an observed average stoichiometry of RDOC : RDON : RDOP = 1373–3511 : 10–202 : 1 (Aminot and Kérouel, 2004; Hopkinson and Vallino, 2005; Liang et al., 2023; Lønborg and Álvarez-Salgado, 2012).

Despite its high carbon content, RDOM only acts as a minor source of inorganic carbon and nutrients on sub-millennial timescales due to its slow formation and decomposition (Hopkinson and Vallino, 2005). In contrast, LDOM, with an observed average stoichiometry of LDOC : LDON : LDOP = 179–199 : 20 : 1 (Hopkinson and Vallino, 2005; Liang et al., 2023) in the global surface ocean, acts as the major control on the recycling of carbon and nutrients on shorter timescales. Consequently, the majority of OM cycling on the annual to decadal timescales considered here occurs at an intermediate stoichiometry between the composition of bulk DOM and elemental Redfield ratios (Hopkinson and Vallino, 2005). The balance between concentrations of RDOM and LDOM to a large extent determines the vertical gradient in bulk DOM stoichiometry (Aminot and Kérouel, 2004). High LDOM concentrations are only observed in surface waters, while RDOM concentrations are instead vertically homogeneous (Aminot and Kérouel, 2004; Hansell and Carlson, 1998). Hence, the fraction of RDOM, and with that the relative carbon content in bulk DOM, increase with depth (Aminot and Kérouel, 2004; Hopkinson and Vallino, 2005; Hung et al., 2003; Liang et al., 2023).

In marginal seas such as the North Sea and Baltic Sea, river discharge and water residence times may further control bulk DOM stoichiometry (Voss et al., 2021). Regions of freshwater influence exhibit higher carbon contents, with DOC : DON : DOP = 1199–3714 : 52–221 : 1 (Stepanauskas et al., 2002; Voss et al., 2021). This is attributed to the elevated C : N ratios of 30–60 : 1 observed in riverine OM (Bauer et al., 2013). Long residence times in the Baltic Sea facilitate the accumulation of riverine organic matter, in contrast to the relatively short residence times in the North Sea, which reduce the influence of riverine inputs on bulk OM stoichiometry. These factors contribute to the large regional variations, for which we provide an overview in the literature compilation.

2.2.2 Simulated organic matter stoichiometry

To ascertain a realistic magnitude of the preferential remineralization and the release of carbon-enriched DOM, we identified parameter settings for which the simulated stoichiometry adheres to observational bounds for LDOM and POM. Accordingly, we reduced the contribution of each mechanism in the ER&PR configuration to ensure consistency across all configurations. We found that using the parameter settings from the individual configurations in the combined ER&PR configuration resulted in C : N and C : P ratios significantly exceeding those that were observed and in the other configurations, making their comparison less meaningful.

It should be noted that the DOM simulated in ECOSMO is fully biodegradable, with the majority of DOM produced being respired within 1 year. Consequently, the simulated DOM

represents a spectrum of only labile and semi-labile DOM but not RDOM. The latter is not currently considered, as its impact on the carbon and nutrient cycles is assumed to be negligible on the timescales in question. Therefore, we assess the simulated DOM concentrations and stoichiometry with respect to observations of LDOM. Given the large discrepancies in C : N : P stoichiometry of bulk DOM, LDOM, and RDOM, we assume this to be the most reasonable approach.

As a representation of the simulated OM stoichiometry, we present the time-averaged horizontal distribution of column-integrated C : N, C : P, and N : P ratios, as well as vertical profiles of horizontally averaged ratios over the northern, central, and southern North Sea. Figures 4 and 5 show these distributions for the ER, PR, and ER&PR configurations for DOM and POM, respectively. Observations do not allow us to resolve regional vertical profiles. For this reason, we compare the simulated stoichiometry to observed ranges and, where available, the observed mean composition, independent of depth. In the NWES, observations of DOM stoichiometry are limited to bulk DOM, without a distinction between LDOM and RDOM (Chaichana et al., 2019; Davis et al., 2014, 2019; Painter et al., 2018; Suratman et al., 2009). Thus, we compare the vertical distribution of DOM stoichiometry to globally estimated ranges for LDOM from Hopkinson and Vallino (2005) and Liang et al. (2023). In contrast, for POM stoichiometry, we provide both global estimates from Liang et al. (2023), and regional estimates from the Hebrides Shelf (Painter et al., 2017) and the Celtic Sea (Davis et al., 2014, 2019). This is because direct observations for the North Sea are limited to C : N ratios and do not provide estimated mean compositions (Chaichana et al., 2019; Suratman et al., 2009).

Overall, the simulated DOM stoichiometry reproduces the observed range within reasonable limits (Fig. 4). The mean simulated DOC : DON ratios of 10.2–11.2 compare well with the observed means and ranges of 8.9 (5.4–12.0) and 10.7 (8.7–14.1). Similarly, simulated mean DOC : DOP ratios of 198–232 agree with the observational estimates of 179 (83–414) and 199 (154–245). In both cases, the ER&PR configuration is on the upper end of the range, with the ER and PR configurations being more central. In terms of the DON : DOP ratios, all configurations reproduce the observed means of 20 (15–49) and 20 (16–25), with mean simulated DON : DOP ratios of 19.5–20.7. For all three elemental ratios, the PR configuration shows the observed increase with depth as N and P are preferentially removed. This is not the case for the ER configuration, where the additional DOM is only released in the euphotic zone. In terms of the horizontal distribution, the carbon enrichment is highest for the ER configuration in the central and northern parts of the North Sea, as well as in the deep parts of the Atlantic Ocean. This shows a higher DOC accumulation in nutrient depleted areas, as expected from the implementation. For the PR configuration, instead, the carbon contents are highest in the Norwegian Trench and along the shelf edge, where OM respiration is generally high, which amplifies the difference in remineralization rates. The average composition is close to the surface DOM composition, as DOM concentrations rapidly decrease with depth below the euphotic zone.

The simulated POM stoichiometry is also consistent with the observed ranges but is more challenging for the observed mean ratios, as only one global study explicitly provides an average composition (Fig. 5). Simulated mean POC : PON ratios of 7.4–8.1 are consistent with the global mean of 7.7 (6.1–9.2) and the ranges of 8.3–13.7 and 4.3–11.6 for the Hebrides Shelf and the Celtic Sea. Likewise, the simulated POC : POP ratios of 139–158 are within the center of the observed mean and ranges of 160 (73–295), (142–260), and (63–283), with the PR configuration being closest to the estimated mean. The increased PON : POP ratios compared to Redfield stoichiometry are reproduced in all configurations. Simulated PON : POP ratios of 19.0–19.6 are comparable to the observational estimates, with a mean and ranges of 21 (10–37), (16–26), and (10–47). For all three elemental ratios, the PR configuration shows the highest and the ER configuration the lowest horizontal averages across all vertical levels. As for DOM, the increasing ratios with depth indicated by DOM and POM observations are reproduced by the PR but not the ER configuration. The horizontal distribution for the ER configuration shows the highest carbon enrichment in the central and northern North Sea, the same as for DOM. In contrast, the PR configuration instead shows homogeneous elemental ratios across the NWES but high carbon enrichment in the deep, open Atlantic. Altogether, simulated DOM and POM stoichiometry both reasonably represent the available observations.

2.3 Impact on model performance

The ability of SCHISM-ECOSMO-CO_2 to reproduce the observed variability in temperature, nutrients, and carbonate system variables in the NWES has already been established in Kossack et al. (2023, 2024). As the extended OM representation in the variable stoichiometry ECOSMO II version may have consequences for the model validation, we here describe the effects of the model extension on the model validation in the ER, PR, and ER&PR configurations compared to the RS reference configuration. With the primary objective being to investigate the consequences of the proposed modifications on marine carbon cycling, particularly with regard to the biological uptake of inorganic carbon, we provide a more comprehensive account of the carbonate system validation. Differences in the model representation compared to Kossack et al. (2023, 2024) may also be linked to the different data availability in the simulated time period, to the monthly resolved surface deposition, and to a reduced remineralization rate for DOM. The latter was adjusted for a better representation of DOC concentrations, which are essential for assessing the effects of variable stoichiometry. This is

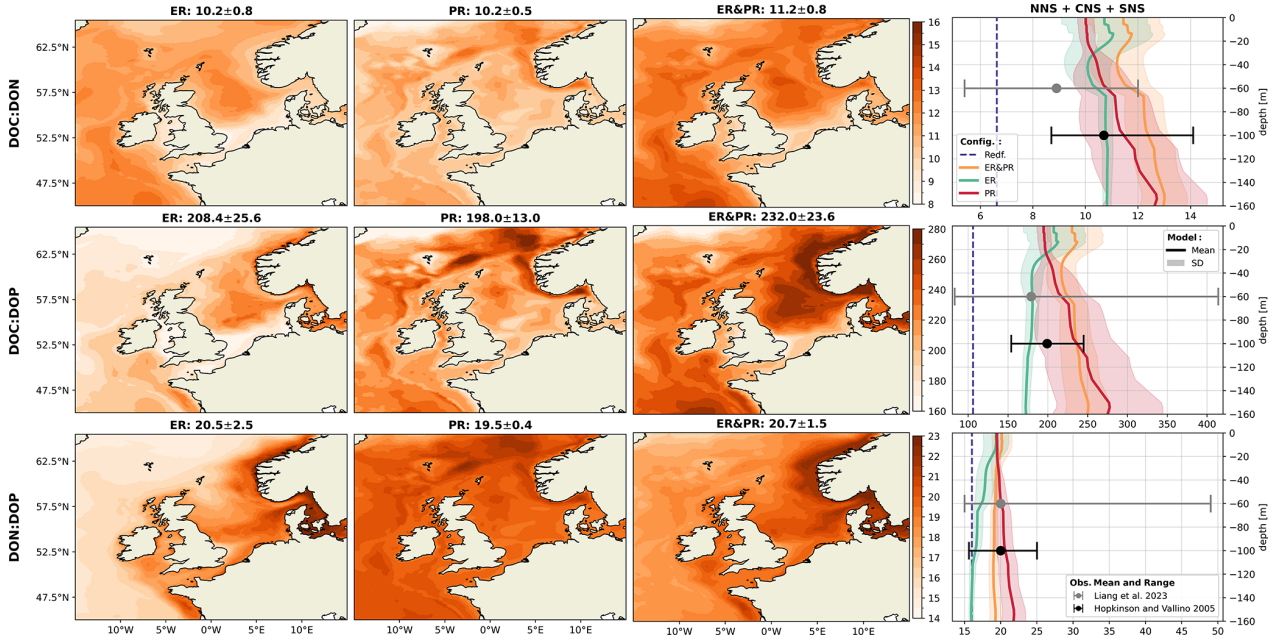

Figure 4. Mean DOM stoichiometry for the ER, PR, and ER&PR configurations over the simulation period of 2000–2010. The first three columns show the vertically integrated horizontal distribution. For each elemental ratio and configuration, the titles display the mean values and the respective standard deviations over the NWES. The last column shows the vertical distribution of simulated horizontal mean stoichiometry and the corresponding standard deviation over the NNS, CNS, and SNS sub-areas. Observed depth-independent ranges in DOM stoichiometry and the estimated mean composition from Hopkinson and Vallino (2005) and Liang et al. (2023) are represented by the error bars. The corresponding Redfield ratios of C : N = 6.625, C : P = 106, and N : P = 16 are indicated by the dashed blue lines in the vertical profiles. The horizontal means and standard deviations over the entire NWES are listed above the horizontal distributions. For the vertical profiles, the horizontal standard deviation is represented by the shaded area around the solid lines.

associated with a decrease in nutrient availability and hence productivity.

Based on surface, bottle, and pump data from the ocean hydrochemistry data collection of the International Council for the Exploration of the Sea (ICES), we find that there is no significant improvement or deterioration in the model representation of phosphate and nitrate for any of the three variable stoichiometry configurations with respect to the reference configuration. For these variables we provide the horizontal distribution of seasonal model biases at co-located data points and corresponding Taylor diagrams in the Supplement (Figs. S1–S6). The spatial distribution of regional and seasonal biases is persistent across all configurations, which results in overall negligible differences in the resulting model performance. We include temperature and salinity for the RS configuration, as it may have a relevant influence on the carbonate system calculations. All other configurations are excluded for the physical variables, as the physical simulations are equivalent.

In the validation for the carbonate system, we assess DIC, TA, and pCO_2. While we do not discuss TA in the results of this study, it is used to derive the simulated pCO_2 and, as such, is relevant to the model performance. We compare the simulated DIC and TA concentrations to a total of 5685 and 5110 observations from the Global Ocean Data Analysis Project (GLODAP). Additionally, we validate the simulated CO_2 concentrations against 772 202 CO_2 fugacity (fCO_2) measurements from the Surface Ocean CO_2 Atlas (SOCAT). For this, the observed fCO_2 values are converted to pCO_2 using the Python library PyCO2SYS (Humphreys et al., 2022, 2024). Simulated surface CO_2 concentrations are converted to pCO_2 according to Eqs. (15)–(16) from the guide to best practices by Dickson et al. (2007) and an updated water vapor pressure equation as a function of temperature from Huang (2018). Here, xCO_2 is the simulated dry mole fraction, p_{air} and p_{H_2O} are the air and water vapor pressure, and T is the simulated temperature.

$$pCO_2 = xCO_2 \times (p_{air} - p_{H_2O}) \tag{15}$$

$$p_{H_2O} = 9.869 \times \exp\left(34.494 - \frac{4924.99}{T + 237.1}\right) \times (T + 105)^{-1.57} \tag{16}$$

In stark contrast to the nutrient validation, there is a significant discrepancy between the model configurations with respect to DIC and pCO_2 related to changes in the inorganic carbon uptake. TA validation, however, does not differ significantly between configurations. This is demonstrated by the

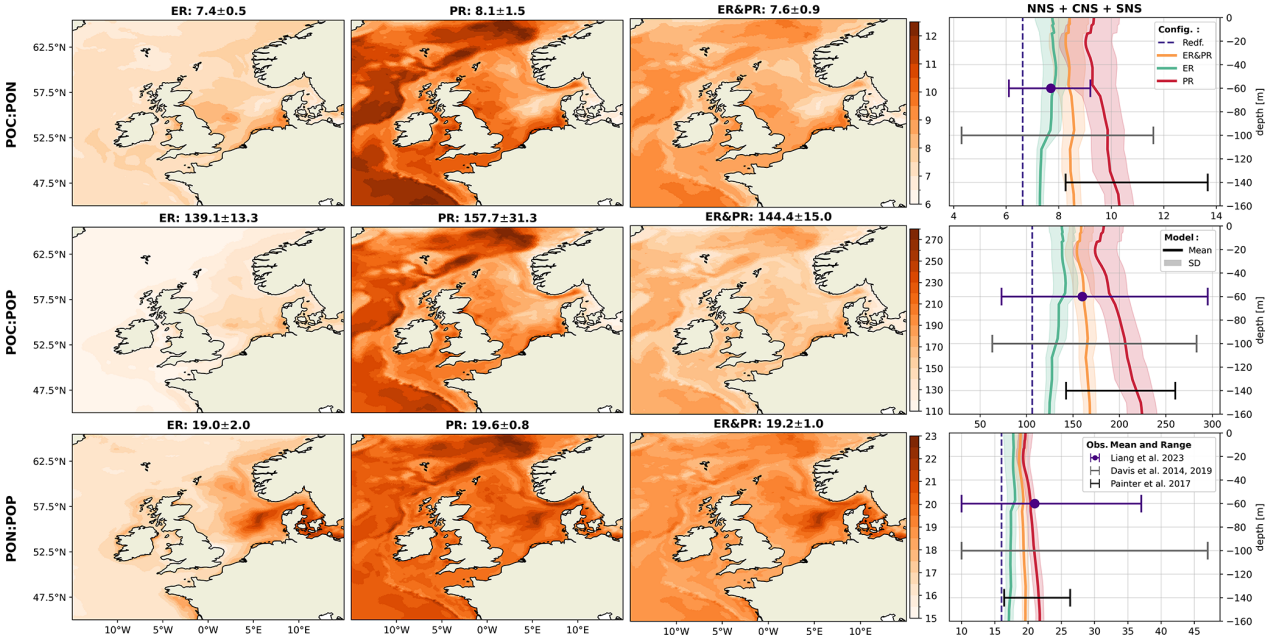

Figure 5. Mean POM stoichiometry for the ER, PR, and ER&PR configurations over the simulation period of 2000–2010. The first three columns show the vertically integrated horizontal distribution. For each elemental ratio and configuration, the titles display the mean values and the respective standard deviation over the NWES. The last column shows the vertical distribution of simulated horizontal mean stoichiometry and the corresponding standard deviation over the NNS, CNS, and SNS sub-areas. Observed depth-independent ranges in POM stoichiometry and the estimated mean composition from Liang et al. (2023), Davis et al. (2014, 2019), and Painter et al. (2017) are represented by the error bars. The corresponding Redfield ratios of $C:N = 6.625$, $C:P = 106$, and $N:P = 16$ are indicated by the dashed blue lines in the vertical profiles. The horizontal means and standard deviations over the entire NWES are listed above the horizontal distributions. For the vertical profiles, the horizontal standard deviation is represented by the shaded area around the solid lines.

changes in the corresponding Taylor diagrams in Fig. 6. The Taylor diagrams represent the model performance in terms of the correlation, normalized standard deviation (NSD) with respect to the observations, and their normalized and centered root-mean-squared difference (RMSD). As complementary indicators of the model performance, we provide the seasonal co-located model biases and the mean percentage biases in the Supplement (Figs. S7–S9 and Table 2).

With regard to DIC, the RS configuration underestimates the observed variability in the NNS, CNS, SNS, and NT, with an NSD of 0.48–0.80 (Fig. 6). Compared to this, the configurations allowing for variable OM stoichiometry show a consistent improvement in the represented variability, with an NSD of 0.70–0.98, 0.55–0.85, and 0.63–0.90 for the ER, PR, and ER&PR configurations, respectively (Fig. 6). With an average increase in NSD of 0.07–0.21, these more closely reproduce the range of observed variability across all sub-regions. The improvement is consistently largest for the ER and smallest for the PR configuration. This range of improvement is proportional to the additional DIC uptake from biological carbon fixation, which is discussed below. Only in the SK sub-region does the NSD exceed 1 in the RS configuration, showing an increase from 1.17 to 1.21–1.32, which adds to the overestimation of the observed variability. Differences in the correlation between the configurations are negligible, with correlation coefficients of 0.81–0.88 for the NNS, CNS, and NT sub-regions (Fig. 6). For the SK and SNS, the correlation is weaker, with correlation coefficients of 0.71–0.72 and 0.60–0.66, respectively. Improvements in the correlation may be limited due to an expected mismatch between the small-scale variability captured in measurements and simulated average concentrations on much larger scales. The model's percentage bias in DIC is generally between 0.6 % and 1.3 % and does not show any conclusive differences between configurations (Table S2).

Differences in the model performance for TA are negligible and inconsistent across sub-regions, ranging from 0.002 to 0.013 in the NSD and 0.001 to 0.003 in the correlation coefficients (Fig. 6). The correlation is generally weaker for TA than for DIC, which can be attributed to both missing constituents in ECOSMO II that contribute to changes in TA (Wolf-Gladrow et al., 2007) and to uncertainties in terrestrial TA sources. In the SNS and NT sub-regions, the correlation coefficients of 0.60 and 0.82 are on the higher end. In comparison, the NNS and CNS have correlation coefficients of 0.29 and 0.40, which are more influenced by exchange with the Atlantic and less by river discharge. This may suggest

that not only terrestrial sources contribute to the lower correlation but local alkalinity generation also contributes.

As pCO_2 is largely dependent on DIC, improvements in the representation of DIC are expected to be reflected, to some extent, in the representation of pCO_2. However, given the considerably greater data availability for pCO_2, we provide a validation here explicitly. For the simulated surface pCO_2, as for DIC, there is an improvement in the representation of the observed variability in most of the sub-regions. Additionally, several sub-regions show a significant increase in correlation in combination with a small but consistent decrease of approximately 0.2 %–3.3 % (Table S2) in the percentage bias across all sub-regions except from the SK and SWC regions. The correlation coefficients for the NNS, CNS, SNS, NT, SK, EC, and AS regions increase significantly from 0.66, 0.60, 0.36, 0.21, 0.34, 0.43, and −0.06 in the RS configuration to 0.78, 0.76, 0.53, 0.42, 0.44, 0.59, and 0.39 in the ER configuration (Fig. 6). This increase in correlation is similarly dependent on the increase in inorganic carbon uptake, the same as for the changes in standard deviation for DIC. The PR and ER&PR configurations yield intermediate results, with the lowest increase in correlation for the PR configuration. Only for the SWC does the correlation remain rather consistent. Likewise, the observed standard deviation is more closely represented in the NNS, CNS, SNS, EC, SWC, and AS sub-regions by variable OM stoichiometry. The corresponding NSD increases from 0.67, 0.81, 0.70, 0.65, 0.75, and 0.37 in the RS configuration up to 1.10, 1.08, 0.87, 0.74, 1.14, and 0.48 in the ER configuration (Fig. 6). Variability is generally overestimated in the NT and SK sub-regions, likely due to the representation of rivers as point sources rather than explicitly resolved estuaries.

In summary, the variable stoichiometry configurations consistently improve model performance in terms of the represented range of variability for DIC and pCO_2, represented by the NSD, as well as the correlation with observations for pCO_2. The magnitude of the improvement is lowest in the PR and highest in the ER configuration, which is related to the corresponding increase in biological uptake of inorganic carbon, as discussed below. This supports the need to account for carbon overconsumption compared to estimates based on Redfield stoichiometry. While variable OM stoichiometry here improves the representation in terms of the range of variability, some challenges remain in representing the timing of DIC release in autumn. This is further discussed below with respect to surface DIC concentrations. Overall, the changes in TA are negligible, indicating that the implementation has a minimal impact on TA.

2.4 Net community production

Net community production (NCP), defined as the difference between carbon fixation and respiration, is a metric used to assess whether a system is net autotrophic (NCP >0), with a net production of organic carbon, or net heterotrophic (NCP <0), with a net respiration of organic carbon (Smith and Hollibaugh, 1993). Net autotrophic regions typically act as a sink for inorganic carbon, while net heterotrophic regions increase the inorganic carbon content respired from additional imported organic carbon (Thomas et al., 2005). For this study we define NCP as carbon fixation through primary production and the extracellular release of DOC minus carbon respiration, which consists of pelagic and benthic remineralization as well as zooplankton excretion contributing to DIC release (Fig. 3).

3 Results

3.1 Annual carbon fluxes

As a first step towards quantifying the large-scale effects of both pathways for variable OM stoichiometry on OM cycling and the resulting changes in the air–sea CO_2 exchange, we assess their influence on key annual carbon fluxes and their seasonal variability. In particular, we examine the effects on vertically integrated carbon fixation, carbon respiration, NCP, and the air–sea CO_2 exchange. We begin by assessing changes in the balance between organic carbon production and respiration to understand how the associated uptake and release of inorganic carbon contributes to resulting changes in the oceanic CO_2 uptake.

3.1.1 Biological carbon fixation

Biological carbon fixation exhibits a consistent percentage increase between the North Sea and the entire NWES for each of the variable stoichiometry configurations (Fig. 7). However, the magnitude of this increase varies considerably, with the PR configuration showing the smallest and the ER configuration showing the largest increase. In comparison to the vertically integrated carbon fixation in the North Sea of 4.5 Tmol C yr^{-1} for the RS configuration, the PR, ER&PR, and ER configurations exhibit a notable increase, reaching 4.9 (+10 %), 6.0 (+34 %), and 6.9 Tmol C yr^{-1} (+55 %), respectively. For the entire NWES, the corresponding reference carbon fixation of 9.7 Tmol C yr^{-1} increases to 10.6 (+9 %), 12.8 (+32 %), and 14.8 Tmol C yr^{-1} (+52 %).

In the RS reference configuration, carbon fixation is highest in the shallow and well-mixed shelf regions (Fig. 8a), including the SNS, EC, AS, CS, IS, ISS, and NWA sub-areas (Fig. 2). The highest annual sub-region mean is reached in the Celtic Sea, with a mean value of 9.1 mol C m^{-2} yr^{-1}. In contrast, the lowest annual mean of carbon fixation is found in the deeper central North Sea, with a value of 7.2 mol C m^{-2} yr^{-1}. This is due to the seasonal stratification, which promotes nutrient limitation. The spatial distribution of simulated carbon fixation is consistent with the established physical controls on primary production and its characteristic spatial pattern in the NWES (Holt et al., 2012).

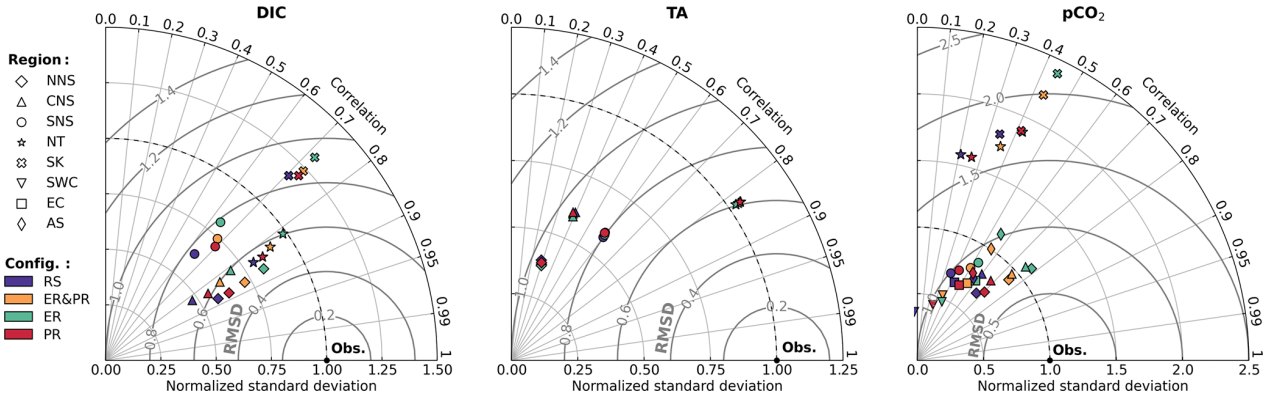

Figure 6. Taylor diagrams for simulated dissolved inorganic carbon (DIC), total alkalinity (TA), and partial pressure of CO_2 (pCO_2) in comparison to the GLODAPv2022 and SOCATv2023 datasets, including all four model configurations. The model performance is represented in terms of correlation, normalized standard deviation, and normalized and centered root mean square difference (RMSD), with respect to the observations. Regions were selected based on sufficient data availability. The results are differentiated by configuration, as indicated by color, and sub-region, as indicated by shape.

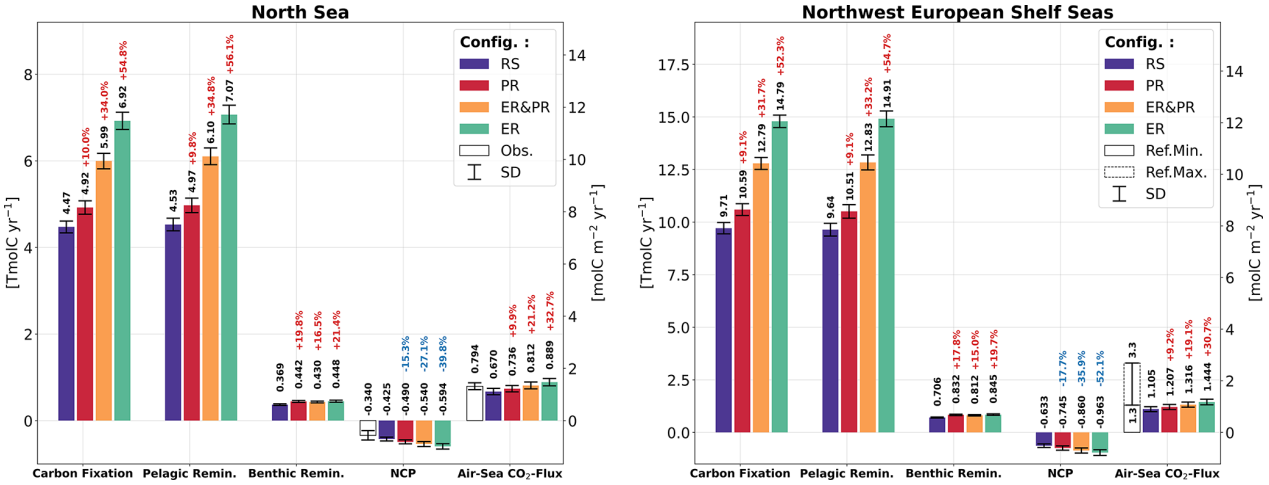

Figure 7. Simulated annual vertically integrated carbon fixation, pelagic and benthic remineralization, net community production (NCP), and net air–sea CO_2 exchange for all four model configurations, averaged over the simulated period of 2000–2010. The air–sea CO_2 flux is defined downward such that positive values indicate an oceanic uptake and negative values an outgassing of CO_2. The error bars show the corresponding standard deviation. White bars show the literature estimates and ranges for NCP and the air–sea CO_2 exchange in the North Sea from Thomas et al. (2005) and the estimated range of the air–sea CO_2 exchange in the NWES from Legge et al. (2020), with reference to both modeling and observational studies. The annual time series for selected sub-regions and the average fluxes for all sub-regions are provided in the Supplement (Figs. S10–S14 and Tables S11–S15).

Across the North Sea area, the carbon fixation response differs considerably between the PR and ER configurations. For the ER configuration, the largest increase in carbon fixation here is observed in the CNS, NNS, and NT sub-regions, with values ranging from 3.9 to 4.7 mol C m^{-2} yr^{-1} (Fig. 8a). In contrast, the SNS sub-region exhibits a smaller increase, with a value of 3.2 mol C m^{-2} yr^{-1}. Conversely, the PR configuration exhibits the highest increase of 0.9 mol C m^{-2} yr^{-1} in the SNS and smaller increases of 0.4–0.7 mol C m^{-2} yr^{-1} in the CNS, NNS, and NT sub-regions. Consequently, the north–south gradient in productivity is weakened in the ER configuration but strengthened in the PR configuration. There is an evenly distributed positive response in the outer shelf regions, while some inner shelf regions, including the EC, IS, and ISS, show a much weaker response. All configurations further show a large increase in carbon fixation in the AS region, from 1.2 to 5.6 mol C m^{-2} yr^{-1}. Consistent with the mean annual changes, the amplitude of these changes is largest in the ER and smallest in the PR configuration.

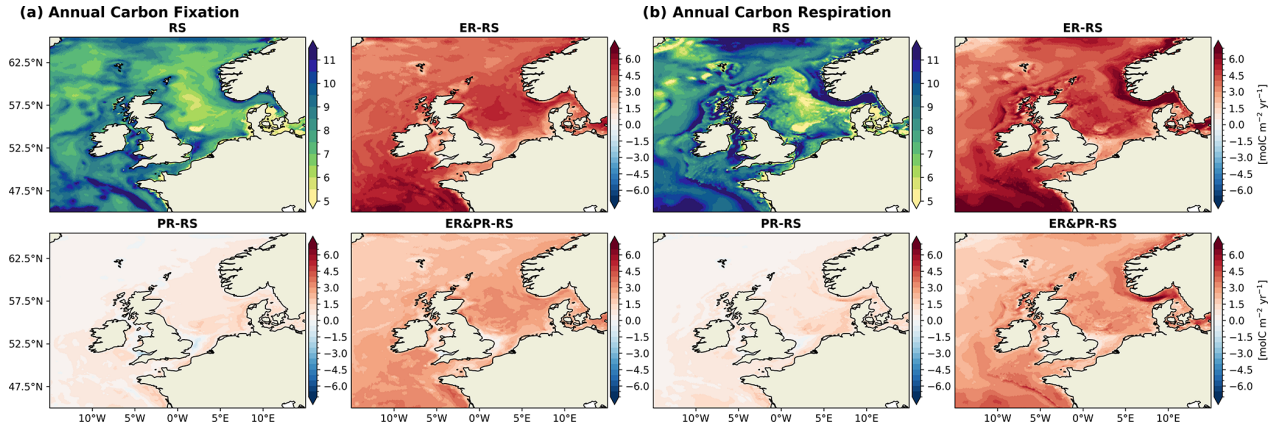

Figure 8. Spatial distribution of annual mean vertically integrated **(a)** carbon fixation and **(b)** respiration, including pelagic and benthic remineralization, for the RS configuration and differences for the ER, PR, and ER&PR configurations over the simulation period of 2000–2010. The respective seasonal means for carbon fixation and respiration are provided in the Supplement (Figs. S15 and S16).

3.1.2 Carbon respiration

The rate of carbon respiration exceeds the rate of carbon fixation in the North Sea and the entire NWES in all configurations (Fig. 7). In the RS configuration, the magnitude of pelagic remineralization is comparable to that of carbon fixation, with annual means of 4.5 Tmol C yr^{-1} in the North Sea and 9.6 Tmol C yr^{-1} across the entire NWES. The additional benthic remineralization of 0.37 and 0.70 Tmol C yr^{-1}, however, results in a total respiration that surpasses carbon fixation. In comparison, the variable stoichiometry configurations exhibit higher pelagic remineralization, reaching values of 5.0 (+10 %), 6.1 (+35 %), and 7.1 Tmol C yr^{-1} (+56 %) for the North Sea in the PR, ER&PR, and ER configurations, respectively. In the entire the NWES, the corresponding values are 10.5 (+9 %), 12.8 (+33 %), and 14.9 Tmol C yr^{-1} (+55 %). In contrast, the increases in benthic remineralization are equal across configurations and thus do not match this percentage increase. The annual means of benthic remineralization are 0.44 (+20 %), 0.43 (+17 %), and 0.45 Tmol C yr^{-1} (+21 %) in the North Sea and 0.83 (+18 %), 0.81 (+15 %), and 0.85 Tmol C yr^{-1} (+20 %) in the NWES. This is likely linked to a comparable increase in POC concentrations, which is further discussed below.

The pattern of the RS reference carbon respiration (Fig. 8b) resembles the distribution of carbon fixation, with the exception of the NT region. Similar to carbon fixation, respiration is particularly low in the CNS, 7.5 mol C m^{-2} yr^{-1}, and particularly high in the western outer shelf regions, up to 9.3 mol C m^{-2} yr^{-1} in the SWC. However, respiration reaches its maximum in the NT, with an average rate of 11.1 mol C m^{-2} yr^{-1} despite only moderate carbon fixation. The north–south gradient in the impact of carbon respiration across the North Sea is positive in the PR configuration and negative in the ER and ER&PR configurations. The preferential remineralization thus increases the north–south gradient in production and respiration. Conversely, the extracellular release of DOC promotes production and respiration in the otherwise nutrient-depleted and less biologically productive areas. The strong respiration in the NT is further enhanced by 16.1 mol C m^{-2} yr^{-1} in the variable stoichiometry configurations. Otherwise, the differences are consistent with the increases in carbon fixation.

Shifts in the balance between carbon fixation and respiration rather than either process alone play a crucial role in air–sea CO_2 exchange, influencing whether specific locations act as sources or sinks of DIC. Therefore, we will further assess the annual NCP, focusing on both vertically integrated values and the vertical gradient between the surface and sub-surface layers.

3.1.3 NCP

Overall, the North Sea and the entire NWES are net heterotrophic in all configurations, with a corresponding NCP of −0.43 and −0.63 Tmol C yr^{-1} in the RS configuration (Fig. 7). For the North Sea, this value is situated at the lower end of the uncertainty range from observations, with an estimated NCP of -0.34 ± 0.11 Tmol C yr^{-1} reported in Thomas et al. (2005). The PR, ER&PR, and ER configurations exhibit a stronger net heterotrophy (i.e., lower NCP), with NCP values of −0.49 (−15 %), −0.54 (−27 %), and −0.59 Tmol C yr^{-1} (−40 %) in the North Sea. In the NWES, the percentage decrease in NCP is even more pronounced, with an annual NCP of −0.75 (−18 %), −0.86 (−36 %), and −0.96 Tmol C yr^{-1} (−52 %).

In the RS configuration, net autotrophic regions are found in the shallow coastal areas of the SNS, EC, CS, IS, and NWA sub-regions; the shelf edge; and the Dogger Bank (Fig. 9a). The most pronounced net autotrophic region is a broad band in the North Sea along the Norwegian Trench.

Conversely, beyond the 200 m isobath, the NT and the deep parts of the SK region are the most net heterotrophic regions across the entire shelf. This results in a large NCP gradient across the slope. Similarly, portions of the shelf slope and the deeper central IS, ISS, and NWA sub-regions exhibit comparatively elevated net heterotrophy, with net autotrophy observed in adjacent, shallower areas. The remaining shelf area is largely weakly net heterotrophic or nearly neutral.

The most notable NCP response is the intensification of the aforementioned gradient between net autotrophy along the edge of the NT region and the net heterotrophy inside the NT region. This feature indicates an increase in OM that is produced in the CNS, transported into the NT, and subsequently remineralized. The variable stoichiometry configurations demonstrate a reinforcement of the pre-existing pattern of NCP across the entire shelf area. This is expressed by an increase in NCP in net autotrophic and a decrease in NCP in net heterotrophic regions. The RS reference NCP is lowest in the NT and SK regions, with annual means of -3.2 and $-1.0\,\mathrm{mol\,C\,m^{-2}\,yr^{-1}}$, respectively. These regions also exhibit the most pronounced NCP response, with decreases of -0.3 to $-1.6\,\mathrm{mol\,C\,m^{-2}\,yr^{-1}}$ in the NT and -0.3 to $-1.0\,\mathrm{mol\,C\,m^{-2}\,yr^{-1}}$ in the SK subregion. In accordance with the response in carbon fixation and respiration, the PR configuration overall shows the weakest decrease, while the ER configuration shows the strongest decrease. Nevertheless, even in the PR configuration, the largest decrease in NCP is shown in the NT and SK regions, thereby amplifying the pre-existing NCP gradient. In the SNS, IS, and ISS, the impact is intermediate, with values ranging from -0.1 to $-0.2\,\mathrm{mol\,C\,m^{-2}\,yr^{-1}}$, and it is less significant in the remaining regions. The ER configuration shows an increase in the CNS and AS, with a range of 3–$0.05\,\mathrm{mol\,C\,m^{-2}\,yr^{-1}}$. A significant decrease can be seen in the NNS, SNS, SWC, IS, ISS, HS, and MS, with a range of -0.2 to $-0.4\,\mathrm{mol\,C\,m^{-2}\,yr^{-1}}$.

While the increase in carbon fixation is limited to the euphotic zone, where sufficient light and nutrients are available, respiration increases in both the surface and sub-surface layers (Fig. 10). In the upper 50 m, pelagic remineralization is approximately 10 %–61 % higher in the variable stoichiometry configurations. Below 50 m, the remaining water column shows a smaller increase in pelagic remineralization of approximately 5 %–41 %. The separation into carbon fixation at the surface only and respiration across various depths leads to opposite changes in the pelagic NCP (i.e., excluding benthic remineralization) between the surface and sub-surface layers. The net autotrophic surface layer above 50 m becomes increasingly autotrophic, by 7 %–34 %, while the remaining water column becomes more net heterotrophic, by 6 %–41 %. This enhanced vertical gradient in NCP suggests a stronger depletion of DIC in surface waters and a stronger release of DIC at depth, implying a stronger biological control on surface pCO_2 and an increase in the resulting oceanic CO_2 uptake.

3.1.4 Enhanced seasonal organic matter cycling

The impacts of variable stoichiometry on the annual means result from marked changes in the seasonality of carbon fixation and respiration. Across all configurations, carbon fixation in the North Sea and the NWES exceeds respiration between mid-January and the end of May, reaching its maximum at the beginning of May (Fig. 9b). Carbon respiration accordingly surpasses carbon fixation at the end of May and remains higher until mid-January, with the maximum reached in July. This results in a range of approximately 4.5 months of net autotrophy, with the maximum NCP in April, and 7.5 months of net heterotrophy, with minimum NCP in October.

Considering the observed OM stoichiometry in our simulations leads to an intensification of seasonal carbon fixation, respiration, and NCP. As with the annual mean fluxes, the intensification is lowest for the PR configuration and highest for the ER configuration. The maximum reference carbon fixation of $16.3\,\mathrm{mol\,C\,m^{-2}\,yr^{-1}}$ reached in May increases to a range of 18.3 (+12 %) to $26.2\,\mathrm{mol\,C\,m^{-2}\,yr^{-1}}$ (+60 %) in the NWES. Similarly, the maximum carbon respiration of $15.1\,\mathrm{mol\,C\,m^{-2}\,yr^{-1}}$ in July increases to values of 16.9 (+12 %) to $23.3\,\mathrm{mol\,C\,m^{-2}\,yr^{-1}}$ (+54 %). For NCP, both the maximum of $7.1\,\mathrm{mol\,C\,m^{-2}\,yr^{-1}}$ in April and the minimum of $-4.3\,\mathrm{mol\,C\,m^{-2}\,yr^{-1}}$ in October are enhanced. The seasonal maximum in NCP increases to a range of 7.7 (+8 %) to $12.3\,\mathrm{mol\,C\,m^{-2}\,yr^{-1}}$ (+72 %) in the variable stoichiometry configurations. At the same time, the seasonal minimum decreases to an amplitude of -4.8 (-13 %) to $-7.3\,\mathrm{mol\,C\,m^{-2}\,yr^{-1}}$ (-72 %). The response is nearly identical in the North Sea. In conclusion, these results indicate that variable OM stoichiometry intensifies both the seasonal biological production of organic carbon and its subsequent degradation. In combination with the lateral and vertical gradient in NCP, this finding suggests an increased biological control of the seasonal pCO_2 and the resulting air–sea CO_2 exchange.

3.1.5 Net air–sea CO_2 exchange

In response to the enhanced OM cycling, all variable stoichiometry configurations result in an increased net oceanic CO_2 uptake from the atmosphere. The magnitude of this increase in the CO_2 uptake, compared across configurations, is proportional to the increase in carbon fixation and respiration (Figs. 7–9) and the resulting increase in the vertical gradient of NCP (Fig. 10). The reference simulation yields an average net CO_2 uptake by the ocean of $0.67\,\mathrm{Tmol\,C\,yr^{-1}}$ for the North Sea and $1.11\,\mathrm{Tmol\,C\,yr^{-1}}$ for the entire NWES. These values are slightly below observational estimates of $0.79\,\mathrm{Tmol\,C\,yr^{-1}}$ for the North Sea (Thomas et al., 2005) and 1.3 to $3.3\,\mathrm{Tmol\,C\,yr^{-1}}$ for the NWES (Legge et al., 2020). In the variable stoichiometry configurations, the enhanced CO_2 uptake is in good agreement with the literature estimates in

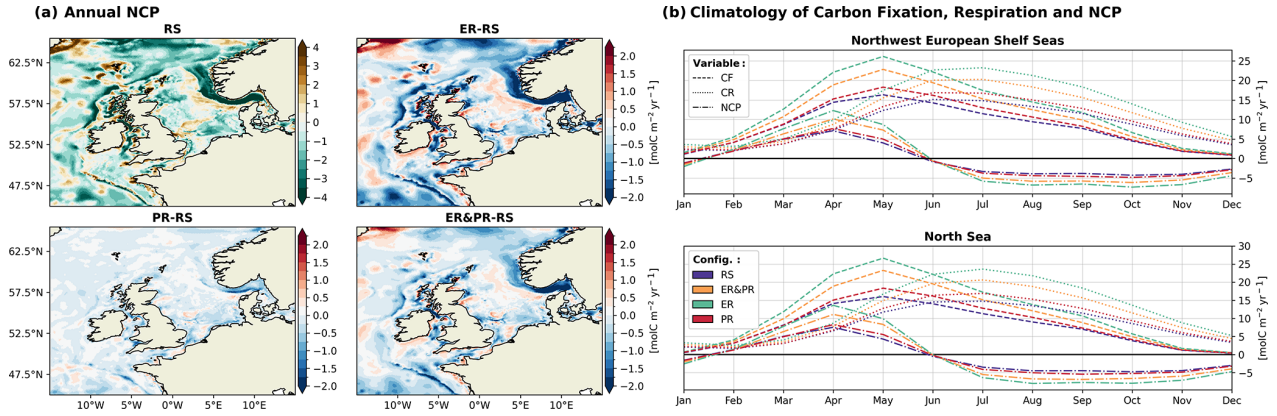

Figure 9. **(a)** Spatial distribution of annual vertically integrated NCP for the RS configuration and differences for the ER, PR, and ER&PR configurations over the simulation period of 2000–2010. **(b)** Respective monthly 11-year mean of carbon fixation (CF, dashed); carbon respiration (CR, dotted), including benthic and pelagic remineralization; and NCP (dash–dot). The respective seasonal means of NCP are provided in the Supplement (Fig. S17).

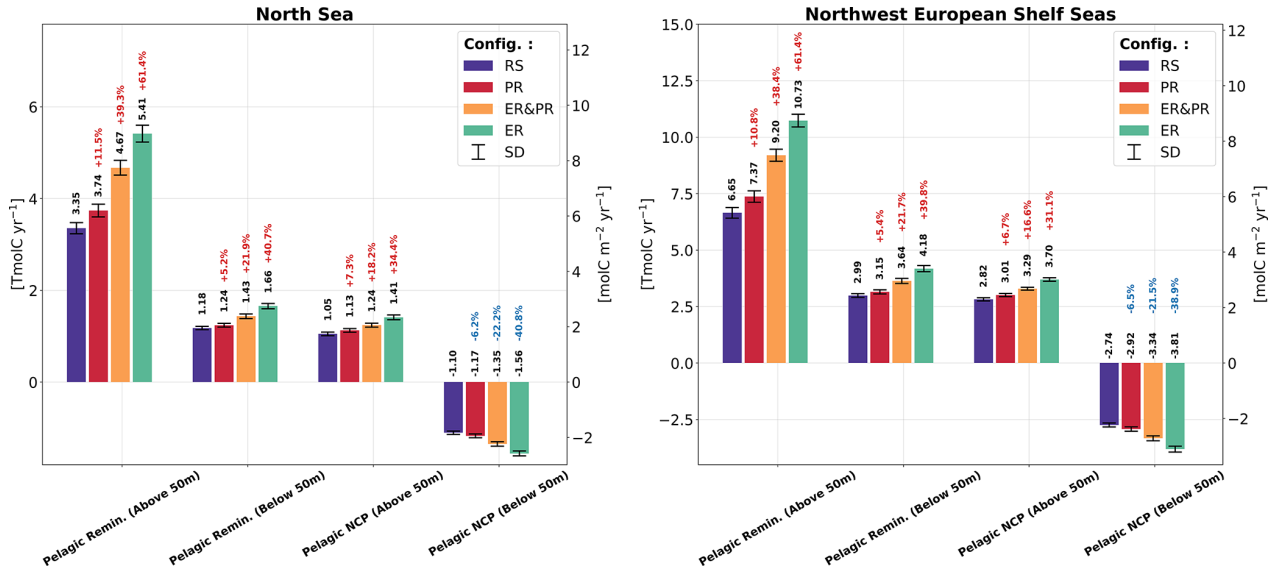

Figure 10. Simulated annual vertically integrated pelagic remineralization and pelagic NCP, separated into above and below 50 m depth and averaged over the simulated period of 2000–2010 for all four model configurations. The error bars show the corresponding standard deviation. In contrast to the NCP shown with all vertically integrated fluxes in Fig. 9, pelagic NCP here does not include benthic remineralization.

the North Sea, with an annual CO_2 uptake of 0.74 (+10 %) to 0.89 Tmol C yr^{-1} (+33 %). In the NWES, the annual CO_2-uptake is on the lower end of the literature estimates, 1.21 (+9 %) to 1.44 Tmol C yr^{-1} (+31 %). Thus, considering the observed stoichiometry improves the representation of the annual net air–sea CO_2 exchange both for the North Sea and the entire NWES.

In terms of the spatial distribution, the increase in CO_2 uptake is not uniform across the shelf but instead amplifies existing regional differences (Fig. 11). The reference configuration reproduces the observed north–south gradient across the North Sea, with the annual CO_2 uptake decreasing from the NNS and NT sub-regions towards the SNS sub-region (Kitidis et al., 2019; Schiettecatte et al., 2007; Thomas et al., 2004). All variable stoichiometry configurations consistently strengthen this latitudinal gradient in the air–sea CO_2 exchange. However, the amplitude of this effect varies consistently with the magnitude of the increased annual uptake. The largest increase in CO_2 uptake is consistently shown in the deeper central shelf areas and parts of the outer shelf regions including the NNS, CNS, NT, SWC, MS, AS, and WI. In the ER configuration, the mean CO_2 up-

take increases by 0.3 to 0.5 mol C m^{-2} yr^{-1} in these regions. Here, the CNS shows the greatest average increase, ranging from 0.1 mol C m^{-2} yr^{-1} in the PR to 0.5 mol C m^{-2} yr^{-1} in the ER configuration. Smaller but consistent increases are displayed for the southern and near-coastal regions including the SNS, SK, and SWC regions. A persistent increase in CO_2 outgassing or decrease in CO_2 uptake is only shown in a narrow band along the Norwegian coast, near the Elbe estuary, and in inner shelf regions including the EC and IS. In the Atlantic Ocean, the CO_2 uptake consistently increases. Overall, the variable OM stoichiometry configurations demonstrate an increase in the annual net CO_2 uptake, with an intensification of the north–south gradient across the North Sea. This is consistent with the enhanced NCP gradient across the slope of the Norwegian Trench (Fig. 9) and between surface and sub-surface NCP (Fig. 10). The latter suggest additional drawdown of DIC with potential for a stronger CO_2 uptake, especially in but not limited to this region.

3.1.6 Seasonal air–sea CO_2 exchange

In addition to the net annual changes, the seasonal intensification of OM cycling also results in a shifted seasonality of the air–sea CO_2 exchange. This can be attributed to an intensification of the biological contribution to changes in pCO_2 relative to the influence of temperature, which is further discussed below. The RS reference configuration shows the strongest CO_2 uptake during winter and spring (Fig. 12), with averages of 1.7 and 2.4 mol C m^{-2} yr^{-1}, respectively. In winter, the highest uptake occurs in the NNS and SNS, with the CNS exhibiting the lowest uptake. For the remaining year, there is a consistent north–south gradient, with the highest uptake rates shown in the northern half and weaker uptake or outgassing in the southern half. In summer and autumn, the southern parts and inner shelf areas of the NWES including the SNS, SK, EC, IS, and parts of the CNS display an outgassing of CO_2. The extent of this outgassing is greatest in summer, while the intensity is greatest in autumn. On average, there is a net outgassing of -0.2 mol C m^{-2} yr^{-1} in summer and autumn. This qualitative pattern with a pronounced north–south gradient is overall in good agreement with previous monthly estimates from observations (Kitidis et al., 2019). However, the seasonality indicates that in the reference configuration, the effect of biological carbon fixation on the air–sea CO_2 exchange is underestimated relative to the influence of temperature. This is demonstrated by the majority of uptake occurring during winter and spring, although observations also suggest that significant uptake continues during summer (Kitidis et al., 2019; Thomas et al., 2004).

The seasonal impact of variable stoichiometry is consistent across configurations, with differences in amplitude proportional to the annual changes. For each season, the smallest differences in uptake and outgassing are shown in the PR configuration, while the largest are seen in the ER configuration. In winter, the CO_2 uptake is reduced by 0.2 to 0.8 mol C m^{-2} yr^{-1} across the entire NWES. The strongest reduction is shown in the central and outer shelf areas, as well as the Norwegian Trench. During the spring and summer months, the CO_2 uptake is significantly stronger, with the most pronounced increases in the central North Sea and the Norwegian Trench. The average increase is 0.1 to 0.7 mol C m^{-2} yr^{-1} in spring and 0.4 to 1.3 mol C m^{-2} yr^{-1} in summer, resulting in a shift from net outgassing to net uptake in summer. In autumn, the gradient between uptake in the northern and outgassing in the southern parts is enhanced, with an average decrease in uptake or increase in outgassing of up to 0.2 mol C m^{-2} yr^{-1}. This is consistent with the increased autotrophy in spring and summer and increased heterotrophy during autumn and winter. These shifts in the seasonal air–sea CO_2 exchange indicate that the additional drawdown of DIC through increased carbon fixation enhances CO_2 uptake and decreases outgassing during the productive season, while additional respiration reduces uptake and promotes outgassing in autumn and winter. This implies that the air–sea CO_2 flux becomes less temperature controlled and more biologically controlled. This indication is supported by the intensified seasonal carbon fixation and respiration (Figs. 9 and S15–S17), as well as the increased vertical gradient in NCP (Fig. 10). In the absence of biological carbon fixation, seasonal temperature variations would lead to a high CO_2 uptake due to the low temperatures in winter and a lower uptake or higher outgassing due to high temperatures in summer. By depleting the surface waters of DIC during the productive season, the biological pump drives the seasonality in the opposite direction. Thus, with the increased carbon fixation in the variable stoichiometry configurations, the CO_2 uptake shifts towards the productive season.

3.2 Organic and inorganic carbon concentrations

The seasonal variations in organic and inorganic carbon concentrations are regulated by the balance between biological carbon fixation and respiration. Consequently, the intensification of the annual and seasonal OM cycling as described above has implications for the transformation and transport of both organic and inorganic carbon. In turn, these carbon pools determine carbon fluxes, which are of relevance for the regional carbon budget. Therefore, we assess the changes in organic and inorganic carbon contents in the context of the enhanced OM cycling and identify further potential consequences for marine carbon cycling in the NWES. Our analysis focuses on changes in the surface DIC and pCO_2, which are relevant for the air–sea CO_2 exchange, as well as seasonal vertical gradients in DIC, which influence cross-shelf exchanges of inorganic carbon. With regard to organic carbon contents, we assess the seasonal vertical distribution of both DOC and POC, which represent how long inorganic carbon uptake is seasonally retained in OM and control cross-shelf transports and sedimentation of organic carbon.

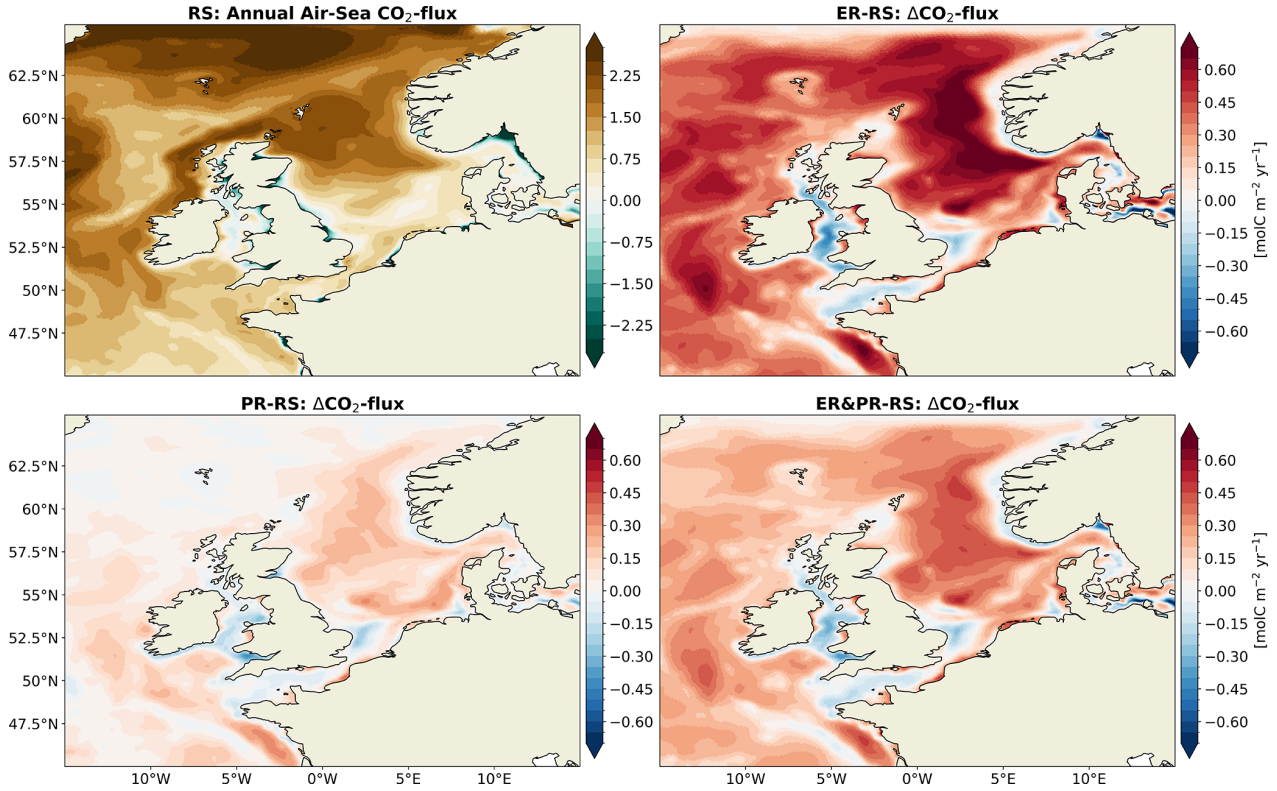

Figure 11. Annual mean air–sea CO_2 exchange for the RS configuration and differences for the ER, PR, and ER&PR configurations over the simulation period of 2000–2010. The direction of the flux is defined as downward, meaning a positive air–sea CO_2 exchange indicates an oceanic uptake and a negative one an outgassing of CO_2. Similarly, positive differences represent an increase in uptake or a decrease in outgassing and vice versa.

3.2.1 Surface inorganic carbon seasonality

Biogeochemical models constrained to elemental Redfield ratios tend to underestimate the seasonal uptake of DIC by biological carbon fixation in surface waters (Bozec et al., 2006; Kähler and Koeve, 2001; Prowe et al., 2009). Here, the RS reference configuration demonstrates this underestimation of seasonal variability in surface DIC concentrations and ΔpCO_2 (Fig. 13). While ΔpCO_2 in winter agrees well with observational estimates, the seasonal minimum between April and October is strongly underestimated in the RS configuration for both DIC and ΔpCO_2.

The variable stoichiometry configurations demonstrate a higher reduction in surface DIC concentrations during summer in proportion to the increased seasonal carbon fixation described above. The decreased summer ΔpCO_2 relative to the RS configuration increases the potential for CO_2 uptake in summer, which is consistent with the abovementioned shift from the maximum CO_2 uptake in winter and spring towards spring and summer, connected to a more pronounced biological contribution. The additional DIC uptake leads to a reduction in the RMSD of ΔpCO_2 between simulated and observed monthly means, dropping from 57, 21, 41, and 66 µatm in the NT, NNS, CNS, and SNS regions to 37–50, 16–19, 21–32, and 47–58 µatm, respectively. This improvement is most significant in the ER configuration and least significant in the PR configuration. In contrast, the RMSD for DIC shows smaller, less consistent differences. This is likely due to a small general overestimation of surface DIC concentrations and an overestimation of DIC during the second half of the year.

Although reproducing the observed OM stoichiometry improves the representation of summer minima in ΔpCO_2 and DIC, even with variable stoichiometry, simulated DIC increases more rapidly than observed levels do in the second half of the year. This DIC overestimation can be attributed to a lack of organic carbon retention, such that respiration exceeds production too early, thereby releasing DIC back into the water column. One factor limiting the retention of organic carbon may be the missing representation of higher trophic levels including pelagic fish stocks and macrobenthos. Incorporating these and explicitly representing the microbial loop instead of solely relying on bulk remineralization rates for DOM and POM may further improve the model's ability to

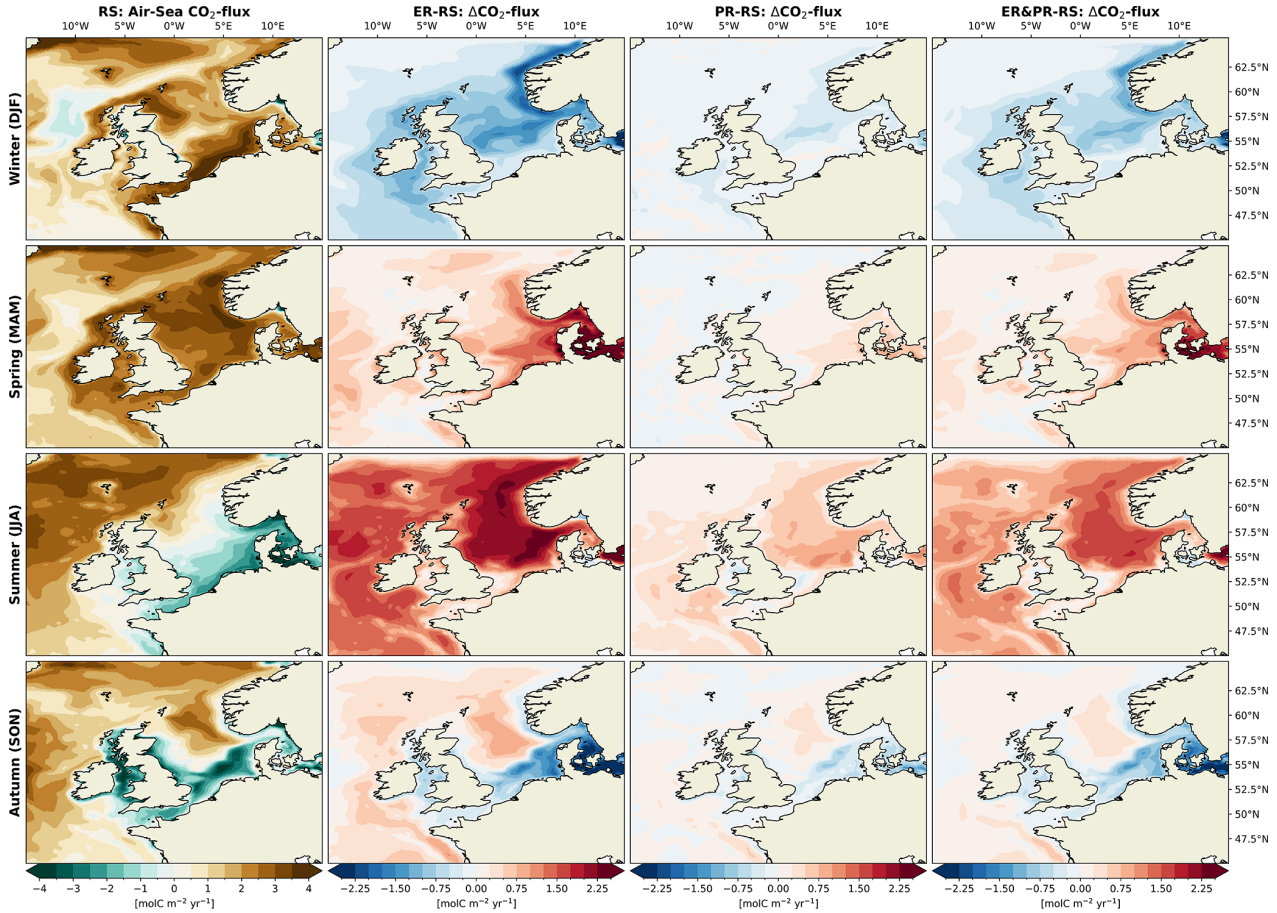

Figure 12. Seasonal mean air–sea CO_2 exchange for the RS configuration and differences for the ER, PR, and ER&PR configurations over the simulation period of 2000–2010. The CO_2 exchange for each configuration is shown in the Supplement (Fig. S18).

capture the seasonal dynamics of inorganic carbon, particularly in late summer and autumn.

3.2.2 Seasonal vertical DIC gradient

In the deep and seasonally stratified central and northern parts of the North Sea, the separation of OM production in the euphotic zone and respiration in deeper layers leads to a seasonal vertical DIC gradient (Thomas et al., 2004). The high productivity in spring and summer reduce DIC in the surface waters, exporting OM to the sub-surface layer, where subsequent respiration increases DIC concentrations at depths. Vertical mixing in autumn and winter then reduces the gradient and finally restores the nearly homogeneous vertical distribution in winter. This qualitative pattern is reproduced in the RS reference configuration (Fig. 14) but with an underestimated seasonal inorganic carbon drawdown. Because observations are limited and represent only parts of each season, often covering a single month, direct comparisons of seasonally averaged gradients are of limited value. Therefore, we focus here on the representation of the maximum DIC drawdown in summer and the implications of variable stoichiometry for DIC drawdown to sub-surface layers.

In both sub-regions, the vertical DIC gradient in summer is more closely reproduced in the variable stoichiometry configurations, with the closest representation in the ER configuration. Compared to the RS configuration, the additional carbon fixation leads to a reduction in the vertically integrated DIC content in the upper 50 m during summer by 122 to 564 mmol m^{-2} in the NT and 169 to 820 mmol m^{-2} in the combined NNS and CNS sub-regions. Conversely, in autumn and winter, bottom DIC concentrations are significantly higher compared to those in the RS configuration due to additional respiration. This increase in bottom DIC concentrations is more pronounced in the NT region. The vertically integrated autumn DIC concentrations below 50 m in the NT show a large increase of 1367 to 3855 mmol m^{-2} compared to the reference configuration. In the NNS and CNS regions, this increase only ranges from 176 to 384 mmol m^{-2}. The much larger increase in bottom DIC concentrations in the

NT indicates additional external sources of DIC to this region from additional downwelling of organic carbon. An intensification of the vertical DIC gradient overall suggests a higher biological drawdown of DIC, with the potential for higher DIC concentrations in waters exported to the North Atlantic.

3.2.3 Seasonal organic carbon production

The enhanced seasonal carbon fixation in the variable stoichiometry configurations also results in an increased seasonal accumulation of DOC in both the well-mixed and seasonally stratified regions, with the greatest accumulation occurring in the euphotic zone (Fig. 15). For the purpose of comparison, we present the means and ranges of derived (semi-)labile DOC (LDOC) concentrations in surface and bottom waters in August from 2 consecutive years. These observational ranges demonstrate considerable interannual variability. The ranges from both years demonstrate that the simulated DOC concentrations are a reasonable representation of concentrations during the summer months. The RS stoichiometry is situated at the lower end of the estimated range, while the ER configuration is situated at the upper end.

In the combined NNS and CNS region, the water-column-integrated DOC content during summer exhibits a 68 % to 123 % increase in the ER&PR and ER configurations relative to the reference simulation. In contrast, the PR configuration exhibits a small decrease of 1.2 % in the total summer DOC content, with concentrations increasing in the surface layer but decreasing in the sub-surface layer. A consistent increase in the entire water column is observed in the variable stoichiometry configurations, resulting in a 4 %, 48 %, and 82 % increase in the vertically integrated DOC content in the SNS during summer for the PR, ER&PR, and ER configurations, respectively. The surface DOC content approximately doubles in the SNS and triples in the NNS and CNS during all seasons for the ER configuration, with a maximum increase of approximately 25 % in the PR and an intermediate increase in the combined configuration. The increased DOC concentrations are likely to contribute to carbon export from surface waters through downwelling transport. By retaining more organic carbon in the water column that can be redistributed and respired elsewhere, this likely contributes to the greater depletion of surface DIC concentrations and hence higher CO_2 uptake.

The enhanced seasonal carbon fixation in the variable stoichiometry configurations further increases the POC content during spring and summer (Fig. 16). Simulated summer POC concentrations are consistent with observations across all configurations in the CNS. In the SNS, the reference configuration underestimates the mean POC concentrations, which are more closely represented in all variable stoichiometry configurations. The vertically integrated POC content is 22 % to 31 % higher in the CNS, with the largest increase in the PR and the smallest increase in the ER configuration. In the SNS, increases are larger and more consistent across configurations, with a range of 55 % to 66 %. The increases are smaller in spring and autumn and negligible in winter. The overall larger POC concentrations in the variable stoichiometry configurations suggest a higher availability of organic carbon for lateral and vertical transports, as well as sedimentation of POC. An increased export from surface waters and subsequent respiration of POC likely contribute to the abovementioned higher drawdown of DIC and the resulting increase in CO_2 uptake. The comparable increase in POC concentrations for the variable stoichiometry configurations with a varying increase in CO_2 uptake indicates that both POC and DOC production contribute to the drawdown of DIC, which is relevant for the enhanced CO_2 uptake. This also corroborates the high additional accumulation of DIC from downwelling into and subsequent respiration of organic carbon from the Norwegian Trench.

4 Discussion

For the first time, this study provides a comprehensive modeling assessment of how observed variations in the C : N : P stoichiometry of OM impact model-based carbon cycle estimates in the NWES compared to OM cycling at fixed Redfield ratios. We focus on changes in OM cycling in terms of carbon fixation, respiration, NCP, the resulting export of DIC to sub-surface layers, and its consequences for the air–sea CO_2 exchange.

By implementing two pathways for variable C : N : P stoichiometry in the production and respiration of OM (Fig. 3), we demonstrate that variable stoichiometry consistently results in an increased oceanic CO_2 uptake, with a range of 10 %–33 % in the North Sea and 9 %–31 % in the entire NWES. This additional CO_2 uptake is driven by an enhanced biological drawdown of CO_2 through intensified surface production and sub-surface respiration of organic carbon (Figs. 7–10). With the increase in OM cycling, both the North Sea and the entire NWES become more net heterotrophic (Figs. 7–9), with an increased NCP in net autotrophic regions and a decreased NCP in net heterotrophic regions (Fig. 9). This amplifies the pre-existing gradient in NCP, especially along the border between the central North Sea and the Norwegian Trench. Further, the vertical gradient between the net autotrophic surface layer and net heterotrophic sub-surface layer increases, leading to increased DIC uptake at the surface and increased DIC release at depth (Fig. 10). Seasonally, there is an increase in net autotrophy during spring and early summer, while net heterotrophy increases during the rest of the year. This increase in the seasonal amplitude in NCP appears without a notable shift in the timing of the transition from net autotrophy to net heterotrophy. The resulting changes in both organic and inorganic carbon concentrations (Figs. 13–16) have implications for marine carbon cycling in the NWES.

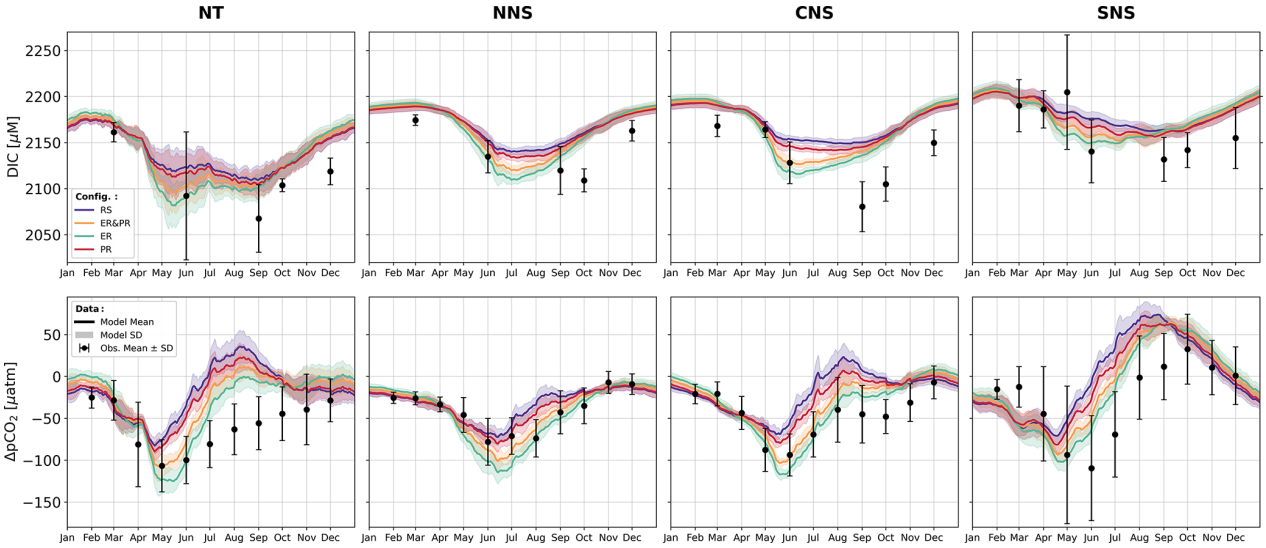

Figure 13. Simulated daily 11-year mean of horizontal means and standard deviations of DIC concentrations and differences between simulated surface pCO_2 and prescribed atmospheric concentrations from the Mace Head measurement station (Lan et al., 2023) for all four model configurations. The error bars indicate monthly means and standard deviations of corresponding GLODAP and SOCAT observations for DIC and pCO_2. The conversion from simulated CO_2 concentrations and observed fCO_2 to pCO_2 was conducted in accordance with the methodology described above for the carbonate system validation. For the derivation of the ΔpCO_2 from observed pCO_2, the same monthly atmospheric concentrations were subtracted as for the simulated ΔpCO_2. Both variables are shown for the Norwegian Trench (NT) as well as the northern (NNS), central (CNS), and southern North Sea (SNS).

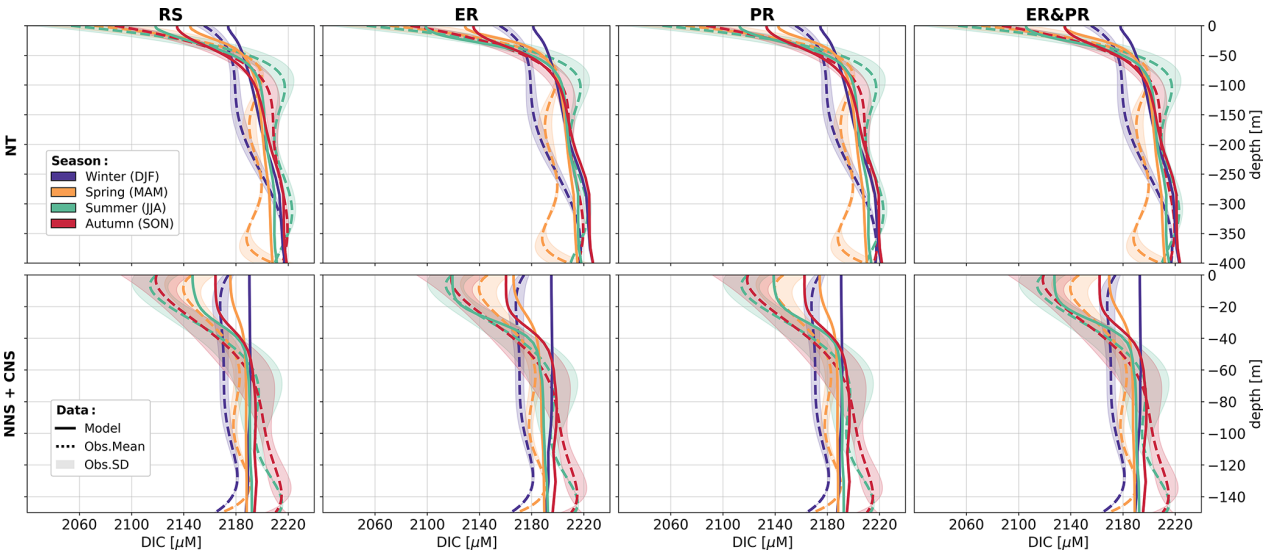

Figure 14. Simulated and observed horizontally averaged seasonal DIC gradients in the Norwegian Trench (NT) and the combined northern (NNS) and central North Sea (CNS) sub-regions for all four model configurations. Solid lines represent the simulated concentrations, while dashed lines and the shaded area indicate observed concentrations and their corresponding standard deviation. The observed vertical profiles were generated by firstly calculating the mean concentrations and standard deviation within every meter of depth and, secondly, generating a fifth-order polynomial fit for the vertical profiles of means and standard deviations using numpy.polyfit for each season. The polynomial coefficients are listed in the Supplement (Table S16).

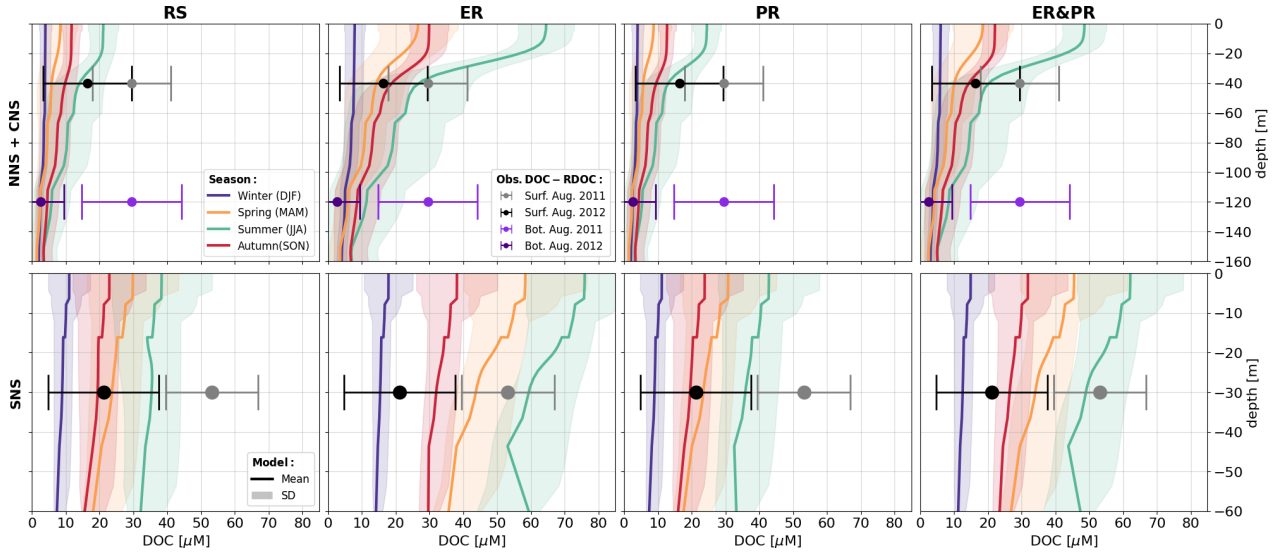

Figure 15. Vertical distribution of the horizontally averaged seasonal mean (solid) and standard deviation (shaded) of DOC concentrations for all four model configurations over the simulation period from 2000 to 2010 in the southern North Sea (SNS) and over the combined northern (NNS) and central North Sea (CNS) sub-regions. The error bars indicate derived estimates of mean LDOC concentrations and observed ranges. These estimates were derived from observed seasonal bulk DOC concentrations in the seasonally stratified and well-mixed regions of the North Sea from Chaichana et al. (2019) by subtracting an average surface ocean refractory or recalcitrant DOC (RDOC) concentration of 44.3 µM from three observational estimates (Aminot and Kérouel, 2004; Hopkinson and Vallino, 2005; Liang et al., 2023).

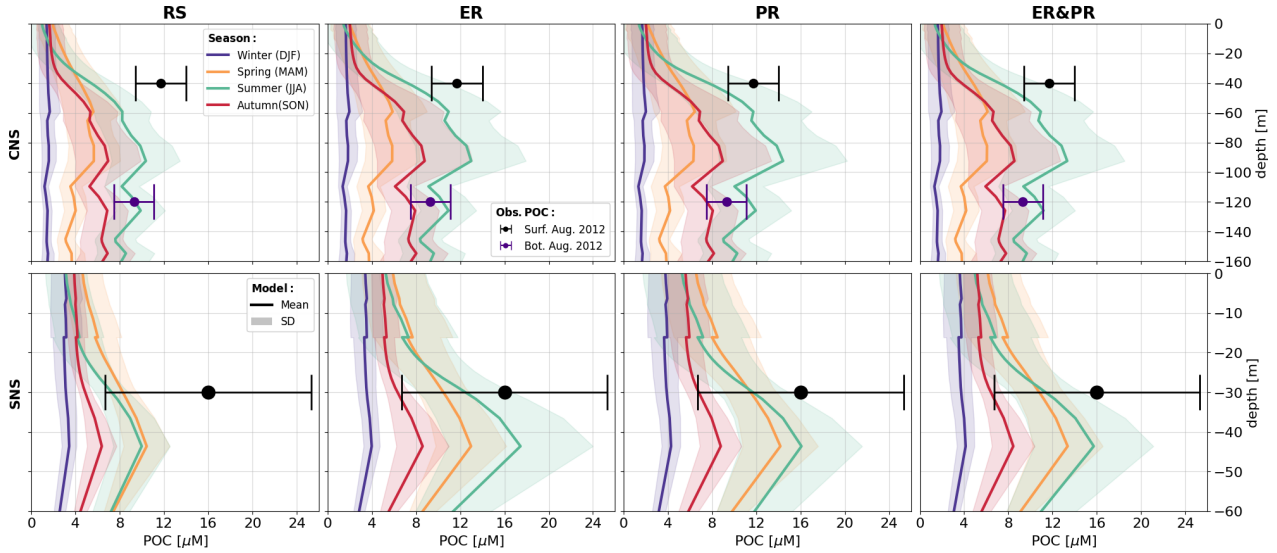

Figure 16. Vertical distribution of horizontally averaged seasonal mean and standard deviation of POC concentrations in the central (CNS) and southern North Sea (SNS) for all four model configurations. The error bars indicate estimated mean POC concentrations and observed ranges from Chaichana et al. (2019).

Firstly, the reduction in surface DIC concentrations and hence in ΔpCO_2 enhances the annual net CO_2 uptake (Figs. 7 and 11) and additionally shifts the seasonality to be more biologically controlled and therefore less dominated by temperature. This is expressed by an increased CO_2 uptake in spring and summer and a reduced CO_2 uptake in winter. Furthermore, there is a stronger north–south gradient, with the maximum uptake in the stratified northern regions where export of organic carbon to deeper layers is most efficient (Fig. 12). Secondly, a higher seasonal accumulation

of both DOC and POC indicates greater availability of OM contents for lateral transport, the export from surface waters through sinking and downwelling, and the sedimentation of POC (Figs. 13–16). Since comparable simulated POC concentrations with different DOC concentrations show large differences in air–sea CO_2 exchange, these results suggest that both additional POC and DOC production and the resulting carbon export from surface waters contribute significantly to seasonal DIC reduction in surface waters.

In particular, an increase in sub-surface DIC in seasonally stratified areas (Fig. 14) in combination with higher availability of organic carbon (Figs. 15–16) and a stronger vertical (Fig. 10) and lateral gradient in NCP across the slope of the Norwegian Trench (Fig. 9) indicate an intensification of the shelf carbon pump mechanism. This is likely due to additional degradation of OM in the Norwegian Trench imported from the North Atlantic and other parts of the North Sea, resulting in DIC enrichment of deeper shelf waters, which are subsequently exported to the North Atlantic. The increased export of DIC to the open ocean and potentially to sediments is likely responsible for the net uptake of atmospheric CO_2.

The reason for the increased productivity varies between the two mechanisms. The preferential remineralization of organic nitrogen and phosphorus increases production through higher nutrient availability, while the extracellular release of DOM allows for additional carbon fixation beyond nutrient limitation, which additionally reduces surface nutrient concentrations (Supplement Fig. S19). For a comparable range in OM stoichiometry, which reflects the observed variations in the composition of LDOM and POM (Figs. 4 and 5), the impact described is of a higher amplitude for the extracellular release of DOM than for the preferential remineralization of organic nitrogen and phosphorus across all of these carbon fluxes (Fig. 7). As expected, the combined configuration, with a reduced contribution of each mechanism, consistently reproduces intermediate changes between the two individual configurations. While the extracellular release of DOM more effectively accounts for the underestimated reduction in DIC in surface waters, the preferential remineralization better reflects the vertical increase in C : N and C : P ratios with depth and, as such, age of the material. Since both mechanisms have been suggested by observational and experimental studies and reproduce relevant features of OM cycling, the consideration of variable stoichiometry in both production and decomposition of OM is likely necessary for an adequate model representation of marine carbon cycling.

While previous studies have considered carbon fixation beyond elemental Redfield ratios in the North Sea and Baltic Sea (Neumann et al., 2022; Prowe et al., 2009), here we explicitly quantify the impact on regional carbon cycling across the NWES and assess the individual and combined contributions of two contributing mechanisms. Our findings regarding the regional impact on marine carbon cycling are consistent with previous global Earth system model experiments considering the preferential remineralization of organic nitrogen and phosphorus, as well as with proposed consequences of higher C : N and C : P ratios in OM from observational studies. In particular, our results regionally support the suggestion that increased carbon content relative to elemental Redfield ratios would imply higher export production, an associated drawdown of inorganic carbon, and increased availability of organic carbon for lateral carbon transport (Hopkinson and Vallino, 2005; Letscher and Moore, 2015; Tanioka et al., 2021; Zakem and Levine, 2019). Beyond the large-scale effects, we highlight how the regional carbon export mechanism determines the response to variable OM stoichiometry in terms of spatial distribution and seasonality and, as such, needs to be considered regionally as well as globally.

Given the significant impact on major carbon fluxes, we show that estimates of regional carbon budgets are sensitive to a reasonable representation of OM stoichiometry. These findings not only underscore the importance of the elemental composition of OM in regional carbon cycling but also suggest that global carbon budget models may need to be re-evaluated to account for its accurate representation. The pronounced seasonal shifts in CO_2 uptake driven by variable OM stoichiometry highlight the need for its consideration in carbon modeling in temperate shelf seas globally.

Future research efforts should focus on identifying the contribution of different processes to the observed OM stoichiometry and their spatiotemporal variability. Other effects on OM composition that are beyond the scope of this study include the quality of imported OM from land (Painter et al., 2018), the effect of variable stoichiometry in prey on higher trophic levels (Schindler and Eby, 1997), and pathways for variable stoichiometry in phyto- and zooplankton (Moreno and Martiny, 2018). The latter pathways include the direct uptake of DON and DOP by phytoplankton (Fitzsimons et al., 2020), as well as variable C : N : P ratios in zooplankton grazing and excretion (Anderson et al., 2005; Elser and Urabe, 1999). Another important factor to consider is the role of community composition in shaping ecosystem stoichiometry (Kwiatkowski et al., 2018). All of these contributions may be subject to regional and interannual variability, as well as long-term trends imposed by climate change (Sardans et al., 2012). Additionally, spatiotemporal variations in ecosystem processes, such as the partitioning of new detritus into POM and DOM, grazing rates, and temperature-dependent remineralization rates, could introduce regional and interannual variability not explicitly accounted for in this study. While these processes contribute to organic matter cycling and could influence our findings, the model's accurate representation of OM concentrations and stoichiometry ensures that the broader conclusions regarding regional carbon fluxes remain robust.

While this study offers valuable insights into the drawdown of inorganic carbon and explores changes in both organic and inorganic carbon concentrations, it does not fully quantify the impact on the carbon budget of the NWES.

Specifically, the study has not yet established key fluxes explicitly, such as lateral cross-shelf transports of dissolved organic carbon (DOC) and particulate organic carbon (POC), vertical POC sedimentation rates, and the export of dissolved inorganic carbon (DIC) to the open ocean. Future research should aim to quantify these fluxes to provide a more comprehensive understanding of the impact on the full carbon budget of the NWES. Setting these impacts in the context of multiple anthropogenic stressors including climate change impacts will be crucial for refining carbon budget estimates and predicting long-term carbon sequestration in this region and their significance for global carbon cycling.

5 Conclusions

This study highlights the significant impact of the observed variations in C : N : P stoichiometry of OM on carbon cycling in the NWES. By incorporating two pathways for variable OM stoichiometry into the regional 3D physical–biogeochemical modeling system SCHISM-ECOSMO-CO_2, we reproduce the observed stoichiometry of LDOM and POM. In comparison to fixed Redfield stoichiometry, our results show an enhanced biological drawdown of DIC and a resulting increase in the oceanic CO_2 uptake. This additional CO_2 uptake is driven by an intensification of OM cycling and the resulting increase in seasonal, lateral, and vertical NCP gradients, which enhances the seasonal DIC gradient. With an increased biological contribution to the seasonality of pCO_2, CO_2 uptake shifts from winter towards spring and summer. This is particularly evident in the deep and seasonally stratified regions of the North Sea. Despite the difference in the pathways for variable stoichiometry in the production and respiration of OM, the model response shows a consistent impact on OM cycling and the resulting air–sea CO_2 exchange, with noticeable differences only in their magnitude. To determine the amplitude of these changes, a deeper understanding of the individual process contributions to variable stoichiometry is required.

Our findings underscore the limitations of using fixed Redfield stoichiometry for simulating OM cycling, revealing that the observed variations in OM stoichiometry have a profound influence on marine carbon cycling in the NWES. Incorporating variable OM stoichiometry into biogeochemical models will be essential for an accurate representation of carbon cycling, regional carbon budgets, and their spatiotemporal variations. This will be a crucial aspect when evaluating the impact of multiple anthropogenic stressors on the marine ecosystem and the role of OM stoichiometry in future carbon budgets under changing environmental conditions. As the results are largely determined by the pre-existing regional physical controls and the resulting structure of biogeochemical cycles, we emphasize that regional assessments are key to understanding the role of OM stoichiometry in regional carbon cycling and should be incorporated into the representation of the coastal ocean in global modeling studies.

Data availability. All datasets used to generate the figures and results in this study are openly accessible via Zenodo at https://doi.org/10.5281/zenodo.14916290 (Demir, 2025). The code used for the model simulations and data analysis is available from the corresponding author upon reasonable request.

Supplement. The supplement related to this article is available online at https://doi.org/10.5194/bg-22-2569-2025-supplement.

Author contributions. KTD was responsible for the conceptualization of the study, while the methodology was developed collaboratively by KTD, MM, JK, and CSc. Software development was undertaken by KTD, JK, FL, and CSt, with the validation carried out by KTD, JK, and FL. KTD performed the formal analysis, and the investigation was conducted by KTD, MM, CSc, and HT. MM and CSc provided the necessary resources, and data curation was managed by KTD. The original draft of the manuscript was prepared by KTD, and subsequent writing, review, and editing were contributed by KTD, MM, JK, FL, UD, CSt, HT, and CSc. KTD also took responsibility for visualization. Supervision of the project was provided by MM, UD, HT, and CSc. Finally, CSc handled the project administration and funding acquisition.

Competing interests. The contact author has declared that none of the authors has any competing interests.

Disclaimer. Publisher's note: Copernicus Publications remains neutral with regard to jurisdictional claims made in the text, published maps, institutional affiliations, or any other geographical representation in this paper. While Copernicus Publications makes every effort to include appropriate place names, the final responsibility lies with the authors.

Acknowledgements. Computational resources for this work were made available by the German Climate Computing Center (DKRZ) through support from the German Federal Ministry of Education and Research (BMBF). We would like to thank ICDC, CEN, and the University of Hamburg for data support. This study has been conducted using data from the Global Ocean Data Analysis Project (GLODAP), the Surface Ocean CO_2 Atlas (SOCAT), and the International Council for the Exploration of the Sea (ICES). The research was funded by the Deutsche Forschungsgemeinschaft (DFG, German Research Foundation) under Germany's Excellence Strategy – EXC 2037 "CLICCS – Climate, Climatic Change, and Society", project number 390683824 and contributes to the CLICCS subproject A5, The Land–Ocean Transition Zone. Feifei Liu received funding from the BMBF project RETAKE (grant no. 03F0895C).

Financial support. This research has been supported by the Deutsche Forschungsgemeinschaft (grant no. 390683824) and the German Federal Ministry of Education and Research (BMBF) (grant no. 03F0895C).

The article processing charges for this open-access publication were covered by the Helmholtz-Zentrum Hereon.

Review statement. This paper was edited by Liuqian Yu and reviewed by two anonymous referees.

References

Aminot, A. and Kérouel, R.: Dissolved organic carbon, nitrogen and phosphorus in the N-E Atlantic and the N-W Mediterranean with particular reference to non-refractory fractions and degradation, Deep-Sea Res. Pt. I, 51, 1975–1999, https://doi.org/10.1016/j.dsr.2004.07.016, 2004.

Anderson, T. R. and Pondaven, P.: Non-Redfield carbon and nitrogen cycling in the Sargasso Sea: Pelagic imbalances and export flux, Deep-Sea Res. Pt. I, 50, 573–591, https://doi.org/10.1016/S0967-0637(03)00034-7, 2003.

Anderson, T. R., Hessen, D. O., Elser, J. J., and Urabe, J.: Metabolic Stoichiometry and the Fate of Excess Carbon and Nutrients in Consumers, Am. Nat., 165, 1–15, https://doi.org/10.2307/3473193, 2005.

Aricò, S., Watson, A. J., Wanninkhof, R., Thomas, H., Shutler, J. D., Schuster, U., Schoo, K. L., Sanders, R., Sabine, C., Robinson, C., Monteiro, P., McKinley, G. A., Jiao, N., Ishii, M., Isensee, K., Gruber, N., Dai, M., Chai, F., Cotrim da Cunha, L., Boyd, P. W., Bakker, D. C. E., Arrieta, J. M., and Lauvset, S. K.: Integrated Ocean Carbon Research: A Summary of Ocean Carbon Research, and Vision of Coordinated Ocean Carbon Research and Observations for the Next Decade, UNESCO, https://unesdoc.unesco.org/ark:/48223/pf0000376708 (last access: 14 November 2023), 2021.

Artioli, Y., Blackford, J. C., Butenschön, M., Holt, J. T., Wakelin, S. L., Thomas, H., Borges, A. V., and Allen, J. I.: The carbonate system in the North Sea: Sensitivity and model validation, J. Marine Syst., 102–104, 1–13, https://doi.org/10.1016/j.jmarsys.2012.04.006, 2012.

Artioli, Y., Blackford, J. C., Nondal, G., Bellerby, R. G. J., Wakelin, S. L., Holt, J. T., Butenschön, M., and Allen, J. I.: Heterogeneity of impacts of high CO_2 on the North Western European Shelf, Biogeosciences, 11, 601–612, https://doi.org/10.5194/bg-11-601-2014, 2014.

Barrón, C. and Duarte, C. M.: Dissolved organic carbon pools and export from the coastal ocean, Global Biogeochem. Cy., 29, 1725–1738, https://doi.org/10.1002/2014GB005056, 2015.

Bauer, J., Williams, P., and Druffel, E.: ^{14}C activity of dissolved organic carbon fractions in the North Central Pacific and Sargasso Sea, Nature, 357, 667–670, https://doi.org/10.1038/357667a0, 1992.

Bauer, J. E., Cai, W.-J., Raymond, P. A., Bianchi, T. S., Hopkinson, C. S., and Regnier, P. A. G.: The changing carbon cycle of the coastal ocean, Nature, 504, 61–70, https://doi.org/10.1038/nature12857, 2013.

Blackford, J., Artioli, Y., Clark, J., and De Mora, L.: Monitoring of offshore geological carbon storage integrity: Implications of natural variability in the marine system and the assessment of anomaly detection criteria, Int. J. Greenh. Gas Con., 64, 99–112, https://doi.org/10.1016/j.ijggc.2017.06.020, 2017.

Blackford, J. C. and Gilbert, F. J.: pH variability and CO_2 induced acidification in the North Sea, J. Marine Syst., 64, 229–241, https://doi.org/10.1016/j.jmarsys.2006.03.016, 2007.

Børsheim, K. Y., Vadstein, O., Myklestad, S. M., Reinertsen, H., Kirkvold, S., and Olsen, Y.: Photosynthetic algal production, accumulation and release of phytoplankton storage carbohydrates and bacterial production in a gradient in daily nutrient supply, J. Plankton Res., 27, 743–755, https://doi.org/10.1093/plankt/fbi047, 2005.

Bozec, Y., Thomas, H., Elkalay, K., and de Baar, H. J. W.: The continental shelf pump for CO_2 in the North Sea – evidence from summer observation, Mar. Chem., 93, 131–147, https://doi.org/10.1016/j.marchem.2004.07.006, 2005.

Bozec, Y., Thomas, H., Schiettecatte, L.-S., Borges, A. V., Elkalay, K., and De Baar, H. J. W.: Assessment of the processes controlling the seasonal variations of dissolved inorganic carbon in the North Sea, Limnol. Oceanogr., 51, 2746–2762, https://doi.org/10.4319/lo.2006.51.6.2746, 2006.

Broullón, D., Pérez, F. F., Velo, A., Hoppema, M., Olsen, A., Takahashi, T., Key, R. M., Tanhua, T., González-Dávila, M., Jeansson, E., Kozyr, A., and van Heuven, S. M. A. C.: A global monthly climatology of total alkalinity: a neural network approach, Earth Syst. Sci. Data, 11, 1109–1127, https://doi.org/10.5194/essd-11-1109-2019, 2019.

Broullón, D., Pérez, F. F., Velo, A., Hoppema, M., Olsen, A., Takahashi, T., Key, R. M., Tanhua, T., Santana-Casiano, J. M., and Kozyr, A.: A global monthly climatology of oceanic total dissolved inorganic carbon: a neural network approach, Earth Syst. Sci. Data, 12, 1725–1743, https://doi.org/10.5194/essd-12-1725-2020, 2020.

Bruggeman, J. and Bolding, K.: A general framework for aquatic biogeochemical models, Environ. Modell. Softw., 61, 249–265, https://doi.org/10.1016/j.envsoft.2014.04.002, 2014.

Butenschön, M., Clark, J., Aldridge, J. N., Allen, J. I., Artioli, Y., Blackford, J., Bruggeman, J., Cazenave, P., Ciavatta, S., Kay, S., Lessin, G., van Leeuwen, S., van der Molen, J., de Mora, L., Polimene, L., Sailley, S., Stephens, N., and Torres, R.: ERSEM 15.06: a generic model for marine biogeochemistry and the ecosystem dynamics of the lower trophic levels, Geosci. Model Dev., 9, 1293–1339, https://doi.org/10.5194/gmd-9-1293-2016, 2016.

Cai, R. and Jiao, N.: Recalcitrant dissolved organic matter and its major production and removal processes in the ocean, Deep-Sea Res. Pt. I, 191, 103922, https://doi.org/10.1016/j.dsr.2022.103922, 2023.

Canuel, E. A., Cammer, S. S., McIntosh, H. A., and Pondell, C. R.: Climate change impacts on the organic carbon cycle at the land-ocean interface, Annu. Rev. Earth Pl. Sc., 40, 685–711, https://doi.org/10.1146/annurev-earth-042711-105511, 2012.

Carlson, C. A. and Hansell, D. A.: Chapter 3 – DOM Sources, Sinks, Reactivity, and Budgets, in: Biogeochemistry of Marine Dissolved Organic Matter (Second Edition), edited by: Hansell, D. A. and Carlson, C. A., Academic Press, Boston, 65–126, https://doi.org/10.1016/B978-0-12-405940-5.00003-0, 2015.

Chaichana, S., Jickells, T., and Johnson, M.: Interannual variability in the summer dissolved organic matter inventory of the North Sea: implications for the continental shelf pump, Biogeosciences, 16, 1073–1096, https://doi.org/10.5194/bg-16-1073-2019, 2019.

Clark, L. L., Ingall, E. D., and Benner, R.: Marine phosphorus is selectively remineralized, Nature, 393, 426–426, https://doi.org/10.1038/30881, 1998.

Daewel, U. and Schrum, C.: Simulating long-term dynamics of the coupled North Sea and Baltic Sea ecosystem with ECOSMO II: Model description and validation, J. Marine Syst., 119–120, 30–49, https://doi.org/10.1016/j.jmarsys.2013.03.008, 2013.

Dai, M., Su, J., Zhao, Y., Hofmann, E. E., Cao, Z., Cai, W.-J., Gan, J., Lacroix, F., Laruelle, G. G., Meng, F., Müller, J. D., Regnier, P. A. G., Wang, G., and Wang, Z.: Carbon Fluxes in the Coastal Ocean: Synthesis, Boundary Processes, and Future Trends, Annu. Rev. Earth Pl. Sc., 50, 593–626, https://doi.org/10.1146/annurev-earth-032320-090746, 2022.

Davis, C. E., Mahaffey, C., Wolff, G. A., and Sharples, J.: A storm in a shelf sea: Variation in phosphorus distribution and organic matter stoichiometry, Geophys. Res. Lett., 41, 8452–8459, https://doi.org/10.1002/2014GL061949, 2014.

Davis, C. E., Blackbird, S., Wolff, G., Woodward, M., and Mahaffey, C.: Seasonal organic matter dynamics in a temperate shelf sea, Prog. Oceanogr., 177, 101925, https://doi.org/10.1016/j.pocean.2018.02.021, 2019.

del Giorgio, P. A. and Duarte, C. M.: Respiration in the open ocean, Nature, 420, 379–384, https://doi.org/10.1038/nature01165, 2002.

Demir, K. T.: Dataset for the study: Variable organic matter stoichiometry enhances the biological drawdown of CO_2 in the northwest European shelf seas, Zenodo [data set], https://doi.org/10.5281/zenodo.14916290, 2025.

Dickson, A. G., Sabine, C. L., and Christian, J. R.: Guide to Best Practices for Ocean CO_2 Measurements, PICES Special Publication 3, 191 pp., https://www.ncei.noaa.gov/access/ocean-carbon-acidification-data-system/oceans/Handbook_2007.html (last access: 26 June 2024), 2007.

Elser, J. J. and Urabe, J.: The Stoichiometry of Consumer-Driven Nutrient Recycling: Theory, Observations, and Consequences, Ecology, 80, 735–751, https://doi.org/10.1890/0012-9658(1999)080[0735:TSOCDN]2.0.CO;2, 1999.

Engel, A.: Direct relationship between CO_2 uptake and transparent exopolymer particles production in natural phytoplankton, J. Plankton Res., 24, 49–53, https://doi.org/10.1093/plankt/24.1.49, 2002.

Fajon, C., Cauwet, G., Lebaron, P., Terzic, S., Ahel, M., Malej, A., Mozetic, P., and Turk, V.: The accumulation and release of polysaccharides by planktonic cells and the subsequent bacterial response during a controlled experiment, FEMS Microbiol. Ecol., 29, 351–363, https://doi.org/10.1016/S0168-6496(99)00029-X, 1999.

Falkowski, P. G., Barber, R. T., and Smetacek, V.: Biogeochemical Controls and Feedbacks on Ocean Primary Production, Science, 281, 200–206, https://doi.org/10.1126/science.281.5374.200, 1998.

Finkel, Z. V., Beardall, J., Flynn, K. J., Quigg, A., Rees, T. A. V., and Raven, J. A.: Phytoplankton in a changing world: cell size and elemental stoichiometry, J. Plankton Res., 32, 119–137, https://doi.org/10.1093/plankt/fbp098, 2010.

Fitzsimons, M. F., Probert, I., Gaillard, F., and Rees, A. P.: Dissolved organic phosphorus uptake by marine phytoplankton is enhanced by the presence of dissolved organic nitrogen, J. Exp. Mar. Biol. Ecol., 530–531, 151434, https://doi.org/10.1016/j.jembe.2020.151434, 2020.

Frankignoulle, M. and Borges, A. V.: European continental shelf as a significant sink for atmospheric carbon dioxide, Global Biogeochem. Cy., 15, 569–576, https://doi.org/10.1029/2000GB001307, 2001.

Friedlingstein, P., O'Sullivan, M., Jones, M. W., Andrew, R. M., Bakker, D. C. E., Hauck, J., Landschützer, P., Le Quéré, C., Luijkx, I. T., Peters, G. P., Peters, W., Pongratz, J., Schwingshackl, C., Sitch, S., Canadell, J. G., Ciais, P., Jackson, R. B., Alin, S. R., Anthoni, P., Barbero, L., Bates, N. R., Becker, M., Bellouin, N., Decharme, B., Bopp, L., Brasika, I. B. M., Cadule, P., Chamberlain, M. A., Chandra, N., Chau, T.-T.-T., Chevallier, F., Chini, L. P., Cronin, M., Dou, X., Enyo, K., Evans, W., Falk, S., Feely, R. A., Feng, L., Ford, D. J., Gasser, T., Ghattas, J., Gkritzalis, T., Grassi, G., Gregor, L., Gruber, N., Gürses, Ö., Harris, I., Hefner, M., Heinke, J., Houghton, R. A., Hurtt, G. C., Iida, Y., Ilyina, T., Jacobson, A. R., Jain, A., Jarníková, T., Jersild, A., Jiang, F., Jin, Z., Joos, F., Kato, E., Keeling, R. F., Kennedy, D., Klein Goldewijk, K., Knauer, J., Korsbakken, J. I., Körtzinger, A., Lan, X., Lefèvre, N., Li, H., Liu, J., Liu, Z., Ma, L., Marland, G., Mayot, N., McGuire, P. C., McKinley, G. A., Meyer, G., Morgan, E. J., Munro, D. R., Nakaoka, S.-I., Niwa, Y., O'Brien, K. M., Olsen, A., Omar, A. M., Ono, T., Paulsen, M., Pierrot, D., Pocock, K., Poulter, B., Powis, C. M., Rehder, G., Resplandy, L., Robertson, E., Rödenbeck, C., Rosan, T. M., Schwinger, J., Séférian, R., Smallman, T. L., Smith, S. M., Sospedra-Alfonso, R., Sun, Q., Sutton, A. J., Sweeney, C., Takao, S., Tans, P. P., Tian, H., Tilbrook, B., Tsujino, H., Tubiello, F., van der Werf, G. R., van Ooijen, E., Wanninkhof, R., Watanabe, M., Wimart-Rousseau, C., Yang, D., Yang, X., Yuan, W., Yue, X., Zaehle, S., Zeng, J., and Zheng, B.: Global Carbon Budget 2023, Earth Syst. Sci. Data, 15, 5301–5369, https://doi.org/10.5194/essd-15-5301-2023, 2023.

Garcia, H., Weathers, K., Paver, C., Smolyar, I., Boyer, T., Locarnini, M., Zweng, M., Mishonov, A., Baranova, O., Seidov, D., and Reagan, J.: World Ocean Atlas 2018. Volume 4: Dissolved Inorganic Nutrients (phosphate, nitrate and nitrate+nitrite, silicate), Mishonov, A., Technical Ed., NOAA Atlas NESDIS 84, 35 pp., https://doi.org/10.25923/ng6j-ey81, 2018a.

Garcia, H., Weathers, K., Paver, C., Smolyar, I., Boyer, T., Locarnini, M., Zweng, M., Mishonov, A., Baranova, O., Seidov, D., and Reagan, J.: World Ocean Atlas 2018, Volume 3: Dissolved Oxygen, Apparent Oxygen Utilization, and Dissolved Oxygen Saturation, Mishonov, A., Technical Ed., NOAA Atlas NESDIS 83, 38 pp., https://doi.org/10.25923/qspr-pn52, 2018b.

Gattuso, J.-P., Frankignoulle, M., and Wollast, R.: Carbon and Carbonate Metabolism in Coastal Aquatic Ecosystems, Annu. Rev. Ecol. Evol. S., 29, 405–434, https://doi.org/10.1146/annurev.ecolsys.29.1.405, 1998.

Geider, R. and La Roche, J.: Redfield revisited: variability of C : N : P in marine microalgae and its biochemical basis, Eur. J. Phycol., 37, 1–17, https://doi.org/10.1017/S0967026201003456, 2002.

Gustafsson, E.: Modelling the marine CO_2 system in BALTSEM, Baltic Nest Institute Technical Report No. 9, Stockholm University, Stockholm, Sweden, ISBN 978-91-86655-08-2, https://su.diva-portal.org/smash/record.jsf?pid=diva2:1598412 (last access: 12 April 2022), 2013.

Hach, P. F., Marchant, H. K., Krupke, A., Riedel, T., Meier, D. V., Lavik, G., Holtappels, M., Dittmar, T., and Kuypers, M. M. M.: Rapid microbial diversification of dissolved organic matter in oceanic surface waters leads to carbon sequestration, Sci. Rep., 10, 13025, https://doi.org/10.1038/s41598-020-69930-y, 2020.

Hansell, D., Carlson, C., Repeta, D., and Schlitzer, R.: Dissolved Organic Matter in the Ocean: A Controversy Stimulates New Insights, Oceanography, 22, 202–211, https://doi.org/10.5670/oceanog.2009.109, 2009.

Hansell, D. A. and Carlson, C. A.: Deep-ocean gradients in the concentration of dissolved organic carbon, Nature, 395, 263–266, https://doi.org/10.1038/26200, 1998.

Hjalmarsson, S., Wesslander, K., Anderson, L. G., Omstedt, A., Perttilä, M., and Mintrop, L.: Distribution, long-term development and mass balance calculation of total alkalinity in the Baltic Sea, Cont. Shelf Res., 28, 593–601, https://doi.org/10.1016/j.csr.2007.11.010, 2008.

Ho, T.-Y., Quigg, A., Finkel, Z. V., Milligan, A. J., Wyman, K., Falkowski, P. G., and Morel, F. M. M.: The Elemental Composition of Some Marine Phytoplankton, J. Phycol., 39, 1145–1159, https://doi.org/10.1111/j.0022-3646.2003.03-090.x, 2003.

Holt, J., Butenschön, M., Wakelin, S. L., Artioli, Y., and Allen, J. I.: Oceanic controls on the primary production of the northwest European continental shelf: model experiments under recent past conditions and a potential future scenario, Biogeosciences, 9, 97–117, https://doi.org/10.5194/bg-9-97-2012, 2012.

Hopkinson, C. S. and Vallino, J. J.: Efficient export of carbon to the deep ocean through dissolved organic matter, Nature, 433, 142–145, https://doi.org/10.1038/nature03191, 2005.

Hopkinson, C. S., Fry, B., and Nolin, A. L.: Stoichiometry of dissolved organic matter dynamics on the continental shelf of the northeastern U.S.A., Cont. Shelf Res., 17, 473–489, https://doi.org/10.1016/S0278-4343(96)00046-5, 1997.

Hopkinson, C. S., Vallino, J. J., and Nolin, A.: Decomposition of dissolved organic matter from the continental margin, Deep-Sea Res. Pt. II, 49, 4461–4478, https://doi.org/10.1016/S0967-0645(02)00125-X, 2002.

Huang, J.: A Simple Accurate Formula for Calculating Saturation Vapor Pressure of Water and Ice, J. Appl. Meteorol. Clim., 57, 1265–1272, https://doi.org/10.1175/JAMC-D-17-0334.1, 2018.

Humphreys, M. P., Achterberg, E. P., Hopkins, J. E., Chowdhury, M. Z. H., Griffiths, A. M., Hartman, S. E., Hull, T., Smilenova, A., Wihsgott, J. U., Woodward, E. M. S., and Moore, C. M.: Mechanisms for a nutrient-conserving carbon pump in a seasonally stratified, temperate continental shelf sea, Prog. Oceanogr., 177, 101961, https://doi.org/10.1016/j.pocean.2018.05.001, 2019.

Humphreys, M. P., Lewis, E. R., Sharp, J. D., and Pierrot, D.: PyCO2SYS v1.8: marine carbonate system calculations in Python, Geosci. Model Dev., 15, 15–43, https://doi.org/10.5194/gmd-15-15-2022, 2022.

Humphreys, M. P., Schiller, A. J., Sandborn, D., Gregor, L., Pierrot, D., van Heuven, S. M. A. C., Lewis, E. R., and Wallace, D. W. R.: PyCO2SYS: marine carbonate system calculations in Python, Zenodo [code], https://doi.org/10.5281/zenodo.10671397, 2024.

Hung, J.-J., Chen, C.-H., Gong, G.-C., Sheu, D.-D., and Shiah, F.-K.: Distributions, stoichiometric patterns and cross-shelf exports of dissolved organic matter in the East China Sea, Deep-Sea Res. Pt. II, 50, 1127–1145, https://doi.org/10.1016/S0967-0645(03)00014-6, 2003.

Ingri, N., Kakolowicz, W., Sillén, L. G., and Warnqvist, B.: High-speed computers as a supplement to graphical methods – V1Haltafall, a general program for calculating the composition of equilibrium mixtures, Talanta, 14, 1261–1286, https://doi.org/10.1016/0039-9140(67)80203-0, 1967.

Kähler, P. and Koeve, W.: Marine dissolved organic matter: can its C : N ratio explain carbon overconsumption?, Deep-Sea Res. Pt. I, 48, 49–62, https://doi.org/10.1016/S0967-0637(00)00034-0, 2001.

Kitidis, V., Shutler, J. D., Ashton, I., Warren, M., Brown, I., Findlay, H., Hartman, S. E., Sanders, R., Humphreys, M., Kivimäe, C., Greenwood, N., Hull, T., Pearce, D., McGrath, T., Stewart, B. M., Walsham, P., McGovern, E., Bozec, Y., Gac, J.-P., van Heuven, S. M. A. C., Hoppema, M., Schuster, U., Johannessen, T., Omar, A., Lauvset, S. K., Skjelvan, I., Olsen, A., Steinhoff, T., Körtzinger, A., Becker, M., Lefevre, N., Diverrès, D., Gkritzalis, T., Cattrijsse, A., Petersen, W., Voynova, Y. G., Chapron, B., Grouazel, A., Land, P. E., Sharples, J., and Nightingale, P. D.: Winter weather controls net influx of atmospheric CO_2 on the north-west European shelf, Sci. Rep., 9, 20153, https://doi.org/10.1038/s41598-019-56363-5, 2019.

Kossack, J., Mathis, M., Daewel, U., Zhang, Y., and Schrum, C.: Barotropic and baroclinic tides increase primary production on the Northwest European Shelf, Front. Mar. Sci., 10, 1206062, https://doi.org/10.3389/fmars.2023.1206062, 2023.

Kossack, J., Mathis, M., Daewel, U., Liu, F., Demir, K. T., Thomas, H., and Schrum, C.: Tidal impacts on air-sea CO_2 exchange on the North-West European shelf, Front. Mar. Sci., 11, 1406896, https://doi.org/10.3389/fmars.2024.1406896, 2024.

Kühn, W., Pätsch, J., Thomas, H., Borges, A. V., Schiettecatte, L. S., Bozec, Y., and Prowe, A. E. F.: Nitrogen and carbon cycling in the North Sea and exchange with the North Atlantic-A model study, Part II: Carbon budget and fluxes, Cont. Shelf Res., 30, 1701–1716, https://doi.org/10.1016/j.csr.2010.07.001, 2010.

Kwiatkowski, L., Aumont, O., Bopp, L., and Ciais, P.: The Impact of Variable Phytoplankton Stoichiometry on Projections of Primary Production, Food Quality, and Carbon Uptake in the Global Ocean, Global Biogeochem. Cy., 32, 516–528, https://doi.org/10.1002/2017GB005799, 2018.

Lacroix, F., Ilyina, T., Mathis, M., Laruelle, G. G., and Regnier, P.: Historical increases in land-derived nutrient inputs may alleviate effects of a changing physical climate on the oceanic carbon cycle, Glob. Change Biol., 27, 5491–5513, https://doi.org/10.1111/gcb.15822, 2021.

Lan, X., Mund, J., Crotwell, A., Crotwell, M., Moglia, E., Madronich, M., Neff, D., and Thoning, K.: Atmospheric Carbon Dioxide Dry Air Mole Fractions from the NOAA GML Carbon Cycle Cooperative Global Air Sampling Network, 1968–2022, Version: 2023-08-28, NOAA [data set], https://doi.org/10.15138/wkgj-f215, 2023.

Laruelle, G. G., Lauerwald, R., Pfeil, B., and Regnier, P.: Regionalized global budget of the CO_2 exchange at the air-water interface in continental shelf seas, Global Biogeochem. Cy., 28, 1199–1214, https://doi.org/10.1002/2014GB004832, 2014.

Laruelle, G. G., Cai, W.-J., Hu, X., Gruber, N., Mackenzie, F. T., and Regnier, P.: Continental shelves as a variable but increasing global sink for atmospheric carbon dioxide, Nat. Commun., 9, 454, https://doi.org/10.1038/s41467-017-02738-z, 2018.

Legge, O., Johnson, M., Hicks, N., Jickells, T., Diesing, M., Aldridge, J., Andrews, J., Artioli, Y., Bakker, D. C. E., Burrows, M. T., Carr, N., Cripps, G., Felgate, S. L., Fernand, L., Greenwood, N., Hartman, S., Kröger, S., Lessin, G., Mahaffey, C., Mayor, D. J., Parker, R., Queirós, A. M., Shutler, J. D., Silva, T., Stahl, H., Tinker, J., Underwood, G. J. C., Molen, J. V. D., Wakelin, S., Weston, K., and Williamson, P.: Carbon on the Northwest European Shelf: Contemporary Budget and Future Influences, Frontiers in Marine Science, 7, 143, https://doi.org/10.3389/fmars.2020.00143, 2020.

Letscher, R. T. and Moore, J. K.: Preferential remineralization of dissolved organic phosphorus and non-Redfield DOM dynamics in the global ocean: Impacts on marine productivity, nitrogen fixation, and carbon export, Global Biogeochem. Cy., 29, 325–340, https://doi.org/10.1002/2014GB004904, 2015.

Letscher, R. T., Moore, J. K., Teng, Y.-C., and Primeau, F.: Variable C : N : P stoichiometry of dissolved organic matter cycling in the Community Earth System Model, Biogeosciences, 12, 209–221, https://doi.org/10.5194/bg-12-209-2015, 2015.

Liang, Z., Letscher, R. T., and Knapp, A. N.: Global Patterns of Surface Ocean Dissolved Organic Matter Stoichiometry, Global Biogeochem. Cy., 37, e2023GB007788, https://doi.org/10.1029/2023GB007788, 2023.

Locarnini, M., Mishonov, A., Baranova, O., Boyer, T., Zweng, M., Garcia, H., Reagan, J., Seidov, D., Weathers, K., Paver, C., and Smolyar, I.: World Ocean Atlas 2018, Volume 1: Temperature, NOAA Atlas NESDIS 81, 52 pp., https://doi.org/10.25923/e5rn-9711, 2018.

Loh, A. N. and Bauer, J. E.: Distribution, partitioning and fluxes of dissolved and particulate organic C, N and P in the eastern North Pacific and Southern Oceans, Deep-Sea Res. Pt. I, 47, 2287–2316, https://doi.org/10.1016/S0967-0637(00)00027-3, 2000.

Lønborg, C. and Álvarez-Salgado, X. A.: Recycling versus export of bioavailable dissolved organic matter in the coastal ocean and efficiency of the continental shelf pump, Global Biogeochem. Cy., 26, GB3018, https://doi.org/10.1029/2012GB004353, 2012.

Lønborg, C., Álvarez-Salgado, X. A., Davidson, K., and Miller, A. E. J.: Production of bioavailable and refractory dissolved organic matter by coastal heterotrophic microbial populations, Estuar. Coast. Shelf S., 82, 682–688, https://doi.org/10.1016/j.ecss.2009.02.026, 2009.

Lønborg, C., Carreira, C., Abril, G., Agustí, S., Amaral, V., Andersson, A., Arístegui, J., Bhadury, P., Bif, M. B., Borges, A. V., Bouillon, S., Calleja, M. Ll., Cotovicz Jr., L. C., Cozzi, S., Doval, M., Duarte, C. M., Eyre, B., Fichot, C. G., García-Martín, E. E., Garzon-Garcia, A., Giani, M., Gonçalves-Araujo, R., Gruber, R., Hansell, D. A., Hashihama, F., He, D., Holding, J. M., Hunter, W. R., Ibánhez, J. S. P., Ibello, V., Jiang, S., Kim, G., Klun, K., Kowalczuk, P., Kubo, A., Lee, C.-W., Lopes, C. B., Maggioni, F., Magni, P., Marrase, C., Martin, P., McCallister, S. L., McCallum, R., Medeiros, P. M., Morán, X. A. G., Muller-Karger, F. E., Myers-Pigg, A., Norli, M., Oakes, J. M., Osterholz, H., Park, H., Lund Paulsen, M., Rosentreter, J. A., Ross, J. D., Rueda-Roa, D., Santinelli, C., Shen, Y., Teira, E., Tinta, T., Uher, G., Wakita, M., Ward, N., Watanabe, K., Xin, Y., Yamashita, Y., Yang, L., Yeo, J., Yuan, H., Zheng, Q., and Álvarez-Salgado, X. A.: A global database of dissolved organic matter (DOM) concentration measurements in coastal waters (CoastDOM v1), Earth Syst. Sci. Data, 16, 1107–1119, https://doi.org/10.5194/essd-16-1107-2024, 2024.

Lorkowski, I., Pätsch, J., Moll, A., and Kühn, W.: Interannual variability of carbon fluxes in the North Sea from 1970 to 2006 – Competing effects of abiotic and biotic drivers on the gas-exchange of CO_2, Estuar. Coast. Shelf S., 100, 38–57, https://doi.org/10.1016/j.ecss.2011.11.037, 2012.

Mari, X., Passow, U., Migon, C., Burd, A. B., and Legendre, L.: Transparent exopolymer particles: Effects on carbon cycling in the ocean, Prog. Oceanogr., 151, 13–37, https://doi.org/10.1016/j.pocean.2016.11.002, 2017.

Martiny, A. C., Pham, C. T. A., Primeau, F. W., Vrugt, J. A., Moore, J. K., Levin, S. A., and Lomas, M. W.: Strong latitudinal patterns in the elemental ratios of marine plankton and organic matter, Nat. Geosci., 6, 279–283, https://doi.org/10.1038/ngeo1757, 2013.

Martiny, A. C., Vrugt, J. A., and Lomas, M. W.: Concentrations and ratios of particulate organic carbon, nitrogen, and phosphorus in the global ocean, Sci. Data, 1, 140048, https://doi.org/10.1038/sdata.2014.48, 2014.

Mathis, M., Logemann, K., Maerz, J., Lacroix, F., Hagemann, S., Chegini, F., Ramme, L., Ilyina, T., Korn, P., and Schrum, C.: Seamless Integration of the Coastal Ocean in Global Marine Carbon Cycle Modeling, J. Adv. Model. Earth Sy., 14, e2021MS002789, https://doi.org/10.1029/2021MS002789, 2022.

Mathis, M., Lacroix, F., Hagemann, S., Nielsen, D. M., Ilyina, T., and Schrum, C.: Enhanced CO_2 uptake of the coastal ocean is dominated by biological carbon fixation, Nat. Clim. Change, 14, 373–379, https://doi.org/10.1038/s41558-024-01956-w, 2024.

Millero, F. J., Graham, T. B., Huang, F., Bustos-Serrano, H., and Pierrot, D.: Dissociation constants of carbonic acid in seawater as a function of salinity and temperature, Mar. Chem., 100, 80–94, https://doi.org/10.1016/j.marchem.2005.12.001, 2006.

Moreno, A. R. and Martiny, A. C.: Ecological Stoichiometry of Ocean Plankton, Annu. Rev. Mar. Sci., 10, 43–69, https://doi.org/10.1146/annurev-marine-121916-063126, 2018.

Myklestad, S. M.: Release of extracellular products by phytoplankton with special emphasis on polysaccharides, Sci. Total Environ., 165, 155–164, https://doi.org/10.1016/0048-9697(95)04549-G, 1995.

Neal, C. and Davies, H.: Water quality fluxes for eastern UK rivers entering the North Sea: a summary of information from the Land Ocean Interaction Study (LOIS), Sci. Total Environ., 314–316, 821–882, https://doi.org/10.1016/S0048-9697(03)00086-X, 2003.

Neumann, T., Radtke, H., Cahill, B., Schmidt, M., and Rehder, G.: Non-Redfieldian carbon model for the Baltic Sea (ERGOM version 1.2) – implementation and budget estimates, Geosci. Model Dev., 15, 8473–8540, https://doi.org/10.5194/gmd-15-8473-2022, 2022.

Painter, S. C., Hartman, S. E., Kivimäe, C., Salt, L. A., Clargo, N. M., Daniels, C. J., Bozec, Y., Daniels, L., Allen, S., Hemsley, V. S., Moschonas, G., and Davidson, K.: The elemental stoichiometry (C, Si, N, P) of the Hebrides Shelf and

its role in carbon export, Prog. Oceanogr., 159, 154–177, https://doi.org/10.1016/j.pocean.2017.10.001, 2017.

Painter, S. C., Lapworth, D. J., Woodward, E. M. S., Kroeger, S., Evans, C. D., Mayor, D. J., and Sanders, R. J.: Terrestrial dissolved organic matter distribution in the North Sea, Sci. Total Environ., 630, 630–647, https://doi.org/10.1016/j.scitotenv.2018.02.237, 2018.

Pätsch, J. and Lenhart, H.: Daily Loads of Nutrients, Total Alkalinity, Dissolved Inorganic Carbon and Dissolved Organic Carbon of the European Continental Rivers for the Years 1977-2002, Berichte aus dem Zentrum für Meeres- und Klimaforschung, Reihe B, Ozeanographie, 2004.

Porz, L., Zhang, W., Christiansen, N., Kossack, J., Daewel, U., and Schrum, C.: Quantification and mitigation of bottom-trawling impacts on sedimentary organic carbon stocks in the North Sea, Biogeosciences, 21, 2547–2570, https://doi.org/10.5194/bg-21-2547-2024, 2024.

Prowe, A. E. F., Thomas, H., Pätsch, J., Kühn, W., Bozec, Y., Schiettecatte, L. S., Borges, A. V., and Baar, H. J. W. de: Mechanisms controlling the air-sea CO_2 flux in the North Sea, Cont. Shelf Res., 29, 1801–1808, https://doi.org/10.1016/j.csr.2009.06.003, 2009.

Redfield, A. C.: The influence of organisms on the composition of seawater, The Sea, 2, 26–77, 1963.

Samuelsen, A., Schrum, C., Yumruktepe, V. Ç., Daewel, U., and Roberts, E. M.: Environmental Change at Deep-Sea Sponge Habitats Over the Last Half Century: A Model Hindcast Study for the Age of Anthropogenic Climate Change, Front. Mar. Sci., 9, 737164, https://doi.org/10.3389/fmars.2022.737164, 2022.

Sardans, J., Rivas-Ubach, A., and Peñuelas, J.: The C : N : P stoichiometry of organisms and ecosystems in a changing world: A review and perspectives, Perspect. Plant Ecol., 14, 33–47, https://doi.org/10.1016/j.ppees.2011.08.002, 2012.

Sardans, J., Janssens, I. A., Ciais, P., Obersteiner, M., and Peñuelas, J.: Recent advances and future research in ecological stoichiometry, Perspectives in Plant Ecology, Evolution and Systematics, 50, 125611, https://doi.org/10.1016/j.ppees.2021.125611, 2021.

Schiettecatte, L.-S., Thomas, H., Bozec, Y., and Borges, A. V.: High temporal coverage of carbon dioxide measurements in the Southern Bight of the North Sea, Mar. Chem., 106, 161–173, https://doi.org/10.1016/j.marchem.2007.01.001, 2007.

Schindler, D. E. and Eby, L. A.: Stoichiometry of Fishes and Their Prey: Implications for Nutrient Recycling, Ecology, 78, 1816–1831, https://doi.org/10.1890/0012-9658(1997)078[1816:SOFATP]2.0.CO;2, 1997.

Schrum, C., Alekseeva, I., and John, M. S.: Development of a coupled physical-biological ecosystem model ECOSMO. Part I: Model description and validation for the North Sea, J. Marine Syst., 61, 79–99, https://doi.org/10.1016/j.jmarsys.2006.01.005, 2006.

Simpson, D., Benedictow, A., Berge, H., Bergström, R., Emberson, L. D., Fagerli, H., Flechard, C. R., Hayman, G. D., Gauss, M., Jonson, J. E., Jenkin, M. E., Nyíri, A., Richter, C., Semeena, V. S., Tsyro, S., Tuovinen, J.-P., Valdebenito, Á., and Wind, P.: The EMEP MSC-W chemical transport model – technical description, Atmos. Chem. Phys., 12, 7825–7865, https://doi.org/10.5194/acp-12-7825-2012, 2012.

Singh, A., Baer, S. E., Riebesell, U., Martiny, A. C., and Lomas, M. W.: C : N : P stoichiometry at the Bermuda Atlantic Time-series Study station in the North Atlantic Ocean, Biogeosciences, 12, 6389–6403, https://doi.org/10.5194/bg-12-6389-2015, 2015.

Smith, S. V. and Hollibaugh, J. T.: Coastal metabolism and the oceanic organic carbon balance, Rev. Geophys., 31, 75–89, https://doi.org/10.1029/92RG02584, 1993.

Søndergaard, M., Williams, P. J. le B., Cauwet, G., Riemann, B., Robinson, C., Terzic, S., Woodward, E. M. S., and Worm, J.: Net accumulation and flux of dissolved organic carbon and dissolved organic nitrogen in marine plankton communities, Limnol. Oceanogr., 45, 1097–1111, https://doi.org/10.4319/lo.2000.45.5.1097, 2000.

Stepanauskas, R., JØrgensen, N. O. G., Eigaard, O. R., Žvikas, A., Tranvik, L. J., and Leonardson, L.: Summer Inputs of Riverine Nutrients to the Baltic Sea: Bioavailability and Eutrophication Relevance, Ecol. Monogr., 72, 579–597, https://doi.org/10.1890/0012-9615(2002)072[0579:SIORNT]2.0.CO;2, 2002.

Suratman, S., Weston, K., Jickells, T., and Fernand, L.: Spatial and seasonal changes of dissolved and particulate organic C in the North Sea, Hydrobiologia, 628, 13–25, https://doi.org/10.1007/s10750-009-9730-z, 2009.

Tanioka, T., Matsumoto, K., and Lomas, M. W.: Drawdown of Atmospheric pCO_2 Via Variable Particle Flux Stoichiometry in the Ocean Twilight Zone, Geophys. Res. Lett., 48, e2021GL094924, https://doi.org/10.1029/2021GL094924, 2021.

Tanioka, T., Larkin, A. A., Moreno, A. R., Brock, M. L., Fagan, A. J., Garcia, C. A., Garcia, N. S., Gerace, S. D., Lee, J. A., Lomas, M. W., and Martiny, A. C.: Global Ocean Particulate Organic Phosphorus, Carbon, Oxygen for Respiration, and Nitrogen (GO-POPCORN), Sci. Data, 9, 688, https://doi.org/10.1038/s41597-022-01809-1, 2022a.

Tanioka, T., Garcia, C. A., Larkin, A. A., Garcia, N. S., Fagan, A. J., and Martiny, A. C.: Global patterns and predictors of C : N : P in marine ecosystems, Communications Earth & Environment, 3, 271, https://doi.org/10.1038/s43247-022-00603-6, 2022b.

Thomas, H., Ittekkot, V., Osterroht, C., and Schneider, B.: Preferential recycling of nutrients – the ocean's way to increase new production and to pass nutrient limitation?, Limnol. Oceanogr., 44, 1999–2004, https://doi.org/10.4319/lo.1999.44.8.1999, 1999.

Thomas, H., Bozec, Y., Elkalay, K., and Baar, H. J. W. D.: Enhanced Open Ocean Storage of CO_2 from Shelf Sea Pumping, Science, 304, 1005–1008, https://doi.org/10.1126/science.1095491, 2004.

Thomas, H., Bozec, Y., de Baar, H. J. W., Elkalay, K., Frankignoulle, M., Schiettecatte, L.-S., Kattner, G., and Borges, A. V.: The carbon budget of the North Sea, Biogeosciences, 2, 87–96, https://doi.org/10.5194/bg-2-87-2005, 2005.

Tsunogai, S., Watanabe, S., and Sato, T.: Is there a "continental shelf pump" for the absorption of atmospheric CO_2?, Tellus B, 51, 701–712, https://doi.org/10.3402/tellusb.v51i3.16468, 1999.

Voss, M., Asmala, E., Bartl, I., Carstensen, J., Conley, D. J., Dippner, J. W., Humborg, C., Lukkari, K., Petkuviene, J., Reader, H., Stedmon, C., Vybernaite-Lubiene, I., Wannicke, N., and Zilius, M.: Origin and fate of dissolved organic matter in four shallow Baltic Sea estuaries, Biogeochemistry, 154, 385–403, https://doi.org/10.1007/s10533-020-00703-5, 2021.

Wakelin, S. L., Holt, J. T., Blackford, J. C., Allen, J. I., Butenschön, M., and Artioli, Y.: Modeling the carbon fluxes of the northwest European continental shelf: Valida-

tion and budgets, J. Geophys. Res., 117, 2011JC007402, https://doi.org/10.1029/2011JC007402, 2012.

Wang, H., Gong, D., Friedrichs, M. A. M., Harris, C. K., Miles, T., Yu, H.-C., and Zhang, Y.: A Cycle of Wind-Driven Canyon Upwelling and Downwelling at Wilmington Canyon and the Evolution of Canyon-Upwelled Dense Water on the MAB Shelf, Front. Mar. Sci., 9, 866075, https://doi.org/10.3389/fmars.2022.866075, 2022.

Wanninkhof, R.: Relationship between wind speed and gas exchange over the ocean revisited, Limnology & Ocean Methods, 12, 351–362, https://doi.org/10.4319/lom.2014.12.351, 2014.

Wear, E. K., Carlson, C. A., Windecker, L. A., and Brzezinski, M. A.: Roles of diatom nutrient stress and species identity in determining the short- and long-term bioavailability of diatom exudates to bacterioplankton, Mar. Chem., 177, 335–348, https://doi.org/10.1016/j.marchem.2015.09.001, 2015a.

Wear, E. K., Carlson, C. A., James, A. K., Brzezinski, M. A., Windecker, L. A., and Nelson, C. E.: Synchronous shifts in dissolved organic carbon bioavailability and bacterial community responses over the course of an upwelling-driven phytoplankton bloom, Limnol. Oceanogr., 60, 657–677, https://doi.org/10.1002/lno.10042, 2015b.

Williams, P., Carlucci, A., and Olson, R.: A deep profile of some biologically important properties in the central North Pacific gyre, Oceanol. Acta, 3, 471–476, 1980.

Williams, P. J. leB.: Evidence for the seasonal accumulation of carbon-rich dissolved organic material, its scale in comparison with changes in particulate material and the consequential effect on net CN assimilation ratios, Mar. Chem., 51, 17–29, https://doi.org/10.1016/0304-4203(95)00046-T, 1995.

Wolf-Gladrow, D. A., Zeebe, R. E., Klaas, C., Körtzinger, A., and Dickson, A. G.: Total alkalinity: The explicit conservative expression and its application to biogeochemical processes, Mar. Chem., 106, 287–300, https://doi.org/10.1016/j.marchem.2007.01.006, 2007.

Ye, F., Zhang, Y. J., He, R., Wang, Z., Wang, H. V., and Du, J.: Third-order WENO transport scheme for simulating the baroclinic eddying ocean on an unstructured grid, Ocean Model., 143, 101466, https://doi.org/10.1016/j.ocemod.2019.101466, 2019.

Zakem, E. J. and Levine, N. M.: Systematic Variation in Marine Dissolved Organic Matter Stoichiometry and Remineralization Ratios as a Function of Lability, Global Biogeochem. Cy., 33, 1389–1407, https://doi.org/10.1029/2019GB006375, 2019.

Zhang, Y. J., Ateljevich, E., Yu, H.-C., Wu, C. H., and Yu, J. C. S.: A new vertical coordinate system for a 3D unstructured-grid model, Ocean Model., 85, 16–31, https://doi.org/10.1016/j.ocemod.2014.10.003, 2015.

Zhang, Y. J., Ye, F., Stanev, E. V., and Grashorn, S.: Seamless cross-scale modeling with SCHISM, Ocean Model., 102, 64–81, https://doi.org/10.1016/j.ocemod.2016.05.002, 2016a.

Zhang, Y. J., Stanev, E. V., and Grashorn, S.: Unstructured-grid model for the North Sea and Baltic Sea: Validation against observations, Ocean Model., 97, 91–108, https://doi.org/10.1016/j.ocemod.2015.11.009, 2016b.

Zhao, C., Daewel, U., and Schrum, C.: Tidal impacts on primary production in the North Sea, Earth Syst. Dynam., 10, 287–317, https://doi.org/10.5194/esd-10-287-2019, 2019.

Zweng, M. M., Reagan, J. R., Seidov, D., Boyer, T. P., Locarnini, R. A., Garcia, H. E., Mishonov, A. V., Baranova, O. K., Weathers, K., Paver, C. R., and Smolyar, I.: World Ocean Atlas 2018, Volume 2: Salinity, NOAA Atlas NESDIS 82, 50 pp., https://doi.org/10.25923/9pgv-1224, 2019.

Supplement of Biogeosciences, 22, 2569–2599, 2025
https://doi.org/10.5194/bg-22-2569-2025-supplement

Biogeosciences Open Access EGU

Supplement of

Variable organic matter stoichiometry enhances the biological drawdown of CO_2 in the northwest European shelf seas

Kubilay Timur Demir et al.

Correspondence to: Kubilay Timur Demir (kubilay.demir@hereon.de)

S1 Supplementary Figures and Tables

S1.1 Supplementary Figures

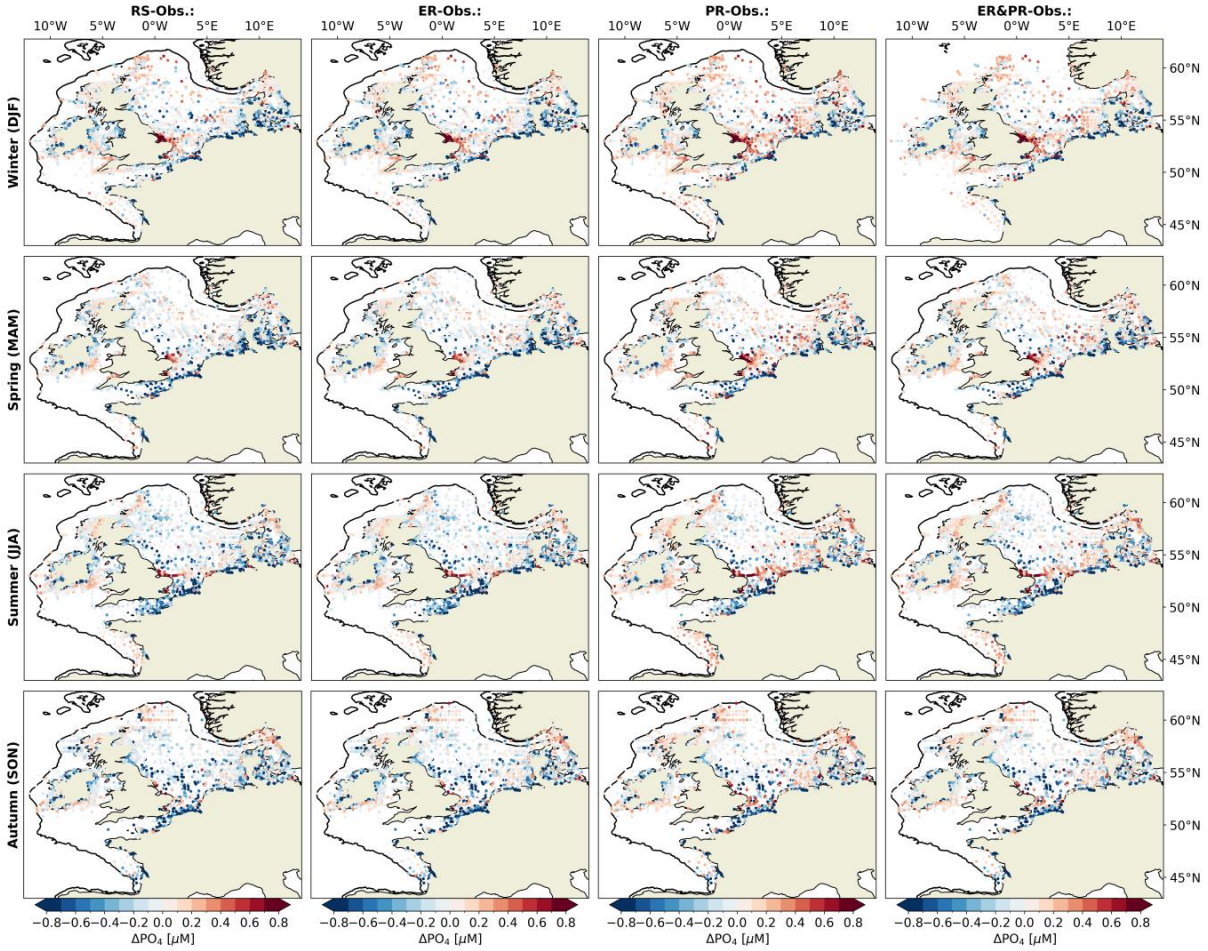

Figure S1: Differences between simulated and observed seasonal phosphate (PO_4) concentrations over 2000–2010. The total of 161,152 data points from the International Council for the Exploration of the Sea (ICES) are compared to respective model output, co-located by a horizontal and vertical nearest neighbor search, for all four configurations: Redfield Stoichiometry (RS), Extracellular Release (ER), Preferential Remineralization (PR), and the combined configuration (ER&PR). The data includes both bottle and pump data from the ocean hydrochemistry data collection.

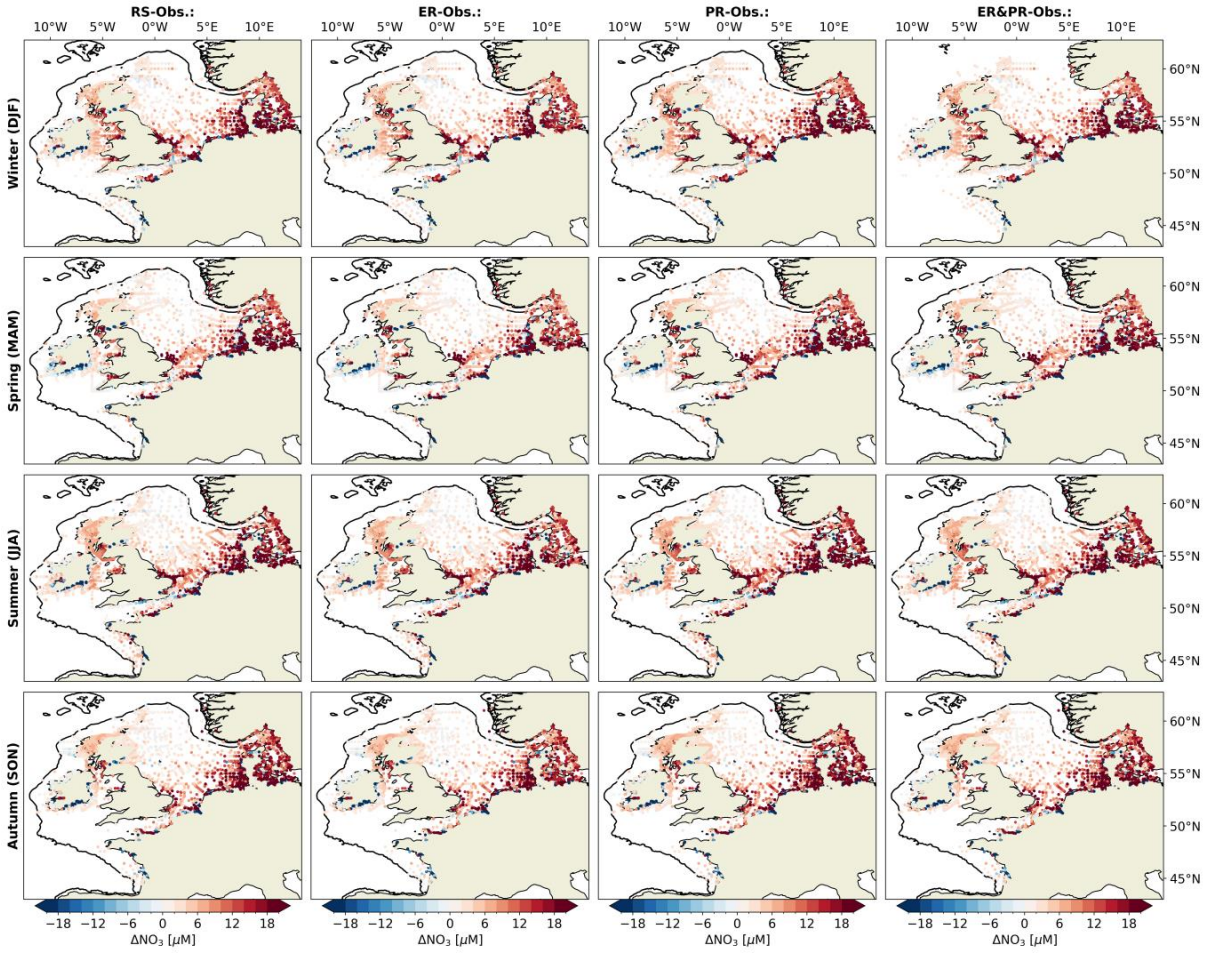

Figure S2: Differences between simulated and observed seasonal nitrate (NO_3) concentrations over 2000–2010. The total of 135,469 data points from the International Council for the Exploration of the Sea (ICES) are compared to respective model output, co-located by a horizontal and vertical nearest neighbor search, for all four configurations: Redfield Stoichiometry (RS), Extracellular Release (ER), Preferential Remineralization (PR), and the combined configuration (ER&PR). The data includes both bottle and pump data from the ocean hydrochemistry data collection.

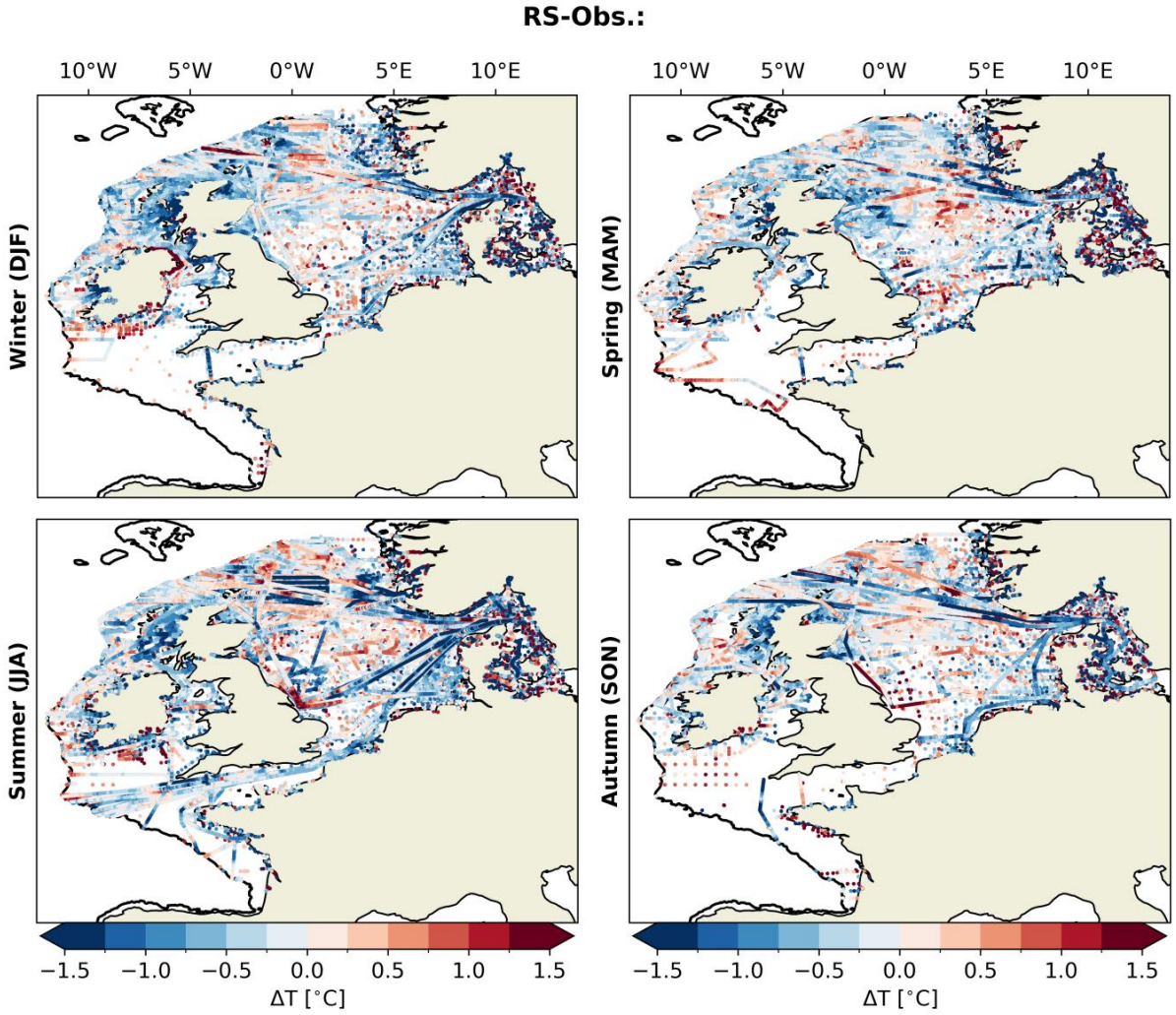

Figure S3: Differences between simulated and observed seasonal in situ temperature (T) over 2000–2010. The total of 2,153,726 data points from the International Council for the Exploration of the Sea (ICES) are compared to respective model output, co-located by a horizontal and vertical nearest neighbor search for the Redfield Stoichiometry (RS) configuration. As the physical simulation is consistent between all four simulations, it is not shown for each of the configurations. The data includes the surface, bottle, and pump data from the ocean hydrochemistry data collection.

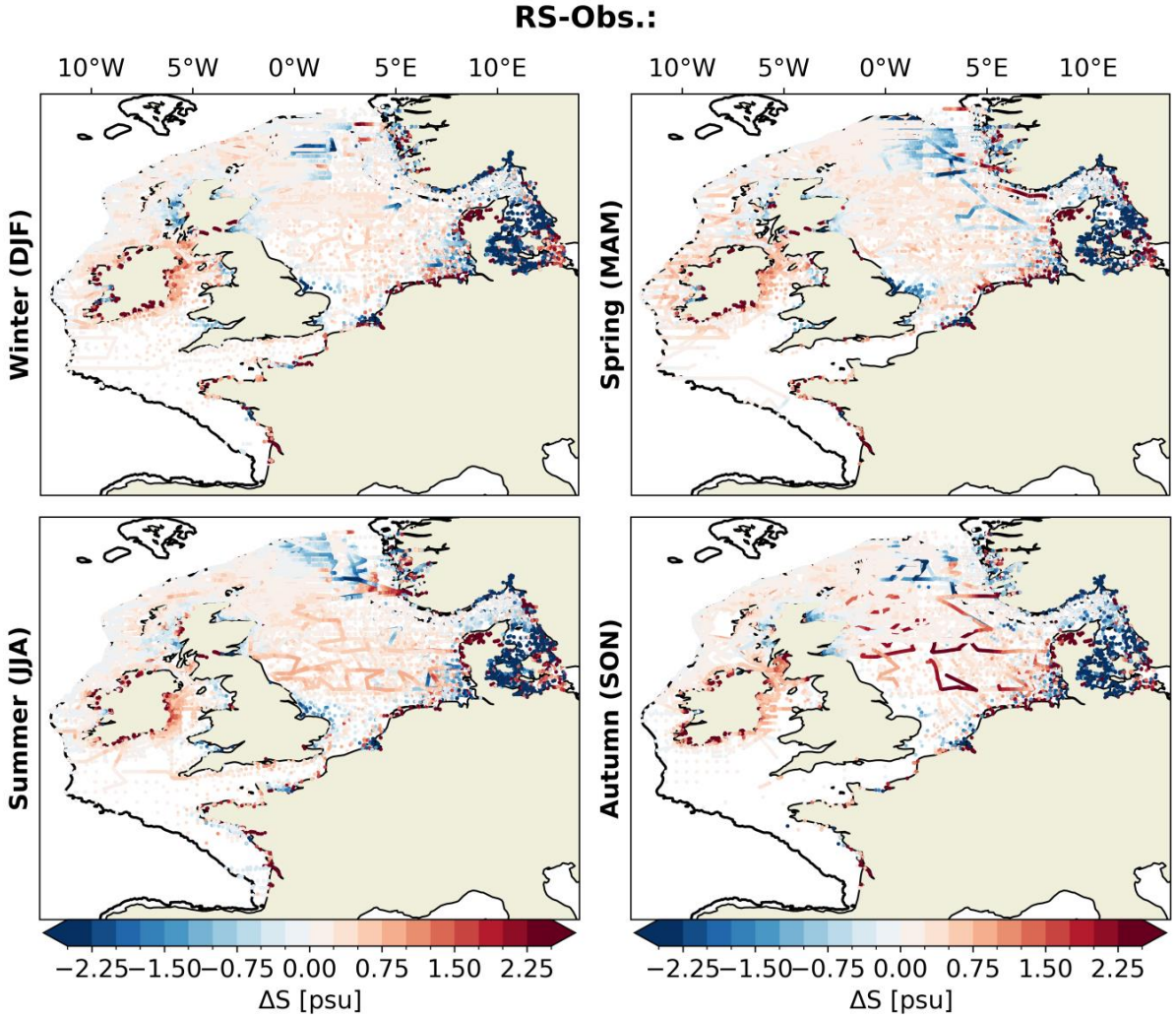

Figure S4: Differences between simulated and observed seasonal salinity (S) over 2000–2010. The total of 1,913,297 data points from the International Council for the Exploration of the Sea (ICES) are compared to respective model output, co-located by a horizontal and vertical nearest neighbor search for the Redfield Stoichiometry (RS) configuration. As the physical simulation is consistent between all four simulations, it is not shown for each of the configurations. The data includes the bottle and pump data from the ocean hydrochemistry data collection.

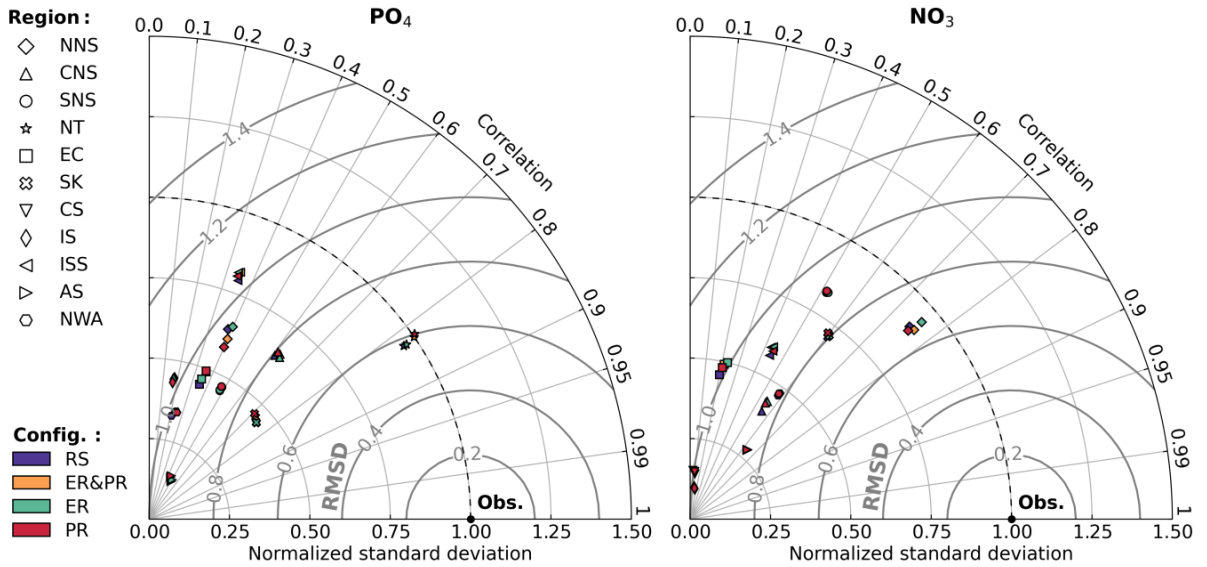

Figure S5: Taylor diagrams for phosphate (PO_4) and nitrate (NO_3), both limiting nutrients for primary production, showing correlation, root mean squared difference (RMSD), and normalized standard deviation of the model output with respect to observations. For each of the variables, the respective observations from Figures S1 and S2 are combined for all seasons and compared to the co-located model output using a horizontal and vertical nearest neighbor search. The model performance is differentiated by configuration, as indicated by color, and subregion, as indicated by shape.

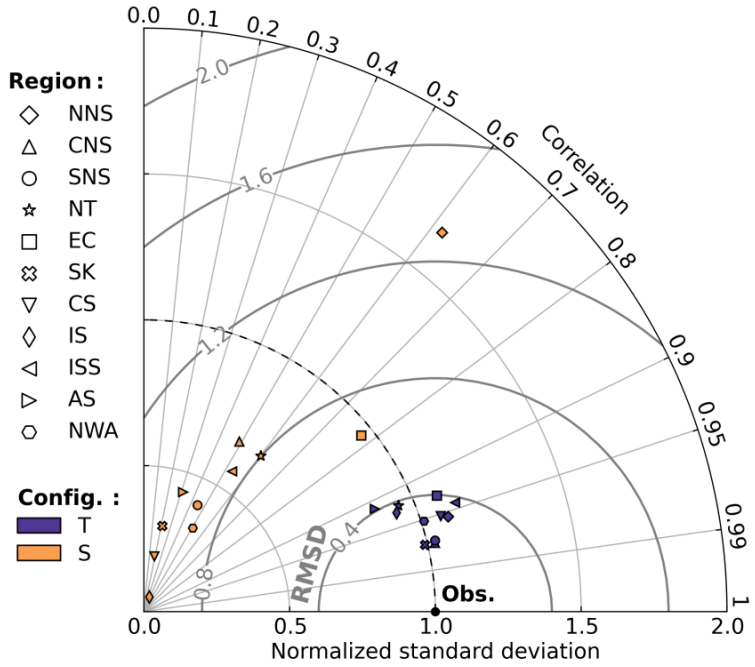

Figure S6: Taylor diagrams for the physical variables in situ temperature (T) and salinity (S), showing correlation, root mean squared difference (RMSD), and normalized standard deviation of the model output with respect to observations. For each of the variables, the respective observations from Figures S3 and S4 are combined for all seasons and compared to the co-located model output. As all four physical model configurations are consistent, we here only show the results for the Redfield Stoichiometry (RS) configuration.

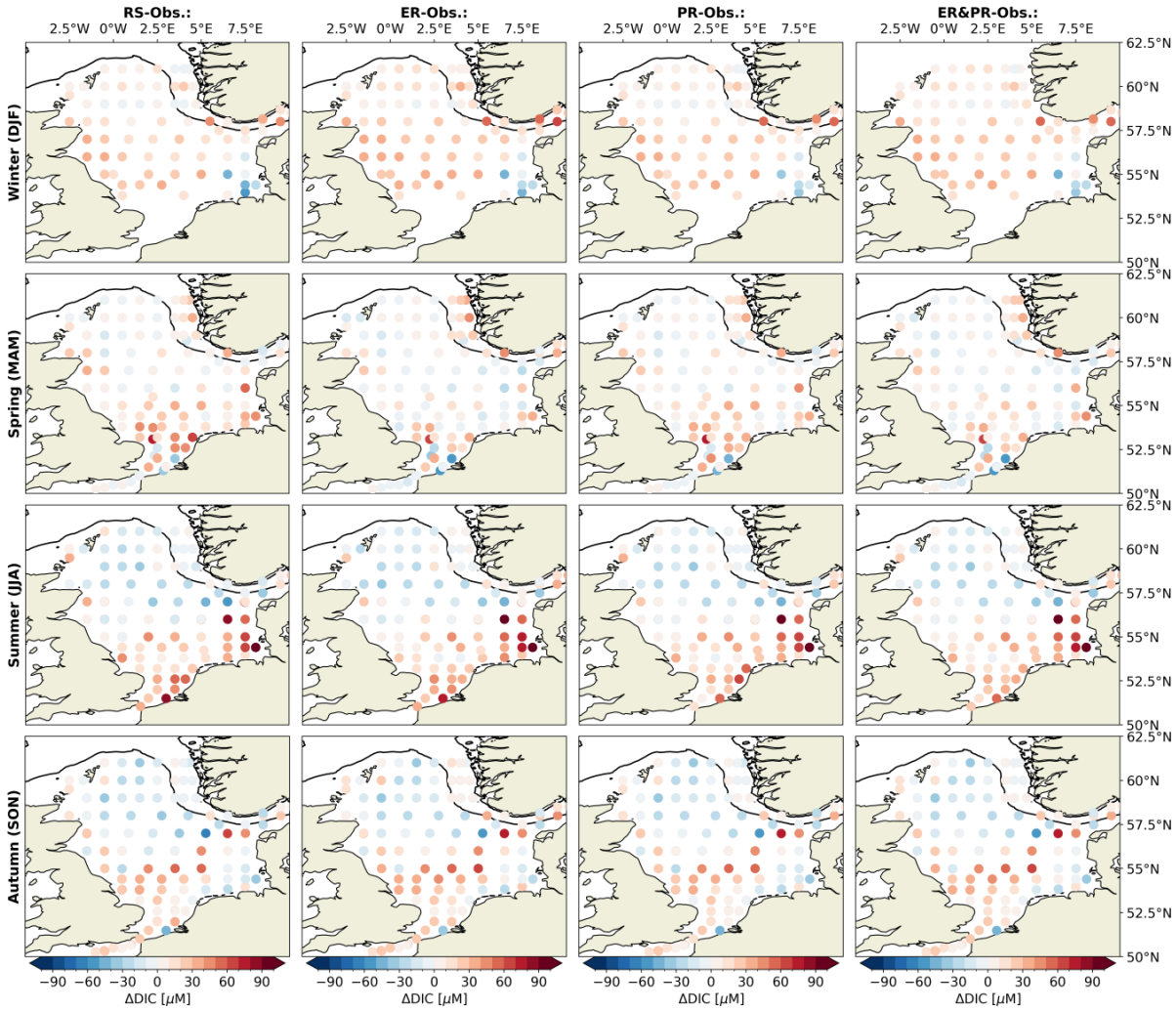

Figure S7: Differences between simulated and observed seasonal dissolved inorganic carbon (DIC) concentrations over 2000–2010. The total of 5,685 data points from the Global Ocean Data Analysis Project (GLODAP) are compared to respective model output, co-located by a horizontal and vertical nearest neighbor search, for all four configurations: Redfield Stoichiometry (RS), Extracellular Release (ER), Preferential Remineralization (PR), and the combined configuration (ER&PR).

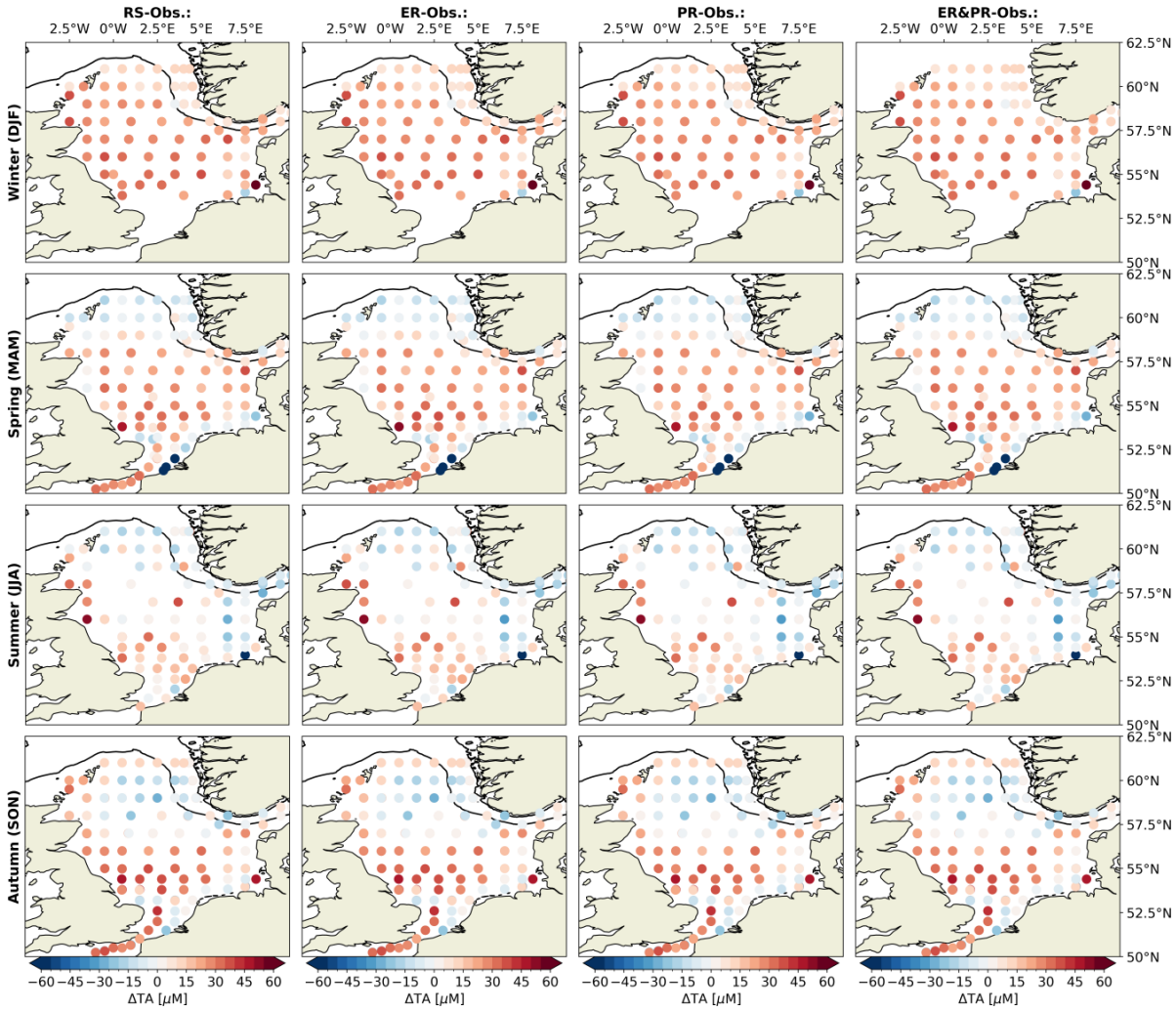

Figure S8: Differences between simulated and observed seasonal total alkalinity (TA) over 2000–2010. The total of 5,110 data points from the Global Ocean Data Analysis Project (GLODAP) are compared to respective model output, co-located by a horizontal and vertical nearest neighbor search, for all four configurations: Redfield Stoichiometry (RS), Extracellular Release (ER), Preferential Remineralization (PR), and the combined configuration (ER&PR).

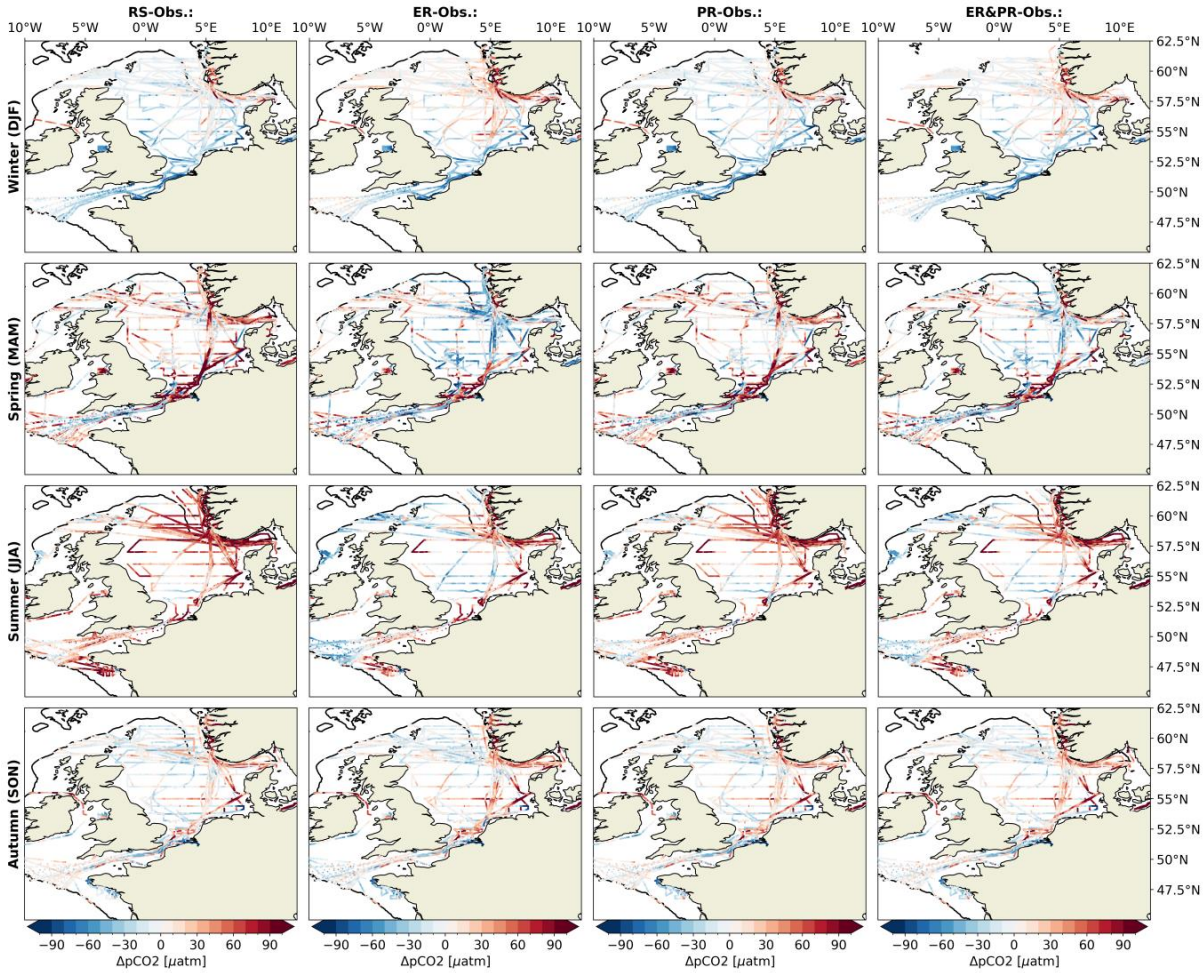

Figure S9: Differences between simulated and observed seasonal surface partial pressure of CO_2 (pCO_2) over 2000–2010. The total of 772,202 data points in the northwest European shelf seas from the Surface Ocean CO_2 Atlas (SOCAT) are compared to respective model output, co-located by a horizontal nearest neighbor search, for all four configurations: Redfield Stoichiometry (RS), Extracellular Release (ER), Preferential Remineralization (PR), and the combined configuration (ER&PR). Observations were converted from fCO_2 to pCO_2 using PyCO2SYS (Humphreys et al., 2022, 2024). Model CO_2 concentrations in parts per million were converted to pCO_2 using Eq. 15-16, based on the conversion suggested by PyCO2SYS (Humphreys et al., 2022, 2024) and an improved temperature-dependent saturation vapor pressure equation (Huang, 2018).

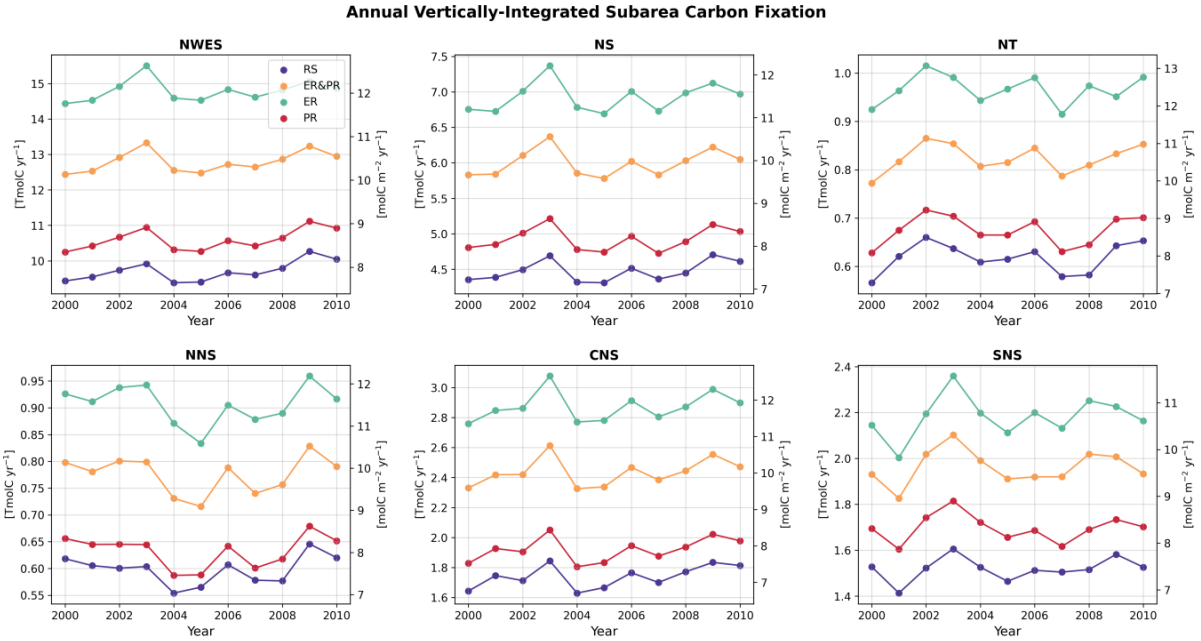

Figure S10: Time Series of annual vertically-integrated carbon fixation for the entire northwest European shelf seas (NWES), the North Sea (NS), the Norwegian Trench (NT), and the northern, central and southern North Sea (NNS, CNS, SNS). These include all four configurations: Redfield Stoichiometry (RS), Extracellular Release (ER), Preferential Remineralization (PR), and the combined configuration (ER&PR).

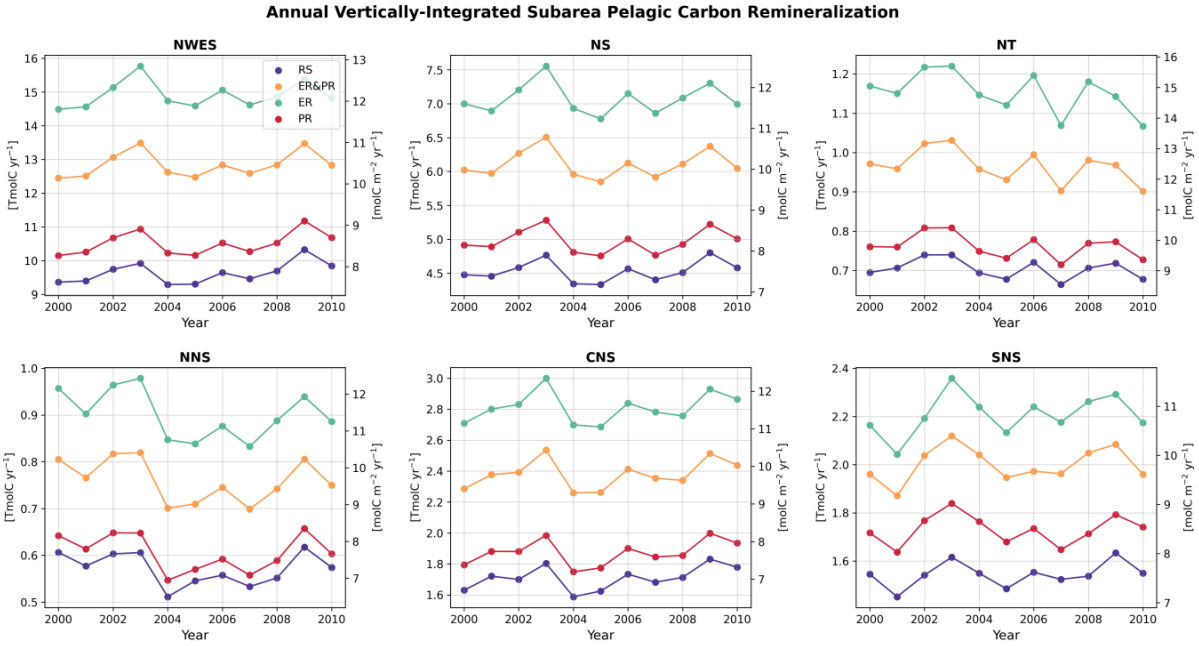

Figure S11: Time Series of annual vertically-integrated pelagic carbon remineralization for the entire northwest European shelf seas (NWES), the North Sea (NS), the Norwegian Trench (NT), and the northern, central and southern North Sea (NNS, CNS, SNS). These include all four configurations: Redfield Stoichiometry (RS), Extracellular Release (ER), Preferential Remineralization (PR), and the combined configuration (ER&PR).

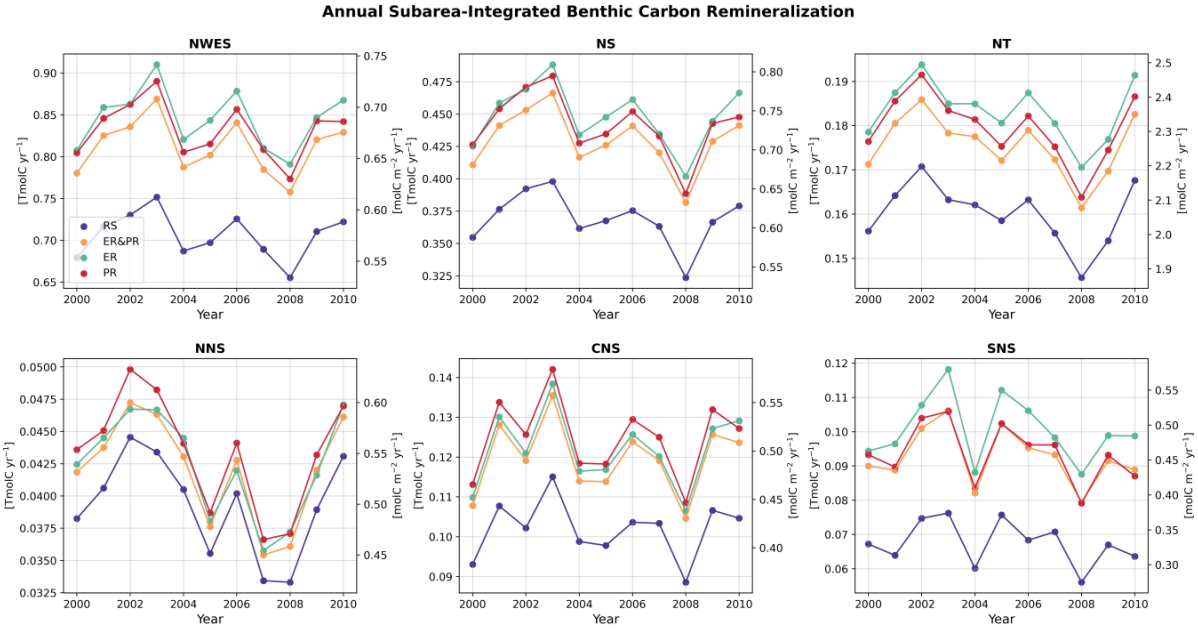

Figure S12: Time Series of annual subarea-integrated benthic carbon remineralization for the entire northwest European shelf seas (NWES), the North Sea (NS), the Norwegian Trench (NT), and the northern, central and southern North Sea (NNS, CNS, SNS). These include all four configurations: Redfield Stoichiometry (RS), Extracellular Release (ER), Preferential Remineralization (PR), and the combined configuration (ER&PR).

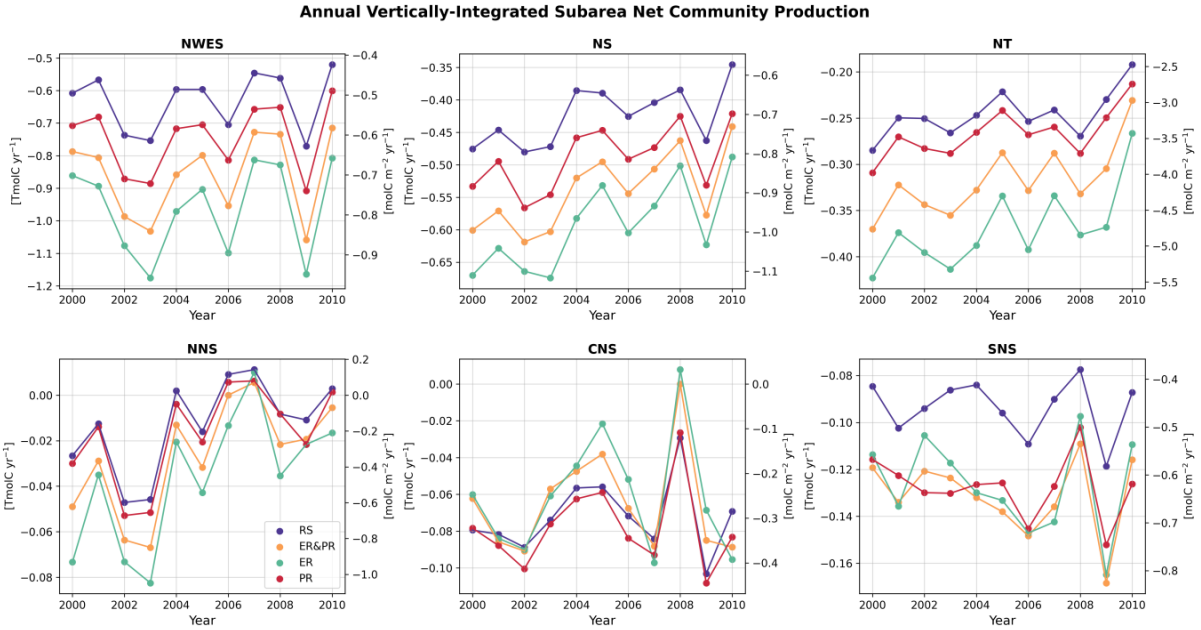

Figure S13: Time Series of annual vertically-integrated net community production for the entire northwest European shelf seas (NWES), the North Sea (NS), the Norwegian Trench (NT), and the northern, central and southern North Sea (NNS, CNS, SNS). These include all four configurations: Redfield Stoichiometry (RS), Extracellular Release (ER), Preferential Remineralization (PR), and the combined configuration (ER&PR).

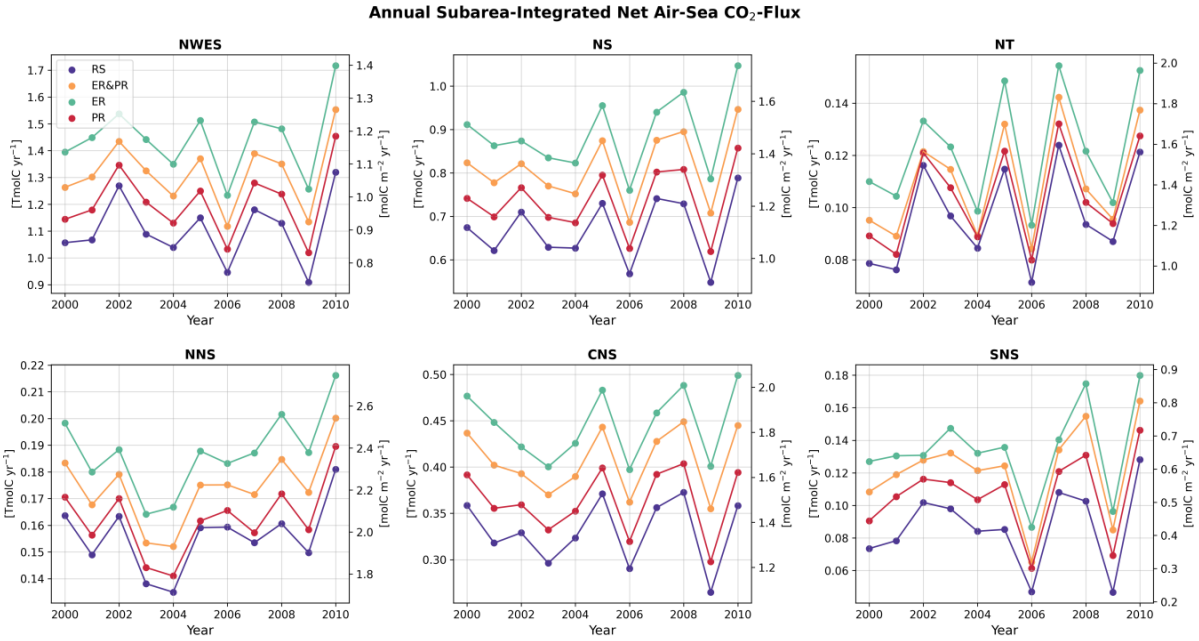

Figure S14: Time Series of subarea-integrated annual net air-sea CO_2 flux for the entire northwest European shelf seas (NWES), the North Sea (NS), the Norwegian Trench (NT), and the northern, central and southern North Sea (NNS, CNS, SNS). These include all four configurations: Redfield Stoichiometry (RS), Extracellular Release (ER), Preferential Remineralization (PR), and the combined configuration (ER&PR).

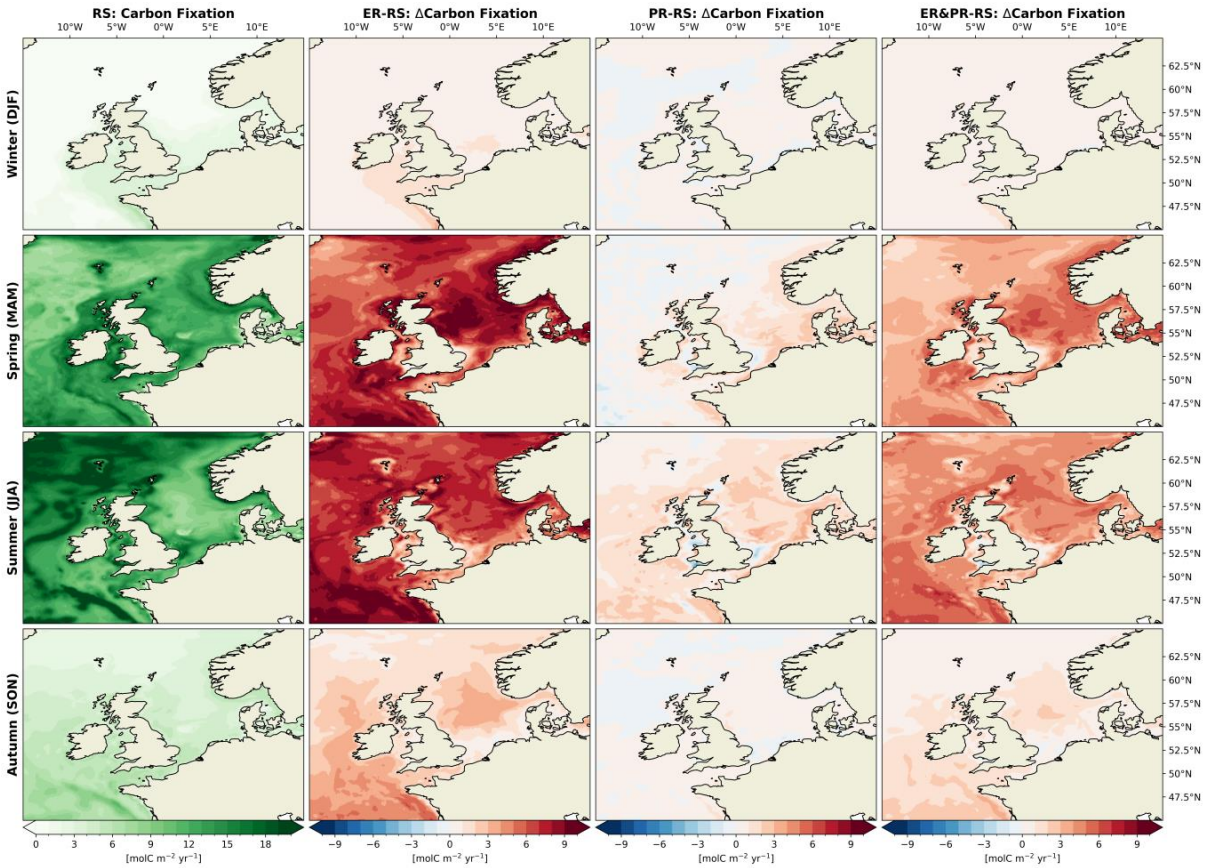

Figure S15: Simulated spatial distribution of seasonal means of vertically-integrated carbon fixation for the Redfield Stoichiometry (RS) configuration and differences for the Extracellular Release (ER), Preferential Remineralization (PR), and the combined (ER&PR) configurations. In the ER and ER&PR configurations, the carbon fixation includes the extracellular release of DOC.

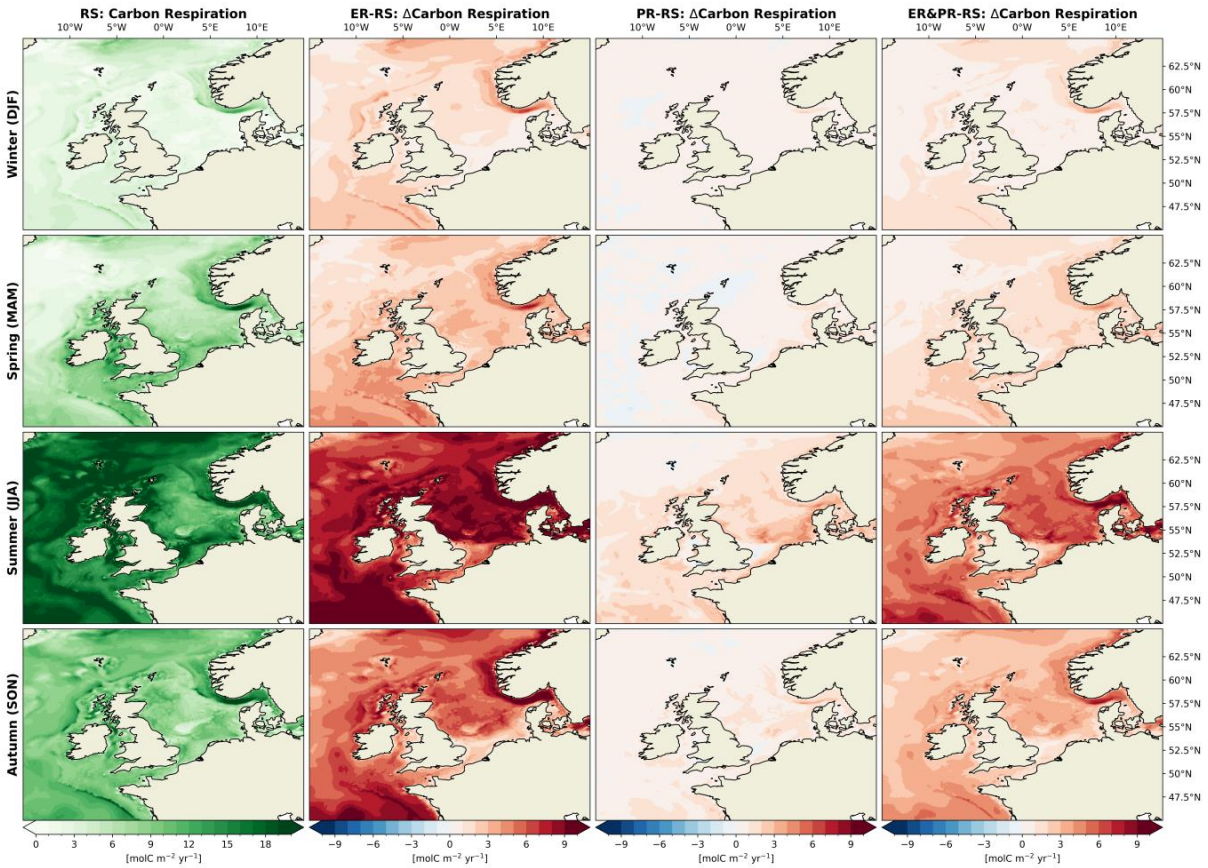

Figure S16: Simulated spatial distribution of seasonal means of vertically-integrated carbon respiration for the Redfield Stoichiometry (RS) configuration and differences for the Extracellular Release (ER), Preferential Remineralization (PR), and the combined (ER&PR) configurations. Carbon respiration here includes both pelagic and benthic heterotrophic remineralization.

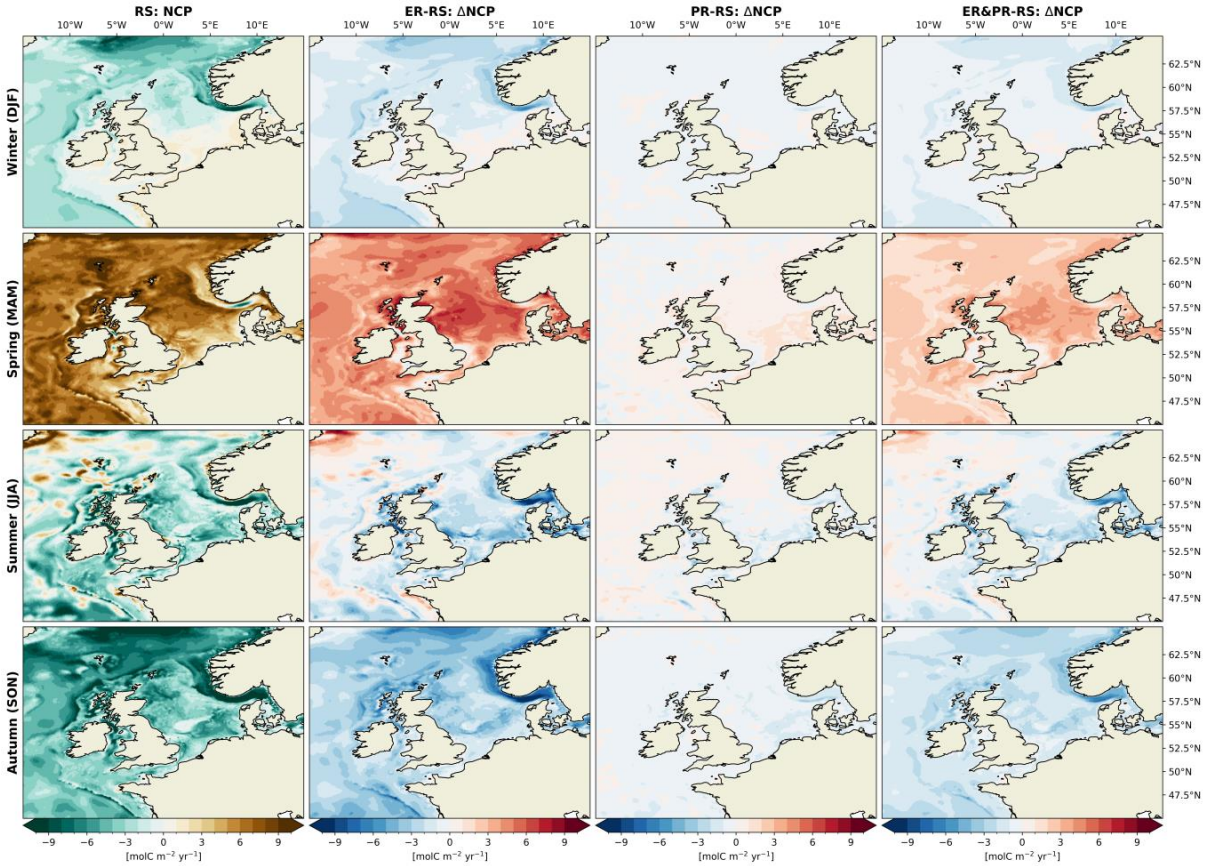

Figure S17: Simulated spatial distribution of seasonal means of vertically-integrated net community production (NCP) for the Redfield Stoichiometry (RS) configuration and differences for the Extracellular Release (ER), Preferential Remineralization (PR), and the combined (ER&PR) configurations. Net community production is here defined as carbon fixation minus respiration, where carbon respiration includes both pelagic and benthic heterotrophic remineralization.

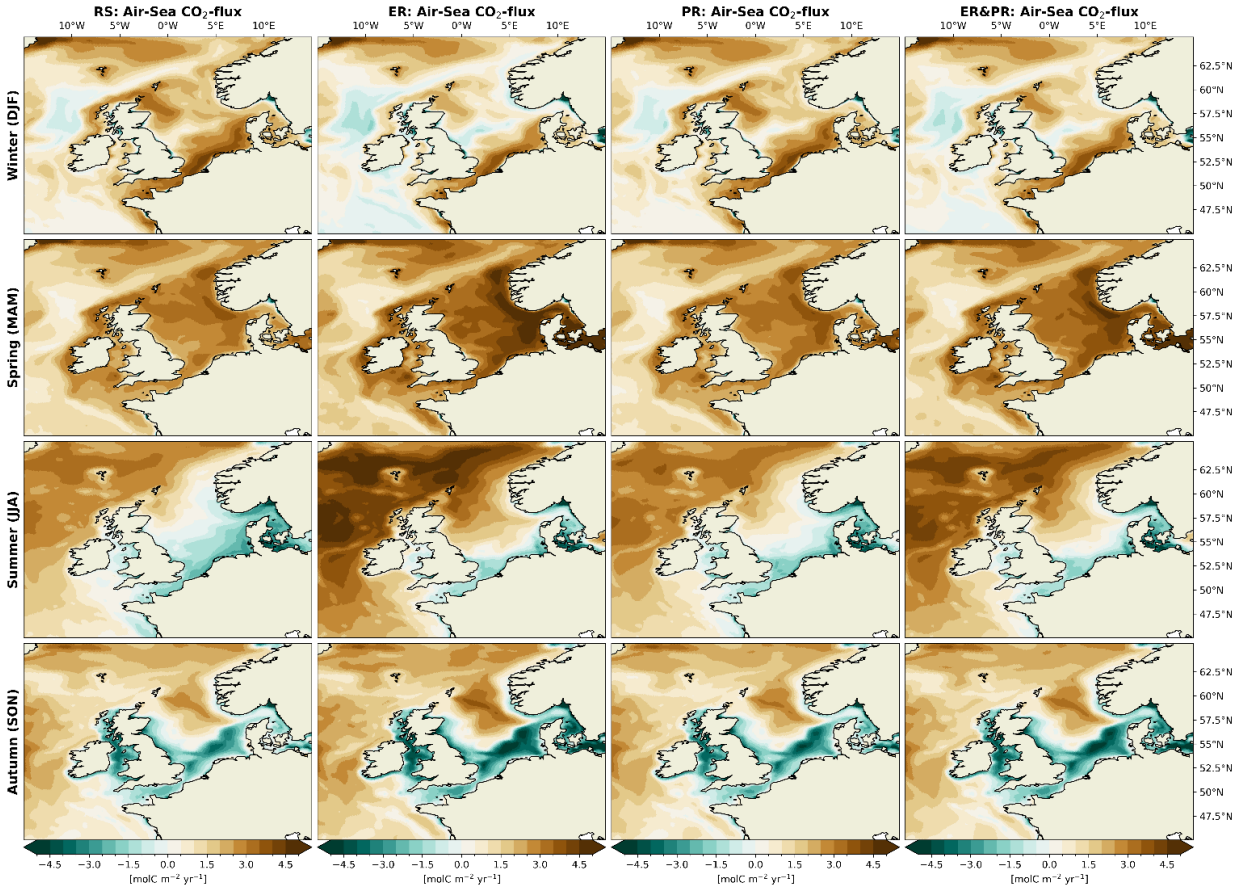

Figure S18: Simulated spatial distribution of the respective seasonal means of the air-sea CO_2 exchange for all four configurations: the Redfield Stoichiometry (RS), Extracellular Release (ER), Preferential Remineralization (PR), and the combined (ER&PR) configuration.

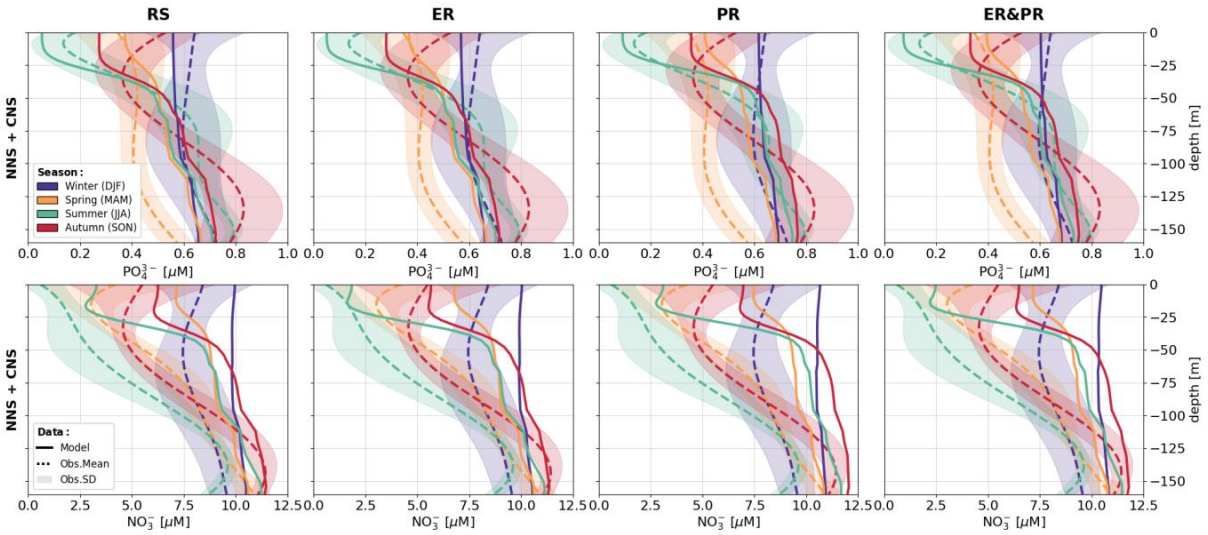

Figure S19: Vertical distribution of observed and simulated, seasonally and subarea-averaged NO_3 and PO_4 concentrations for all four model configurations: Redfield Stoichiometry (RS), Extracellular Release (ER), Preferential Remineralization (PR), and the combined configuration (ER&PR). Both model output and observational data are averages over the simulated period 2000–2010 for the respective season. For the combined Northern (NNS) and central North Sea (CNS) sub-regions 11,636 and 11,065 data points were selected for PO_4 and NO_3 respectively from the bottle and pump data in the ocean hydrochemistry data collection of the International Council for the Exploration of the Sea (ICES). The vertical profiles were generated by firstly calculating the mean concentrations and standard deviation within every meter of depth, and secondly, generating a fifth-order polynomial fit for the vertical profiles of means and standard deviations using *numpy.polyfit* for each season. The coefficients are listed below in Table S16.

S1.2 Supplementary Tables

Table S1: Summary of the ECOSMO II parameter set used for this study. Values in square brackets indicate different configurations for the respective experiments. This means, the first value is for the Redfield-based model, the second for the model with preferential remineralization only, the third with both preferential remineralization and extracellular release and the fourth with extracellular release only. For the variable stoichiometry ECOSMO II model description, see below in section S2 of the Supplementary Material.

Definition	Abbr.	Value	Unit
Maximum growth rate for P_2 (diatoms)	σ_{P_2}	1.30	$[d^{-1}]$
Maximum growth rate for P_1 (flagellates)	σ_{P_1}	1.10	$[d^{-1}]$
Photosynthesis efficiency	α	0.01	$[m^2\ W^{-1}]$
Phytoplankton self-shading	κ_{phyto}	0.03	$[m^2\ (mmolC)^{-1}]$
Particulate organic matter (POM) self-shading	κ_{POM}	0.20	$[m^2\ (mmolC)^{-1}]$
Dissolved organic matter (DOM) self-shading	κ_{DOM}	0.29	$[m^2\ (mmolC)^{-1}]$
Water background light extinction coefficient	κ_W	0.03	$[m^{-1}]$
External suspended particulate matter (SPM) light extinction coefficient	κ_{SPM}	0.0	$[mg\ l^{-1}\ m^{-1}]$
Photosynthetically active radiation (PAR) fraction of incident light	par_fraction	0.6	-
Ammonium (NH_4) half saturation const.	$r_{\mathrm{NH_4}}$	0.20	$[mmolN\ m^{-3}]$
Nitrate (NO_3) half saturation const.	$r_{\mathrm{NO_3}}$	0.5	$[mmolN\ m^{-3}]$
Ammonium (NH_4) inhibition parameter	Ψ	3.0	$[m^3\ (mmolN)^{-1}]$
Diatom mortality rate	m_{P_2}	0.04	$[d^{-1}]$
Flagellate mortality rate	m_{P_1}	0.08	$[d^{-1}]$
Grazing rate of meso-zooplankton on phytoplankton	$\sigma_{Z_2,P}$	0.8	$[d^{-1}]$
Grazing rate of micro-zooplankton on phytoplankton	$\sigma_{Z_1,P}$	1.0	$[d^{-1}]$
Grazing rate of meso-zooplankton on micro-zooplankton	σ_{Z_2,Z_1}	0.5	$[d^{-1}]$
Zooplankton half saturation constant	r_Z	0.5	$[mmolC\ m^{-3}]$
Meso-zooplankton mortality rate	m_{Z_2}	0.1	$[d^{-1}]$
Micro-zooplankton mortality rate	m_{Z_1}	0.2	$[d^{-1}]$
Meso-zooplankton excretion rate	μ_{Z_2}	0.06	$[d^{-1}]$
Micro-zooplankton excretion rate	μ_{Z_1}	0.08	$[d^{-1}]$
Meso-zooplankton assimilation efficiency on plankton	$\gamma_{Z_2,P}$	0.75	-
Micro-zooplankton assimilation efficiency on plankton	$\gamma_{Z_1,P}$	0.75	-
Zooplankton assimilation efficiency on POM	$\gamma_{Z,POM}$	0.75	-
POC remineralization rate	ε_{POC}	0.003	$[d^{-1}]$

POM sinking rate	w_{POM}	5.0	$[m\ d^{-1}]$
Phosphate (PO_4) half saturation const.	$r_{\mathrm{PO_4}}$	0.05	$[mmolP\ m^{-3}]$
Silicate (SiO_2) half saturation const.	r_{Si}	0.5	$[mmolSi\ m^{-3}]$
Silicate (SiO_2) remineralization rate	$\varepsilon_{\mathrm{Si}}$	0.015	$[d^{-1}]$
Maximum growth rate of cyanobacteria	σ_{P_3}	1.0	$[d^{-1}]$
Cyanobacteria temperature control	T_{ctrl,P_3}	1.0	$[°\mathrm{C}^{-1}]$
Cyanobacteria reference temperature	T_{ref,P_3}	0.0	$[°C]$
Cyanobacteria maximum grazing rate	β_{P_3}	0.3	$[d^{-1}]$
Cyanobacteria mortality rate	m_{P_3}	0.08	$[d^{-1}]$
Critical bottom shear stress for resuspension	τ_{crit}	0.007	$[N\ m^{-2}]$
Resuspension rate for $\tau > \tau_{crit}$	λ_{res}	25.0	$[d^{-1}]$
Sedimentation rate for $\tau \leq \tau_{crit}$	λ_{dep}	3.5	$[m\ d^{-1}]$
Burial rate	δ_{bur}	0.00001	$[d^{-1}]$
Sediment base remineralization rate	$\varepsilon_{\mathrm{Sed}}$	0.001	$[d^{-1}]$
Temperature control of denitrification	$T_{\mathrm{ref,denit}}$	0.15	$[°C^{-1}]$
Sed. PIP release parameter p1	RelSEDp1	0.15	-
Sed. PIP release parameter p2	RelSEDp2	0.10	-
Sed. remineralization rate Si	ε_{Sed3}	0.0002	$[d^{-1}]$
Biogenic opal ($SiO_2 \cdot 2H_2O$) sinking rate	w_{Opal}	5.0	$[m\ d^{-1}]$
Cyanobacteria sinking rate	w_{P_3}	-1.0	$[m\ d^{-1}]$
Diatom sinking rate	w_{P2}	0.0	$[m\ d^{-1}]$
Grazing preference of micro-zooplankton on flagellates	a_{Z_1,P_1}	0.7	-
Grazing preference of micro-zooplankton on diatoms	a_{Z_1,P_2}	0.25	-
Grazing preference of micro-zooplankton on particulate organic matter	$a_{Z_1,\mathrm{POM}}$	0.1	-
Grazing preference of micro-zooplankton on cyanobacteria	a_{Z_1,P_3}	0.3	-
Grazing preference of meso-zooplankton on flagellates	a_{Z_2,P_1}	0.1	-
Grazing preference of meso-zooplankton on diatoms	a_{Z_2,P_2}	0.85	-
Grazing preference of meso-zooplankton on micro-zooplankton	a_{Z_2,Z_1}	0.15	-
Grazing preference of meso-zooplankton on particulate organic matter	$a_{Z_2,\mathrm{POM}}$	0.1	-
Grazing preference of meso-zooplankton on cyanobacteria	a_{Z_2,P_3}	0.3	-
Fraction of dissolved organic matter from new detrital matter	a_{DOM}	0.4	-

Fraction of particulate organic matter from new detrital matter	$a_{\mathrm{POM}} = (1 - a_{\mathrm{DOM}})$	0.6	-
Surface deposition of nitrate (here provided from monthly observations instead)	$\mathrm{Surf}_{\mathrm{NO}_3}$	0.08	$[mmolN\ m^{-2}\ d^{-1}]$
Surface deposition of ammonium (here provided from monthly observations instead)	$\mathrm{Surf}_{\mathrm{NH}_4}$	0.05	$[mmolN\ m^{-2}\ d^{-1}]$
Surface deposition of phosphate	$\mathrm{Surf}_{\mathrm{PO}_4}$	0.0	$[mmolP\ m^{-2}\ d^{-1}]$
Surface deposition of silicate	$\mathrm{Surf}_{\mathrm{SiO}_2}$	0.0	$[mmolSi\ m^{-2}\ d^{-1}]$
Minimum daily radiation for cyanobacteria growth	I_{P_3}	120	$[W\ m^{-2}]$
Minimum daily photosynthetically active radiation for nitrogen fixation	$\mathrm{PAR}_{\mathrm{P}_3}$	120	$[W\ m^{-2}]$
Remineralization ratio of DOC to POC	$\epsilon_{\mathrm{DOC:POC}}$	0.5	-
Remineralization ratio of POC to PON	$\epsilon_{\mathrm{POC:PON}}$	[1, 0.625, 0.7692, 1]	-
Remineralization ratio of POC to POP	$\epsilon_{\mathrm{POC:POP}}$	[1, 0.5, 0.6666, 1]	-
Remineralization ratio of DOC to DON	$\epsilon_{\mathrm{DOC:DON}}$	[1, 0.625, 0.7692, 1]	-
Remineralization ratio of DOC to DOP	$\epsilon_{\mathrm{DOC:DOP}}$	[1, 0.5, 0.6666, 1]	-
Rate of flocculation from DOM to POM	F_{DOM2POM}	[0, 0, 0.02, 0.02]	-
Extracellular release scaling factor	B_{ER}	[0, 0, 0.2, 0.4]	-

Table S2: Model percentage biases for all four configurations RS, ER, PR and ER&PR with respect to observations for dissolved inorganic carbon (DIC), total alkalinity (TA), and surface partial pressure of CO_2 (pCO_2) across different subareas of the northwest European shelf seas. Both DIC and TA observations are from the Global Ocean Data Analysis Project (GLODAP), whereas pCO_2 measurements are from the Surface Ocean CO_2 Atlas (SOCAT).

Model percentage bias [%] compared to co-located observational data from GLODAP, SOCAT and ICES					
Variable	Sub-Region	RS	ER	PR	ER&PR
DIC	NNS	0.661	0.596	0.630	0.610
	CNS	1.105	0.947	1.025	0.967
	SNS	1.254	1.149	1.100	1.101
	NT	0.870	0.975	0.871	0.916
	SK	1.115	1.319	1.140	1.195
TA	NNS	0.544	0.542	0.542	0.541
	CNS	0.884	0.891	0.856	0.869
	SNS	0.872	0.882	0.850	0.866
	NT	0.666	0.664	0.660	0.660
	SK	0.917	0.909	0.914	0.912
pCO_2	NNS	4.492	4.337	4.313	4.100
	CNS	7.993	6.341	6.978	6.297
	SNS	15.119	13.441	14.002	13.379
	NT	18.701	16.709	17.723	16.700
	SK	24.801	29.812	24.277	27.552
	EC	11.591	10.076	11.118	10.520
	SWC	7.158	9.202	7.167	7.608
	AS	16.642	13.367	14.731	13.718

Table S3: Literature compilation of observational data on concentrations of bulk dissolved organic carbon (DOC), nitrogen (DON), and phosphorus (DOP), including both the (semi-) labile and refractory fractions of dissolved organic matter (DOM). Individual numbers without parentheses represent averages over regions or a series of measurements, whereas values in parentheses show ranges between individual measurements or sub-regions. Ranges of concentrations with a double-asterisk represent estimates from figures in the respective references. For the data from Lønborg et al. (2024), we report the median along with the 25th and 75th percentiles, as these better represent the distribution of the large dataset, avoiding the influence of outliers on the mean and range.

Location	Sub-Region or Focus	Bulk DOM Concentrations			Source
		DOC $[\mu M]$	DON $[\mu M]$	DOP $[\mu M]$	
Global Ocean	Surface Ocean Biogeochemical Regions	65.8 (52.4–73.5)	4.5 (3.7–5.3)	0.17 (0.11–0.27)	(Liang et al., 2023)
	Full Water Column	(46.2–65.3)	(2.1–4.5)	(0.04–0.19)	(Letscher et al., 2015; Letscher and Moore, 2015)
	Coastal Ocean	(50–60)	(4.5–45)	(0.08–0.50)	(Lønborg and Álvarez-Salgado, 2012)
	Coastal Ocean	103 (77–228)	8.0 (5.5–15.8)	0.18 (0.11–0.30)	(Lønborg et al., 2024)
	Shelf, Slope and Open Ocean (surface only 0–100m)	(30–160)**	(1–11)**	(0.00–0.45)**	(Hopkinson and Vallino, 2005)
Atlantic Ocean	Georges Bank (Surface Ocean)	65–92	5	0.17	(Hopkinson et al., 1997)
	Georges Bank (Deep Waters)	50	3	0.02	(Hopkinson et al., 1997)
	Middle Atlantic Bight (Surface Ocean)	125 (81–201)	10.2 (7.1–14.3)	0.30 (0.14–0.42)	(Hopkinson et al., 2002)
	Middle Atlantic Bight (Deep Slope Waters)	46.7	2.76	0.03	(Hopkinson et al., 2002)
	Northeast Atlantic (Surface Waters)	(61–83)	(4.2–6.1)	(0.07–0.14)	(Aminot and Kérouel, 2004)
	Northeast Atlantic (Deep Waters)	(41–55)	(2.6–4.0)	(0.01–0.08)	(Aminot and Kérouel, 2004)
Pacific Ocean	Eastern North Pacific	(35–72)	(1.5–4.5)	(0.013–0.229)	(Loh and Bauer, 2000)
	North Pacific Subtropical Gyre	(63–105)	(3.7–6.2)	(0.10–0.27)	(Church et al., 2002)
Southern Ocean	-	(39–53)	(2.5–5.2)	(0.061–0.225)	(Loh and Bauer, 2000)
Mediterranean Sea	Southern Adriatic Basin (Surface)	(49–79)	(2.3–7.2)	(0.02–0.08)	(Santinelli et al., 2012)
	Southern Adriatic Basin (Intermediate Waters)	(45–54)	(1.8–5.3)	(0.02–0.06)	(Santinelli et al., 2012)
	Southern Adriatic Basin (Deep Waters)	(47–60)	(2.9–6.2)	(0.02–0.08)	(Santinelli et al., 2012)
	Northwestern Mediterranean	(44–95)	(2.8–6.2)	-	(Doval et al., 1999)
	Northwestern Mediterranean	(40–120)**	(0–6)**	(0.0–0.4)**	(Lucea et al., 2003)
	Northwestern Mediterranean (Surface Waters)	(67–69)	(4.0–4.2)	(0.08–0.08)	(Aminot and Kérouel, 2004)

	Northwestern Mediterranean (Deep Waters)	(46–48)	(2.7–3.0)	(0.03–0.04)	(Aminot and Kérouel, 2004)
	Northwestern Mediterranean	(80–100)	(4.5–5.5)	(0.06–0.10)	(Raimbault et al., 1999)
	Western Basin	(37.6–69.4)	(2.5–5.5)	(0–0.09)	(Pujo-Pay et al., 2011)
	Eastern Basin	(37.5–72.4)	(2.1–6.3)	(0–0.10)	(Pujo-Pay et al., 2011)
East China Sea	-	(60–120)	(6–9.6)	(0.05–0.25)	(Hung et al., 2003)
South China Sea	Northern Parts	(43–132)	-	-	(Hung et al., 2007)
northwest European shelf seas	Norwegian Coastal Waters	-	(8–11.5)**	-	(Frigstad et al., 2013)
	Celtic Sea	(65–70)	(3.9–6)	(0.19–0.35)	(Davis et al., 2019)
	North Sea	46.9–107.5 (32.7–224.8)	5.2–9.0 (2.8–13.7)	-	(Chaichana et al., 2017, 2019)
	northern North Sea (Surface)	60.7–73.8 (32.7–104.2)	5.3–6.6 (3.0–8.7)	-	(Chaichana et al., 2017, 2019)
	northern North Sea (Bottom)	46.9–73.8 (36.8–120.1)	5.2–5.9 (1.0–11.7)	-	(Chaichana et al., 2017, 2019)
	southern North Sea	65.5–97.5 (36.3–224.8)	5.3–9.0 (2.8–13.7)	-	(Chaichana et al., 2017, 2019)
	central North Sea	(68–318)	(2–11)**	-	(Suratman et al., 2009)
	North Sea	108.7 (61.7–185.0)	6.6 (3.5–16.4)	0.26 (0.13–0.46)	(Painter et al., 2018)
Baltic Sea	Bothnian Sea	466	-	-	(Rowe et al., 2018)
	Bothnian Bay	416	-	-	(Rowe et al., 2018)
	Gulf of Finland	(290–724)	(8.6–38.5)	(0.06–0.80)	(Hoikkala et al., 2012, 2015)
	Gulf of Bothnia	(241–520)	(7.8–14.8)	(0.12–0.18)	(Hoikkala et al., 2015)
	Gulf of Riga	(400–1230)	(10–38)	(0.5–0.9)	(Hoikkala et al., 2015)
	Baltic Proper	(259–708)	(10.2–203)	-	(Hoikkala et al., 2015; Rowe et al., 2018)
	Estuaries	(318.41–736.74)	(14.14–45.22)	(0.14–0.38)	(Voss et al., 2021)
	Southwestern Baltic Sea (Heiligendamm)	290	17.2	-	(Osterholz et al., 2021)
	Gotland Basin	-	-	(0.20–0.29)	(Nausch et al., 2008)

Table S4: Literature compilation of observational data on concentrations of biodegradable or (semi-)labile dissolved organic carbon (LDOC), nitrogen (LDON), and phosphorus (LDOP). Individual numbers or ranges (e.g., between sub-regions or different years) without parentheses represent averages over regions or a series of measurements whereas values in parentheses show ranges between individual measurements. The given percentage indicates the fraction of labile dissolved organic carbon, nitrogen, and phosphorus in relation to the bulk pool.

Location	Sub-Region or Focus	Biodegradable or (Semi-)Labile DOM Concentrations			Source
		LDOC $[\mu M]$	LDON $[\mu M]$	LDOP $[\mu M]$	
Global Ocean	Surface Ocean Biogeochemical Regions	25.0 (10.5–29.1)	2.8 (1.9–3.5)	0.14 (0.06–0.22)	(Liang et al., 2023)
	Shelf, Slope and Open Ocean	(15–80)	-	-	(Hopkinson and Vallino, 2005)
	Coastal Ocean	(1–199) (2–51%)	(0.6–15.2) (10–65%)	(0.04–0.33) (30–96%)	(Lønborg and Álvarez-Salgado, 2012)
Atlantic Ocean	Northeast Atlantic	(16.0–16.3) (26–27%)	(1.5–1.6) (34–36%)	(0.04–0.10) (60–78%)	(Aminot and Kérouel, 2004)
Mediterranean Sea	Northwestern Mediterranean	23.3 34%	1.2 30%	0.04 60%	(Aminot and Kérouel, 2004)
Baltic Sea	Open Sea Only	(0–82) (0–17%)	(0–6.5) (0–41%)	(0.01–0.34) (8–65%)	(Hoikkala et al., 2012, 2015)

Table S5: Literature compilation of observational data on concentrations of refractory or recalcitrant dissolved organic carbon (RDOC), nitrogen (RDON), and phosphorus (RDOP). Individual numbers or ranges (e.g., between sub-regions or different years) without parentheses represent averages over regions or a series of measurements whereas values in parentheses show ranges between individual measurements.

Location	Sub-Region or Focus	Refractory or Recalcitrant DOM Concentrations			Source
		RDOC $[\mu M]$	RDON $[\mu M]$	RDOP $[\mu M]$	
Global Ocean	Surface Ocean	46 (45–49)	2.7 (2.5–2.8)	-	(Liang et al., 2023)
	Deep Ocean	42	3.0	0.05	(Liang et al., 2023)
	Surface Ocean	42	-	-	(Hopkinson and Vallino, 2005)
	Deep Ocean	34	-	-	(Hopkinson and Vallino, 2005)
	Deep Ocean	(33.8–48.1)	-	-	(Hansell and Carlson, 1998)
Atlantic and Mediterranean	NE Atlantic and NW Mediterranean	44.9 (43.8–45.9)	2.85 (2.73–3.00)	0.029 (0.023–0.034)	(Aminot and Kérouel, 2004)

Table S6: Literature compilation of observational data on concentrations of particulate organic carbon (POC), nitrogen (PON), and phosphorus (POP). Individual numbers or ranges (e.g., between sub-regions or different years) without parentheses represent averages over regions or a series of measurements whereas values in parentheses show ranges between individual measurements. Ranges of concentrations with a double-asterisk represent estimates from figures in the respective references. Strong outliers in the measurement referenced as "Patch" were excluded from (Nausch et al., 2008).

Location	Sub-Region or Focus	POM Concentrations			Source
		POC $[\mu M]$	PON $[\mu M]$	POP $[nM]$	
Global Ocean	Surface Ocean Biogeochemical Regions	6.4 (2.3–17.2)	0.83 (0.32–2.2)	40 (10–170)	(Liang et al., 2023; Martiny et al., 2014; Tanioka et al., 2022)
Pacific Ocean	Eastern North Pacific	(0.09–5.76)	(0.012–0.917)	(0.45–37.32)	(Loh and Bauer, 2000)
Southern Ocean	South of the Tasman Sea	(0.05–3.48)	(0.004–0.490)	(0.25–13.48)	(Loh and Bauer, 2000)
Mediterranean Sea	NW Mediterranean	(0.9–14.9)	(0.1–1.7)	-	(Doval et al., 1999)
	NW Mediterranean	(4–15)**	(0.2–0.7)**	(0–55)**	(Lucea et al., 2003)
	Western Basin	(0.74–8.70)	(0.01–0.87)	(1–45)	(Pujo-Pay et al., 2011)
	Eastern Basin	(0.70–5.41)	(0.01–0.66)	(1–30)	(Pujo-Pay et al., 2011)
South China Sea	Northern Parts	(1.1–13)	-	-	(Hung et al., 2007)
northwest European shelf seas	Hebrides Shelf	(4.73–6.74)	(0.37–0.76)	(1–10)	(Painter et al., 2017)
	Norwegian Coastal Waters	(6–14)**	(0.8–2.5)**	(6–14)**	(Frigstad et al., 2013)
	Celtic Sea	(2–15)**	(0.2–3)**	(1–13)**	(Davis et al., 2019)
	North Sea	7.3–16.0 (1.1–43.8)	1.5–2.2 (0.3–5.9)	-	(Chaichana et al., 2017, 2019)
	northern North Sea (Surface)	10.5 (2.7–21.8)	2.0 (0.6–2.9)	-	(Chaichana et al., 2017, 2019)
	northern North Sea (Bottom)	7.3 (1.1–16.2)	1.5 (0.3–2.7)	-	(Chaichana et al., 2017, 2019)
	southern North Sea	16.0 (5.8–43.8)	2.2 (0.6–5.9)	-	(Chaichana et al., 2017, 2019)
	central North Sea	(1.9–38.4)	(0.2–5.8)**	-	(Suratman et al., 2009)
Baltic Sea	Estuaries	(29.8–388)	-	-	(Voss et al., 2021)
	Gotland and Gdansk Deep	(8.3–79.9)	(0.7–11.4)	-	(Winogradow et al., 2019)
	SW Baltic Sea (Heiligendamm)	33	4.8	-	(Osterholz et al., 2021)
	Gotland Basin	(27.98–93.92)	(3.88–13.42)	(140–390)	(Nausch et al., 2008)

Table S7: Literature compilation of observational data on elemental ratios of carbon, nitrogen, and phosphorus in bulk dissolved organic matter (DOM). Individual numbers or ranges (e.g., between sub-regions or different years) without parentheses represent averages over regions or a series of measurements whereas values in parentheses show ranges between individual measurements. A single asterisk indicates implicit estimates of individual C:N, C:P or N:P ratios from provided ranges of C:N:P ratios where they were not provided explicitly. Ranges of values with a double-asterisk represent estimates from figures in the respective references. For the data from Lønborg et al. (2024), we report the median along with the 25th and 75th percentiles, as these better represent the distribution of the large dataset, avoiding the influence of outliers on the mean and range.

Location	Sub-region or focus	Bulk DOM stoichiometry			Source
		DOC:DON	DOC:DOP	DON:DOP	
Global ocean	Global surface ocean (biogeochemical regions)	14.6 (13.0–16.1)	387 (251–638)	26 (17–44)	(Liang et al., 2023)
	Full water column	17*	810	48	(Letscher et al., 2015; Letscher and Moore, 2015)
	Coastal ocean	9*	1164	123	(Lønborg and Álvarez-Salgado, 2012)
	Coastal ocean	14 (11–18)	583 (401–1034)	47 (30–78)	(Lønborg et al., 2024)
	Shelf, slope, and open ocean	14*	778	54	(Hopkinson and Vallino, 2005)
	Shelf, slope, and open ocean (surface only 0–100m)	14	374	27	(Hopkinson and Vallino, 2005)
Atlantic Ocean	Georges Bank (Surface Ocean)	(11–15)	(400–800)	(24–55)	(Hopkinson et al., 1997)
	Geroges Bank (Deep Waters)	(14–20)	(700–2500)	(40–140)	(Hopkinson et al., 1997)
	Middle Atlantic Bight (Surface Ocean)	12 (9–14)*	431 (290–1101)	36 (25.8–86.7)	(Hopkinson et al., 2002)
	Middle Atlantic Bight (Deep Slope Waters)	13 (12–14)*	2700 (986–4404)	215 (70–360)	(Hopkinson et al., 2002)
	NE Atlantic (Surface Waters)	(13.1–14.3)	(440–850)	(31–62)	(Aminot and Kérouel, 2004)
	NE Atlantic (Deep Waters)	(12.6–16.4)	(640–3100)	(45–200)	(Aminot and Kérouel, 2004)
Pacific Ocean	Eastern North Pacific	(13–30)	(277–537)	(13–34)	(Loh and Bauer, 2000)
	North Pacific Subtropical Gyre	(14.8–16.4)	(390–483)	(24.0–31.4)	(Church et al., 2002)
Southern Ocean	South of the Tasman Sea	(9–18)	(229–682)	(12–49)	(Loh and Bauer, 2000)
Mediterranean Sea	Southern Adriatic Basin (Surface)	(14–16)	(1189–1411)	(86–88)	(Santinelli et al., 2012)
	Southern Adriatic Basin (Intermediate Waters)	(13–14)	(1107–1279)	(83–97)	(Santinelli et al., 2012)
	Southern Adriatic Basin (Deep Waters)	(11–15)	(993–1693)	(85–108)	(Santinelli et al., 2012)
	NW Mediterranean	15.5	-	-	(Doval et al., 1999)
	NW Mediterranean	(30–60)*	(1510–1984)	(25–66)	(Lucea et al., 2003)

	NW Mediterranean (Surface Waters)	(16.7–16.9)	(920–970)	(55–57)	(Aminot and Kérouel, 2004)
	NW Mediterranean (Deep Waters)	(15.1–17.2)	(1100–1800)	(64–106)	(Aminot and Kérouel, 2004)
	Western Basin	12.1	1941	162.7	(Pujo-Pay et al., 2011)
	Eastern Basin	13.0	2055	160.8	(Pujo-Pay et al., 2011)
East China Sea	-	(8.9–15.3)	(200–853)	(19–83.6)	(Hung et al., 2003)
South China Sea	Northern Parts	(11–13)*	(322–510)	(29–39)	(Hung et al., 2007)
Sea of Japan (East Sea)	-	17*	374	22	(Kim and Kim, 2013)
northwest European shelf seas	Norwegian Coastal Waters	-	-	(59.8–73.6)	(Frigstad et al., 2013)
	Celtic Sea	(12–17)*	(281–416)	(17–33)	(Davis et al., 2014)
	Celtic Sea	(11.0–17.4)	(147–377)	(11.7–31.7)	(Davis et al., 2019)
	North Sea	(5.9–36.5)	-	-	(Chaichana et al., 2017, 2019)
	central North Sea	(9.5–67.4)	-	-	(Suratman et al., 2009)
	North Sea	(10–25)**	(200–900)**	(15–75)**	(Painter et al., 2018)
Baltic Sea	Baltic Proper	31.6	527.0	16.6	(Rowe et al., 2018)
	Bothnian Sea	21.3	402.6	18.9	(Rowe et al., 2018)
	Bothnian Bay	23.1	780.7	33.8	(Rowe et al., 2018)
	Gulf of Finland	(10–54)	-	(25–419)	(Hoikkala et al., 2012, 2015)
	Gulf of Bothnia	(25–28)	-	100	(Hoikkala et al., 2015)
	Gulf of Riga	-	-	(20–60)	(Hoikkala et al., 2015)
	Baltic Proper	(17–26)	-	(20–30)	(Hoikkala et al., 2015)
	Estuaries	(16–23)*	(1199–3714)	(52–221)	(Voss et al., 2021)
	Rivers	31*	2790	91	(Stepanauskas et al., 2002)
	Southwestern Baltic Sea (Heiligendamm)	(12.5–20)**	-	-	(Osterholz et al., 2021)

Table S8: Literature compilation of observational data on elemental ratios of carbon, nitrogen, and phosphorus in biodegradable or (semi-)labile dissolved organic matter (LDOM). Individual numbers or ranges (e.g., between sub-regions or different years) without parentheses represent averages over regions or a series of measurements whereas values in parentheses show ranges between individual measurements. A single asterisk indicates implicit estimates from provided ranges of C:N:P ratios where they were not provided explicitly.

Location	Sub-region or focus	Biodegradable or (semi-)labile DOM stoichiometry			Source
		LDOC:LDON	LDOC:LDOP	LDON:LDOP	
Global ocean	Global surface ocean (biogeochemical regions)	8.9 (5.4–12.0)	179 (83–414)	20 (15–49)	(Liang et al., 2023)
	Coastal ocean	(8–9)*	(197–216)	(24–25)	(Lønborg and Álvarez-Salgado, 2012)
	Shelf, slope, and open ocean	10.7 (8.7–14.1)	199 (154–245)	20 (15.6–25)	(Hopkinson and Vallino, 2005)
Atlantic	NE Atlantic	(10.1–10.7)	(159–380)	(14.8–38)	(Aminot and Kérouel, 2004)
	Middle Atlantic Bight	(10.0–14.1)	(193–203)	(15.6–20.2)	(Hopkinson and Vallino, 2005)
	Georges Bank	9.8	245	25	(Hopkinson and Vallino, 2005)
Pacific Ocean	Hawaiian Ocean	8.7	154	17.8	(Hopkinson and Vallino, 2005)
Mediterranean Sea	NW Mediterranean	19.2	530	28	(Aminot and Kérouel, 2004)
Baltic Sea	Gulf of Finland	(0.8–11.7)	-	-	(Hoikkala et al., 2012, 2015)

Table S9: Literature compilation of observational data on elemental ratios of carbon, nitrogen, and phosphorus in refractory or recalcitrant dissolved organic matter (RDOM). Individual numbers or ranges (e.g., between sub-regions or different years) without parentheses represent averages over regions or a series of measurements whereas values in parentheses show ranges between individual measurements. A single asterisk indicates implicit estimates from provided ranges of C:N:P ratios where they were not provided explicitly.

Location	Refractory or recalcitrant DOM stoichiometry			Source
	RDOC:RDON	RDOC:RDOP	RDON:RDOP	
Global ocean	17.0 (16.5–18.1)	1373 (900–2300)	82 (50–140)	(Liang et al., 2023)
Coastal ocean	18*	2835	159	(Lønborg and Álvarez-Salgado, 2012)
Shelf, slope, and open ocean	17*	3511	202	(Hopkinson and Vallino, 2005)
NE Atlantic and NW Mediterranean	15.7	1570	10	(Aminot and Kérouel, 2004)

Table S10: Literature compilation of observational data on elemental ratios of carbon, nitrogen, and phosphorus in particulate organic matter (POM). Individual numbers represent averages over regions or a series of measurements whereas values in parentheses show ranges between sub-regions or measurements. A single asterisk indicates implicit estimates from provided ranges of C:N:P ratios where they were not provided as individual ratios explicitly. Ranges of values with a double-asterisk represent estimates from figures in the respective references.

Location	Sub-region or focus	POM stoichiometry			Source
		POC:PON	POC:POP	PON:POP	
Global Ocean	Surface ocean	7.7 (6.1–9.2)	160 (73–295)	21 (10–37)	(Liang et al., 2023; Martiny et al., 2014; Tanioka et al., 2022)
	-	6.6	163	22	(Martiny et al., 2014)
	Surface layer (50m)	-	146	-	(Tanioka et al., 2021)
	Twilight zone (100-1000m)	-	294 (83–500)	-	(Tanioka et al., 2021)
	Bermuda Atlantic	6 (1–19)	210 (45–532)	36 (7–140)	(Singh et al., 2015)
Pacific Ocean	Eastern North Pacific	(6–10)	(117–630)	(12–74)	(Loh and Bauer, 2000)
Southern Ocean	-	(4–14)	(59–336)	(6–46)	(Loh and Bauer, 2000)
Mediterranean Sea	NW Mediterranean	8.6	-	-	(Doval et al., 1999)
	NW Mediterranean	(14–19)*	(220–426)	(15–22)	(Lucea et al., 2003)
	Western Basin	13.3	256	19.8	(Pujo-Pay et al., 2011)
	Eastern Basin	14.0	235	18.8	(Pujo-Pay et al., 2011)
South China Sea	Northern Parts	(8–12)*	(148–502)	(18–42)	(Hung et al., 2007)
northwest European shelf seas	Hebrides Shelf	(8.26–13.67)	(142.4–259.97)	(16.4–26.32)	(Painter et al., 2017)
	Norwegian Coastal Waters	(7.1–7.4)	(110.8–125.2)	(14.6–17.6)	(Frigstad et al., 2013)
	Celtic Sea	(5–6)*	(63–223)	(10–38)	(Davis et al., 2014)
	Celtic Sea	(4.3–11.6)	(144–283)	(24–47)	(Davis et al., 2019)
	North Sea	(0.7–16.8)	-	-	(Chaichana et al., 2017, 2019)
	central North Sea	(2.5–34.9)	-	-	(Suratman et al., 2009)
Baltic Sea	Estuaries	6*	253	39	(Voss et al., 2021)
	Gotland and Gdansk Deep	(5.8–10.8)	-	-	(Winogradow et al., 2019)
	SW Baltic Sea (Heiligendamm)	(2.5–11)**	-	-	(Osterholz et al., 2021)

Table S11: Annual vertically- and subarea-integrated carbon fixation averaged over the simulation period 2000–2010 for all four model configurations: Redfield Stoichiometry (RS), Extracellular Release (ER), Preferential Remineralization (PR), and the combined configuration (ER&PR). For each configuration, the mean is provided both area-integrated and per area. The variable stoichiometry configurations also include the per area difference with respect to the RS configuration.

Annual vertically- and subarea-integrated carbon fixation averaged over 2000–2010											
Subarea	RS		ER			PR			ER&PR		
	Total $[Tmol C\ yr^{-1}]$	Per Area $[mol C\ m^{-2} yr^{-1}]$	Total $[Tmol C\ yr^{-1}]$	Per Area $[mol C\ m^{-2} yr^{-1}]$	Difference $[mol C\ m^{-2} yr^{-1}]$	Total $[Tmol C\ yr^{-1}]$	Per Area $[mol C\ m^{-2} yr^{-1}]$	Difference $[mol C\ m^{-2} yr^{-1}]$	Total $[Tmol C\ yr^{-1}]$	Per Area $[mol C\ m^{-2} yr^{-1}]$	Difference $[mol C\ m^{-2} yr^{-1}]$
Entire NWES	9.708	7.909	14.790	12.049	+4.141	10.593	8.630	+0.721	12.786	10.416	+2.508
Entire North Sea	4.473	7.413	6.923	11.474	+4.061	4.922	8.158	+0.745	5.994	9.935	+2.522
northern North Sea	0.598	7.591	0.907	11.515	+3.924	0.632	8.033	+0.441	0.775	9.849	+2.257
central North Sea	1.739	7.155	2.870	11.807	+4.652	1.919	7.896	+0.741	2.434	10.013	+2.858
southern North Sea	1.518	7.446	2.180	10.694	+3.248	1.696	8.321	+0.874	1.962	9.621	+2.175
Norwegian Trench	0.618	7.951	0.966	12.437	+4.486	0.674	8.682	+0.731	0.823	10.600	+2.649
English Channel	0.676	8.210	0.952	11.562	+3.352	0.737	8.947	+0.737	0.850	10.323	+2.113
Skagerrak Kattegat	0.471	6.056	0.747	9.601	+3.546	0.535	6.875	+0.820	0.644	8.275	+2.220
NE Celtic Sea	0.973	9.078	1.448	13.510	+4.432	1.045	9.746	+0.668	1.252	11.684	+2.605
SW Celtic Sea	0.832	9.101	1.320	14.439	+5.338	0.886	9.694	+0.594	1.105	12.097	+2.996
Irish Sea	0.408	8.547	0.533	11.175	+2.627	0.429	8.980	+0.432	0.479	10.035	+1.487
Inner Seas (Scotland)	0.382	8.630	0.541	12.212	+3.582	0.405	9.140	+0.509	0.474	10.705	+2.075
Armorican Shelf	0.603	8.626	0.992	14.190	+5.564	0.685	9.807	+1.181	0.838	11.987	+3.361
Hebrides Shelf	0.302	8.491	0.453	12.749	+4.257	0.321	9.025	+0.534	0.391	10.990	+2.499
Malin Shelf	0.190	8.960	0.282	13.264	+4.304	0.199	9.387	+0.427	0.241	11.360	+2.400
West Irish Shelf	0.401	8.507	0.603	12.815	+4.308	0.432	9.175	+0.668	0.520	11.052	+2.545

Table S12: Annual vertically- and subarea-integrated pelagic carbon remineralization averaged over the simulation period 2000–2010 for all four model configurations: Redfield Stoichiometry (RS), Extracellular Release (ER), Preferential Remineralization (PR), and the combined configuration (ER&PR). For each configuration, the mean is provided both area-integrated and per area. The variable stoichiometry configurations also include the per area difference with respect to the RS configuration.

Annual vertically- and subarea-integrated pelagic carbon remineralization averaged over 2000–2010											
Subarea	RS		ER			PR			ER&PR		
	Total [$Tmol C\ yr^{-1}$]	Per Area [$mol C\ m^{-2} yr^{-1}$]	Total [$Tmol C\ yr^{-1}$]	Per Area [$mol C\ m^{-2} yr^{-1}$]	Difference [$mol C\ m^{-2} yr^{-1}$]	Total [$Tmol C\ yr^{-1}$]	Per Area [$mol C\ m^{-2} yr^{-1}$]	Difference [$mol C\ m^{-2} yr^{-1}$]	Total [$Tmol C\ yr^{-1}$]	Per Area [$mol C\ m^{-2} yr^{-1}$]	Difference [$mol C\ m^{-2} yr^{-1}$]
Entire NWES	9.635	7.849	14.908	12.145	+4.296	10.507	8.560	+0.710	12.834	10.455	+2.606
Entire North Sea	4.528	7.505	7.068	11.715	+4.210	4.971	8.238	+0.733	6.104	10.118	+2.612
northern North Sea	0.571	7.257	0.901	11.443	+4.186	0.606	7.700	+0.443	0.760	9.655	+2.398
central North Sea	1.709	7.032	2.808	11.555	+4.522	1.872	7.703	+0.671	2.379	9.787	+2.755
southern North Sea	1.544	7.574	2.207	10.823	+3.249	1.730	8.487	+0.913	2.000	9.811	+2.237
Norwegian Trench	0.704	9.056	1.152	14.834	+5.777	0.762	9.805	+0.749	0.965	12.425	+3.368
English Channel	0.665	8.077	0.942	11.443	+3.366	0.727	8.833	+0.756	0.840	10.197	+2.121
Skagerrak Kattegat	0.416	5.341	0.731	9.394	+4.053	0.479	6.156	+0.815	0.619	7.948	+2.608
NE Celtic Sea	0.975	9.094	1.449	13.525	+4.430	1.051	9.804	+0.710	1.254	11.705	+2.611
SW Celtic Sea	0.843	9.227	1.364	14.924	+5.697	0.904	9.889	+0.662	1.142	12.495	+3.268
Irish Sea	0.433	9.062	0.569	11.916	+2.854	0.457	9.574	+0.512	0.513	10.738	+1.676
Inner Seas (Scotland)	0.375	8.460	0.545	12.313	+3.853	0.394	8.889	+0.439	0.472	10.665	+2.205
Armorican Shelf	0.556	7.950	0.935	13.377	+5.427	0.627	8.969	+1.019	0.781	11.170	+3.220
Hebrides Shelf	0.299	8.406	0.461	12.966	+4.560	0.315	8.873	+0.466	0.391	10.991	+2.584
Malin Shelf	0.179	8.400	0.279	13.113	+4.713	0.189	8.898	+0.498	0.233	10.959	+2.559
West Irish Shelf	0.364	7.734	0.564	11.981	+4.246	0.391	8.298	+0.564	0.483	10.252	+2.518

Table S13: Annual subarea-integrated benthic carbon remineralization averaged over the simulation period 2000–2010 for all four model configurations: Redfield Stoichiometry (RS), Extracellular Release (ER), Preferential Remineralization (PR), and the combined configuration (ER&PR). For each configuration, the mean is provided both area-integrated and per area. The variable stoichiometry configurations also include the per area difference with respect to the RS configuration.

Annual subarea-integrated benthic carbon remineralization averaged over 2000–2010											
Subarea	RS		ER			PR			ER&PR		
	Total [$Tmol C\ yr^{-1}$]	Per Area [$mol C\ m^{-2} yr^{-1}$]	Total [$Tmol C\ yr^{-1}$]	Per Area [$mol C\ m^{-2} yr^{-1}$]	Difference [$mol C\ m^{-2} yr^{-1}$]	Total [$Tmol C\ yr^{-1}$]	Per Area [$mol C\ m^{-2} yr^{-1}$]	Difference [$mol C\ m^{-2} yr^{-1}$]	Total [$Tmol C\ yr^{-1}$]	Per Area [$mol C\ m^{-2} yr^{-1}$]	Difference [$mol C\ m^{-2} yr^{-1}$]
Entire NWES	0.706	0.575	0.845	0.689	+0.114	0.832	0.678	+0.102	0.812	0.662	+0.086
Entire North Sea	0.369	0.611	0.448	0.743	+0.132	0.442	0.732	+0.120	0.430	0.712	+0.101
northern North Sea	0.039	0.499	0.042	0.539	+0.040	0.043	0.551	+0.053	0.042	0.534	+0.035
central North Sea	0.102	0.419	0.122	0.502	+0.082	0.125	0.514	+0.094	0.120	0.492	+0.072
southern North Sea	0.068	0.332	0.101	0.493	+0.162	0.094	0.459	+0.128	0.093	0.454	+0.123
Norwegian Trench	0.160	2.061	0.183	2.360	+0.299	0.180	2.312	+0.251	0.176	2.259	+0.198
English Channel	0.002	0.027	0.003	0.032	+0.005	0.003	0.036	+0.009	0.003	0.034	+0.007
Skagerrak Kattegat	0.135	1.734	0.175	2.246	+0.512	0.155	1.989	+0.255	0.158	2.029	+0.295
NE Celtic Sea	0.011	0.105	0.013	0.119	+0.013	0.014	0.130	+0.025	0.013	0.123	+0.018
SW Celtic Sea	0.008	0.084	0.008	0.085	+0.001	0.008	0.089	+0.005	0.008	0.085	+0.001
Irish Sea	0.005	0.114	0.007	0.138	+0.023	0.007	0.147	+0.033	0.007	0.140	+0.025
Inner Seas (Scotland)	0.044	0.982	0.048	1.084	+0.102	0.051	1.157	+0.175	0.049	1.105	+0.123
Armorican Shelf	0.059	0.847	0.067	0.953	+0.106	0.070	1.007	+0.160	0.067	0.959	+0.112
Hebrides Shelf	0.018	0.508	0.019	0.538	+0.030	0.020	0.569	+0.061	0.019	0.545	+0.037
Malin Shelf	0.013	0.612	0.014	0.642	+0.030	0.014	0.681	+0.069	0.014	0.648	+0.036
West Irish Shelf	0.042	0.889	0.045	0.962	+0.073	0.047	0.997	+0.108	0.045	0.958	+0.069

Table S14: Annual vertically- and subarea-integrated net community production (NCP) averaged over the simulation period 2000–2010 for all four model configurations: Redfield Stoichiometry (RS), Extracellular Release (ER), Preferential Remineralization (PR), and the combined configuration (ER&PR). For each configuration, the mean is provided both area-integrated and per area. The variable stoichiometry configurations also include the per area difference with respect to the RS configuration.

Annual vertically- and subarea-integrated net community production averaged over 2000–2010											
Subarea	RS		ER			PR			ER&PR		
	Total [$Tmol C\ yr^{-1}$]	Per Area [$molC\ m^{-2}yr^{-1}$]	Total [$Tmol C\ yr^{-1}$]	Per Area [$molC\ m^{-2}yr^{-1}$]	Difference [$molC\ m^{-2}yr^{-1}$]	Total [$Tmol C\ yr^{-1}$]	Per Area [$molC\ m^{-2}yr^{-1}$]	Difference [$molC\ m^{-2}yr^{-1}$]	Total [$Tmol C\ yr^{-1}$]	Per Area [$molC\ m^{-2}yr^{-1}$]	Difference [$molC\ m^{-2}yr^{-1}$]
Entire NWES	−0.633	−0.516	−0.963	−0.785	−0.269	−0.745	−0.607	−0.092	−0.860	−0.701	−0.185
Entire North Sea	−0.425	−0.704	−0.594	−0.984	−0.280	−0.490	−0.812	−0.108	−0.540	−0.895	−0.191
northern North Sea	−0.013	−0.164	−0.037	−0.467	−0.303	−0.017	−0.219	−0.054	−0.027	−0.340	−0.175
central North Sea	−0.072	−0.297	−0.061	−0.249	+0.048	−0.078	−0.321	−0.024	−0.065	−0.266	+0.031
southern North Sea	−0.094	−0.459	−0.127	−0.623	−0.163	−0.128	−0.626	−0.167	−0.131	−0.644	−0.185
Norwegian Trench	−0.246	−3.166	−0.370	−4.757	−1.591	−0.267	−3.436	−0.270	−0.317	−4.084	−0.918
English Channel	0.009	0.106	0.007	0.088	−0.018	0.006	0.078	−0.028	0.008	0.092	−0.014
Skagerrak Kattegat	−0.079	−1.019	−0.159	−2.039	−1.020	−0.099	−1.270	−0.251	−0.132	−1.702	−0.682
NE Celtic Sea	−0.013	−0.121	−0.014	−0.133	−0.012	−0.020	−0.188	−0.067	−0.015	−0.144	−0.023
SW Celtic Sea	−0.019	−0.210	−0.052	−0.570	−0.360	−0.026	−0.284	−0.074	−0.044	−0.484	−0.274
Irish Sea	−0.030	−0.629	−0.042	−0.879	−0.250	−0.035	−0.741	−0.113	−0.040	−0.843	−0.214
Inner Seas (Scotland)	−0.036	−0.812	−0.053	−1.185	−0.373	−0.041	−0.916	−0.104	−0.047	−1.065	−0.253
Armorican Shelf	−0.012	−0.171	−0.010	−0.139	+0.031	−0.012	−0.168	+0.002	−0.001	−0.142	+0.029
Hebrides Shelf	−0.015	−0.423	−0.027	−0.756	−0.332	−0.015	−0.417	+0.007	−0.019	−0.545	−0.122
Malin Shelf	−0.007	−0.312	−0.014	−0.648	−0.336	−0.008	−0.386	−0.075	−0.011	−0.495	−0.183
West Irish Shelf	−0.005	−0.116	−0.006	−0.127	−0.011	−0.006	−0.121	−0.005	−0.007	−0.158	−0.042

Table S15: Annual subarea-integrated air-sea CO_2 flux averaged over the simulation period 2000–2010 for all four model configurations: Redfield Stoichiometry (RS), Extracellular Release (ER), Preferential Remineralization (PR), and the combined configuration (ER&PR). For each configuration, the mean is provided both area-integrated and per area. The variable stoichiometry configurations also include the per area difference with respect to the RS configuration.

Annual subarea-integrated air-sea CO_2 exchange averaged over 2000–2010												
Subarea	RS		ER			PR			ER&PR			
	Total $[Tmol C\ yr^{-1}]$	Per Area $[mol C\ m^{-2} yr^{-1}]$	Total $[Tmol C\ yr^{-1}]$	Per Area $[mol C\ m^{-2} yr^{-1}]$	Difference $[mol C\ m^{-2} yr^{-1}]$	Total $[Tmol C\ yr^{-1}]$	Per Area $[mol C\ m^{-2} yr^{-1}]$	Difference $[mol C\ m^{-2} yr^{-1}]$	Total $[Tmol C\ yr^{-1}]$	Per Area $[mol C\ m^{-2} yr^{-1}]$	Difference $[mol C\ m^{-2} yr^{-1}]$
Entire NWES	1.105	0.900	1.444	1.176	+0.276	1.207	0.984	+0.083	1.316	1.072	+0.171
Entire North Sea	0.670	1.110	0.889	1.474	+0.364	0.736	1.221	+0.110	0.812	1.346	+0.236
northern North Sea	0.156	1.977	0.187	2.379	+0.402	0.162	2.063	+0.085	0.174	2.211	+0.234
central North Sea	0.331	1.361	0.445	1.833	+0.472	0.363	1.495	+0.134	0.407	1.673	+0.312
southern North Sea	0.087	0.425	0.135	0.661	+0.236	0.106	0.522	+0.097	0.121	0.596	+0.171
Norwegian Trench	0.097	1.245	0.122	1.570	+0.325	0.104	1.341	+0.095	0.110	1.414	+0.168
English Channel	0.056	0.685	0.058	0.702	+0.017	0.057	0.691	+0.007	0.057	0.692	+0.008
Skagerrak Kattegat	−0.051	−0.651	−0.042	−0.537	+0.114	−0.048	−0.615	+0.036	−0.046	−0.588	+0.063
NE Celtic Sea	0.085	0.790	0.101	0.945	+0.155	0.088	0.817	+0.028	0.094	0.873	+0.083
SW Celtic Sea	0.105	1.145	0.135	1.480	+0.335	0.116	1.272	+0.127	0.124	1.357	+0.212
Irish Sea	0.001	0.028	−0.001	−0.017	−0.045	−0.001	−0.020	−0.048	−0.001	−0.030	−0.058
Inner Seas (Scotland)	0.023	0.522	0.025	0.562	+0.040	0.023	0.530	+0.008	0.024	0.532	+0.010
Armorican Shelf	0.044	0.624	0.073	1.039	+0.416	0.056	0.805	+0.181	0.062	0.892	+0.268
Hebrides Shelf	0.069	1.939	0.079	2.227	+0.289	0.071	1.992	+0.054	0.074	2.095	+0.156
Malin Shelf	0.037	1.757	0.044	2.063	+0.306	0.038	1.794	+0.037	0.040	1.903	+0.146
West Irish Shelf	0.066	1.408	0.082	1.752	+0.343	0.071	1.503	+0.095	0.076	1.608	+0.200

Table S16: Polynomial fit coefficients for seasonally and subarea-averaged vertical profiles of DIC, PO_4 and NO_3 in Fig. 12 and S15. Each variable is given by a function $\boldsymbol{f(z)}$ as defined below with depth $\boldsymbol{z}$ and polynomial coefficients $\boldsymbol{C_N}$.

Polynomial fit coefficients of function $f(z)$ for seasonally and subarea-averaged vertical profiles of DIC, PO_4 and NO_3									
$f(z) = C_5 \times z^5 + C_4 \times z^4 + C_3 \times z^3 + C_2 \times z^2 + C_1 \times z^1 + C_0$									
Variable		Subarea	Season	C_5	C_4	C_3	C_2	C_1	C_0
DIC	Mean	NT	Winter (DJF)	-8.501×10^{-11}	-1.081×10^{-7}	-4.813×10^{-5}	-8.865×10^{-3}	-7.422×10^{-1}	2155.466
			Spring (MAM)	-6.082×10^{-10}	-6.708×10^{-7}	-2.746×10^{-4}	-5.125×10^{-2}	-4.264	2071.123
			Summer (JJA)	-3.553×10^{-10}	-4.544×10^{-7}	-2.158×10^{-4}	-4.683×10^{-2}	-4.581	2053.557
			Autumn (SON)	-1.250×10^{-10}	-1.764×10^{-7}	-9.315×10^{-5}	-2.294×10^{-2}	-2.685	2087.112
		NNS + CNS	Winter (DJF)	1.307×10^{-11}	1.787×10^{-8}	8.678×10^{-6}	1.732×10^{-3}	1.283×10^{-1}	6.088
			Spring (MAM)	1.062×10^{-10}	1.390×10^{-7}	6.476×10^{-5}	1.324×10^{-2}	1.165	37.925
			Summer (JJA)	-3.300×10^{-11}	-3.122×10^{-8}	-8.317×10^{-6}	1.009×10^{-4}	2.911×10^{-1}	29.286
			Autumn (SON)	-1.119×10^{-11}	-1.588×10^{-8}	-8.153×10^{-6}	-1.746×10^{-3}	-1.029×10^{-1}	8.571
	SD	NT	Winter (DJF)	1.731×10^{-8}	5.925×10^{-6}	7.261×10^{-4}	3.926×10^{-2}	8.554×10^{-1}	2174.176
			Spring (MAM)	5.204×10^{-8}	1.950×10^{-5}	2.563×10^{-3}	1.341×10^{-1}	1.749	2146.274
			Summer (JJA)	4.971×10^{-8}	2.015×10^{-5}	2.854×10^{-3}	1.580×10^{-1}	1.676	2119.107
			Autumn (SON)	2.894×10^{-8}	1.159×10^{-5}	1.640×10^{-3}	9.021×10^{-2}	4.800×10^{-1}	2119.163
		NNS + CNS	Winter (DJF)	-4.945×10^{-9}	-1.923×10^{-6}	-2.668×10^{-4}	-1.574×10^{-2}	-3.270×10^{-1}	3.823
			Spring (MAM)	7.860×10^{-10}	4.200×10^{-7}	8.976×10^{-5}	9.472×10^{-3}	5.431×10^{-1}	17.771
			Summer (JJA)	8.581×10^{-9}	3.947×10^{-6}	6.208×10^{-3}	3.719×10^{-2}	6.910×10^{-1}	16.854
			Autumn (SON)	3.858×10^{-8}	1.471×10^{-5}	1.993×10^{-3}	1.126×10^{-1}	2.417	27.440
PO_4	Mean	NNS + CNS	Winter (DJF)	1.543×10^{-11}	5.092×10^{-9}	4.692×10^{-7}	1.669×10^{-5}	8.289×10^{-4}	6.420×10^{-1}
			Spring (MAM)	1.295×10^{-11}	4.443×10^{-9}	2.278×10^{-7}	-3.684×10^{-5}	-3.438×10^{-3}	3.455×10^{-1}
			Summer (JJA)	2.356×10^{-10}	1.011×10^{-7}	1.531×10^{-5}	9.266×10^{-4}	1.236×10^{-2}	1.828×10^{-1}
			Autumn (SON)	-3.862×10^{-11}	-1.422×10^{-8}	-9.474×10^{-7}	1.247×10^{-4}	9.711×10^{-3}	5.298×10^{-1}
	SD	NNS + CNS	Winter (DJF)	4.952×10^{-11}	2.624×10^{-8}	5.055×10^{-6}	4.170×10^{-4}	1.303×10^{-2}	1.930×10^{-1}
			Spring (MAM)	2.932×10^{-12}	6.676×10^{-10}	3.308×10^{-8}	1.007×10^{-5}	2.239×10^{-3}	1.656×10^{-1}
			Summer (JJA)	3.750×10^{-11}	1.584×10^{-8}	2.202×10^{-6}	9.837×10^{-5}	2.461×10^{-4}	1.187×10^{-1}
			Autumn (SON)	-2.413×10^{-11}	-1.177×10^{-8}	-1.909×10^{-6}	-1.087×10^{-4}	-9.343×10^{-4}	1.350×10^{-1}
NO_3	Mean	NNS + CNS	Winter (DJF)	-3.479×10^{-10}	-1.539×10^{-7}	-2.202×10^{-5}	-8.834×10^{-4}	1.298×10^{-2}	8.414
			Spring (MAM)	1.271×10^{-9}	6.194×10^{-7}	1.096×10^{-4}	8.300×10^{-3}	1.842×10^{-1}	4.268
			Summer (JJA)	-6.435×10^{-10}	-3.310×10^{-7}	-5.331×10^{-5}	-3.027×10^{-3}	-1.045×10^{-1}	5.854×10^{-1}
			Autumn (SON)	-5.051×10^{-10}	-2.309×10^{-7}	-2.912×10^{-5}	-3.413×10^{-4}	4.106×10^{-2}	5.507
	SD	NNS + CNS	Winter (DJF)	4.146×10^{-10}	2.243×10^{-7}	4.467×10^{-5}	3.863×10^{-3}	1.315×10^{-1}	2.406
			Spring (MAM)	9.102×10^{-10}	4.563×10^{-7}	8.320×10^{-5}	6.706×10^{-3}	2.320×10^{-1}	3.504
			Summer (JJA)	1.081×10^{-9}	4.807×10^{-7}	7.366×10^{-5}	4.320×10^{-3}	7.011×10^{-2}	1.109
			Autumn (SON)	6.768×10^{-11}	9.436×10^{-8}	3.034×10^{-5}	3.737×10^{-3}	1.827×10^{-1}	3.542

S2 Ecosystem model equations: variable stoichiometry ECOSMO II

The here introduced variable stoichiometry version of ECOSMO II is an extension to the model presented in Daewel and Schrum (2013). Dissolved and particulate organic matter, formerly constrained to constant Redfield stoichiometry (Redfield, 1963), are now separated into individual variables for carbon, nitrogen, and phosphorus contents in both pelagic and benthic reservoirs. While primary and secondary production remain at Redfield stoichiometry, we here introduce two pathways for variable organic matter stoichiometry: firstly, we allow for carbon fixation beyond nutrient limitation in form of an extracellular release of carbon-enriched dissolved organic matter. This implementation represents the release of carbohydrates observed in phytoplankton blooms under nutrient stress (Børsheim et al., 2005; Fajon et al., 1999; Søndergaard et al., 2000) and was adapted from the model parametrization in Neumann et al. (2022). With this, we also include the suggested particle formation from dissolved to particulate organic matter as transparent exopolymer particles (Engel, 2002; Neumann et al., 2022), and add a dependence on the nutrient state as for the DIC uptake by the extracellular release itself. Secondly, we consider the observed preferential remineralization of nitrogen and phosphorus with the sequence P > N > C (Clark et al., 1998; Hopkinson et al., 2002; Loh and Bauer, 2000; Thomas et al., 1999; Williams et al., 1980) with a constant ratio between the remineralization rates of carbon, nitrogen and phosphorus. By considering variable stoichiometry in the production and degradation of organic matter, the model can represent variations in organic matter composition and their control on the coupling of elemental fluxes. It further incorporates the additional variables dissolved inorganic carbon (DIC) and total alkalinity (TA) introduced in Kossack et al. (2024) for the coupling to a carbonate system model (Blackford and Gilbert, 2007). This enables the analysis of the effects of variable stoichiometry on inorganic carbon contents and carbon cycling.

The model integrates a total of twenty-four prognostic equations for tracer concentrations of different functional groups. Besides DIC and TA, these include three phytoplankton (flagellates, diatoms, and cyanobacteria), two zooplankton (micro- and meso-zooplankton), seven detritus (pelagic DOC, DON, DOP, POC, PON, POP, and biogenic opal), five sediment (benthic POC, PON, POP, PIP, and opal), and four nutrient variables (NO_3^-, NH_4^+, PO_4^{3-}, SiO_2) in addition to oxygen. Each tracer concentration C is integrated in time based on a prognostic equation of the form:

(1) $C_t + (v \cdot \nabla)C + w_d C_z = (A_v C_z)_z + R_C,$

where subscripts of time t and depth z represent derivatives d/dt and d/dz respectively. Here, $v=(u,v,w)$ is the three-dimensional velocity field, A_v the sub-scale diffusion coefficient, w_d a constant sinking velocity and R_C the local sources and sinks. The sinking velocity w_d is only non-zero for particulate organic matter, cyanobacteria, and opal. Whereas the physical model component provides physical transports by advection $(v \cdot \nabla)C$, diffusion $(A_v C_z)_z$, and sinking $w_d C_z$, the ECOSMO II module describes the biogeochemical processes in R_C that act as local sources and sinks. The table below summarizes these terms R_C for all twenty-four tracers. For a more detailed description of the primary production, secondary

production, and nutrient limitation dynamics, the reader is referred to the original ECOSMO II model description (Daewel and Schrum, 2013).

Local sink and source terms R_C for all tracer concentrations C_X of tracer X		
Variable	Definition	Unit
Primary Production		
C_{P_j}: biomass of phytoplankton group P_j	$R_{P_j} = \sigma_j \beta_{T_j} \Phi_{P_j} C_{P_j} - \sum_{i=1}^{2} G_i(C_{P_j}) C_{Z_i} - m_{P_j} C_{P_j}$ for j in [1, 2, 3]	$[mg\ C\ m^{-3}]$
C_{P_1}: flagellate biomass	$\Phi_{P_1} = \min(\alpha(I), \beta_N, \beta_P)$	$[mg\ C\ m^{-3}]$
C_{P_2}: diatom biomass	$\Phi_{P_2} = \min(\alpha(I), \beta_N, \beta_P, \beta_{Si})$	$[mg\ C\ m^{-3}]$
C_{P_3}: cyanobacteria biomass	$\Phi_{P_3} = \begin{cases} 0, & if\ C_{\mathrm{Sal}} > 10.0 \text{ or } I_s(x,y) < 120\ Wm^{-2} \\ \min(\alpha(I), \beta_P), & \text{else if } n_z = N_z \\ \min(\alpha(I), \beta_N, \beta_P), & \text{else} \end{cases}$ with C_{Sal} provided by the physical model.	$[mg\ C\ m^{-3}]$
α(I): light limitation	$\alpha(I) = \tanh(\alpha \cdot I(x,y,z,t))$	-
$I(x,y,z,t)$: photosynthetically active radiation	$I(x,y,z,t) = \frac{I_s(x,y)}{2} \exp(-k_w z - k_{\mathrm{phyto}} \int_z^0 \sum_{j=1}^{3} C_{P_j} \partial z)$	$[Wm^{-2}]$
β_N: nitrogen limitation	$\beta_N = \beta_{NH_4} + \beta_{NO_3}$	-
β_{NH_4}: ammonium limitation	$\beta_{NH_4} = \frac{C_{NH_4}}{r_{NH_4} + C_{NH_4}}$	-
β_{NO_3}: nitrate limitation	$\beta_{NO_3} = \frac{C_{NO_3}}{r_{NO_3} + C_{NO_3}} \exp(-\Psi \cdot C_{NH_4})$	-
β_P: phosphorus limitation	$\beta_{PO_4} = \frac{C_{PO_4}}{r_{PO_4} + C_{PO_4}}$	-
β_{Si}: silicate limitation	$\beta_{Si} = \max(0, \frac{C_{SiO_2} - R_{SiO_2}}{r_{SiO_2} + C_{SiO_2}})$	-
$\beta_{T_{1,2,3}}$: temperature dependence	$\beta_{T_1} = 1,\ \beta_{T_2} = 1,\ \beta_{T_3}(T) = \frac{1}{1+\exp(-T)}$	-
σ_{P_j}: maximum growth rate of phytoplankton group P_j	$\sigma_{P_1} = 1.10,\ \sigma_{P_2} = 1.30,\ \sigma_{P_3} = 1.00$	$[d^{-1}]$
m_{P_j}: mortality rate of phytoplankton group P_j	$m_{P_1} = 0.08,\ m_{P_2} = 0.05,\ m_{P_3} = 0.08$	$[d^{-1}]$
$I_s(x,y)$: short wave radiation	Prescribed fields loaded from file.	$[Wm^{-2}]$
α: Photosynthesis efficiency	$\alpha = 0.01$	$[(Wm^{-2})^{-1}]$
k_w: water background light extinction coefficient	$k_w = 0.05$	$[m^{-1}]$
k_{phyto}: phytoplankton light extinction coefficient	$k_{\mathrm{phyto}} = 0.20$	$[m^2(mmol\ C)^{-1}]$
Ψ: NH_4 inhibition parameter	$\Psi = 3.00$	$[m^3(mmol\ N)^{-1}]$

r_{NO_3}: NO_3 half saturation constant	$r_{NO_3} = 0.50$	$[mmol\ N\ m^{-3}]$
r_{NH_4}: NH_4 half saturation constant	$r_{NH_4} = 0.20$	$[mmol\ N\ m^{-3}]$
r_{PO_4}: PO_4 half saturation constant	$r_{PO_4} = 0.05$	$[mmol\ P\ m^{-3}]$
r_{SiO_2}: SiO_2 half saturation constant	$r_{SiO_2} = 0.50$	$[mmol\ Si\ m^{-3}]$
Rr_{SiO_2}: SiO_2 constant	$Rr_{SiO_2} = 1.00$	$[mmol\ Si\ m^{-3}]$
Secondary Production		
C_{Z_1}: micro-zooplankton biomass	$R_{Z_1} = \gamma_1 C_{Z_1} \sum_{j=1}^{3} G_1\left(C_{P_j}\right) + \gamma_2 G_1(\min(C_{\mathrm{POC}}, C_{\mathrm{PON}}, C_{\mathrm{POP}}))C_{Z_1} - G_2(C_{Z_1})C_{Z_2} - \mu_1 C_{Z_1} - m_{Z_1} C_{Z_1}$	$[mg\ C\ m^{-3}]$
C_{Z_2}: meso-zooplankton biomass	$R_{Z_2} = \gamma_1 C_{Z_2} \sum_{j=1}^{3} G_2\left(C_{P_j}\right) + \gamma_1 G_2(C_{Z_1})C_{Z_2} + \gamma_2 G_2(\min(C_{\mathrm{POC}}, C_{\mathrm{PON}}, C_{\mathrm{POP}}))C_{Z_2} - \mu_2 C_{Z_2} - m_{Z_2} C_{Z_2}$	$[mg\ C\ m^{-3}]$
$G_i(C_X)$: zooplankton grazing rates	$G_i(C_X) = \sigma_{i,X} \frac{a_{i,X} C_X}{r_i + H_i}$ with $H_i = \sum_X a_{i,X} C_X$	-
r_Z: zooplankton half saturation constant	$r_Z = 3.3$	$[mmol\ C\ m^{-3}]$
m_{Z_i}: zooplankton mortality rate of group Z_i	$m_{Z_1} = 0.2,\ m_{Z_2} = 0.1$	$[d^{-1}]$
μ_{Z_i}: zooplankton excretion rate of group Z_i	$\mu_{Z_1} = 0.08,\ \mu_{Z_2} = 0.06$	$[d^{-1}]$
γ_1: assimilation efficiency of grazing on $P_{1,2,3}$ and Z_1	$\gamma_1 = 0.75$	-
γ_2: assimilation efficiency of grazing on POC	$\gamma_2 = 0.30$	-
$\sigma_{Z_1,X}$: grazing parameter of Z_1 on X	$\sigma_{Z_1,P_1} = 1.00,\ \sigma_{Z_1,P_2} = 1.00,\ \sigma_{Z_1,P_3} = 0.30,\ \sigma_{Z_1,Z_1} = 0.00,\ \sigma_{Z_1,\mathrm{POC}} = 1.00$	-
$a_{Z_1,X}$: grazing parameter of Z_1 on X	$a_{Z_1,P_1} = 0.70,\ a_{Z_1,P_2} = 0.25,\ a_{Z_1,P_3} = 0.30,\ a_{Z_1,Z_1} = 0.00,\ a_{Z_1,\mathrm{POC}} = 0.10$	-
$\sigma_{Z_2,X}$: grazing parameter of Z_2 on X	$\sigma_{Z_2,P_1} = 0.80,\ \sigma_{Z_2,P_2} = 0.80,\ \sigma_{Z_2,P_3} = 0.30,\ \sigma_{Z_2,Z_1} = 0.50,\ \sigma_{Z_2,\mathrm{POC}} = 0.80$	-
$a_{Z_2,X}$: grazing parameter of Z_2 on X	$a_{Z_2,P_1} = 0.10,\ a_{Z_2,P_2} = 0.85,\ a_{Z_2,P_3} = 0.30,\ a_{Z_2,Z_1} = 0.15,\ a_{Z_2,\mathrm{POC}} = 0.10$	-
Degradation Products		
C_{DOC}: dissolved organic carbon concentration	$R_{\mathrm{DOC}} = a_{\mathrm{DOM}} R_{\mathrm{OM}}^{+} - \epsilon_{\mathrm{DOC}} C_{\mathrm{DOC}} + E_{\mathrm{DOC}} - F_{\mathrm{DOC2POC}}$	$[mg\ C\ m^{-3}]$
C_{DON}: dissolved organic nitrogen concentration	$R_{\mathrm{DON}} = a_{\mathrm{DOM}} R_{\mathrm{OM}}^{+} - \epsilon_{\mathrm{DON}} C_{\mathrm{DON}} + E_{\mathrm{DON}} - F_{\mathrm{DON2PON}}$	$[mg\ C\ m^{-3}]$
C_{DOP}: dissolved organic phosphorus concentration	$R_{\mathrm{DOP}} = a_{\mathrm{DOM}} R_{\mathrm{OM}}^{+} - \epsilon_{\mathrm{DOP}} C_{\mathrm{DOP}} + E_{\mathrm{DOP}} - F_{\mathrm{DOP2POP}}$	$[mg\ C\ m^{-3}]$
C_{POC}: particulate organic carbon concentration	$R_{\mathrm{POC}} = (1 - a_{\mathrm{DOM}}) R_{\mathrm{OM}}^{+} - R_{\mathrm{POC}}^{-} + \left[\frac{\lambda_{\mathrm{res}} C_{\mathrm{Sed.POC}} - \lambda_{\mathrm{dep}} C_{\mathrm{POC}}}{dz}\right]_{n_z=0} + F_{\mathrm{DOC2POC}}$	$[mg\ C\ m^{-3}]$
C_{PON}: particulate organic nitrogen concentration	$R_{\mathrm{PON}} = (1 - a_{\mathrm{DOM}}) R_{\mathrm{OM}}^{+} - R_{\mathrm{PON}}^{-} + \left[\frac{\lambda_{\mathrm{res}} C_{\mathrm{Sed.PON}} - \lambda_{\mathrm{dep}} C_{\mathrm{PON}}}{dz}\right]_{n_z=0} + F_{\mathrm{DON2PON}}$	$[mg\ C\ m^{-3}]$

C_{POP}: particulate organic phosphorus concentration	$R_{\mathrm{POP}} = (1 - a_{\mathrm{DOM}})R^{+}_{\mathrm{OM}} - R^{-}_{\mathrm{POP}} + \left[\frac{\lambda_{\mathrm{res}} C_{\mathrm{Sed.POP}} - \lambda_{\mathrm{dep}} C_{\mathrm{POP}}}{dz}\right]_{n_z=0} + F_{\mathrm{DOP2POP}}$	$[mg\ C\ m^{-3}]$
C_{Opal}: biogenic opal concentration	$R_{\mathrm{Opal}} = \frac{1}{\mathrm{REDF_{C:Si}}}\left[\sum_{i=1}^{2} G_i(P_2) C_{Z_i} + m_2 P_2 - \epsilon_{\mathrm{Si}} C_{\mathrm{Opal}}\right] + \left[\frac{\lambda_{\mathrm{res}} C_{\mathrm{Sed.SiO_2}} - \lambda_{\mathrm{dep}} C_{\mathrm{Opal}}}{dz}\right]_{n_z=0}$	$[mg\ C\ m^{-3}]$
R^{+}_{OM}: new detrital matter from assimilation losses and mortality	$R^{+}_{\mathrm{OM}} = (1-\gamma_1)\left(\sum_{i=1}^{2} C_{Z_i} \sum_{j=1}^{3} G_i\left(C_{P_j}\right) + G_2\left(C_{Z_1}\right)\right) + (1-\gamma_2)\sum_{i=1}^{2} C_{Z_i} G_i(\min(C_{\mathrm{POC}}, C_{\mathrm{PON}}, C_{\mathrm{POP}})) + \sum_{j=1}^{3} m_{P_j} C_{P_j} + \sum_{i=1}^{2} m_{Z_i} C_{Z_i}$	$[mg\ C\ m^{-3} s^{-1}]$
R^{-}_{X}: POM losses through grazing and remineralization	$R^{-}_{X} = \sum_{i=1}^{2} C_{Z_i} G_i(\min(C_{\mathrm{POC}}, C_{\mathrm{PON}}, C_{\mathrm{POP}})) + \epsilon_X(T) C_X$ for X in [POC, PON, POP]	$[mg\ C\ m^{-3} s^{-1}]$
$\epsilon_{\mathrm{POC}}(T)$: remineralization rate of POC	$\epsilon_{\mathrm{POC}}(T) = 0.006 \times (1 + 20 \times (\frac{T^2}{T_{\mathrm{ref}}^2 + T^2}))$	$[d^{-1}]$
$\epsilon_{\mathrm{PON}}(T)$: remineralization rate of PON	$\epsilon_{\mathrm{PON}}(T) = \frac{\epsilon_{\mathrm{POC}}(T)}{\epsilon_{\mathrm{POC:PON}}}$ with parameter $\epsilon_{\mathrm{POC:PON}}$ specified in configuration	$[d^{-1}]$
$\epsilon_{\mathrm{POP}}(T)$: remineralization rate of POP	$\epsilon_{POP}(T) = \frac{\epsilon_{\mathrm{POC}}(T)}{\epsilon_{\mathrm{POC:POP}}}$ with parameter $\epsilon_{\mathrm{POC:POP}}$ specified in configuration	$[d^{-1}]$
$\epsilon_{\mathrm{DOC}}(T)$: remineralization rate of DOC	$\epsilon_{\mathrm{DOC}}(T) = \epsilon_{\mathrm{DOC:POC}} \epsilon_{POC}(T)$ with parameter $\epsilon_{\mathrm{DOC:POC}}$ specified in configuration	$[d^{-1}]$
$\epsilon_{\mathrm{DON}}(T)$: remineralization rate of DON	$\epsilon_{\mathrm{DON}}(T) = \frac{\epsilon_{\mathrm{DOC}}(T)}{\epsilon_{\mathrm{DOC:DON}}}$ with parameter $\epsilon_{\mathrm{DOC:DON}}$ specified in configuration	$[d^{-1}]$
$\epsilon_{\mathrm{DOP}}(T)$: remineralization rate of DOP	$\epsilon_{\mathrm{DOP}}(T) = \frac{\epsilon_{DOC}(T)}{\epsilon_{DOC:\mathrm{DOP}}}$ with parameter $\epsilon_{\mathrm{DOC:DOP}}$ specified in configuration	$[d^{-1}]$
ϵ_{Si}: remineralization rate of opal	$\epsilon_{\mathrm{Si}} = 0.015$	$[d^{-1}]$
a_{DOM}: fraction of dissolved organic matter from new detrital matter	$a_{\mathrm{DOM}} = 0.4$	-
T_{ref}: reference temperature for remineralization	$T_{\mathrm{ref}} = 13$	$[°C]$
w_D: sinking rate of particulate organics and opal	$w_D = 5$	$[md^{-1}]$
n_z: depth index with bottom index $n_z = 0$, surface index $n_z = N_z$	Provided by the physical model component.	-
dz: vertical step size at depth level n_z	Provided by the physical model component.	$[m]$
Extracellular Release and Flocculation		
E: extracellular release base rate	$E = \mathrm{B_{ER}} \times \Sigma_{j=1}^{3}(\sigma_j C_{P_j} \beta_{Tj})$ with temperature limitation β_{Tj} of phytoplankton group P_j where applicable	$[mg\ C\ m^{-3} s^{-1}]$
E_{DON}: extracellular release of DON	$E_{\mathrm{DON}} = \begin{cases} E \times \min(1-\beta_{\mathrm{P}},\ \beta_{\mathrm{N}},\ \alpha(I)),\ \beta_N > 0.1 \text{ and } \beta_{\mathrm{P}} < 1 \\ 0,\ \beta_N \le 0.1 \text{ or } \beta_{\mathrm{P}} \ge 1 \end{cases}$	$[mg\ C\ m^{-3} s^{-1}]$
E_{DOP}: extracellular release of DOP	$E_{\mathrm{DOP}} = \begin{cases} E \times \min(\beta_{\mathrm{P}},\ 1.1-\beta_{\mathrm{N}},\ \alpha(I)),\ \beta_{\mathrm{P}} > 0.1 \text{ and } \beta_{\mathrm{N}} < 1.1 \\ 0,\ \beta_{\mathrm{P}} \le 0.1 \text{ or } \beta_{\mathrm{N}} \ge 1.1 \end{cases}$	$[mg\ C\ m^{-3} s^{-1}]$
E_{DOC}: extracellular release of DOC	$E_{\mathrm{DOC}} = E_{\mathrm{DON}} + E_{\mathrm{DOP}} + \begin{cases} E \times \min(\max(1-\beta_{\mathrm{P}},\ 1.1-\beta_{\mathrm{N}}),\ \alpha(I)),\ \beta_{\mathrm{P}} < 1 \text{ and } \beta_{\mathrm{N}} < 1.1 \\ 0,\ \beta_{\mathrm{P}} \ge 1 \text{ or } \beta_{\mathrm{N}} \ge 1.1 \end{cases}$	$[mg\ C\ m^{-3} s^{-1}]$
F: flocculation base rate	$F = F_{\mathrm{DOM2POM}} \times B_{\mathrm{ER}}$	$[s^{-1}]$
F_{DON2PON}: flocculation from DON to PON	$F_{\mathrm{DON2PON}} = \begin{cases} F \times \mathrm{C_{DON}} \times \min(1-\beta_{\mathrm{P}},\ \beta_{\mathrm{N}},\ \alpha(I)), & \beta_{\mathrm{N}} > 0.1 \text{ and } \beta_{\mathrm{P}} < 1 \\ 0, & \beta_{\mathrm{N}} \le 0.1 \text{ or } \beta_{\mathrm{P}} \ge 1 \end{cases}$	$[mg\ C\ m^{-3} s^{-1}]$

F_{DOP2POP}: flocculation from DOP to POP	$F_{\mathrm{DOP2POP}} = \begin{cases} F \times \mathrm{C_{DOP}} \times \min(\beta_{\mathrm{P}},\ 1.1 - \beta_{\mathrm{N}},\ \alpha(I)), & \beta_{\mathrm{P}} > 0.1 \text{ and } \beta_{\mathrm{N}} < 1.1 \\ 0, & \beta_{\mathrm{P}} \le 0.1 \text{ or } \beta_{\mathrm{N}} \ge 1.1 \end{cases}$	$[mg\ C\ m^{-3}s^{-1}]$
F_{DOC2POC}: flocculation from DOC to POC	$F_{\mathrm{DOC2POC}} = F_{\mathrm{DON2PON}} + F_{\mathrm{DOP2POP}} + \begin{cases} F \times \mathrm{C_{DOC}} \times \min(\max(1 - \beta_{\mathrm{P}},\ 1.1 - \beta_{\mathrm{N}}),\ \alpha(I)), & \beta_{\mathrm{P}} < 1 \text{ and } \beta_{\mathrm{N}} < 1.1 \\ 0, & \beta_{\mathrm{P}} \ge 1 \text{ or } \beta_{\mathrm{N}} \ge 1.1 \end{cases}$	$[mg\ C\ m^{-3}s^{-1}]$
B_{ER}: extracellular release scaling factor	Specified in configuration.	-
F_{DOM2POM}: flocculation scaling factor	Specified in configuration.	$[d^{-1}]$
Nutrients		
$\mathrm{C_{NH_4}}$: ammonium concentration	$R_{\mathrm{NH_4}} = -\frac{\beta_{\mathrm{NH_4}}}{\beta_{\mathrm{N}}}(\sum_{j=1}^{3}\sigma_j\beta_{\mathrm{T_j}}\Phi_{P_j}C_{P_j} + E_{\mathrm{DON}}) + \sum_{i=1}^{2}\mu_i C_{Z_i} + \epsilon_{\mathrm{PON}}C_{\mathrm{PON}} + \epsilon_{\mathrm{DON}}C_{\mathrm{DON}} - \Omega_a(\mathrm{O_2},T)C_{\mathrm{NH_4}} + \left[\frac{C_{\mathrm{Sed.PON}}(\theta(\mathrm{O_2})\epsilon_{\mathrm{Sed.Ox}}}{dz}\right]_{n_z=0} + \left[\frac{\theta(-\mathrm{O_2})\epsilon_{\mathrm{Sed.Anox}})}{dz}\right]_{n_z=0} + \mathrm{SurfNH_4}$ with surface deposition $\mathrm{SurfNH_4}$ provided from observational data.	$[mgC\ m^{-3}]$
$\mathrm{C_{NO_3}}$: nitrate concentration	$R_{\mathrm{NO_3}} = -\frac{\beta_{\mathrm{NO_3}}}{\beta_{\mathrm{N}}}\left(\sum_{j=1}^{3}\sigma_j\beta_{\mathrm{T_j}}\Phi_{P_j}C_{P_j} + E_{\mathrm{DON}}\right) + \Omega_a(\mathrm{O_2},T)C_{\mathrm{NH_4}} - \theta(-\mathrm{O_2})\theta(\mathrm{NO_3})a_{\mathrm{denit}}(\epsilon_{\mathrm{POC}}C_{\mathrm{POC}} + \epsilon_{\mathrm{DOC}}C_{\mathrm{DOC}}) - \left[\frac{-\theta(-O_2)\theta(\mathrm{NO_3})a_{\mathrm{denit}}\epsilon_{\mathrm{Sed.Anox}}C_{\mathrm{Sed.PON}}}{dz}\right]_{n_z=0} + \mathrm{SurfNO_3}$ with surface deposition $\mathrm{SurfNO_3}$ provided from observational data.	$[mgC\ m^{-3}]$
$\mathrm{C_{PO_4}}$: phosphate concentration	$R_{\mathrm{PO_4}} = \left[-\sum_{j=1}^{3}\sigma_j\beta_{\mathrm{T_j}}\Phi_{P_j}C_{P_j} - E_{\mathrm{DOP}} + \epsilon_{\mathrm{POP}}C_{\mathrm{POP}} + \epsilon_{\mathrm{DOP}}C_{\mathrm{DOP}} + \sum_{i=1}^{2}\mu_i C_{Z_i}\right] + \left[\frac{\theta(O_2)\epsilon_P(1-0.15\sigma)C_{\mathrm{Sed.PIP}}}{dz}\right]_{n_z=0} + \left[\frac{\theta(-O_2)\epsilon_{\mathrm{PIP}}C_{\mathrm{Sed.PIP}}}{dz}\right]_{n_z=0}$	$[mgC\ m^{-3}]$
$\mathrm{C_{SiO_2}}$: silicate concentration	$R_{\mathrm{SiO_2}} = \left[-\Phi_2\sigma_2 P_2 + \epsilon_{\mathrm{Si}}C_{\mathrm{Opal}}\right] + \left[\frac{\epsilon_{\mathrm{Sed.SiO_2}}C_{\mathrm{Sed.SiO_2}}}{dz}\right]_{n_z=0}$	$[mgC\ m^{-3}]$
$\mathrm{C_{O_2}}$: oxygen concentration	$R_{\mathrm{O_2}} = \frac{1}{\mathrm{REDF_{C:O_2}REDF_{C:N}}}\left(\frac{6.625\beta_{\mathrm{NH_4}}+8.125\beta_{\mathrm{NO_3}}}{\beta_{\mathrm{N}}}\sum_{j=1}^{3}\sigma_j\beta_{\mathrm{T_j}}\Phi_{P_j}C_{P_j} - \theta(\mathrm{O_2})\left(6.625\left(\epsilon_{\mathrm{POC}}C_{\mathrm{POC}} + \epsilon_{\mathrm{DOC}}C_{\mathrm{DOC}} + \sum_{i=1}^{2}\mu_i C_{Z_i}\right) + 2\Omega_a(\mathrm{O_2},T)C_{\mathrm{NH_4}}\right)\right) + \frac{E_{\mathrm{DOC}}}{\mathrm{REDF_{C:O_2}}} + \mathrm{SurfO_2} + \mathrm{BottomO_2}$	$[mmolO_2\ m^{-3}]$
$\Omega_{\mathrm{a}}(\mathrm{O_2},\mathrm{T})$: oxygen and temperature scaling	$\Omega_{\mathrm{a}}(\mathrm{O_2},\mathrm{T}) = 0.1 \times \theta(\mathrm{O_2})\exp(0.11 \times T)\frac{C_{\mathrm{O_2}}}{0.01+C_{\mathrm{O_2}}}$	-
$\theta(x)$: distinction for oxygen and nitrogen conditions	$\theta(x) = \begin{cases} 1, & \forall x > 0 \\ 0, & \forall x \le 0 \end{cases}$	-
$\mathrm{SurfO_2}$: air-sea $\mathrm{O_2}$ exchange	$\mathrm{SurfO_2} = \left[\frac{v_P}{dz(\mathrm{O_{2sat}}(T,S)-C_{O_2})}\right]_{n_z=N_z}$	$[mmolO_2\ m^{-3}d^{-1}]$
$\mathrm{BottomO_2}$: benthic-pelagic $\mathrm{O_2}$ exchange flux	$\mathrm{BottomO_2} = -\left[\frac{\theta(\mathrm{O_2})(2\times6.625\times\epsilon_{\mathrm{Sed.Ox}}C_{\mathrm{Sed.POC}}+\Omega_a(\mathrm{O_2},T)\epsilon_{\mathrm{Sed.Ox}}C_{\mathrm{Sed.POC}})}{dz\,\mathrm{REDF_{C:O_2}REDF_{C:N}}}\right]_{n_z=0} - \left[\frac{\theta(-\mathrm{O_2})\theta(-\mathrm{NO_3})6.625\times\epsilon_{\mathrm{Sed.Anox}}C_{\mathrm{Sed.POC}}}{dz\,\mathrm{REDF_{C:O_2}REDF_{C:N}}}\right]_{n_z=0}$	$[mmolO_2\ m^{-3}d^{-1}]$
$\mathrm{O_{2sat}}(T,S)$: oxygen saturation	$\mathrm{O_{2sat}}(T,S) = \exp\left(-135.90205 + 1.575701\times10^5\times T_{\mathrm{O_2}} - 6.642308\times10^7\times T_{\mathrm{O_2}}^2 + 1.2438\times10^{10}\times T_{\mathrm{O_2}}^3 - 8.621949\times10^{11}\times T_{\mathrm{O_2}}^4 - C_{\mathrm{Sal}}\left(1.7674\times10^{-2} - 10.754\times T_{\mathrm{O_2}} + 2140.7\times T_{\mathrm{O_2}}^2\right)\right)$ with $T_{\mathrm{O_2}}(T) = \frac{1}{T+273.15}$	$[mmolO_2\ m^{-3}]$
a_{denit}: increased nitrate loss as oxidation agent under anoxic conditions	$a_{\mathrm{denit}} = 5$	-
Ω_{aMax}: $\mathrm{NH_4}$ maximum oxidation rate	$\Omega_{\mathrm{aMax}} = 0.05$	$[d^{-1}]$
Ω_{nMax}: NO_2 maximum oxidation rate	$\Omega_{\mathrm{nMax}} = 0.10$	$[d^{-1}]$
Ω_{rMax}: NO_3 maximum reduction rate	$\Omega_{\mathrm{rMax}} = 0.01$	$[d^{-1}]$
Ω_{dMax}: NO_2 maximum reduction rate	$\Omega_{\mathrm{dMax}} = 0.01$	$[d^{-1}]$

v_P: oxygen piston velocity	$v_P = 5$	$[md^{-1}]$
$\mathrm{REDF_{C:N}}$: Redfield ratio of carbon to nitrogen	$\mathrm{REDF_{C:N}} = 6.625$	$[\frac{mol\ C}{mol\ N}]$
$\mathrm{REDF_{C:P}}$: Redfield ratio of carbon to phosphorus	$\mathrm{REDF_{C:P}} = 106$	$[\frac{mol\ C}{mol\ P}]$
$\mathrm{REDF_{C:Si}}$: Redfield ratio of carbon to silicon	$\mathrm{REDF_{C:Si}} = 6.625$	$[\frac{mol\ C}{mol\ Si}]$
$\mathrm{REDF_{C:O_2}}$: molar mass of carbon	$\mathrm{REDF_{C:O_2}} = 12.01$	$[\frac{g\ C}{mol\ C}]$
Sediment Processes		
$C_{\mathrm{Sed.POC}}$: benthic POC concentration	$R_{\mathrm{Sed.POC}} = \lambda_{\mathrm{dep}} C_{POC} - C_{\mathrm{Sed.POC}}(\lambda_{\mathrm{res}} + \theta(O_2)2\epsilon_{\mathrm{Sed.Ox}} + \theta(-O_2)\epsilon_{\mathrm{Sed.Anox}} + \delta_{\mathrm{bur}})$	$[mg\ C\ m^{-2}]$
$C_{\mathrm{Sed.PON}}$: benthic PON concentration	$R_{\mathrm{Sed.PON}} = \lambda_{\mathrm{dep}} C_{PON} - C_{\mathrm{Sed.PON}}(\lambda_{\mathrm{res}} + \theta(O_2)\epsilon_{\mathrm{Sed.Ox}} + \theta(-O_2)\epsilon_{\mathrm{Sed.Anox}} + \delta_{\mathrm{bur}})$	$[mg\ C\ m^{-2}]$
$C_{\mathrm{Sed.POP}}$: benthic POP concentration	$R_{\mathrm{Sed.POP}} = \lambda_{\mathrm{dep}} C_{POP} - C_{\mathrm{Sed.POP}}(\lambda_{\mathrm{res}} + \theta(O_2)2\epsilon_{\mathrm{Sed.Ox}} + \theta(-O_2)\epsilon_{\mathrm{Sed.Anox}} + \delta_{\mathrm{bur}})$	$[mg\ C\ m^{-2}]$
$C_{\mathrm{Sed.PIP}}$: benthic inorganic iron-bound phosphate concentration	$R_{\mathrm{Sed.PIP}} = \theta(O_2)(2\epsilon_{\mathrm{Sed.Ox}} C_{\mathrm{Sed.POP}} - \epsilon_{\mathrm{PIP}}(1 - 0.15\sigma) C_{\mathrm{Sed.PIP}}) + \theta(-O_2)(\epsilon_{\mathrm{Sed.Anox}} C_{\mathrm{Sed.POP}} - \epsilon_{\mathrm{PIP}} C_{\mathrm{Sed.PIP}})$	$[mg\ C\ m^{-2}]$
$C_{\mathrm{Sed.SiO_2}}$: benthic opal concentration	$R_{\mathrm{Sed.SiO_2}} = \lambda_{\mathrm{dep}} C_{Opal} - C_{\mathrm{Sed.SiO_2}}(\lambda_{\mathrm{res}} + \epsilon_{\mathrm{Sed.SiO_2}} + \delta_{\mathrm{bur}})$	$[mg\ C\ m^{-2}]$
$\epsilon_{\mathrm{Sed.Ox}}(T)$: organic sediment remineralization under oxic conditions	$\epsilon_{\mathrm{Sed.Ox}}(T) = 0.001 \times \exp(0.15 \times T)$	$[d^{-1}]$
$\epsilon_{\mathrm{Sed.Anox}}(T)$: organic sediment remineralization under anoxic conditions	$\epsilon_{\mathrm{Sed.Anox}}(T) = 2 \times \epsilon_{\mathrm{Sed.Ox}}(T)$	$[d^{-1}]$
$\epsilon_{\mathrm{PIP}}(T)$: release of phosphate from benthic PIP into the water column	$\epsilon_{\mathrm{PIP}}(T) = 2 \times \epsilon_{\mathrm{Sed.Ox}}(T)$	$[d^{-1}]$
σ: oxygen dependence of organic sediment phosphorous remineralization	$\sigma = \frac{\left(\frac{C_{O_2}}{375}\right)^2}{0.1^2 + \left(\frac{C_{O_2}}{375}\right)^2}$	-
$\epsilon_{\mathrm{Sed.SiO_2}}$: sediment opal remineralization rate	$\epsilon_{\mathrm{Sed.SiO_2}} = 0.0002$	$[d^{-1}]$
λ_{dep}: sedimentation rate below critical bottom shear stress	$\lambda_{\mathrm{dep}} = \begin{cases} 3.5, & \tau < \tau_{\mathrm{crit}} \\ 0, & \tau \geq \tau_{\mathrm{crit}} \end{cases}$	$[d^{-1}]$
λ_{res}: resuspension rate above critical bottom shear stress	$\lambda_{\mathrm{res}} = \begin{cases} 0, & \tau < \tau_{\mathrm{crit}} \\ 25, & \tau \geq \tau_{\mathrm{crit}} \end{cases}$	$[d^{-1}]$
τ_{crit}: critical bottom shear stress	$\tau_{\mathrm{crit}} = 0.007$	$[Nm^{-2}]$
δ_{bur}: burial rate	$\delta_{\mathrm{bur}} = 10^{-5}$	$[d^{-1}]$
Carbonate System Variables		
C_{DIC}: dissolved inorganic carbon concentration	$R_{\mathrm{DIC}} = \frac{1}{\mathrm{REDF_{C:O_2}}}\left(\sum_{i=1}^{2} \mu_i C_{Z_i} + \epsilon_{\mathrm{DOC}} C_{\mathrm{DOC}} + \epsilon_{\mathrm{POC}} C_{\mathrm{POC}} - \sum_{j=1}^{3} \sigma_j \beta_{\mathrm{T_j}} \Phi_{P_j} C_{P_j} - E_{\mathrm{DOC}}\right) + \frac{1}{\mathrm{REDF_{C:O_2}}}\left[\frac{\theta(O_2)(2\epsilon_{\mathrm{Sed.Ox}} C_{\mathrm{Sed.POC}})}{dz}\right]_{n_z=0} +$	$[mmol\ C\ m^{-3}]$

	$\frac{1}{\mathrm{REDF_{C:O_2}}}\left[\frac{\theta(-O_2)(\epsilon_{\mathrm{Sed.Anox}}C_{\mathrm{Sed.POC}})}{dz}\right]_{n_z=0}$	
C_{TA}: total alkalinity	$R_{\mathrm{TA}} = \frac{R^*_{\mathrm{NH_4}} - R^*_{\mathrm{NO_3}}}{\mathrm{REDF_{C:O_2}REDF_{C:N}}} - 0.5 \times \theta(-\mathrm{O_2})R_{\mathrm{O_2}} - \frac{R^*_{\mathrm{PO_4}}}{\mathrm{REDF_{C:O_2}REDF_{C:P}}} + \mathrm{BottomTA}$ where terms with * exclude surface and bottom exchange fluxes	$[mmol\ m^{-3}]$
BottomTA: benthic-pelagic total alkalinity exchange flux	$\mathrm{BottomTA} = \left[\frac{\theta(\mathrm{O_2})(\epsilon_{\mathrm{Sed.Ox}}C_{\mathrm{Sed.PON}})}{dz\ \mathrm{REDF_{C:O_2}REDF_{C:N}}}\right]_{n_z} + \left[\frac{\theta(-\mathrm{O_2})(\epsilon_{\mathrm{Sed.Anox}}C_{\mathrm{Sed.PON}})}{dz\ \mathrm{REDF_{C:O_2}REDF_{C:N}}}\right]_{n_z} + \left[\frac{\theta(-\mathrm{O_2})\theta(\mathrm{NO_3})(a_{\mathrm{denit}}\epsilon_{\mathrm{Sed.Anox}}C_{\mathrm{Sed.PON}})}{dz\ \mathrm{REDF_{C:O_2}REDF_{C:N}}}\right]_{n_z} - 0.5 \times \theta(-\mathrm{O_2})\mathrm{BottomO_2}$	$[mmol\ m^{-3}s^{-1}]$

References

Aminot, A. and Kérouel, R.: Dissolved organic carbon, nitrogen and phosphorus in the N-E Atlantic and the N-W Mediterranean with particular reference to non-refractory fractions and degradation, Deep Sea Research Part I: Oceanographic Research Papers, 51, 1975–1999, https://doi.org/10.1016/j.dsr.2004.07.016, 2004.

Blackford, J. C. and Gilbert, F. J.: pH variability and CO2 induced acidification in the North Sea, Journal of Marine Systems, 64, 229–241, https://doi.org/10.1016/j.jmarsys.2006.03.016, 2007.

Børsheim, K. Y., Vadstein, O., Myklestad, S. M., Reinertsen, H., Kirkvold, S., and Olsen, Y.: Photosynthetic algal production, accumulation and release of phytoplankton storage carbohydrates and bacterial production in a gradient in daily nutrient supply, Journal of Plankton Research, 27, 743–755, https://doi.org/10.1093/plankt/fbi047, 2005.

Chaichana, S., Jickells, T., and Johnson, M.: Distribution and C/N stoichiometry of dissolved organic matter in the North Sea in summer 2011-12, Biogeosciences Discuss, 1–33, https://doi.org/10.5194/bg-2017-387, 2017.

Chaichana, S., Jickells, T., and Johnson, M.: Interannual variability in the summer dissolved organic matter inventory of the North Sea: Implications for the continental shelf pump, Biogeosciences, 16, 1073–1096, https://doi.org/10.5194/bg-16-1073-2019, 2019.

Church, M. J., Ducklow, H. W., and Karl, D. M.: Multiyear increases in dissolved organic matter inventories at Station ALOHA in the North Pacific Subtropical Gyre, Limnology and Oceanography, 47, 1–10, https://doi.org/10.4319/lo.2002.47.1.0001, 2002.

Clark, L. L., Ingall, E. D., and Benner, R.: Marine phosphorus is selectively remineralized, Nature, 393, 426–426, https://doi.org/10.1038/30881, 1998.

Daewel, U. and Schrum, C.: Simulating long-term dynamics of the coupled North Sea and Baltic Sea ecosystem with ECOSMO II: Model description and validation, Journal of Marine Systems, 119–120, 30–49, https://doi.org/10.1016/j.jmarsys.2013.03.008, 2013.

Davis, C. E., Mahaffey, C., Wolff, G. A., and Sharples, J.: A storm in a shelf sea: Variation in phosphorus distribution and organic matter stoichiometry, Geophysical Research Letters, 41, 8452–8459, https://doi.org/10.1002/2014GL061949, 2014.

Davis, C. E., Blackbird, S., Wolff, G., Woodward, M., and Mahaffey, C.: Seasonal organic matter dynamics in a temperate shelf sea, Progress in Oceanography, 177, https://doi.org/10.1016/j.pocean.2018.02.021, 2019.

Doval, M. D., Pérez, F. F., and Berdalet, E.: Dissolved and particulate organic carbon and nitrogen in the Northwestern Mediterranean, Deep Sea Research Part I: Oceanographic Research Papers, 46, 511–527, https://doi.org/10.1016/S0967-0637(98)00072-7, 1999.

Engel, A.: Direct relationship between CO2 uptake and transparent exopolymer particles production in natural phytoplankton, Journal of Plankton Research, 24, 49–53, https://doi.org/10.1093/plankt/24.1.49, 2002.

Fajon, C., Cauwet, G., Lebaron, P., Terzic, S., Ahel, M., Malej, A., Mozetic, P., and Turk, V.: The accumulation and release of polysaccharides by planktonic cells and the subsequent bacterial response during a controlled experiment, FEMS Microbiology Ecology, 29, 351–363, https://doi.org/10.1016/S0168-6496(99)00029-X, 1999.

Frigstad, H., Andersen, T., Hessen, D. O., Jeansson, E., Skogen, M., Naustvoll, L.-J., Miles, M. W., Johannessen, T., and Bellerby, R. G. J.: Long-term trends in carbon, nutrients and stoichiometry in Norwegian coastal waters: Evidence of a regime shift, Progress in Oceanography, 111, 113–124, https://doi.org/10.1016/j.pocean.2013.01.006, 2013.

Hansell, D. A. and Carlson, C. A.: Deep-ocean gradients in the concentration of dissolved organic carbon, Nature, 395, 263–266, https://doi.org/10.1038/26200, 1998.

Hoikkala, L., Lahtinen, T., Perttilä, M., and Lignell, R.: Seasonal dynamics of dissolved organic matter on a coastal salinity gradient in the northern Baltic Sea, Continental Shelf Research, 45, 1–14, https://doi.org/10.1016/j.csr.2012.04.008, 2012.

Hoikkala, L., Kortelainen, P., Soinne, H., and Kuosa, H.: Dissolved organic matter in the Baltic Sea, Journal of Marine Systems, 142, 47–61, https://doi.org/10.1016/j.jmarsys.2014.10.005, 2015.

Hopkinson, C. S. and Vallino, J. J.: Efficient export of carbon to the deep ocean through dissolved organic matter, Nature, 433, 142–145, https://doi.org/10.1038/nature03191, 2005.

Hopkinson, C. S., Fry, B., and Nolin, A. L.: Stoichiometry of dissolved organic matter dynamics on the continental shelf of the northeastern U.S.A., 17, 473–489, https://doi.org/10.1016/S0278-4343(96)00046-5, 1997.

Hopkinson, C. S., Vallino, J. J., and Nolin, A.: Decomposition of dissolved organic matter from the continental margin, Deep Sea Research Part II: Topical Studies in Oceanography, 49, 4461–4478, https://doi.org/10.1016/S0967-0645(02)00125-X, 2002.

Huang, J.: A Simple Accurate Formula for Calculating Saturation Vapor Pressure of Water and Ice, Journal of Applied Meteorology and Climatology, 57, 1265–1272, https://doi.org/10.1175/JAMC-D-17-0334.1, 2018.

Humphreys, M. P., Lewis, E. R., Sharp, J. D., and Pierrot, D.: PyCO2SYS v1.8: marine carbonate system calculations in Python, Geoscientific Model Development, 15, 15–43, https://doi.org/10.5194/gmd-15-15-2022, 2022.

Humphreys, M. P., Schiller, A. J., Sandborn, D., Gregor, L., Pierrot, D., van Heuven, S. M. A. C., Lewis, E. R., and Wallace, D. W. R.: PyCO2SYS: marine carbonate system calculations in Python, , https://doi.org/10.5281/zenodo.10671397, 2024.

Hung, J.-J., Chen, C.-H., Gong, G.-C., Sheu, D.-D., and Shiah, F.-K.: Distributions, stoichiometric patterns and cross-shelf exports of dissolved organic matter in the East China Sea, Deep Sea Research Part II: Topical Studies in Oceanography, 50, 1127–1145, https://doi.org/10.1016/S0967-0645(03)00014-6, 2003.

Hung, J.-J., Wang, S.-M., and Chen, Y.-L.: Biogeochemical controls on distributions and fluxes of dissolved and particulate organic carbon in the Northern South China Sea, Deep Sea Research Part II: Topical Studies in Oceanography, 54, 1486–1503, https://doi.org/10.1016/j.dsr2.2007.05.006, 2007.

Kim, T.-H. and Kim, G.: Factors controlling the C:N:P stoichiometry of dissolved organic matter in the N-limited, cyanobacteria-dominated East/Japan Sea, Journal of Marine Systems, 115–116, 1–9, https://doi.org/10.1016/j.jmarsys.2013.01.002, 2013.

Kossack, J., Mathis, M., Daewel, U., Liu, F., Demir, K. T., Thomas, H., and Schrum, C.: Tidal impacts on air-sea CO2 exchange on the North-West European shelf, Front. Mar. Sci., 11, 1406896, https://doi.org/10.3389/fmars.2024.1406896, 2024.

Letscher, R. T. and Moore, J. K.: Preferential remineralization of dissolved organic phosphorus and non-Redfield DOM dynamics in the global ocean: Impacts on marine productivity, nitrogen fixation, and carbon export, Global Biogeochemical Cycles, 29, 325–340, https://doi.org/10.1002/2014GB004904, 2015.

Letscher, R. T., Moore, J. K., Teng, Y.-C., and Primeau, F.: Variable C : N : P stoichiometry of dissolved organic matter cycling in the Community Earth System Model, Biogeosciences, 12, 209–221, https://doi.org/10.5194/bg-12-209-2015, 2015.

Liang, Z., Letscher, R. T., and Knapp, A. N.: Global Patterns of Surface Ocean Dissolved Organic Matter Stoichiometry, Global Biogeochemical Cycles, 37, e2023GB007788, https://doi.org/10.1029/2023GB007788, 2023.

Loh, A. N. and Bauer, J. E.: Distribution, partitioning and fluxes of dissolved and particulate organic C, N and P in the eastern North Pacific and Southern Oceans, Deep Sea Res. Pt. I, 47, 2287–2316, https://doi.org/10.1016/S0967-0637(00)00027-3, 2000.

Lønborg, C. and Álvarez-Salgado, X. A.: Recycling versus export of bioavailable dissolved organic matter in the coastal ocean and efficiency of the continental shelf pump, Global Biogeochemical Cycles, 26, GB3018, https://doi.org/10.1029/2012GB004353, 2012.

Lønborg, C., Carreira, C., Abril, G., Agustí, S., Amaral, V., Andersson, A., Arístegui, J., Bhadury, P., Bif, M. B., Borges, A. V., Bouillon, S., Calleja, M. L., Cotovicz Jr., L. C., Cozzi, S., Doval, M., Duarte, C. M., Eyre, B., Fichot, C. G., García-Martín, E. E., Garzon-Garcia, A., Giani, M., Gonçalves-Araujo, R., Gruber, R., Hansell, D. A., Hashihama, F., He, D., Holding, J. M., Hunter, W. R., Ibánhez, J. S. P., Ibello, V., Jiang, S., Kim, G., Klun, K., Kowalczuk, P., Kubo, A., Lee, C.-W., Lopes, C. B., Maggioni, F., Magni, P., Marrase, C., Martin, P., McCallister, S. L., McCallum, R., Medeiros, P. M., Morán, X. A. G., Muller-Karger, F. E., Myers-Pigg, A., Norli, M., Oakes, J. M., Osterholz, H., Park, H., Lund Paulsen, M., Rosentreter, J. A., Ross, J. D., Rueda-Roa, D., Santinelli, C., Shen, Y., Teira, E., Tinta, T., Uher, G., Wakita, M., Ward, N., Watanabe, K., Xin, Y., Yamashita, Y., Yang, L., Yeo, J., Yuan, H., Zheng, Q., and Álvarez-Salgado, X. A.: A global database of dissolved organic matter (DOM) concentration measurements in coastal waters (CoastDOM v1), Earth System Science Data, 16, 1107–1119, https://doi.org/10.5194/essd-16-1107-2024, 2024.

Lucea, A., Duarte, C. M., Agustí, S., and Søndergaard, M.: Nutrient (N, P and Si) and carbon partitioning in the stratified NW Mediterranean, Journal of Sea Research, 49, 157–170, https://doi.org/10.1016/S1385-1101(03)00005-4, 2003.

Martiny, A. C., Vrugt, J. A., and Lomas, M. W.: Concentrations and ratios of particulate organic carbon, nitrogen, and phosphorus in the global ocean, Sci Data, 1, 140048, https://doi.org/10.1038/sdata.2014.48, 2014.

Nausch, M., Nausch, G., Wasmund, N., and Nagel, K.: Phosphorus pool variations and their relation to cyanobacteria development in the Baltic Sea: A three-year study, Journal of Marine Systems, 71, 99–111, https://doi.org/10.1016/j.jmarsys.2007.06.004, 2008.

Neumann, T., Radtke, H., Cahill, B., Schmidt, M., and Rehder, G.: Non-Redfieldian carbon model for the Baltic Sea (ERGOM version 1.2) – implementation and budget estimates, Geosci. Model Dev., 15, 8473–8540, https://doi.org/10.5194/gmd-15-8473-2022, 2022.

Osterholz, H., Burmeister, C., Busch, S., Dierken, M., Frazão, H. C., Hansen, R., Jeschek, J., Kremp, A., Kreuzer, L., Sadkowiak, B., Waniek, J. J., and Schulz-Bull, D. E.: Nearshore Dissolved and Particulate Organic Matter Dynamics in the Southwestern Baltic Sea: Environmental Drivers and Time Series Analysis (2010–2020), Frontiers in Marine Science, 8:795028, https://doi.org/10.3389/fmars.2021.795028, 2021.

Painter, S. C., Hartman, S. E., Kivimäe, C., Salt, L. A., Clargo, N. M., Daniels, C. J., Bozec, Y., Daniels, L., Allen, S., Hemsley, V. S., Moschonas, G., and Davidson, K.: The elemental stoichiometry (C, Si, N, P) of the Hebrides Shelf and its role in carbon export, Progress in Oceanography, 159, 154–177, https://doi.org/10.1016/j.pocean.2017.10.001, 2017.

Painter, S. C., Lapworth, D. J., Woodward, E. M. S., Kroeger, S., Evans, C. D., Mayor, D. J., and Sanders, R. J.: Terrestrial dissolved organic matter distribution in the North Sea, Science of The Total Environment, 630, 630–647, https://doi.org/10.1016/j.scitotenv.2018.02.237, 2018.

Pujo-Pay, M., Conan, P., Oriol, L., Cornet-Barthaux, V., Falco, C., Ghiglione, J.-F., Goyet, C., Moutin, T., and Prieur, L.: Integrated survey of elemental stoichiometry (C, N, P) from the western to eastern Mediterranean Sea, Biogeosciences, 8, 883–899, https://doi.org/10.5194/bg-8-883-2011, 2011.

Raimbault, P., Pouvesle, W., Diaz, F., Garcia, N., and Sempéré, R.: Wet-oxidation and automated colorimetry for simultaneous determination of organic carbon, nitrogen and phosphorus dissolved in seawater, Marine Chemistry, 66, 161–169, https://doi.org/10.1016/S0304-4203(99)00038-9, 1999.

Redfield, A. C.: The influence of organisms on the composition of seawater, The sea, 2, 26–77, 1963.

Rowe, O. F., Dinasquet, J., Paczkowska, J., Figueroa, D., Riemann, L., and Andersson, A.: Major differences in dissolved organic matter characteristics and bacterial processing over an extensive brackish water gradient, the Baltic Sea, Marine Chemistry, 202, 27–36, https://doi.org/10.1016/j.marchem.2018.01.010, 2018.

Santinelli, C., Ibello, V., Lavezza, R., Civitarese, G., and Seritti, A.: New insights into C, N and P stoichiometry in the Mediterranean Sea: The Adriatic Sea case, Continental Shelf Research, 44, 83–93, https://doi.org/10.1016/j.csr.2012.02.015, 2012.

Singh, A., Baer, S. E., Riebesell, U., Martiny, A. C., and Lomas, M. W.: C : N : P stoichiometry at the Bermuda Atlantic Time-series Study station in the North Atlantic Ocean, Biogeosciences, 12, 6389–6403, https://doi.org/10.5194/bg-12-6389-2015, 2015.

Søndergaard, M., Williams, P. J. le B., Cauwet, G., Riemann, B., Robinson, C., Terzic, S., Woodward, E. M. S., and Worm, J.: Net accumulation and flux of dissolved organic carbon and dissolved organic nitrogen in marine plankton communities, Limnology and Oceanography, 45, 1097–1111, https://doi.org/10.4319/lo.2000.45.5.1097, 2000.

Stepanauskas, R., JØrgensen, N. O. G., Eigaard, O. R., Žvikas, A., Tranvik, L. J., and Leonardson, L.: Summer Inputs of Riverine Nutrients to the Baltic Sea: Bioavailability and Eutrophication Relevance, Ecological Monographs, 72, 579–597, https://doi.org/10.1890/0012-9615(2002)072[0579:SIORNT]2.0.CO;2, 2002.

Suratman, S., Weston, K., Jickells, T., and Fernand, L.: Spatial and seasonal changes of dissolved and particulate organic C in the North Sea, Hydrobiologia, 628, 13–25, https://doi.org/10.1007/s10750-009-9730-z, 2009.

Tanioka, T., Matsumoto, K., and Lomas, M. W.: Drawdown of Atmospheric pCO2 Via Variable Particle Flux Stoichiometry in the Ocean Twilight Zone, Geophysical Research Letters, 48, e2021GL094924, https://doi.org/10.1029/2021GL094924, 2021.

Tanioka, T., Larkin, A. A., Moreno, A. R., Brock, M. L., Fagan, A. J., Garcia, C. A., Garcia, N. S., Gerace, S. D., Lee, J. A., Lomas, M. W., and Martiny, A. C.: Global Ocean Particulate Organic Phosphorus, Carbon, Oxygen for Respiration, and Nitrogen (GO-POPCORN), Sci Data, 9, 688, https://doi.org/10.1038/s41597-022-01809-1, 2022.

Thomas, H., Ittekkot, V., Osterroht, C., and Schneider, B.: Preferential recycling of nutrients—the ocean's way to increase new production and to pass nutrient limitation?, Limnology and Oceanography, 44, 1999–2004, https://doi.org/10.4319/lo.1999.44.8.1999, 1999.

Voss, M., Asmala, E., Bartl, I., Carstensen, J., Conley, D. J., Dippner, J. W., Humborg, C., Lukkari, K., Petkuviene, J., Reader, H., Stedmon, C., Vybernaite-Lubiene, I., Wannicke, N., and Zilius, M.: Origin and fate of dissolved organic matter in four shallow Baltic Sea estuaries, Biogeochemistry, 154, 385–403, https://doi.org/10.1007/s10533-020-00703-5, 2021.

Williams, P. M., Carlucci, A. F., and Olson, R.: A deep profile of some biologically important properties in the central North Pacific gyre, Oceanologica Acta, 3, 471–476, https://archimer.ifremer.fr/doc/00122/23291/21119.pdf, 1980.

Winogradow, A., Mackiewicz, A., and Pempkowiak, J.: Seasonal changes in particulate organic matter (POM) concentrations and properties measured from deep areas of the Baltic Sea, Oceanologia, 61, 505–521, https://doi.org/10.1016/j.oceano.2019.05.004, 2019.

Appendix C: *Article* III

This appendix contains the following article currently under review in Global Biogeochemical Cycles:

Demir, K. T., Mathis, M., Kossack, J., Liu, F., Daewel, U., Stegert, C., Thomas, H., and Schrum, C. (2025a). Organic matter stoichiometry regulates the continental shelf carbon pump efficiency of the northwest European shelf seas. ESS Open Archive [Preprint]. Submitted to *Global Biogeochemical Cycles* (*under review*), doi: 10.22541/essoar.175088438.85557149/v1

The author contributions of Kubilay Timur Demir (KTD) and others to this paper are as follows:

KTD was responsible for the conceptualization of the study, while the methodology was developed collaboratively by KTD, MM, JK, and CSc. Software development was undertaken by KTD, JK, FL, and CSt, with the validation carried out by KTD, JK, and FL. KTD performed the formal analysis, and the investigation was conducted by KTD, MM, CSc, and HT. MM and CSc provided the necessary resources, and data curation was managed by KTD. The original draft of the manuscript was prepared by KTD, and subsequent writing, review, and editing were contributed by KTD, MM, JK, FL, UD, CSt, HT, and CSc. KTD also took responsibility for visualization. Supervision of the project was provided by MM, UD, HT, and CSc. Finally, CSc handled the project administration and funding acquisition.

Organic matter stoichiometry regulates the continental shelf carbon pump efficiency of the northwest European shelf seas

Kubilay Timur Demir[1], Moritz Mathis[1], Jan Kossack[1], Feifei Liu[1], Ute Daewel[2], Christoph Stegert[3], Helmuth Thomas[4], and Corinna Schrum[1]

[1]Helmholtz-Zentrum Hereon
[2]Helmholtz Centre Hereon
[3]Bundesamt für Seeschifffahrt und Hydrographie
[4]Institute of Carbon Cycles, Helmholtz-Zentrum Hereon, Geesthacht, Germany

June 25, 2025

Abstract

Variations in the elemental C:N:P ratios of organic matter (OM) influence carbon cycling and the coupling of carbon and nutrient cycles in the global coastal and open oceans. In this study, we assess the relevance of OM stoichiometry for regional carbon cycling in the northwest European shelf seas (NWES), with a focus on the efficiency of the continental shelf carbon pump mechanism. We incorporate two pathways for variable OM stoichiometry into the coupled regional physical-biogeochemical modeling system SCHISM-ECOSMO-CO2: the extracellular release of carbon-enriched dissolved organic matter under nutrient limitation and the preferential remineralization of organic nitrogen and phosphorus over carbon. Observational and experimental evidence demonstrate that these mechanisms enhance nutrient recycling, new production, and carbon fixation beyond nutrient co-limitation. We assess the changes in both the organic and inorganic carbon budgets of the NWES and link the previously demonstrated increase in CO2 uptake of approximately 10–30% through intensified OM cycling to a proportionate increase in the subsequent export of dissolved inorganic carbon. Depending on the relative contribution of the two mechanisms, roughly 60–90% of the additional CO2 uptake is exported across the shelf break, primarily via the Norwegian Trench. In contrast, the organic carbon budget shows smaller and more variable contributions in time. These results demonstrate that OM stoichiometry regulates the efficiency of the continental shelf carbon pump mechanism in the NWES. Our study emphasizes the importance of OM stoichiometry for carbon fluxes and export in the coastal and open oceans, highlighting its impact on regional and global carbon cycling.

Organic matter stoichiometry regulates the continental shelf carbon pump efficiency of the northwest European shelf seas

K. T. Demir[1], M. Mathis[1], J. Kossack[1], F. Liu[1], U. Daewel[1], C. Stegert[2], H. Thomas[3,4] and C. Schrum[1,5]

[1]Institute of Coastal Systems—Analysis and Modeling, Helmholtz-Zentrum Hereon, Geesthacht, Germany

[2]Bundesamt für Seeschifffahrt und Hydrographie, Hamburg, Germany

[3]Institute of Carbon Cycles, Helmholtz-Zentrum Hereon, Geesthacht, Germany

[4]Institute for Chemistry and Biology of the Marine Environment, Carl von Ossietzky University of Oldenburg, Oldenburg, Germany

[5]Institute of Oceanography, University of Hamburg, Hamburg, Germany

Corresponding author: Kubilay Timur Demir (Kubilay.Demir@hereon.de)

Key Points:

- The efficiency of carbon export in the northwest European shelf seas is regulated by the C:N:P stoichiometry of organic matter.
- Preferential remineralization of organic N and P, and carbon-enriched DOM release enhance CO_2 uptake by approximately 10–30%.
- Roughly 60–90% of the additional CO_2 uptake is exported as DIC across the shelf break, primarily via the Norwegian Trench.

Abstract

Variations in the elemental C:N:P ratios of organic matter (OM) influence carbon cycling and the coupling of carbon and nutrient cycles in the global coastal and open oceans. In this study, we assess the relevance of OM stoichiometry for regional carbon cycling in the northwest European shelf seas (NWES), with a focus on the efficiency of the continental shelf carbon pump mechanism. We incorporate two pathways for variable OM stoichiometry into the coupled regional physical-biogeochemical modeling system SCHISM-ECOSMO-CO_2: the extracellular release of carbon-enriched dissolved organic matter under nutrient limitation and the preferential remineralization of organic nitrogen and phosphorus over carbon. Observational and experimental evidence demonstrate that these mechanisms enhance nutrient recycling, new production, and carbon fixation beyond nutrient co-limitation. We assess the changes in both the organic and inorganic carbon budgets of the NWES and link the previously demonstrated increase in CO_2 uptake of approximately 10–30% through intensified OM cycling to a proportionate increase in the subsequent export of dissolved inorganic carbon. Depending on the relative contribution of the two mechanisms, roughly 60–90% of the additional CO_2 uptake is exported across the shelf break, primarily via the Norwegian Trench. In contrast, the organic carbon budget shows smaller and more variable contributions in time. These results demonstrate that OM stoichiometry regulates the efficiency of the continental shelf carbon pump mechanism in the NWES. Our study emphasizes the importance of OM stoichiometry for carbon fluxes and export in the coastal and open oceans, highlighting its impact on regional and global carbon cycling.

Plain Language Summary

Variations in the ratios of carbon, nitrogen, and phosphorus in marine organic matter influence carbon cycling in the northwest European shelf seas. This study builds on previous findings, linking the 10–30% increase in carbon dioxide uptake to an increased export of dissolved inorganic carbon across the shelf break. Approximately 60–90% of the additional CO_2 uptake is exported, primarily via the Norwegian Trench. The results show that these changes in the

elemental composition of organic matter regulate the efficiency of carbon export, demonstrating its relevance for regional and global carbon cycles.

1 Introduction

The global coastal ocean acts as a sink for atmospheric CO_2, primarily through the export of carbon via advective transport to the deep ocean and burial of particulate organic carbon (POC) in sediments (Bauer et al., 2013; Chen & Borges, 2009; Dai et al., 2022; Laruelle et al., 2014, 2018; Resplandy et al., 2024; Roobaert et al., 2019; Roobaert, Resplandy, et al., 2024). Observational reconstructions and model assessments suggest that it has shifted from a pre-industrial source of CO_2 to a contemporary, increasing sink (Bauer et al., 2013; Laruelle et al., 2018), driven by rising atmospheric CO_2 concentrations, climate-driven changes in circulation, and increased terrestrial nutrient inputs (Lacroix et al., 2021; Mathis et al., 2024). Uptake is strongest at temperate and high latitudes, where changes in temperature and net community production (NCP), which represents the difference between carbon fixation and respiration, cause large seasonal variations (Dai et al., 2022; Resplandy et al., 2024; Roobaert et al., 2019). While positive NCP, and an advective export of accumulated organic carbon (OC) primarily drive the increasing CO_2 sequestration in the global coastal ocean (Mathis et al., 2024), the dominant pathways for regional carbon export are varied and depend on both biogeochemical and physical processes (Bauer et al., 2013; Dai et al., 2022; Roobaert et al., 2019; Roobaert, Resplandy, et al., 2024).

In particular, the northwest European shelf seas (NWES) efficiently export atmospheric CO_2 to the northeastern Atlantic Ocean through the continental shelf carbon pump mechanism (Holt et al., 2009; Legge et al., 2020; Thomas et al., 2004, 2005; Wakelin et al., 2012). In the seasonally stratified northern North Sea, the separation between surface organic matter (OM) production and sub-surface respiration generates a seasonal vertical gradient in dissolved inorganic carbon (DIC). Positive NCP at the surface results in net carbon fixation and DIC consumption, while negative NCP below the surface layer results in net carbon respiration and DIC release at depth (Thomas et al., 2004). This vertical DIC gradient, combined with the regional circulation

77 characterized by net on-shelf transport of surface waters low in DIC, and off-shelf transport of
78 DIC-rich waters at depth, drives the net DIC export across the shelf edge (Holt et al., 2009;
79 Thomas et al., 2004; Wakelin et al., 2012). DIC export is further fueled by river and Baltic Sea
80 discharge, and net heterotrophy, where imported organic carbon from cross-shelf transport is
81 respired, further adding DIC to the system (Thomas et al., 2005). A smaller contribution to carbon
82 sequestration is attributed to POC export to sediments, primarily in the Norwegian Trench, the
83 Skagerrak, and along the shelf edge (de Haas et al., 2002; Legge et al., 2020; Thomas et al., 2005).
84 However, the magnitude of this contribution is uncertain, strongly regionally variable, and is likely
85 to become more significant when considering centennial or millennial time scales (Diesing et al.,
86 2017, 2021; de Haas et al., 1997, 2002; Legge et al., 2020; Müller et al., 2025; Thomas et al.,
87 2005).

88 A major uncertainty in quantifying the efficiency of oceanic carbon sequestration and export
89 fluxes is the C:N:P stoichiometry of marine OM in its production and decomposition (Hopkinson
90 & Vallino, 2005). The balance between OM production and respiration regulates carbon
91 transformation and transports (del Giorgio & Duarte, 2002; Hansell et al., 2009), with its
92 stoichiometry controlling the coupling between carbon and nutrient cycles (Hopkinson & Vallino,
93 2005). Despite strong observational evidence for substantial variations in elemental C:N:P ratios
94 of dissolved (DOM) and particulate organic matter (POM), with differences across fractions of
95 size and lability (Aminot & Kérouel, 2004; Clark et al., 1998; Hopkinson & Vallino, 2005; Liang et
96 al., 2023; Loh & Bauer, 2000; Martiny et al., 2013; Tanioka et al., 2022), many biogeochemical
97 models constrain all represented OM pools to elemental Redfield ratios of C:N:P=106:16:1 or
98 similar (Redfield, 1958, 1963).

99 As a result, carbon fixation is often underestimated, particularly during nutrient limitation in late
100 summer, which manifests as a deficiency in representing the seasonality of DIC concentrations
101 and partial pressure of CO_2 (pCO_2) in surface waters (Anderson & Pondaven, 2003; Bozec et al.,
102 2006; Fransner et al., 2018; Kähler & Koeve, 2001; Prowe et al., 2009). This underestimation has
103 been linked to an underrepresentation of new production and the export of DOC and POC to sub-
104 surface waters, due to the omission of increasing carbon content of OM with depth. The failure

105 to account for the variable quality of exported DOM (Anderson & Pondaven, 2003; Hopkinson &
106 Vallino, 2005; Letscher & Moore, 2015) and POM (Anderson & Pondaven, 2003; Matsumoto,
107 Tanioka, et al., 2020; Osterroht & Thomas, 2000; Schneider et al., 2004; Tanioka et al., 2021;
108 Thomas et al., 1999; P. M. Williams et al., 1980) has been highlighted as a major inconsistency of
109 the Redfield stoichiometry assumption. Accounting for the observed OM stoichiometry is
110 therefore crucial for more accurately representing vertical carbon export and the coupling of
111 biogeochemical cycles, including the regional carbon and nutrient budgets of the NWES (Bozec
112 et al., 2006; Kühn et al., 2010; Prowe et al., 2009; Thomas et al., 1999).

113 For the global ocean, Earth system models show that considering globally observed carbon-
114 enrichment in DOM and POM compared to Redfield ratio-based estimates, through a preferential
115 recycling of nutrients or flexible phytoplankton stoichiometry, enhances carbon and nitrogen
116 fixation, export production, and the drawdown of inorganic carbon (Letscher et al., 2015;
117 Letscher & Moore, 2015; Liang et al., 2025; Matsumoto, Tanioka, et al., 2020; Sullivan et al., 2024;
118 Tanioka et al., 2021; Teng et al., 2014). Yet, the regional impact on coastal seas and its
119 spatiotemporal variability remain uncertain, largely due to insufficient measurements and
120 limited consideration in regional assessments (Aricò et al., 2021). Some previous studies have
121 addressed carbon fixation beyond elemental Redfield ratios in the North and Baltic Seas
122 (Butenschön et al., 2016; Fransner et al., 2018; Kühn et al., 2010; Lorkowski et al., 2012; Neumann
123 et al., 2022; Prowe et al., 2009). However, a comprehensive assessment of the implications of
124 variable stoichiometry in both production and respiration of OM for carbon cycling in the NWES,
125 including regional and interannual variability, is still lacking. Considering variable OM
126 stoichiometry in model-based carbon budget estimates is crucial for quantifying the efficiency of
127 the continental shelf carbon pump of the NWES, potentially altering both the estimated CO_2
128 uptake and carbon export fluxes to the open ocean.

129 In a first comprehensive assessment of the implications of variable OM stoichiometry on carbon
130 cycling in the NWES, Demir et al. (2025) demonstrated that incorporating two pathways for
131 variable organic matter stoichiometry into a regional biogeochemical modeling system for the
132 NWES resulted in a 9–31% increase in annual CO_2 uptake, with the seasonal maximum shifting

toward the spring and summer months. These new implementations accounted for the extracellular release of carbon-enriched DOM under nutrient limitation (Børsheim et al., 2005; Carlson et al., 2024; Fajon et al., 1999; Myklestad, 1995; Søndergaard et al., 2000; Thornton, 2014; Wear, Carlson, James, et al., 2015; Wear, Carlson, Windecker, et al., 2015; P. J. Williams, 1995), and the preferential remineralization of organic nitrogen and phosphorus (Clark et al., 1998; Hach et al., 2020; Hopkinson et al., 1997, 2002; Loh & Bauer, 2000; Lønborg & Álvarez-Salgado, 2012; Thomas et al., 1999; P. M. Williams et al., 1980). Under consideration of these two processes, the model showed an intensification of OM cycling, which strengthened the seasonal vertical and lateral gradients in NCP. This resulted in higher net autotrophy in surface waters and greater net heterotrophy in sub-surface layers, thereby enhancing the biological drawdown of CO_2, and the resulting oceanic CO_2 uptake. Furthermore, the maximum uptake was shifted from winter to spring and summer. The additional CO_2 uptake was particularly pronounced in the Norwegian Trench, suggesting a potential increase in cross-shelf DIC export.

This study extends this assessment of the impact of variable OM stoichiometry on carbon cycling in the NWES, based on the SCHISM-ECOSMO-CO_2 coupled modeling system, with the experimental setup and configurations inherited from Demir et al. (2025). As a first step, we evaluate net volume fluxes across individual shelf break sections, in comparison to previous studies on cross-shelf exchanges (Graham et al., 2018; Holt et al., 2009, 2018; Huthnance et al., 2009, 2022), to validate the basis for the resulting tracer fluxes. From there, we establish the organic and inorganic carbon budgets by evaluating net tracer exchanges across the shelf edge of the NWES with the North Atlantic and net exchanges with the Baltic Sea, along with benthic-pelagic coupling and trends in carbon stocks, which were not addressed in the previous study. We compare the differences in export fluxes between model configurations to identify the dominant mechanisms enabling the additional CO_2 uptake. To evaluate the consistency of these changes in carbon export over time, we examine their interannual variability. Ultimately, we aim to understand how changes in OM stoichiometry influence the carbon sequestration and export efficiency of the continental shelf carbon pump, which controls the amount of DIC exported from the NWES to the intermediate and deep waters of the Atlantic Ocean. There, it may be temporarily stored out of contact with the atmosphere for durations limited by, but likely far

below the ocean mixing timescale, which is estimated at up to 800 years in the deep waters of the Atlantic Ocean (DeVries & Primeau, 2011). This work builds on earlier global findings on the role of OM stoichiometry in carbon cycling and vertical export, highlighting regional variability in its impact depending on the dominant regional carbon export pathways.

2 Materials and Methods

2.1 SCHISM-ECOSMO-CO_2 Modeling System

The SCHISM-ECOSMO-CO_2 modeling system integrates three-dimensional hydrodynamics, biogeochemical processes, and carbonate system dynamics, all coupled through the Framework for Aquatic Biogeochemical Models (Bruggeman & Bolding, 2014). This approach, as detailed in Demir et al. (2025) and Kossack et al. (2023, 2024), enables the simulation of ecosystem and carbon dynamics in response to variable physical forcing conditions, as well as the influence of OM cycling and the physical state on the carbonate system dynamics and air-sea CO_2 exchange.

The hydrodynamic component is based on the SCHISM model (Zhang, Stanev, et al., 2016; Zhang, Ye, et al., 2016), which efficiently resolves 3D-baroclinic ocean circulation across a wide range of scales and depths, from shallow regions like the southern North Sea to the eddying regime of the deep Atlantic Ocean (Ye et al., 2019). The physical grid and forcing configuration for this study, based on the NWES-LR setup from Kossack et al. (2023, 2024), utilizes SCHISM's unstructured triangular horizontal grid, Localized Sigma Coordinates with shaved cells (LSC^2) for vertical resolution, and a third-order finite volume transport scheme built upon the Weighted Essentially Non-Oscillatory (WENO) formalism (Ye et al., 2019). This allows for the accurate representation of cross-shelf transports, mesoscale eddies, and the complex topography of regions such as the Norwegian Trench and the Skagerrak. The model domain spans 40° to 66°N and 20°W to 30°E, covering the NWES, Baltic Sea, and northeastern Atlantic. All model configurations simulate the period from 1995 to 2010 with a time step of 200 seconds, with the first five years treated as a spin-up period. The horizontal resolution ranges from 4.5 km to 10 km on the shelf, and up to 15 km in the Atlantic, totaling 140,152 grid elements and up to 53 vertical layers. As such, it

efficiently captures physical processes such as bottom and slope currents, which are critical for the representation of tracer transports and benthic-pelagic coupling.

The lower-trophic-level ecosystem model, ECOSMO II (Daewel & Schrum, 2013, 2017; Schrum, Alekseeva, et al., 2006; Schrum, John, et al., 2006), simulates nutrient cycles (phosphorus, nitrogen, silicon, and oxygen), phytoplankton, zooplankton, and detritus in the pelagic zone and a surface sediment layer. It includes three functional groups of phytoplankton (flagellates, diatoms, and cyanobacteria), with diatoms additionally limited by silicate and cyanobacteria capable of fixing nitrogen from the atmosphere. There are two functional zooplankton groups with herbivorous and omnivorous feeding behaviors. The model differentiates detritus into POM, DOM, and biogenic opal, each with its own remineralization and sediment dynamics. Simulated DOM represents a combination of the seasonally produced and decomposed labile and semi-labile fractions, characterized by turnover times ranging from hours to weeks and months to years, respectively, with highest concentrations in surface waters. It excludes refractory DOM, which sequesters carbon over centennial to millennial timescales and contributes to vertically uniform background concentrations throughout the water column (Dittmar et al., 2021; Hansell, 2013; Nagata, 2008). Benthic remineralization releases DIC and silicate, with nitrogen and phosphorus release depending on oxygen conditions, allowing for the representation of sediment processes such as denitrification under varying oxygen levels. With the recent extension in Demir et al. (2025), pelagic and benthic particulate organic carbon (POC), nitrogen (PON), and phosphorus (POP), as well as pelagic dissolved organic carbon (DOC), nitrogen (DON), and phosphorus (DOP), are now treated as independent state variables to enable the representation of observed variations in OM stoichiometry.

ECOSMO II further prognostically calculates DIC and total alkalinity (TA) as required inputs for the carbonate system model, following Blackford & Gilbert (2007). DIC is taken up by biological carbon fixation and released through OM remineralization and zooplankton excretion. Changes in TA result from biological uptake and release of nitrate, ammonium, and phosphate, as described by Wolf-Gladrow (2007) and Gustafsson (2013). Using DIC and TA, the carbonate system model diagnostically estimates the speciation of DIC into carbonic acid, bicarbonate, and

carbonate ions under equilibrium conditions based on the HALTAFALL algorithm for equilibrium mixtures (Ingri et al., 1967), and subsequently calculates pCO_2 and pH. Finally, air-sea exchange is calculated depending on the difference in atmospheric and oceanic pCO_2, along with wind speed, following the parameterization of Wanninkhof (2014). A comprehensive description of the modeling system, configuration, and carbonate system validation can be found in to Demir et al. (2025) and Kossack et al. (2023, 2024).

2.2 Variable organic matter stoichiometry in ECOSMO

The extended ECOSMO II formulation accounts for variability in DOM and POM stoichiometry through two key pathways: first, the extracellular release of carbon-enriched DOM under nutrient limitation, with an associated particle aggregation linked to transparent exopolymer particles (TEPs), and second, the preferential remineralization of organic nitrogen and phosphorus (Demir et al., 2025). These pathways are based on experimental and observational evidence showing that such processes drive stoichiometric variability and influence carbon and nutrient cycling (Carlson et al., 2024; Hopkinson & Vallino, 2005; Moran, Kujawinski, et al., 2022; Tanioka et al., 2021; Thornton, 2014; Wear, Carlson, Windecker, et al., 2015).

The extracellular release of DOM by phytoplankton is recognized as a significant component of marine primary productivity (Borchard & Engel, 2012; Carlson et al., 2024; Granum et al., 2002; Moran, Ferrer-González, et al., 2022; Moran, Kujawinski, et al., 2022; Mühlenbruch et al., 2018; Obernosterer & Herndl, 1995; Thornton, 2014; Wear, Carlson, Windecker, et al., 2015). Mechanisms of DOM release are commonly classified into passive and active release (Carlson et al., 2024; Thornton, 2014; Wear, Carlson, Windecker, et al., 2015). Passive release involves diffusion across the cell membrane, driven by concentration gradients, and typically yields DOM with a stoichiometry similar to that of the cell interior (Carlson et al., 2024; Thornton, 2014). Active release includes both the production of carbon-rich exopolysaccharides, functioning as a carbon overflow mechanism to dissipate excess energy and maintain internal stoichiometric

241 balance, and the active exudation of DOM that provides extracellular benefits to the cell (Carlson
242 et al., 2024; Mühlenbruch et al., 2018; Thornton, 2014).

243 However, the relative contributions of these pathways and their physiological regulation remain
244 uncertain (Carlson et al., 2024; Mühlenbruch et al., 2018; Thornton, 2014; Wear, Carlson,
245 Windecker, et al., 2015). Estimates of phytoplankton-derived DOM contributions to primary
246 production (percentage extracellular release; PER) vary widely. Some studies report averages of
247 10–20%, with values temporarily reaching up to 80% (Wear, Carlson, James, et al., 2015; Wear,
248 Carlson, Windecker, et al., 2015), while others estimate a lower range of 2–50%, with varying
249 average contributions of 3.7–11.0%, 13%, or 25% based on a collection of studies (Baines & Pace,
250 1991; Borchard & Engel, 2012; Moran, Ferrer-González, et al., 2022; Thornton, 2014).

251 The release of carbohydrate-rich, and thus carbon-rich, DOM by phytoplankton has been widely
252 observed across laboratory cultures, microcosm and mesocosm studies, as well as field
253 measurements during phytoplankton blooms, particularly under nutrient stress (Baines & Pace,
254 1991; Børsheim et al., 2005; Fajon et al., 1999; Granum et al., 2002; Meador & Aluwihare, 2014;
255 Moran, Ferrer-González, et al., 2022; Myklestad, 1995; Obernosterer & Herndl, 1995;
256 Søndergaard et al., 2000; Wear, Carlson, James, et al., 2015). Among the DOM released, some
257 extracellular polymeric substances act as precursors for TEPs (Mari et al., 2017; Passow, 2002),
258 which promote particle aggregation and coagulation. This facilitates the formation of larger
259 particles or aggregates and enhances the sinking and export of POC to sub-surface waters
260 (Borchard & Engel, 2012; Engel, 2002; He et al., 2016; Mari et al., 2017; Thornton, 2014; Verdugo
261 et al., 2004).

262 ECOSMO represents the extracellular release by a direct uptake of DIC and nutrients into DOM
263 under nutrient limitation and the particle formation as a flocculation from DOM to POM, both
264 modified from Neumann et al. (2022). Release rates depend on phytoplankton biomass and
265 nutrient conditions. Under nutrient-replete conditions, carbon fixation is dominated by primary
266 production at Redfield stoichiometry, which is co-limited by nitrogen and phosphorus sources.
267 With increasing limitation of one nutrient source, DOM release for the other nutrient source
268 increases. In the absence of both nitrogen and phosphorus sources, DOM release shifts to DOC

only, consistent with the dependence on nutrient availability described in Myklestad (1995) and Thornton (2014). Any release of DON and DOP also releases DOC, such that total DOM release is always carbon-rich relative to Redfield ratios. Because the release rate scales with phytoplankton biomass, but does not generate new plankton biomass, it eventually declines in the absence of primary production. The rates of DOM flocculation to POM depend on the same limitation functions as the release rate itself.

The preferential remineralization of organic nitrogen and phosphorus with the sequence P > N > C has been widely observed for both DOM and POM (Clark et al., 1998; Hopkinson et al., 1997, 2002; Hopkinson & Vallino, 2005; Loh & Bauer, 2000; Thomas et al., 1999; P. M. Williams et al., 1980). Moreover, experimental evidence further confirms that OM containing nitrogen and phosphorus is more bioavailable than carbon-rich OM (Hach et al., 2020; Lønborg, Álvarez-Salgado, et al., 2009; Lønborg & Álvarez-Salgado, 2012). These findings indicate that neglecting preferential remineralization would lead to underestimates of nutrient recycling, new production, and carbon export (Hach et al., 2020; Lønborg & Álvarez-Salgado, 2012). Global studies have demonstrated its impact on carbon export efficiency (Letscher & Moore, 2015; Tanioka et al., 2021).

In ECOSMO, the preferential remineralization is implemented by assigning higher relative base remineralization rates for nitrogen and phosphorus compared to carbon, reflecting their higher bioavailability. As observed (Hopkinson et al., 2002; Lønborg, Davidson, et al., 2009; Lønborg & Álvarez-Salgado, 2012), the increased bioavailability is assumed to be higher for phosphorus than for nitrogen. For further details on the ecosystem model equations and the implementation of variable stoichiometry, the reader is referred to Demir et al. (2025).

2.3 Model configurations

To assess the individual and combined influence of these two pathways for variable OM stoichiometry, we evaluate four model configurations. The first, which serves as the reference simulation, adheres to Redfield stoichiometry (RS), with equal remineralization rates for carbon, nitrogen, and phosphorus, and carbon fixation only by particulate primary production at Redfield

ratios. The second configuration, termed extracellular release (ER), incorporates the release of carbon-enriched DOM, with a scaling factor of 0.4. The third configuration, termed preferential remineralization (PR), adjusts remineralization rates by increasing nitrogen bioavailability by 60% and phosphorus bioavailability by 100%. The fourth and final configuration, ER&PR, combines both processes, with a scaling factor of 0.2 for the extracellular release, and less increased remineralization rates of +30% for nitrogen and +50% for phosphorus. The parameter choices for the relative remineralization rates and the scaling of the extracellular release for these configurations were developed by Demir et al. (2025) to accurately represent OM concentrations and stoichiometry. The contributions in the combined configurations were reduced accordingly to ensure a consistent OM representation and thus a meaningful comparison between configurations. Since no feedback from biogeochemical to physical processes is considered, all physical variables are equivalent across configurations.

2.4 Cross-shelf transport and budget estimates

To quantify cross-shelf volume and tracer transports for the budget calculations, we used vertically integrated transports through pre-defined transects, across the shelf break toward the North Atlantic and between the North and Baltic Seas, based on SCHISM's internal flux calculations. These transects were defined using integer flux flags, which distinguished the regions in front of and behind the transect, as specified with the xmgredit software tool. For further details, we refer to the SCHISM documentation (Zhang, Ye, et al., 2016). At each 200-second model time step, both positive and negative contributions to volume and tracer fluxes were stored for each transect for evaluating the net volume and tracer transports.

For validating the model's representation of residual circulation and to identify regions particularly sensitive to the effects of variable OM stoichiometry, we divided the shelf break into several sub-sections. Budget estimates are based on long-term means of net volume and tracer transports over the simulation period from 2000 to 2010, with additional calculations of annual mean net cross-shelf transports, averaged over tidally neutral phases (i.e., periods defined by consistent tidal phase cutoffs at the start and end of each year). This avoids biases from incomplete tidal cycles and ensures that residual transport estimates consistently reflect the

integrated effect of circulation over full tidal cycles. To quantify interannual variability in these residual transports, we calculated the standard deviation between annual means.

Cross-compartment fluxes, such as air-sea CO_2 exchange, and benthic-pelagic fluxes, including net deposition, burial, and benthic remineralization of POC, were averaged over the entire simulation period. We assess variability in these fluxes by calculating the standard deviation of annual means. Inputs of DIC from rivers were derived from the forcing data, with the bioavailable fraction of riverine DOC assumed to be rapidly remineralized, and thus directly added to DIC. This approach, as detailed in Demir et al. (2025), was chosen to ensure consistency between model configurations, as the study focuses on variable stoichiometry in the production and respiration of OM in the marine environment, without introducing variability in stoichiometry and lability from terrestrial DOM inputs (Bauer et al., 2013; Bianchi, 2011).

Stocks of DIC and TOC were calculated as 11-year averages. TOC includes detritus as both POC and DOC as well as the biomass from all phytoplankton and zooplankton functional groups. Sedimentary TOC only consists of POC. Pelagic NCP was derived as the average closure term between the DIC and TOC budgets, with the uncertainty expressed as the deviation between the two closure terms. Trends in carbon stocks, including their differences and associated uncertainties, represented by the standard error, were estimated using linear regression based on annual mean stocks.

3 Results and Discussion

3.1 Cross-shelf volume fluxes

As a first step in validating the simulated volume and carbon budgets, we examine the spatial distribution and magnitude of annual net volume transports across individual shelf break sections. In the following, net transports represent the mean sum of on- and off-shelf volume and tracer fluxes over the simulation period as well as annual mean values. In addition, we analyze total net cross-shelf transports, which refer to the total net volume and tracer flux summed across all shelf break sections and represent the net exchange between the NWES and

the Atlantic Ocean. Net exchange through the Skagerrak, connecting the North Sea and Baltic Sea, is accounted for separately.

The simulated vertically-integrated net transports are consistent with the characteristic cyclonic, counterclockwise residual circulation in the North Sea (Fig. 1) (Holt et al., 2018; Huthnance et al., 2009, 2022; Thomas et al., 2005; Winther & Johannessen, 2006). The largest net volume inputs originate from the West Shetland Shelf in the north, contributing 0.40 ± 0.08 Sverdrup (Sv, 1 Sv = 10^6 m^3s^{-1}), and from the Celtic Sea in the southwest, contributing 0.56 ± 0.18 Sv. Smaller net on-shelf contributions, ranging from 0.05 to 0.23 Sv, originate from the Hebrides, Malin, and West Irish Shelves. Most of the net off-shelf transport occurs across the Norwegian Trench, with an export of 1.17 ± 0.13 Sv. In comparison, the Armorican Shelf, with a smaller contribution, shows a net cross-shelf volume export of 0.25 ± 0.12 Sv. Minor additional volume sources include the North Sea-Baltic Sea exchange and river discharge into the NWES, adding 0.010 ± 0.004 Sv and 0.005 Sv, respectively.

Overall, the distribution of net volume transports across the shelf break of the NWES (Fig. 1) aligns well with previous assessments of cross-shelf volume exchange (Holt et al., 2009, 2018; Huthnance et al., 2009, 2022; Thomas et al., 2005; Winther & Johannessen, 2006). The net off-shelf flux across the Norwegian Trench of 1.17 ± 0.13 Sv closely matches the estimate of 1.29 Sv from Huthnance et al. (2009), and falls within the 1.09–1.23 Sv range reported by Graham et al. (2018). Similarly, the off-shelf transport across the Armorican Shelf of 0.25 ± 0.12 Sv aligns with the 0.19 Sv estimate from Huthnance et al. (2009), although it is higher than the estimate from Graham et al. (2018), which ranges from 0.02 Sv off-shelf to 0.07 Sv on-shelf, as evaluated across a southern gate at a fixed latitude. For the remaining shelf edge, from the Celtic Sea to the West Shetland Shelf, the estimated net on-shelf flux of 1.41 ± 0.22 Sv compares well with the 1.40 Sv reported by Huthnance et al. (2009), and the range of 1.02–1.24 Sv provided by Graham et al. (2018), which includes surface, internal, and basal fluxes.

Whereas the northwestern inflow of 0.57 ± 0.15 Sv from the Hebrides and West Shetland Shelves (Fig. 1) is consistent with the estimate of 0.47 Sv in Huthnance et al. (2009), their study identifies the strongest influx along the southwestern edge in the Malin Shelf. In contrast, our estimates

show the strongest influx in the Celtic Sea, indicating a different distribution of inflow along the western shelf break. The net Baltic Sea inflow and river discharge of 0.010 ± 0.004 and 0.005 Sv are slightly lower than the estimates of 0.016 and 0.010 Sv from Thomas et al. (2005), and the estimated net volume input of 0.014 Sv to the Baltic Sea from 1950 to 1990 (Bergström & Carlsson, 1994). This may be due to interannual variability, with the possibility of a climate-driven weakening in North Sea-North Atlantic exchange as suggested by Holt et al. (2018) compared to estimates for or from earlier time periods.

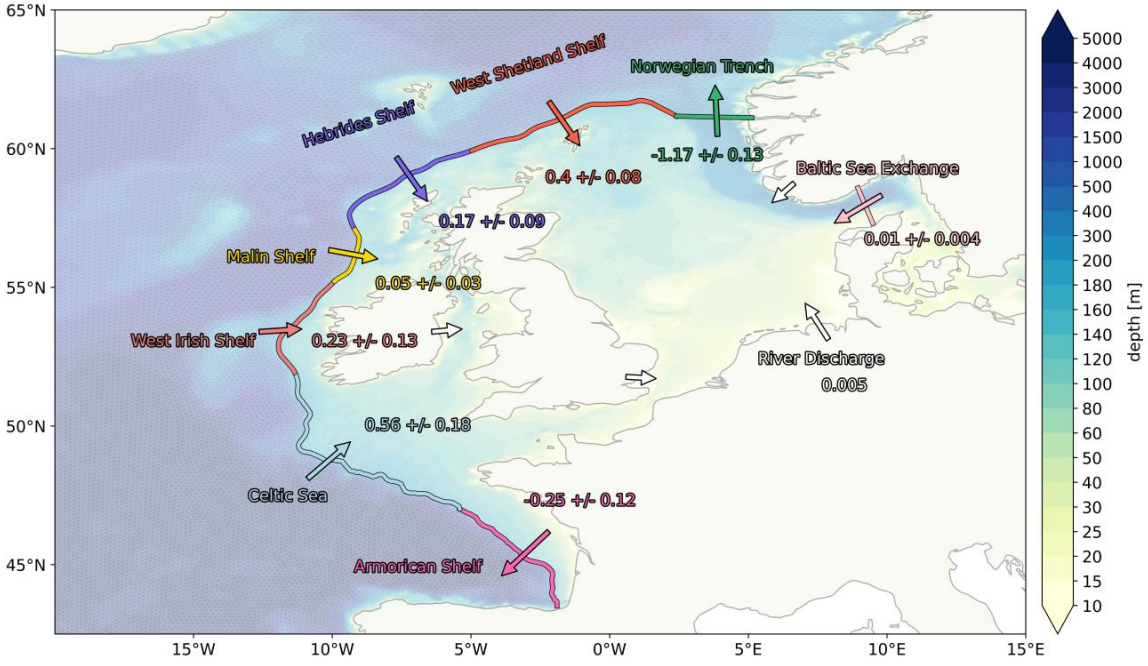

Figure 1. Cross-shelf net volume transports in Sverdrup (Sv, 1 Sv = 10^6 m^3s^{-1}) across shelf break sections of the northwest European shelf seas (NWES) and North Sea-Baltic Sea net volume exchange. All vertically-integrated net transports are presented as 11-year means, with standard deviations between annual means indicating interannual variability. River discharge from continental Europe, Norway, the United Kingdom, and Ireland is indicated by white arrows, but reported as a single total value for the volume budget. Arrow direction indicates net transport

direction, while the colormap shows bathymetry and lines delineate individual triangular grid cells.

While previous studies have emphasized seasonal (Graham et al., 2018) or long-term circulation trends (Holt et al., 2018), we focus here on interannual variability in cross-shelf volume fluxes. This variability is crucial for understanding year-to-year changes in carbon inventories and for identifying regions where fluctuations in circulation may exert the strongest control on carbon flux variability.

Although the overall structure of the residual circulation remains consistent across the simulated period, there are notable interannual variations in the intensity of cross-shelf exchange (Fig. 2). This is reflected by a range of 0.03–0.18 Sv in the standard deviations between annual means across the different subregions (Fig. 1–2). The largest variations in volume exchange, considering both the absolute values of the standard deviation and its relative magnitude compared to the mean, occur in the southwestern inflow and outflow, with 0.12–0.18 Sv or 32–57% variation between the West Irish and Armorican Shelves. In contrast, the West Shetland Shelf and Norwegian Trench exhibit smaller variations of 0.08–0.13 Sv or 11–20%, indicating more stable exchanges between the Northern North Sea and the North Atlantic. The Malin and Hebrides Shelves show a high relative variability of 53–60%, but with smaller absolute changes of 0.03–0.09 Sv, contributing less to the overall exchange with the North Atlantic. A particularly notable finding is the low exchange rates across both the northern and southwestern shelf edges in the final year of the simulation, which may suggest intermittent cross-shelf exchanges, as proposed by Chaichana et al. (2019), and could be a key factor in driving interannual variability in carbon inventories. The net cross-shelf exchange shows considerable fluctuation, with an export of 0.015 ± 0.017 Sv, likely in part controlled by variability in the net North Sea-Baltic Sea exchange.

These cross-shelf volume fluxes, as key physical controls on carbon transport, are consistent across all model configurations, providing a fixed physical state for comparison. This consistency enables us to isolate the effects of both pathways for variable OM stoichiometry, specifically the

preferential remineralization of organic nitrogen and phosphorus, and the release of carbon-enriched DOM, on the organic and inorganic carbon budgets of the NWES.

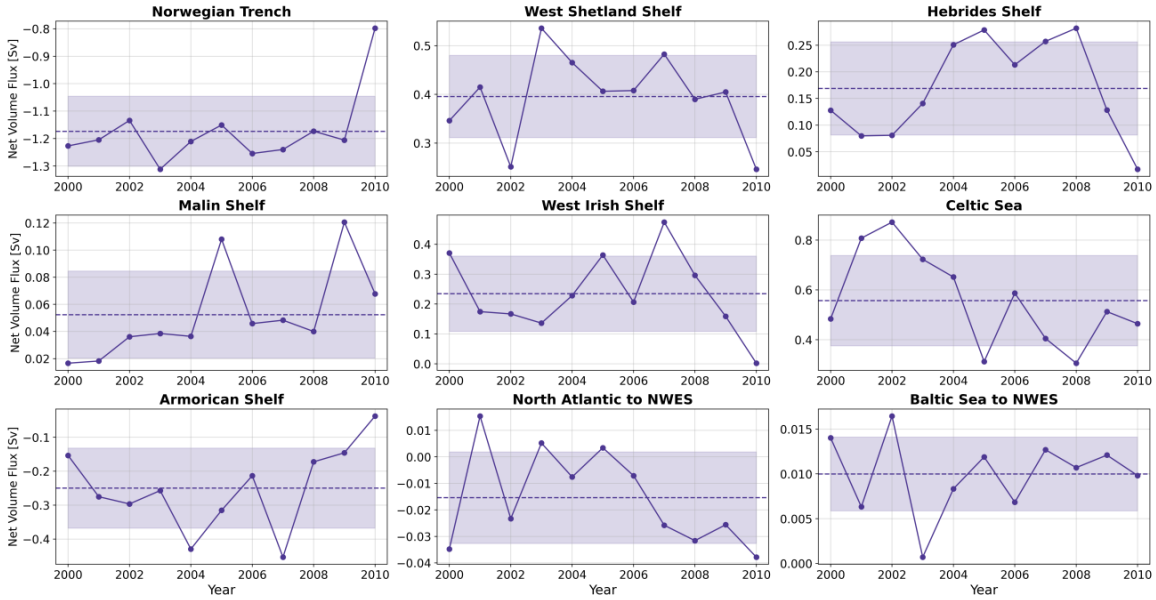

Figure 2. Annual net volume transports across individual shelf break sections of the NWES and net volume exchange with the Atlantic Ocean and the Baltic Sea, shown in Sverdrup (Sv, 1 Sv = 10^6 m^3s^{-1}) over the simulated period from 2000 to 2010. The dashed lines represent the 11-year mean, while the shaded blue areas illustrate the standard deviation between annual means. The volume exchange is only shown for one configuration, as all physical variables are equivalent across configurations.

3.2 Impact on the inorganic carbon budget

Building on the volume transport assessment, we now evaluate how variable OM stoichiometry influences the inorganic carbon budget compared to the Redfield stoichiometry baseline (Fig. 3). In the RS configuration, sources of DIC to the water masses of the NWES include net oceanic CO_2 uptake, contributing 1.105 ± 0.118 Tmol C yr^{-1}, net DIC import from the Baltic Sea, at 0.364 ± 0.238 Tmol C yr^{-1}, river discharge, adding 0.475 Tmol C yr^{-1}, and benthic remineralization, releasing 0.706 ± 0.026 Tmol C yr^{-1}. DIC sinks consist of a net cross-shelf export of 1.850 ± 0.996 Tmol C yr^{-1} and 0.645 Tmol C yr^{-1} taken up by pelagic NCP. The accumulated excess DIC drives a

pelagic DIC trend of 0.153 ± 0.014 Tmol C yr^{-1}, resulting in an increase in the pelagic DIC stock from 245.7 to 247.4 Tmol C between 2000 and 2010 (Fig. 3 and S1). Interannual variability in net DIC export across the shelf edge and import from the Baltic Sea is primarily driven by fluctuations in net volume exchange (Fig. 1 and 2), which likely modulate the net uptake of atmospheric CO_2, alongside changes in the rate of increase in atmospheric concentrations. However, despite these fluctuations, they do not result in a long-term accumulation or removal of DIC on the shelf, as variations in net volume transport must balance out over several years. Consequently, while these short-term variations may affect year-to-year DIC fluxes, they do not alter the long-term DIC trend.

The most significant impact of the variable OM stoichiometry configurations is an increase in the oceanic uptake of CO_2, as shown in Demir et al. (2025), and a resulting increase in the cross-shelf export of DIC (Fig. 3). The amplitude of the additional DIC export varies between 0.060 ± 0.022 and 0.301 ± 0.064 Tmol C between configurations, and largely balances the increase in CO_2 uptake of 0.102 ± 0.016 to 0.339 ± 0.037 Tmol C across configurations. These changes are highest in the ER and lowest in the PR configuration, with an intermediate impact in the combined ER&PR configuration. In contrast, the DIC import from the Baltic Sea increases by 0.005 ± 0.005 to 0.024 ± 0.010 Tmol C yr^{-1}, suggesting a larger reduction in DIC concentrations in the North Sea compared to the Baltic Sea. The introduction of variable OM stoichiometry also enhances the pelagic NCP. The increases of 0.137 ± 0.040 to 0.160 ± 0.076 Tmol C yr^{-1} are almost entirely compensated by increases in benthic remineralization of 0.106 ± 0.006 to 0.139 ± 0.010 Tmol C yr^{-1}, with 0.021 to 0.032 Tmol C yr^{-1} additionally transformed into organic carbon (Fig. 3 and 5). The DIC trend only shows a close to negligible increase of 0.003 ± 0.004 to 0.006 ± 0.005 Tmol C yr^{-1} (Fig. 3 and S1). As differences in the average DIC stocks are only 0.003–0.075 Tmol C, the enhanced CO_2 uptake also compensates for the small additional biological DIC consumption remaining from increasing NCP and benthic remineralization.

Hence, the net impact of variable OM stoichiometry on the inorganic carbon budget is dominated by an increased uptake of CO_2, with the majority subsequently exported across the shelf edge. The consideration of variable C:N:P ratios in the OM representation of our model thus increases

463 the continental shelf carbon pump efficiency of the NWES, with an increase in CO_2 uptake by
464 roughly 10–30%, of which the majority with approximately 60–90% are exported as DIC across
465 the shelf edge. All other net export contributions are of much smaller magnitude and strongly
466 variable.

467 The simulated cross-shelf DIC export of 1.85–2.15 Tmol C yr^{-1} is below the estimated range of
468 3.45–6.4 Tmol C yr^{-1} reported by Legge et al. (2020) in their supplement, based on POLCOMS-
469 ERSEM (Wakelin et al., 2012) and NEMO-ERSEM simulations. This lower estimated DIC export in
470 our simulations likely reflects a combination of the lower oceanic CO_2 uptake of 1.11–1.44 Tmol
471 C yr^{-1}, compared to their reported range of 1.3–3.3 Tmol C yr^{-1}, as well as an underrepresentation
472 of riverine inputs and a lower net DIC import from the Baltic Sea. Notably, the higher estimates
473 range are based on results from Wakelin et al. (2012), which show a combination of stronger
474 seasonal amplitude in NCP, higher net CO_2 uptake, higher terrestrial DIC inputs, and consequently
475 greater DIC export. The large range of estimates on both CO_2 uptake and DIC export

demonstrates the high remaining uncertainty in the strength of the biological pump and resulting carbon export fluxes.

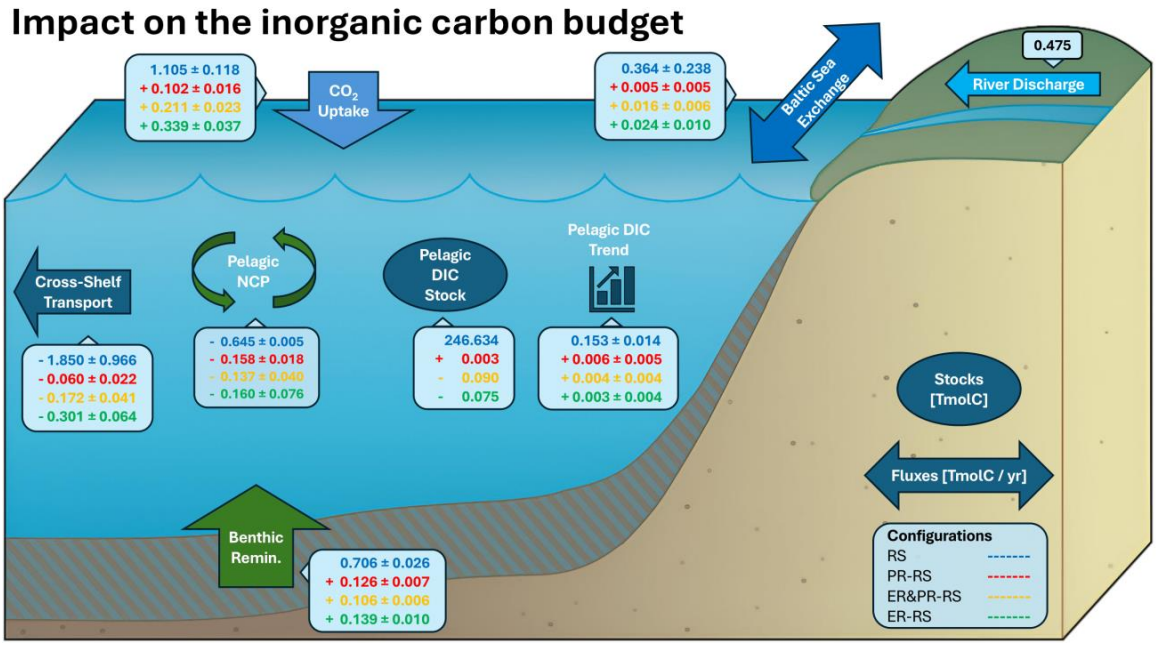

Figure 3. Impacts of variable stoichiometry on the inorganic carbon budget of the NWES. All carbon stocks are shown in Tmol C, and fluxes are provided in Tmol C yr^{-1}. Green arrows indicate the conversion between organic and inorganic carbon. The absolute stocks and fluxes are shown for the Redfield stoichiometry (RS) configuration, with the differences shown for the extracellular release (ER), preferential remineralization (PR), and the combined configuration (ER&PR). The figure background was created in part using modified images from the UMCES IAN Media Library under a Creative Commons license CC BY-SA 4.0.

In addition to the long-term mean of the total cross-shelf exchanges, we examine the contributions of individual shelf break sections to the additional DIC export and their interannual variability. The largest fraction of the additional DIC export occurs through the Norwegian Trench, with 0.040 ± 0.013 to 0.185 ± 0.035 Tmol C yr^{-1} between the PR and ER configurations, respectively (Fig. 4). Across the northwestern shelf break, from the West Shetland Shelf to the West Irish Shelf, there is a consistent overall decrease in DIC imports of 0.022 ± 0.012 Tmol C yr^{-}

492 ^{1} in the PR and 0.135 ± 0.044 Tmol C yr^{-1} in the ER configuration. While there is a net on-shelf
493 volume and hence DIC transport in those regions (Fig. 2 and 4), the concentration-driven export
494 of DIC through its vertical gradient is increased (Demir et al., 2025), thereby decreasing the net
495 on-shelf transport. A small and highly variable increase in net on-shelf DIC transport occurs in the
496 Celtic Sea and Armorican Shelf, with 0.013 ± 0.030 and 0.007 ± 0.013 Tmol C yr^{-1}, respectively, in
497 the ER configuration. Overall, the net contribution to cross-shelf DIC exchange is primarily driven
498 by increased net DIC export across the Norwegian Trench, which accounts for 58–65%, and a
499 decrease in net DIC import across the northern and northwestern shelf edge, accounting for 35–
500 42% of their combined contribution.

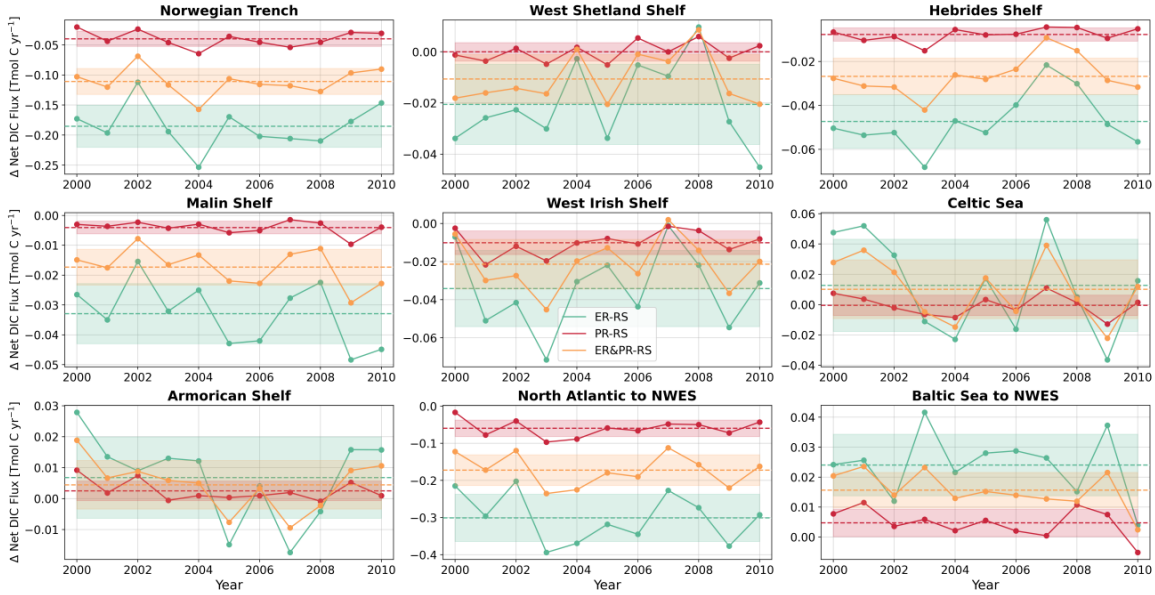

501

502 **Figure 4.** Differences in annual net cross-shelf DIC transports, expressed in Tmol C yr^{-1}, across
503 individual shelf break sections of the NWES and net DIC exchange with the Atlantic Ocean and
504 the Baltic Sea for the ER, PR, and ER&PR configurations compared to the RS configuration. The

505 dashed lines indicate the mean over the simulated period 2000–2010, and the shaded areas show
506 the standard deviation between annual means.

507 **3.3 Impact on the organic carbon budget**

508 Following the assessment of the inorganic budget, we now quantify the changes in the organic
509 carbon budget, focusing on differences in carbon export and their contribution to the additionally
510 sequestered CO_2 (Fig. 5). In the RS reference configuration, the annual mean pelagic TOC stock of
511 2.291 Tmol C is roughly two orders of magnitude smaller than the DIC stock, and shows a
512 negligible negative trend of -0.005 ± 0.006 Tmol C yr^{-1}. TOC sources are the positive pelagic NCP
513 of 0.645 Tmol C yr^{-1}, along with net imported TOC across the shelf edge with 0.056 ± 0.069 Tmol
514 C yr^{-1} and from the Baltic Sea with 0.005 ± 0.018 Tmol C yr^{-1}. This accumulated POC of 0.708 ±
515 0.028 Tmol C yr^{-1} is net deposited in benthic POC. With 0.706 ± 0.026 Tmol C yr^{-1} almost all of the
516 net deposited POC is released as DIC through benthic remineralization, with only 0.001 Tmol C
517 yr^{-1} each contributing to the positive benthic POC trend and long-term burial in sediments. As
518 such, the net imported TOC is respired along with the locally produced and deposited POC in
519 sediments, contributing a source to the pelagic DIC budget.

520 In consistency with the increased seasonal DOC and POC production in Demir et al. (2025), the
521 variable stoichiometry configurations show an increased pelagic TOC stock with an additional
522 0.218 to 1.535 Tmol C, which are each stable over the simulated period (Fig. 5 and S1). There is
523 only a marginal increase in the pelagic TOC trend of 0.005 ± 0.003 to 0.009 ± 0.005 Tmol C yr^{-1},
524 which can be attributed to interannual variability (Fig. S1). In terms of the import of TOC across
525 the shelf edge and from the Baltic Sea, there are opposing responses between the PR and ER
526 configurations. The PR configuration shows a decrease of imported TOC of 0.015 ± 0.010 Tmol C
527 yr^{-1} from the North Atlantic, and a decrease of 0.003 ± 0.005 Tmol C per year from the Baltic Sea.
528 In contrast, the ER configuration shows an increased import of TOC of 0.006 ± 0.079 Tmol C yr^{-1}
529 from the North Atlantic, and 0.020 ± 0.020 Tmol C yr^{-1} from the Baltic Sea, with large interannual
530 variability. As discussed above for the DIC budget, the additionally accumulated TOC through
531 increased pelagic NCP in all configurations is released as DIC through benthic remineralization,
532 with the remaining TOC contributing to the increased trend. There is no additional accumulation

533 of POC in surface sediments, nor an increased POC burial. Overall, there are substantial changes
534 in lateral transports with respect to the magnitude of TOC fluxes, but the potential contribution
535 to the export of the additional CO_2 uptake is much smaller and variable compared to changes in
536 the DIC budget.

537 In agreement with our findings, Wakelin et al. (2012) found that nearly all net deposited POC in
538 the NWES is remineralized, with a pelagic NCP of 1.7 Tmol C yr^{-1}, net POC deposition 1.5 of Tmol
539 C yr^{-1}, and a corresponding benthic DIC release of 1.5 Tmol C yr^{-1}. While this shows a higher overall
540 cycling of POC than in our simulations, this also suggests a negligible long-term sink of POC in
541 sediments. Given that our baseline simulation does not show a significant net accumulation or
542 burial of POC, the increased net deposition under variable OM stoichiometry does not increase
543 the accumulation. However, if the baseline showed a significant long-term sink, it would likely be
544 increased due to the additional POC deposition, or similarly in other shelf sea systems with
545 significant benthic POC accumulation.

546 Estimates of cross-shelf TOC transport to the NWES vary widely, with reported values ranging
547 from a net export of 0.4 ± 0.4 Tmol C yr^{-1} (Wakelin et al., 2012) and 0.01–1.84 Tmol C yr^{-1} (Legge
548 et al., 2020) to a net import of 0.24 Tmol C yr^{-1} to the North Sea (Thomas et al., 2005). In this
549 context, our simulated net import of 0.04–0.06 Tmol C yr^{-1} lies within the broader range of
550 published estimates, especially considering the large interannual variability of 0.07 Tmol C yr^{-1} in
551 the reference simulation. As for the inorganic carbon budget, the wide range of TOC transport

estimates reflects the uncertainty in the efficiency of the biological carbon pump and its control on organic carbon cycling and export.

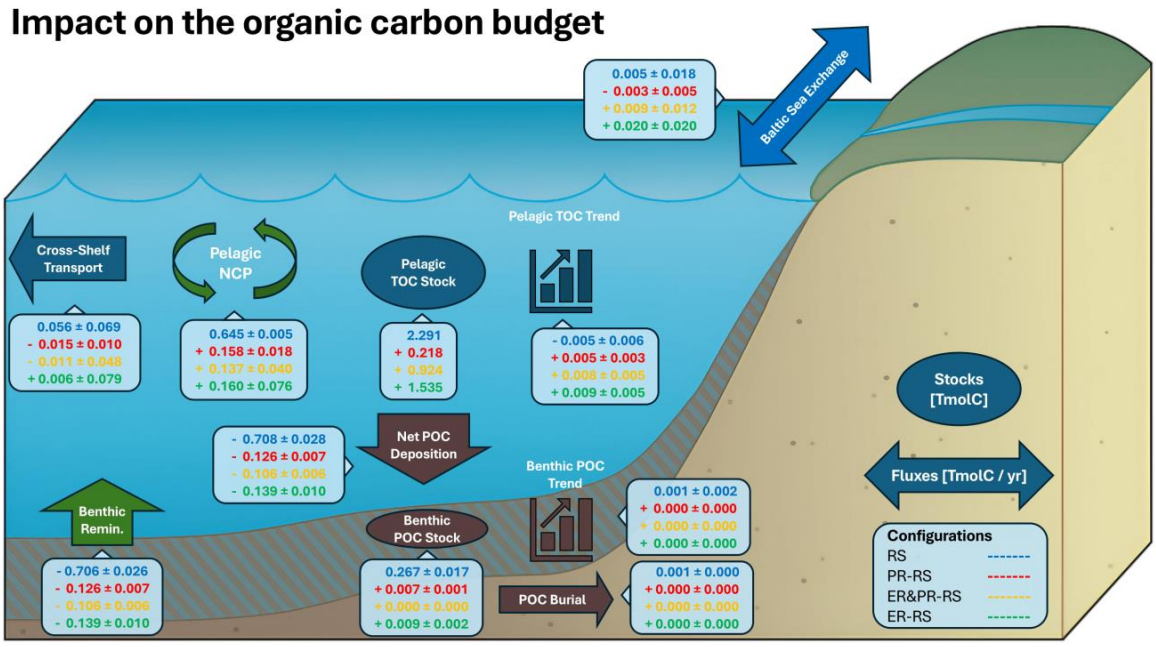

Figure 5. Variable stoichiometry impacts on the organic carbon budget of the northwest European shelf seas. All stocks are shown in Tmol C, and fluxes in Tmol C yr^{-1}. Green arrows represent the conversion between organic and inorganic carbon pools. For the RS reference configuration, the absolute stocks and fluxes are shown, while the differences are shown for all other configurations. The figure background was created in part using modified images from the UMCES IAN Media Library under a Creative Commons license CC BY-SA 4.0.

While the changes in net TOC exchange with the North Atlantic are only moderate, there is a substantial increase in both TOC import and export contributions in the ER and ER&PR configurations, with small relative differences in the PR configuration (Fig. 6). The net off-shelf TOC transport through the Norwegian Trench increases by 0.165 ± 0.024 and 0.289 ± 0.039 Tmol C yr^{-1} in the ER&PR and ER configurations, respectively. For the Armorican Shelf the increase in export is between 0.033 ± 0.012 Tmol C yr^{-1} in the ER&PR and 0.059 ± 0.023 Tmol C yr^{-1} in the ER configuration. The total TOC import through the shelf edge from the West Shetland Shelf to the

Celtic Sea increases by 0.188 ± 0.053 and 0.353 ± 0.083 Tmol C yr^{-1} in the ER&PR and ER configurations, respectively. An increase in standard deviation between annual means across all shelf sections with 0.013 to 0.049 Tmol C yr^{-1} in the ER configuration, and 0.074 Tmol C yr^{-1} for the total net cross-shelf TOC exchange with the Atlantic further indicates an increased variability in net TOC exchange under the consideration of variable OM stoichiometry.

Figure 6. Annual mean net cross-shelf TOC transports, expressed in Tmol C yr^{-1}, across individual shelf break sections of the NWES and net TOC exchange with the Atlantic Ocean and the Baltic Sea for all four configurations. The dashed lines indicate the mean over 2000–2010, while the shaded areas represent the standard deviation between annual means.

3.4 Carbon export contributions

To assess which export fluxes enable the additional CO_2 uptake in the variable stoichiometry configurations, and hence the fate of the additionally sequestered carbon, we compare the differences in each flux relative to the difference in CO_2 uptake in the respective configurations (Fig. 7a). Positive percentages represent additional DIC sources and negative percentages

potential sinks for the CO_2 uptake of 0.102, 0.211, and 0.339 Tmol C yr^{-1} in the PR, ER&PR, and ER configurations, respectively.

Considering the impact on both the inorganic and organic carbon budgets, the dominant export contribution is the increased net export of DIC across the shelf edge with 59 ± 22, 82 ± 19, and 89 ± 19% in the PR, ER&PR, and ER configurations, respectively (Fig. 7a). Only in the PR configuration, there are other large and consistent contributions of 15 ± 10% from a reduced cross-shelf import of TOC, 6 ± 5% from an increased trend in pelagic DIC, and lastly 5 ± 3% from an increased trend in pelagic TOC. For the ER and ER&PR configurations, the contributions of both trend increases only account for a total of roughly 4–6%, and the contribution of cross-shelf TOC exchange is strongly variable. In all configurations, an increased DIC import from the Baltic Sea provides an additional DIC source of 5–8%. Conversely, changes in TOC import from the Baltic Sea range from an export contribution of 3 ± 5% in the PR to an additional import contribution of 6 ± 6% and 4 ± 6% in the ER and ER&PR configurations. Opposing responses in net cross-shelf and Baltic Sea TOC imports result from a consistent increase in net off-shelf transport of POC and plankton biomass. Only in the ER and ER&PR configurations is this increased export offset by a larger increase in net import of DOC, with no such offset in the PR configuration (Fig. S2–S5).

This is consistent with the differences in concentrations found in Demir et al. (2025). The latter showed that while the PR configuration primarily exports additional organic carbon to sub-surface waters as POC through increased nutrient release and hence primary productivity, the ER configuration facilitates additional export of both DOC and POC through enhanced DOM release and subsequent particle formation (Fig. S1). The resulting increase in DOC concentrations is largely confined to surface waters, promoting net on-shelf transport, whereas the additional POC tends to accumulate at depth, thereby enhancing net off-shelf export. The comparatively higher percentage contributions of other export fluxes in the PR configuration reflect the smaller absolute changes in both CO_2 uptake and DIC export, making the influence of interannual variability more pronounced in relative terms (Fig. 3–6).

Given the small and highly variable contribution of changes in TOC export (Fig. 7a), and trends in both organic and inorganic carbon stocks (Fig. 3, 5, and S1), these impacts are likely driven by

611 interannual variability, with their significance likely diminishing over longer time periods. An
612 exception to this is the decrease in net TOC import in the PR configuration, which indicates a
613 larger and more consistent increase in concentration-driven TOC export due to higher POC
614 production and its subsequent export to deep waters. In particular, the changes in trends of all
615 carbon stocks are least likely to contribute, since the differences across configurations remain
616 consistent throughout the entire simulation period (Fig. S1).

617 As cross-shelf DIC export plays a key role in the enhanced CO_2 uptake, we examine the individual
618 contributions of three shelf break sections separately (Fig. 7b): the Norwegian Trench as the main
619 export pathway, the northwestern (NW) shelf break from the West Shetland Shelf to the West
620 Irish Shelf, with a consistent reduction in net on-shelf DIC transport, and lastly the southwestern
621 (SW) shelf break, consisting of the Celtic Sea and the Armorican Shelf, which consistently show
622 an increased net import or decreased net export contribution. The Norwegian Trench alone
623 contributes 39 ± 13, 53 ± 10, and 55 ± 10% to CO_2 sequestration in the PR, ER&PR, and ER
624 configurations. Through a decreased net DIC import by increased concentration-driven export
625 below 50m depth (Demir et al., 2025), the northwestern shelf break contributes an additional 22

± 12, 36 ± 14, and 40 ± 13%. Only the southwestern shelf break contributes a small and strongly variable DIC source of 2 ± 8, 7 ± 9, and 6 ± 9%.

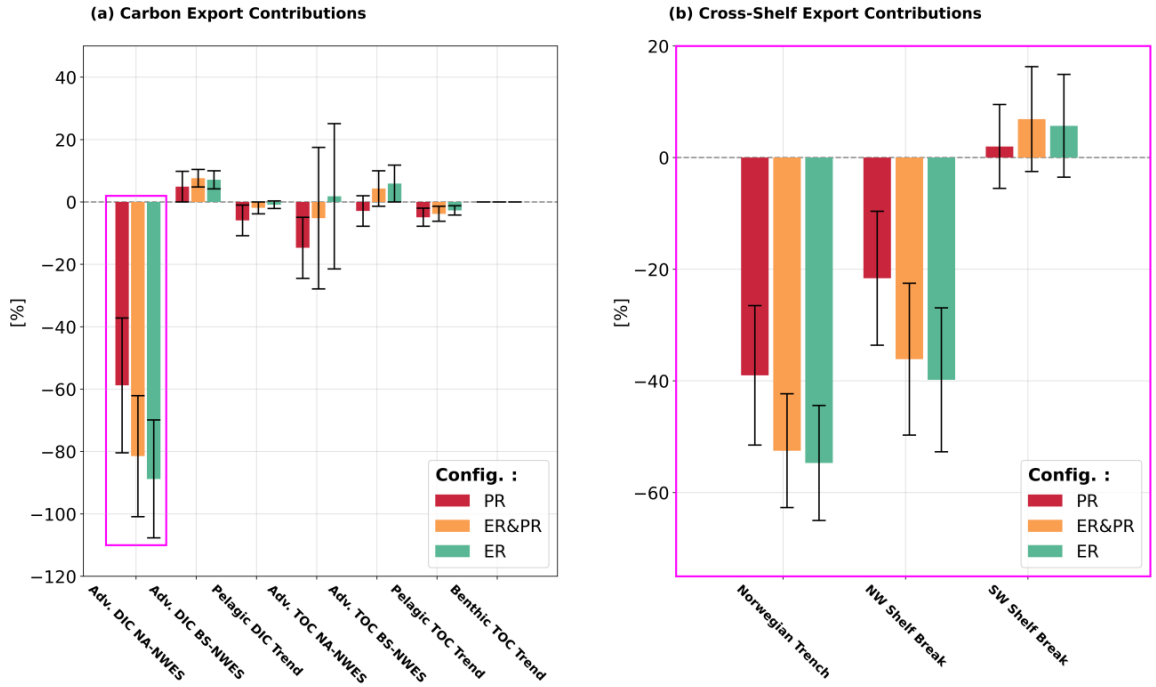

Figure 7. (a) Contributions of export fluxes and trends in carbon stock to the additional uptake of atmospheric CO_2 in the variable stoichiometry configurations. The mean contribution represents the average over the period 2000–2010, with error bars indicating interannual variability as standard deviation for carbon fluxes and normal error for the differences in trends. (b) The advective (Adv.) cross-shelf exchanges of both DIC and TOC are separated into the net cross-shelf exchange with the North Atlantic (NA), and with the Baltic Sea (BS). The northwestern (NW) shelf break ranges from the West Shetland Shelf to the West Irish Shelf, with the southwestern (SW) shelf break including the Celtic Sea and Armorican Shelf.

3.5 Implications for regional and global carbon cycling

Our assessment focuses on the NWES, a highly productive, temperate shelf sea system with large seasonal variability in air-sea CO_2-exchange due to changes in temperature and NCP, and efficient cross-shelf exchange with the northeastern Atlantic Ocean. While the modeled impact of variable

OM stoichiometry, as compared to fixed Redfield stoichiometry, on CO_2 uptake and DIC export is regionally substantial (Fig. 3–7), this outcome is closely tied to the specific carbon export mechanism of the NWES, primarily affecting export via inorganic carbon fluxes rather than organic carbon transport. Shelf sea systems differ widely in their physical and biological characteristics, and dominant drivers of carbon sequestration such as biological productivity, vertical transport, cross-shelf exchange, open ocean and freshwater inputs, and seasonal variations in temperature and NCP vary substantially across latitudes (Bauer et al., 2013; Dai et al., 2022; Resplandy et al., 2024; Roobaert et al., 2019; Roobaert, Regnier, et al., 2024; Roobaert, Resplandy, et al., 2024). Given these regional differences in carbon cycling and export fluxes, the influence of OM stoichiometry on carbon budgets cannot be assumed to scale uniformly across coastal regions, but rather requires region-specific assessments.

Despite this regional variability, incorporating the observed carbon-enrichment of DOM and POM into biogeochemical models consistently yields higher carbon export per unit of nutrients, as originally proposed by Hopkinson and Vallino (2005). For the NWES, our simulations suggest a 10–30% increase in carbon sequestration efficiency, which is consistent with global model studies incorporating flexible internal plankton stoichiometry or preferential remineralization of phosphorus, which report increases in carbon sequestration and export production of 9–20% (Letscher & Moore, 2015; Sullivan et al., 2024; Tanioka et al., 2021). Globally, models also show a reduction in atmospheric pCO_2 of 20 µatm and a 5–18% buffering of declines in carbon sequestration and export under glacial or warming conditions, with regionally variable responses (Matsumoto, Rickaby, et al., 2020; Tanioka & Matsumoto, 2017). This consistency across regional and global scales provides a useful reference for evaluating the limitations of assuming fixed Redfield stoichiometry in estimating carbon sequestration and export. Accurate projections of future changes should thus account for both the sensitivity of export to stoichiometric variation and the impact of environmental change on ecosystem stoichiometry (Matsumoto, Rickaby, et al., 2020; Matsumoto & Tanioka, 2020; Sardans et al., 2012, 2021; Tanioka & Matsumoto, 2017).

Our findings highlight that variable OM stoichiometry is relevant to marine carbon cycling, but, given the large general uncertainty in carbon budgets, it should be addressed alongside other

669 uncertainties in the model representation of OM cycling. Several recent studies point to the
670 importance of DOM fractions, their vertical distribution, composition, reactivity timescales, DOM
671 processing via the microbial carbon pump, and the relative contributions of DOC and POC to
672 vertical carbon export (Cai & Jiao, 2023; Carlson et al., 2024; Dittmar et al., 2021; Dittmar &
673 Lennartz, 2024; Hansell, 2013; Hansell et al., 2009; Moran, Ferrer-González, et al., 2022; Moran,
674 Kujawinski, et al., 2022; Nagata, 2008; Wakeham & Lee, 2019). OM comprises a diverse range of
675 compounds, from highly labile DOM with near-Redfield stoichiometry to carbon-rich, refractory
676 DOM, as well as intermediate semi-labile and semi-refractory fractions, each with distinct roles,
677 elemental compositions, and reactivity timescales that shape nutrient recycling, vertical carbon
678 export, and long-term carbon sequestration (Cai & Jiao, 2023; Carlson et al., 2024; Dittmar et al.,
679 2021; Dittmar & Lennartz, 2024; Hansell, 2013; Hansell et al., 2009; Nagata, 2008). These
680 variations in OM quality and stoichiometry are linked to a broader range of production,
681 transformation, and removal processes, and dynamic POM-DOM exchanges, including microbial
682 OM interactions, higher-trophic-level food web dynamics, aggregation and solubilization,
683 transformation of terrestrial OM, biological interactions with marine sediments, that collectively
684 determine the quality of OM and whether it is recycled or sequestered (Bianchi, 2011; Bianchi et
685 al., 2021; Cai & Jiao, 2023; Carlson et al., 2024; Hansell et al., 2009; He et al., 2016; Wakeham &
686 Lee, 1993, 2019). In this context, our findings underscore the need to improve the representation
687 of OM stoichiometry and other key aspects of OM cycling for accurate estimates of regional and
688 global carbon budgets.

689 **4 Conclusions**

690 In this study, we extend our previous assessment of two pathways for variable OM stoichiometry
691 (Demir et al., 2025) to the full organic and inorganic carbon budgets of the NWES. We assess the
692 impact on cross-shelf exchange, benthic-pelagic coupling, and trends in carbon stocks to identify
693 the carbon export pathways which enable the previously shown increase of approximately 10–
694 30% in CO_2 sequestration. Our earlier findings demonstrated that preferential remineralization
695 of organic nitrogen and phosphorus, along with the extracellular release of carbon-rich DOM,
696 enhances biological drawdown of DIC, and consequently, the CO_2 uptake from the atmosphere

(Demir et al., 2025). The present study reveals that this increased drawdown of DIC results in an increased cross-shelf export of DIC, which drives roughly 60–90% of the additional CO_2 uptake. Our results show that this increased off-shelf DIC transport is strongest across the northern boundary of the Norwegian Trench, with additional significant contributions from the export of DIC-rich deeper water masses across the northwestern shelf edge, spanning from the West Shetland Shelf to the West Irish Shelf. This is consistent with the previously identified intensified lateral gradient in NCP between the Central North Sea and the Norwegian Trench, as well as the seasonal vertical gradient of both NCP and DIC. Smaller and more variable contributions from changes in lateral TOC transports, as well as in DIC and TOC trends, are likely influenced by interannual variability, and their significance would diminish over longer timescales. When considering the preferential remineralization of organic nitrogen and phosphorus, we also found a significant contribution from concentration driven export of POC, while this was outbalanced by increased DOC import when considering a release of carbon-enriched DOM.

These findings provide a more complete understanding of how OM stoichiometry affect carbon cycling in the NWES. They demonstrate that variable OM stoichiometry in the production and respiration of OM regulates the continental shelf carbon pump efficiency, linking increased CO_2 uptake and biological DIC drawdown to its subsequent export across the shelf edge. This further highlights the importance of improving the representation of OM stoichiometry and other key processes in regional and global carbon cycle assessments, as this would enable more reliable estimates of regional and global carbon sequestration and export. The significance of the continental shelf carbon pump mechanism to our results suggests that the role of OM stoichiometry is strongly linked to the prevailing regional carbon export pathways, supporting the need for region-specific assessments rather than estimates based on global upscaling. At the same time, the consistent increases in carbon sequestration and export across regional and global models provide a useful reference for quantifying the uncertainty associated with assuming fixed Redfield stoichiometry.

Acknowledgments

Computational resources for this work were made available by the German Climate Computing Center (DKRZ) through support from the German Federal Ministry of Education and Research (BMBF). We would like to thank ICDC, CEN, University Hamburg, for data support. The research was funded by the Deutsche Forschungsgemeinschaft (DFG, German Research Foundation) under Germany's Excellence Strategy – EXC 2037 'CLICCS - Climate, Climatic Change, and Society'–Project Number: 390683824 and contributes to the CLICCS subproject A5 The Land-Ocean Transition Zone. Feifei Liu received funding from the BMBF project RETAKE (Grant 03F0895C).

Open Research

The SCHISM-ECOSMO-CO_2 modeling system used in this study combines independently developed model components. The hydrodynamic model SCHISM is described in Zhang, Ye, et al. (2016), and is available on GitHub at https://github.com/schism-dev/schism. Both the lower-trophic-level ecosystem model ECOSMO II (Daewel & Schrum, 2013) and the carbonate system module (Blackford & Gilbert, 2007) are implemented as part of the FABM framework, published in Bruggeman and Bolding (2014), which is available on GitHub at https://github.com/fabm-model/fabm. The updated variable stoichiometry version of ECOSMO II used in this study, including the parameter settings for all four configurations, is described in the Supplement of Demir et al. (2025). All processed model output and the related Jupyter Notebooks used for the analysis and generating the figures for this study are available in a supporting Zenodo dataset (Demir, 2025): https://doi.org/10.5281/zenodo.15685047.

Competing Interests

The contact author has declared that none of the authors has any competing interests.

Author Contributions

KD was responsible for the conceptualization of the study, while the methodology was developed collaboratively by KD, MM, JK, and CSc. Software development was undertaken by KD, JK, FL, and

CSt, with the validation carried out by KD, JK, and FL. KD performed the formal analysis, and the investigation was conducted by KD, MM, CSc, and HT. MM and CSc provided the necessary resources, and data curation was managed by KD. The original draft of the manuscript was prepared by KD, and subsequent writing, review, and editing were contributed by KD, MM, JK, FL, UD, CSt, HT, and CSc. KD also took responsibility for visualization. Supervision of the project was provided by MM, UD, HT, and CSc. Finally, CSc handled the project administration and funding acquisition.

References

Aminot, A., & Kérouel, R. (2004). Dissolved organic carbon, nitrogen and phosphorus in the N-E Atlantic and the N-W Mediterranean with particular reference to non-refractory fractions and degradation. *Deep Sea Research Part I: Oceanographic Research Papers*, *51*(12), 1975–1999. https://doi.org/10.1016/j.dsr.2004.07.016

Anderson, T. R., & Pondaven, P. (2003). Non-Redfield carbon and nitrogen cycling in the Sargasso Sea: Pelagic imbalances and export flux. *Deep-Sea Research Part I: Oceanographic Research Papers*, *50*(5), 573–591. https://doi.org/10.1016/S0967-0637(03)00034-7

Aricò, S., Watson, A. J., Wanninkhof, R., Thomas, H., Shutler, J. D., Schuster, U., et al. (2021). *Integrated Ocean Carbon Research: A Summary of Ocean Carbon Research, and Vision of Coordinated Ocean Carbon Research and Observations for the Next Decade*. UNESCO. Retrieved from https://doi.org/10.25607/h0gj-pq41

Baines, S. B., & Pace, M. L. (1991). The production of dissolved organic matter by phytoplankton and its importance to bacteria: Patterns across marine and freshwater systems. *Limnology and Oceanography*, *36*(6), 1078–1090. https://doi.org/10.4319/lo.1991.36.6.1078

Bauer, J. E., Cai, W.-J., Raymond, P. A., Bianchi, T. S., Hopkinson, C. S., & Regnier, P. A. G. (2013). The changing carbon cycle of the coastal ocean. *Nature*, *504*(7478), 61–70. https://doi.org/10.1038/nature12857

Bergström, S., & Carlsson, B. (1994). River runoff to the Baltic Sea: 1950-1990. *Ambio*, *23*(4–5), 280–287. https://www.diva-portal.org/smash/record.jsf?pid=diva2%3A897362&dswid=-9536

775 Bianchi, T. S. (2011). The role of terrestrially derived organic carbon in the coastal ocean: A changing paradigm and
776 the priming effect. *Proceedings of the National Academy of Sciences*, *108*(49), 19473–19481.
777 https://doi.org/10.1073/pnas.1017982108
778 Bianchi, T. S., Aller, R. C., Atwood, T. B., Brown, C. J., Buatois, L. A., Levin, L. A., et al. (2021). What global
779 biogeochemical consequences will marine animal–sediment interactions have during climate change?
780 *Elementa: Science of the Anthropocene*, *9*(1), 00180. https://doi.org/10.1525/elementa.2020.00180
781 Blackford, J. C., & Gilbert, F. J. (2007). pH variability and CO2 induced acidification in the North Sea. *Journal of*
782 *Marine Systems*, *64*(1), 229–241. https://doi.org/10.1016/j.jmarsys.2006.03.016
783 Borchard, C., & Engel, A. (2012). Organic matter exudation by Emiliania huxleyi under simulated future ocean
784 conditions. *Biogeosciences*, *9*(8), 3405–3423. https://doi.org/10.5194/bg-9-3405-2012
785 Børsheim, K. Y., Vadstein, O., Myklestad, S. M., Reinertsen, H., Kirkvold, S., & Olsen, Y. (2005). Photosynthetic
786 algal production, accumulation and release of phytoplankton storage carbohydrates and bacterial
787 production in a gradient in daily nutrient supply. *Journal of Plankton Research*, *27*(8), 743–755.
788 https://doi.org/10.1093/plankt/fbi047
789 Bozec, Y., Thomas, H., Schiettecatte, L.-S., Borges, A. V., Elkalay, K., & De Baar, H. J. W. (2006). Assessment of
790 the processes controlling the seasonal variations of dissolved inorganic carbon in the North Sea. *Limnology*
791 *and Oceanography*, *51*(6), 2746–2762. https://doi.org/10.4319/lo.2006.51.6.2746
792 Bruggeman, J., & Bolding, K. (2014). A general framework for aquatic biogeochemical models. *Environmental*
793 *Modelling & Software*, *61*, 249–265. https://doi.org/10.1016/j.envsoft.2014.04.002
794 Butenschön, M., Clark, J., Aldridge, J. N., Allen, J. I., Artioli, Y., Blackford, J., et al. (2016). ERSEM 15.06: A
795 generic model for marine biogeochemistry and the ecosystem dynamics of the lower trophic levels.
796 *Geoscientific Model Development*, *9*(4), 1293–1339. https://doi.org/10.5194/gmd-9-1293-2016
797 Cai, R., & Jiao, N. (2023). Recalcitrant dissolved organic matter and its major production and removal processes in
798 the ocean. *Deep Sea Research Part I: Oceanographic Research Papers*, *191*, 103922.
799 https://doi.org/10.1016/j.dsr.2022.103922
800 Carlson, C. A., Liu, S., Stephens, B. M., & English, C. J. (2024). Chapter 5 - DOM production, removal, and
801 transformation processes in marine systems. In D. A. Hansell & C. A. Carlson (Eds.), *Biogeochemistry of*

Marine Dissolved Organic Matter (Third Edition) (pp. 137–246). Academic Press. https://doi.org/10.1016/B978-0-443-13858-4.00013-7

Chaichana, S., Jickells, T., & Johnson, M. (2019). Interannual variability in the summer dissolved organic matter inventory of the North Sea: Implications for the continental shelf pump. *Biogeosciences*, *16*(5), 1073–1096. https://doi.org/10.5194/bg-16-1073-2019

Chen, C.-T. A., & Borges, A. V. (2009). Reconciling opposing views on carbon cycling in the coastal ocean: Continental shelves as sinks and near-shore ecosystems as sources of atmospheric CO2. *Deep Sea Research Part II: Topical Studies in Oceanography*, *56*(8), 578–590. https://doi.org/10.1016/j.dsr2.2009.01.001

Clark, L. L., Ingall, E. D., & Benner, R. (1998). Marine phosphorus is selectively remineralized. *Nature*, *393*(6684), 426–426. https://doi.org/10.1038/30881

Daewel, U., & Schrum, C. (2013). Simulating long-term dynamics of the coupled North Sea and Baltic Sea ecosystem with ECOSMO II: Model description and validation. *Journal of Marine Systems*, *119–120*, 30–49. https://doi.org/10.1016/j.jmarsys.2013.03.008

Daewel, U., & Schrum, C. (2017). Low-frequency variability in North Sea and Baltic Sea identified through simulations with the 3-D coupled physical-biogeochemical model ECOSMO. *Earth System Dynamics*, *8*(3), 801–815. https://doi.org/10.5194/esd-8-801-2017

Dai, M., Su, J., Zhao, Y., Hofmann, E. E., Cao, Z., Cai, W.-J., et al. (2022). Carbon Fluxes in the Coastal Ocean: Synthesis, Boundary Processes, and Future Trends. *Annual Review of Earth and Planetary Sciences*, *50*(1), 593–626. https://doi.org/10.1146/annurev-earth-032320-090746

Demir, K. T. (2025). Dataset for the study: Organic matter stoichiometry regulates the continental shelf carbon pump efficiency of the northwest European shelf seas [Data set]. Zenodo. https://doi.org/10.5281/zenodo.15685046

Demir, K. T., Mathis, M., Kossack, J., Liu, F., Daewel, U., Stegert, C., et al. (2025). Variable organic matter stoichiometry enhances the biological drawdown of CO_2 in the northwest European shelf seas. *Biogeosciences*, *22*(11), 2569–2599. https://doi.org/10.5194/bg-22-2569-2025

DeVries, T., & Primeau, F. (2011). Dynamically and Observationally Constrained Estimates of Water-Mass Distributions and Ages in the Global Ocean. https://doi.org/10.1175/JPO-D-10-05011.1

Diesing, M., Kröger, S., Parker, R., Jenkins, C., Mason, C., & Weston, K. (2017). Predicting the standing stock of organic carbon in surface sediments of the North–West European continental shelf. *Biogeochemistry*, *135*(1), 183–200. https://doi.org/10.1007/s10533-017-0310-4

Diesing, M., Thorsnes, T., & Bjarnadóttir, L. R. (2021). Organic carbon densities and accumulation rates in surface sediments of the North Sea and Skagerrak. *Biogeosciences*, *18*(6), 2139–2160. https://doi.org/10.5194/bg-18-2139-2021

Dittmar, T., & Lennartz, S. T. (2024). Chapter 13 - Reasons behind the long-term stability of dissolved organic matter. In D. A. Hansell & C. A. Carlson (Eds.), *Biogeochemistry of Marine Dissolved Organic Matter (Third Edition)* (pp. 613–655). Academic Press. https://doi.org/10.1016/B978-0-443-13858-4.00006-X

Dittmar, T., Lennartz, S. T., Buck-Wiese, H., Hansell, D. A., Santinelli, C., Vanni, C., et al. (2021). Enigmatic persistence of dissolved organic matter in the ocean. *Nature Reviews Earth & Environment*, *2*(8), 570–583. https://doi.org/10.1038/s43017-021-00183-7

Engel, A. (2002). Direct relationship between CO2 uptake and transparent exopolymer particles production in natural phytoplankton. *Journal of Plankton Research*, *24*(1), 49–53. https://doi.org/10.1093/plankt/24.1.49

Fajon, C., Cauwet, G., Lebaron, P., Terzic, S., Ahel, M., Malej, A., et al. (1999). The accumulation and release of polysaccharides by planktonic cells and the subsequent bacterial response during a controlled experiment. *FEMS Microbiology Ecology*, *29*(4), 351–363. https://doi.org/10.1016/S0168-6496(99)00029-X

Fransner, F., Gustafsson, E., Tedesco, L., Vichi, M., Hordoir, R., Roquet, F., et al. (2018). Non-Redfieldian Dynamics Explain Seasonal pCO2 Drawdown in the Gulf of Bothnia. *Journal of Geophysical Research: Oceans*, *123*(1), 166–188. https://doi.org/10.1002/2017JC013019

del Giorgio, P. A., & Duarte, C. M. (2002). Respiration in the open ocean. *Nature*, *420*(6914), 379–384. https://doi.org/10.1038/nature01165

Graham, J. A., Rosser, J. P., O'Dea, E., & Hewitt, H. T. (2018). Resolving Shelf Break Exchange Around the European Northwest Shelf. *Geophysical Research Letters*, *45*(22), 12,386-12,395. https://doi.org/10.1029/2018GL079399

Granum, E., Kirkvold, S., & Myklestad, S. M. (2002). Cellular and extracellular production of carbohydrates and amino acids by the marine diatom Skeletonema costatum: diel variations and effects of N depletion. *Marine Ecology Progress Series*, *242*, 83–94. https://doi.org/10.3354/meps242083

Gustafsson, E. (2013). *Modelling the marine CO2 system in BALTSEM* (Baltic Nest Institute Technical Report No. 9) (p. 26). Stockholm University, Baltic Nest Institute. Retrieved from https://su.diva-portal.org/smash/record.jsf?pid=diva2%3A1598412&dswid=-735

de Haas, H., Boer, W., & van Weering, T. C. E. (1997). Recent sedimentation and organic carbon burial in a shelf sea: the North Sea. *Marine Geology*, *144*(1), 131–146. https://doi.org/10.1016/S0025-3227(97)00082-0

de Haas, H., Van Weering, T. C. E., & De Stigter, H. (2002). Organic carbon in shelf seas: sinks or sources, processes and products. *Continental Shelf Research*, *22*(5), 691–717. https://doi.org/10.1016/S0278-4343(01)00093-0

Hach, P. F., Marchant, H. K., Krupke, A., Riedel, T., Meier, D. V., Lavik, G., et al. (2020). Rapid microbial diversification of dissolved organic matter in oceanic surface waters leads to carbon sequestration. *Scientific Reports*, *10*(1), 13025. https://doi.org/10.1038/s41598-020-69930-y

Hansell, D. A. (2013). Recalcitrant Dissolved Organic Carbon Fractions. *Annual Review of Marine Science*, *5*(Volume 5, 2013), 421–445. https://doi.org/10.1146/annurev-marine-120710-100757

Hansell, D. A., Carlson, C., Repeta, D., & Schlitzer, R. (2009). Dissolved Organic Matter in the Ocean: A Controversy Stimulates New Insights. *Oceanography*, *22*(4), 202–211. https://doi.org/10.5670/oceanog.2009.109

He, W., Chen, M., Schlautman, M. A., & Hur, J. (2016). Dynamic exchanges between DOM and POM pools in coastal and inland aquatic ecosystems: A review. *Science of The Total Environment*, *551–552*, 415–428. https://doi.org/10.1016/j.scitotenv.2016.02.031

Holt, J., Wakelin, S., & Huthnance, J. (2009). Down-welling circulation of the northwest European continental shelf: A driving mechanism for the continental shelf carbon pump. *Geophysical Research Letters*, *36*(14). https://doi.org/10.1029/2009GL038997

Holt, J., Polton, J., Huthnance, J., Wakelin, S., O'Dea, E., Harle, J., et al. (2018). Climate-Driven Change in the North Atlantic and Arctic Oceans Can Greatly Reduce the Circulation of the North Sea. *Geophysical Research Letters*, *45*(21), 11,827-11,836. https://doi.org/10.1029/2018GL078878

Hopkinson, C. S., & Vallino, J. J. (2005). Efficient export of carbon to the deep ocean through dissolved organic matter. *Nature*, *433*(7022), 142–145. https://doi.org/10.1038/nature03191

Hopkinson, C. S., Fry, B., & Nolin, A. L. (1997). Stoichiometry of dissolved organic matter dynamics on the continental shelf of the northeastern U.S.A., *17*(5), 473–489. https://doi.org/10.1016/S0278-4343(96)00046-5

Hopkinson, C. S., Vallino, J. J., & Nolin, A. (2002). Decomposition of dissolved organic matter from the continental margin. *Deep Sea Research Part II: Topical Studies in Oceanography*, *49*(20), 4461–4478. https://doi.org/10.1016/S0967-0645(02)00125-X

Huthnance, J. M., Holt, J. T., & Wakelin, S. L. (2009). Deep ocean exchange with west-European shelf seas. *Ocean Science*, *5*(4), 621–634. https://doi.org/10.5194/os-5-621-2009

Huthnance, J. M., Hopkins, J., Berx, B., Dale, A., Holt, J., Hosegood, P., et al. (2022). Ocean shelf exchange, NW European shelf seas: Measurements, estimates and comparisons. *Progress in Oceanography*, *202*. https://doi.org/10.1016/j.pocean.2022.102760

Ingri, N., Kakolowicz, W., Sillén, L. G., & Warnqvist, B. (1967). High-speed computers as a supplement to graphical methods—V1Haltafall, a general program for calculating the composition of equilibrium mixtures. *Talanta*, *14*(11), 1261–1286. https://doi.org/10.1016/0039-9140(67)80203-0

Kähler, P., & Koeve, W. (2001). Marine dissolved organic matter: can its C:N ratio explain carbon overconsumption? *Deep Sea Research Part I: Oceanographic Research Papers*, *48*(1), 49–62. https://doi.org/10.1016/S0967-0637(00)00034-0

Kossack, J., Mathis, M., Daewel, U., Zhang, Y., & Schrum, C. (2023). Barotropic and baroclinic tides increase primary production on the Northwest European Shelf. *Frontiers in Marine Science*, *10*. https://doi.org/10.3389/fmars.2023.1206062

Kossack, J., Mathis, M., Daewel, U., Liu, F., Demir, K. T., Thomas, H., & Schrum, C. (2024). Tidal impacts on air-sea CO2 exchange on the North-West European shelf. *Frontiers in Marine Science*, *11*, 1406896. https://doi.org/10.3389/fmars.2024.1406896

Kühn, W., Pätsch, J., Thomas, H., Borges, A. V., Schiettecatte, L. S., Bozec, Y., & Prowe, A. E. F. (2010). Nitrogen and carbon cycling in the North Sea and exchange with the North Atlantic-A model study, Part II: Carbon budget and fluxes. *Continental Shelf Research*, *30*(16), 1701–1716. https://doi.org/10.1016/j.csr.2010.07.001

Lacroix, F., Ilyina, T., Mathis, M., Laruelle, G. G., & Regnier, P. (2021). Historical increases in land-derived nutrient inputs may alleviate effects of a changing physical climate on the oceanic carbon cycle. *Global Change Biology*, *27*(21), 5491–5513. https://doi.org/10.1111/gcb.15822

Laruelle, G. G., Lauerwald, R., Pfeil, B., & Regnier, P. (2014). Regionalized global budget of the CO2 exchange at the air-water interface in continental shelf seas. *Global Biogeochemical Cycles*, *28*(11), 1199–1214. https://doi.org/10.1002/2014GB004832

Laruelle, G. G., Cai, W.-J., Hu, X., Gruber, N., Mackenzie, F. T., & Regnier, P. (2018). Continental shelves as a variable but increasing global sink for atmospheric carbon dioxide. *Nature Communications*, *9*(1), 454. https://doi.org/10.1038/s41467-017-02738-z

Legge, O., Johnson, M., Hicks, N., Jickells, T., Diesing, M., Aldridge, J., et al. (2020). Carbon on the Northwest European Shelf: Contemporary Budget and Future Influences. *Frontiers in Marine Science*, *7*. https://doi.org/10.3389/fmars.2020.00143

Letscher, R. T., & Moore, J. K. (2015). Preferential remineralization of dissolved organic phosphorus and non-Redfield DOM dynamics in the global ocean: Impacts on marine productivity, nitrogen fixation, and carbon export. *Global Biogeochemical Cycles*, *29*(3), 325–340. https://doi.org/10.1002/2014GB004904

Letscher, R. T., Moore, J. K., Teng, Y.-C., & Primeau, F. (2015). Variable C : N : P stoichiometry of dissolved organic matter cycling in the Community Earth System Model. *Biogeosciences*, *12*(1), 209–221. https://doi.org/10.5194/bg-12-209-2015

Liang, Z., Letscher, R. T., & Knapp, A. N. (2023). Global Patterns of Surface Ocean Dissolved Organic Matter Stoichiometry. *Global Biogeochemical Cycles*, *37*(12), e2023GB007788. https://doi.org/10.1029/2023GB007788

Liang, Z., Letscher, R. T., & Knapp, A. N. (2025). Oligotrophic Ocean New Production Supported by Lateral Transport of Dissolved Organic Nutrients. *Global Biogeochemical Cycles*, *39*(6), e2024GB008345. https://doi.org/10.1029/2024GB008345

Loh, A. N., & Bauer, J. E. (2000). Distribution, partitioning and fluxes of dissolved and particulate organic C, N and P in the eastern North Pacific and Southern Oceans. *Deep Sea Res. Pt. I*, *47*(12), 2287–2316. https://doi.org/10.1016/S0967-0637(00)00027-3

938 Lønborg, C., & Álvarez-Salgado, X. A. (2012). Recycling versus export of bioavailable dissolved organic matter in
939 the coastal ocean and efficiency of the continental shelf pump. *Global Biogeochemical Cycles*, *26*(3),
940 GB3018. https://doi.org/10.1029/2012GB004353
941 Lønborg, C., Davidson, K., Álvarez–Salgado, X. A., & Miller, A. E. J. (2009). Bioavailability and bacterial
942 degradation rates of dissolved organic matter in a temperate coastal area during an annual cycle. *Marine*
943 *Chemistry*, *113*(3–4), 219–226. https://doi.org/10.1016/j.marchem.2009.02.003
944 Lønborg, C., Álvarez-Salgado, X. A., Davidson, K., & Miller, A. E. J. (2009). Production of bioavailable and
945 refractory dissolved organic matter by coastal heterotrophic microbial populations. *Estuarine, Coastal and*
946 *Shelf Science*, *82*(4), 682–688. https://doi.org/10.1016/j.ecss.2009.02.026
947 Lorkowski, I., Pätsch, J., Moll, A., & Kühn, W. (2012). Interannual variability of carbon fluxes in the North Sea
948 from 1970 to 2006 - Competing effects of abiotic and biotic drivers on the gas-exchange of CO 2.
949 *Estuarine, Coastal and Shelf Science*, *100*, 38–57. https://doi.org/10.1016/j.ecss.2011.11.037
950 Mari, X., Passow, U., Migon, C., Burd, A. B., & Legendre, L. (2017). Transparent exopolymer particles: Effects on
951 carbon cycling in the ocean. *Progress in Oceanography*, *151*, 13–37.
952 https://doi.org/10.1016/j.pocean.2016.11.002
953 Martiny, A. C., Pham, C. T. A., Primeau, F. W., Vrugt, J. A., Moore, J. K., Levin, S. A., & Lomas, M. W. (2013).
954 Strong latitudinal patterns in the elemental ratios of marine plankton and organic matter. *Nature*
955 *Geoscience*, *6*(4), 279–283. https://doi.org/10.1038/ngeo1757
956 Mathis, M., Lacroix, F., Hagemann, S., Nielsen, D. M., Ilyina, T., & Schrum, C. (2024). Enhanced CO2 uptake of
957 the coastal ocean is dominated by biological carbon fixation. *Nature Climate Change*, *14*(4), 373–379.
958 https://doi.org/10.1038/s41558-024-01956-w
959 Matsumoto, K., & Tanioka, T. (2020). Shifts in regional production as a driver of future global ocean production
960 stoichiometry. *Environmental Research Letters*, *15*(12), 124027. https://doi.org/10.1088/1748-9326/abc4b0
961 Matsumoto, K., Rickaby, R., & Tanioka, T. (2020). Carbon Export Buffering and CO2 Drawdown by Flexible
962 Phytoplankton C:N:P Under Glacial Conditions. *Paleoceanography and Paleoclimatology*, *35*(7),
963 e2019PA003823. https://doi.org/10.1029/2019PA003823

964 Matsumoto, K., Tanioka, T., & Rickaby, R. (2020). Linkages Between Dynamic Phytoplankton C:N:P and the
965 Ocean Carbon Cycle Under Climate Change. *Oceanography*, *33*(2), 44–52.
966 https://www.jstor.org/stable/26937739
967 Meador, T. B., & Aluwihare, L. I. (2014). Production of dissolved organic carbon enriched in deoxy sugars
968 representing an additional sink for biological C drawdown in the Amazon River plume. *Global*
969 *Biogeochemical Cycles*, *28*(10), 1149–1161. https://doi.org/10.1002/2013GB004778
970 Moran, M. A., Kujawinski, E. B., Schroer, W. F., Amin, S. A., Bates, N. R., Bertrand, E. M., et al. (2022). Microbial
971 metabolites in the marine carbon cycle. *Nature Microbiology*, *7*(4), 508–523.
972 https://doi.org/10.1038/s41564-022-01090-3
973 Moran, M. A., Ferrer-González, F. X., Fu, H., Nowinski, B., Olofsson, M., Powers, M. A., et al. (2022). The
974 Ocean's labile DOC supply chain. *Limnology and Oceanography*, *67*(5), 1007–1021.
975 https://doi.org/10.1002/lno.12053
976 Mühlenbruch, M., Grossart, H.-P., Eigemann, F., & Voss, M. (2018). Mini-review: Phytoplankton-derived
977 polysaccharides in the marine environment and their interactions with heterotrophic bacteria.
978 *Environmental Microbiology*, *20*(8), 2671–2685. https://doi.org/10.1111/1462-2920.14302
979 Müller, D., Liu, B., Geibert, W., Holtappels, M., Sander, L., Miramontes, E., et al. (2025). Depositional controls and
980 budget of organic carbon burial in fine-grained sediments of the North Sea – the Helgoland Mud Area as a
981 natural laboratory. *Biogeosciences*, *22*(11), 2541–2567. https://doi.org/10.5194/bg-22-2541-2025
982 Myklestad, S. M. (1995). Release of extracellular products by phytoplankton with special emphasis on
983 polysaccharides. *Science of The Total Environment*, *165*(1–3), 155–164. https://doi.org/10.1016/0048-
984 9697(95)04549-G
985 Nagata, T. (2008). Organic Matter–Bacteria Interactions in Seawater. In *Microbial Ecology of the Oceans* (pp. 207–
986 241). John Wiley & Sons, Ltd. https://doi.org/10.1002/9780470281840.ch7
987 Neumann, T., Radtke, H., Cahill, B., Schmidt, M., & Rehder, G. (2022). Non-Redfieldian carbon model for the
988 Baltic Sea (ERGOM version 1.2) – implementation and budget estimates. *Geoscientific Model*
989 *Development*, *15*(22), 8473–8540. https://doi.org/10.5194/gmd-15-8473-2022
990 Obernosterer, I., & Herndl, G. (1995). Phytoplankton extracellular release and bacterial growth: dependence on the
991 inorganic N: P ratio. *Marine Ecology Progress Series*, *116*, 247–257. https://doi.org/10.3354/meps116247

992 Osterroht, C., & Thomas, H. (2000). New production enhanced by nutrient supply from non-Redfield
993 remineralisation of freshly produced organic material. *Journal of Marine Systems*, *25*(1), 33–46.
994 https://doi.org/10.1016/S0924-7963(00)00007-5
995 Passow, U. (2002). Transparent exopolymer particles (TEP) in aquatic environments. *Progress in Oceanography*,
996 *55*(3), 287–333. https://doi.org/10.1016/S0079-6611(02)00138-6
997 Prowe, A. E. F., Thomas, H., Pätsch, J., Kühn, W., Bozec, Y., Schiettecatte, L.-S., et al. (2009). Mechanisms
998 controlling the air–sea CO2 flux in the North Sea. *Continental Shelf Research*, *29*(15), 1801–1808.
999 https://doi.org/10.1016/j.csr.2009.06.003
1000 Redfield, A. C. (1958). *THE BIOLOGICAL CONTROL OF CHEMICAL FACTORS IN THE ENVIRONMENT* (Vol.
1001 46, pp. 205–221). Retrieved from http://www.jstor.org/stable/27827150
1002 Redfield, A. C. (1963). The influence of organisms on the composition of seawater. *The Sea*, *2*, 26–77.
1003 Resplandy, L., Hogikyan, A., Müller, J. D., Najjar, R. G., Bange, H. W., Bianchi, D., et al. (2024). A Synthesis of
1004 Global Coastal Ocean Greenhouse Gas Fluxes. *Global Biogeochemical Cycles*, *38*(1), e2023GB007803.
1005 https://doi.org/10.1029/2023GB007803
1006 Roobaert, A., Laruelle, G. G., Landschützer, P., Gruber, N., Chou, L., & Regnier, P. (2019). The Spatiotemporal
1007 Dynamics of the Sources and Sinks of CO2 in the Global Coastal Ocean. *Global Biogeochemical Cycles*,
1008 *33*(12), 1693–1714. https://doi.org/10.1029/2019GB006239
1009 Roobaert, A., Regnier, P., Landschützer, P., & Laruelle, G. G. (2024). A novel sea surface pCO_2-product for the
1010 global coastal ocean resolving trends over 1982–2020. *Earth System Science Data*, *16*(1), 421–441.
1011 https://doi.org/10.5194/essd-16-421-2024
1012 Roobaert, A., Resplandy, L., Laruelle, G. G., Liao, E., & Regnier, P. (2024). Unraveling the Physical and Biological
1013 Controls of the Global Coastal CO2 Sink. *Global Biogeochemical Cycles*, *38*(3), e2023GB007799.
1014 https://doi.org/10.1029/2023GB007799
1015 Sardans, J., Rivas-Ubach, A., & Peñuelas, J. (2012). The C:N:P stoichiometry of organisms and ecosystems in a
1016 changing world: A review and perspectives. *Perspectives in Plant Ecology, Evolution and Systematics*,
1017 *14*(1), 33–47. https://doi.org/10.1016/j.ppees.2011.08.002

1018 Sardans, J., Janssens, I. A., Ciais, P., Obersteiner, M., & Peñuelas, J. (2021). Recent advances and future research in
1019 ecological stoichiometry. *Perspectives in Plant Ecology, Evolution and Systematics*, *50*, 125611.
1020 https://doi.org/10.1016/j.ppees.2021.125611
1021 Schneider, B., Engel, A., & Schlitzer, R. (2004). Effects of depth- and CO2-dependent C:N ratios of particulate
1022 organic matter (POM) on the marine carbon cycle. *Global Biogeochemical Cycles*, *18*(2).
1023 https://doi.org/10.1029/2003GB002184
1024 Schrum, C., Alekseeva, I., & John, M. S. (2006). Development of a coupled physical-biological ecosystem model
1025 ECOSMO. Part I: Model description and validation for the North Sea. *Journal of Marine Systems*, *61*(1–2),
1026 79–99. https://doi.org/10.1016/j.jmarsys.2006.01.005
1027 Schrum, C., John, M. S., & Alekseeva, I. (2006). ECOSMO, a coupled ecosystem model of the North Sea and Baltic
1028 Sea: Part II. Spatial-seasonal characteristics in the North Sea as revealed by EOF analysis. *Journal of*
1029 *Marine Systems*, *61*(1–2), 100–113. https://doi.org/10.1016/j.jmarsys.2006.01.004
1030 Søndergaard, M., Williams, P. J. le B., Cauwet, G., Riemann, B., Robinson, C., Terzic, S., et al. (2000). Net
1031 accumulation and flux of dissolved organic carbon and dissolved organic nitrogen in marine plankton
1032 communities. *Limnology and Oceanography*, *45*(5), 1097–1111. https://doi.org/10.4319/lo.2000.45.5.1097
1033 Sullivan, M. R., Primeau, F. W., Hagstrom, G. I., Wang, W.-L., & Martiny, A. C. (2024). Integrating Trait-Based
1034 Stoichiometry in a Biogeochemical Inverse Model Reveals Links Between Phytoplankton Physiology and
1035 Global Carbon Export. *Global Biogeochemical Cycles*, *38*(3), e2023GB007986.
1036 https://doi.org/10.1029/2023GB007986
1037 Tanioka, T., & Matsumoto, K. (2017). Buffering of Ocean Export Production by Flexible Elemental Stoichiometry
1038 of Particulate Organic Matter. *Global Biogeochemical Cycles*, *31*(10), 1528–1542.
1039 https://doi.org/10.1002/2017GB005670
1040 Tanioka, T., Matsumoto, K., & Lomas, M. W. (2021). Drawdown of Atmospheric pCO2 Via Variable Particle Flux
1041 Stoichiometry in the Ocean Twilight Zone. *Geophysical Research Letters*, *48*(22), e2021GL094924.
1042 https://doi.org/10.1029/2021GL094924
1043 Tanioka, T., Garcia, C. A., Larkin, A. A., Garcia, N. S., Fagan, A. J., & Martiny, A. C. (2022). Global patterns and
1044 predictors of C:N:P in marine ecosystems. *Communications Earth & Environment*, *3*(1), 271.
1045 https://doi.org/10.1038/s43247-022-00603-6

1046 Teng, Y.-C., Primeau, F. W., Moore, J. K., Lomas, M. W., & Martiny, A. C. (2014). Global-scale variations of the
1047 ratios of carbon to phosphorus in exported marine organic matter. *Nature Geoscience*, *7*(12), 895–898.
1048 https://doi.org/10.1038/ngeo2303
1049 Thomas, H., Ittekkot, V., Osterroht, C., & Schneider, B. (1999). Preferential recycling of nutrients—the ocean's way
1050 to increase new production and to pass nutrient limitation? *Limnology and Oceanography*, *44*(8), 1999–
1051 2004. https://doi.org/10.4319/lo.1999.44.8.1999
1052 Thomas, H., Bozec, Y., Elkalay, K., & Baar, H. J. W. D. (2004). Enhanced Open Ocean Storage of CO2 from Shelf
1053 Sea Pumping. *Science*, *304*(5673), 1005–1008. https://doi.org/10.1126/science.1095491
1054 Thomas, H., Bozec, Y., Baar, H. J. W. de, Elkalay, K., Frankignoulle, M., Schiettecatte, L.-S., et al. (2005). The
1055 carbon budget of the North Sea. *Biogeosciences*, *2*(1), 87–96. https://doi.org/10.5194/bg-2-87-2005
1056 Thornton, D. C. O. (2014). Dissolved organic matter (DOM) release by phytoplankton in the contemporary and
1057 future ocean. *European Journal of Phycology*, *49*(1), 20–46.
1058 https://doi.org/10.1080/09670262.2013.875596
1059 Verdugo, P., Alldredge, A. L., Azam, F., Kirchman, D. L., Passow, U., & Santschi, P. H. (2004). The oceanic gel
1060 phase: a bridge in the DOM–POM continuum. *Marine Chemistry*, *92*(1–4), 67–85.
1061 https://doi.org/10.1016/j.marchem.2004.06.017
1062 Wakeham, S. G., & Lee, C. (1993). Production, Transport, and Alteration of Particulate Organic Matter in the
1063 Marine Water Column. In M. H. Engel & S. A. Macko (Eds.), *Organic Geochemistry* (Vol. 11, pp. 145–
1064 169). Boston, MA: Springer US. https://doi.org/10.1007/978-1-4615-2890-6_6
1065 Wakeham, S. G., & Lee, C. (2019). Limits of our knowledge, part 2: Selected frontiers in marine organic
1066 biogeochemistry. *Marine Chemistry*, *212*, 16–46. https://doi.org/10.1016/j.marchem.2019.02.005
1067 Wakelin, S. L., Holt, J. T., Blackford, J. C., Allen, J. I., Butenschön, M., & Artioli, Y. (2012). Modeling the carbon
1068 fluxes of the northwest European continental shelf: Validation and budgets. *Journal of Geophysical*
1069 *Research: Oceans*, *117*(C5), 2011JC007402. https://doi.org/10.1029/2011JC007402
1070 Wanninkhof, R. (2014). Relationship between wind speed and gas exchange over the ocean revisited. *Limnology*
1071 *and Oceanography: Methods*, *12*(6), 351–362. https://doi.org/10.4319/lom.2014.12.351

Wear, E. K., Carlson, C. A., Windecker, L. A., & Brzezinski, M. A. (2015). Roles of diatom nutrient stress and species identity in determining the short- and long-term bioavailability of diatom exudates to bacterioplankton. *Marine Chemistry*, *177*, 335–348. https://doi.org/10.1016/j.marchem.2015.09.001

Wear, E. K., Carlson, C. A., James, A. K., Brzezinski, M. A., Windecker, L. A., & Nelson, C. E. (2015). Synchronous shifts in dissolved organic carbon bioavailability and bacterial community responses over the course of an upwelling-driven phytoplankton bloom. *Limnology and Oceanography*, *60*(2), 657–677. https://doi.org/10.1002/lno.10042

Williams, P. J. (1995). Evidence for the seasonal accumulation of carbon-rich dissolved organic material, its scale in comparison with changes in particulate material and the consequential effect on net CN assimilation ratios. *Marine Chemistry*, *51*(1), 17–29. https://doi.org/10.1016/0304-4203(95)00046-T

Williams, P. M., Carlucci, A. F., & Olson, R. (1980). A deep profile of some biologically important properties in the central North Pacific gyre. *Oceanologica Acta*, *3*(4), 471–476. https://archimer.ifremer.fr/doc/00122/23291/21119.pdf

Winther, N. G., & Johannessen, J. A. (2006). North Sea circulation: Atlantic inflow and its destination. *Journal of Geophysical Research: Oceans*, *111*(C12), 2005JC003310. https://doi.org/10.1029/2005JC003310

Wolf-Gladrow, D. A., Zeebe, R. E., Klaas, C., Körtzinger, A., & Dickson, A. G. (2007). Total alkalinity: The explicit conservative expression and its application to biogeochemical processes. *Marine Chemistry*, *106*(1–2), 287–300. https://doi.org/10.1016/j.marchem.2007.01.006

Ye, F., Zhang, Y. J., He, R., Wang, Z., Wang, H. V., & Du, J. (2019). Third-order WENO transport scheme for simulating the baroclinic eddying ocean on an unstructured grid. *Ocean Modelling*, *143*, 101466. https://doi.org/10.1016/j.ocemod.2019.101466

Zhang, Y. J., Ye, F., Stanev, E. V., & Grashorn, S. (2016). Seamless cross-scale modeling with SCHISM. *Ocean Modelling*, *102*, 64–81. https://doi.org/10.1016/j.ocemod.2016.05.002

Zhang, Y. J., Stanev, E. V., & Grashorn, S. (2016). Unstructured-grid model for the North Sea and Baltic Sea: Validation against observations. *Ocean Modelling*, *97*, 91–108. https://doi.org/10.1016/j.ocemod.2015.11.009

Global Biogeochemical Cycles

Supporting Information for

Organic matter stoichiometry regulates the continental shelf carbon pump efficiency of the northwest European shelf seas

K. T. Demir[1], M. Mathis[1], J. Kossack[1], F. Liu[1], U. Daewel[1], C. Stegert[2], H. Thomas[3,4] and C. Schrum[1,5]

[1]Institute of Coastal Systems—Analysis and Modeling, Helmholtz-Zentrum Hereon, Geesthacht, Germany
[2]Bundesamt für Seeschifffahrt und Hydrographie, Hamburg, Germany
[3]Institute of Carbon Cycles, Helmholtz-Zentrum Hereon, Geesthacht, Germany
[4]Institute for Chemistry and Biology of the Marine Environment, Carl von Ossietzky University of Oldenburg, Oldenburg, Germany
[5]Institute of Oceanography, University of Hamburg, Hamburg, Germany

Contents of this file

Supplementary Figures S1 to S5

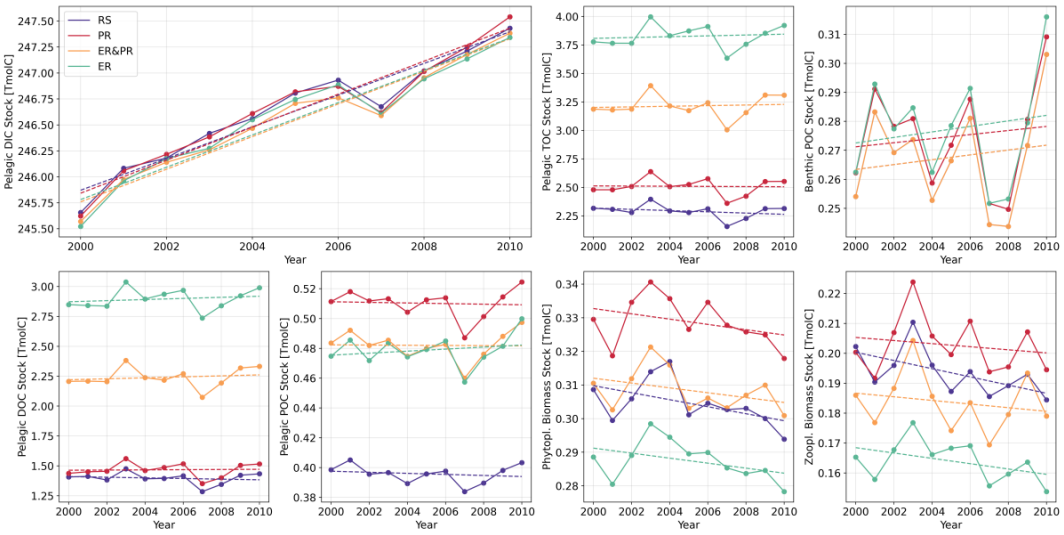

Figure S1. Annual mean organic and inorganic carbon stocks of the northwest European shelf seas (NWES) (solid lines and dots, in Tmol C) and trend lines (dashed), based on linear regression, for all configurations: extracellular release (ER), preferential remineralization (PR), the combined configuration (ER&PR), and the Redfield stoichiometry (RS) configuration. The stocks include pelagic dissolved inorganic carbon (DIC), pelagic total organic carbon (TOC), and benthic particulate organic carbon (POC). For the pelagic TOC stock, the four contributing organic carbon stocks are shown: detritus as dissolved organic carbon (DOC) and POC, along with total phytoplankton and zooplankton biomass, including all functional groups. The DOC pool represents a combination of the seasonally produced and respired labile and semi-labile DOC, with lifetimes of days to years, but not the refractory DOC, which maintains long-lived background concentrations. The average stocks and trends in Figures 3 and 5 are based on these stocks, trends, and their differences.

Figure S2. Differences in annual net cross-shelf DOC transports (solid lines and dots), expressed in Tmol C yr^{-1}, across individual shelf break sections of the northwest European shelf seas (NWES) and net DOC exchange with the Atlantic Ocean and the Baltic Sea for the extracellular release (ER), preferential remineralization (PR), and the combined configuration (ER&PR) compared to the Redfield stoichiometry (RS) configuration. The dashed lines indicate the mean over the simulated period 2000–2010, and the shaded areas show the standard deviation between annual means.

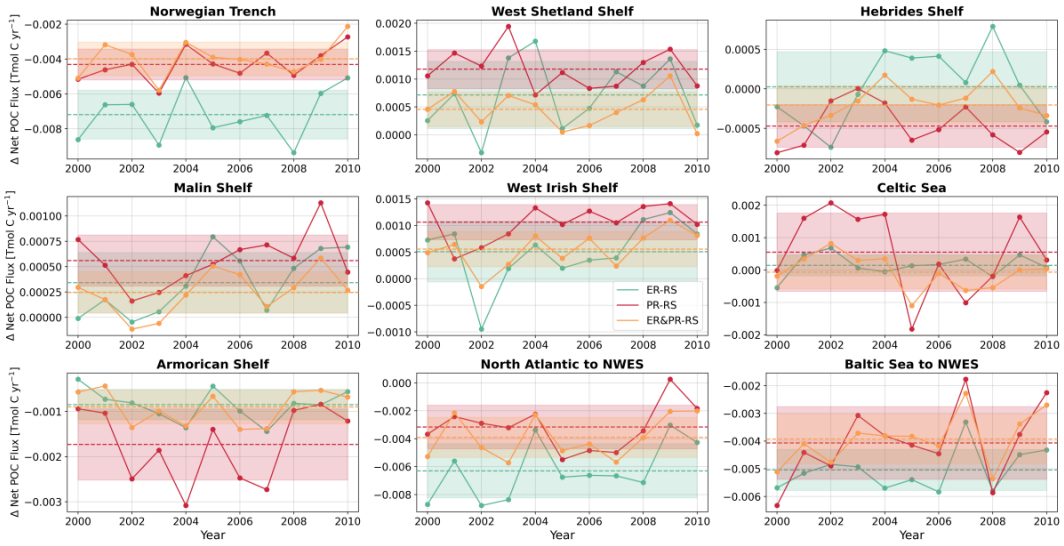

Figure S3. Differences in annual net cross-shelf POC transports (solid lines and dots), expressed in Tmol C yr^{-1}, across individual shelf break sections of the northwest European shelf seas (NWES) and net POC exchange with the Atlantic Ocean and the Baltic Sea for the extracellular release (ER), preferential remineralization (PR), and the combined configuration (ER&PR) compared to the Redfield stoichiometry (RS) configuration. The dashed lines indicate the mean over the simulated period 2000–2010, and the shaded areas show the standard deviation between annual means.

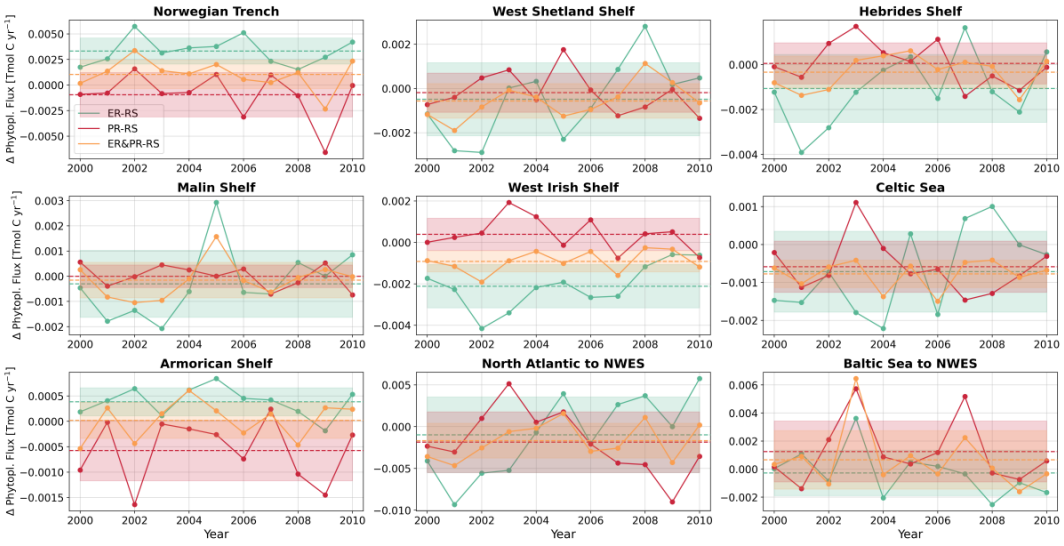

Figure S4. Differences in annual net cross-shelf phytoplankton biomass transports (solid lines and dots), expressed in Tmol C yr^{-1}, across individual shelf break sections of the northwest European shelf seas (NWES) and net phytoplankton biomass exchange with the Atlantic Ocean and the Baltic Sea for the extracellular release (ER), preferential remineralization (PR), and the combined configuration (ER&PR) compared to the Redfield stoichiometry (RS) configuration. The dashed lines indicate the mean over the simulated period 2000–2010, and the shaded areas show the standard deviation between annual means.

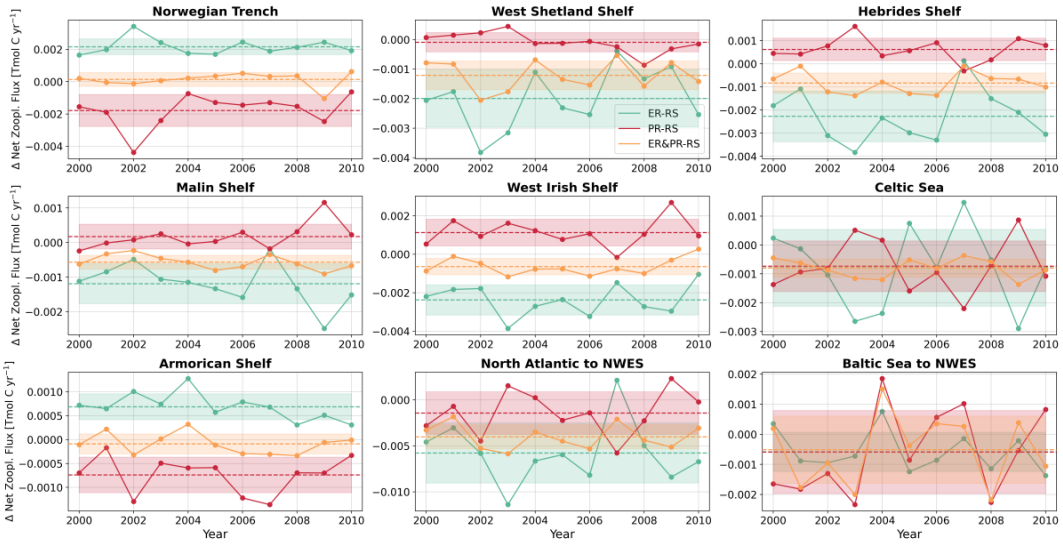

Figure S5. Differences in annual net cross-shelf zooplankton biomass transports (solid lines and dots), expressed in Tmol C yr^{-1}, across individual shelf break sections of the northwest European shelf seas (NWES) and net zooplankton biomass exchange with the Atlantic Ocean and the Baltic Sea for the extracellular release (ER), preferential remineralization (PR), and the combined configuration (ER&PR) compared to the Redfield stoichiometry (RS) configuration. The dashed lines indicate the mean over the simulated period 2000–2010, and the shaded areas show the standard deviation between annual means.

Acknowledgements

I wish to acknowledge with gratitude the individuals and institutions who have supported me during the completion of this dissertation. My supervisor Corinna Schrum provided invaluable guidance and expertise in coupled physical–biogeochemical and ecosystem models, while my co-supervisor Helmuth Thomas offered key insights on the interpretation of observations and their role in advancing model-based understanding. The extensive and insightful discussions with my second co-supervisor Moritz Mathis were fundamental in shaping this work and situating it within the broader context of the carbon cycle in the global coastal ocean. In addition, I am grateful to Ute Daewel for her guidance in understanding primary producers and food web dynamics, which greatly enriched the ecological perspective of this work.

I also thank Jan Kossack and Feifei Liu for the collaborative work and stimulating discussions on carbonate system dynamics and their implementation. Furthermore, I am thankful to the SICSS graduate school for providing a unique program and the opportunity to connect with a broad community of researchers in climate and Earth sciences. Being part of the excellence cluster CLICCS has offered a highly interdisciplinary research environment, broadening my perspective and enriching my approach to complex interactions of biogeochemistry and climate. I would like to thank the Helmholtz-Zentrum Hereon for the opportunities to participate in a total of three summer schools, which strongly supported my academic and professional development and reflects the institute's appreciation for continued qualification.

Finally, I owe special gratitude to my parents for their unwavering support in my pursuit of an academic career and for instilling in me the value of education from the very beginning. Most of all, I would like to thank Christine for supporting me through every hardship and for inspiring me in all aspects of life and science.

Eidesstattliche Versicherung | Declaration on oath

Hiermit erkläre ich an Eides statt, dass ich die vorliegende Dissertationsschrift selbst verfasst und keine anderen als die angegebenen Quellen und Hilfsmittel benutzt habe. Sofern im Zuge der Erstellung der vorliegenden Dissertationsschrift generative Künstliche Intelligenz (gKI) basierte elektronische Hilfsmittel verwendet wurden, versichere ich, dass meine eigene Leistung im Vordergrund stand und dass eine vollständige Dokumentation aller verwendeten Hilfsmittel gemäß der Guten wissenschaftlichen Praxis vorliegt. Ich trage die Verantwortung für eventuell durch die gKI generierte fehlerhafte oder verzerrte Inhalte, fehlerhafte Referenzen, Verstöße gegen das Datenschutz- und Urheberrecht oder Plagiate.

I hereby declare and affirm that this doctoral dissertation is my own work and that I have not used any aids and sources other than those indicated. If electronic resources based on generative artificial intelligence (gAI) were used in the course of writing this dissertation, I confirm that my own work was the main and value-adding contribution and that complete documentation of all resources used is available in accordance with good scientific practice. I am responsible for any erroneous or distorted content, incorrect references, violations of data protection and copyright law or plagiarism that may have been generated by the gAI.

Hamburg, den 15.09.25

Ort, Datum | City, Date

Unterschrift | Signature